

The Continental Shelf: a Conveyor and/or Filter of Sediment to Deep- Water?

Grace Isabel Emma Cosgrove

Submitted in accordance with the requirement for the degree of
Doctor of Philosophy

The University of Leeds
Institute of Applied Geoscience
School of Earth and Environment

March 2019

The candidate confirms that the work submitted is his/her own, except where work which has formed part of jointly-authored publications has been included. The contribution of the candidate and the other authors to this work has been explicitly indicated below. The candidate confirms that appropriate credit has been given within the thesis where reference has been made to the work of others. Contributors to jointly-authored publications are outlined below.

Chapter Three

G.I.E. Cosgrove: principal investigator, collected and analysed all grain character data and main author.

D.M. Hodgson: discussion, manuscript review.

M.P. Poyatos-Moré: discussion, manuscript review.

N.P. Mountney: discussion, manuscript review.

W.D. McCaffrey: discussion, manuscript review.

Chapter Four

G.I.E. Cosgrove: principal investigator, collected and analysed all grain character data and main author.

D.M. Hodgson: discussion, manuscript review.

N.P. Mountney: discussion, manuscript review.

W.D. McCaffrey: discussion, manuscript review.

Chapter Five

G.I.E. Cosgrove: principal investigator, collected and analysed all grain character data and main author.

M.P. Poyatos-Moré: fieldwork assistance, discussion, manuscript review.

D. Lee: fieldwork assistance, manuscript review.

D.M. Hodgson: fieldwork assistance, discussion, manuscript review.

N.P. Mountney: discussion, manuscript review.

W.D. McCaffrey: discussion, manuscript review.

This copy has been supplied on the understanding that it is copyright material and that no quotation from the thesis may be published without proper acknowledgement.

The right of Grace Cosgrove to be identified as Author of this work has been asserted by her in accordance with the Copyright, Designs and Patents Act 1988.

© 2019 The University of Leeds and Grace Isabel Emma Cosgrove

Acknowledgements

I would like to thank my supervisors, David Hodgson, Nigel Mountney and Bill McCaffrey for their guidance and support throughout the course of my PhD. I would also like to thank Miquel Poyatos-Moré and David Lee for their assistance in the field and contributions to manuscripts.

The Bremen Core Repository (University of Bremen), the Cohen Lab (University of Leeds), the Sorby Lab (University of Leeds) and the Leeds Electron Microscopy and Spectroscopy Centre (University of Leeds) and John Wyn-Williams (University of Leeds) are also thanked for their assistance with sample collection, preparation and analysis. IAG at the University of Leeds are also thanked for their financial contribution towards fieldwork in the Pyrenees.

Big love to my parents Caroline and Steve, to the wider Cosgrove clan, to the residents of 3 Roxholme Road, and all of my beautiful friends at Leeds University and beyond.

Abstract

Outcrop and core-based studies of clinothems provide valuable archives basin-margin evolution. However, published quantitative grain character data (including grain size, grain shape, sorting, and sand-to-mud-ratios) are limited, and grain character variation across complete clinothem systems remains poorly constrained. Novel quantitative grain character datasets are presented here for core (Miocene intrashelf clinothems, offshore New Jersey) and outcrop (Eocene clinothems, Sobrarbe Deltaic Complex, Spain) case studies, which target quasi-coeval topset, foreset and bottomset deposits of prograding clinothems.

Grain character datasets reveal that basin-scale and intraclinothem variations in sedimentary fabric are dependent on the dominant process-regime in operation at the shelf-edge. At basin-scales, shelf process-regime plays a more important role than clinofom trajectory in determining the location and timing of coarse-grained sediment delivery; river-dominated clinothems effectively convey coarse-grained sediment downdip under both rising and falling clinofom rollover trajectories. At intraclinothem scales abrupt stratigraphic changes in process-regime significantly impact the distribution of grain character across the complete depositional profile, forming observable and quantifiable intraclinothem chronostratigraphic surfaces.

The grain-character dataset has been used to: i) compile unique databases of grain size, grain shape, and sorting statistics, which can be applied to test and refine numerical forward models of sediment distribution, which seek to improve prediction of lithology distribution; ii) quantitatively define intraclinothem surfaces at a higher resolution than is possible using chronostratigraphic techniques; iii) refine the placement of sequence boundaries, and iv) develop a model of clinothem evolution, in which the nature of the flows, and dominant process-regime in the shelf, control the downdip and vertical distribution of sand and mud. This study challenges widely held paradigms that link accommodation, sediment supply, and clinofom rollover trajectories to the distribution of sediment on basin margins. The results highlight the critical role played by the shelf process-regime in determining how and when sediment of different calibre and maturity is transported downdip.

Chapter 1 Contents

Chapter 1 Introduction	1
1.1 Introduction	2
1.1.1 Source-to-Sink Systems.....	2
1.1.2 The Continental Shelf as a Conveyor or Filter	2
1.1.3 Clinoforms and Clinothems.....	4
1.1.4 Shelf and Topset Process-Regime.....	6
1.1.5 Grain character along the Depositional Profile.....	7
1.2 Aims and Objectives	8
1.2.1 Research Question One	8
1.2.2 Research Question Two	10
1.2.3 Research Question Three.....	11
1.2.4 Research Question Four.....	12
1.3 Literature Review	13
1.3.1 Clinoforms and Clinothems.....	13
1.3.2 Clinothems: Fundamental Components of Stratigraphy	15
1.3.3 Prediction of Deep-Water Sands in Clinoforms.....	23
1.3.4 Controls on the Delivery of Sediment to Deep-Water.....	29
1.3.5 Shelf Process-Regime.....	33
1.4 Thesis Layout.....	47
1.4.1 Chapter One	48
1.4.2 Chapter Two	48
1.4.3 Chapter Three.....	48
1.4.4 Chapter Four.....	48
1.4.5 Chapter Five	49
1.4.6 Chapter Six	49
Chapter 2 Materials and Methods	50
2.1 Introduction	51
2.1.1 IODP Expedition 313, Offshore New Jersey	51
2.1.2 Sobrarbe Deltaic Complex, South Central Pyrenees, Spain	53
2.2 Offshore New Jersey Dataset.....	53

2.2.1 Materials	54
2.2.2 Methods	57
2.2.3 Grain size and Shape Analysis	63
2.2.4 Clinoform Rollover Trajectory Analysis	70
2.2.5 Sedimentological Interpretations	70
2.3 Sobrarbe Deltaic Complex (Ainsa Basin) Dataset	70
2.3.1 Introduction	70
2.3.2 Materials	72
2.3.3 Methods	72
2.4. Sample Storage	74
Chapter 3 Manuscript One	76
3.1 Abstract	77
3.2 Introduction	77
3.2.1 Nomenclature	79
3.3 Geological Setting	80
3.3.1 Sequence Boundaries	81
3.4 Data and Methods	81
3.4.1 Materials	81
3.4.2 Methods	82
3.5 Results	86
3.5.1 Sequence m5.7	86
3.5.2 Sequence m5.45	91
3.5.3 Sequence m5.4	97
3.5.4 Sequence m5.3	104
3.5.5 Clinothem Groupings	109
3.6 Discussion	112
3.6.1 Controls on Differences between Type A and B Clinothems	112
3.6.2 Lateral Variability in Process-Regime	113
3.6.3 Interaction of Shelf Process-regime and Clinoform Rollover Trajectory	114
3.7 Conclusions	119
Chapter 4 Manuscript Two	121
4.1 Abstract	122
4.2 Introduction	122
4.3 Geological Setting	125

4.4 Sequence m5.4.....	127
4.4.1 Site M27	127
4.4.2 Site M28	128
4.4.3 Site M29	130
4.5 Methods.....	130
4.5.1 Facies Associations and Depositional Environments.....	130
4.5.2 Grain-Character Analysis.....	131
4.6 Results	132
4.6.1 Topset Deposits (Core M27): Description	133
4.6.2 Topset Deposits (Core M27): Interpretation.....	133
4.6.3 Foreset Deposits (Core M28): Description.....	134
4.6.4 Foreset Deposits (Core M28): Interpretation.....	134
4.6.5 Bottomset Deposits (Core M29): Description	139
4.6.6 Bottomset Deposits (Core M29): Interpretation.....	139
4.6.7 Process Summary	139
4.6.8 Grain Character	143
4.6.9 Correlations Across Topset-Foreset-Bottomset Profiles.....	144
4.6.10 Up-Core Grain-Size Patterns.....	151
4.7 Discussion	154
4.7.1 How Does Intraclinothem Topset Process-Regime Influence Downdip Grain Character?	154
4.7.2 How Can High-Resolution Grain Character Data Be Used As An Additional Correlation Tool?	158
4.7.3 How Can High-Resolution Grain Character Data Be Used As An Additional Tool To Refine Sequence Boundaries?	160
4.8 Conclusions	166
Chapter 5 Manuscript Three.....	168
5.1 Abstract.....	169
5.2 Introduction	169
5.2.1 Nomenclature.....	171
5.3 Geological Setting.....	172
5.4 Methods.....	174
5.5 Clinothem Geometry	176
5.5.1 Description	176
5.5.2 Interpretation.....	176

5.6 Facies Associations and Descriptions	176
5.6.1 Shelf Deposits	178
5.6.2 Slope Deposits	182
5.7 Process-Regime Variability	190
5.8 Basinward Change	190
5.8.1 Grain Size.....	191
5.8.2 Sorting.....	191
5.9 Discussion	191
5.9.1 Mixed-Process Clinothem Evolution.....	191
5.9.2 Sediment Bypass at the Clinof orm Rollover.....	192
5.9.3 Allo genic and Autogen ic Process Regime Variability.....	195
5.10 Conclusions	196
5.11 Supplementary Information.....	198
Chapter 6 Discussion, Conclusions and Future Work.....	200
6.1 Discussion	201
6.1.1 Research Question One	201
6.1.2 Research Question Two	225
6.1.3 Research Question Three	238
6.1.4 Research Question Four.....	253
6.2 Conclusions	257
6.2.1 What are intermediate-scale clinothems?.....	258
6.2.2 What role does process-regime play in regulating the timing of sand transfer, and in controlling the character of grains delivered, to the slope and basin-floor settings?	259
6.2.3 How can grain-character be used to improve understanding of clinothem evolution?	259
6.2.4 What value do high-resolution quantitative grain-character datasets offer to sedimentology and stratigraphy?	260
6.2.5 Final Remarks	261
6.3 Future Work.....	261
6.3.1 Lateral Variability.....	261
6.3.2 Expanding the New Jersey Dataset.....	263
6.3.3 Expanding the Sobrarbe Deltaic Complex Dataset.....	264
6.3.4 Geochemical Datasets	265
6.3.5 Conclusions	268
Chapter 7 References	270

List of Tables

Table 2.1: Advantages and disadvantages of various methods of grain character analysis.	64
Table 2.2: Mathematical parameters used by the CamsizerXT software to calculate the grain size distribution of a sediment sample.	68
Table 3.1: Data on grain size and grain character for M5.7	90
Table 3.2: Data on grain size and grain character for M5.45	96
Table 3.3: Data on grain size and grain character for M5.4.	101
Table 3.4: Data on grain size and grain character for M5.3	109
Table 4.1: Summary of the observed lithology and sedimentary texture of the Core M27.	135
Table 4.2 Summary of the observed lithology and sedimentary texture of the Core M28.	137
Table 4.3: Summary of the observed lithology and sedimentary texture of the Core M29.	138
Table 4.4: Summary of grain character for topset deposits (sedimentary package M27a-c)	140
Table 4.5: Summary of grain character for foreset deposits (sedimentary package M28a-c).....	141
Table 4.6: Summary of grain character for bottomset deposits (sedimentary package M29a-c)..	142
Table 5.1: Descriptions and interpretations of shelf and slope facies associations (FA A – FA F)..	177
Table 5.2: Supplementary information showing the georeferenced sample locations. The sampling locations and sampling numbers are shown in Figure 5.16.	199
Table 6.1: Comparison of various clinothem parameters between clinothem classes	203
Table 6.2: Comparison of various clinothem parameters between a series of intermediate-scale clinothems. Adapted from: Dreyer et al., 1999; Steel et al., 2000; Mellere et al., 2003; Dreyer et al., 2005; Pyles.....	207
Table 6.3: Comparison of various clinothem parameters between a series of seismically imaged intermediate-scale clinothems.	211
Table 6.4: Comparison of various clinothem parameters between clinothem classes; modified from Table 6.1, with the intrashelf clinothem class included.....	225
Table 6.5: Glauconite maturity in relation to depositional setting and the sequence stratigraphic framework. Adapted from Amorosi (1995).	266

List of Figures

Figure 1.1: Genetically linked segments within the source-to-sink system	3
Figure 1.2: Simplified dip-parallel profile showing different scales of compound clinoform systems	4
Figure 1.3: Clinoforms within a sedimentary prism of a prograding basin margin.	7
Figure 1.4: Regional cross-section, showing idealised clinoform systems, highlighting delta-scale, shelf-edge and shelf-slope-basin clinoforms.....	15
Figure 1.5: Parasequence stacking patterns in parasequence sets showing depositional cross-section, schematic log and clinoform expression.....	20
Figure 1.6: Simplified clinothem model displaying systems tracts and major sequence stratigraphic surfaces.	22
Figure 1.7: Estimations of sand delivery to the deep-water environment	23
Figure 1.8: Scales of trajectory analysis within prograding systems.	26
Figure 1.9: Examples of dip-parallel seismic sections displaying well-defined clinoforms and clinoform trajectories.....	27
Figure 1.10: Internal clinoforms within a sedimentary prism of a prograding basin margin.....	28
Figure 1.11: Established clinoform rollover trajectory model.....	29
Figure 1.12: Clinoform datasets used by Dixon et al. (2012a).....	32
Figure 1.13: Ternary diagram illustrating river-, wave- and tide-dominated deltas.....	34
Figure 1.14: Schematic diagram showing morphology of a modern wave-dominated delta	35
Figure 1.15: Eocene Porcupine Basin, Offshore Ireland.....	36
Figure 1.16: Tide-dominated Ganges-Brahmaputra river delta.	37
Figure 1.17: Schematic cross-section illustrating major morphologic and physiographic features of a tide-dominated delta system.....	39
Figure 1.18: Schematic diagram showing a simplified river-dominated delta	40
Figure 1.19: Schematic diagram of a downwelling hyperpycnal flow	41
Figure 1.20: Deposits of Eocene Central Basin of Spitsbergen.....	42
Figure 1.21: Schematic Logs depicting classic wave-, tide- and river-dominated deltas.....	44
Figure 1.22: Simplified diagram of a mixed-energy deltaic system	45
Figure 1.23: Evolution of the Mississippi Delta during the Holocene	46
Figure 1.24: Chimney Rock Member, showing an ancient example of autogenic change in process-regime from wave- to river-dominated.	47
Figure 2.1: Location map of the New Jersey sea level transect.....	51
Figure 2.2: Seismic line Oc270 529	52
Figure 2.3: Seismic line Oc270 529. Sequence boundaries relevant to Chapter Four are highlighted in red. Depositional sequence m5.4 is highlighted in blue.	52
Figure 2.4: Geological map of the Sobrarbe Deltaic Complex and surrounding formations	53
Figure 2.5: Seismically imaged clinothems of the New Jersey Margin	54
Figure 2.6: Representative core photographs of different the five dominant lithofacies. a) Silt lithofacies.	55
Figure 2.7: Illustration of the sampling strategy used in this investigation. The sampling frequency is plotted against core depth (mcd).....	57

Figure 2.8: Photographs illustrating methodology of sample preparation and pretreatment prior to grain size and grain shape analysis..	62
Figure 2.9: Comparison of optical microscopy and DIA techniques.	65
Figure 2.10: Schematic diagram of CamsizerXT.	66
Figure 2.11: Image shows the how the mathematical parameters ‘maximum chord’ (X_c) and ‘minimum chord’ ($X_{c\ min}$) are defined.	68
Figure 2.12: Schematic diagram showing how shape parameters are calculated from a particle converted into binary format.	69
Figure 2.13: Photographs illustrating methodology of sample collection and preparation for grain size analysis	75
Figure 3.1: Location map of New Jersey sea-level transect,	80
Figure 3.2: Seismic line Oc270 529	81
Figure 3.3: Representative core photographs of Clinothem sequences m5.7 (a-c), m5.45 (d-f), m5.4 (g-i) and m5.3 (j-l)	84
Figure 3.4: Average grain size distribution plots for the topset, foreset, and bottomset deposits of Sequences m5.7.	85
Figure 3.5: Box and whisker plots for Sequence m5.7	90
Figure 3.6: Grain size cumulative frequency plot for topset (5a), foreset (5b) and bottomset (5c) deposits of Sequence m5.7.	91
Figure 3.7 Box and whisker plots for Sequence m5.45	96
Figure 3.8: Grain-size cumulative frequency plot for topset (5a), foreset (5b), and bottomset (5c) deposits of Sequence m5.45	97
Figure 3.9: Box and whisker plots for Sequence m5.4	102
Figure 3.10: Grain size cumulative frequency plot for topset (5a), foreset (5b) and bottomset (5c) deposits of Sequence m5.4.	103
Figure 3.11: Grain-size cumulative frequency plot for topset (5a), foreset (5b) and bottomset (5c) deposits of Sequence m5.3.	105
Figure 3.12: Box and whisker plots for Sequence m5.3	109
Figure 3.13: Plots of average grain size distribution comparing the topset, foreset, and bottomset deposits of Type A and Type B clinothems.	110
Figure 3.14: Idealised Type A and B clinothem sequences and associated downdip grain character changes.	117
Figure 4.1: Schematic diagram of a clinothem sequence	123
Figure 4.2: Location map of New Jersey sea level transect.	125
Figure 4.3: Location map of New Jersey sea level transect, modified from Expedition 313 Scientists (2010). Study sites used in this paper (Integrated Ocean Drilling Program [IODP] Expedition 313 Sites M27, M28 and M29) are presented as blue circles.	126
Figure 4.4: Correlation panel displaying various authors’ composite sequence boundary (m5.3 and m5.4) and sequence boundary (m5.4-1, m5.34 and m5.33) interpretations	129
Figure 4.5: Simplified lithologic columns of Sites M27 (a), M28 (b) and M29 (c). The purple lines illustrate the boundaries of the core described in Tables 4.1 – 4. 3.	132
Figure 4.6: Representative core photographs	133
Figure 4.7: Average grain-size distribution profiles	145
Figure 4.8: Correlation panel.	146
Figure 4.9: Box and whisker plot for sedimentary packages M27a, M27b and M27c (topset deposits).	147

Figure 4.10: Pie charts showing average sand-to-mud composition by percentage volume.	148
Figure 4.11: Box and whisker plot for sedimentary packages M28a, M28b and M28c (foreset deposits).....	149
Figure 4.12: Box and whisker plot for sedimentary packages M29a, M29b and M29c (bottomset deposits).....	150
Figure 4.13: Box and whisker plot for sedimentary packages M27-M29a.....	151
Figure 4.14: Box and whisker plot for sedimentary packages M27-M29b (topset-bottomset profile)	152
Figure 4.15: Box and whisker plot for sedimentary packages M27-M29c (topset-bottomset profile)	153
Figure 4.16: Comparison of the ‘original general lithology’ (Mountain et al., 2010), ‘original cumulative lithology’ (Miller et al., 2013b) and ‘new cumulative grain-size patterns’ (this study)..	160
Figure 4.17: Pie-charts showing average sand-to-mud composition by percentage volume across the candidate sequence boundaries.....	161
Figure 4.18: Percentage difference in grain character across candidate sequence boundaries....	164
Figure 5.1: Map showing the location of the Ainsa Basin and the key neighbouring structural features.	171
Figure 5.2: Simplified Geological map of the study area	172
Figure 5.3: Regional cross-section showing the Sobrarbe Deltaic Complex stratigraphy.....	173
Figure 5.4: Outcrop model constructed from UAV photographs showing the study site and total log thickness at each logging and sampling location.....	175
Figure 5.5: Pie charts illustrating differences in grain-size composition between Facies A-E.....	178
Figure 5.6: Grain size and sorting for Facies A-E.....	178
Figure 5.7: Sedimentary logs showing stratigraphic and dip-parallel facies distributions in Cycle LG-1.	180
Figure 5.8: Representative facies photographs (FA A and FA B)	181
Figure 5.9: Representative facies photographs (FA C)	182
Figure 5.10: Basinward trends in grain size and sorting for Facies A-E of Cycle LG-1.....	184
Figure 5.11: Representative facies photographs (FA D).....	185
Figure 5.12: Representative facies photographs (FA E).	187
Figure 5.13: Grain-size cumulative frequency plot showing basinward changes in grain size at each sampling location.	189
Figure 5.14: Basinward trends in grain-size and sorting data.	190
Figure 5.15: Clinothem model based on Cycle LG-1, including schematic grain-size logs.	194
Figure 5.16: Supplementary information illustrating sample numbers and sample locations within sedimentary logs.....	198
Figure 6.1: Comparison of the scale, architecture and relative position on the shelf, of the New Jersey clinothems with subaqueous, shelf-edge and mid-shelf clinothems	202
Figure 6.2: Examples of ramp style intermediate-scale clinothems..	213
Figure 6.3: Idealised ramp and slope style clinothems.	214
Figure 6.4: Examples of slope intermediate-scale clinothems	215
Figure 6.5: Interpreted systems tracts (as per Proust et al. 2018), overlain onto sedimentary log (Mountain et al., 2010) and quantitative cumulative grain size data (this thesis).	219
Figure 6.6: Alternative scenario of New Jersey clinothem formation.	221

Figure 6.7: Relationship between clinofrom rollover trajectory, process-regime and sand- and mud distribution.	227
Figure 6.8: Box and whisker plots illustrating the difference in grain-size across topset (M27), foreset (M28) and bottomset (M29) deposits between the river- and wave-dominated portions of an individual clinothem sequence (Sequence m5.4).	229
Figure 6.9: Box and whisker plots illustrating the grain roundness and sorting of topset (shelf), foreset (slope) and bottomset (basin-floor) deposits in river-dominated and wave-dominated clinothems.	Error! Bookmark not defined.
Figure 6.10: Box and whisker plots illustrating the grain sphericity and roundness of topset (shelf), foreset (slope) and bottomset (basin-floor) deposits in river-dominated and wave-dominated clinothems.	231
Figure 6.11: Heterogeneity within river-dominated topset deposits (Core M27) in Sequences m5.7 and m5.3.	232
Figure 6.12: Box and whisker plots illustrating the difference in grain character attributes between the topset (Core M27) deposits of river-dominated Sequences m5.7 and m5.3.	233
Figure 6.13: Summary diagram illustrating the sedimentological, architectural and grain character attributes of river-dominated Sequences m5.7 and m5.3.	236
Figure 6.14: Summary diagram illustrating the sedimentological, architectural and grain character attributes of river-dominated Cycle LG-1.	237
Figure 6.15: a) Summary diagram illustrating the sedimentological, architectural and grain character attributes of wave-dominated Sequences m5.45 and m5.4.	238
Figure 6.16: Tripartite classification scheme of Galloway (1975). The black lines illustrate the stratigraphic evolution of the dominant process-regime within Sequence m5.4 and Cycle LG-1.	239
Figure 6.17: Core (a-f) and outcrop (g-j) facies photos, showing river- and wave-dominated facies within Sequence m5.4 and Cycle LG-1.	240
Figure 6.18: box and whisker plots illustrating grain size (a-c) and sorting (d-f) in the topset (shelf), foreset (slope) and bottomset (basin-floor) deposits of Sequence m5.4 and Cycle LG-1, comparing the river- and wave-dominated portions of each clinothem, respectively.	243
Figure 6.19: Summary diagram illustrating the differences in grain-size composition between river- and wave-dominated deposits within a single clinothem (Sequence m5.4).	244
Figure 6.20: Summary diagram illustrating the differences in mean grain-size and sphericity between river- and wave-dominated deposits, within a single clinothem (Sequence m5.4).	245
Figure 6.21: Summary diagram illustrating the differences in mean roundness and sorting between river- and wave-dominated deposits, within a single clinothem (Sequence m5.4).	246
Figure 6.22: Summary diagram showing the geometric, downdip and stratigraphic distribution of river- and wave-dominated facies with Cycle LG-1.	248
Figure 6.23: Difference in grain size for wave-dominated and river-dominated sedimentary packages. The river-dominated sedimentary packages are subdivided into sustained and episodic hyperpycnal flows.	249
Figure 6.24: Summary diagram showing lateral (along strike), temporal (stratigraphic) and downdip variability associated with river-dominated, mixed-energy and wave-dominated clinothem sequences.	252
Figure 6.25: Summary diagram showing the differences in grain-size composition between a) sedimentary logs (qualitative; Mountain et al., 2010), b) cumulative lithologies (qualitative/ semi quantitative; Browning et al., 2013) and c) the new quantitative dataset presented in this thesis.	256

Figure 6.26: Three dip-parallel cross-sections of the lower Waterford Formation, capturing along-strike variation in sedimentary facies. Inset shows the location of the lower Waterford Formation. Adapted from Jones et al. (2015).....	263
Figure 6.27: Location map illustrating location of planned 3-D seismic survey, which encompasses the IODP Expedition 313 drill sites. The Expedition 313 drill sites exist within grids of 2-D seismic profiles (violet, yellow and grey lines).	264
Figure 6.28: Progressive stages of glauconitisation, showing the four stages of glauconite evolution. X-ray diffractogram for glauconite evolution are shown, as are cartoons of glauconite grains at various stages of evolution. Adapted from Odin and Matter (1981) and McCracken et al. (1996)	267

Chapter 1 Introduction

This introductory chapter outlines the main aims, objectives and research questions addressed in this PhD thesis; a summary of each chapter is also provided. A literature review is included, covering the major areas of research explored in this thesis. This includes: an i) introduction to clinoforms and clinothems; ii) sequence stratigraphy and clinothems; iii) prediction of deep-water sands using clinothem trajectory; iv) clinoform trajectory analysis; and v) shelf and topset process-regime types.

1.1 Introduction

1.1.1 Source-to-Sink Systems

The source-to-sink system, or sediment routing system (e.g., Meade, 1972, 1982; Allen, 1997, 2005, 2008; Densmore et al., 2007; Sømme et al., 2009; Martinsen et al., 2011) comprises genetically linked segments (Moore, 1969), which together encompass the erosion, transportation and deposition of sediments (Allen, 2008). Underpinning source-to-sink analysis is the idea that the entire sedimentary system, from the continental upstream source to the deep-marine sink, is intrinsically linked (Sømme et al., 2009). As such, processes affecting one segment of the source-to-sink system (i.e. catchment, shelf, slope, basin-floor) cause morphological modifications to one, or all, adjacent segments within the source-to-sink system (Fig. 1.1).

The source-to-sink system typically initiates in mountainous upland areas in drainage basins. Sediment, weathered via a variety of physical, chemical and biological processes, is eroded via rivers and streams and transported to lower relief areas of the catchment, which are governed by bypass (transport) and deposition (storage) (Romans and Graham, 2013). These subaerial, transport-dominated areas transition in a basinward direction to the subaqueous shelf, slope and basin-floor settings, which are dominated by sediment accumulation, long-term sediment storage, burial and lithification (Romans et al., 2009; Sømme et al., 2009). Alternatively, the sink, within the source-to-sink system, could be lacustrine, or even non-marine (e.g., a terminal fluvial fan).

1.1.2 The Continental Shelf as a Conveyor or Filter

Throughout the depositional profile, a number of key transitional zones exist, which demarcate the transition between the various segments (i.e. catchment, shelf, slope, basin-floor; Fig. 1.1) of the source-to-sink system. The focus of this research is the transitional zone between the subaqueous shelf and the slope and basin-floor settings. In systems that pass into marine settings, the shelf (or alternatively the marine ramp) represents a key interface between terrestrial sediment source areas and deep-water systems (Covault and Fildani, 2014); as such, shelves connect the subaerial and submarine segments of the source-to-sink system, and act as staging areas for the delivery of sediment to deeper-water settings (Posamentier and Kolla, 2003). In the context of the source-to-sink system, the shelf can either be a sediment conveyor, where sediment is efficiently distributed basinward, or a sediment filter, where sediment is (partially) reworked and/or stored on the continental shelf

(Posamentier and Kolla, 2003; Plink-Björklund and Steel, 2004; Petter and Steel, 2006; Covault and Fildani, 2014; Dixon et al., 2012a; Jones et al., 2015 Gong et al., 2016).

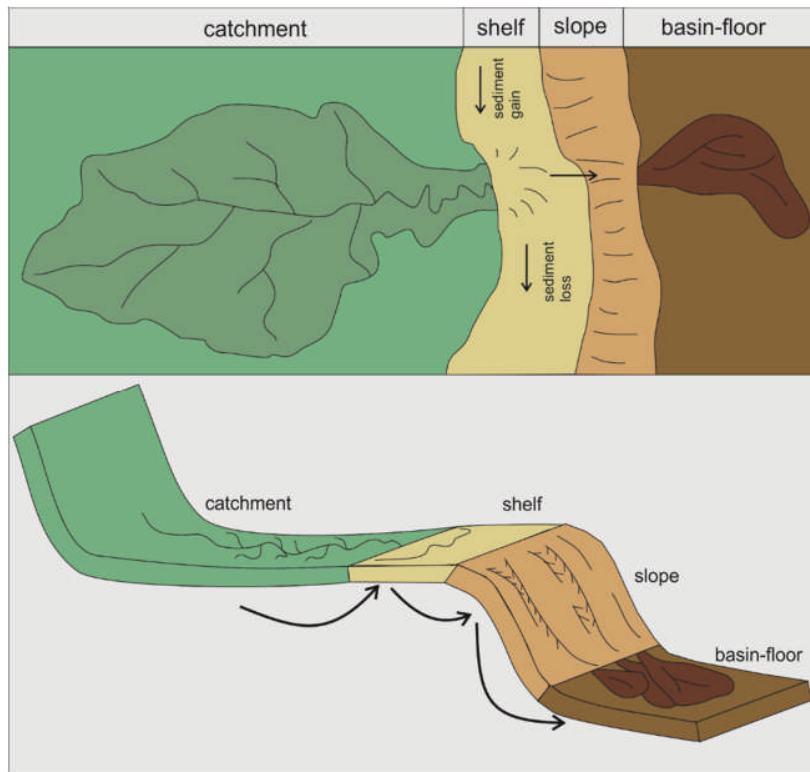


Figure 1.1: Genetically linked segments within the source-to-sink system; modification to one of the segments, through processes of deposition and erosion, will affect adjacent segments, resulting in modification to the system as a whole. Adapted from Sømme et al., (2009) and Martinsen et al., (2011).

Despite recent advancements in analyses of source-to-sink systems, the critical role played by the continental shelf in regulating sediment transfer to deep-water settings remains relatively poorly understood and largely unquantified. There is a need to better-constrain the buffering role played by the shelf on sediment dispersal patterns, in terms of both morphological and sedimentological parameters. The key question to be answered is ‘how and when is sediment of different calibre and maturity transported off the shelf into deeper-water settings?’

To help address this question, this study will focus on two seawardly prograding clinothem systems. Quantitative grain character databases have been produced using samples recovered from core (offshore New Jersey, USA, Western Atlantic Ocean) and outcrop (Cycle LG-1, Sobrarbe Deltaic Complex, South-Central Pyrenees, Spain). The first study area is offshore New Jersey, where a series of seawardly prograding, Miocene, intrashelf clinothems have been cored and logged during IODP (International Ocean Drilling Project) Expedition 313. The second study area is the Eocene Sobrarbe Deltaic Complex, where a series of sandy sediment packages representative of prograding clinoforms crop out along a dip-parallel transect, and capture the transition from fluvio-deltaic to lower slope facies. Collectively, these locations

provide the opportunity to: i) characterise sediment of stratigraphically linked shelf (topset), foreset (slope) and basin-floor (bottomset) deposits under variable shelf process-regimes, and ii) to assess how grain character changes stratigraphically and spatially, along the depositional profile.

1.1.3 Clinofolds and Clinothems

1.1.3.1 Nomenclature

The term clinoform is hereafter used to describe basinward-dipping chronostratigraphic stratal surfaces, and the term clinothem to describe the sedimentary packages that are found between these surfaces (e.g., Gilbert, 1885; Rich, 1951; Mitchum et al., 1977; Pirmez et al., 1998; Patruno et al., 2015). Clinothems are typically composed of three constituent parts: topset (updip, gently dipping), foreset (central component, seaward-dipping, typically at $\sim 1-3^\circ$) and bottomset (downdip, gently dipping) deposits (Fig. 1.2; Gilbert, 1885; Steel and Olsen, 2002). The clinoform rollover zone (Fig. 1.2), also termed offlap-break, shelf-break, shelf-edge and platform-edge, signifies an area of gradient increase and the uppermost break-in-slope between the topset and foreset segments (Van Wagoner et al., 1990; Pirmez et al., 1998; Plink-Björklund et al., 2001; Glørstad-Clark et al., 2010, Glørstad-Clark et al., 2011; Anell and Midtkandal, 2015; Jones et al., 2015).

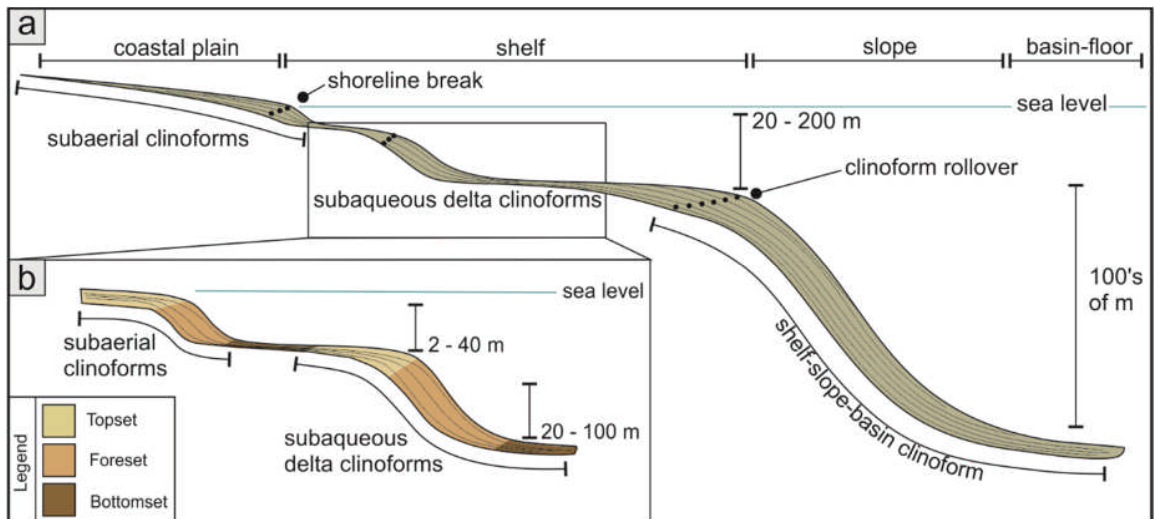


Figure 1.2: Simplified dip-parallel profile showing different scales of compound clinoform systems. a) Idealised regional cross-section showing three scales of clinoform development: subaerial (shoreline) clinoforms, subaqueous delta (intrashelf) clinoforms and shelf-slope-basin (continental margin) clinoform. b) Compound delta-scale clinoform system, showing subaerial and subaqueous delta clinoforms. Adapted from Helland-Hansen and Hampson (2009) and Patruno et al. (2015a).

Clinofolds develop at variable scales (Fig. 1.2), ranging from shelf-delta clinoforms (< 10s of m in height) to basin-margin or shelf-slope-basin clinoforms (ranging from ~ 100 s of m to > 1 km in height) (e.g., Pirmez et al., 1998; Steel and Olsen, 2002; Helland-Hansen and Hampson

2009; Henriksen et al., 2009; Anell and Midtkandal, 2015; Patruno et al., 2015a). An additional scale of clinothem exists, which forms seaward of a subaqueous delta clinothem and landwards of the shelf-edge. This intermediate-scale of clinothem (~ 100 – 400 m), situated in an intra-shelf setting, is known by a variety of nomenclatural terms, including mid-shelf (Proust et al., 2018), intra-shelf (Hodgson et al., 2018), shelf-prism (Patruno et al., 2015a) and shelf-edge (Helland-Hansen and Patruno, 2018).

1.1.3.2 Clinothems in Stratigraphy

Clinothems form the principal architectural building blocks of many shelf-to-basin successions (Fig. 1.3a; e.g., Gilbert, 1885; Rich, 1951; Bates, 1953; Asquith, 1970; Mitchum et al., 1977; Pirmez et al., 1998; Adams and Schlager, 2000; Bhattacharya, 2006; Patruno et al., 2015), and form valuable archives of basin margin evolution. The geometry and trajectory of successive clinoform rollovers, and the resulting stacking patterns of clinothems, have been used extensively to predict the spatial location and temporal evolution of sand bodies in basin-margin successions, both in outcrop and subsurface (Fig. 1.3; e.g., Steel and Olsen, 2002; Johannessen and Steel, 2005; Helland-Hansen and Hampson, 2009; Koo et al., 2016; Chen et al., 2018; Pellegrini et al., 2017). In both sequence stratigraphic frameworks (e.g., Vail et al., 1977; Van Wagoner et al., 1988; Posamentier et al., 1992; Johannessen and Steel, 2005; Catuneanu et al., 2009) and clinoform trajectory approaches (e.g., Burgess and Hovius, 1998; Mellere et al., 2002; Steel and Olsen, 2002; Bullimore et al., 2005; Carvajal and Steel, 2006; Uroza and Steel, 2008; Helland-Hansen and Hampson, 2009; Ryan et al., 2009) emphasis has been largely placed on the relative roles played by the interplay (expressed as a ratio) between the rate of accommodation generation and the rate of sediment supply.

Sequence stratigraphy (e.g., Vail et al., 1977; Posamentier and Vail, 1988; Van Wagoner et al., 1988; Galloway, 1989; Martinsen and Helland-Hansen, 1995; Posamentier and Allen, 1999; Steel and Olsen, 2002; Johannessen and Steel, 2005; Catuneanu et al., 2009) and clinoform trajectory analysis (e.g., Helland-Hansen and Gjelberg, 1994; Helland-Hansen and Hampson, 2009) are the most commonly applied approaches used to predict the presence or absence of deep-water, sand-rich deposits. These models emphasise fluctuations in relative sea level and sediment supply as the dominant mechanisms governing when and how sediment of different calibre and maturity is transported downdip, or is stored on the continental shelf.

The basic principles underpinning sequence stratigraphic and trajectory approaches are outlined below. Clinoform rollover trajectories, formed by the accretion of successive clinothems (Fig. 1.3a), which have flat to falling trajectories (negative gradient), indicate a relative sea level that is stable or falling through time (Fig. 1.3c, d) and point to favourable

conditions for sand-delivery into the deep-water setting (Fig. 1.3e). Flat or falling clinoform rollover trajectories are often associated with shelf-edge incision; as such, sediment is delivered across the shelf within fluvial channel systems that have the potential to be directly linked to slope-channel systems (Johannessen and Steel, 2005). If the supply of sediment remains channelized during downslope transit, large volumes of sand can be bypassed across the shelf to the base-of-slope and the basin-floor (Steel and Olsen, 2002).

Clinoform rollover trajectories, created by the accretion of successive clinothem, which have a rising trajectory (positive gradient), indicate a relative sea-level that is rising through time (Fig. 1.3b), with less favourable conditions for the bypass of sand into the deep-water setting (Johannessen and Steel, 2005). A rising shelf-edge trajectory is associated with the preferential storage of a large proportion of the sediment budget on the shelf and coastal plain, with little or no sand bypassed into the deep-water setting (Steel and Olsen, 2002).

1.1.4 Shelf and Topset Process-Regime

Recent studies have highlighted that the topset and shelf process-regime (resulting from the cumulative effects of fluvial, wave, tidal, and oceanographic currents) is an important parameter to consider when predicting the presence or absence of coarse-grained sediment in downdip locations (e.g., Dixon et al., 2012a; Jones et al., 2015; Gomis-Cartesio et al., 2016; Hodgson et al., 2018). For example, Dixon et al. (2012a) suggest that a river-dominated shelf process-regime is critical to sand delivery into the deep-water setting. Conversely, wave- or storm-dominated shelf process-regimes are cited as ineffective conveyors of sediment to deep-water, instead filtering and redistributing sediment alongshore (Plink-Björklund and Steel, 2004; Petter and Steel, 2006; Dixon et al., 2012a; Gong et al., 2016).

Rapid spatial and temporal changes in shelf process-regime can occur at intraclinothem scales (Ta et al., 2002; Ainsworth et al., 2008; 2011; Olariu, 2014; Jones et al., 2015; Gomis-Cartesio et al., 2016). The topset or shelf process-regime may be dominated by river-, wave- or tide-processes at a specific location. However the dominant process-regime can vary temporally (e.g., Olariu, 2014; Rossi and Steel, 2016) and spatially, along-strike, in the same system (e.g., Jones et al., 2015; Gomis-Cartesio, 2017).

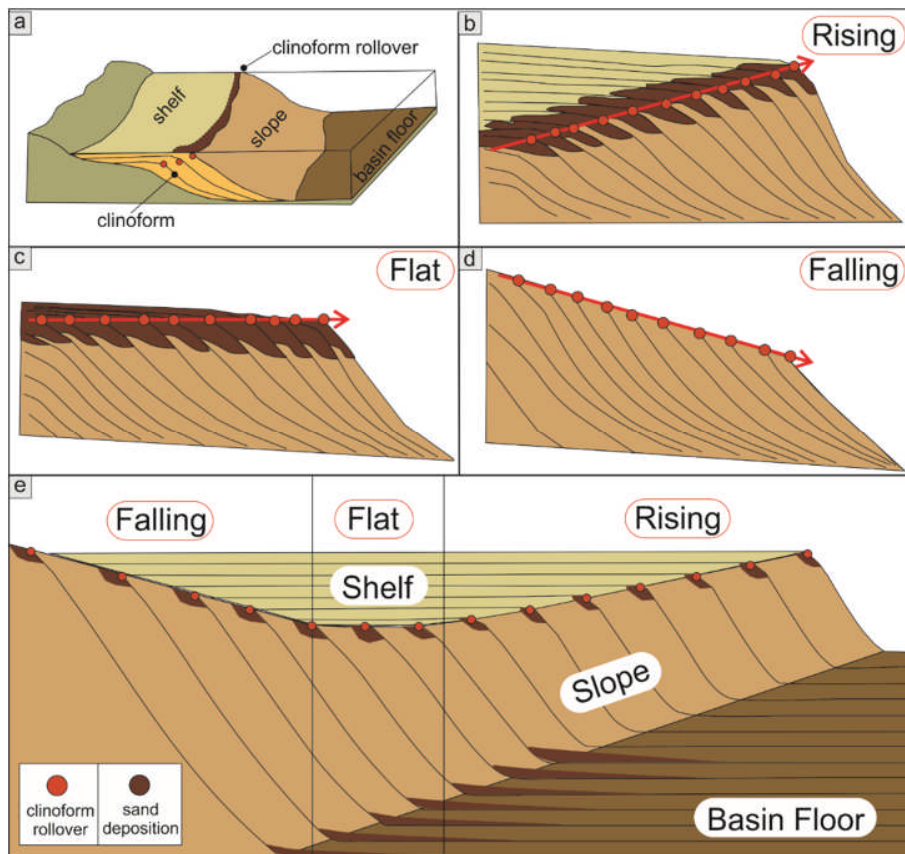


Figure 1.3: a) Clinoforms within a sedimentary prism of a prograding basin margin. b) Rising (positive) clinoform rollover trajectory, associated with relative sea-level rise, shelf accommodation and limited delivery of coarse-grained sediment into the deeper-water setting. c) Flat clinoform rollover trajectory, associated with relative sea-level standstill, limited shelf accommodation and delivery of coarse-grained sediment into the deeper-water setting. d) Falling (negative) clinoform rollover trajectory, associated with relative sea-level fall, no shelf accommodation and delivery of coarse-grained sediment into the deeper-water setting. e) Established clinoform rollover trajectory model; deposition of coarse-grained sediment on the basin-floor occurs only when the clinoform rollover trajectory is falling or flat (associated with relative sea-level fall and standstill respectively); rising clinoform rollover trajectories (associated with relative sea-level rise) display basin-floor sediment starvation. Adapted from Steel and Olsen (2002), Helland-Hansen and Hampson (2009) and Dixon et al. (2012a).

1.1.5 Grain character along the Depositional Profile

Seismic and well-log data have been used extensively to study clinothem successions in the subsurface (e.g., Erskine and Vail, 1988; Ross et al., 1995; Pinous et al., 2001; Donovan, 2003; Jennette et al., 2003; Hadler-Jacobsen et al., 2005). However, clinothems remain relatively understudied in outcrop and core; this is partly due to scale constraints and the rarity of exhumed, or continuously cored, dip-parallel, laterally continuous clinothem sequences (e.g., Dreyer et al., 1999; Mellere, et al., 2002; Deibert et al., 2003; Johannessen and Steel, 2005; Carvajal and Steel, 2006; Uroza and Steel, 2008; Couvalt et al., 2009; Hubbard et al., 2010; Jones et al., 2013).

Although outcrop and core analogues of complete clinothem successions are relatively limited, they are valuable archives of basin-margin evolution, as they can reveal the nature of

shelf-slope-basin transitions at unparalleled spatial and stratigraphic scales (e.g., Helland-Hansen, 1992; Dreyer et al., 1999; Pyles and Slatt, 2007; Pontén and Plink-Björklund, 2009; Hubbard et al., 2010). Despite the potential afforded by outcrop and core analogues, limited quantitative grain character data (including grain size, grain shape and sorting) is currently available in the literature. As such, grain character variation across clinothem systems remains a poorly constrained and largely unquantified parameter (Catuneanu et al., 2009). Predicting grain character changes along the depositional profile of a clinothem is further complicated by spatial and temporal changes in the dominant shelf process-regime (cf. Dixon et al., 2012a). Changes in the dominant topset and shelf process-regime can occur at inter- and intraclinothem scales (Ta et al., 2002; Ainsworth et al., 2008; 2011; Dixon et al., 2012a; Olariu, 2014; Jones et al., 2015). Stratigraphic and along-strike variability in topset and shelf process-regime fundamentally affects how and when sediment of different calibre and maturity is transferred down-dip. In the absence of quantitative analysis of grain character across clinothems, prediction of sediment distribution at different positions along the topset-to-bottomset profile is tied to conceptual models.

1.2 Aims and Objectives

The overarching aim of this research project is to understand how and when sediments of different calibre and maturity bypass the continental shelf and are delivered into deep-water settings. This fundamental research aim will be accomplished through the development of quantitative grain character datasets from core and outcrop examples of intermediate-scale clinothem sequences. Four specific objectives are outlined: i) to improve understanding of the formation, architecture and sediment partitioning within intermediate-scale clinothems; ii) to assess the role played by the topset process-regime in regulating sediment transfer beyond the clinof orm rollover; iii) to understand the causes of sedimentological and textural grain character variability within individual clinothem sequences; and iv) to highlight the applications and value of grain character datasets in sedimentology studies.

1.2.1 Research Question One

What are intermediate-scale clinothems?

1.2.1.1 Rationale

Intermediate-scale (~ 100 – 400 m foreset height) clinothems are a suite of clinothems observed in many basin margins between the scale of shoreline and basin-margin clinothems (e.g., Steel et al., 1985; Helland-Hansen, 1990; Dreyer et al., 1999; Mellere et al., 2002; Plink-Björklund and Steel, 2003; Petter and Steel, 2006; Pyles and Slatt, 2007; Pyles et al., 2010; Patruno et al., 2015b). The origin and evolution of intermediate-scale clinothems is poorly

understood and this problem has been exacerbated by the nomenclatural confusion that shrouds the classification of intermediate-scale clinothems. For example the New Jersey clinothems have been classified as ‘subaqueous clinothems’ (see Hodgson et al., 2018), ‘midshelf clinothems’ (sensu Porębski and Steel, 2006), ‘shelf-prism clinothems’ (see Patruno et al., 2015a) and ‘shelf-edge clinothems’ (see Patruno and Helland-Hansen 2018). However, the scale and architecture and relative location of the Miocene New Jersey clinothems on the continental shelf means that they do not fit simply into current clinothem classification schemes and they exhibit a variety of features that span a number of the categories of clinothems.

In the wider literature intermediate-scale clinothems are variably referred to as: i) subaqueous clinothems (e.g., Sognefjord Formation; Patruno et al., 2015b; ii) shelf-prism clinothems (e.g., Florida-Hatteras Slope; Patruno et al., 2015a); iii) mid-shelf clinothems (e.g., offshore New Jersey; Proust et al., 2018) and shelf-edge clinothems (e.g., the Van Kuelenfjorden outcrop transect from Spitsbergen, Svalbard Islands; Steel and Olsen, 2002). Many ancient examples of intermediate-scale clinothems are classified as shelf-edge clinothems (see Dreyer et al., 1999; Petter and Steel, 2006; Pyles and Slatt, 2007; Pyles et al., 2010). However, uncertainty surrounds this ‘shelf-edge’ classification, due to the difficulty in discerning the location of the contemporaneous structural shelf-edge break in ancient outcrop examples. The lack of definitive proof of clinothem deposition at the true shelf-edge, leaves the possibility open that these intermediate-scale clinothems may have been deposited landwards of the true shelf-edge. If these intermediate-scale clinothems are not true ‘shelf-edge’ clinothems (sensu Dixon et al., 2012b), then how and why are clinothems of this scale able to develop landwards of the true shelf-edge, i.e. in an intrashelf setting?

The formation of intermediate-scale clinoforms also remains, as yet, to be fully resolved; commonly, repeated interactions between smaller-scale subaerial and subaqueous clinoforms are cited as the mechanism of formation of intermediate-scale clinothems, within the intrashelf setting (e.g., Burgess and Hovius, 1998; Steel et al., 2000, 2003, 2008; Porębski and Steel, 2003, 2006; Johannessen and Steel, 2005; Olariu and Steel, 2009; Oliveira et al., 2011; Helland-Hansen et al., 2012; Proust et al., 2018). However, this scenario does not fully account for what is observed in the stratigraphic record; intermediate-scale clinothems are larger in scale than both subaerial and subaqueous clinothems and differ in depositional architecture (e.g., Petter and Steel, 2006; Pyles and Slatt, 2007; Pyles et al., 2010). Efforts to further clarify the formation of intermediate-scale clinothems, and determine their role as sedimentary conveyors or filters, will aid understanding of sediment partitioning between the shelf, slope and basin-floor.

To address the difficulties in i) classifying and ii) understanding the formation of intermediate-scale intrashelf clinothems, this study will primarily focus on the Miocene clinothems of offshore New Jersey. During IODP Expedition 313, the seawardly prograding Miocene clinothems were continuously cored and logged in three research boreholes, which intersect the topset, foreset and bottomset deposits of the intermediate-scale clinothems; the research boreholes follow a transect along a seismic reflection line oriented dip-parallel to the prograding Miocene clinothems. In order to better define intermediate scale clinothems it is necessary to: i) critique clinothem classification schemes; ii) compare the characteristics of intermediate scale clinothems from different systems; and iii) evaluate their mechanisms of formation.

1.2.2 Research Question Two

What role does process-regime play in regulating the timing and grain character of sand transfer to slope and basin-floor settings?

1.2.2.1 Rationale

The geometry and trajectory of successive clinoform rollovers in outcrop and subsurface data, and the resulting stacking patterns of clinothems, have been used extensively to predict the spatial location and temporal evolution of sand bodies in basin-margin successions (e.g., Steel and Olsen, 2002; Johannessen and Steel, 2005; Helland-Hansen and Hampson, 2009; Koo et al., 2016; Chen et al., 2018; Pellegrini et al., 2017). In both clinoform trajectory approaches (e.g., Burgess and Hovius, 1998; Mellere et al., 2002; Steel and Olsen, 2002; Bullimore et al., 2005; Carvajal and Steel, 2006; Uroza and Steel, 2008; Helland-Hansen and Hampson, 2009; Ryan et al., 2009) and sequence stratigraphic approaches (e.g., Vail et al., 1977; Van Wagoner et al., 1988; Posamentier et al., 1992; Johannessen and Steel, 2005; Catuneanu et al., 2009), the temporal distribution of coarse-grained sediment (i.e., fine grained sand or coarser) is thought to be governed by the balance of accommodation and sediment supply.

In addition, the shelf process-regime plays a significant, but often understated, role in determining how and when sediment of different calibre and maturity is transported downdip (Helland-Hansen and Hampson 2009; Dixon et al 2012a; Covault and Fildani 2014; Gong et al., 2016; Peng et al., 2017). Shelf process-regime can be a mix, or dominated by river, wave or tide processes at the shelf-edge regardless of the clinoform-rollover trajectory.

Despite the topset (shelf) process-regime being acknowledged as a key parameter determining styles of deep-water sedimentation (i.e. sand vs. mud deposition), quantification of grain character (including grain-size, sorting, grain-shape and sand-to-mud ratios) remains largely neglected. The offshore New Jersey dataset provides the opportunity to: i) assess

variability in grain character under end-member shelf process-regime conditions across a series of clinothem sequences, and ii) check for associations between grain character and clinof orm rollover trajectories. Furthermore, due to the retrieval of samples from quasi-coeval topset, foreset and bottomset deposits, the offshore New Jersey dataset allows variation in grain character under end-member process-regime conditions to be quantified across the complete depositional profile. The Sobrarbe Deltaic Complex deposits provide an outcrop example of a river-dominated shelf; the continuous exposure from fluvio-deltaic to distal-slope deposits, allows basinward changes in grain character to be quantified along the continuous depositional profile.

To answer this research question, the following points will be addressed: i) the interactions between process-regime, clinof orm rollover trajectory and the downdip distribution of sand and mud will be evaluated; ii) the architecture and sedimentological and grain character attributes of river- and wave-dominated conditions, across the complete depositional profile will be assessed; and iii) a quantitative grain character database, comparing wave- and river-dominated clinothem sequences will be presented.

1.2.3 Research Question Three

How can grain character be used to improve understanding of clinothem evolution?

1.2.3.1 Rationale

Previous studies of clinothem sequences have emphasised basin-scale relationships across multiple successive clinothems (e.g., Steel and Olsen, 2002; Johannessen and Steel, 2005; Helland-Hansen and Hampson, 2009; Dixon et al., 2012b; Koo et al., 2016; Chen et al., 2017; Pellegrini et al., 2017). The reservoir-driven focus for understanding basin-scale sand distribution across clinothems, has dominated over variability in sedimentological processes and grain character within individual clinothem sequences. As such, the documentation of intraclinothem scale grain character variability and evaluation of its causes remain largely unaddressed. This limited understanding is exacerbated by a paucity of sedimentological and stratigraphic documentation of individual clinothems with preserved coeval topset (shelf), foreset (slope) and bottomset (basin-floor) deposits (e.g., Carvajal and Steel, 2009; Carvajal et al., 2009; Wild et al., 2009; Grundvåg et al., 2014; Prélat et al., 2015; Koo et al., 2016).

Understanding the internal sedimentological complexities of complete topset-foreset-bottomset clinothem sequences, and of the shelf-to-slope transition, is key to understanding how and when sediment is transferred basinward. Such understanding might also help to better constrain the spatio-temporal sedimentary correlations of stratal units, and their bounding surfaces at a resolution that is higher than conventional chronostratigraphic

approaches. High-resolution sampling plus detailed sedimentological analysis of the New Jersey (core-based) and the Sobrarbe Deltaic Complex (outcrop-based) clinothems provides two quantitative databases, which document grain character variability at an intraclinothem scale. To address this research question: i) the sedimentological variability associated with mixed-energy clinothems will be documented; ii) changes in intraclinothem grain character will be documented, and tied to changes in the dominant topset (shelf) process-regime and flow style; and iii) intraclinothem sedimentary packages across the complete depositional profile will be correlated using grain character.

1.2.4 Research Question Four

What value do high-resolution quantitative grain character datasets offer to sedimentology and stratigraphy?

1.2.4.1 Rationale

Grain character (including grain size, grain shape, sorting and sand-to-mud ratios) is a fundamental physical property of any sedimentary deposit. Grain character at any point along the source-to-sink profile records a combination of the source ('parent') material, the previous erosion and transport processes, and the hydrodynamic characteristics of deposition (Watson et al., 2013). Grain character, particularly grain size, is a parameter considered in almost all sedimentological studies. However, there is a relative paucity of quantitative grain character data, particularly in outcrop-based studies (e.g., Dreyer et al., 1999; Pyles and Slatt, 2007; Wild et al., 2009; Shiers et al., 2017; Burns et al., 2017; Brooks et al., 2018, amongst many others); many studies rely simply on visual estimations of grain size, sorting, sand-to-mud ratios and grain roundness and grain sphericity. In core-based studies too, qualitative (or at best semi-quantitative) methodologies are commonly used to produce sedimentary logs, upon which further interpretations are based (e.g., Mountain et al., 2010; Browning et al., 2013). Because the use of qualitative grain character data is widespread, human-error in grain character estimation can introduce significant error into grain size and grain shape values. As the field of sedimentology moves away from models based on subjective observation, to those more firmly based on numerical datasets, quantitative grain character datasets will come into play. However, as yet, quantitative grain character datasets are relatively limited in studies of clinothem deposits (Catuneanu et al., 2009). Outcrop and core-based studies that capture coeval, genetically linked topset-foreset-bottomset deposits are particularly rare (e.g., Helland-Hansen, 1992; Dreyer et al., 1999; Pyles and Slatt, 2007; Pontén and Plink-Björklund, 2009; Hubbard et al., 2010) and very limited quantitative grain character data is currently available from such outcrop and core studies. As such, grain character variation across

clinothem systems remains poorly constrained; it is effectively a largely unquantified parameter (Catuneanu et al., 2009). This research question aims to: i) outline the value of quantitative grain character databases; ii) apply quantitative databases to improve the placement of sequence boundaries and iii) compare traditional qualitative logging techniques with quantitative grain character databases

1.3 Literature Review

1.3.1 Clinoforms and Clinothems

1.3.1.1 *What is a Clinoform?*

The term clinoform is used to describe a chronostratigraphic, stratal surface and is applied to both sigmoid sedimentary slopes and any accretionary feature with sigmoidal bounding surfaces (e.g., Gilbert, 1885; Rich, 1951; Bates, 1953; Asquith, 1970; Mitchum et al., 1977; Pirmez et al.; 1998, Patruno et al., 2015). Whilst clinoform is used a descriptor of shape, the term clinothem is used expressly to reference a specific body of rock and its accompanying lithology. The term clinothem describes a seawardly-prograding, coarsening-upward sedimentary sequence that is composed of interbedded sands and muds (Rich, 1951). The clinothem is obliquely cut by sigmoidal clinoforms, which represent chronostratigraphic surfaces (Slingerland et al., 2008). The cross-sectional shape of clinoforms fall into three fundamental categories: linear, oblique and sigmoidal.

1.3.1.2 *Clinoform Geometry*

Shelf-slope-basin clinothems comprise three fundamental geometric components: topsets, foresets and bottomsets (Gilbert, 1885). Topset deposits form the upper portion of the clinothem; the depositional slopes of topset deposits dip gently seaward (typical dip is less than 0.3°). Foreset deposits form the steepest part of the clinothem sigmoid (typical dip is 1-3° at the clinoform inflection point), and can be referred to as the clinothem slope. Bottomset deposits dip gently seaward, and include the toe-of-slope (Steel and Olsen, 2002). The progression from topset to foreset is marked by the locus of maximum curvature (Anell and Midtkandal, 2015), which has multiple names (shelf-edge break, platform edge or offlap break), but is most commonly referred to as the (clinoform) rollover (Van Wagoner et al., 1990; Pirmez et al., 1998; Plink-Björklund et al., 2001; Glørstad-Clark et al., 2010, Glørstad-Clark et al., 2011; Anell and Midtkandal, 2015). The lower clinoform break in slope, which defines the transition between foreset and bottomset, is referred to as the base-of-slope.

1.3.1.3 *Clinoform Scale*

The definitions of clinoform and clinothem have been expanded to include a variety of scales, ranging from bedform features of centimetre scale, to continental-margin accumulations (Fig.

1.4; shelf-slope-basin clinoforms) that are kilometres deep (Pirmez et al., 1998). The latter dip basinward and facilitate platform construction through the formation of sedimentary prisms at the basin margin (Anell and Midtkandal, 2015); as such, clinoform deposits are referred to as the fundamental building blocks of the infill of sedimentary basins (Pirmez et al., 1998) and form the principal architectural element of many deltaic-to-continental slope successions (e.g., Gilbert, 1885; Rich, 1951; Mitchum et al., 1977; Pirmez et al., 1998).

The range of vertical scales exhibited by clinoforms and clinothems can result in three or four scales of clinoform that synchronously prograde from shallow- to deep-marine, increasing in scale downdip (Fig. 1.4; Henriksen et al., 2009; Patruno et al., 2015). In systems such as these, referred to as compound clinoforms, the bottomset deposits of one up-dip clinoform corresponds to the topset deposits of a downdip, larger clinoform; as such, compound clinoforms are morphologically and genetically linked (Swenson et al., 2005; Helland-Hansen and Hampson, 2009; Henriksen et al., 2009; Helland-Hansen and Gjelberg, 2012; Patruno et al., 2015). Moving in a basinward direction and increasing in scale, these clinoforms are: i) shoreline deltas (subaerial deltas); ii) subaqueous deltas (intrashelf clinothems); and iii) shelf-slope-basin clinoforms (continental margins) (Helland-Hansen and Gjelberg, 2012).

The vertical relief of delta-scale clinoforms (both subaerial and subaqueous) is on the order of tens of metres. Typically, delta-scale clinoforms prograde and retrograde in cycles lasting 10^2 – 10^5 years (e.g., Burgess and Hovius, 1998; Hampson and Storms, 2003). Subaerial deltas have their clinoform rollovers situated in the proximity of the shoreline break and often display irregular geometries. In contrast, the rollovers of subaqueous clinoforms are situated at water depths of between 40 – 60 m, and tend to display more regular geometries (Helland-Hansen and Gjelberg, 2012; Mitchell et al., 2012). Where deltas prograde to the shelf-edge, this can form shelf-edge clinoforms (shelf-edge deltas sensu Porębski and Steel, 2003; Burgess and Steel, 2008). Shelf-edge clinoforms typically have heights of between ~100 – 500 m and typically prograde and retrograde in cycles lasting 10^4 – 10^6 years (e.g., Steel and Olsen, 2002). Shelf-slope-basin clinoforms, i.e. those which compose continental margins, typically have heights on the magnitude of several thousand metres and typically prograde and retrograde in cycles lasting 10^6 – 10^8 years (Henriksen et al., 2009; Helland-Hansen and Gjelberg, 2012).

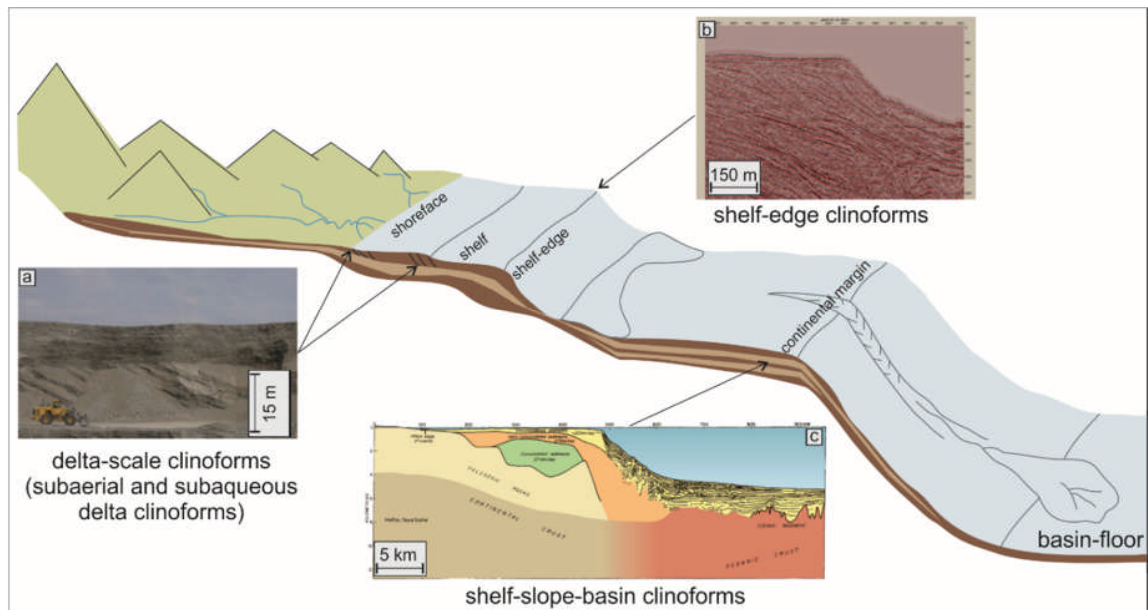


Figure 1.4: Regional cross-section, showing idealised clinoform systems, highlighting delta-scale, shelf-edge and shelf-slope-basin clinoforms. a) Delta-scale clinoforms, Varanger Peninsula, Norway (Late Proterozoic). b) Shelf-edge clinoforms, Mid-Norwegian Shelf (Neogene). c) Shelf-slope-basin clinoform. Adapted from Patruno and Helland-Hansen (2018).

As clinoforms increase in scale (i.e. basinward), the architecture becomes decreasingly affected by autogenic controls, resulting in relatively simpler clinoform architectures and clinoform trajectories (Patruno et al., 2015). Shelf-edge and continental margin clinoforms can only either prograde, or remain at a relatively fixed position through time (Helland-Hansen and Hampson, 2009). Contrastingly, delta-scale clinoforms are able to both prograde and retrograde. The aggradation of shelf sediments is therefore a product of the stacking of successive deltaic and shoreline clinothem vertically (Bullimore et al., 2005; Helland-Hansen and Hampson, 2009). Multiple episodes of delta and shoreline regression and transgression across the shelf is the principal cause of continental-shelf outbuilding (Johannessen and Steel, 2005). Over time, this process can result in basinward progradation, and the architectural evolution of the spatially and temporally larger-scale shelf-prism and continental-margin clinoforms (Olariu and Steel, 2009).

1.3.2 Clinothem: Fundamental Components of Stratigraphy

Clinofom surfaces are chronostratigraphic, depositional surfaces, described by Patruno and Helland-Hansen (2018, p. 204) as ‘frozen palaeo-bathymetric profiles.’ The geometry of clinoforms provides direct information regarding palaeo-shoreface and palaeo-shelf morphologies. The stratigraphic architecture of clinoform successions aids understanding of how and when sediments are partitioned between topset and bottomset deposition (i.e. the balance between degradational topset bypass and aggradational topset storage). Clinoforms reflect fundamental external forcings and provide a physical record of the interactions

between sea-level change, subsidence and uplift, basin physiography, sediment flux and climate, amongst other factors (e.g., Mitchum et al., 1977; Ross et al., 1994; Postma, 1995; Pirmez et al., 1998; Adams and Schlager, 2000; Steel and Olsen, 2002; Bullimore et al., 2005; Anell and Midtkandal, 2017).

Clinofolds are important surfaces in a sequence stratigraphic context, and their stratal terminations, geometries, and stacking patterns permit the identification of fundamental stratigraphic units (Patrino and Helland-Hansen, 2018). Within a stratigraphic succession, clinofolds characterise simple regressive-transgressive building blocks (Steel and Olsen, 2002). These sequence stratigraphic building blocks, most often observed in seismic reflection data (e.g. offshore New Jersey, USA; Steckler et al., 1998), allow chronostratigraphic time-lines within stratigraphy to be pictured

1.3.2.1 Sequence Stratigraphy: an Introduction

The development of sequence stratigraphy originates from the seminal advances published in AAPG (American Association of Petroleum Geologists) Memoir 26. Sequence stratigraphy introduced a new methodology in which seismic units were mapped laterally along surfaces interpreted to represent erosion or nondeposition. The methodology of Payton (1977) and others, permitted the sedimentary record to be viewed genetically and at greater scale than had previously been possible through outcrop, core and well-log data. Sequence stratigraphy created a new methodology to map, correlate and subdivide sediments (Vail et al., 1977). Sequence stratigraphy is now widely applied as an analytical tool for the study of rock successions and basin analysis. Although sequence stratigraphy was developed originally from the identification of patterns of repeating seismic reflector styles from early, regional 2-D seismic reflection surveys, its principles have subsequently been applied to well-log datasets, core and outcrop (e.g., Van Wagoner et al., 1990; Johnson et al., 2001; Droz et al., 2003)

1.3.2.2 Sequence Stratigraphic Nomenclature

Sequence stratigraphy comprises the study of genetically-related stratal successions within the context of a chronostratigraphic framework (Van Wagoner et al., 1988). Such stratal successions are delimited by unconformities (including both erosional surfaces and depositional hiatuses and excluding localised events of deposition and erosion e.g., dune migration, development of point bars or distributary channels) and their correlative conformities (Van Wagoner et al., 1988).

The primary unit of sequence stratigraphy is the depositional sequence, which is composed of the parasequence and parasequence sets. A parasequence is defined as a succession of

relatively conformable and genetically related beds or bedsets, which are frequently delimited by prominent marine flooding surfaces and their correlative surfaces (Van Wagoner, 1985; Van Wagoner et al., 1990). A marine flooding surface defines a prominent change in facies, which suggests decreasing rates of sediment supply or an increase in water depth (Van Wagoner et al., 1988).

1.3.2.3 Sequence Boundaries

The sequence boundary is a fundamental stratigraphic surface, produced by a fall in relative sea-level, which results in decreased accommodation (Posamentier et al., 1988). Relative sea-level fall causes forced regression of the system in a basinward direction; this results in a dislocation of facies basinward, where proximal facies immediately overlie relatively distal facies and no intervening succession of coarsening and thickening upward strata are preserved. In the shallow-marine environment, a sequence boundary may be identified by the abrupt juxtaposition of subaerial fluvial deposits and/or palaeosols above offshore mudstone facies. The sequence boundary is laterally extensive and can be traced to downdip locations (Mitchum, 1977). In circumstances where the updip supply regime has the ability to deliver significant volumes of sediment out into the basin, the correlative conformity may be identified by a dramatic increase in the sand content.

In the earlier sequence stratigraphic literature sequence boundaries were subdivided into type one (SB1) and type two (SB2) sequence boundaries (e.g., Posamentier et al., 1988; Posamentier and Vail, 1988; Mitchum and Van Wagoner, 1990). The former (SB1) are unconformities characterised by the rejuvenation of streams and fluvial incision of the shelf, which results in sedimentary bypass of the continental shelf. SB1 are associated with the abrupt basinward shift of facies and are interpreted to form where the eustatic rate of sea-level fall is greater than the rate of basin subsidence at the depositional shoreline break; as such, at a given location, a relative fall in sea-level occurs (Posamentier et al., 1988). SB1 form when relative sea level falls below the preceding depositional systems tract (Mitchum and Van Wagoner, 1990). The latter (SB2) are unconformities characterised by subaerial exposure, but lack the subaerial erosion associated with stream rejuvenation. SB2 are interpreted to form where the eustatic rate of sea-level fall is lesser than the basin subsidence rate at the depositional shoreline break; as such, at a given location, no relative fall in sea-level occurs (Posamentier and Vail, 1988). SB2 form when relative sea-level does not fall below the preceding depositional inflection (Mitchum and Van Wagoner, 1990). SB2 are not commonly recognised in the more recent stratigraphic literature, and as such, the subdivision of

sequence boundaries will not be considered further (Posamentier and Allen, 1999; Catuneanu et al., 2009).

1.3.2.4 Flooding Surfaces

In the shallow-marine realm, a flooding surface is recognised by the juxtaposition shallow-water or emergent facies overlain by finer-grained offshore mud facies. A flooding surface is the result of the landward migration of the system, resulting from relative sea-level rise, sometimes in combination with a decrease in the rate of sediment supply (Mitchum, 1977). A flooding surface that separates a highstand systems tract above from a transgressive system below is called the maximum flooding surface. A flooding surface that occurs within a parasequence shows a marked increase in water depth and separates older and younger sedimentary deposits, which reflect this (Posamentier et al., 1988). Typically, the flooding surface is expressed in the stratigraphic record as condensed horizon, which reflects slow rates of deposition; the parasequence flooding surface commonly separates two fining and thinning upwards units and/or two coarsening and thickening upward units (Van Wagoner et al., 1990).

1.3.2.5 Transgressive Surface

Identification of the first marine deposits to overlie non-marine deposits demarcates the transgressive surface (TS) on the shelf; the transgressive surface on the shelf may also be identified where the underlying regressive shoreline deposits are flooded by mud-rich, back-barrier sedimentary deposits (Johannessen and Steel, 2005). As transgression progresses, wave and/or tidal ravinement surfaces may develop above the primary transgressive surface (Steel et al., 2008). Landwards of the shelf, the transgressive surface and subaerial sequence boundary can merge. Basinwards of the shelf, the transgressive surface and the sequence boundary become increasingly separated, such that a sedimentary package exists between the two stratigraphic surfaces at the shelf margin (Johannessen and Steel, 2005).

1.3.2.6 Parasequences

In shoreface and deltaic settings, parasequences are usually characterised by thickening and coarsening upwards packages (Fig. 1.5), which are interpreted to signify one episode of shoreline progradation (Van Wagoner, 1985; Van Wagoner et al., 1990). Episodes of repeated shoreline progradation produce a parasequence set, which has a distinctive stacking pattern and is composed of a succession of genetically related parasequences. Typically, parasequence sets are bounded by major marine flooding surfaces and their correlative surfaces (Van Wagoner et al., 1988). When viewed in a dip-parallel orientation, the stacking-pattern can be

described as progradational, aggradational or retrogradational. The observed stacking pattern is a product of the horizontal and vertical migration of the shoreline.

1.3.2.7 Progradational Parasequence Sets

A progradational parasequence set is a product of consecutive parasequences increasingly progressing basinward (Van Wagoner et al., 1990; Fig. 1.5a, b). In cross-section, a progradational parasequence set will show the basinward migration of facies belts in successive parasequences; in vertical section, successive parasequences display a greater proportion of shallow-water facies upward across each successive parasequence. The formation of a progradational stacking pattern is the result of the long-term rate of sediment supply exceeding the generation rate of accommodation (Van Wagoner et al., 1990).

1.3.2.8 Retrogradational Parasequence Sets

A retrogradational parasequence set is a product of consecutive parasequences increasingly moving landwards (Fig. 1.5c, d). In cross-section, a retrogradational parasequence set will show the landward migration of facies belts in successive parasequences; in vertical section, successive parasequences display an increasing proportion of deep-water (offshore) facies upward across each successive parasequence. The formation of a retrogradational stacking pattern is the result of the generation rate of accommodation exceeding the long-term rate of sediment supply (Van Wagoner et al., 1990).

1.3.2.9 Aggradational Parasequence Sets

An aggradational parasequence set is a product of consecutive parasequences reaching a similar position as that of each underlying parasequence (Fig. 1.5e, f); as a result of this, the distribution of facies shown by each parasequence is similar. The formation of an aggradational stacking pattern is the result of an equal balance between the long-term rate of sediment supply and the generation rate of accommodation (Van Wagoner et al., 1990).

1.3.2.10 Systems Tracts and Depositional Sequences

Each depositional sequence records one complete cycle of relative sea-level change. The sequence (a relatively conformable succession of strata, which are genetically related and bounded by unconformities, or their correlative conformities) can be subdivided into a number of predictable systems tracts, which are separated by key stratigraphic surfaces. The stacking patterns of parasequence sets, in association with facies assemblages, key surface boundaries and the location within a sequence, are used to identify systems tracts.

Initially, a three systems tract scheme was proposed, in which a one complete relative sea-level cycle is divided into an isochronous sequence boundary (SB), overlain by a Lowstand Systems Tract (LST), succeeded by a Transgressive Systems Tract (TST) and finally a Maximum Flooding Surface (MFS) followed by a Highstand Systems Tract (HST) (Vail et al., 1977; Jervey, 1988; Posamentier et al., 1988; Mitchum and Van Wagoner, 1990; Van Wagoner et al., 1990; Vail et al., 1991). This scheme was revised and a four systems tract scheme is now widely advocated for SB1, in which the HST terminates with the onset of relative sea-level fall; a Falling Stage Systems Tract (FSST) is thus proposed (see Plint and Nummedal, 2000). The FSST begins with the onset of a fall in relative sea-level and concludes with the end of the relative fall in sea-level; this is associated with a regressive surface of marine erosion (SB) or a subaerial unconformity.

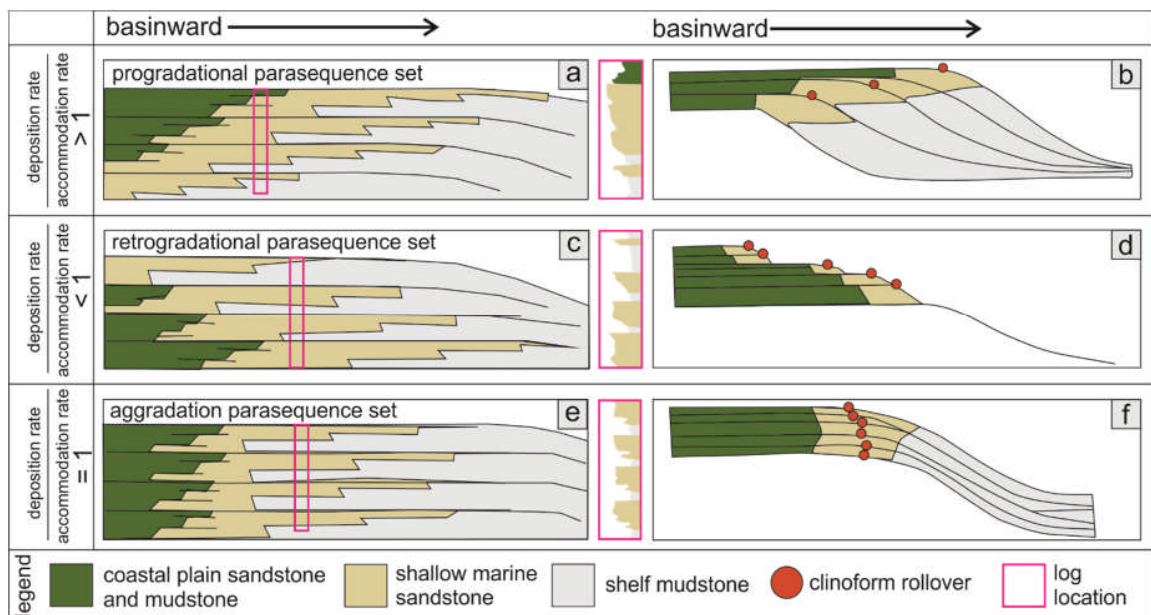


Figure 1.5: Parasequence stacking patterns in parasequence sets showing depositional cross-section, schematic log and clinoform expression. Figures a) and b) show progradation; c) and d) show retrogradation; Figures e) and f) show aggradation. Adapted from Van Wagoner et al. (1990) and Steel and Olsen (2002).

1.3.2.11 Lowstand Systems Tract (LST)

Within the four systems tract model, the LST is the initial depositional system to develop following the formation of a type 1 sequence boundary (SB1); the LST is active during a period of relative sea-level fall, which surpasses the shelf break and results in the development of incised valleys and widespread erosion as the emergent shelf becomes fully exposed. The rapid initial fall in relative sea-level is associated with basin-floor and slope deposition, as sediments are transported across the shelf and quickly deposited in the deep-water setting. If there is adequate sea level fall, the LST is comprised of a prograding wedge complex, a slope-fan and basin-floor-fan (Vail et al., 1991). The LST is therefore considered to

be an extremely attractive target for hydrocarbon exploration, due to the prediction of such sand-rich facies. This conceptual model is readily applied to the petroleum industry and is used in both mature and frontier basins (Shanmugam et al., 1996). The LST is associated with a typically retrogradational stacking pattern (Van Wagoner et al., 1990). However, a progradational stacking pattern can be produced where the initial rate of relative sea-level rise after the lowstand is slow, relative to the rate at which sediment is delivered to the basin-floor (Coe et al., 2003).

1.3.2.12 Transgressive Systems Tract (TST)

The TST directly overlies the LST and represents a period of continued relative sea-level rise; the boundary between the LST and TST is defined by the transgressive surface, which is identified by the first marine deposits to overlie non-marine deposits on the shelf. The TST concludes with the formation of the maximum flooding surface (MFS) during the period of maximum marine transgression (Vail et al., 1991). The MFS is defined as a surface of deposition at the time the shoreline is at its maximum landward position (Posamentier and Allen, 1999) and is often defined by organic rich shales, glauconite and hardgrounds (Helland-Hansen and Martinsen, 1996; Catuneanu et al., 2006).

1.3.2.13 Highstand Systems Tract (HST)

The HST overlies the MFS. Typically, the rate of relative sea-level rise decreases following the MFS and sediment supply progressively begins to outpace the rate of accommodation generation. However, the HST can also form due to a heightened rate of sediment delivery, which pushes the coastline basinwards (i.e., a decreased rate of relative sea-level rise is not required). The HST is initially associated with a stacking pattern that is broadly aggradational; the stacking pattern becomes increasingly progradational during sea-level transgression (Posamentier et al., 1988).

1.3.2.14 Falling Stage Systems Tract (FSST)

The FSST overlies the HST and is marked by a fall in relative sea-level. The FSST is associated with an increasingly progradational stacking pattern as shelf-accommodation decreases. The fall in relative sea-level exposes updip sediments subaerially, leading to increased fluvial incision. The subaerial exposure of sediment, and its erosion by fluvial systems, feeds the rapidly prograding shoreline. The high rates of sediment supply and the limited accommodation on the shelf facilitates the rapid progradation of deltaic systems across the continental shelf (Van Wagoner et al., 1990).

1.3.2.15 Sequence Stratigraphic Concepts Applied to Clinotherms

Relative sea-level fall and rise are recorded in clinotherm sequences by key stratigraphic surfaces (Fig. 1.6; SB, MFS and transgressive surfaces (TS)). When viewed in seismic profile, the identification of key reflector terminations (downlap, onlap, toplap, offlap and erosional truncation), in addition to corehole and log data, allows such key stratigraphic surfaces to be identified (Vail et al., 1977; Mitchum et al., 1977; Vail, 1987; Van Wagoner et al., 1987; Carvajal et al., 2009; Miller et al., 2013a). The sedimentary intervals (parasequences) sandwiched between these stratigraphic surfaces display specific stacking patterns and may be subdivided into systems tracts (Van Wagoner et al., 1987; Posamentier et al., 1988).

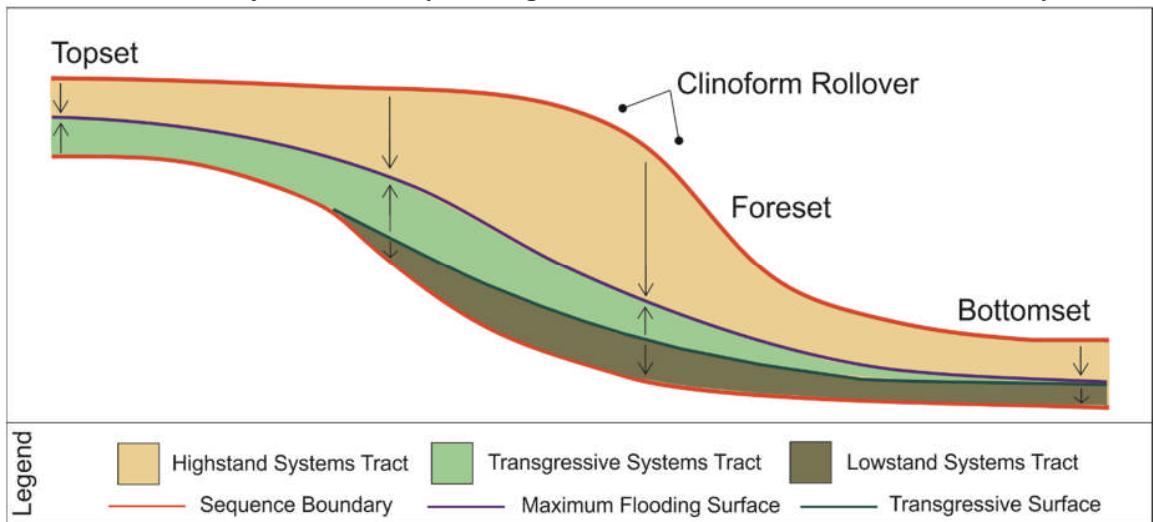


Figure 1.6: Simplified clinotherm model displaying systems tracts and major sequence stratigraphic surfaces. Arrows indicate direction of fining. Adapted from Miller et al. (2018).

1.3.2.16 Limitations of Sequence Stratigraphy

Early sequence stratigraphic models (see Vail et al., 1977; Vail and Todd, 1981) were underpinned by a set of key assumptions, including: i) sinusoidal variations in eustatic sea-level; ii) a constant rate of sediment supply; iii) a shelf-slope-basin physiography; and iv) that deposition of sediment in the deep-water setting occurred only during periods of sea-level fall and sea-level lowstand. These assumptions are now considered to be an oversimplification of the complex interplay of forcing mechanisms that govern patterns of deep-water sedimentation. For example, deep-water sand deposition during periods of relative sea-level rise and/or sea-level highstand were discussed by Kolla and Macurda (1988), Galloway (1989) and Burgess and Hovius (1998), amongst others. Additionally, the role of sediment supply in determining sediment delivery to deep water was emphasized by a number of authors including Galloway (1989) and Schlager (1993) amongst others. Hunt and Tucker (1992) and Posamentier et al. (1992) highlighted examples of significant sediment deposition

in the coastal and shallow-marine environment during episodes of sea-level fall. The aforementioned publications, amongst many others, called into question the ideals of the lowstand basin-floor fan hypothesis, consequently leading to broader discussions of the controls on stratal architectures.

1.3.3 Prediction of Deep-Water Sands in Clinofolds

When a single clinothem is considered, estimations of sand-delivery to the deep-water environment (i.e. lower slope and/or basin-floor) requires the extent of base-level (Shanley and McCabe, 1994) fall below the pre-existing platform shelf-edge to be evaluated (Steel et al., 2000; Porębski et al., 2002). If base-level does not fall below the outer-shelf platform, the propensity for incision of the falling-stage deltas (situated on the shelf-margin) is reduced (Fig. 1.7; Steel and Olsen, 2002). The lack of adequate incision of falling-stage deltas prevents the formation of sufficient connections between the distributary channels of the deltas and any slope channels or canyons; as such, the presence of deep-water sands is unlikely (Steel and Olsen, 2002).

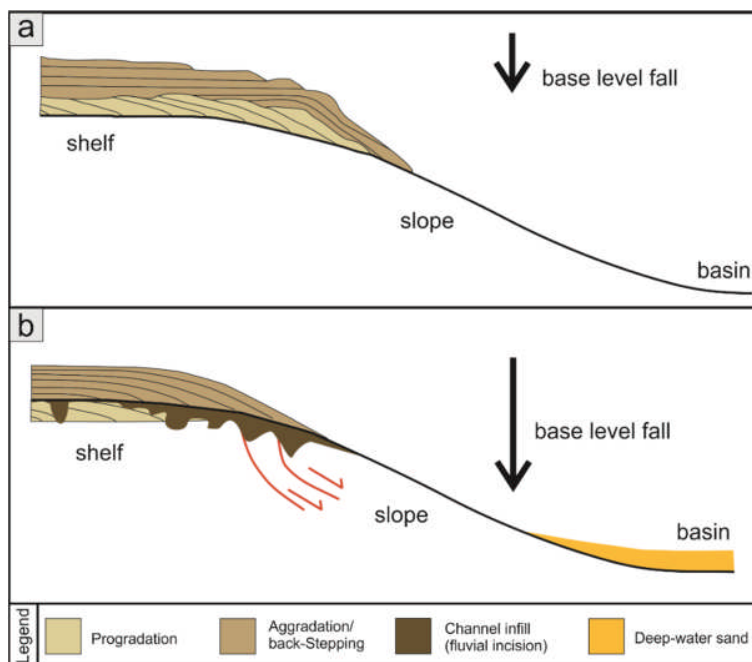


Figure 1.7: Estimations of sand delivery to the deep-water environment. The black arrow indicates the magnitude of base-level fall. The red lines indicate fault-blocks. a) Scenario in which base-level does not fall below shelf-edge; this is associated with a lack of fluvial incision on the shelf and limited/no bypass of coarse-grained sediment into the deep-water setting. b) Scenario in which base-level does fall below shelf-edge; this is associated with fluvial incision of shelf-edge and underlying deltas, leading to significant bypass of coarse-grained sediment into the deep-water setting. Adapted from Steel et al. (2008).

The aforementioned conditions instead promote deposition on the middle- and upper-slope. This occurs due to the progradation of the shelf-margin deltas across the clinoform rollover. The delta-fronts in these circumstances are generally turbidite-prone and can shed significant

volumes of sand basinward. However, the turbidite-prone delta front sands tend to pinchout laterally before reaching the lower slope (Mellere et al., 2002). During subsequent relative base-level rise, aggradation of the shelf-margin deltas occurs, ultimately leading to back-stepping across the shelf as lagoonal barrier systems or estuaries (Schellpeper and Steel, 2001).

The conditions associated with little or no deep-water sand deposition are suggested to be associated with the following attributes: i) the shelf-edge and upper-slope form a smooth profile; ii) there is little or no evidence of shelf-edge incision or fluvial erosion; and iii) up to the clinoform rollover, there is a well-preserved, progradational delta architecture, which subsequently has a back-stepping or aggradational architecture (Fig. 1.7; Plink-Björklund and Steel, 2002; Porębski and Steel, 2003; Steel and Olsen, 2002).

If relative base-level falls below the clinoform rollover of the pre-existing platform shelf-edge, the propensity for incision of the falling-stage deltas (situated on the shelf-margin) is increased (Steel and Olsen, 2002). Under these conditions, shelf-margin deltas typically become incised and cannibalised by the distributary channels of the shelf-margin delta; this leads to the basinwards migration of the depocentre. Incision of the shelf-edge by river systems potentially leads to a connection between valleys situated on the shelf and any channels or canyons situated on the slope. The potential linkage between shelf and slope facilitates the direct delivery of sediment into the deep-water setting (Kolla, 1993; Steel et al., 2000). During subsequent base-level rise, late-stage shelf-margin deltas form again, but onlap onto the incised slope.

The conditions associated with significant deep-water sand deposition are suggested to be associated with the following attributes: i) fluvial incision of the shelf-edge falling stage deltas; ii) prominent collapse of the slope; iii) the formation of growth faults and block rotation (Fig. 1.9b); and iv) an aggradational to back-stepping shelf-margin delta architecture (Fig. 1.7; Nemec et al., 1988; Steel et al., 2000; Johannessen and Steel, 2002; Porębski et al., 2003).

1.3.3.1 Trajectory Analysis and Sequence Stratigraphy

Clinoform rollover trajectory analysis is an objective methodology that complements sequence stratigraphic approaches, whilst also taking into account rates of sediment supply. Conventional sequence stratigraphic analysis assigns strata to various systems tracts (TST, HST, FSST and LST) with the aim of producing predictive models. The concept of clinoform rollover (shelf-edge) trajectory analysis permits the established sequence stratigraphic systems tracts to be visualised within the context of a more continuous depositional spectrum during relative sea-level change (Henriksen et al., 2009). Analysis of clinoform rollover

trajectory and the depositional products associated with a relative sea-level rise, stillstand, or fall in the migratory pathway taken by the clinoform rollover provides an effective methodology for the prediction of lithologies in shallow- and deep-water settings.

1.3.3.2 Trajectory Analysis: an Introduction

Trajectory analysis combines the examination of the vertical and lateral migratory pathways of geomorphological features (Helland-Hansen and Hampson, 2009), and can improve understanding of temporal variations in facies distributions and palaeoenvironment. Trajectory analysis can be attempted from small scale (e.g., ripple migration and aggrading fluvial bars), through intermediate scale (e.g., prograding delta front and shelf-edge clinoforms), to large scale (e.g., progradation of continental margins) (Fig. 1.8). However, trajectory analysis is most commonly used for the study of 2-D dip-parallel depositional sequences at two scales: i) shoreline trajectories, where the migratory pathways of shorelines and related coastal depositional systems are analysed in cross-section (e.g., Helland-Hansen and Gjelberg, 1994; Helland-Hansen and Martinsen, 1996) and ii) clinoform rollover trajectories, where the migratory pathways of the clinoform rollover are analysed within a series of clinoforms (e.g., Mellere et al., 2002; Steel and Olsen, 2002; Johannessen and Steel, 2005).

Shoreline and clinoform rollover trajectory analysis have a number of attributes that make this approach advantageous for the study of migratory pathways: i) both systems have a physiographic break-in-slope, and ii) the clinoform rollover and the shoreline are both characterised by marked variations in depositional processes and products (Helland-Hansen and Hampson, 2009). The significant changes in depositional character that occur at both the clinoform rollover and at the shoreline, facilitate the mapping of the lateral and vertical shifts of the breaks-in-slope within dip-parallel seismic sections. Additionally, the fundamental differences in depositional character across the clinoform rollover and shoreline enable breaks-in-slope to be identified in well-log, core and outcrop data, in cases where the geometries of migratory pathways cannot be directly observed. In such circumstances, the migratory pathway of the clinoform rollover or shoreline trajectory may be constructed by proxy, using changes in facies distribution to identify breaks-in-slope (Helland-Hansen and Hampson, 2009).

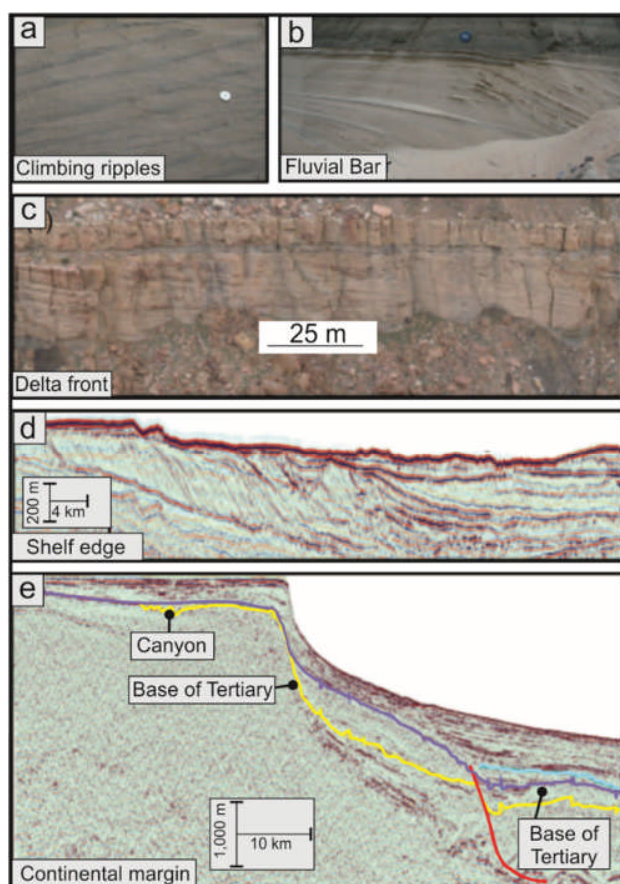


Figure 1.8: Scales of trajectory analysis within prograding systems. a) Climbing ripples (lens cap for scale) from Tana River, Northern Norway. b) Aggrading fluvial bar (lens cap for scale) from Tana River, Northern Norway. c) Prograding delta front clinoforms from Cretaceous Ferron Sandstone, Utah, USA. d) Prograding shelf-edge clinoforms from Norwegian Sea (Neogene). e) Prograding continental margin from offshore Brazil. Adapted from Henriksen et al. (2009).

1.3.3.3 Clinoform Trajectory Analysis and Deep-Water Sands

The clinoform rollover trajectory is defined as the pathway of migration taken by the clinoform rollover as a series of accreting clinoforms develop (Fig. 1.9; Steel and Olsen, 2002; Sydow et al., 2003; Johannessen and Steel, 2005; Helland-Hansen and Hampson, 2009). The shelf-edge trajectory can exhibit variation in its gradient and the relative rise, or relative fall, of the location of successive shelf-edges can be used as a proxy for relative sea-level rise and fall respectively.

The following conclusions regarding the relationship between clinoform rollover trajectory and the partitioning of the sediment budget between the shallow- and deep-water settings are discussed in Steel and Olsen (2002). Clinoform rollover trajectories formed by the accretion of successive clinoforms that have a flat to downward trajectory (Fig. 1.10c, d; negative gradient) indicate a relative sea-level that is stable or falling, through time. Clinoform rollover trajectories with low-gradients are suggested to represent the most favourable conditions for sand-delivery into the deep-water setting (Fig. 1.11). Flat or falling clinoform rollover

trajectories are often associated with shelf-edge incision; as such, sediment is delivered across the shelf within fluvial channel systems that have the potential to be directly linked to slope channel systems (Johannessen and Steel, 2005). If the supply of sediment remains channelized during downslope transit, large volumes of sand can be bypassed to the base-of-slope and the basin-floor.

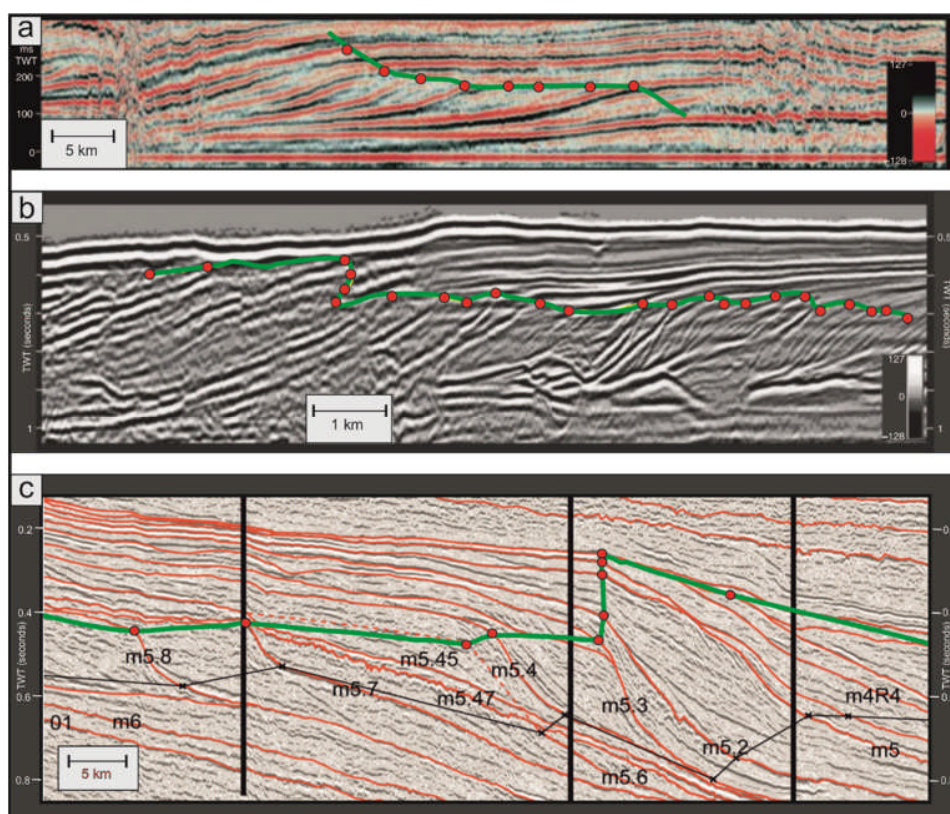


Figure 1.9: Examples of dip-parallel seismic sections displaying well-defined clinoforms and clinoform trajectories. The red dots indicate the position of the clinoform rollover (shelf-edge). The green line illustrates the migratory pathway taken of the shelf-edge. a) Anisian, Barents shelf. b) Oligocene-Miocene, mid-Norwegian shelf. c) Miocene, offshore New Jersey. Seismic images a) and b) adapted from Helland-Hansen and Hampson (2009).

In contrast to the previous example, clinoform rollover trajectories, formed by the accretion of successive clinoforms, which have a rising trajectory (Fig. 1.10b; positive gradient), indicate a relative sea-level rise. Clinoform rollover trajectories with rising gradients are suggested to reflect poor conditions for the bypass of sand into the deep-water setting (Fig. 1.11; Johannessen and Steel, 2005). A rising shelf-edge trajectory is associated with the storage of a large proportion of the sediment budget on the shelf and coastal plain, with little or no sand bypassed into the deep-water setting (Steel and Olsen, 2002).

1.3.3.4 Limitations of Clinoform Rollover Trajectory Analysis

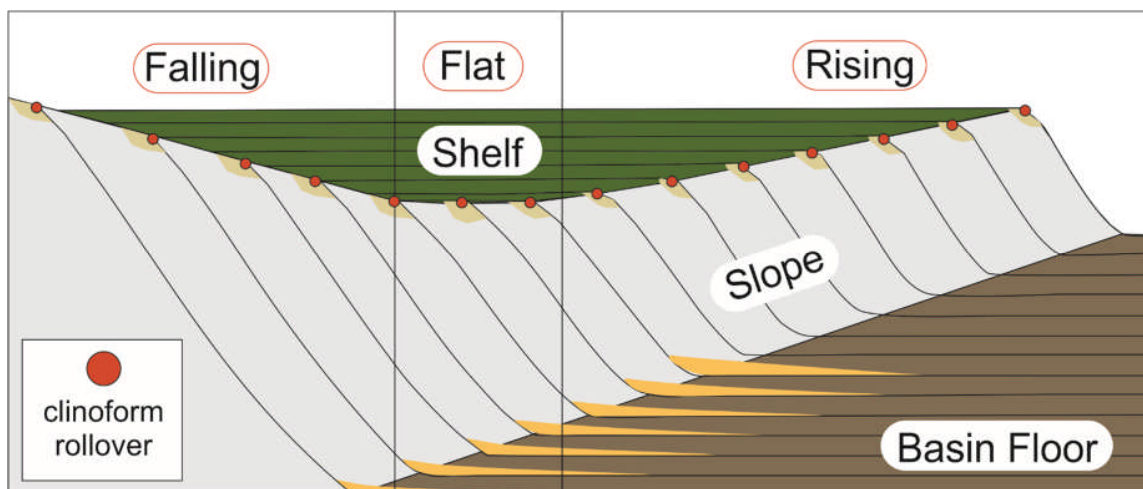


Figure 1.10: a) Internal clinoforms within a sedimentary prism of a prograding basin margin. b) Rising (positive) clinoform rollover trajectory, associated with relative sea-level rise, shelf accommodation and limited delivery of coarse-grained sediment basinward. c) Flat clinoform rollover trajectory, associated with a relative sea-level standstill, limited shelf accommodation and delivery of coarse-grained sediment basinward. d) Falling (negative) clinoform rollover trajectory, associated with relative sea-level fall, no shelf accommodation and delivery of coarse-grained sediment basinward. Adapted from Steel and Olsen (2002) and Helland-Hansen and Hampson (2009).

Despite the many advantages of clinoform rollover trajectory analysis as a methodology for the description and interpretation of successions of strata, there are a number of caveats associated with clinoform rollover trajectory analysis; these are discussed in Helland-Hansen and Hampson (2009) and Henriksen et al. (2009). A brief summary of some of the limitations of trajectory analysis are provided below. i) The choice of reference point used for the reconstruction of the trajectory path may vary. This is a particular problem in circumstances where there is not a well-defined clinoform rollover, such as in poorly-exposed outcrop data or within cores. ii) The clinoform rollover is not a point per se, but a zone; as such, there may be some variation as to where the clinoform rollover is identified by different authors. iii) Compaction of sediment post-deposition may change the original gradients of surfaces and affect the perceived relationships between strata; studies indicate that clinothem decompaction should be undertaken prior to any interpretations of clinoform trajectory (Steckler et al., 1999; Klausen and Helland-Hansen, 2018). iv) Lateral or along-strike variability cannot be accounted for in a single 2-D, dip-parallel transect. The majority of modern and ancient shelf-edges are not linear features and can vary significantly along-strike; as such, an apparent 2-D dip-parallel profile is likely to be, at least somewhat, oblique to the true direction of depositional dip. Variability in three dimensions can affect clinoform rollover trajectories to the extent that the same succession can seem to have either rising, flat or falling trajectories in different cross-sections taken along-strike. v) The geometry of the depositional

clinoform rollover may be significantly altered by erosion. This can be mitigated by careful evaluation of the stratigraphic interval in the context of the evolving shelf-edge succession.

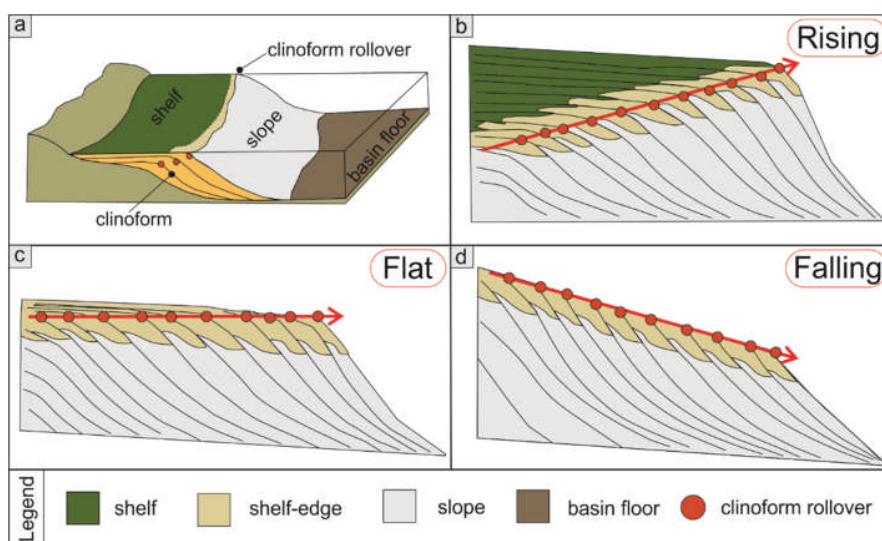


Figure 1.11: Established clinoform rollover trajectory model. Deposition of coarse-grained sediment on the basin-floor occurs only when the clinoform rollover trajectory is falling or flat (associated with relative sea-level fall and standstill respectively). Rising clinoform rollover trajectories (associated with relative sea-level rise) display basin-floor sediment starvation. Adapted from Dixon et al. (2012a).

1.3.4 Controls on the Delivery of Sediment to Deep-Water

Despite the widespread use of sequence stratigraphic and clinoform trajectory concepts, the fundamental controls determining the delivery of shelf-edge sands into the deep-water setting is still debated. This is in spite of the fact that deep-water (slope and basin-floor) sandstones host > 15 % of global siliciclastic hydrocarbon reservoirs, and remain valuable targets for exploration (e.g., Richards et al., 1998; Carvajal and Steel, 2006; Sømme et al., 2009; Martinsen et al., 2011). Authors considering the conditions necessary to deliver coarse-grained sand into slope and basin-floor settings fall into three fundamental categories: accommodation-driven, supply-driven, and process-regime-driven.

1.3.4.1 Accommodation-Driven Mechanisms

The accommodation-driven mechanism of sand delivery is underpinned by early sequence stratigraphic concepts, developed when researchers at ExxonMobil noticed a global pattern in seismic datasets. The seismic datasets suggested that a fall in relative sea-level on or below the continental shelf-edge was the fundamental control on sand delivery to the deep-water environment (e.g., Vail et al., 1997; Van Wagoner et al., 1990; Posamentier et al., 1992; Catuneanu et al., 2009; Steel and Milliken, 2013). The accommodation-driven mechanism is effective under Icehouse conditions, when the magnitude of eustatic sea-level change is between 70 and 120 m (Coe et al., 2003). Under Greenhouse conditions, however, the accommodation driven-mechanism is less certain, as the magnitudes of relative sea-level fall

were a few tens of metres (e.g., Coe et al., 2003; Carvajal and Steel, 2006; Gong et al., 2016). The magnitudes of sea-level fall under Greenhouse conditions are not sufficient to drive delta progradation across continental shelves, which typically have widths exceeding 200 km. Despite this, thick turbiditic successions are equally documented in stratigraphic intervals associated with both Icehouse and Greenhouse conditions (Gong et al., 2016).

1.3.4.2 Supply-Driven Mechanisms

During the late 1990's it became apparent that the accommodation-driven mechanisms of deep-water coarse-grained sand delivery could not account for the observed formation of deep-water fans during periods of rising clinoform rollover trajectory, associated with sea-level rise or highstand (Burgess and Hovius, 1998; Carvajal and Steel, 2006; Covault and Graham, 2010). Equally, accommodation-driven mechanisms could not account for the absence of basin-floor fans under falling clinoform rollover trajectories, associated with relative sea-level fall below the shelf-edge (Plink-Björklund and Steel, 2002). The supply-driven mechanism of sediment delivery to the deep-sea was born from outcrop (Carvajal and Steel, 2006), shallow seismic (Covault et al., 2007), experimental (Burgess and Hovius, 1998), and deep-sea, late Quaternary depositional-rate (Covault and Graham, 2010) datasets. These datasets showed that deltas could prograde to, and maintain a position at the shelf-edge, and effectively deliver sand into the deep-water setting during sea-level rise or highstand.

The supply-driven mechanism requires: i) a narrow shelf, and/or ii) a large sediment discharge (e.g., Burgess and Hovius, 1998; Muto and Steel, 2002; Covault and Graham, 2010; Kim et al., 2013; Gong et al., 2016). Narrow shelves permit rapid delta progradation to the shelf-edge, and in the absence of auto-retreat (*sensu* Muto and Steel, 1997, 2002) deltas can be sustained at the shelf-edge during falling or rising relative sea-level. Deep-water coarse-grained deposits are documented in the Californian Borderlands, USA (Covault, et al., 2007; Normark et al., 2009; Covault and Graham, 2010) irrespective of sea-level. A number of factors contribute to the development and maintenance of such highstand fans in the Californian Borderlands; these include a narrow shelf, resulting in a relatively short distance between the canyon head and littoral zone, and the high sediment discharge provided by the tectonically active Californian margin (Covault et al., 2007).

Deltas that prograde to the shelf-edge during relative sea-level rise due to high rates of sediment discharge (supply-dominated), can cross moderately-wide continental shelves. Favourable conditions for high sediment supply include optimal climatic conditions (Kolla and Perlmutter, 1993) and episodes of significant tectonism (e.g., Winker, 1989; Marzo and Steel, 2000). The application of the supply-driven model in different depositional

environments led to the development of the ‘highstand fan’ concept (e.g., Bullimore et al., 2005; Carvajal and Steel, 2006; Covault et al., 2007; Boyd et al., 2008). Examples of highstand fans, associated with high sediment-supply rates include: southeast Australian margin fans (Boyd et al., 2008); Lewis Shale fans, southern Wyoming, USA (Carvajal and Steel, 2006); and the Bengal fan, Bay of Bengal (Weber, 2006).

1.3.4.3 Shelf Process-Regime-Driven

Typically, where the morphological shelf is >100 km (i.e. a wide shelf) the most effective shelf process-regimes for delivering sediment to the shelf-margin are river-dominated deltas (Burgess and Hovius, 1998; Muto and Steel, 2002). Where the morphological shelf is ~ 10 km (i.e. a narrow shelf) sediment delivery to the shelf-edge can be governed by tidal currents (e.g., Berne et al., 1998), wind-driven currents (e.g., Snedden et al., 1988) and wave-orbital currents (e.g., Drake et al., 1985). Regardless of the mechanisms and rate of sediment supply to the shelf-edge, the automatic bypass of this sediment into the deep-water setting is not guaranteed at that location; in part, this is due to the dominant process-regime in operation at the shelf-edge (e.g., Dixon et al., 2012a; Laugier and Plink-Björklund, 2016).

Wave-dominated shelf process-regimes, associated with open ocean conditions, are considered to be ineffective at bypassing sediment into the deep-water setting (e.g., Plink-Björklund and Steel, 2004; Petter and Steel, 2006; Dixon et al., 2012a; Gong et al., 2016). Open ocean waves create a shelf-edge energy-fence, which inhibits the bypass of sediment into the deep-water setting. Under wave-dominated conditions, sediment preferentially accumulates on the shelf, due to the prevalence of longshore-drift currents (e.g., Carvajal and Steel, 2009; Dixon et al., 2012a; Laugier and Plink-Björklund, 2016). The dominance of strike-parallel sediment transport under wave-dominated conditions is typically only associated with sediment transport into the deep-water setting where longshore currents intersect a canyon or channel (Carvajal and Steel, 2009; Dixon et al., 2012a; Jones et al., 2015).

In contrast to wave-dominated shelf process-regime conditions, river-dominated shelves are considered to be effective conveyors of sediment into the deep-water setting. Dixon et al. (2012a) compiled a review of 29 shelf-edge deltas (Fig. 1.12) and associated basin-floor sediments, with a range of clinoform rollover trajectories and shelf process-regimes. The review paper of Dixon et al. (2012a) classified the 29 shelf-edges as being either fluviially-, wave-, or tidally-dominated, according to the tripartite classification of Galloway (1975). In 34% of the examples presented in Dixon et al. (2012a), a breakdown in the established relationship between clinoform rollover trajectory and deep-water deposition is documented. This established model assumes that flat to falling clinoform rollover trajectories (indicating

relative sea-level standstill and fall respectively) are associated with significant deposition of coarse-grained sediment in the basin-floor setting. Conversely, the established model assumes that rising clinof orm rollover trajectories (indicating relative sea-level rise) are associated with sediment starvation in the basin-floor setting.

Shelf-edge deltas 20, 21, 24, 25 and 26 (Fig. 1.12) show the formation of basin-floor fans during periods with rising clinof orm rollover trajectories. Shelf edge deltas 4, 5, 10, 13 and 14 (Fig. 1.12) show basin-floor sediment starvation, despite having flat to falling clinof orm rollover trajectories; these deltas are, however, associated with the deposition of sand on the middle- and upper-slope (Dixon et al., 2012a). The deposition of basin-floor fans during episodes of rising clinof orm rollover trajectory are attributed by Dixon et al. (2012a) to high sediment flux, associated with either narrow shelf-widths or high rates of fluvial discharge.

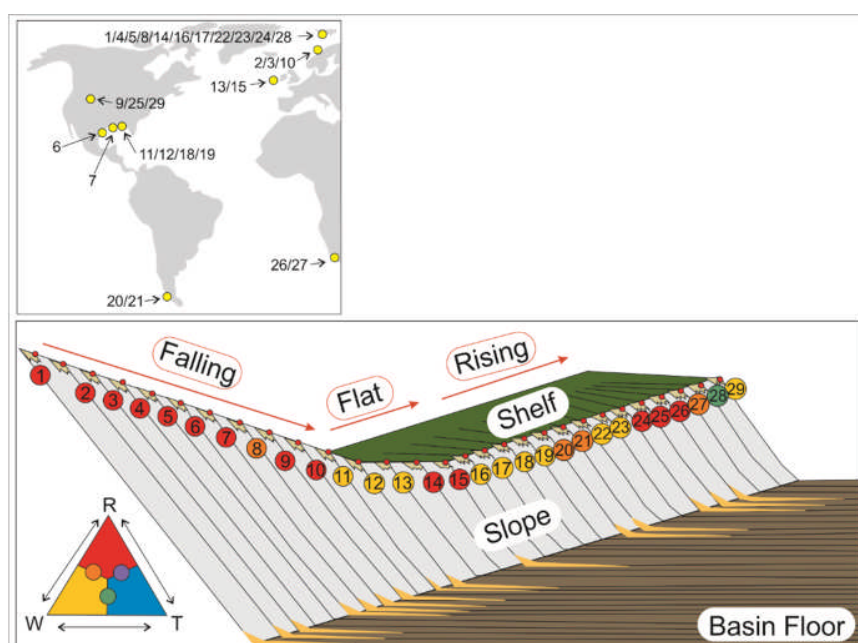


Figure 1.12: Clinoform datasets used by Dixon et al. (2012a). Map illustrates the geographic location of the examples used by Dixon et al. (2012a). The ternary diagram illustrates the colour coding system: river-dominated is red; wave-dominated is yellow; tide-dominated is blue. Where the various processes interact, an intermediate colour is indicated (e.g., the interaction of river and tide processes creates a purple colour and the interaction of wave and tide processes creates a green colour). The shelf-edge trajectory is also schematically illustrated. Each number corresponds with a geographic location (as illustrated on the map). The presence (or absence) of sandy deposits in the slope and basin-floor setting is illustrated. Adapted from Dixon et al. (2012a).

The dataset presented by Dixon et al. (2012a) includes 15 shelf-margins that display significant basin-floor fan deposition; 80% of these shelf margins are associated with a river-dominated shelf process-regime. The river-dominated shelf process-regime is most likely to be present when the clinof orm rollover displays a falling trajectory (associated with relative sea-level fall); however, the river-dominated shelf process-regime can occur when the clinof orm rollover trajectory is either flat, falling or rising. The results presented in Dixon et

al. (2012a) highlight the need for caution when attempting to predict the presence or absence of basin floor fans from clinoform rollover trajectory alone.

River-dominated shelf process-regimes are suggested by Dixon et al. (2012a) to be effective at delivering coarse-grained sediment into the deep-water setting over a range of clinoform rollover trajectories, primarily due to the presence of channels, gullies and canyons on the slope, which are fed by river-systems that generate both delta-front turbidity currents and hyperpycnal flows. The river-dominated shelf process-regime thus promotes direct connectivity (through either non-incised shelf-edge deltas or incised river valleys on the outer shelf) between the shelf and slope conduits, which effectively deliver coarse-grained sediment into the deep-water setting. The shelf process-regime plays a significant role in sediment partitioning across the depositional profile and in determining how and when sediment is transported from the staging area of the continental shelf (Dixon et al., 2012a; Laugier and Plink-Björklund., 2016).

1.3.5 Shelf Process-Regime

Deltaic systems have been classified according to the tripartite classification systems developed in the 1970's by Coleman and Wright (1975) and Galloway (1975), which subdivided modern deltas into those that are river-, wave-, or tide-dominated (Fig. 1.13). Subdivision of delta systems using the Galloway (1975) ternary classification system is achieved through qualitative interpretations of sedimentary structures, coastal processes, and delta-morphology. Modern variations of the traditional ternary classification scheme have been developed to consider: grain size, sea-level, and sediment supply (Boyd et al., 1992, 2006; Orton and Reading, 1993). Many examples of modern delta systems display intermediate characteristics and are consequently classified as mixed-energy; additionally, large delta systems may be mixed-energy, where there is a spatial and morphological partitioning of the river-, wave- and tidal-processes (Bhattacharya and Giosan, 2003).

1.3.5.1 Wave-Dominated Systems

A wave-dominated shoreline is found where wave action dominates over tidal influences to redistribute sediment discharged at the river mouth (Heward, 1981). A wave-dominated system is typically associated with open-ocean facing conditions, where there is potential for higher wave-energy and less influence from fluvial sources. Wave-dominated process-regimes are characterised morphologically by foreshore sands that advance basinward with the active delta lobe in a wide coast-parallel front (Einsele, 2013).

In wave-dominated systems immediate mixing of fresh and salt water occurs where breaking waves interact with fluvial discharge; this mixing results in the rapid deceleration of fresh

water flow velocity, typically producing a bar adjacent to the distributary mouth of the fluvial system. Sediment delivered by the fluvial system is transported in a shore-parallel direction and is deposited to form beach and bar deposits (Fig. 1.14). The typically oblique angles of wave approach can produce beach ridges that have asymmetric morphologies, and can result in the progradation of a spit across the river mouth (Davis and Hayes, 1984).

Due to the oblique angles of wave approach and along-shore drift, sediment is delivered to a section of wave-dominated coast not only from the adjacent river mouth (Fig. 1.14, 1.15), but also neighbouring river mouths (Bhattacharya and Giosan, 2003). The high energy of wave-reworking transports sediment away from the river mouth, and forms sediment ridges sub-parallel to the shoreline with distinctive arcuate to linear planform morphologies (Coleman and Wright, 1975). With increasing distance from the river mouth, the linear sediment ridges become increasingly narrow (Bhattacharya and Giosan, 2003). Finer-grained sediment is carried offshore, forming the subaqueous parts of the wave-dominated delta.

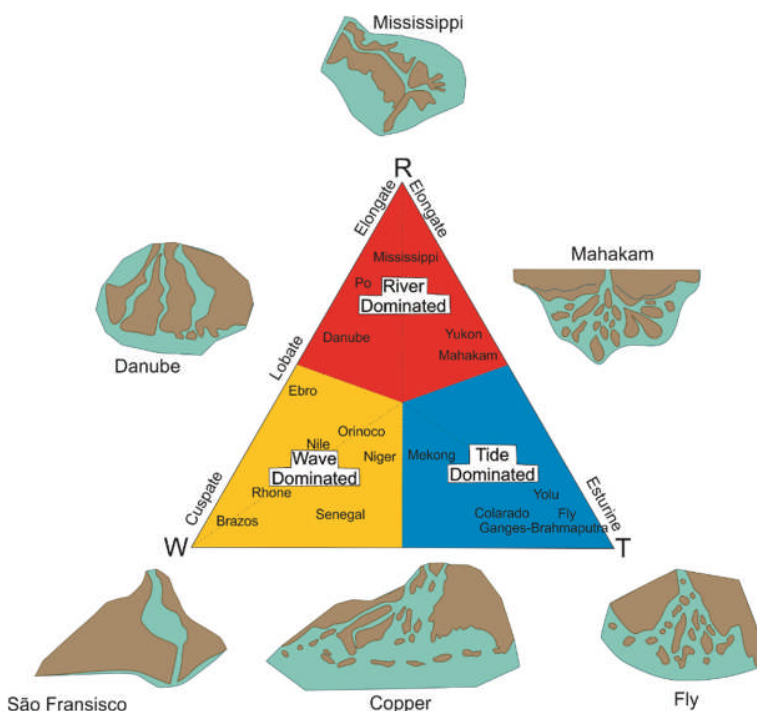


Figure 1.13: Ternary diagram illustrating river-, wave- and tide-dominated deltas. Examples of modern river-, wave- and tide-dominated deltas are illustrated alongside the classic morphology associated with the dominant process-regime. Adapted from Galloway, (1975)

Modern examples of wave-dominated deltas systems include: the New Brazos delta, Texas, USA; the Guadiana delta, Spain/Portugal; the Nile delta, Egypt; Senegal delta, Senegal; the Rio Grijalva, Mexico and the Paraibo do Sul delta, east Brazilian coast. These modern examples are characterised by prominent longshore drift, resulting in continuous sheet-like sands updrift of

the river mouth and linear sands interfingered with muddy facies downdrift of the river mouth (Li et al., 2011).

The river system discharging into a section of wave-dominated coast cannot deliver sediment ad infinitum into the ocean due to the decreasing gradient and decreasing capacity of river flow; as such, the river system relocates (autogenic switching) to a higher gradient location (Olariu, 2014). Typically, autogenic switching takes place during a flooding event where, inland, the river breaks its natural levee and advances to the ocean via a new course. When autogenic switching occurs, the site of active sedimentation is also relocated with the river system; the section of the delta system left behind is eroded by wave and current energy.

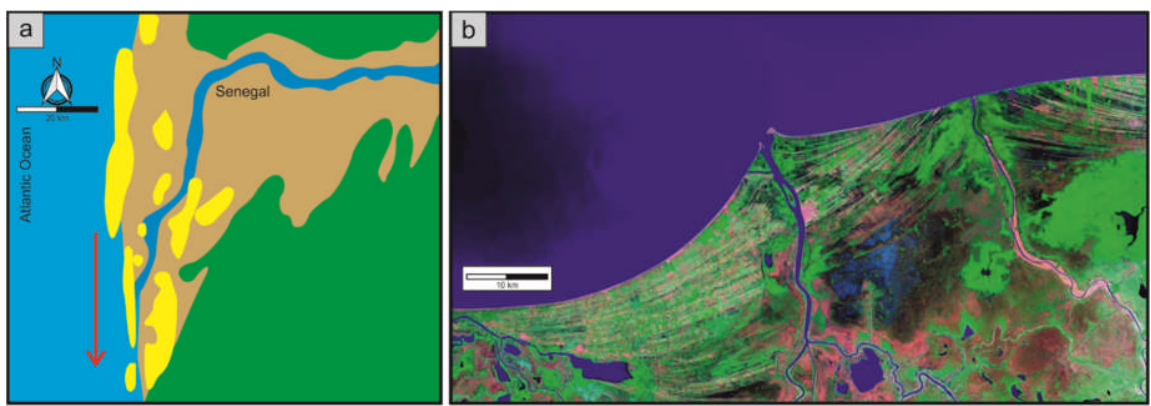


Figure 1.14: Schematic diagram showing morphology of a modern wave-dominated delta (Senegal delta, Senegal). Sand bodies are illustrated in yellow; deltaic plain features are illustrated in brown; areas that are not part of the modern Senegal deltaic system are illustrated in green; the red arrow indicates the dominant longshore drift direction. The Senegal delta is characterised by rapid southward transport of sediment by longshore currents, resulting in shore-parallel barrier islands. Adapted from Li et al. (2011). b) Landsat image of the Rio Grijalva, Mexico; land vegetation is shown in pink; the deltaic deposits are shown in green; the surrounding water is shown in dark blue. Image adapted from the European Space Agency.

In outcrop and core, wave-dominated deltas are recognised as sharp-based sand-bodies, which coarsen-upwards abruptly as a result of shoreface progradation (Davis and Hayes, 1984). The delta-fronts of wave-dominated deposits are characteristically sandy, with few mudstone deposits. Commonly, sedimentary structures associated with wave-dominated systems include abundant hummocky and swaley cross-stratification and symmetrical wave-ripples (Bhattacharya and Walker, 1992; Deibert et al., 2003; Li et al., 2011). Intensive wave-reworking produces better sorted and more mature sediment than those deposited within river-dominated deltas. Additionally, wave-dominated deposits typically contain abundant shell debris, associated with in-situ shallow-water organisms; shell debris also accumulates through processes of shore-parallel sand transport (Einsele, 2013).

The deeper-water counterparts of the wave-dominated shelf (i.e. the slope and basin-floor) lack substantial sandy basin-floor fan deposits (Carvajal and Steel, 2009; Dixon et al., 2012). Relative to river-dominated systems, wave-dominated deltas have a reduced capacity to channelize the shelf-edge, and are therefore less likely to develop conduits to bypass sand downdip (Carvajal and Steel, 2009). Typically, slope and basin-floor deposits associated with wave-dominated shelves are dominated by mud and silt deposits, and contain only rare, thin sand sheets associated with turbidity currents (Deibert et al., 2003; Uroza and Steel, 2008).

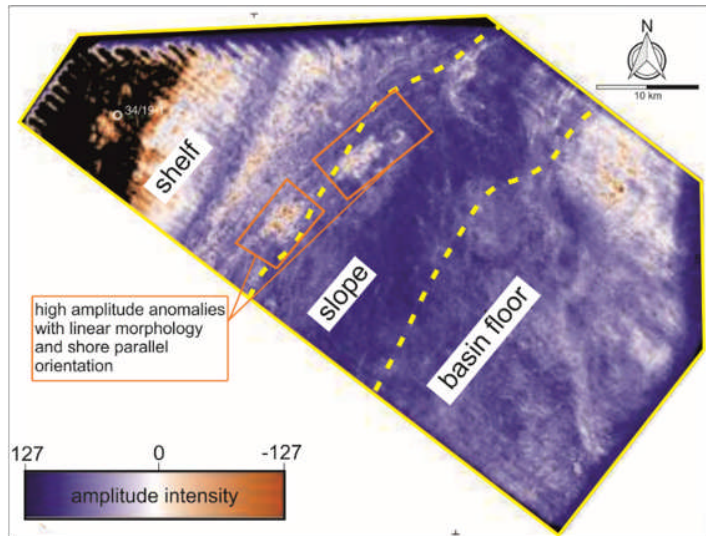


Figure 1.15: Eocene Porcupine Basin, Offshore Ireland. The orange boxes highlight high amplitude, strike-elongate features, interpreted as wave-generated sand-ridges located parallel to the shelf-edge, and positioned at the clinoform rollover. Adapted from Ryan et al. (2009).

Large accumulations of shore parallel sand deposits are rarely bypassed into the deep-water setting under wave-dominated conditions (Dixon et al., 2012). Bullimore et al. (2005) document sand-rich slump deposits present on over steepened upper-slope segments in the Molo Formation (mid-Norwegian continental shelf). Additionally, wave-dominated shelves can deliver significant volumes of sand into the deep-water setting where sediment supplied via longshore drift intersect with canyon heads (Carvajal and Steel, 2009; Dixon et al., 2012; Jones et al., 2015). An additional example of deep-water bypass under wave-dominated conditions comes from the east Australian longshore transport system, where compositionally and texturally mature sands are bypassed to deep water in the absence of fluvial processes; in this case shore-parallel sourced sands interact with tidal currents at an estuarine embayment, formed by barrier elongation, and are transported over the shelf-edge (Boyd et al., 2008).

The development of a wave-dominated shelf process-regime, and preservation of wave-dominated architectures, is most likely to occur under conditions where relative sea level is rising. Highstand, or rising sea-level, favours the development of aggrading sedimentary

packages of substantial thickness, in which longshore drift can continue along the linear and open coasts for great distances (Carvajal and Steel, 2009). Under conditions of falling relative sea-level, an incised shelf-edge coast tends to develop, leading to relatively thinner and less well developed delta systems; the influence of wave-processes is inhibited by the development of areas of protected coastline and consequently diminishes the shore-parallel distribution of sand (Carvajal and Steel, 2009).

1.3.5.2 Tide-Dominated Systems

Tide-dominated deltas are characterised morphologically by wide river mouths, which taper significantly upstream, and by the presence of islands and channel bars. The tide-dominated delta operates under mesotidal to macrotidal conditions in open shorelines; this is associated with high rates of sediment supply, discharged from large rivers. As such, the tide-dominated delta is associated with constant sediment transport and tidal-exchange (Goodbred and Saito, 2011).

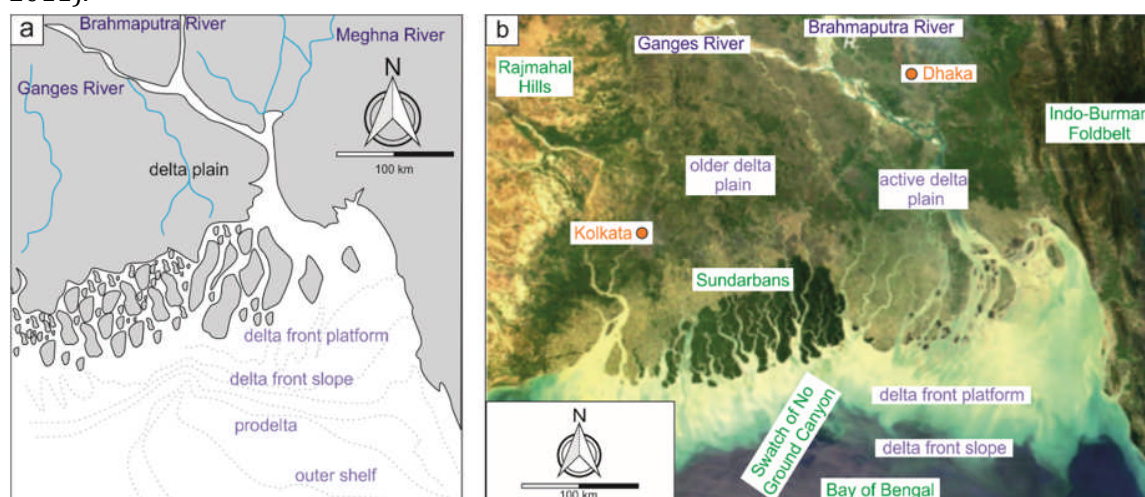


Figure 1.16: Tide-dominated Ganges-Brahmaputra river delta, characterised by a large muddy clinothem deposit (~10's of km) forming off the river-mouth. a) Physiographic map illustrating the funnel-shaped river-mouth morphology. b) MODIS satellite image (19/03/02, dry season) with labelling of the prominent physiographic and geographic features of the delta. Adapted from Goodbred and Saito (2011).

Modern tide-dominated deltas are located in low-latitude and tectonically active regions, including Australasia and South and East Asia. In low latitude regions, the principal lunar semi-diurnal tide (M2 tide) is amplified in areas with large tidal-ranges. This is supported by the presence of shallow and wide continental shelves, which typically exhibit a narrowing in width towards their apex, and are well-connected to the ocean (Goodbred and Saito, 2011); examples include East China Sea (Changjiang), Bay of Bengal (Ganges-Brahmaputra; Fig. 1.16), and the Gulf of Papua (Fly).

Mountainous and tectonically active regions supply the necessary sediment yield required to form tide-dominated deltas in high-energy coastal environments; an example is the

Indonesian Archipelago, which receives an exceptionally high rate of sediment supply (Milliman and Syvitski, 1992), associated with the Himalayan-Tibetan uplift.

Ancient tide-dominated deltas are recognised in the stratigraphic record by the presence of interbedded sand and mud deposits (heterolithic deposits) on the delta front. Sedimentary structures used to recognise tide-dominated deltas include: i) bi-directional and/or land-facing palaeocurrents (e.g., Bhattacharya and Walker, 1992); ii) stacking of high-angle cross-strata, with associated mud-drapes, located on the mid and upper delta front (Willis, 2005); iii) ripple-laminae sets, with associated mud-drapes, located on the lower delta-front (Willis, 2005); iv) ichnofacies associated with brackish conditions (MacEachern, et al., 2005); and v) sand and mud ridges situated parallel to the palaeo-shoreline (Coleman and Wright, 1975). Modern examples of tide-dominated deltas display slowly prograding subaerial delta plains, and relatively rapid progradation of subaqueous clinothems, which are typically mud-dominated and heterolithic (e.g., Fly, Gulf of Papua). However, rare examples, including the Ganges-Brahmapura (Bay of Bengal), have a large coarse-grained sand content. In the ancient record, tide-dominated deltas are invariably associated with interbedded sand and mud deposits on the delta front (e.g., Willis, 2005) and consequently have a significant coarse-grained component. The dominance of ancient examples that are coarse-grained is suggested by Goodbred and Saito (2011) to result from the difficulty in discriminating between other mud-dominated sedimentary facies, and those which are tide-dominated. Additionally, recognising tide-dominated deltas in outcrop is challenging, due the large distances over which they develop.

Observations of modern tide-dominated deltas suggests that the majority of cross-shelf sediment transport is gravity-driven (Wright and Friedrichs, 2006); the requirements for gravity-driven cross-shelf sediment transport are encountered when there is peak riverine sediment discharge onto an energetic, tide-dominated delta-margin (Harris et al., 2004). The high sediment discharge and energetic conditions associated with gravity-driven sediment transport promote the development of compound clinothem morphologies (Fig. 1.17; Swenson et al., 2005). As such, tide-dominated systems are associated with subaqueous deltas located offshore that are distinct from the commonly described subaerial counterparts (Nittrouer et al., 1986; Prior et al., 1986). The tide-dominated subaqueous delta occurs at the

boundary between shallow-marine (i.e. tidal-current transport) and deep-marine (i.e. gravity-dominated processes, such as mass wasting) processes (Swenson et al., 2005).

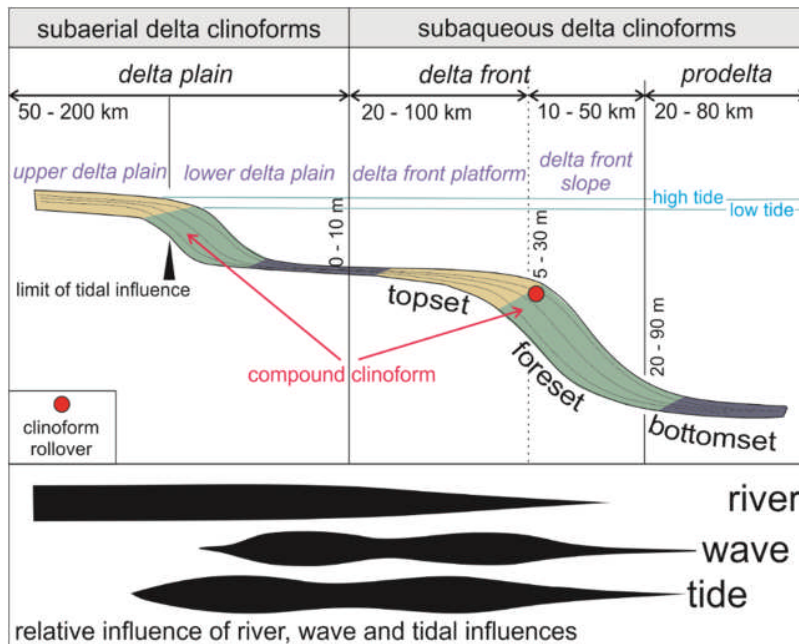


Figure 1.17: Schematic cross-section illustrating major morphologic and physiographic features of a tide-dominated delta system. The delta system is characterised by a well-developed, prograding subaerial and subaqueous compound delta. Adapted from Goodbred and Saito (2011)

In the ancient record, tide-dominated delta systems are not recognised frequently in a shelf-edge location, however rare examples (e.g., Nova Scotia shelf margin; Cummings et al., 2006) have been documented. The absence of preserved shelf-margin tide-dominated delta-systems has been the subject of some confusion, as previous studies have noted that the shelf-edge is associated with maximum tidal current velocities (Fleming and Revelle, 1939; Reynaud and Dalrymple, 2011). In rare documented examples of ancient tide-dominated deltas situated at or near the shelf-margin, sand is largely retained within topset deposits (e.g., Cummings et al., 2006; Petter and Steel, 2006) and there is minimal downdip sand-transport.

1.3.5.3 River-Dominated Systems

A river-dominated shelf process-regime is classified as one in which there is no significant tidal- or wave-reworking of suspended and bedload sediment deposited at the river mouth; as such, the river delta progrades into a basin with relatively low tidal and/or wave energy. The river-dominated delta has a characteristic planform morphology (Fig. 1.18), in which multiple terminal distributary channels form complex dendritic distributary networks that are lobate in shape, or form extended deltaic systems perpendicular to the shoreline (Coleman and Wright, 1975; Olariu and Bhattacharya, 2006).

River systems are the dominant mechanism responsible for the transfer of sediment from terrestrial source areas to marine basins; modern river systems transfer ~ 25 GT/year of sediment to the ocean, representing $> 90\%$ of the total terrestrial sediment influx to the ocean (Syvitski, 2003). River mouths have been traditionally considered as areas of sediment sequestration, due to the loss of confinement and rapid flow deceleration. However, studies have demonstrated that river deltas with large sediment bedloads, typically during periods of river-flooding, can bypass the coastal area and transfer large volumes of sediment basinward (Normark and Piper, 1991; Mulder and Syvitski, 1995). This scenario arises when the bulk density of fluvial discharge exceeds that of the lower-density receiving basinal water, forming a hyperpycnal flow (after Bates, 1953).

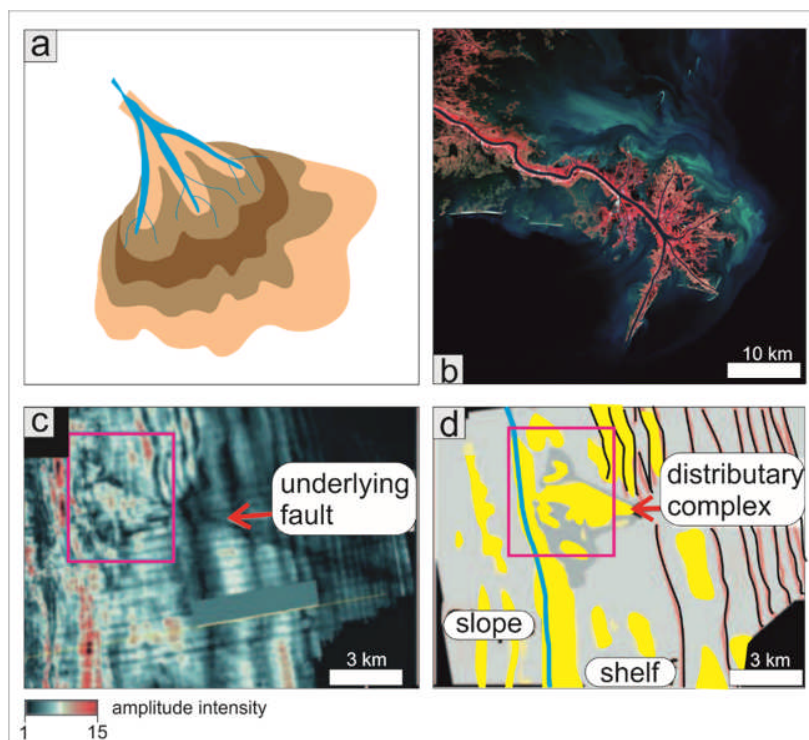


Figure 1.18: Schematic diagram showing a simplified river-dominated delta. River-dominated deltas have many (10's – 100's) of terminal distributary channels, which disperse sediment into the basin. The darker shades of brown indicate thicker sediment deposition. Adapted from Olariu and Bhattacharya (2006). b) Landsat image of the Mississippi River Delta (October 2011); land vegetation is shown in pink, sediment dispersed into the surrounding water is shown in turquoise and royal blue. Image taken from the European Space Agency. c) Un-interpreted seismic data of Molo Formation (offshore Norway). d) Interpreted depositional features of the Molo Formation as shown in c). Figures c and d adapted from Bullimore et al., (2005) and Dixon et al., (2012a).

The potential for basinward sediment transport during hyperpycnal flow events has been documented in 230 modern river systems, in which 84 % of river systems produced episodic hyperpycnal discharges (Mulder and Chapron, 2011). Additionally, in a study of the Var River, France, Mulder (2003) documented a single hyperpycnal flow event (with a duration of 18 hours), in which the particle load was 11-14 times greater than that typically transported under normal conditions. Modern studies of hyperpycnal flows suggest they have the

potential to travel long distances in a basinward direction; as an example, hyperpycnal flow deposits were documented 700 km downdip from the associated river canyon system in the Japan Sea (Nakajima, 2006).

Studies of modern systems suggest that hyperpycnal flow events should be commonly documented in the ancient record (Mulder and Chapron, 2011; Mulder, 2003; Nakajima, 2006). The recent appreciation of the sediment transport potential and widespread occurrence of hyperpycnal flows represents an important paradigm shift in our understanding of how and when sediment is transferred from source to sink. In the ancient record, the deposits of sandy hyperpycnal flows have been increasingly recognised in the literature since the early 2000's (e.g., Mulder and Alexander, 2001; Mulder et al., 2003; Mutti et al., 2003); examples include: the Misoa Formation, Argentina (Eocene; Gamero et al., 2006) and the Central Basin of Spitsbergen (Eocene; Plink-Björklund and Steel, 2004).

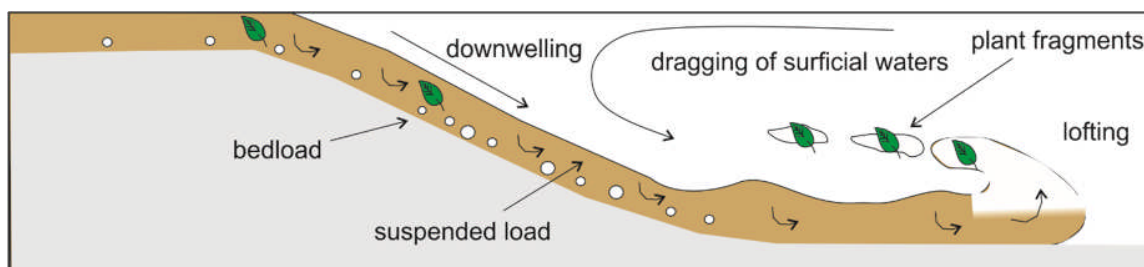


Figure 1.19: Schematic diagram of a downwelling hyperpycnal flow, illustrating the basinward transfer of terrestrial sediment, including sandy bedload and lofted plant debris. Adapted from Zavala and Pan (2018).

Hyperpycnal flows associated with a delta system located at the shelf-edge typically result in the deposition of thin-bedded turbidites on the slope or on the delta front (Normark and Piper, 1991; Mulder and Syvitski, 1995). Delta front deposits associated with hyperpycnal flows can also result in the deposition of sandy turbidites (either channelized or tabular) that are interbedded with silt and mud deposits (e.g., Plink-Björklund and Steel, 2004; Petter and Steel, 2006; Dixon et al., 2012b). Hyperpycnal flows associated with shelf-edge delta systems can also result in slope instability and delta-front collapse, leading to the deposition of associated debritic deposits (e.g., Mayall et al., 1992; Petter and Steel, 2006; Dixon et al., 2012b). The propensity for coarse-grained sediment transfer (transported as bedload sediment) and deposition in the deep-water setting during hyperpycnal flow events is increased when the river delta progrades to the shelf-edge. Under these circumstances, the slope of the delta front and slope of the basin margin can merge, resulting in slope channel systems that act as conduits for sand transport to the basin floor (e.g., Mellere et al., 2003). Hyperpycnites can be sandy or muddy, depending on the entrained grain size. The diagnostic features associated with sandy hyperpycnites have been the subject of much discussion (see Zavala and Pan, 2018). This has resulted in previous misinterpretations of hyperpycnites as

fluvial, estuarine or shoreface deposits and sandy debrites in the literature. However, the presence of reverse-to-normal grading at bed-scale, suggesting the presence of accelerating (waxing) and decelerating (waning) flow regimes (cf. Kneller, 1995) is also associated with sandy hyperpycnites. A waxing period of river-mouth discharge will deposit a coarsening-up unit within an event bed (Mulder et al., 2001) and a waning period of river-mouth discharge will deposit a fining-up unit above within the same event bed.

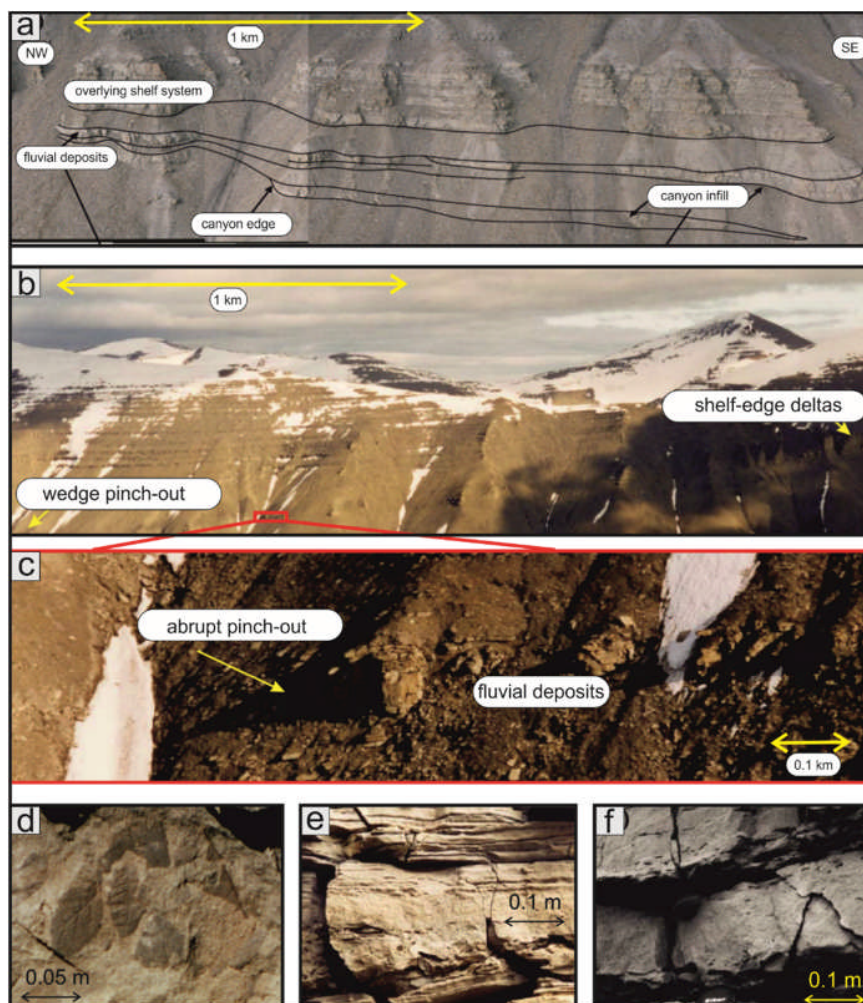


Figure 1.20: Deposits of Eocene Central Basin of Spitsbergen. a) Thick sandstone beds show the same lateral thickness over significant lateral thicknesses and then thin abruptly. d) Plant fragments. e) Coal fragments. f) Clay chips and coal fragments aligned parallel to bedding surfaces. Adapted from Plink-Björklund (2008).

Another diagnostic feature associated with hyperpycnal flows is the presence of terrestrial organic matter (Fig. 1.19). Terrestrial organic matter (including plant fragments, wood chunks, charcoal and lignite) is now widely suggested to be transported into the marine setting via hyperpycnal flows (e.g., Normark and Piper, 1991; Mulder and Syvitski, 1995; Mulder et al., 2003; Plink-Björklund and Steel, 2004), associated with sustained periods of high river discharge (e.g., Mulder et al., 2003; Plink-Björklund and Steel, 2004; Lamb et al.,

2008; Zavala and Arcuri, 2016). The hyperpycnites of the Eocene Central Basin, Spitsbergen (Fig. 1.20; Plink-Björklund and Steel, 2004), offer laterally continuous outcrop, permitting both downdip and along-strike changes in architecture and sedimentary texture and structure to be documented. The criteria used to identify the Eocene deposits as hyperpycnites are as follows: i) direct connectivity between shelf-edge fluvial and slope channels; ii) sandy beds, which remain the same thickness laterally (~ 1 -5 m) and then pinch-out rapidly over ~ 0.2 km distance; iii) downdip variation in sedimentary structure from parallel laminated beds, to interbedded massive and laminated beds, to graded or structureless beds; iv) rare occurrence of debris flow and slumped deposits and v) common occurrence of terrestrial organic matter, including fragments of coal and plant material (Fig. 1.20; see Plink-Björklund and Steel, 2004).

1.3.5.4 Process-Regime Classification Schemes

The classic ternary classification scheme of Galloway (1975) classifies deltas as being 'river-dominated', 'wave-dominated' or 'tide-dominated' (Fig. 1.13), and is popular amongst sedimentologists; it has also been adapted for fan delta systems (e.g., Orton, 1988). Despite the popularity of the Galloway (1975) scheme it has some disadvantages, particularly when applied to the ancient record.

Firstly, the scheme has a heavy reliance on the ability of a researcher to make suitable estimates of 'the degree of reworking' of the delta front by tidal- and wave-processes; even with good exposure, estimating the degree of reworking from the ancient record is subjective. Secondly, the scheme necessitates that delta systems are plotted onto the diagram (semi-) quantitatively, however, there is ambiguity surrounding how the 'degree of reworking' is quantified. Previous authors have interpreted this to mean the relative thickness of preserved tide- or wave-reworked sediment, although this is not explicitly outlined in the classification scheme. Furthermore, delta-front facies have a low preservation potential, due to the tendency for shoreline deposits to be eroded by delta-plain distributaries. Additionally, deltas with steep-faces are often subject to processes of re-sedimentation, adding additional complexity to the stratigraphic record.

Finally, although the Galloway (1975) classification scheme allows mixed-energy systems to be plotted, it has largely promoted the use of end-member descriptors of ancient systems (Fig. 1.21; i.e. river-, wave- or tide-dominated). The use of end-member descriptors has led to many previous authors neglecting to account for temporal and spatial variability in the dominant process-regime of a delta-system (Fig. 1.22). As such, relatively few ancient systems have been interpreted as being mixed-energy (e.g., Ta et al., 2002; Bhattacharya and Giosan, 2003; Gani and Bhattacharya, 2007; Ainsworth et al., 2008; Carvajal and Steel, 2009; Ainsworth et al., 2011; Vakarelov and Ainsworth, 2013; Olariu, 2014; Jones et al. 2015).

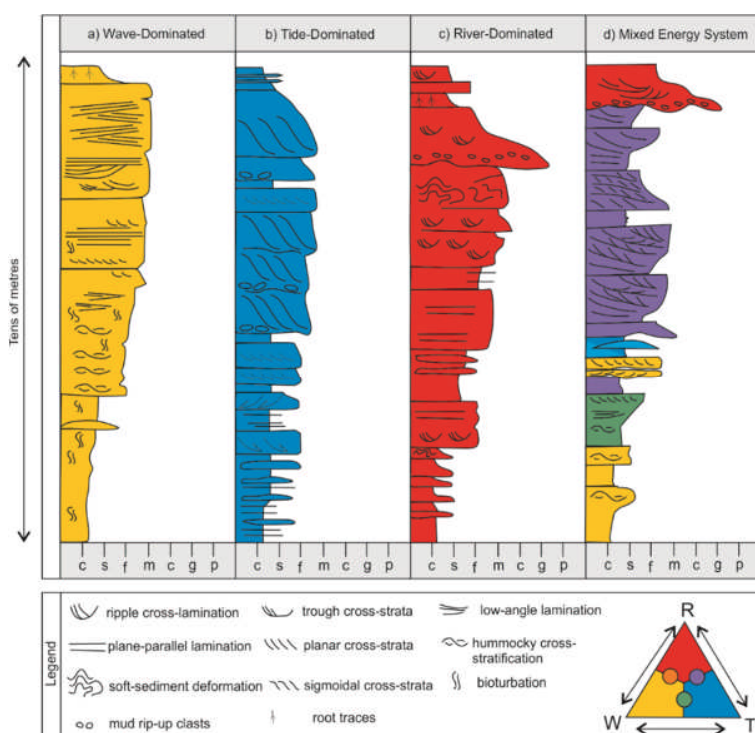


Figure 1.21: Schematic Logs depicting classic wave-, tide- and river-dominated deltas (based on Willis, 2005; Bhattacharya, 2010; Charvin et al., 2010; Olariu et al., 2010) and a mixed-energy delta (Rossi and Steel, 2016). The ternary diagram illustrates the colour coding system: river-dominated is red; wave-dominated is yellow; tide-dominated is blue. Where the various processes interact, an intermediate colour is indicated (e.g., the interaction of river and tide processes creates a purple colour and the interaction of wave and tide processes creates a green colour). Adapted from Rossi and Steel (2016).

The delta shoreline or shelf process-regime may be dominated by river, wave or tide processes at a specific location. However, the dominant process can change temporally, during the process of delta evolution (Fig. 1.22; e.g., Olariu, 2014; Rossi and Steel, 2016). The dominant process can also change spatially, along-strike, in the same system (e.g., Jones et al. 2015; Gomis-Cartesio, 2017). The acknowledgement of the possibility for multiple processes to dominate a system, or influence a system, resulted in the Ainsworth et al. (2011) classification system, which has 22 system classifications. The Ainsworth et al. (2011) scheme of subdivision subdivides the classic Galloway (1975) ternary diagram into multiple categories; in each category a system is assigned a dominant process, and one or two

secondary processes (an influencer and a modifier respectively). This scheme was applied to a modern system in the Gulf of Carpentaria, Australia (Mitchell River Delta). The Ainsworth et al. (2011) scheme classifies the Mitchell River Delta as tide-dominated, river-influenced and wave-modified; 62 %, 25 % and 13 % of the system was covered by tide-dominated, river-dominated and wave-dominated elements respectively. Although this classification scheme provides improved understanding of process variability in a system, it does not adequately describe the spatio-temporal dynamic evolution of systems.

1.3.5.5 Autogenic Process-Regime Change

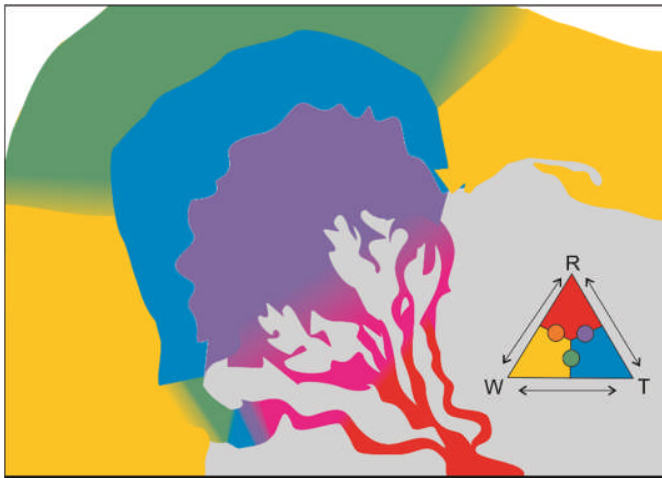


Figure 1.22: Simplified diagram of a mixed-energy deltaic system, illustrating where river, wave and tidal processes overlap and are active at the same time. River, wave and tidal processes can be active at the same time and vary spatially across the delta system and/or can be active in the same location and vary temporally. The ternary diagram illustrates the colour coding system: river-dominated is red; wave-dominated is yellow; tide-dominated is blue. Where the various processes interact, an intermediate colour is indicated (e.g., the interaction of river and tide processes creates a purple colour and the interaction of wave and tide processes creates a green colour). Adapted from Rossi and Steel (2016).

The causes of variability in process-regime have largely been attributed to the ratio between accommodation (A) and sediment supply (S) and consequent changes in the equilibrium profile; the A/S ratio describes terms linked in a non-linear manner, which produce shoreline behaviours that are complex (Muto and Steel, 1997). However, it is now acknowledged that changes in process-dominance within a system can occur without changes in the A/S ratio (external, allogenic forcings); i.e. non-equilibrium changes (autogenic responses) can also result in system process-variability (Muto and Steel, 2014). As such, autogenic responses can result in changes in the relative importance of river-, wave-, and tide-processes even when external forcings are in a steady state (Muto and Steel, 2014; Olariu, 2014). Autogenic causes of process-regime change are of significance due to the propensity for different dominant process-regimes to impact the efficiency of cross-shelf sediment transport, and consequently the calibre and maturity of sediment transported beyond the clinoform rollover and into deep-water. Additionally, it is important to differentiate allogenic and autogenic process-

regime change, as the former affect depositional systems at basin scale, while the latter affect only relatively small localities within a single system.

1.3.5.6 Modern Examples

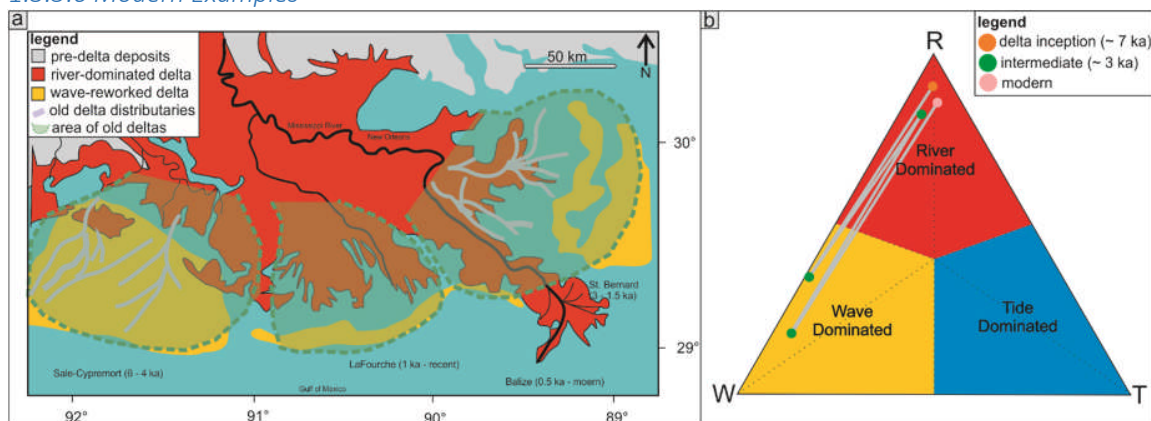


Figure 1.23: Evolution of the Mississippi Delta during the Holocene. a) Autogenic variability in process-regime from river- to wave-dominated. b) Variation in process-regime overlain onto the Galloway (1975) ternary diagram. Adapted from Olariu et al. (2014).

During the last ~ 7.5 ka of the Holocene, allogenic forcings are considered to be relatively stable; climatic conditions (and by-proxy sediment supply) did not significantly change, and sea level rise was relatively constant (2.5 mm/year; Fairbanks, 1989). Due to the relatively stable external forcings of the Holocene, variability in process-regime change for a specific delta system is attributed to autogenic forcings (Olariu, 2014). An example of river- to wave-dominated process-regime is the Mississippi delta (see Coleman, 1988; Roberts, 1997, 1998). Mississippi delta inception was initiated at approximately 7.5 ka, 300 km landward of the position of the modern shoreline. The Mississippi has numerous lobes, and is widely used as the quintessential example of a river-dominated delta that has multiple distributary channels (Galloway, 1975; Coleman and Wright, 1975).

The Holocene evolution of the Mississippi delta (Fig. 1.23) is governed by the transition from a river-dominated lobe to a wave-dominated lobe; as such, older lobes of the Mississippi complex (Sale-Cypremort, Teche, St Bernard Lafourche) were river-dominated during progradation and transitioned to be wave-dominated following abandonment (Olariu, 2014). The transition from a river- to a wave-dominated process-regime results from the autogenic process of avulsion, which results in a decrease in discharge to the active delta. Avulsion is followed by compaction and subsidence, eventually resulting in the complete abandonment of said lobe; this process likely occurs over hundreds of years (Roberts, 1997).

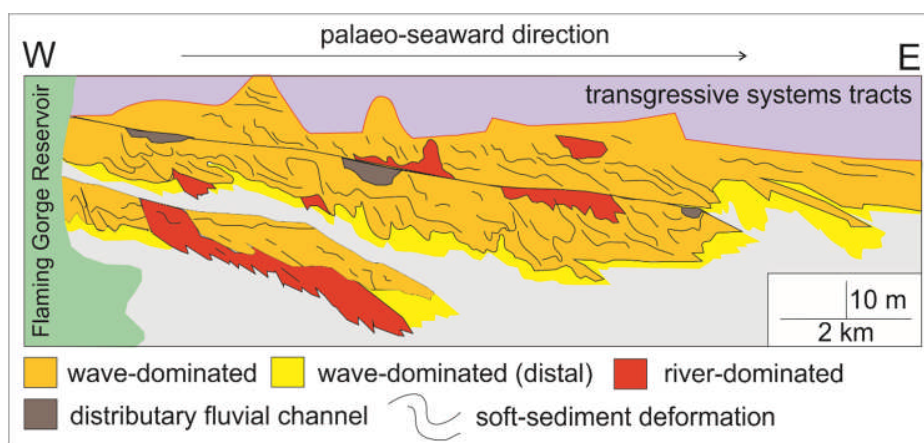


Figure 1.24: Chimney Rock Member, showing an ancient example of autogenic change in process-regime from wave- to river-dominated. Adapted from Plink-Björklund (2008) and Olariu (2014).

1.3.5.7 Ancient Examples

In ancient systems process-regime change resulting from autogenic processes can be assumed when delta-front facies show clear variations in character within the same parasequence (Plink-Björklund, 2008; Charvin et al., 2010; Olariu, 2014). Additionally, autogenic processes can be inferred when changes in the dominant process-regime do not occur at a basin-wide scale, but rather, impact a relatively small area of the system. Process-regime change has been attributed to autogenic responses in the ancient record in numerous cases, examples include: Campanian Chimney Rock Delta, Utah (Fig. 1.24; Plink-Björklund, 2008), the Aberdeen Member of the Blackhawk Formation, Utah (Charvin et al., 2010) and the Fox Hills Formation of the Washakie Basin, South Wyoming (Carvajal and Steel, 2009; Olariu et al., 2012). The Campanian Chimney Rock Delta is an outcrop record of the ancient shoreline of the Cretaceous Western Interior Seaway, which has been interpreted to be predominantly wave-dominated (Plink-Björklund, 2008). The regressive portion of the Chimney Rock Delta does, however, show a change in delta front facies to become river-dominated in two intervals (Fig. 1.24; Plink-Björklund, 2008). The transition from wave-dominated delta front deposits to river-dominated gravity flow deposits and fluvial moth bar deposits occurs laterally over a 2-3 km distance (Plink-Björklund, 2008). The localised lateral transition between wave- and river-dominated facies is attributed to an autogenic response to delta-complex progradation (Olariu, 2014).

1.4 Thesis Layout

This thesis contains six chapters; chapters three, four and five are based on scientific papers that have been submitted to international journals for publication. At the time of thesis submission, chapter three has been published in *The Journal of Sedimentary Research* (published August 2018; entitled 'Filter or conveyor? Establishing relationships between

clinoform rollover trajectory, sedimentary process-regime, and grain character within intrashelf clinothems, offshore New Jersey, USA'; referenced in thesis as Cosgrove et al., 2018); chapter four has been accepted for publication in *Geosphere* (accepted January 2019; entitled 'High-resolution correlations of strata within a sand-rich sequence clinothem using grain fabric data, offshore New Jersey, USA'; referenced in thesis as Cosgrove et al., 2019) and is currently in press; and chapter five has been accepted for publication in *Sedimentology* (accepted March 2019; entitled 'Grain Character and Process-Regime Change Recorded down Clinothem Slope Profiles'; referenced in thesis as Cosgrove et al., in review), pending revisions.

1.4.1 Chapter One

The first chapter outlines the aims and objectives addressed in this PhD thesis. A literature review is included, covering the major areas of research explored in this thesis. This includes: an i) introduction to clinoforms and clinothems; ii) sequence stratigraphy in clinothems; iii) prediction of deep-water sands in clinothems; iv) clinoform trajectory analysis; and v) shelf and topset process-regime.

1.4.2 Chapter Two

The second chapter outlines the methodological approaches used for data collection during the course of this thesis. The methodology of sample collection, laboratory-based sample preparation and grain character analysis are discussed in detail for both the New Jersey dataset and the Sobrarbe Deltaic Complex dataset.

1.4.3 Chapter Three

The third chapter uses the New Jersey grain character dataset to understand basin-scale interactions between clinoform rollover trajectory, process-regime and grain character; this integrated dataset is used to assess the role of topset process-regime in determining sand distribution and sediment character across clinothems. Four successive clinothem sequences were targeted in this investigation: m5.7, m5.45, m5.4 and m5.3. In this chapter, three overarching research questions are addressed. 1) What are the major controls that determine clinothem architecture? 2) How does the interaction between the dominant topset process-regime and clinoform trajectory affect the timing and delivery of coarse-grained sediment to deeper-water settings? 3) How do downdip grain character profiles differ between clinothem sequences deposited under different dominant topset process-regime conditions?

1.4.4 Chapter Four

The fourth chapter uses the New Jersey grain character dataset to understand intraclinothem variations in grain character within an individual clinothem sequence (Sequence m5.4). The

grain character dataset is used to produce high-resolution correlations of strata within a sand-rich sequence and to refine the placement of sequence boundaries. This chapter aims to highlight how quantitative grain character data can be used to better understand the cause(s) of intra-sequence textural complexities. In this chapter four overarching research questions are addressed. 1) How are topset process-regime signals (including depositional architecture and grain character) propagated downdip into foreset and bottomset deposits? 2) How does topset process-regime variability impact sediment texture down the complete 2-D, dip parallel, depositional profile? 3) How can grain character be used to correlate intraclinothem, time equivalent surfaces? 4) How can high-resolution grain character data be used as an additional tool to refine the placement of sequence boundaries?

1.4.5 Chapter Five

The fifth chapter assesses intraclinothem process-regime variability along the continuous depositional profile of the Sobrarbe Deltaic Complex. This study uses quantitative grain size and sorting data from a sandy clinothem from the Eocene Sobrarbe Deltaic Complex, which crops out along a > 5 km dip-parallel transect, and captures the transition from fluvio-deltaic to slope depositional facies. This chapter uses both dip-parallel and stratigraphic changes in quantitative grain character data in order to address three overarching research questions. 1) Can simple shelf-slope-basin (topset-foreset-bottomset) models of clinothems be improved to better capture sediment grain size distributions? 2) Can grain character data be used to identify sediment bypass at the clinoform rollover? 3) How do changes in the dominant shelf process regime affect the nature, timing and delivery of sand basinward? This outcrop-based grain character study provides new insights into the evolution of individual clinothems, and may be used as a predictive reference for subsurface exploration and basin evolution models.

1.4.6 Chapter Six

The sixth chapter combines the findings of the previous chapters in order to address the four research questions outlined in Chapter One. A succinct conclusion is also provided, to summarise the overall findings of the project. Finally, recommendations are made for potential future research endeavours, which would build upon the findings presented and discussed in this thesis.

Chapter 2 Materials and Methods

This chapter outlines the methodological approaches used for data collection during the research programme.

2.1 Introduction

In this thesis, two datasets have been collected. The first dataset is an integrated sedimentological and grain character dataset from IODP (International Ocean Discovery Program) Expedition 313 (Offshore New Jersey, USA), which is presented in Chapters 3 and 4 (Figs. 2.1, 2.2, 2.3). The second dataset is an integrated sedimentological and grain size and sorting dataset from the Sobrarbe Deltaic Complex (South-Central Pyrenees, Spain), which is presented in Chapter 5 (Fig. 2.4).

2.1.1 IODP Expedition 313, Offshore New Jersey

2.1.1.1 Chapter Three

In Chapter Three, seismic reflection data was combined with core analysis and grain character data, derived from 664 samples. This study targets the topset, foreset, and bottomset deposits of four successive Miocene intrashelf clinothem sequences (m5.7, m5.4, m5.45 and m5.3; Monteverde et al., 2008; Mountain et al., 2010; Miller et al., 2013a; Fig. 2.2), which represent deposition under either river-dominated or wave-dominated conditions.

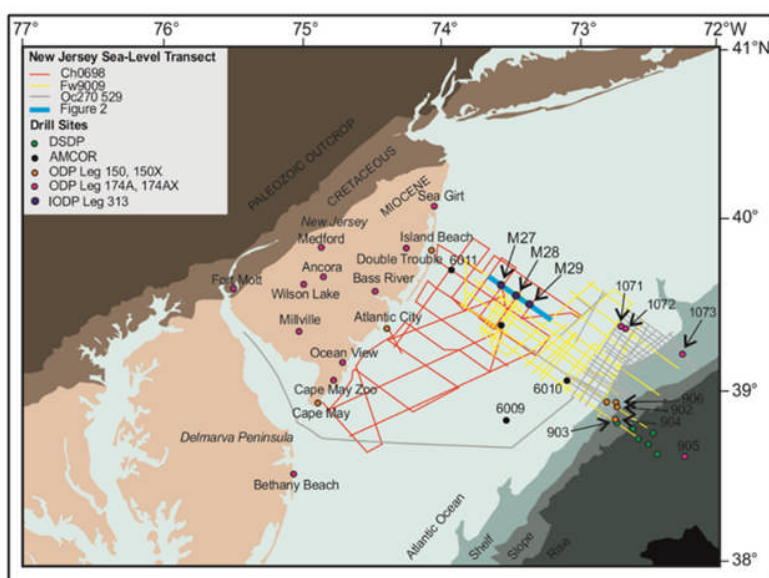


Figure 2.1: Location map of the New Jersey sea level transect, modified from Mountain et al. (2010). Study sites used in Chapters Three and Four (IODP Expedition 313 Sites M27, M28 and M29) are presented as purple circles. The seismic line transecting the core sites M27-M29 (Oc270 529) is indicated in blue. This seismic transect is shown in Figures 2.2 and 2.3.

Two principal methodological approaches were used in this study: high-resolution grain character analysis and clinoform trajectory analysis. The grain character analysis has been used primarily to produce longitudinal sediment profiles and grain size distribution profiles, which are supplemented by core descriptions (Mountain et al., 2010) and published seismic reflection (Monteverde et al., 2008; Mountain et al., 2010; Miller et al., 2013a), and core

sedimentology (Mountain et al., 2010; Browning et al., 2013; Hodgson et al. 2018) interpretations.

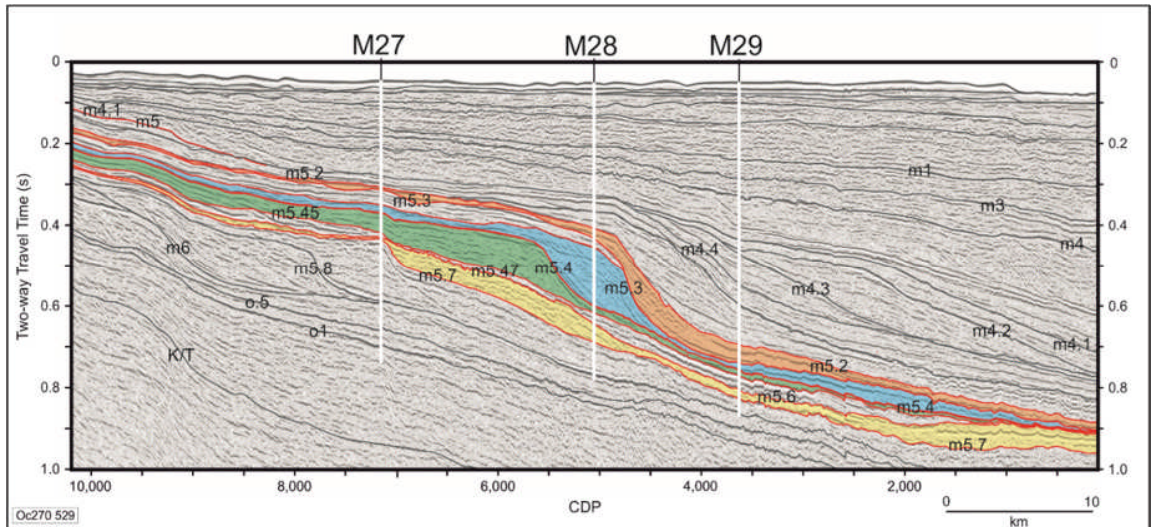


Figure 2.2: Seismic line Oc270 529. Sequence boundaries relevant to Chapter Three are highlighted in red. Depositional sequences analysed in Chapter Three are highlighted in various colours, where the yellow clinothem is Sequence m5.7, the green clinothem is Sequence m5.45, the blue clinothem is Sequence m5.4 and the orange clinothem is Sequence m5.3. Depositional sequences are named in according to their basal reflector boundary, for example Sequence m5.7 lies on reflector m5.7. All seismic interpretations are from Monteverde et al. (2008), Mountain et al. (2010) and Browning et al. (2013).

2.1.1.2 Chapter Four

Chapter Four uses high-resolution, core-based analyses of 267 samples from the topset, foreset and bottomset deposits of a single clinothem (Sequence m5.4; Fig. 2.3; Monteverde et al., 2008; Mountain et al., 2010; Miller et al., 2013a), integrated with core-based interpretations of sedimentary texture and structure (Mountain et al., 2010; Browning et al., 2013; Hodgson et al. 2018).

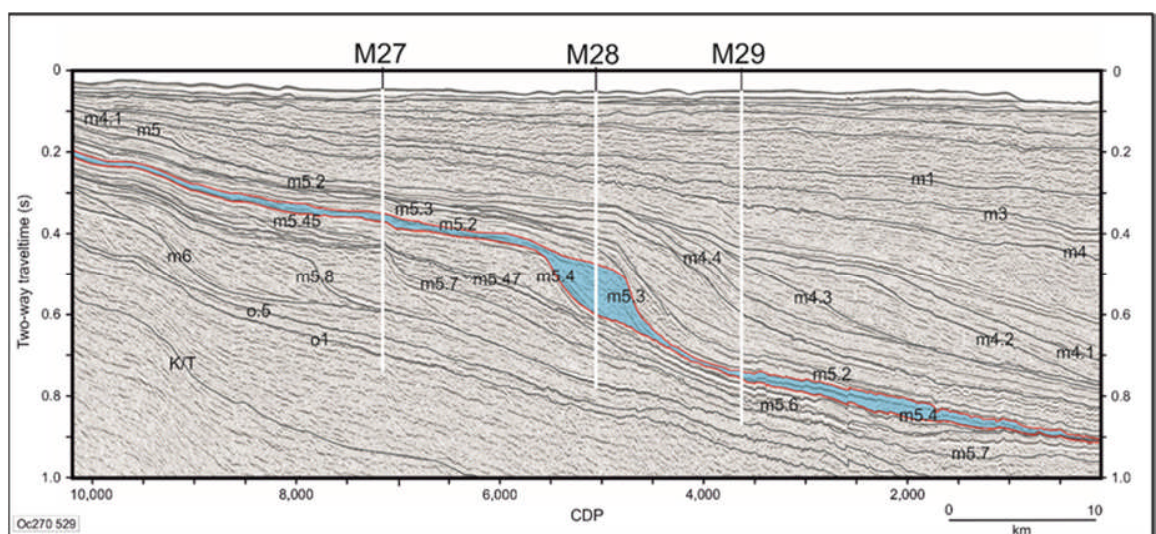


Figure 2.3: Seismic line Oc270 529. Sequence boundaries relevant to Chapter Four are highlighted in red. Depositional sequence m5.4 is highlighted in blue.

2.1.2 Sobrarbe Deltaic Complex, South Central Pyrenees, Spain

2.1.2.1 Chapter Five

Chapter Five uses quantitative grain size and sorting data (derived from 36 rock samples) recovered from a sandy clinothem from the Eocene Sobrarbe Deltaic Complex (Ainsa Basin, south-central Pyrenees, Spain; Fig. 2.4). Quantitative grain size and sorting data are presented for Cycle 1 of the Las Gorgas Composite Sequence (Cycle LG-1).

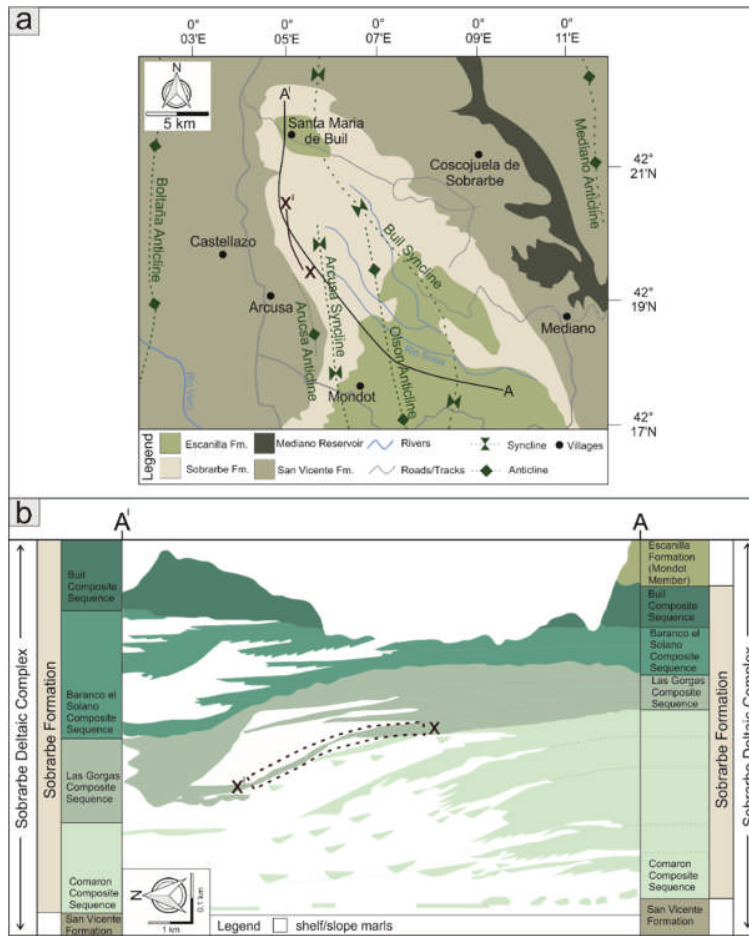


Figure 2.4: a) Geological map of the Sobrarbe Deltaic Complex and surrounding formations. Lines X-X¹ indicates the location of the dip-parallel outcrop transect sampled in Chapter Five (Cycle LG-1). Line A-A¹ transects the Sobrarbe Deltaic Complex and composite sequences therein. b) Line A-A¹, showing Sobrarbe Deltaic Complex stratigraphy. The Sobrarbe Deltaic Complex comprises a number of composite sequences: Comaron, Las Gorgas, Baranco el Solano and Buit. The sampling location (lines X-X¹; Cycle LG-1) is shown. Adapted from Dreyer et al. (1999).

2.2 Offshore New Jersey Dataset

The New Jersey Atlantic margin is an example of a mid-latitude, siliciclastic-dominated, prograding passive margin, and is an ideal location to study high-resolution grain character variability for the following reasons: i) rapid rates of deposition, which have resulted in thick accumulated sedimentary sequences (Miller and Mountain, 1994; Austin et al., 1998); ii) the tectonic dormancy of the New Jersey margin, which is in the late stages of thermal cooling

(Katz et al., 2013); iii) good chronostratigraphic control on the timing of sedimentation (Browning et al., 2013); and iv) a significant volume of previously published literature that includes seismic reflection transects, outcrop and well data (Mountain et al., 2010) in which the general geological setting can be framed. In 2009, IODP Expedition 313 continuously cored and logged a nearshore portion of the New Jersey shelf-margin transect (Fig. 2.1). The clinothems intersected during IODP Expedition 313 and studied here are seaward-prograding, intrashelf sequences of Miocene age (Mountain et al. 2010). The three cores (M27, M28 and M29) intersect topset, foreset, and bottomset deposits (ca. 12-22 Ma) along seismic line Oc270 529 (Fig. 2.5; Mountain et al., 2010; Kominz et al., 2016).

2.2.1 Materials

2.2.1.1 Grain character Analysis

In total, 965 sediment samples were collected from the working half of three cores recovered during IODP Expedition 313, offshore New Jersey. The three cores, kept in cold storage at the University of Bremen, are from Sites M27, M28 and M29 (Figs. 2.1, 2.5). The sampling process was completed in February 2016, over a two-week period.

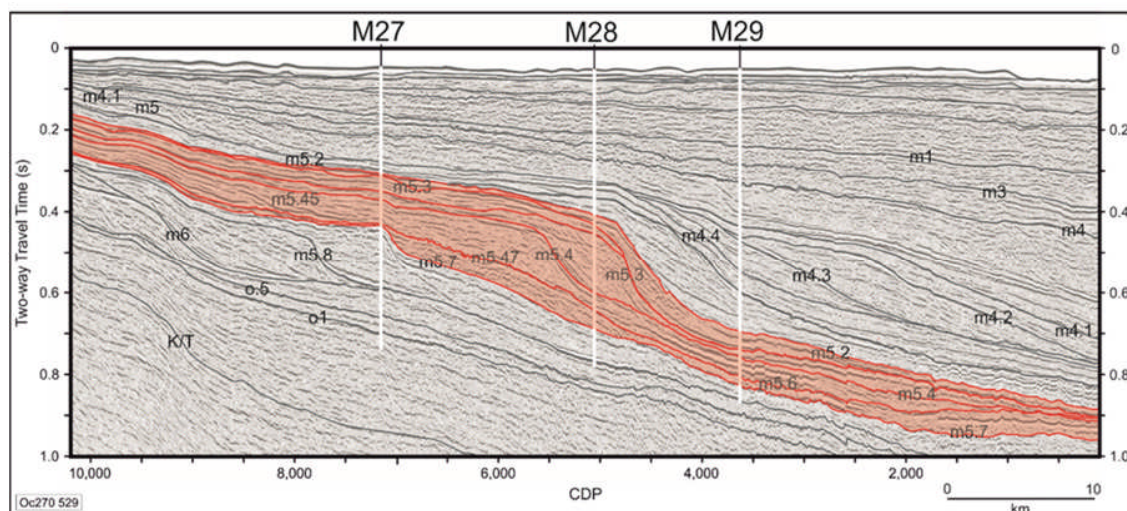


Figure 2.5: Seismically imaged clinothems of the New Jersey Margin. The grey lines indicate major seismic sequence boundaries (Monteverde et al., 2008; Mountain et al., 2010; Miller et al., 2013a). The highlighted area indicates the total stratigraphic range sampled during this investigation. The red lines within the highlighted area indicate the associated major seismic sequence boundaries that bound and intersect the stratigraphic range sampled during this investigation, corresponding to major sequence boundaries m5.7, m5.6, m5.45, m5.4, m5.3 and m5.2.

The stratigraphic horizons targeted during this investigation were exclusively Miocene in age, corresponding to depths of 225 – 365 mcd (metres core depth), 312 – 600 mcd and 600 – 730 mcd in cores M27, M28 and M29 respectively (Fig. 2.5). Collectively, a total of 560 m of core has been sampled. With reference to the seismic clinothem model presented in Miller et al. (2013a), these stratigraphic depths correspond to the interval between major seismic

sequence boundaries m5.7 – m5.2. Rudimentary sedimentary descriptions of the targeted intervals of M27 – M29 show 5 different lithofacies that dominate continuous successions: 1) silt, 2) sandy-silt 3) sand, 4) glauconite-rich sandstone, 5) glauconite-rich gravelly sandstone (Fig. 2.6). The recovered samples of all lithofacies were semi-lithified.

2.2.1.2 Site M27

A total of 209 sediment samples were recovered from Cores 313-M27A-80-1 (224 mcd) to 313-M27A-129-2 (377 mcd; 152 m thick). Recovered samples vary in lithology and grain size throughout the stratigraphic interval sampled. The upper ~ 110 m (~ 225 – ~ 335 mcd) is dominated by graded and scoured sand and silts, corresponding to Lithofacies Types 1 – 3 (Fig. 2.6a, b, c). The lower ~40 m (~ 335 – ~ 368 mcd) of stratigraphy shows a prominent change in lithology to glauconite-rich sandstones, corresponding to Lithofacies Types 4 – 5 (Fig. 2.6d, e).

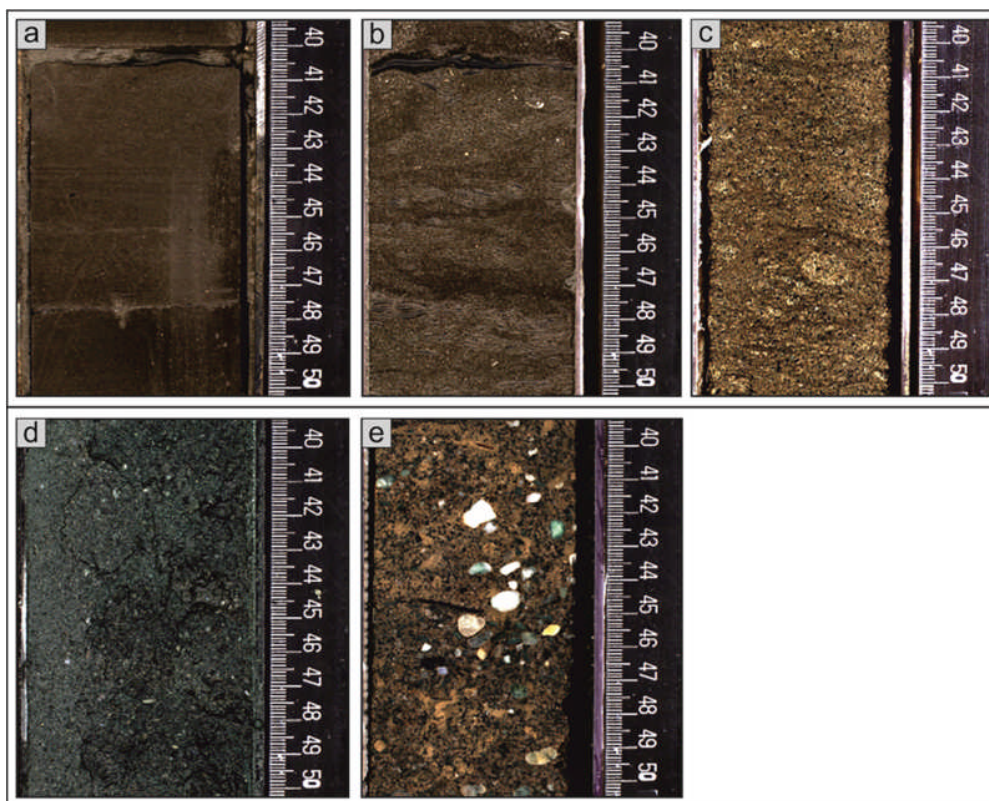


Figure 2.6: Representative core photographs of different the five dominant lithofacies. a) Silt lithofacies (Core 313_M27A_90-3_40-50). b) Sandy-silt lithofacies (Core 313_M28A_84-2_40-50). c) Sand lithofacies (Core 313_M29A_207-1_40-50). d) Glauconite-rich sandstone lithofacies (Core 313_M27A_125-1_40-50). e) Glauconite-rich gravelly sandstone lithofacies (Core 313_M28A_41-2_40-50).

2.2.1.3 Site M28

A total of 498 sediment samples were recovered from Cores 313-M28A-35-1 (311 mcd) to 313-M28A-147-1 (600 mcd; 288 m thick). Recovered samples vary in lithology and grain size

throughout the stratigraphic interval sampled. The upper ~ 100 m (311 – 412 mcd) of the cored interval is dominated by coarse sands, containing variable percentages of glauconite (typically ~ 25 – 85 %). The size of glauconite grains within the sands also vary considerably downcore and range in size from ~ 1 mm to ~ 7 mm. The upper ~ 100 m corresponds with Lithofacies Types 4 – 5 (Fig. 2.6d, e). At 413 mcd there is a prominent change in lithology to Lithofacies Types 1 – 3 (Fig. 2.6a, b, c), which contain little (< 1 %) or no glauconite. Lithology Types 1-3 are pervasive for ~ 110 m, until ~ 523 mcd. There is another prominent change in lithology towards the lower ~ 75 m of stratigraphy (523 – 600 mcd), marked by the reappearance of glauconite. This lower portion of the cored interval is dominated by Lithofacies Types 4 – 5 (Fig. 2.6e, d). From ~ 529 – ~534 mcd (Cores 313-M28A-118-1 – 313-M28A-120-1) the glauconite-rich sands become well stratified and exhibit prominent grading.

2.2.1.4 Site M29

A total of 258 sediment samples were recovered from Cores 313-M29A-161-1 (600 mcd) to 313-M28A-208-1 (730 mcd; 130 m thick). Recovered samples vary in lithology and grain size throughout the stratigraphic interval sampled. The upper ~ 45 m (~ 600 – ~ 645 mcd) of the cored interval is dominated by semi-consolidated, glauconite-rich sands, corresponding to Lithofacies Type 4 (Fig. 2.6d). The lower ~ 85 m (~ 645 – ~ 730 mcd) of stratigraphy is composed of alternating units of silt (Lithofacies Type 1; Fig. 2.6a) and coarse sands, which contain variable amounts of glauconite, ranging between ~ 5 – 25 % (Lithofacies Types 3 – 4; Fig. 2.6c, d). Throughout the lower ~ 85 m of core, there are significant proportions of stratigraphy disrupted by biscuiting disturbance, which refers to the interaction of drilling fluid with the cored sediment; biscuiting predominantly affects the silt-rich units.

2.2.1.5 Clinoform Rollover Trajectory Analysis

The analysis of clinoform trajectory is based on the geometric properties of clinothems; clinoform trajectory analysis is completed through the identification of the clinoform rollover position on each seismic reflector, and its evolution through time along successive intrashelf clinothem sequences. Trajectory analysis was performed on high-resolution 2-D, dip-parallel seismic data (Fig. 2.2).

The sequence boundaries of the clinothems were recognised in multichannel seismic profiles based on the location of reflector terminations (truncation, onlap, downlap, and toplap) (Miller et al., 2013a). The positions of sequence boundaries were confirmed through in-core identification, on the premise of physical stratigraphy and age breaks (Mountain et al., 2010; Browning et al., 2013; Miller et al., 2013a). Miller et al. (2013a) concluded that they could successfully match most core and log surfaces unequivocally with seismic sequence

boundaries. The sequence stratigraphic framework presented in Miller et al. (2013a) provides a means of subdividing the stratigraphic record, and thus contrasting changes in grain character and clinothem rollover trajectory between individual clinothem sequences. The timings of sequence boundaries have been shown to correlate with major positive excursions in the $\delta^{18}\text{O}$ deep-sea record, suggesting that observed changes in relative sea level ($\sim 5 - 20$ m) are predominantly controlled by sea-level variations of allogenic origin, resulting from the waxing and waning of Antarctic ice sheets (Browning et al., 2013; Kominz et al., 2016).

2.2.1.6 Sedimentological Interpretations

The visual core descriptions and interpretations of the Expedition 313 sedimentologists were used to inform interpretations of topset process-regime. In addition, original core observations of the sedimentary texture and structure of the Expedition 313 core were used.

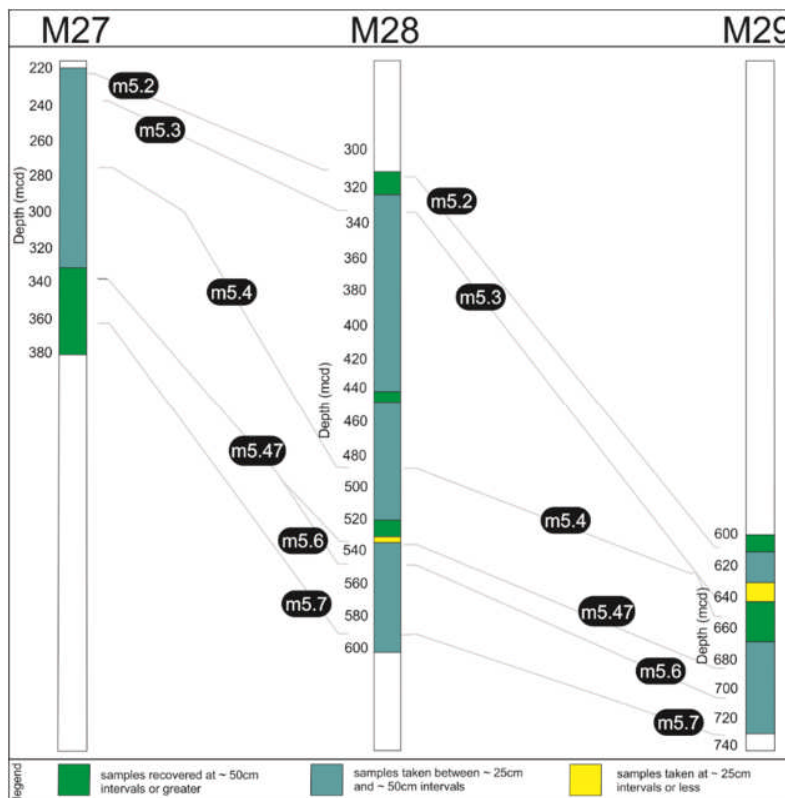


Figure 2.7: Illustration of the sampling strategy used in this investigation. The sampling frequency is plotted against core depth (mcd). The blue colour indicates the standard sampling strategy, where sediment slices were subsampled at an average of 50 cm intervals. The green colour indicates core sections where the sampling density was increased to between 25 cm and 50 cm intervals. The increase in sampling density is associated with prominent lithofacies change. The yellow colour indicates core sections where sampling density was increased to intervals of less than 25 cm. This very high sampling density is associated with sampling of well stratified sands within the core section.

2.2.2 Methods

The methodological approaches of high-resolution grain character analysis, clinofom trajectory analysis and sedimentological interpretations are outlined in detail below.

2.2.2.1 Grain Character Analysis

The analysis of grain character involved multiple steps and processes. Outlined below are: i) the methodology of sample collection; ii) the laboratory analyses required to remove calcitic cement and organic debris and iii) the method of grain character analysis.

2.2.2.2 Sampling Strategy

Where no prominent grain size change was recorded in either the cumulative lithology presented in Miller et al. (2013) or core descriptions (Mountain et al., 2010), the strategy for sample collection was to remove 15 x 15 x 15 mm sediment slices, subsampled at ~ 500 mm intervals down-core. The sampling strategy was amended to target stratigraphic depths where grain size change was most prominent. At these intervals, highlighted by the broad patterns of down-core lithological and grain size change (Mountain et al., 2010; Browning et al., 2013; Miller et al., 2013a), sampling density was increased to ~ 300 mm intervals. The sampling strategy is illustrated in Figure 2.7. During the sampling process there was some deviation from this sampling configuration in order to avoid 1) horizons of cementation, (2) biscuiting disturbance, 3) key stratigraphic surfaces and 4) heavily sampled intervals.

2.2.2.3 Sample Pre-Treatment

Sample pre-treatment comprised the manual and chemical disaggregation of the semi-lithified samples. Sample pre-treatment prior to grain size analysis is required to i) liberate individual grains, ii) remove calcareous cement, iii) remove calcareous debris and iv) remove organic matter. The method of 'best practice' in circumstances where samples are semi-lithified is to combine a form mechanical disaggregation with a form of chemical disaggregation (Green, 2001). It was deemed necessary to remove all calcitic cements and organic matter residues, as these components can result in the agglomeration of individual sediment grains; sediment agglomerations would consequently result in artificially large grain-sizes being recorded during grain character analysis. Additionally, the removal of calcareous debris (e.g., shell hash) was required prior to grain character analysis as these components would alter the recorded grain shape values, leading to artificial values of grain shape and grain roundness.

2.2.2.4 Manual Sample Disaggregation

The most critical feature of any disaggregation process is to ensure that original grain sizes and mineral constituents of a sediment sample are preserved. Methodologies for the effective and reliable disaggregation of sedimentary rocks have been extensively discussed in the literature (e.g., Krumbein, 1933; Krumbein and Pettijohn, 1938; Gray, 1965; Harris and Sweet, 1989; Yang and Aplin, 1997; Jiang and Liu, 2011 amongst others), however, there is no consensus on the best method of manual sample disaggregation. As disaggregation processes

have a direct impact upon resulting grain size distributions, it is critical that the most applicable method of manual sample disaggregation is selected.

2.2.2.5 Mortar and Pestle

Mechanical disaggregation using a mortar and pestle is the traditional method used to disaggregate (semi-)lithified samples (Sahu, 1964). When a mortar and pestle approach is used, samples are disaggregated to the point that aggregates are broken, but individual grains remain intact and are not broken. Gentle mechanical disaggregation using a mortar and pestle is often cited as the best method to disaggregate sediments (e.g., Nelson, 1983) and has been used extensively in the published literature (e.g., Sahu, 1964; Wilson and Pittman, 1977; Frey and Payne, 1996; Ando et al., 2014 amongst others). The 'best practice' method when completing mortar and pestle disaggregation is to ensure that hitting and shearing of the sediment sample is avoided, to ensure individual grains are not broken or damaged. There has been some debate on the suitability of mortar and pestle disaggregation for fine-grained sediments (e.g., Moston and Johnson, 1964). It has been suggested that mechanical disaggregation alone may not be sufficient to ensure the complete disaggregation of sediment samples of silt grade and below (e.g., Nelson, 1983).

2.2.2.6 Ultrasonic Disaggregation

Ultrasonic disaggregation employs the use of high-frequency sound waves to disaggregate sediment samples. Ultrasonic disaggregation is typically used for the finest grain size fractions (silt grade and below). Moston and Johnson (1964) compared mortar and pestle disaggregation with ultrasonic disaggregation and found that ultrasonic disaggregation yields results that have a smaller average grain size. This is typically expressed as lower percentage of silt grade sediment relative to clay grade sediment. When direct comparisons between the methods were made, the clay content of the same sample increased by ~20% when ultrasonic disaggregation was used, relative to mortar and pestle disaggregation.

Ultrasonic disaggregation has a number of associated disadvantages. Firstly, ultrasonic disaggregation has been shown to impact grain shape and can lead to artificial grain rounding of sandstones and siltstones (Savage, 1969). Secondly, ultrasonic disaggregation can lead to the complete break-down of softer minerals through abrasion (Savage, 1969), and the breakage of individual grains (Ando et al., 2014). Thirdly, ultrasonic disaggregation is most commonly used for silt-grade sediments and would therefore not be applicable for use on sand-grade sediment samples. Based on these associated disadvantages, ultrasonic disaggregation was rejected as a method of mechanical disaggregation in this investigation.

2.2.2.7 Freeze-Drying

Freeze drying, or lyophilisation, is a dehydration and desiccation process that works by freezing a material and then reducing the ambient pressure surrounding the material to allow any frozen water contained within the material to undergo an endothermic phase transition and sublimate from the solid phase directly into the gas phase (Hansen et al., 2015). Freeze-drying has a wide number of applications across a variety of disciplines.

In geoscience, freeze-drying has been used as an effective means of drying fine-grained sediment; during the freeze-drying process the sediment becomes disaggregated. In some cases, this can equate to the total disaggregation of the sediment, and eliminate the need to use further mechanical or chemical disaggregation (Simon et al. 2013). In many instances, freeze-drying will only result in the partial disaggregation of sediments and subsequent mechanical disaggregation is required to ensure that sediment samples are fully disaggregated (e.g., Walling and Horowitz, 2005). Freeze-drying was rejected for use during this investigation as freeze-drying is only applicable for use on grain sizes of fine-grained silt and below.

2.2.2.8 SELFRAG (SElective FRAGmentation Technology)

SELFRAG (see <http://www.selfrag.com/>) is a new technology that utilises high voltage pulse power technology to liberate or weaken a material along natural grain boundaries. Repetitive electrical discharges are pulsed into the sediment and defects along grain boundaries lead to the development of discontinuities in the electrical and acoustical properties. The development of these discontinuities enhances electrical fields at grain boundaries; this combines with a shock wave to produce high tensile stresses at grain boundaries. Thus, individual grains are liberated along grain boundaries.

The use of SELFRAG may have been applicable for use in this investigation due to (i) the recovery of intact grains from sediment samples and (ii) the ease of operation, including rapidity of sample disaggregation. However, SELFRAG is a new technology and there are currently no peer-reviewed papers discussing the efficacy and reliability of SELFRAG technology for use in grain size distribution analyses. Due to the lack of peer-reviewed literature regarding SELFRAG technology, refer to <http://www.selfrag.com/> for more information.

2.2.2.9 Summary of Mechanical Disaggregation

The most applicable form of mechanical sediment disaggregation for use in this investigation is the mortar and pestle methodology; this conclusion has been reached based on an appraisal of all available methods for use in sediment disaggregation for grain size analyses. The use of

mortar and pestle mechanical disaggregation has several advantages. Firstly, mortar and pestle disaggregation can be used for samples of all grain size, spanning clay to gravel; this ensures that all samples are subject to the same methodological approaches during sample preparation, making all results directly comparable. Secondly, mortar and pestle mechanical disaggregation is the method most widely used for sediment disaggregation within peer-reviewed grain size analyses (e.g., Sahu, 1964; Wilson and Pittman, 1977; Frey and Payne, 1996; Ando et al., 2014 amongst others). Finally, other potential methods of sediment disaggregation (e.g., ultrasonic disaggregation, freeze-drying and SELFRAG) were accompanied by unwanted secondary effects, or had not been subject to reliable peer-review.

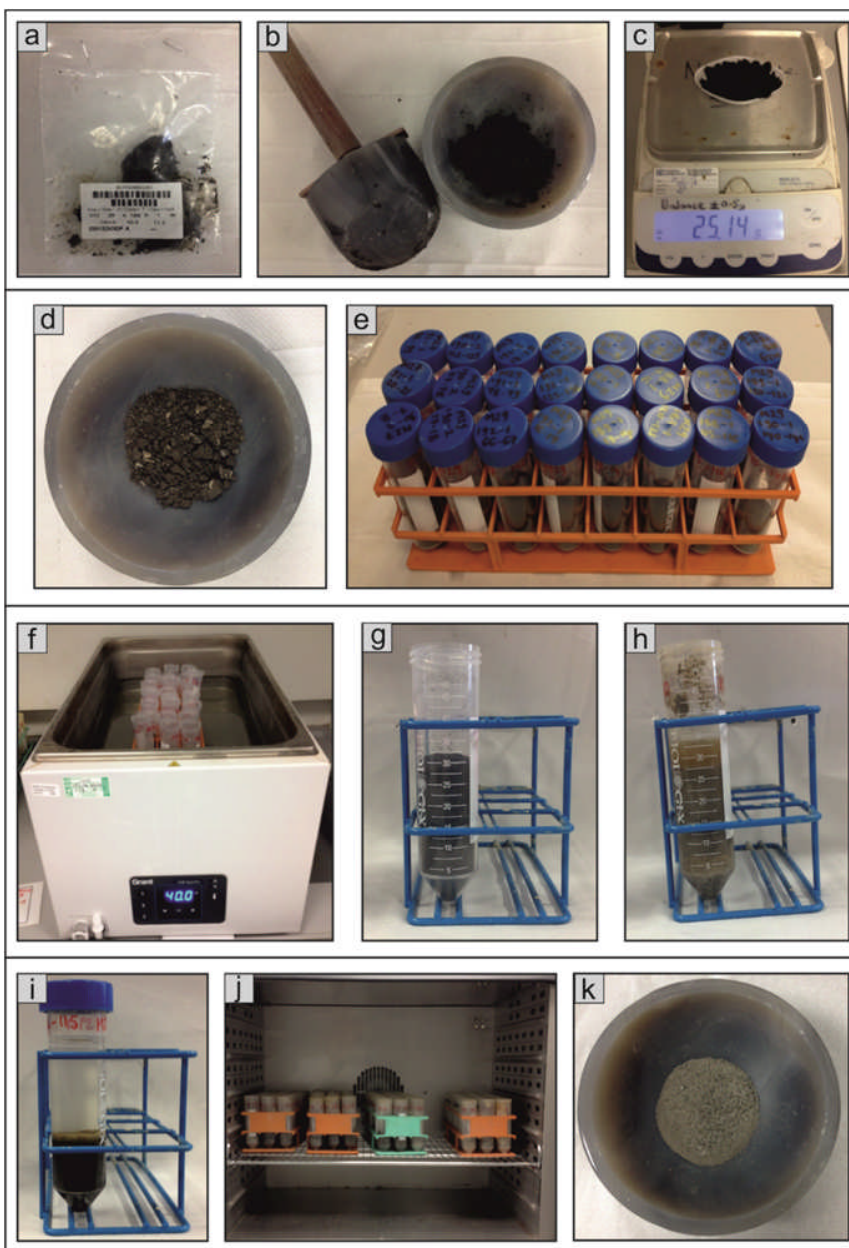


Figure 2.8: Photographs illustrating methodology of sample preparation and pretreatment prior to grain size and grain shape analysis. a) Sample 313_M29A_169-1_10-11 in sample bag prior to any pre-treatment. b) Sample 313_M29A_169-1_10-11 after manual disaggregation using agate mortar and pestle. Note that after the first stage of sample disaggregation some small aggregates of sediment still remain intact; these aggregates represent the portion of the sample more resistant to manual disaggregation. The persistent aggregates are broken down during chemical treatment and the final stage of manual disaggregation after oven-drying. The reason for leaving these small aggregates is to ensure that manual disaggregation does not break individual sediment grains to an artificially small size. c) Sediment aliquot weighing 25 g (\pm 0.5 g) in plastic weigh-boat. d) Sample 313_M27A_89-1_40-41; this is an example of a sample that would undergo manual picking to remove shell fragments. The large chunks within the sample are shell fragments. e) Sample aliquots within standard 50 mL centrifuge tubes, prior to addition of 15 mL of a 10 % weight to volume HCl solution. f) Samples in heated water bath, following the in situ addition of 15 mL of a 10 % weight to volume HCl solution. g) Sample 313_M29A_207-1_12-13 prior to the addition of a 30 % weight to volume H₂O₂ solution. h) Sample 313_M29A_207-1_12-13 after treatment with a 30 % weight to volume H₂O₂ solution; note the bleached appearance of the sample relative to its appearance in previous image. i) Sample 313_M28A_39-1_114-115 after centrifuging process. Note the clear supernatant above the sediment, indicating the complete oxidation of OM. j) Samples drying in the convection oven for 48 hours at a constant temperature of 60° C. k) Sample 313_M28A_49-2_54-55 after oven drying and final disaggregation using mortar and pestle. The sample shown in Photo K is an example of a 'gravelly sand' and contains glauconite grains of \sim 1.5 mm.

To ensure best practice when using mortar and pestle manual disaggregation, methodological protocols were put in place; mechanical disaggregation was done carefully and gently at all times, and hitting and shearing of the sediment was avoided at all times. The process of mechanical disaggregation was as follows. The semi-lithified samples were carefully disaggregated using an agate mortar and pestle (Fig. 2.8b). Sediment aliquots, of 25g (\pm 0.5g), were then weighed out from the mechanically disaggregated sample (Fig. 2.8c). Due to the semi-lithified nature of the sediment samples only \sim 30 % of samples required manual disaggregation.

2.2.2.10 Chemical Disaggregation

The presence of biogenic material within the siliciclastic sediment samples recovered from Sites M27 – M29 necessitates chemical pre-treatment of samples in order to remove bioclasts (e.g., macrofossils, microfossils and nanofossils), calcitic cements and organic matter (OM). The removal of organic and inorganic calcite is achieved through the addition of Hydrochloric Acid (HCl); the removal of OM is achieved through the addition of concentrated Hydrogen Peroxide (Pedrogen; H₂O₂). In order to ensure 'best practice' the method of chemical disaggregation was completed following techniques outlined in peer reviewed literature and the correct chemical molarities were used (e.g., Schumacher, 2002; Vaasma, 2008; Gray et al., 2009). The process of chemical disaggregation is outlined below.

2.2.2.11 Removal of Carbonate

The removal of carbonate was initiated by the manual picking, using tweezers, of visible biogenic calcite debris (e.g., shell fragments; Fig. 2.8d) from samples. Samples were then transferred into 50 ml centrifuge tubes, where they underwent decalcification (Fig. 2.8e). This comprised the in situ addition of 15 mL of a 10% weight to volume HCl solution. Samples were then transferred into a heated water bath, maintained at 40°C, and left for 48 hours (Fig.

2.8f). Samples were then removed from the water bath and left to stand for a further 24 hours. Samples were then centrifuged for 1 hour at 3,600 rpm shaking. The resulting supernatant was decanted and the samples were washed with deionised water.

2.2.2.12 Oxidation of Organic Matter

Following the various processes of carbonate removal, the removal of OM was achieved through the in-situ dropwise addition of a 30 % weight to volume H₂O₂ solution, using a dropping pipette. The dropwise addition of H₂O₂ continued over a period of two to three days until each sample was saturated with the H₂O₂ solution (Fig. 2.8h). Samples were then left to stand for 24 hours. Following this, each sample was treated with a further 5 mL of H₂O₂, until no effervescence was observed and no residual OM remained. Samples were then left to stand at room temperature for a further 24 hours. At this stage, the samples were a bleached colour relative to their original appearance, indicating that the reaction had proceeded until completion (Fig. 2.8h).

2.2.2.13 Final Sample Preparations

Following the carbonate and OM removal, 40 mL of de-ionised (DI) water was added to each sample and samples were left for 24 hours. Samples were then centrifuged for 1 hour at 3,600 rpm shaking. The resulting clear supernatant was decanted and the sample was washed with DI water (Fig. 2.8i). This process was repeated a further two times. Samples were then dried for 48 hours at 60° C to remove any residual moisture (Fig. 2.8j). Following this, samples were once again carefully disaggregated using an agate mortar and pestle to ensure that samples were fully disaggregated and no particle aggregates remained (Fig. 2.8k).

2.2.3 Grain size and Shape Analysis

The grain size and shape distributions of the sediment samples were determined using a Retsch CamsizerXT, located in the Sorby Laboratory at the University of Leeds. The CamsizerXT is an optically based dynamic image analyser, capable of measuring a wide range grain sizes, spanning 1 µm – 8 mm) and yields results fully comparable to those produced by traditional sieving analyses.

The CamsizerXT was selected as the instrument of choice for this investigation, as it has several advantages over sieving and other alternative methods of grain size analysis, such as optical microscopy and laser diffraction; these are summarised in Table 2.1. The principal advantages include: i) the rapidity of sample measurement times (typically < 3 minutes per sample, where a sample contains a few million grains); ii) the precision of digital imaging processing over a wide particle measurement range and iii) the repeatability and reliability of

results. The CamsizerXT has been shown to yield grain size and grain shape analyses with an accuracy of $\pm 1\%$ (Moore et al., 2011).

Measurement Characteristic	CamsizerXT	Laser Diffraction	Sieving	Optical Microscopy
Wide particle measurement range	✓✓	✓✓	✓	✗
Repeatability and reproducibility of results	✓✓	✓✓	✓	✗
Particle shape analysis	✓✓	✗	✗	✓✓
Direct measurement of samples	✓✓	✗	✗	✓✓
Comparability of results with other measurement techniques	✓	✗	✗	✗
Rapidity of sample measurement	✓✓	✓✓	✗	✗
High resolution for narrow particle size distributions	✓✓	✗	✗	✓✓

Table 2.1: Advantages and disadvantages of various methods of grain character analysis.

2.2.3.1 Dynamic Image Analysis

The principal underpinning Dynamic Image Analysis (DIA) can be compared to that of optical microscopy: grains are photographed by a camera that produces enlarged images (Fig. 2.9a). However, during conventional microscopy, grains remain static on the object plate and do not move relative to the optics. In contrast to this, during DIA the particles are photographed whilst in motion, as they pass an illuminated interrogation zone (Fig. 2.9b). The software accompanying the CamsizerXT then uses these images to calculate parameters of size and shape for each individual grain. It is possible to measure thousands of images per minute as particles move in a stream; the stream is generated by either gravity or air pressure (Westermann, 2013).

During grain-flow transit through the measuring fields, grains are illuminated from one side, as a camera simultaneously photographs grains from the alternate side. The internal software of the CamsizerXT then rapidly analyses the particle projections to ascertain grain size distributions. In real time, 277 images are processed per second and each particle within each image is analysed to provide rapid statistical analyses. The CamsizerXT is able to measure a wider grain size range, with more precise statistical analyses, at a higher accuracy (i.e. reproducibility of results), than any alternative image processing systems (Westermann, 2013).

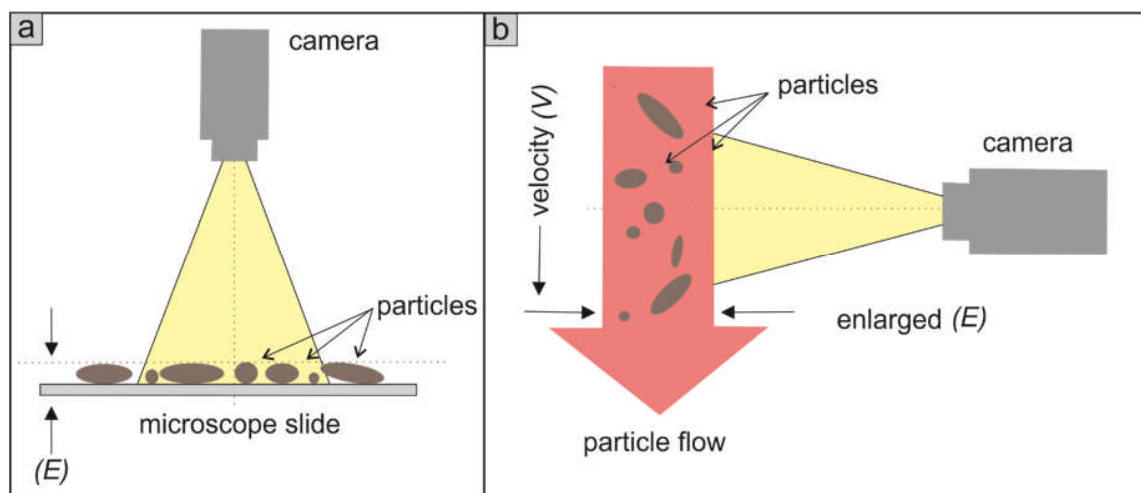


Figure 2.9: Comparison of optical microscopy and DIA techniques. a) Optical microscope, where static grains are photographed on the object plate (microscope slide). b) DIA, where moving grains are photographed as they move in a stream past an illuminated interrogation zone.

The advanced DIA system of the CamsizerXT contains two cameras, which have different levels of magnification in order to maximise the particle measuring range. This comprises: i) a lower magnification camera, or basic camera, (Fig. 2.10) with a wide viewing width to analyse larger particles and ii) a higher magnification camera, or zoom camera, (Fig. 2.10) for the simultaneous evaluation of smaller grains. The dual camera system ensures that image analysis is optimised for both small and large particles, without compromising particle detection probability or image resolution (Westermann, 2013).

Prior to analysis using the CamsizerXT, sediment samples were visually examined to determine an estimate of grain size. Sediment samples that were composed of grain sizes spanning fine-grained sand (> 0.125 mm) to fine-grained gravel (< 8 mm) were analysed using the X-Fall module. Sediment samples that were composed of grain sizes spanning medium-grained silt (> 0.03 mm) to very fine-grained sand (< 0.125 mm) were analysed using the X-Jet module. The different modules, discussed below, affect the dispersion of sediment samples as they pass the DIA system of the CamsizerXT; dispersion is defined as the

separation of grains whilst travelling past the measurement area. The correct dispersion of grains during DIA is essential to ensure reliable and accurate grain size and grain shape data.

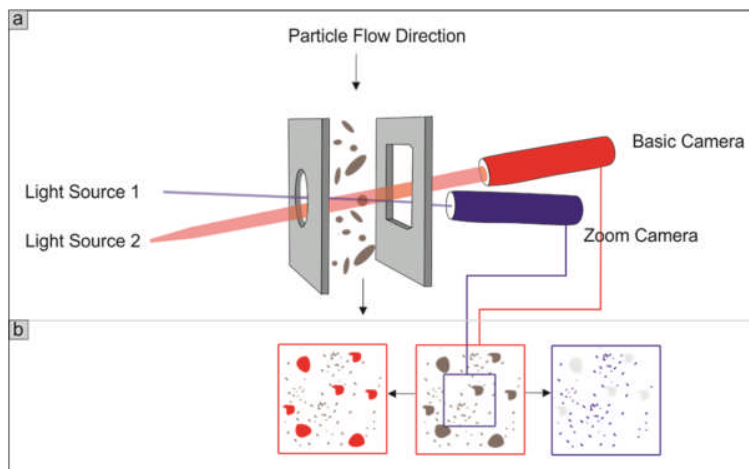


Figure 2.10: Schematic diagram of CamsizerXT. a) Measurement system of the CamsizerXT, including the arrangement of optics and the position of the basic and zoom camera. The grains move past the cameras, either under gravity (X-Fall) or facilitated by compressed air (X-Jet). b) Simplified schematic of the interaction of the basic and zoom cameras. Both cameras simultaneously record grain-flow. The basic camera, depicted in red, is used for the detection of larger grains. The zoom camera, depicted in blue, is used to analyse smaller grains. The combined use and different image scale of these cameras allows the high resolution capture of both small and large grains and substantially increases the dynamic measurement range. Per minute, the dual camera system processes tens of thousands of images, allowing the measurement (size and shape) of millions of particles per sample. Adapted from Westermann (2013).

2.2.3.2 CamsizerXT X-Fall Module

The X-Fall module operates using gravity, such that particles fall through the field of view of the DIA camera system under gravity. Sediment samples are fed into a vibrating dry powder feeder, which slowly feeds particles into the camera interrogation zone. As the X-Fall module is reserved for particle sizes exceeding fine-grained sand, as sediment clumping and agglomeration does not take place at these grain sizes.

2.2.3.3 CamsizerXT X-Jet Module

The X-Jet module operates using air pressure dispersion, which accelerates grains through the field of view of the DIA camera system. Sediment samples are fed into a vibrating dry powder feeder and then pass through a dispersion nozzle, which counteracts the negative effects of particle clumping, aggregation and agglomeration. This is achieved by the dragging action of compressed air, which induces shear forces on the sediment samples and consequently breaks up sediment agglomerations. The use of the X-Jet module increases particle velocity up to ~ 50 m/sec.

2.2.3.4 Grain Size Analysis

Grain size distribution analysis using the CamsizerXT is completed by using the DIA technique; grains fall randomly through the feed chute, in front of the white backlight. As this occurs, grains shadow the white backlight and this image is recorded by the two cameras of

the CamsizerXT. The image then undergoes conversion into binary format and is processed by the internal software to produce grain size data. Each individual grain photographed by the CamsizerXT is analysed using a specific set of parameters (outlined in Table 2.2). These data are then processed internally by the CamsizerXT software to give grain size distributions.

2.2.3.5 Grain Shape Analysis

Shape parameters are presented as numerical values, which describe defined shape characteristics. The shape characteristics used in this investigation are sphericity and roundness.

Parameter Name	Equation	Parameter Description
Particle Diameter (X_{area})	$X_{area} = \sqrt{\frac{4A}{\pi}}$	Particle diameter is calculated from the area of a particle projection; A is the diameter of an equivalent circle.
Width/Breadth (X_{cmin})	-	The shortest chord out of a measured set of maximum chords as measured from a particle projection (Fig. 2.11a).
Width/Breadth ($X_{Ma min}$)	-	$X_{Ma min}$ is calculated from the area of particle projection. The shortest martin diameter is measured (Fig. 2.11a).
Width/Breadth ($X_{Fe min}$)	-	$X_{Fe min}$ is calculated from the area of particle projection. It is the shortest feret diameter out of the measured set of feret diameters (Fig. 2.11b).
Length ($X_{Fe max}$)	-	$X_{Fe max}$ is calculated from the area of particle projection. It is the longest feret diameter out of the measured set of feret diameters.
Length (X_{length})	$X_{length} = \sqrt{X_{Femax}^2 - X_{cmin}^2}$	X_{length} is calculated from the area of particle projection, by subtracting the smallest martin diameter from the largest feret diameter.
Length ($X_{length2}$)	$X_{length2} = \sqrt{X_{Femax}^2 - X_{cmin}^2}$	X_{length} is calculated from the area of particle projection, by subtracting the smallest martin diameter from the largest feret diameter.

Length (X_{stretch})	-	X_{stretch} is calculated from the area of particle projection of each particle, which is divided by the smallest martin diameter (Fig. 2.11c)
Length ($X_{\text{stretch}2}$)	-	$X_{\text{stretch}2}$ is calculated from the area of particle projection of each particle, which is divided by the smallest of all maximum chords

Table 2.2: Mathematical parameters used by the CamsizerXT software to calculate the grain size distribution of a sediment sample.

2.2.3.6 Sphericity and Roundness

The roundness and sphericity of particles is determined using a statistically reliable algorithm, which produces a fully quantitative value of sphericity and roundness (Fig. 2.12a). The parameters of roundness and sphericity are associated with the chart for visual inspection of roundness and sphericity (Fig. 2.12b) according to Krumbein and Sloss (1951). The roundness and sphericity of a particle define its geometric form.

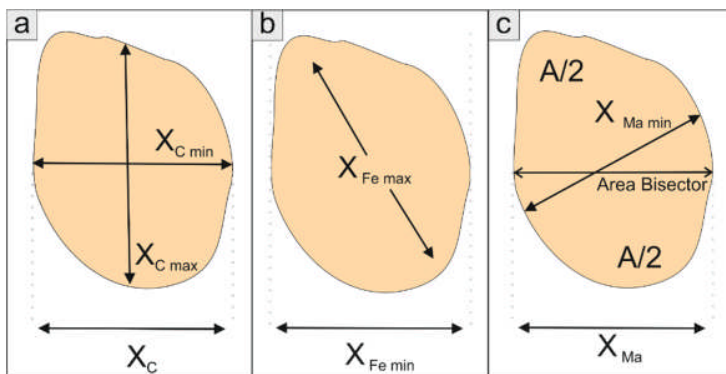


Figure 2.11: a) Image shows the how the mathematical parameters 'maximum chord' (X_C) and 'minimum chord' ($X_{C \min}$) are defined; where the maximum chord is the longest chord in a measuring direction and the minimum chord is the shortest chord out of the total measured set of maximum chords. b) Image shows how the mathematical parameter 'feret diameter' (X_{Fe}) is defined; where the feret diameter is calculated by placing two tangential lines perpendicular to the direction of measurement. $X_{Fe \max}$ is the longest feret diameter out of the total measured set of feret diameters. c) Image shows how the mathematical parameter 'martin diameter' (X_{Ma}) is defined; where the martin diameter is defined as the length of the area bisector in the measuring direction. $X_{Ma \min}$ is the shortest martin diameter out of the total measured set of martin diameters; A is the area. Adapted from Westermann (2013).

The sphericity of a grain is defined by the following equation: $4\pi A/P^2$; A is the measured area covered by a particle projection and P is the measured circumference of a particle (Fig. 2.12c). A particle is given a value between 0 and 1, where a perfect sphere would have a value of 1 and a thin, needle-like particle would have a sphericity value of 0.

The roundness of a grain is defined by the following equation: $\sum(r_i/R)/n$; R is the radius of the largest inscribed sphere, r_i is the radius of curvature of particle corners and n is the total number of particle corners measured (Fig. 2.12d; Krumbein, 1940). The roundness characteristic is used to describe the smoothness of a particle, i.e. the relative roundness or sharpness of a particles edges and corners. A particle is given a value between 0 and 1, where a perfectly smooth particle (e.g., a circle) would have a value of 1 and totally angular particle (e.g., a square) would have a value of 0.

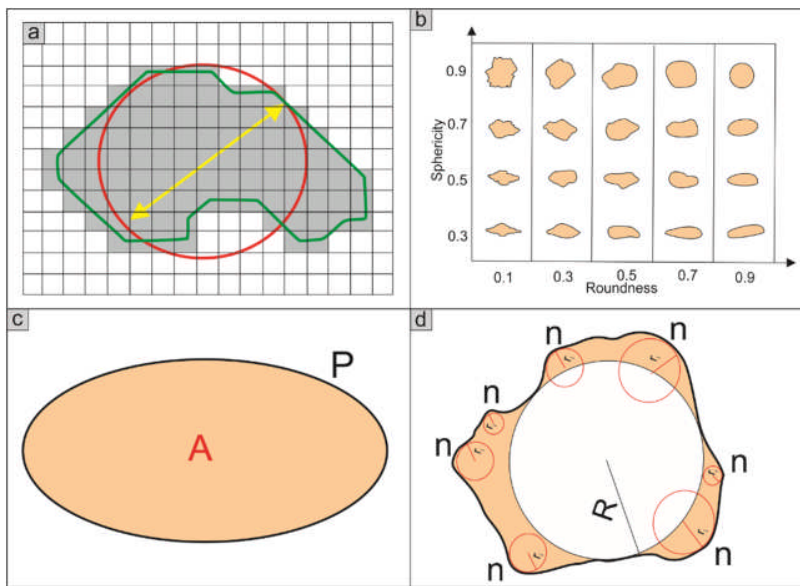


Figure 2.12: a) Schematic diagram showing how shape parameters are calculated from a particle converted into binary format. The grey shadowed area shows the area of the particle. The green line indicates the particle perimeter. The red circle indicates a circle with the same area as the particle. The yellow arrow indicates the diameter of the circle with the same area as the particle. b) The chart for visual inspection of roundness and sphericity according to Krumbein and Sloss (1956), where the Y-axis displays values of sphericity and the X-axis displays values of roundness. c) Image shows how the mathematical parameter of Sphericity is calculated. P is the measured perimeter of a particle projection; A is the measured area covered by the particle projection. d) Image shows how the mathematical parameter of Roundness is calculated. R is the radius of the largest inscribed sphere; r_i is the radius of curvature of particle corners and n is the total number of particle corners measured. Adapted from Krumbein (1940).

2.2.3.7 Statistical Analysis of Grain size and Grain shape

The statistical grain size distribution analysis of all CamsizerXT output files was completed using the GRADISTAT computer program, developed by Blott and Pye (2001). The GRADISTAT program enables the rapid analysis of grain size statistics from multiple sediment samples and produces numerical values of the mean, mode, median, sorting, standard deviation, skewness and kurtosis. Statistical parameters are calculated arithmetically, geometrically and logarithmically, using both Folk and Ward (1957) and moment graphical methodologies (Blott and Pye, 2001). Each sample is also given the relevant descriptive term according to Folk and Ward (1957). The statistical analysis of grain shape parameters was

completed using Microsoft Excel software, to give numerical values of the mean, mode, median and standard deviation for each sample.

2.2.4 Clinoform Rollover Trajectory Analysis

The position of the clinoform rollover is marked by the point of maximum curvature between the topset and foreset (Pirmez et al., 1998); however, delineating this position can be challenging (Olariu and Steel, 2009). To ensure consistency and repeatability, the clinoform rollover has been identified following the methodology of Anell and Midtkandal (2017, p. 282); as such, the position of the clinoform rollover is identified “as a point that is perpendicular to the intersection of straight lines extrapolated from the inflection point of the topset and foreset of the clinoform.”

2.2.5 Sedimentological Interpretations

The IODP Expedition 313 scientists produced sedimentological interpretations of topset depositional environment using assemblages of sedimentary structures, sediment composition and texture, fossil content, and ichnofabric (see Mountain et al., 2010). Sedimentary facies associations presented in Mountain et al. (2010) indicate that the topset depositional environments of the New Jersey clinoforms varies between sequences. Relevant to this investigation, the topset deposits of Sequences m5.45 and m5.4 share features associated with wave-dominated shoreline facies models (e.g., Reineck and Singh, 1972; McCubbin, 1982; Browning et al., 2006). Key diagnostic features of wave-dominated deposits (in the shoreface and shoreface to offshore transition facies) include the following: interbedded fine and very fine sands; shell debris; convex-upward laminae; low angle cross-beds; symmetrical ripple lamination, and moderate to heavy bioturbation (4 to 6 on the standard bioturbation index). Relevant to this investigation, the topset deposits of Sequences m5.7 and m5.3 share features associated with mixed river and wave delta facies models (e.g., Galloway, 1975; Bhattacharya and Walker, 1992). Key diagnostic features of river-dominated deposits include the following: coarse sands; cut-and-fill surfaces associated with basal gravels and rip-up clasts; micaceous sands; current-ripple lamination; and terrestrial plant material.

2.3 Sobrarbe Deltaic Complex (Ainsa Basin) Dataset

2.3.1 Introduction

The Sobrarbe Deltaic Complex crops out in the western part of the Eocene Ainsa Basin, north-eastern Spain. The Ainsa Basin is a piggyback basin, located in and on top of the easternmost portion of the Gavarnie thrust-sheet-complex, and forms the central sector of the South Pyrenean foreland basin (Vergés and Muñoz, 1990; Muñoz, 1992; Fernández et al., 2004). The

Ainsa Basin is bordered to the west by Jaca-Pamplona Basin and to the east by the Tremp-Graus Basin (Puigdefàbregas, 1975; Brunet, 1986). The western part of the basin is structurally constrained by several fold structure active during deposition: the Añisclo anticline to the north; the Peña Montañesa thrust to the northeast; the Mediano anticline to the east and the Boltaña anticline to the west (Fig. 2.4a; Poblet et al., 1998; Dreyer et al., 1999; Fernández et al., 2004).

The western Ainsa Basin fill is dominated by a ~ 5 km thick succession of Upper Eocene sediments, bounded by the San Vicente Formation at the base (marley lower-slope deposits and turbiditic sandstones) and the Olsón Member of the Escanilla Formation at the top (alluvial red-bed succession) (Dreyer et al., 1999). The Sobrarbe Deltaic Complex comprises the uppermost part of the San Vicente Formation, the Sobrarbe Formation and up to the middle part of Mondot Member of the Escanilla Formation (Van Lunsen, 1970; DeFrederico, 1981; Dreyer et al., 1993; Wadsworth, 1994). The lithostratigraphic units forming the Sobrarbe Deltaic Complex show significant lateral interfingering. The Sobrarbe Deltaic Complex accumulated over a period of ~ 3 million years during the middle Lutetian to lower Bartonian, reaching a maximum thickness of ~ 1 km (Muñoz et al., 1998). It was deposited during the growth of the Boltaña Anticline and the intrabasinal Arcusa Anticline, active during the last stages of deposition of the Escanilla Formation (Moss-Russel, 2009).

The Sobrarbe Deltaic Complex alternates cyclically between mud-rich slope deposits, sand-rich and slumped delta front deposits, carbonates, muddy delta plain deposits and alluvial deposits; these deposits belong to a large-scale axial sediment dispersal system (Dreyer et al., 1999). In the west of the Ainsa Basin this system crops out as a series of well-exposed, approximately dip-parallel clinothems, which show the transition from fluvio-deltaic deposits (Escanilla Formation) in the south to progressively deeper shelf- and slope-deposits (Sobrarbe and San Vicente formations) in the north, and can be divided into topset, foreset and bottomset elements (Dreyer et al., 1999). Dreyer et al. (1999) subdivided the Sobrarbe Deltaic Complex into five so called 'composite sequences': the Comaron, the Las Gorgas, the Barranco El Solano, the Buil and the Escanilla composite sequences. These are separated by major unconformities, representing fluctuations in relative sea-level (Fig. 2.4b; Dreyer et al., 1999).

The composite sequences are in turn subdivided into 'minor sequences' (Dreyer et al., 1999). These smaller-scale sequences are comprised of sandstone units typically interbedded with mudstone and marls. The minor sequences are described as genetic sequences, bounded by maximum transgressive surfaces (Dreyer et al., 1999). The Las Gorgas composite sequence, and minor sequences therein, are specifically relevant to this study.

2.3.2 Materials

The Las Gorgas composite sequence contains 2 exposed minor clinothem sequences, the first of which was investigated and is hereafter referred to as Cycle LG-1 (Fig. 2.14). At each chosen sampling site, detailed sedimentary logs were collected, and between 4 and 7 rock samples were recovered at each sampling site. In total, 36 samples were recovered from Cycle LG-1.

2.3.3 Methods

Two principal methodological approaches were used on the Sobrarbe dataset: i) grain size and sorting analysis and ii) sedimentological interpretations of the depositional facies. The chosen methodology of grain size analysis for the samples collected from the Sobrarbe Deltaic Complex was using the image processing software ImageJ. ImageJ calculates grain size from imported photomicrographs (e.g., Sumner et al., 2012). The use of the CamsizerXT, as per the New Jersey dataset, was not suitable for this investigation due to the fully lithified nature of the recovered samples. The methodology of sample collection and grain size analysis are outlined in detail below. The sedimentological interpretations of depositional facies was based upon sedimentary logs, completed in the field.

2.3.3.1 Sampling and Logging Locations

In Cycle LG-1, 7 sampling and logging locations were chosen along the continuous depositional profile to provide even down-dip coverage of the shelf-to-slope transition. The logging and sampling locations were recorded using handheld GPS. Georeferenced sample locations are included in Chapter Five alongside a figure displaying the sample locations within each sedimentary log.

Extensive aerial drone footage was also taken. Using georeferenced photographs, acquired using a DJI Phantom 3 unmanned aerial vehicle (UAV), a photorealistic three-dimensional outcrop model was constructed using the photogrammetric software Agisoft PhotoScan. The resulting model was analysed using the LIME visualisation software (www.virtualoutcrop.com). Drone-footage has enabled the construction of a high-resolution outcrop model, in which Cycle LG-1 can be traced laterally and the sampling locations can be illustrated (see Chapter Five).

2.3.3.2 Sedimentary Logging

Sedimentary logs, capturing the stratigraphic extent of the sandy LG-1 clinothem, were completed in the field at each chosen sampling site; a total of seven logs were completed along the ~ 5 km transect. The logs were completed at a decimetre scale, using a ruler and a tape measure; all measurements were recorded into a geological notebook. The sedimentary logs include observations of: bed thickness, lithology, texture, structure and fossil content; any

other noteworthy observations were also recorded. In order to ensure consistency and repeatability, observations of grain size were made from fresh, un-weathered surfaces, using a hand-lens and a standard grain size card (Wentworth Scale).

2.3.3.3 Sample Preparation

The rock samples (Fig. 2.13a) were recovered from representative facies, as identified in the sedimentary logs, using a geological hammer. In order to ensure repeatability and consistency, all rock samples, of approximately 100 mm x 100 mm x 100 mm dimensions (Fig. 2.13c), were recovered ~ 0.1 m from the base of each bed chosen to be sampled. Samples were placed in plastic wrapping (Fig. 2.13b) and carefully labelled, according to their location. Prior to grain size analysis, it was necessary to prepare rock samples for SEM imaging, and subsequent analysis using ImageJ software. Small squares (~ 25 mm x 10 mm x 10 mm) were cut from each rock sample (Fig. 2.13d). Samples underwent a polishing process to produce a smooth surface. The polished surface was impregnated with epoxy resin (Fig. 2.13d). Samples were then carbon-coated and mounted on an SEM mount using conductive copper tape (Fig. 2.13e).

2.3.3.4 SEM Analysis

Photomicrographs of samples were taken using a Tescan SEM at the Leeds Electron Microscopy and Spectroscopy Centre (The University of Leeds). Each sample was photographed twice, at two different positions within the sample. All SEM photomicrographs were taken in backscatter mode at a similar contrast, to ensure comparability (Fig. 2.13f). Backscattered electrons comprise electrons of high energy that are fired from the electron beam and are back-scattered (reflected) from the sample. The intensity of electron back-scattering depends on the atomic composition of the sample. Light elements, with low atomic numbers, back-scatter electrons less strongly relative to heavy elements, with high atomic numbers; as such, light elements appear darker in the SEM image. Back-scatter images therefore detect contrasts in elemental composition between different areas of the sample with different chemical compositions (Goldstein et al., 1981). Within the samples recovered from the Sobrarbe Formation, the quartz and feldspar grains can be differentiated from the calcitic cement in which they are housed. As is shown in Figure 2.14f, the quartz and feldspar grains appear darker relative to the calcite cement.

2.3.3.5 Grain Size Analysis

The photomicrographs were imported into the image processing and analysis program ImageJ. Firstly, the scale of the image is set; the scale-bar (typically in microns or mm) is present on the strip of information at the base of the photomicrograph, called the data zone

(Fig. 2.13f). A line is drawn over the scale bar; the length of the line can be set to the correct value in microns. Secondly, the imported photomicrograph is cropped; a rectangular box is drawn around the photomicrograph, excluding the data zone at the base of the image.

Following this, the image is converted into binary format. The grain boundaries of the dark quartz and feldspar grains are identified by the ImageJ software.

Grain size parameters were calculated by the ImageJ software. ImageJ calculates grain size by mapping each individual grain to an equivalently sized ellipse; output parameters include: i) the number of particles, ii) particle areas, iii) particle perimeters and iv) major and minor axes.

2.3.3.6 Statistical Analysis of Grain size

The statistical analysis of all ImageJ results was completed using GRADISTAT computer software (Blott and Pye 2001), which enables the rapid analysis of grain size statistics and produces numerical, geometrically calculated values of the mean, mode, median, and sorting.

2.4. Sample Storage

In the offshore New Jersey dataset, each sample location has: i) a preserved pristine portion of the core and ii) a portion that has been mechanically and geochemically disaggregated. In the Sobrarbe Deltaic Complex, each sample location has: i) pristine samples (offcuts from the sample preparation process) and ii) small polished samples, impregnated with resin. All samples are stored at the University of Leeds, alongside field notebooks. In addition, for the Sobrarbe Deltaic Complex dataset, georeferenced sample locations are included in Chapter Five.



Figure 2.13: Photographs illustrating methodology of sample collection and preparation for grain size analysis. a) Example of a prominent sand-bed as identified in a sedimentary log. b) Sample being labelled and placed into plastic wrapping. c) Example of a rock sample. d) Example of rock sample following cutting and polishing process; note the smooth surface impregnated with epoxy resin. e) Example of a sample following carbon coating and attachment of conductive copper tape. f) Example of an SEM image in backscatter mode; note the dark grey appearance of quartz and feldspar grains relative to the light calcite cement.

Chapter 3 Manuscript One

Filter or conveyor? Establishing relationships between clinoform rollover trajectory, sedimentary process-regime, and grain character within intrashelf clinothem, offshore New Jersey, USA

3.1 Abstract

Clinoform geometries and trajectories are widely used to predict the spatial and temporal evolution of sand distribution, but most analytical approaches underplay the significance of topset and shelf process-regime in determining how and when sediment is conveyed downdip or stored on the continental shelf. We present an integrated study of clinoform rollover trajectory and detailed grain character analysis to assess the role of topset process-regime in determining sand distribution and sediment character across clinothems. This study targets the topset, foreset, and bottomset deposits of four successive Miocene intrashelf clinothem sequences, which represent deposition under either river-dominated or wave-dominated conditions. Seismic reflection data was combined with core analysis and grain character data derived from 664 samples collected from three cored research boreholes. In river-dominated clinothems, the transfer of coarse-grained sediment occurs under both rising and flat-to-falling clinoform rollover trajectories, suggesting that process-regime is more important in determining sediment delivery than clinoform trajectory; river-dominated systems are effective conveyors of sediment into deeper water. Wave-dominated clinothems, deposited exclusively under rising clinoform rollover trajectories, largely retain sand within topset and foreset deposits; wave-dominated systems are effective sediment filters. Notably, deposition under either river- or wave-dominated topset process-regimes results in quantifiable differences in grain character attributes along clinoform profiles. Sediments in river-dominated systems are coarser, less well-rounded, and more poorly sorted, and show greater inter-sequence and intra-sequence variability than those in wave-dominated systems; prediction of sediment character is more challenging in river-dominated systems. This study highlights the need for caution when attempting to predict downdip sand distribution from clinoform trajectory alone, and provides a novel perspective into downdip grain character profiles under end-member topset process-regime conditions. The results of this study can be used to better constrain sediment grain size and grain shape distributions in process-based forward models, and have widespread applications in prediction of reservoir quality in both frontier and mature hydrocarbon basins.

3.2 Introduction

The geometry and trajectory of successive clinoform rollovers, and the resulting stacking patterns of clinothems, have been used extensively to predict the spatial location and temporal evolution of sand bodies in basin-margin successions, both in outcrop and subsurface (e.g., Steel and Olsen, 2002; Johannessen and Steel, 2005; Helland-Hansen and Hampson, 2009; Koo et al., 2016; Chen et al., 2018; Pellegrini et al., 2017). In both clinoform

trajectory models (e.g., Burgess and Hovius, 1998; Mellere et al., 2002; Steel and Olsen, 2002; Bullimore et al., 2005; Carvajal and Steel, 2006; Uroza and Steel, 2008; Helland-Hansen and Hampson, 2009; Ryan et al., 2009) and sequence stratigraphic models (e.g., Vail et al., 1977; Van Wagoner et al., 1988; Posamentier et al., 1992; Johannessen and Steel, 2005; Catuneanu et al., 2009), emphasis has been largely placed on the balance of accommodation and sediment supply. However, the dominant shelf process-regime also plays a key, but under-acknowledged, role in determining when coarse-grained sediment (i.e., fine sand and coarser) is stored on the continental shelf and when it is conveyed downdip (Helland-Hansen and Hampson 2009; Dixon et al 2012a; Covault and Fildani 2014; Gong et al., 2016; Peng et al., 2017).

Recent studies have highlighted that shelf process-regime (resulting from the cumulative effects of fluvial, wave, tidal, and oceanographic currents) is an important parameter to consider when predicting the presence or absence of coarse-grained sediment in downdip locations. For example, Dixon et al. (2012a) suggest that a river-dominated shelf edge is critical to sand delivery into the deep-water setting. Conversely, wave- or storm-dominated shelf process-regimes are cited as ineffective conveyors of sediment to deep water, instead filtering and redistributing sediment alongshore (Plink-Björklund and Steel, 2004; Petter and Steel, 2006; Dixon et al., 2012a; Gong et al., 2016). However, prediction of sediment character (grain size, grain shape, and sorting) at different positions along the depositional profile remains poorly constrained and largely unquantified in the context of a specific shelf process-regime. In part, this is due to the paucity of samples from coeval shelf, slope and basin-floor deposits along a continuous depositional profile (Catuneanu et al., 2009). To understand how and when sediments of different calibre and maturity bypass the shelf and are delivered into deep-water settings, we present new grain character data recovered from three cores (M27, M28, and M29) that intersect shallow- and deep-marine strata from chronostratigraphically defined intrashelf clinothems, offshore New Jersey, USA. Intrashelf clinothems, also referred to as subaqueous deltas, are of intermediate scale and typically have reliefs in the order of tens of metres; intrashelf clinothems are situated seaward of the shoreline break and landward of the continental break (Helland-Hansen and Hampson, 2009; Henriksen et al., 2009; Helland-Hansen and Gjelberg, 2012; Patruno et al., 2015; Hodgson et al., 2018). The IODP Expedition 313 transect offers a rare 'natural laboratory' for studying the interactions of clinoform trajectory (depositional architecture) and grain character variability due to the availability of high-resolution dip-parallel seismic data and integrated core data. High-resolution grain character data are presented for four clinothem sequences, in which the clinoform trajectory has been observed from seismic reflection data, and dominant process-

regimes have been interpreted from core-based observations. Three overarching research questions are addressed. 1) What are the major controls that determine clinothem architecture? 2) How does the interaction between the dominant topset process-regime and clinoform trajectory affect the timing and delivery of coarse-grained sediment to deeper-water settings? 3) How do downdip grain character profiles differ between clinothem sequences deposited under different dominant topset process-regime conditions?

The methodology and grain character data presented here provide a unique database of grain size, grain shape, and sorting statistics. This high-resolution grain character database can be applied to test and refine numerical forward models (e.g., DionisosFlow, Delft2-D) that seek to improve prediction of reservoir characteristics in both mature and frontier hydrocarbon basins.

3.2.1 Nomenclature

Hereafter, the term clinoform is used to describe chronostratigraphic stratal surfaces, which are basinward-dipping (e.g., Gilbert, 1885; Rich, 1951; Mitchum et al., 1977; Pirmez et al., 1998; Patruno et al., 2015). Clinothems, at different scales, are the principal architectural element of many deltaic to continental-slope successions (e.g., Gilbert, 1885; Rich, 1951; Mitchum et al., 1977; Pirmez et al., 1998).

Clinothems comprise three fundamental geometrical components: topset, foreset and bottomset deposits (Gilbert, 1885; Steel and Olsen, 2002). The foreset forms the central seaward-dipping part of the clinothem and is the steepest part of the clinoform sigmoid (typically dipping between one and three degrees at the clinoform inflection point). The clinoform rollover (also referred to as the shelf-edge break, platform edge and offlap break) refers to the uppermost break in slope between the topset and foreset (Wear et al., 1974; Southard and Stanley, 1976; Pirmez et al., 1998; Plink-Björklund et al., 2001; Glørstad-Clark et al., 2010, 2011; Anell and Midtkandal, 2017 and represents a zone of increased gradient (Jones et al., 2015). The base of slope refers to the lowermost break in clinoform slope, between the foreset and the bottomset.

Clinofoms develop at a range of scales (e.g., Pirmez et al., 1998; Steel and Olsen, 2002; Helland-Hansen and Hampson 2009; Henriksen et al., 2009; Anell and Midtkandal, 2017; Patruno et al., 2015), from shoreline clinoforms (one meter to ~ tens of meters in height), to shelf-slope-basin or basin-margin clinoforms (~ hundreds of meters to > 1 km in height). The New Jersey intrashelf clinoforms are typically one hundred to three hundred meters in height (Mountain et al., 2010). This intermediate scale of clinoform are referred to as intrashelf clinoforms, or subaqueous delta clinoforms, and form components of the shelf prism.

Intrashelf clinoforms are commonly located seaward of major river mouths and/or clastic shorelines but landward of the continental shelf-edge break (Hodgson et al., 2018). At the shoreline delta clinoform scale, shallow-marine and fluvial processes are dominant (e.g., wave reworking). By contrast, at the basin-margin scale, sediment gravity flows are dominant.

3.3 Geological Setting

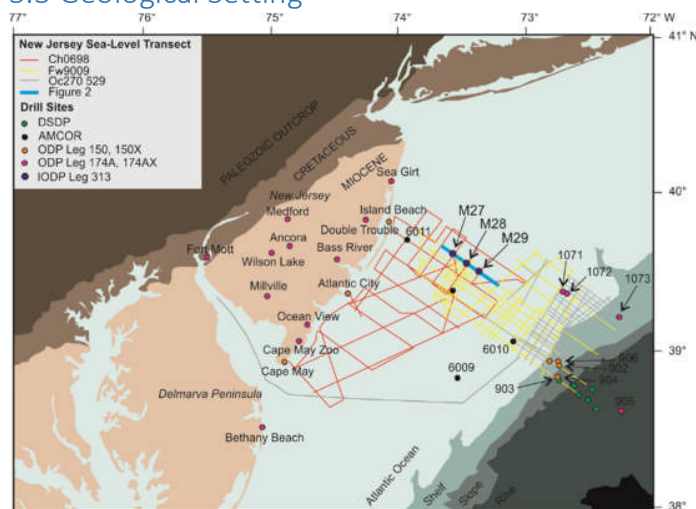


Figure 3.1: Location map of New Jersey sea-level transect, modified from Mountain et al. (2010). Study sites used in this manuscript (IODP Expedition 313 Sites M27, M28, and M29) are presented as purple circles. The seismic profiles show data acquisition from three cruises as part of the New Jersey sea-level transect (R/V Ewing cruise EW9009, R/V Oceanus cruise Oc270 and R/V Cape Hatteras cruise CH0698; Monteverde et al., 2008; Mountain et al., 2010; Miller et al., 2013a). The seismic line transecting the core sites M27-M29 (Oc270 529) is indicated in blue. This seismic transect is shown in Figure 3.2.

The New Jersey Atlantic margin is an example of a mid-latitude, siliciclastic-dominated, prograding passive margin, and is an ideal location to study high-resolution grain character variability for the following reasons: i) rapid rates of deposition, which have resulted in thick accumulated sedimentary sequences (Miller and Mountain, 1994; Austin et al., 1998); ii) the tectonic dormancy of the New Jersey margin, which is in the late stages of thermal cooling (Katz et al., 2013); iii) good chronostratigraphic control on the timing of sedimentation (Browning et al., 2013); and iv) a significant volume of previously published literature that includes seismic reflection transects, outcrop and well data (Mountain et al., 2010) in which the general geological setting can be framed. In 2009, IODP Expedition 313 continuously cored and logged a nearshore portion of the New Jersey shelf-margin transect (Fig. 3.1). The clinothems intersected during Expedition 313, and studied here, are seaward-prograding, intrashelf sequences of Miocene age (Mountain et al. 2010). The three cores (M27, M28 and M29) intersect topset, foreset, and bottomset deposits (ca. 12-22 Ma) along seismic line Oc270 529 (Mountain et al., 2010; Kominz et al., 2016) (Fig. 3.2).

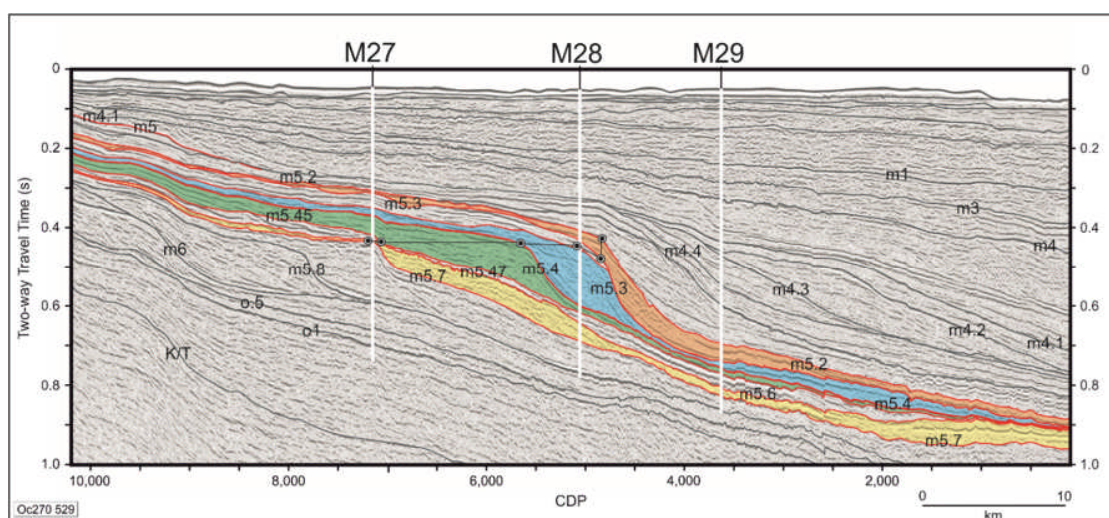


Figure 3.2: Seismic line Oc270 529. Sequence boundaries relevant to this study are highlighted in red. Depositional sequences analysed in this study are highlighted in various colours, where the yellow clinothem is Sequence m5.7, the green clinothem is Sequence m5.45, the blue clinothem is Sequence m5.4, and the orange clinothem is Sequence m5.3. Depositional sequences are named according to their basal reflector boundary, for example Sequence m5.7 lies on reflector m5.7. All seismic interpretations are from Monteverde et al. (2008), Mountain et al. (2010), and Browning et al. (2013). Position of clinoform rollovers are indicated by the grey circles.

3.3.1 Sequence Boundaries

The sequence boundaries of the clinothems were recognized in multichannel seismic profiles based on the location of reflector terminations (truncation, onlap, downlap, and toplap) (Miller et al., 2013a). The positions of sequence boundaries were confirmed through in-core identification, on the premise of physical stratigraphy and age breaks (Mountain et al., 2010; Browning et al., 2013; Miller et al., 2013a). Miller et al. (2013a) concluded that they could successfully match most core and log surfaces unequivocally with seismic sequence boundaries. The sequence stratigraphic framework presented in Miller et al. (2013a) provides a means of subdividing the stratigraphic record, and thus contrasting changes in grain character and clinothem rollover trajectory between individual clinothem sequences. The timings of sequence boundaries have been shown to correlate with major positive excursions in the $\delta^{18}\text{O}$ deep-sea record, suggesting that observed changes in relative sea level ($\sim 5 - 20$ m) are predominantly controlled by sea-level variations of allogenic origin, resulting from the waxing and waning of Antarctic ice sheets (Browning et al., 2013; Kominz et al., 2016).

3.4 Data and Methods

3.4.1 Materials

The stratigraphic successions targeted during this investigation were exclusively Miocene intrashelf clinothems, correlating to depths of 225 – 365 mcd, 312 – 611 mcd and 600 – 730 mcd in cores M27, M28, and M29, respectively. A total of 134 sediment samples were recovered from Cores 313-M27A-80-1 (224 mcd) to 313-M27A-129-2 (377 mcd) (152-m-

thick sampled section). A total of 341 sediment samples were recovered from Cores 313-M28A-35-1 (311 mcd) to 313-M28A-147-1 (600 mcd) (288-m-thick sampled section). A total of 189 sediment samples were recovered from Cores 313-M29A-161-1 (600 mcd) to 313-M29A-208-1 (730 mcd) (130-m-thick sampled section). The stratigraphic interval targeted during this investigation has been subdivided into four depositional sequences based on the depths of the sequence stratigraphic surfaces presented in Browning et al. (2013): m5.7, m5.45, m5.4, and m5.3. In sequence m5.4, Core M27, the data presented here spans from the basal m5.4 sequence boundary to sequence boundary m5.33 (see Miller et al., 2013b). The Miocene clinothems are well-imaged on a grid of seismic reflection profiles (Fig. 3.1). Multichannel seismic profile oc270 529, shot in the region of IODP Expedition 313, transects core sites M27-M29 (Fig. 3.1) and provides a 2-D downdip profile of the clinothem sequences (Fig. 3.2). The seismic interpretations of Monteverde et al. (2008), Mountain et al. (2010), Browning et al. (2013) and Miller et al. (2013b) have been used during this investigation for correlation purposes and to subdivide the stratigraphic record into the aforementioned clinothem sequences.

3.4.2 Methods

Two principal methodological approaches were used in this study: high-resolution grain character analysis and clinof orm trajectory analysis. The grain character analysis has been used primarily to produce longitudinal sediment profiles and grain size distribution profiles, which are supplemented by core descriptions (Expedition 313 Scientists) and published seismic reflection (Monteverde et al., 2008; Mountain et al., 2010; Miller et al., 2013a), and core sedimentology (Expedition 313 Scientists, 2010; Mountain et al., 2010; Browning et al., 2013; Hodgson et al. 2018) interpretations. The analysis of clinof orm trajectory is based on the geometric properties of clinothems and through the identification of the clinof orm rollover position on each seismic reflector and its evolution through time along successive intrashelf clinothem sequences (Fig. 3.2). Trajectory analysis was performed on high-resolution 2-D, dip-parallel seismic data. These quantitative data are supplemented by the visual core descriptions and interpretations of the Expedition 313 sedimentologists and original core observations of the sedimentary texture and structure of the core.

3.4.2.1 Grain character Analysis

The strategy for sample collection was to remove sediment slices (15 mm width), sampled at ~ 0.5 m intervals down-core. In practice, there was some deviation from this sampling configuration to avoid i) horizons of cementation, ii) biscuiting disturbance (interaction of drilling fluid with sediment), iii) key stratigraphic surfaces, and iv) heavily sampled intervals.



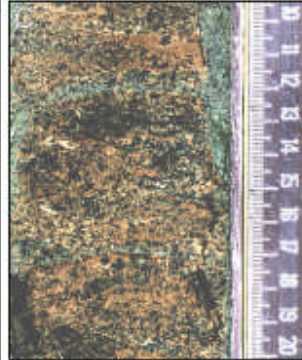









	Topset	Foreset	Bottomset
Sequence m5.7	 <p>Core 313-M27A-116-3</p>	 <p>Core 313-M28A-136-1</p>	 <p>Core 313-M29A-207-3</p>
Sequence m5.45	 <p>Core 313-M27A-107-2</p>	 <p>Core 313-M28A-115-1</p>	 <p>Core 313-M29A-186-2</p>
Sequence m5.4	 <p>Core 313-M27A-96-1</p>	 <p>Core 313-M28A-92-1</p>	 <p>Core 313-M29A-182-2</p>
Sequence m5.3	 <p>Core 313-M27A-85-3</p>	 <p>Core 313-M28A-38-2</p>	 <p>Core 313-M29A-174-1</p>

Figure 3.3: Representative core photographs of Clinothem sequences m5.7 (a-c), m5.45 (d-f), m5.4 (g-i) and m5.3 (j-l), showing topset, foreset, and bottomset deposits. Photographs show: a) gravelly quartz- and glauconite-rich sands; b) gravelly glauconite-rich sands; c) glauconite- and quartz-rich structureless sands; d) convex-up lamination interpreted as hummocky cross-stratification; e) clean fine sands; f) sandy silts with minor glauconite; g) parallel laminae of sand and silt; h) laminated silts; i) structureless fine sands; j) silts containing shell-fragments and organic matter; k) quartz- and glauconite-rich sands; and l) glauconite- and quartz-rich structureless sands.

Due to the pervasive presence of biogenic material (calcareous skeletal remains, shell fragments, and organic matter) it was necessary to undertake sample pre-treatment before grain character measurements, in order to remove these components. Sample pre-treatment comprised the careful manual disaggregation of samples; samples were disaggregated using an agate mortar and pestle (e.g., Sahu, 1964; Wilson and Pittman, 1977; Nelson, 1983; Frey and Payne, 1996; Ando et al., 2014). All samples were treated with hydrochloric acid (10% weight to volume) (e.g., Battarbee, 1986; Battarbee et al., 2001; Schumacher, 2002; Vaasma, 2008) and hydrogen peroxide (30% weight to volume) (e.g., Schumacher, 2002; Vaasma, 2008; Gray et al., 2009), to remove calcareous and non-calcareous organic components, respectively.

Here, grain character is defined as the grain size, grain shape (sphericity and roundness), and sorting of a sample. Grain character analysis was completed using a CamsizerXT (Retsch Technology), which is an optically based dynamic image analyser. The CamsizerXT is capable of measuring the grain size range 1 μm – 8 mm (clay – gravel), with an accuracy of $\pm 1\%$ (Moore et al., 2011). Grain size fractions $< 1 \mu\text{m}$ are lost during the process of analysis. The grain size distributions yielded by the CamsizerXT are comparable with those produced by traditional sieving analyses. However, this instrument provides the additional advantage of simultaneous grain shape analysis (sphericity and roundness). Each sample analysed by the CamsizerXT produces a dataset logarithmically divided into 105 grain size classes, spanning 1 μm – 8 mm. The statistical analysis of all CamsizerXT results was completed using GRADISTAT computer software (Blott and Pye, 2001). The GRADISTAT software enables the rapid analysis of grain size statistics from multiple sediment samples and produces numerical, geometrically calculated values of the mean, mode, and sorting. Grain shape data were analysed using Microsoft Excel software.

3.4.2.2 Trajectory Analysis

The analysis of clinof orm trajectory involves the identification of the clinof orm rollover position on each seismic reflector analysed in this study (Fig. 3.2). The position of the clinof orm rollover is marked by the point of maximum curvature between the topset and foreset (Pirmez et al., 1998); however, delineating this position can be challenging (Olariu and Steel, 2009). To ensure consistency and repeatability, the clinof orm rollover has been identified following the methodology of Anell and Midtkandal (2017, p. 282); as such, the

position of the clinoform rollover is identified “as a point that is perpendicular to the intersection of straight lines extrapolated from the inflection point of the topset and foreset of the clinoform.”

3.4.2.3 Determination of Topset Process-regime

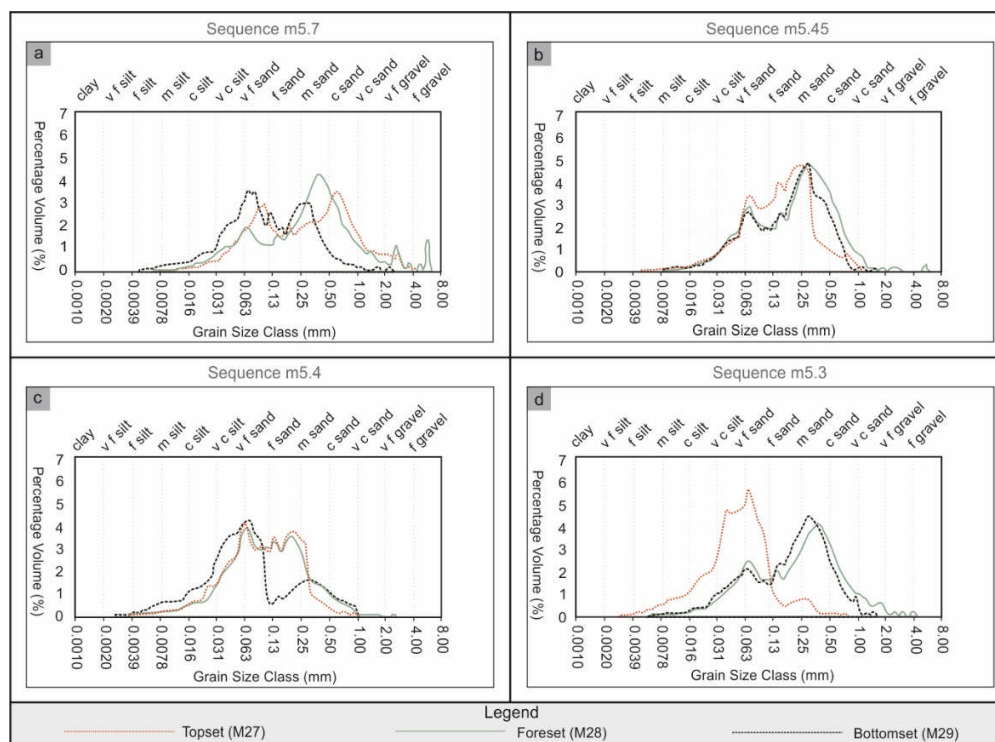


Figure 3.4: Average grain size distribution plots for the topset, foreset, and bottomset deposits of Sequences m5.7 (4a), m5.45 (4b), m5.4 (4c), and m5.3 (4d). Axes are percentage volume (%) and grain size (mm), respectively. Alongside the numerical grain size classes are the descriptive grain size-classes modified from Udden (1914) and Wentworth (1922). Topset, foreset, and bottomset grain size distributions are shown in red, green, and dark brown respectively.

The Expedition 313 scientists produced sedimentological interpretations of topset depositional environment using assemblages of sedimentary structures, sediment composition and texture, fossil content, and ichnofabric (see Mountain et al., 2010). Sedimentary facies associations presented in Mountain et al. (2010) indicate that the topset depositional environments of the New Jersey clinoforms varies between sequences. Relevant to this investigation, the topset deposits of Sequences m5.45 and m5.4 share features associated with wave-dominated shoreline facies models (e.g., Reineck and Singh, 1972; McCubbin, 1982; Browning et al., 2006). Key diagnostic features of wave-dominated deposits (in the shoreface and shoreface to offshore transition facies) include the following: interbedded fine and very fine sands; shell debris; convex-upward laminae; low angle cross-beds; symmetrical ripple lamination, and moderate to heavy bioturbation (4 to 6 on the standard bioturbation index). Relevant to this investigation, the topset deposits of Sequences m5.7 and m5.3 share features associated with mixed river and wave delta facies models (e.g.,

Galloway, 1975; Bhattacharya and Walker, 1992). Key diagnostic features of river-dominated deposits include the following: coarse sands; cut-and-fill surfaces associated with basal gravels and rip-up clasts; micaceous sands; current-ripple lamination; and terrestrial plant material.

3.5 Results

Due to the data-rich nature of this investigation, many of the data have been tabulated and/or are presented in figures. However, important differences in sedimentology (Fig. 3.3) and clinotherm architecture between sequences are highlighted below.

3.5.1 Sequence m5.7

Trajectory analysis of Sequence m5.7 indicates a slightly negative, falling trajectory (Fig. 3.2). At the point of core intersection, Sequence m5.7 has a thickness of 25.2 m, 44.1 m, and 21.0 m in topset, foreset, and bottomset locations respectively. In seismic profile, Sequence m5.7 has relatively thin topset and bottomset deposits and has thicker foreset deposits (Fig. 3.2). The average grain size distribution profiles of topset, foreset, and bottomset deposits show very similar bimodal profiles (Fig. 3.4a). The finer peak is narrower and sits in the very fine sand grain size class, and the coarser peak is broader and spans medium and coarse sand grain size classes (Fig. 3.4a). The grain size distribution profiles show progressive down-dip fining of the average grain size composition (Fig. 3.3a), which corresponds to an increase in sorting (Fig. 3.5b) and a change in modal grain size from medium- or coarse-grained sand in topsets to very fine- or fine-grained sand in bottomset deposits (Table 3.1). Despite the overall down-dip fining trend, the largest (2 – 4 mm) and most angular grains are retained in the foreset position (Figs. 3.4a, 3.5c, d).

Sequence m5.7							
Topset		Relative increase or decrease downdip	Foreset		Relative increase or decrease downdip	Bottomset	
Number of samples	33	increase	Number of samples	56	decrease	Number of samples	29
Mean grain size (mm)	0.22	increase	Mean grain size (mm)	0.29	decrease	Mean grain size (mm)	0.12
Median grain size (n25) (mm)	0.18	increase	Median grain size (n25) (mm)	0.19	decrease	Median grain size (n25) (mm)	0.059

Median grain size (<i>n</i> 50) (mm)	0.21	increase	Median grain size (<i>n</i> 50) (mm)	0.24	decrease	Median grain size (<i>n</i> 50) (mm)	0.15
Median grain size (<i>n</i> 75) (mm)	0.29	increase	Median grain size (<i>n</i> 75) (mm)	0.31	decrease	Median grain size (<i>n</i> 75) (mm)	0.17
Maximum grain size (mm)	0.37	increase	Maximum grain size (mm)	1.3	decrease	Maximum grain size (mm)	0.26
Minimum grain size (mm)	0.042	increase	Minimum grain size (mm)	0.11	decrease	Minimum grain size (mm)	0.029
Standard deviation (σ)	87	increase	Standard deviation (σ)	195	decrease	Standard deviation (σ)	66
Mean sorting (σ)	3.2	increase	Mean sorting (σ)	3.1	increase	Mean sorting (σ)	2.6
Median sorting (<i>n</i> 25) (σ)	2.8	increase	Median sorting (<i>n</i> 25) (σ)	2.7	increase	Median sorting (<i>n</i> 25) (σ)	2.3
Median sorting (<i>n</i> 50) (σ)	3.2	increase	Median sorting (<i>n</i> 50) (σ)	2.9	increase	Median sorting (<i>n</i> 50) (σ)	2.5
Median sorting (<i>n</i> 75) (σ)	3.5	increase	Median sorting (<i>n</i> 75) (σ)	3.3	increase	Median sorting (<i>n</i> 75) (σ)	2.8
Maximum sorting (σ)	1.9	decrease	Maximum sorting (σ)	2.1	increase	Maximum sorting (σ)	1.9
Minimum sorting (σ)	4.2	decrease	Minimum sorting (σ)	4.7	increase	Minimum sorting (σ)	3.5
Standard deviation (σ)	0.53	increase	Standard deviation (σ)	0.56	decrease	Standard deviation (σ)	0.38

Mean sphericity (K)	0.907	increase	Mean sphericity (K)	0.911	increase	Mean sphericity (K)	0.919
Median sphericity (<i>n</i> 25) (K)	0.901	increase	Median sphericity (<i>n</i> 25) (K)	0.907	decrease	Median sphericity (<i>n</i> 25) (K)	0.893
Median sphericity (<i>n</i> 50) (K)	0.908	increase	Median sphericity (<i>n</i> 50) (K)	0.913	increase	Median sphericity (<i>n</i> 50) (K)	0.917
Median sphericity (<i>n</i> 75) (K)	0.915	decrease	Median sphericity (<i>n</i> 75) (K)	0.916	increase	Median sphericity (<i>n</i> 75) (K)	0.942
Maximum sphericity (K)	0.938	decrease	Maximum sphericity (K)	0.925	increase	Maximum sphericity (K)	0.961
Minimum sphericity (K)	0.876	increase	Minimum sphericity (K)	0.891	decrease	Minimum sphericity (K)	0.871
Standard deviation (σ)	0.01	decrease	Standard deviation (σ)	0.007	increase	Standard deviation (σ)	0.03
Mean roundness (K)	0.539	increase	Mean roundness (K)	0.551	increase	Mean roundness (K)	0.644
Median roundness (<i>n</i> 25) (K)	0.506	increase	Median roundness (<i>n</i> 25) (K)	0.514	increase	Median roundness (<i>n</i> 25) (K)	0.54
Median roundness (<i>n</i> 50) (K)	0.527	increase	Median roundness (<i>n</i> 50) (K)	0.532	increase	Median roundness (<i>n</i> 50) (K)	0.637
Median roundness (<i>n</i> 75) (K)	0.56	increase	Median roundness (<i>n</i> 75) (K)	0.561	increase	Median roundness (<i>n</i> 75) (K)	0.726
Maximum roundness (K)	0.691	increase	Maximum roundness (K)	0.904	decrease	Maximum roundness (K)	0.895

Minimum roundness (K)	0.471	decrease	Minimum roundness (K)	0.435	increase	Minimum roundness (K)	0.491
Standard deviation (σ)	0.05	increase	Standard deviation (σ)	0.07	increase	Standard deviation (σ)	0.1
Average glauconite content (%)	~ 15	decrease	Average glauconite content (%)	~ 12	decrease	Average glauconite content (%)	~ 5
Maximum glauconite content (%)	20	increase	Maximum glauconite content (%)	25	increase	Maximum glauconite content (%)	45
Minimum glauconite content (%)	0	increase	Minimum glauconite content (%)	2	decrease	Minimum glauconite content (%)	0
<p>Glauconite Origin: Glauconite is interpreted to be of both allochthonous and autochthonous origin. From the top of the sequence to a depth of ~ 338 mcd, glauconite content remains < 5%. This is interpreted to be autochthonous in origin due to a) its concentration within burrows (Huggett and Gale, 1997) and b) its occurrence in association with a phosphate crust (Amorosi, 1997). Similar autochthonous glauconite is observed towards the base of the sequence (~ 347 - ~ 351mcd). Between ~ 339 and ~ 345 mcd the glauconite content increases to 10 - 20% and is interpreted to be allochthonous in origin, due to a) the presence of glauconite grains of up to</p>			<p>Glauconite Origin: Glauconite is ubiquitous throughout the sequence and varies between 2 - 25%. From the top of the sequence to ~ 593mcd the glauconite is interpreted to be predominantly allochthonous in origin, due to a) the presence of structureless glauconite-rich sands, in which ~ 5.5 mm glauconite grains are found within a silty matrix (Huggett and Gale, 1997) and b) from ~ 570 - ~ 578 mcd glauconite is found in normally graded successions, interbedded with silts (Wermund, 1961). The allochthonous glauconite is associated with quartz granules. From ~ 593 mcd to the base of the sequence, glauconite is interpreted to be autochthonous in origin due to its</p>			<p>Glauconite Origin: From the top of the sequence to ~ 721 mcd the concentration of glauconite within the deposits is low, varying between 0 and 3%. This is interpreted to be autochthonous in origin due to concentration within the burrows of bioturbated sediment (Huggett and Gale, 1997). From ~ 722 mcd to the base of the sequence there is an</p>	

<p>~ 4 mm in a silty matrix (Huggett and Gale, 1997) and b) the presence of glauconite with stratified sequences (Wermund, 1961).</p>	<p>concentration within the burrows of bioturbated sediment (Huggett and Gale, 1997).</p>	<p>abrupt increase in the glauconite content (reaching a maximum of 45%); this is interpreted to be allochthonous in origin due to the presence of glauconite grains of up to ~ 2.5 mm in a silty matrix (Huggett and Gale, 1997).</p>
---	---	--

Table 3.1: Data on grain size and grain character for M5.7. Grain size, sorting, sphericity, roundness, and glauconite content are presented for Sites M27 - M29. It is also indicated if there is a relative increase or decrease in any parameter relative to its downdip counterparts. Data on grain size are presented in millimetres (mm) and has been calculated using GRADISTAT software (Blott and Pye, 2001). Sorting data are presented as a standard deviation (σ) and has been calculated using GRADISTAT software (Blott and Pye, 2001). Data on grain roundness and sphericity are presented according to the Krumbein scale and have been calculated using standard Excel software. Glauconite is given as a percentage of the total sediment volume (%) and has been adapted from qualitative estimates given by the Expedition 313 scientists. Accompanying the glauconite contents are notes on the interpreted origins of glauconite in each core site.

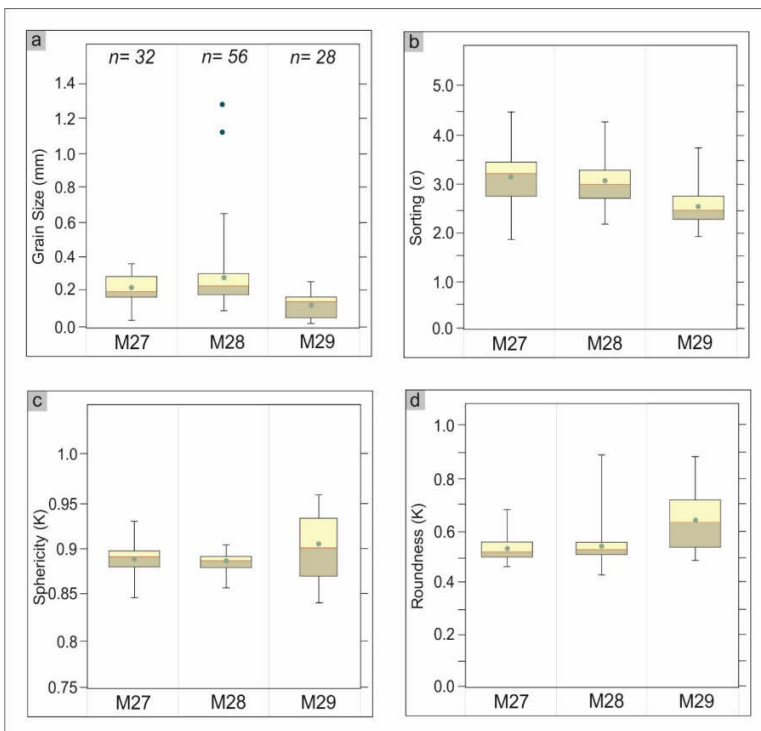


Figure 3.5: Box and whisker plots for Sequence m5.7 showing a) grain size, b) sorting, c) sphericity and d) roundness for Cores M27, M28, and M29. The horizontal red line indicates the median; the mean is shown as a green circle; the boundaries of the box indicate the 25th and 75th percentile; whiskers are minimum and maximum values and outliers are shown as blue circles. $n = x$ represents sample size and is shown in Part 5a.

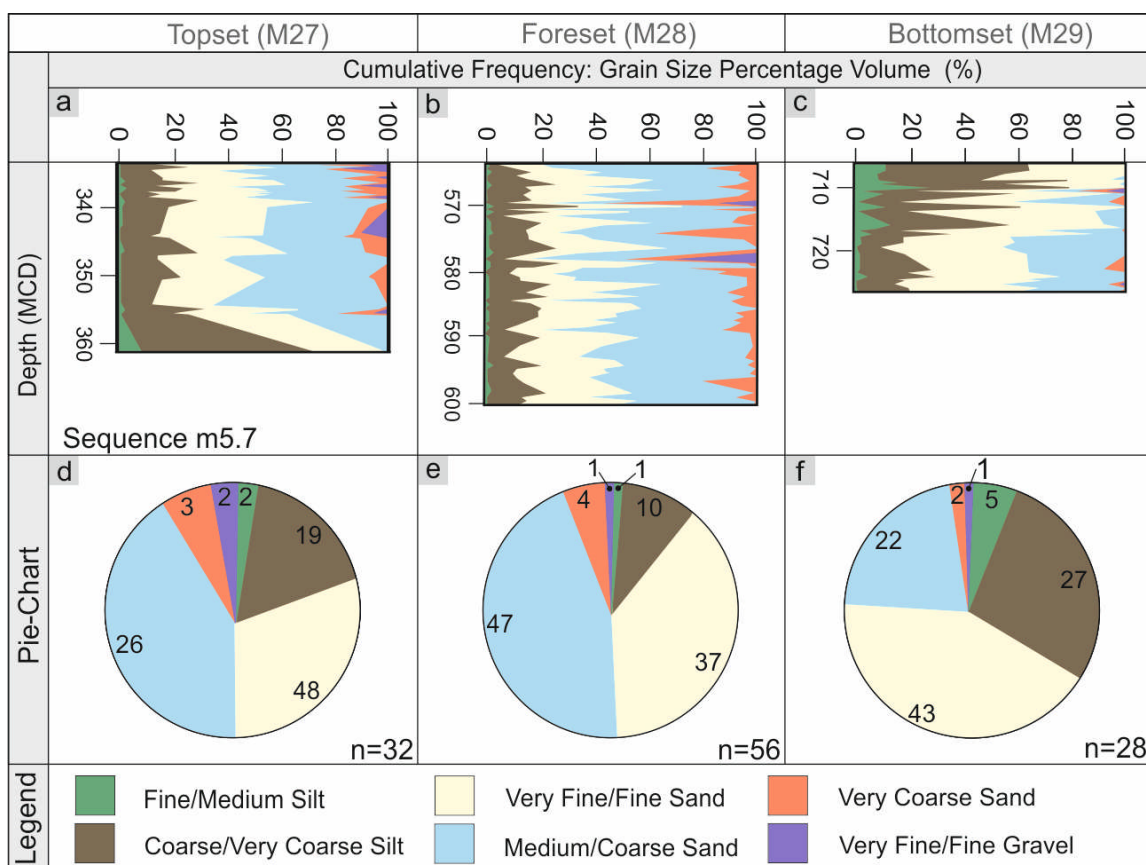


Figure 3.6: Grain size cumulative frequency plot for topset (5a), foreset (5b) and bottomset (5c) deposits of Sequence m5.7. Axes are depth in metres composite depth (mcd) and grain size by percentage (%), respectively. Pie charts showing average grain size composition for topset (4d), foreset (4e), and bottomset (4f) deposits. The percentage volume for each grain size is also indicated numerically. The number of samples is indicated by $n = x$.

3.5.2 Sequence m5.45

Trajectory analysis of Sequence m5.45 indicates a positive, rising trajectory (Fig. 3.2). At the point of core intersection, Sequence m5.45 has a thickness of 41.1 m, 21.3 m, and 11.3 m in topset, foreset, and bottomset locations respectively. In seismic profile, Sequence m5.45 has relatively thick topset and foreset deposits, with relatively thin bottomset deposits (Fig. 3.2). The base of the foreset deposits in Sequence m5.45 has been intersected by the core. The average grain size distribution profiles of topset, foreset, and bottomset deposits are dominated by three narrow peaks in grain size abundance at 0.068 mm (very fine-grained sand), 0.14 mm (fine-grained sand), and 0.2 – 0.35 mm (fine- and medium-grained sand) (Fig. 3.4b). The three peaks are present down-dip from topset to foreset locations with little change along the distribution profile (Fig. 3.4b). The longitudinal depositional profile is consistently dominated by very fine- and fine-grained sand (Figs. 3.3-D, e, f), which is characterized by grains that are highly spherical and well-rounded (Fig. 3.7a, d).

Up-core grain size trends in topset deposits indicate the development of fining-upwards packages, typically ~ 2.5 m thick (Fig. 3.8a). The sedimentary structures associated with these deposits are convex-up laminated sands, containing shell fragments (Fig. 3.3-D). Foreset and bottomset deposits contain numerous packages, which either coarsen or fine upwards, each typically ~ 2 m in thickness (Fig. 3.8b, c). These packages are associated with the occurrence of glauconite-rich sands above erosion surfaces, with some normal grading, and dune-scale cross-stratification in bottomset deposits (Hodgson et al., 2018). There is a greater overall percentage volume of very fine- and fine-grained sand in topset deposits than in foreset and bottomset deposits (Fig. 3.8). Foreset deposits contain a very small contribution of very coarse-grained sand and gravel (1% and 0.5% respectively) (Figs. 3.4b, 3.8). Mean grain sphericity remains high throughout the depositional profile, varying by less than 0.006K from topset to bottomset deposits (Fig. 3.7c, Table 3.2). Mean grain roundness shows greater variability along the depositional profile (Fig. 3.7d). The most angular, least well-rounded grains are found in foreset deposits. The foreset deposits also contain the least well-sorted sediments (Fig. 3.7b, Table 3.2).

Sequence m5.45							
Topset		Relative increase or decrease downdip	Foreset		Relative increase or decrease downdip	Bottomset	
Number of samples	60	decrease	Number of samples	47	decrease	Number of samples	17
Mean grain size (mm)	0.126	increase	Mean grain size (mm)	0.189	decrease	Mean grain size (mm)	0.168
Median grain size (n25) (mm)	0.094	increase	Median grain size (n25) (mm)	0.151	decrease	Median grain size (n25) (mm)	0.127
Median grain size (n50) (mm)	0.124	increase	Median grain size (n50) (mm)	0.174	increase	Median grain size (n50) (mm)	0.177
Median grain size (n75) (mm)	0.145	increase	Median grain size (n75) (mm)	0.214	decrease	Median grain size (n75) (mm)	0.201

Maximum grain size (mm)	0.233	increase	Maximum grain size (mm)	0.654	decrease	Maximum grain size (mm)	0.257
Minimum grain size (mm)	0.039	increase	Minimum grain size (mm)	0.047	increase	Minimum grain size (mm)	0.081
Standard deviation (σ)	46	increase	Standard deviation (σ)	90	decrease	Standard deviation (σ)	50
Mean sorting (σ)	2.28	decrease	Mean sorting (σ)	2.65	increase	Mean sorting (σ)	2.51
Median sorting (n_{25}) (σ)	2.4	decrease	Median sorting (n_{25}) (σ)	2.84	increase	Median sorting (n_{25}) (σ)	2.63
Median sorting (n_{50}) (σ)	2.31	decrease	Median sorting (n_{50}) (σ)	2.56	increase	Median sorting (n_{50}) (σ)	2.54
Median sorting (n_{75}) (σ)	2.17	decrease	Median sorting (n_{75}) (σ)	2.37	constant	Median sorting (n_{75}) (σ)	2.37
Maximum sorting (σ)	1.76	decrease	Maximum sorting (σ)	1.87	decrease	Maximum sorting (σ)	2.13
Minimum sorting (σ)	2.99	decrease	Minimum sorting (σ)	4.04	increase	Minimum sorting (σ)	2.94
Standard deviation (σ)	0.2	increase	Standard deviation (σ)	0.38	decrease	Standard deviation (σ)	0.21
Mean sphericity (K)	0.913	decrease	Mean sphericity (K)	0.912	increase	Mean sphericity (K)	0.914
Median sphericity (n_{25}) (K)	0.893	increase	Median sphericity (n_{25}) (K)	0.903	increase	Median sphericity (n_{25}) (K)	0.904
Median sphericity (n_{50}) (K)	0.918	decrease	Median sphericity (n_{50}) (K)	0.908	increase	Median sphericity (n_{50}) (K)	0.914

Median sphericity (n75) (K)	0.927	decrease	Median sphericity (n75) (K)	0.917	increase	Median sphericity (n75) (K)	0.923
Maximum sphericity (K)	0.948	increase	Maximum sphericity (K)	0.95	decrease	Maximum sphericity (K)	0.944
Minimum sphericity (K)	0.872	increase	Minimum sphericity (K)	0.881	decrease	Minimum sphericity (K)	0.877
Standard deviation (σ)	0.02	constant	Standard deviation (σ)	0.02	constant	Standard deviation (σ)	0.02
Mean roundness (K)	0.636	decrease	Mean roundness (K)	0.594	increase	Mean roundness (K)	0.63
Median roundness (n25) (K)	0.563	increase	Median roundness (n25) (K)	0.546	increase	Median roundness (n25) (K)	0.571
Median roundness (n50) (K)	0.654	decrease	Median roundness (n50) (K)	0.566	increase	Median roundness (n50) (K)	0.609
Median roundness (n75) (K)	0.704	decrease	Median roundness (n75) (K)	0.63	increase	Median roundness (n75) (K)	0.674
Maximum roundness (K)	0.781	decrease	Maximum roundness (K)	0.807	decrease	Maximum roundness (K)	0.771
Minimum roundness (K)	0.484	decrease	Minimum roundness (K)	0.465	increase	Minimum roundness (K)	0.504
Standard deviation (σ)	0.08	constant	Standard deviation (σ)	0.08	constant	Standard deviation (σ)	0.07
Average glauconite content (%)	~ 0.5	increase	Average glauconite content (%)	~ 10	increase	Average glauconite content (%)	~ 25

Maximum glauconite content (%)	2	increase	Maximum glauconite content (%)	80	decrease	Maximum glauconite content (%)	60
Minimum glauconite content (%)	0	constant	Minimum glauconite content (%)	0	increase	Minimum glauconite content (%)	7
<p>Glauconite origin: Glauconite, as a percentage volume of the total sediment composition, is negligible or entirely absent from this deposit. At the base of the deposit the glauconite content reaches a maximum of 2%. The glauconite is interpreted to be autochthonous in origin due to its presence within the burrows of bioturbated sediment, as opposed to within the host sediment (Huggett and Gale, 1997).</p>			<p>Glauconite origin: Glauconite is largely absent from the top of the deposit to a depth of ~ 521 mcd, however there is a minor occurrence (< 4%) of glauconite between the depths of ~ 516 - 518 mcd. This is interpreted to be autochthonous in origin as a) it infills burrows within bioturbated sediment (Huggett and Gale, 1997) and b) it occurs in association with phosphatic grains (Amorosi, 1997). From ~ 521 mcd to the base of the sequence, the glauconite content accounts for between ~ 20 and ~ 80% of the total sediment volume. This glauconite is interpreted to be allochthonous in origin as a) it is present within upward fining sequences (Wermund, 1961) and b) glauconite grains of up to ~ 4 mm are found in a silty matrix (Huggett and Gale, 1997).</p>			<p>Glauconite origin: Within this deposit the glauconite content remains relatively high throughout, varying between ~ 7 and 60%. From the top of the unit to ~ 626 mcd, the glauconite content remains at ~ 7%; this is interpreted to be autochthonous in origin due to its concentration within burrows (Huggett and Gale, 1997). Towards the base of the unit the glauconite content increases, forming a maximum of 60% of the total sediment volume. This is interpreted to be allochthonous in origin due to its presence within cross-laminated</p>	

		<p>packages (Wermund, 1961). Glauconite also occurs in association with quartz grains as a structureless, grain-supported mass.</p>
--	--	--

Table 3.2: Data on grain size and grain character for M5.45. Grain size, sorting, sphericity, roundness, and glauconite content are presented for Sites M27 - M29. It is also indicated if there is a relative increase or decrease in any parameter relative to its downdip counterparts. Data on grain size are presented in millimetres (mm) and has been calculated using GRADISTAT software (Blott and Pye, 2001). Sorting data are presented as a standard deviation (σ) and has been calculated using GRADISTAT software (Blott and Pye, 2001). Data on grain roundness and sphericity are presented according to the Krumbein scale and have been calculated using standard Excel software. Glauconite is given as a percentage of the total sediment volume (%) and has been adapted from qualitative estimates given by the Expedition 313 scientists. Accompanying the glauconite contents are notes on the interpreted origins of glauconite in each core site.

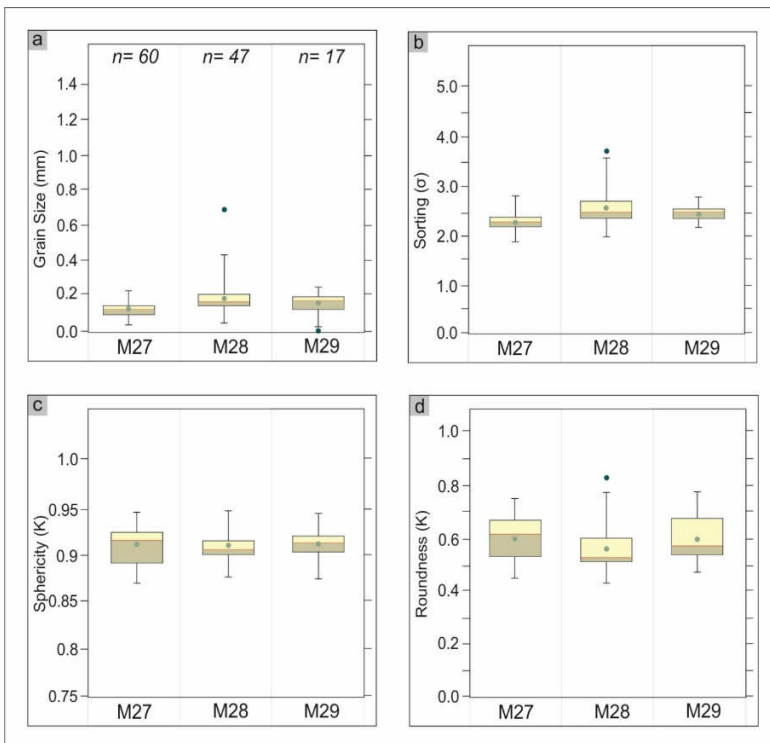


Figure 3.7 Box and whisker plots for Sequence m5.45 showing a) grain size, b) sorting, c) sphericity and d) roundness for Cores M27, M28, and M29. The horizontal red line indicates the median; the mean is shown as a green circle; the boundaries of the box indicate the 25th and 75th percentile; whiskers are minimum and maximum values and outliers are shown as blue circles. The number of samples is indicated by $n = x$ and is shown in Part 3.7a.

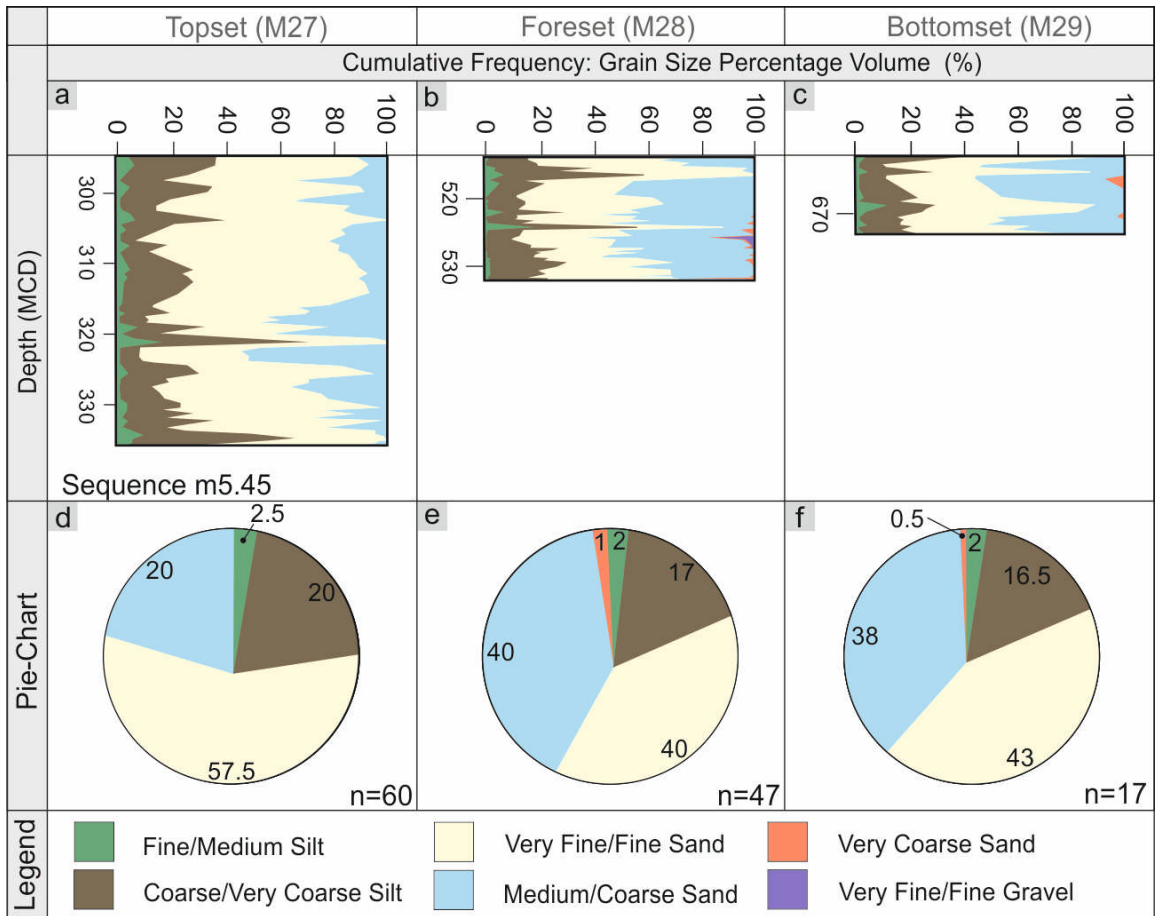


Figure 3.8: Grain-size cumulative frequency plot for topset (5a), foreset (5b), and bottomset (5c) deposits of Sequence m5.45. Axes are depth in metres composite depth (mcd) and grain size by percentage (%), respectively. Pie charts showing average grain-size composition for topset (4d), foreset (4e) and bottomset (4f) deposits. The percentage volume for each grain size is also indicated numerically. The number of samples is indicated by n = x.

3.5.3 Sequence m5.4

Trajectory analysis of Sequence m5.4 indicates a positive, rising trajectory (Fig. 2). In seismic profile, Sequence m5.4 displays relatively thin topset and bottomset deposits with a relatively thick foreset clastic wedge (Fig. 2), which at the point of core intersection are 23.8 m, 149.3 m, and 19.2 m in topset, foreset and bottomset locations, respectively (Fig. 2). The average grain size distribution profile of topset and foreset, deposits is dominated by three narrow peaks in grain size at 0.068 mm (very fine-grained sand), 0.14 mm (fine-grained sand), and 0.2 – 0.35 mm (fine- and medium-grained sand) (Fig. 3.4c). The average grain size distribution profiles remain relatively consistent from topset to foreset locations, i.e., there is little variation in the overall grain size distribution (Fig. 3.4c). This is shown by the median grain size, which varies by < 0.08 mm from topset to bottomset deposits (Fig. 3.9a). The average grain size distribution profile of the bottomset deposits is dominated by a large peak in very coarse-grained silt (Fig. 3.4c).

Sequence m5.4

Topset		Relative increase or decrease downdip	Foreset		Relative increase or decrease downdip	Bottomset	
Number of samples	30	increase	Number of samples	184	decrease	Number of samples	43
Mean grain size (mm)	0.113	increase	Mean grain size (mm)	0.131	decrease	Mean grain size (mm)	0.111
Median grain size (n25) (mm)	0.0836	increase	Median grain size (n25) (mm)	0.0992	decrease	Median grain size (n25) (mm)	0.0363
Median grain size (n50) (mm)	0.101	increase	Median grain size (n50) (mm)	0.121	decrease	Median grain size (n50) (mm)	0.0402
Median grain size (n75) (mm)	0.131	increase	Median grain size (n75) (mm)	0.17	decrease	Median grain size (n75) (mm)	0.206
Maximum grain size (mm)	0.271	increase	Maximum grain size (mm)	0.429	decrease	Maximum grain size (mm)	0.267
Minimum grain size (mm)	0.0446	decrease	Minimum grain size (mm)	0.0397	decrease	Minimum grain size (mm)	0.0329
Standard deviation (σ)	50	increase	Standard deviation (σ)	58	increase	Standard deviation (σ)	91
Mean sorting (σ)	2.3	increase	Mean sorting (σ)	2.2	constant	Mean sorting (σ)	2.2
Median sorting (n25) (σ)	2.5	increase	Median sorting (n25) (σ)	2.4	increase	Median sorting (n25) (σ)	2.3
Median sorting (n50) (σ)	2.4	increase	Median sorting (n50) (σ)	2.2	constant	Median sorting (n50) (σ)	2.2

Median sorting (n75)(σ)	2.2	increase	Median sorting (n75)(σ)	2	decrease	Median sorting (n75)(σ)	2.1
Maximum sorting (σ)	1.7	increase	Maximum sorting (σ)	1.6	decrease	Maximum sorting (σ)	1.7
Minimum sorting (σ)	2.7	decrease	Minimum sorting (σ)	3.8	increase	Minimum sorting (σ)	2.5
Standard deviation (σ)	0.2	increase	Standard deviation (σ)	0.3	decrease	Standard deviation (σ)	0.2
Mean sphericity (K)	0.92	decrease	Mean sphericity (K)	0.916	increase	Mean sphericity (K)	0.922
Median sphericity (n25) (K)	0.908	decrease	Median sphericity (n25) (K)	0.902	increase	Median sphericity (n25) (K)	0.892
Median sphericity (n50) (K)	0.922	decrease	Median sphericity (n50) (K)	0.917	increase	Median sphericity (n50) (K)	0.935
Median sphericity (n75) (K)	0.933	constant	Median sphericity (n75) (K)	0.933	increase	Median sphericity (n75) (K)	0.947
Maximum sphericity (K)	0.943	increase	Maximum sphericity (K)	0.962	decrease	Maximum sphericity (K)	0.959
Minimum sphericity (K)	0.888	decrease	Minimum sphericity (K)	0.78	increase	Minimum sphericity (K)	0.869
Standard deviation (σ)	0.02	constant	Standard deviation (σ)	0.02	increase	Standard deviation (σ)	0.03
Mean roundness (K)	0.655	decrease	Mean roundness (K)	0.622	increase	Mean roundness (K)	0.656
Median roundness (n25) (K)	0.593	decrease	Median roundness (n25) (K)	0.565	decrease	Median roundness (n25) (K)	0.551

Median roundness (n50) (K)	0.658	decrease	Median roundness (n50) (K)	0.627	increase	Median roundness (n50) (K)	0.698
Median roundness (n75) (K)	0.729	decrease	Median roundness (n75) (K)	0.675	increase	Median roundness (n75) (K)	0.731
Maximum roundness (K)	0.779	increase	Maximum roundness (K)	0.801	decrease	Maximum roundness (K)	0.782
Minimum roundness (K)	0.519	decrease	Minimum roundness (K)	0.293	increase	Minimum roundness (K)	0.475
Standard deviation (σ)	0.07	increase	Standard deviation (σ)	0.08	increase	Standard deviation (σ)	0.09
Average glauconite content (%)	~ 0.5	increase	Average glauconite content (%)	~ 1	increase	Average glauconite content (%)	~ 3
Maximum glauconite content (%)	2	increase	Maximum glauconite content (%)	4	increase	Maximum glauconite content (%)	30
Minimum glauconite content (%)	0	constant	Minimum glauconite content (%)	0	constant	Minimum glauconite content (%)	0
Glaucinite origin: Glaucinite, as a percentage volume of the total sediment composition, is negligible or entirely absent from this deposit. At the base of the deposit the glauconite content reaches a maximum of 2%. The glauconite is interpreted to be autochthonous in origin due to its presence within the burrows of			Glaucinite origin: Glaucinite, as a percentage volume of the total sediment composition, remains low or is entirely absent from this deposit. From the top of the unit to ~ 391 mcd, glauconite is present at low levels (< 4%); it is interpreted to be allochthonous in origin as a) it is found within the host sediment and the glauconite			Glaucinite origin: The glauconite content varies between 0 and ~ 10% of the total sediment composition within this deposit. The glauconite is largely concentrated within	

bioturbated sediment, as opposed to within the host sediment (Huggett and Gale, 1997).	grains have similar grain sizes to the surrounding detrital grains, indicating transport (Lebauer, 1964; Amorosi, 1997; Huggett and Gale, 1997)	scours and ripples (~ 660 mcd). The glauconite is interpreted to be predominantly allochthonous in origin due a) its presence within graded sequences (Wermund, 1961) and b) glauconite grains of up to ~ 1.5 mm are found within a silty matrix (Huggett and Gale, 1997).
--	---	--

Table 3.3: Data on grain size and grain character for M5.4. Grain size, sorting, sphericity, roundness, and glauconite content are presented for Sites M27 - M29. It is also indicated if there is a relative increase or decrease in any parameter relative to its downdip counterparts. Data on grain size are presented in millimetres (mm) and has been calculated using GRADISTAT software (Blott and Pye, 2001). Sorting data are presented as a standard deviation (σ) and has been calculated using GRADISTAT software (Blott and Pye, 2001). Data on grain roundness and sphericity are presented according to the Krumbein scale and have been calculated using standard Excel software. Glauconite is given as a percentage of the total sediment volume (%) and has been adapted from qualitative estimates given by the Expedition 313 scientists. Accompanying the glauconite contents are notes on the interpreted origins of glauconite in each core site.

Up-core grain size trends in topset deposits are dominated by fining-upward packages, typically ~ 2.5 m in thickness (Fig. 3.10a). These packages are associated with relatively clean quartz-rich sands, convex-up laminated sands (Fig. 3.3g), terrestrial organic matter, and shell fragments. Foreset deposits are dominated by very fine- and fine-grained sands (Figs. 3.3b, 3.10e). Up-core grain size trends in foreset deposits reveal numerous coarsening- and fining-upward packages, each typically ~ 7 m in thickness (Fig. 3.10b). Bottomset deposits show two silt-rich intervals (Figs. 3.3i, 3.10c), interbedded with thin glauconite-rich, cross-laminated sands (Hodgson et al., 2018).

Grain shape remains relatively similar throughout the depositional profile (Figs. 3.9c, d, Table 3.3), as sediment grains in topset, foreset and bottomset, deposits are highly spherical and rounded (Figs. 3.9c, d). Sorting increases downdip (Fig. 3.9b). Trajectory analysis of Sequence m5.3 indicates a steep rising trajectory (Fig. 3.2). At the point of core intersection, Sequence m5.3 has a thickness of 13.8 m, 39.8 m, and 40.9 m in topset, foreset, and bottomset locations respectively. In seismic profile, Sequence m5.3 has relatively thin topset deposits and relatively thick foreset and bottomset deposits (Fig. 3.2). The average grain size distribution

profile of topset deposits is dominated by very coarse-grained silt and very fine-grained sand (Fig. 3.4d).

Foreset and bottomset deposits are dominated by medium- and coarse-grained sands, (43% and 40% of the total sediment volume in foreset and bottomset deposits respectively; Fig. 3.11e, f). The average grain size distribution profiles of the foreset and bottomset deposits show very similar bimodal profiles, dominated by two broad peaks, corresponding to i) very coarse-grained silt and very fine-grained sand grain size classes, and ii) medium-grained sand grain size classes (Fig. 3.4d). The foreset deposits have a slightly coarser overall profile and contain more very coarse-grained sand and gravel than their bottomset counterparts (Fig. 3.4d). The foreset and bottomset average grain size distribution profiles show a downdip fining trend (Figs. 3.4d, 3.11), coincident with an increase in sorting (Fig. 3.12b) and a decrease in mean grain size (Fig. 3.12a, Table 3.4).

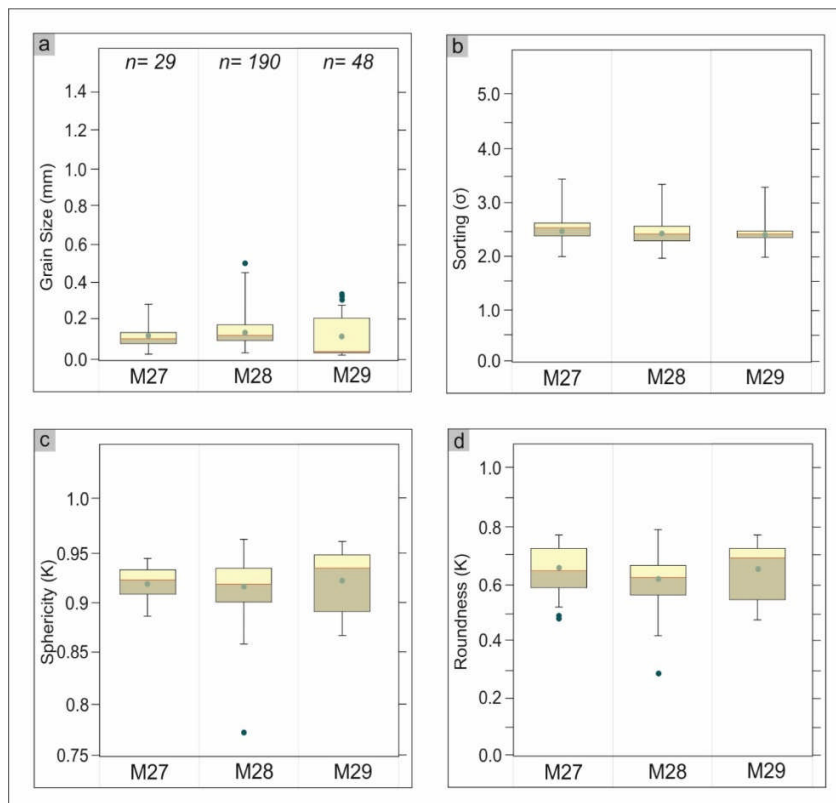


Figure 3.9: Box and whisker plots for Sequence m5.4 showing a) grain size, b) sorting, c) sphericity and d) roundness for Cores M27, M28, and M29. The horizontal red line indicates the median; the mean is shown as a green circle; the boundaries of the box indicate the 25th and 75th percentile; whiskers are minimum and maximum values and outliers are shown as blue circles. The number of samples is indicated by $n = x$ and is shown in Part 3.9a.

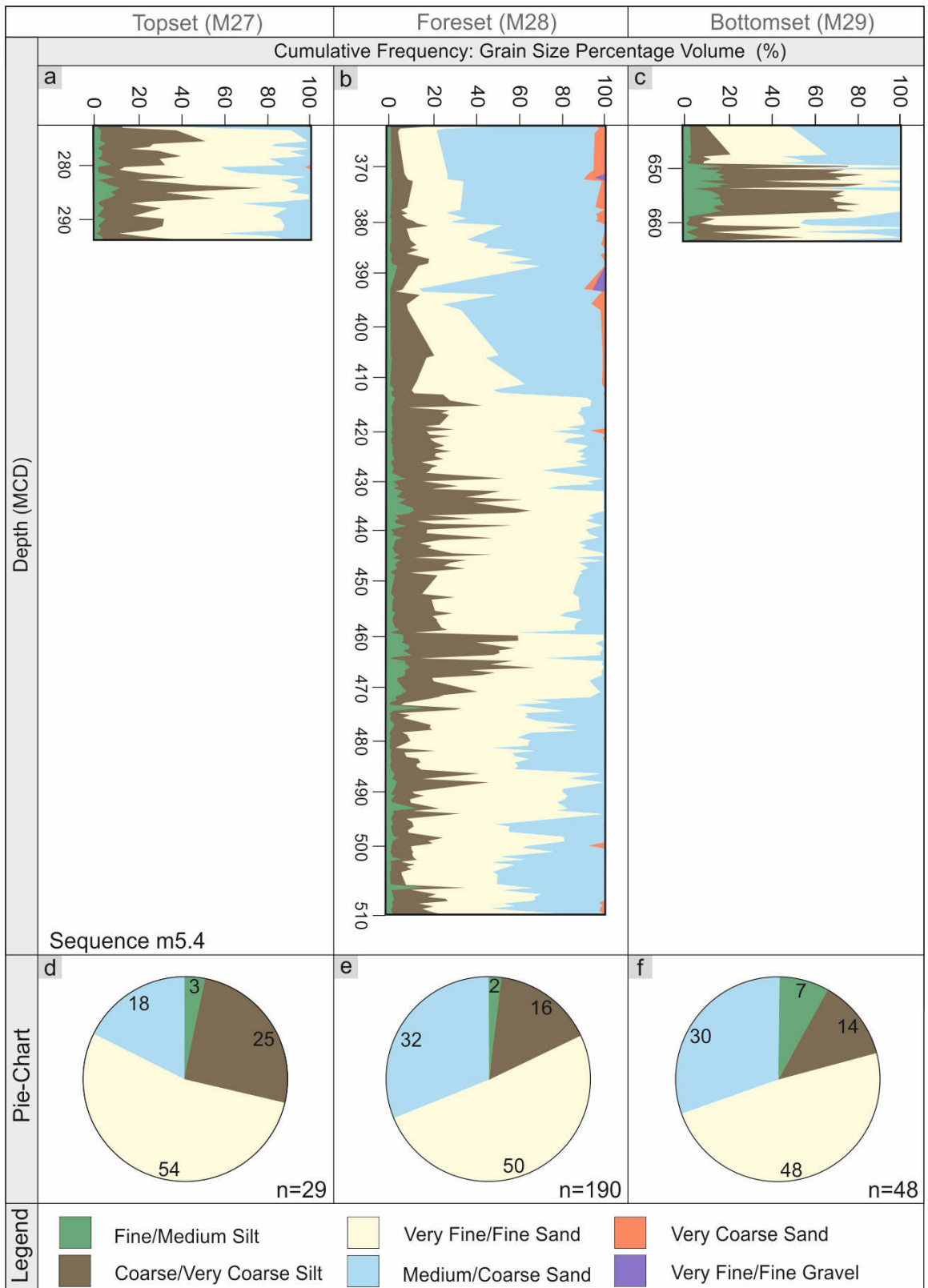


Figure 3.10: Grain size cumulative frequency plot for topset (5a), foreset (5b) and bottomset (5c) deposits of Sequence m5.4. Axes are depth in metres composite depth (mcd) and grain size by percentage (%), respectively. Pie charts showing average grain size composition for topset (4d), foreset (4e), and bottomset (4f) deposits. The percentage volume for each grain size is also indicated numerically. The number of samples is indicated by $n = x$.

3.5.4 Sequence m5.3

Topsets show no obvious trend in up-core grain size and are consistently silt-dominated (Figs. 3.3j, 3.11a). Foreset deposits are dominated by ~ 1 m thick, very coarse sand- and gravel-rich intervals (Fig. 3.11b), which typically contain ~ 15% very coarse-grained sand and gravel by percentage volume (Fig. 3.11e). These coarser-grained intervals are overlain by relatively fine-grained units, which are typically < 1 m thick and contain 20 – 25% silt by percentage volume (Fig. 3.11b). The sedimentary structures associated with these intervals are quartz- and glauconite-rich (Fig. 3.3k), normally graded or cross-stratified sand beds. Bottomset deposits show broadly similar up-core grain size dispersal patterns to those observed in foreset deposits (Fig. 3.11c). However, the coarse intervals are thinner (< 0.7 m) and have a finer grain size composition relative to the coarse intervals observed in foreset deposits (< 0.7 m). The coarse intervals are composed of very coarse-grained sand, with minor gravels (Figs. 3.3l, 3.10c). The mean grain character profile varies longitudinally between parameters. Grains are decreasingly spherical downdip (Fig. 3.12c, Table 3.4). However, grain roundness shows that the most angular grains are retained in the foreset deposits, as there is an increase in roundness from the foreset to bottomset deposits (Fig. 3.12-D, Table 3.4).

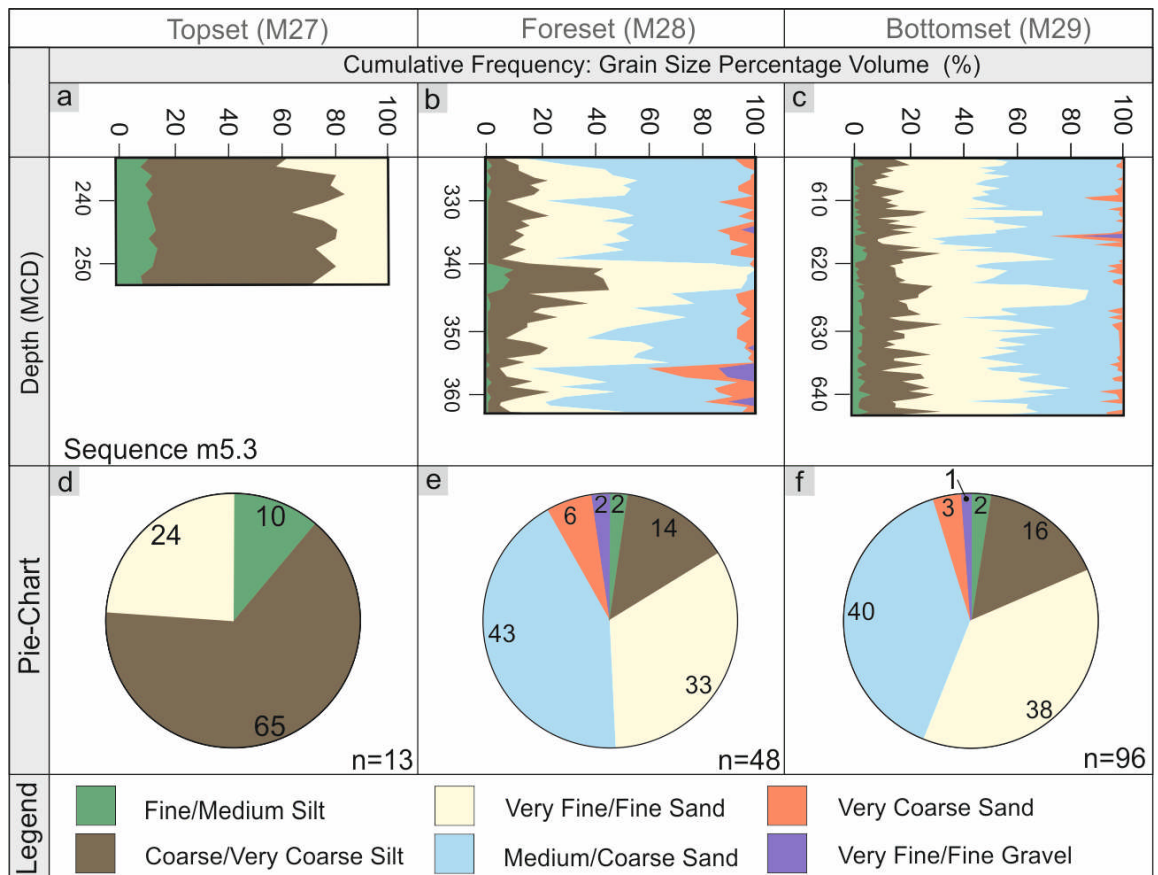


Figure 3.11: Grain-size cumulative frequency plot for topset (5a), foreset (5b) and bottomset (5c) deposits of Sequence m5.3. Axes are depth in metres composite depth (mcd) and grain size by percentage (%), respectively. Pie charts showing average grain-size for topset (4d), foreset (4e) and bottomset (4f) deposits. The percentage volume for each grain size is also indicated numerically. The number of samples is indicated by $n = x$.

Sequence m5.3							
Topset		Relative increase or decrease downdip	Foreset		Relative increase or decrease downdip	Bottomset	
Number of samples	13	increase	Number of samples	46	increase	Number of samples	96
Mean grain size (mm)	0.038	increase	Mean grain size (mm)	0.22	decrease	Mean grain size (mm)	0.19
Median grain size (n_{25}) (mm)	0.035	increase	Median grain size (n_{25}) (mm)	0.16	constant	Median grain size (n_{25}) (mm)	0.16
Median grain size (n_{50}) (mm)	0.37	increase	Median grain size (n_{50}) (mm)	0.19	decrease	Median grain size (n_{50}) (mm)	0.18
Median grain size (n_{75}) (mm)	0.04	increase	Median grain size (n_{75}) (mm)	0.25	decrease	Median grain size (n_{75}) (mm)	0.22
Maximum grain size (mm)	0.046	increase	Maximum grain size (mm)	0.68	decrease	Maximum grain size (mm)	0.37
Minimum grain size (mm)	0.034	increase	Minimum grain size (mm)	0.066	increase	Minimum grain size (mm)	0.077

			size (mm)				
Standard deviation (σ)	3	increase	Standard deviation (σ)	109	decrease	Standard deviation (σ)	53
Mean sorting (σ)	2	decrease	Mean sorting (σ)	2.7	increase	Mean sorting (σ)	2.6
Median sorting ($n25$) (σ)	1.9	decrease	Median sorting ($n25$) (σ)	2.6	increase	Median sorting ($n25$) (σ)	2.3
Median sorting ($n50$) (σ)	2	decrease	Median sorting ($n50$) (σ)	2.8	increase	Median sorting ($n50$) (σ)	2.6
Median sorting ($n75$) (σ)	2.1	decrease	Median sorting ($n75$) (σ)	3.1	increase	Median sorting ($n75$) (σ)	2.9
Maximum sorting (σ)	2.2	decrease	Maximum sorting (σ)	3.7	decrease	Maximum sorting (σ)	4.2
Minimum sorting (σ)	1.9	decrease	Minimum sorting (σ)	2.2	increase	Minimum sorting (σ)	1.9
Standard deviation (σ)	0.1	increase	Standard deviation (σ)	0.3	increase	Standard deviation (σ)	0.4
Mean sphericity (K)	0.947	decrease	Mean sphericity (K)	0.913	decrease	Mean sphericity (K)	0.907
Median sphericity ($n25$) (K)	0.943	decrease	Median sphericity ($n25$) (K)	0.905	decrease	Median sphericity ($n25$) (K)	0.899

Median sphericity ($n50$) (K)	0.949	decrease	Median sphericity ($n50$) (K)	0.912	decrease	Median sphericity ($n50$) (K)	0.907
Median sphericity ($n75$) (K)	0.951	decrease	Median sphericity ($n75$) (K)	0.917	decrease	Median sphericity ($n75$) (K)	0.914
Maximum sphericity (K)	0.954	increase	Maximum sphericity (K)	0.946	decrease	Maximum sphericity (K)	0.944
Minimum sphericity (K)	0.937	decrease	Minimum sphericity (K)	0.898	decrease	Minimum sphericity (K)	0.873
Standard deviation (σ)	0.0006	increase	Standard deviation (σ)	0.01	constant	Standard deviation (σ)	0.01
Mean roundness (K)	0.732	decrease	Mean roundness (K)	0.545	increase	Mean roundness (K)	0.605
Median roundness ($n25$) (K)	0.718	decrease	Median roundness ($n25$) (K)	0.523	increase	Median roundness ($n25$) (K)	0.533
Median roundness ($n50$) (K)	0.737	decrease	Median roundness ($n50$) (K)	0.538	decrease	Median roundness ($n50$) (K)	0.586
Median roundness ($n75$) (K)	0.748	decrease	Median roundness ($n75$) (K)	0.559	increase	Median roundness ($n75$) (K)	0.664
Maximum roundness (K)	0.756	decrease	Maximum roundness (K)	0.719	increase	Maximum roundness (K)	0.901

			roundness (K)			roundness (K)	
Minimum roundness (K)	0.68	decrease	Minimum roundness (K)	0.483	decrease	Minimum roundness (K)	0.47
Standard deviation (σ)	0.02	increase	Standard deviation (σ)	0.04	increase	Standard deviation (σ)	0.08
Average glauconite content (%)	~ 1	increase	Average glauconite content (%)	~ 20	increase	Average glauconite content (%)	~ 40
Maximum glauconite content (%)	3	increase	Maximum glauconite content (%)	40	increase	Maximum glauconite content (%)	90
Minimum glauconite content (%)	0	constant	Minimum glauconite content (%)	0	constant	Minimum glauconite content (%)	0
Glaucanite origin: The glauconite within this deposit is interpreted to be autochthonous in origin due to the concentration of glauconite within bioturbated sediment (Huggett and Gale, 1977).			Glaucanite Origin: Between the top of the sequence and ~ 552 mcd the glauconite content varies significantly between 0 - 40%. The majority of glauconite is interpreted to be predominantly allochthonous due to a) the presence of glauconite within a structureless glauconite-rich sand, in which glauconite grains of up to ~ 4 mm are found within a silty matrix (Huggett and Gale, 1997) and b) at a depth of ~ 332 mcd glauconite grains are found within low-angle cross-beds			Glaucanite Origin: The glauconite within this deposit is interpreted to be predominantly allochthonous in origin, due to a) the presence of glauconite within cross-bedded units and upwardly fining units (Wermund, 1961). Between the depths of ~ 643 - 640 mcd the allochthonous	

	(Wermund, 1961). There is a minor contribution from autochthonous glauconite.	glauconite content reaches 90% of total sediment volume, where glauconite grains and glauconite fragments are found within a silty matrix (Huggett and Gale, 1997).
--	---	---

Table 3.4: Data on grain size and grain character for M5.3. Grain size, sorting, sphericity, roundness, and glauconite content are presented for Sites M27 - M29. It is also indicated if there is a relative increase or decrease in any parameter relative to its downdip counterparts. Data on grain size are presented in millimetres (mm) and has been calculated using GRADISTAT software (Blott and Pye, 2001). Sorting data are presented as a standard deviation (σ) and has been calculated using GRADISTAT software (Blott and Pye, 2001). Data on grain roundness and sphericity are presented according to the Krumbein scale and have been calculated using standard Excel software. Glauconite is given as a percentage of the total sediment volume (%) and has been adapted from qualitative estimates given by the Expedition 313 scientists. Accompanying the glauconite contents are notes on the interpreted origins of glauconite in each core site.

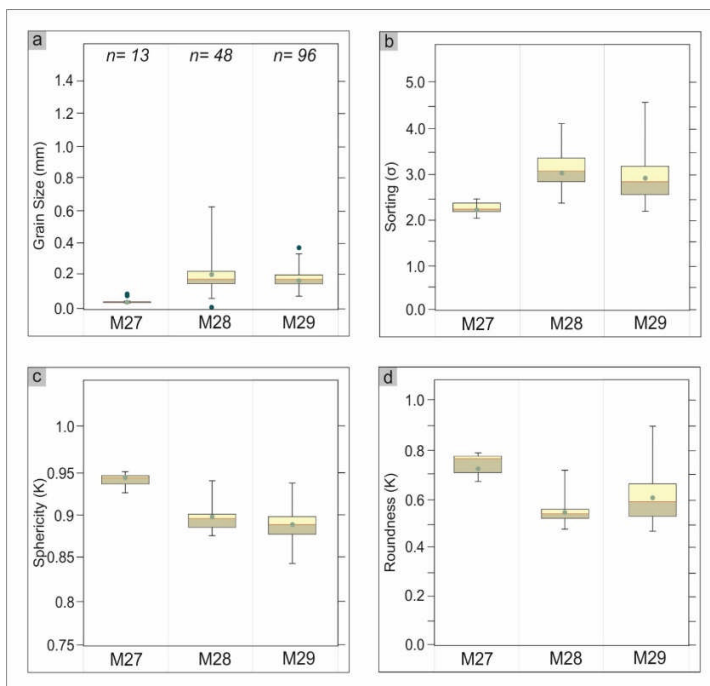


Figure 3.12: Box and whisker plots for Sequence m5.3 showing a) grain size, b) sorting, c) sphericity and d) roundness for Cores M27, M28, and M29. The horizontal red line indicates the median; the mean is shown as a green circle; the boundaries of the box indicate the 25th and 75th percentile; whiskers are minimum and maximum values and outliers are shown as blue circles. The number of samples is indicated by $n = x$ and is shown in Part 3.12a.

3.5.5 Clinotherm Groupings

The four clinotherm sequences (m5.3, m5.4, m5.45, and m5.7) have been separated into two types according to shared geometry in reflection seismic, grain character, and sedimentology.

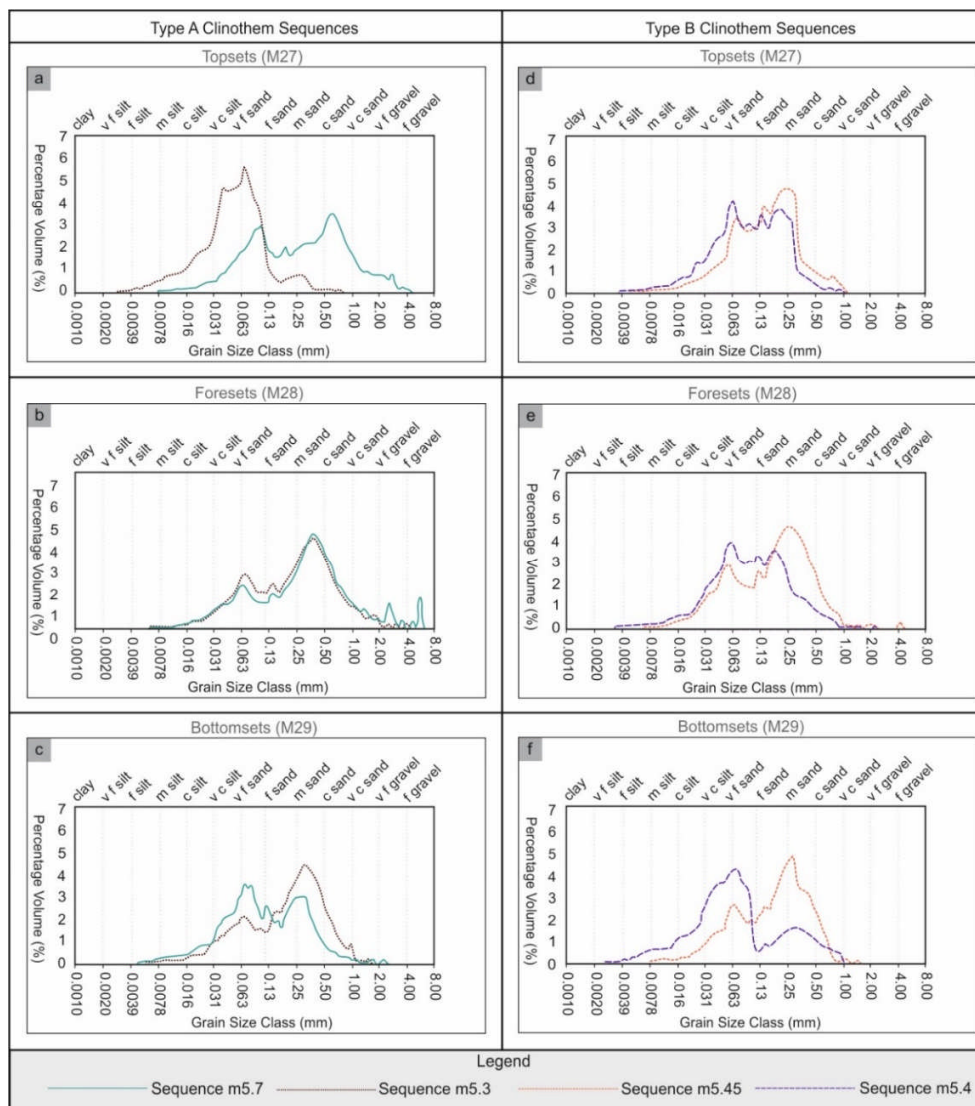


Figure 3.13: Plots of average grain size distribution comparing the topset, foreset, and bottomset deposits of Type A and Type B clinothems. Axes are percentage volume (%) and grain size (mm), respectively. Alongside the numerical grain size classes are the descriptive grain size classes modified from Udden (1914) and Wentworth (1922). Figures 9a, b and c compare the topset, foreset, and bottomset deposits of Type A clinothems respectively. Figures 9d, e and f compare the topset, foreset, and bottomset deposits of Type B clinothems respectively.

3.5.5.1 Type A Clinothem Sequences

Sequences m5.7 and m5.3 constitute Type A clinothems. Core descriptions show that Type A clinothems display the following attributes: i) a lack of any convex-upward laminae (hummocky cross-stratification), low-angle cross-beds (swaley cross-stratification) or symmetrical ripple lamination; ii) cut-and-fill structures overlain by coarse sand and associated with basal gravels (e.g., Sequence m5.3, Core M27; Fig. 3.6a); iii) micaceous sands (e.g., Sequence m5.7, Core M27; Fig. 3.3j); iv) terrestrially derived plant material (e.g., Sequence m5.7, Core M27; Fig. 3.3j); v) foreset channel-fills (e.g., Sequence m5.3, Core M28, 340-344 mcd; Fig. 3.11b) and; v) bottomset deposits dominated by coarse-grained turbidites

and debrites (Mountain et al., 2010; Miller et al., 2013a; Hodgson et al., 2018). The core expression of Type A clinothems shows clear diagnostic characteristics consistent with deposition under a river-dominated topset process-regime; this interpretation is in agreement with that of Mountain et al., (2010). Representative core photos are shown in Figure 3.3.

Sequences m5.7 and m5.3 share similar seismic and core expressions, and grain characters, despite contrasting position in clinoform rollover trajectories (i.e., Sequence m5.7 under a falling trajectory and Sequence m5.3 under a rising trajectory; Fig. 3.2). Type A clinothem sequences have a seismic architecture dominated by relatively thin (14 – 25 m) topset deposits and thickening downdip of foreset (40 – 44 m) and bottomset (21 – 41 m) deposits (Figs. 3.2, 3.4, 3.11).

Type A clinothem sequences share these common attributes: i) average grain size distributions that fine downdip (Figs. 3.4a, b); ii) characteristic bimodal foreset and bottomset grain size distribution plots (Fig. 3.13b); iii) the greatest volume of sand-grade sediment stored in foreset deposits (Figs. 3.6, 3.11); iv) foreset deposits dominated by ~ 1 m-thick very coarse sand and gravel packages overlain by relatively silt-rich packages (Figs. 3.6, 3.11); v) the coarsest (> 1.5 mm) and most angular grains stored in foreset deposits (Figs. 3.5a, d, 3.12a, d); vi) an increase in sorting downdip (Figs. 3.5b, 3.12b, Tables 3.1, 3.4); and vii) glauconite- and quartz-rich structureless sands in bottomsets (Figs. 3.3c, l).

3.5.5.2 Type B Clinothem Sequences

Sequences m5.45 and m5.4 constitute Type B clinothems. Core descriptions show that Type B clinothems display the following attributes: i) widespread convex-upward laminae (hummocky cross-stratification, e.g., Sequence m5.45, Core M27; Fig. 3.3), low-angle cross-beds (swaley cross-stratification) and symmetrical ripple lamination; ii) interbedded fine- and very fine-grained sands (e.g., Sequence m5.4, Core M28; Fig. 3.3h); iii) significant amounts of shell debris; iv) moderate to heavy bioturbation; and v) a lack of substantial foreset or bottomset deposits indicative of gravity-flow origin (Mountain et al., 2010; Miller et al., 2013a; Miller et al., 2013b; Hodgson et al., 2018). The core expression of Type B clinothems shows clear diagnostic characteristics consistent with deposition under a wave-dominated topset process-regime; this interpretation is in agreement with that of Mountain et al., (2010). Representative core photos are shown in Figure 3.3.

Sequences m5.45 and m5.4 share similar core expressions and grain characters; additionally, both Type B clinothems show consistently rising clinoform rollover trajectories. The seismic architecture of Type B clinothems is dominated by relatively thin topset (23 – 42 m) and

bottomset (12 – 19 m) deposits, with significantly thicker foreset (~ 150 m) deposits (Figs. 3.2, 3.8, 3.10).

With reference to the statistical grain character data presented in this paper, Type B clinothems share the following attributes: i) trimodal average grain size distribution profiles; ii) grain size compositions that vary by less than 10% along the longitudinal profile, i.e., limited downdip change in the overall grain size composition and distribution (Figs. 3.4b, c, 3.8, 3.10); iii) limited downdip change in grain character (Figs. 3.7c, d, 3.9c, d), including a < 0.04K change in sphericity and roundness (Tables 3.2, 3.3); iv) the highest mud content within topsets (~ 25%) (Figs. 3.8, 3.10) and v) coarsening- and fining-upward packages in foresets, although these are more numerous and better developed in Sequence m5.4 (Figs. 3.8b, 3.10b).

3.6 Discussion

3.6.1 Controls on Differences between Type A and B Clinothems

Clinothem Types A and B differ fundamentally in many aspects of grain character. Differences in sediment character are controlled by the interplay of accommodation, climate, sediment supply, provenance, and dominant topset process-regime. On the ocean-facing passive-margin location of New Jersey, changes in accommodation are closely tied to changes in eustatic sea level (Browning et al., 2013). Eustasy is largely discounted as a controlling factor to explain differences between Type A and Type B clinothems because each clinothem sequence represents one complete sea-level cycle and associated regression to transgression (Miller et al. 2013a). As such, the effects of eustasy should be common to each sequence. However, it is acknowledged that sea-level fluctuations are not necessarily uniform in amplitude or rate, which could impact differences in clinothem development. A similar argument can be made for climate, as each clinothem sequence theoretically records one complete climatic cycle. However, this argument pertains to regional climatic regime and does not necessarily account for the effects of variability in local climate, which may influence rainfall and consequently sediment supply rates.

Rates of sediment supply have been estimated for Sequences m5.3 (Type A), and Sequences m5.4 and m5.45 (Type B), using integrated strontium-isotope stratigraphy and biostratigraphy age – depth plots (Browning et al., 2013). However, there are not sufficient data available for Sequence m5.7 (Type A) due to poor age constraints. Comparisons between sediment supply rates of sequences were made by averaging sedimentation rates across clinothems. Results indicate that in the bottomset deposits of Sequences m5.4 and m5.45 (Type B), minimum rates of deposition were 96 m/Myr. Similarly, Sequence m5.3 (Type A) had a minimum rate of 100 m/Myr. Topset deposits indicate that Sequences m5.45, m5.4 and

m5.3 (Type A and B) had the same minimum rates of deposition of 43 m/Myr. This suggests that rates of sediment supply did not differ significantly during deposition of clinothem Types A and B in topset and bottomset locations, and therefore that sediment supply rates did not cause the observed differences in grain character between Type A and Type B clinothems. The lack of variability in sediment supply rates also supports the assertion that accommodation and climate did not differentially impact Type A and B clinothems significantly. However, it must be acknowledged that there are significant age-control error margins and there is a lack of data for Sequence m5.7 (Type A) and also that the comparison does not take into account along-strike variability.

Accepting that the Type A and B clinothems appear to have developed under comparable allogenic forcings (i.e., with respect to accommodation and sediment supply) and prograded during the Burdigalian (Browning et al., 2013), a period of time without a recognized large-scale climatic perturbation, the remaining forcing mechanism to consider is that of the dominant process-regime. The expression in core of the four clinothems studied in this investigation permits confident distinction of the dominant process-regime during the development of both Type A and Type B clinothems, which were river- and wave-dominated, respectively (Fig. 3.3). It is therefore suggested that the difference in the dominant topset process-regime had significant bearing on the differences in sediment character and depositional character observed between and within Type A and Type B clinothems.

3.6.2 Lateral Variability in Process-Regime

The dataset presented and discussed, which comprises a 2-D dip-parallel transect of seismic reflection data and three cores that intersect the topset, foreset, and bottomset deposits of prograding clinothems, has both strengths and weaknesses. The New Jersey clinothems are rare examples where the sedimentological and stratigraphic characteristics of coeval topset, foreset, and bottomset deposits have been documented in successive chronostratigraphically constrained clinothems. No previous dataset of such detailed quantitative grain character analysis on genetically linked clinothems has been presented.

There is a network of 2-D seismic reflection lines that allow the 3-D architecture of the clinothems to be constrained (Monteverde et al. 2008). However, the core dataset is from a single 2-D transect. Modern and ancient shallow-marine systems can exhibit high levels of lateral variability, even over relatively short distances of a few hundreds of meters, related to the relative importance of fluvial, wave, and tidal processes (Ta et al., 2002; Bhattacharya and Giosan, 2003; Ainsworth et al., 2008; 2011; Vakarelov and Ainsworth, 2013; Olariu, 2014; Jones et al. 2015). Lateral changes in the process-regime could impact the timing of sand

delivery into the deeper basin (Madof et al., 2016), the location of coarse-grained deposits (Carvajal and Steel 2009; Koo et al., 2016), and the spatial distribution of grain character of the foresets and bottomsets. For example, a wave-dominated system might transition laterally to a river-dominated system in the topsets, but downdip of the wave-dominated system a fan fed by the river-dominated system could be intersected. Nonetheless, the dataset present here has permitted for the first time high-resolution quantitative assessment of grain character to be discussed in relation to clinoform trajectory and topset process-regime. Future investigations into the interplay of lateral variability in process-regime and distribution of grain character will require exceptional exhumed systems with 3-D control, or integrated subsurface datasets of 3-D reflection seismic data and additional research core holes.

3.6.3 Interaction of Shelf Process-regime and Clinoform Rollover Trajectory

3.6.3.1 Type A Clinothem Sequences

Based on core observations, the Type A clinothems (Sequence m5.7 and m5.3) are interpreted to be river-dominated, although lateral variability in process-regime as a control on sediment distribution to the foreset and bottomsets cannot be discounted (e.g., Ainsworth et al., 2011; Olariu, 2014; Jones et al. 2015; Rossi and Steel, 2016). Type A clinothems (river-dominated; Fig. 3.14a) show variability in their clinoform rollover trajectories, such that Sequence m5.7 has a rising trajectory and Sequence m5.3 has a falling trajectory (Fig. 3.2). However, both of the documented Type A clinothems have foreset and bottomset deposits that contain substantial quantities of coarse-grained sediment (Figs. 3.4, 3.11). This indicates that the downdip transport of coarse-grained sediment can occur under both falling and rising clinoform rollover trajectories, in Type A clinothem sequences. This finding would not be predicted by applying conventional sequence stratigraphic models and clinoform trajectory analyses (e.g., Steel and Olsen, 2002; Johannessen and Steel, 2005; Helland-Hansen and Hampson, 2009). In fact, the grain size data presented here show a greater overall proportion of coarse-grained sediment in Sequence m5.3 (rising trajectory) relative to Sequence m5.7 (falling trajectory). The occurrence of coarse-grained sediment in foreset and bottomset deposits implies that a river-dominated process-regime at the clinoform rollover may be a more important factor in determining the delivery of coarse-grained sediment than clinoform trajectory alone, in agreement with Dixon et al. (2012a).

In addition to having different clinoform rollover trajectories, the topset deposits of Sequences m5.7 and m5.3 also differ in grain size composition. Sequence m5.7 has a silt-rich base (355 – 361 mcd), which progressively coarsens upwards, to contain ~ 20% very coarse sand and gravel by percentage volume (336 – 355 mcd) (Fig. 3.4a). By contrast, the topset

deposits of Sequence m5.3 are dominated by silt-prone sediments and lack the coarse-grained sediment components observed in Sequence m5.7 (Fig. 3.11a). The variable nature of the topset deposits of Type A clinothem sequences may reflect along-strike variability in depositional environments of river-dominated process-regimes (Fig. 3.14a); examples of such lateral variability in shelf systems is documented in both modern and ancient delta systems (e.g., Ta et al., 2002; Gani and Bhattacharya, 2007; Carvajal and Steel 2009; Olariu, 2014; Li et al., 2015). Alternatively, or in addition to this, the inter-sequence topset grain size variability may reflect erosive conditions landward of the clinoform rollover, such that the upper topset deposits of Sequence m5.3 may have been eroded during regression or transgression, removing the coarser sediment fractions.

Erosive conditions landward of the clinoform rollover during regression is supported by the presence of significant volumes of allochthonous glauconite in the foreset and bottomset deposits of both Type A clinothem sequences (Hodgson et al., 2018), which can form up to 90% of the total sediment volume (Tables 3.1, 3.4). The presence of reworked glauconite (likely to be originally formed in transgressive shoreface sands in topset environments) in downdip environments is suggestive of erosive conditions in the topset, such that shallow-water glauconite grains are entrained and transported into deeper-water settings. The glauconite-bearing mud-prone sands, which are poorly sorted and poorly stratified, are interpreted to be debrites (debris-flow deposits; Mulder and Alexander, 2001) intercalated with thin turbidites (Hodgson et al., 2018). A predominantly debritic flow regime is further evidenced by the presence of pristine benthic foraminifera and thin-walled articulated shells scattered in the glauconite-bearing mud-prone sands, suggesting a cohesive flow with minimal internal turbulence (see Hodgson et al., 2018). Similar sediment transport processes for Type A clinothem sequences beyond the clinothem rollover is supported by the similar grain size distributions (Figs. 3.13b, c), grain size patterns (Figs. 3.4, 3.11) and core lithologies observed in the foreset and bottomset deposits of Type A clinothem sequences (Fig. 3.3). Despite evidence for debris-flow and turbidity-current processes in operation in the Type A clinothem sequences, seismic and core data do not support the presence of any major incisional features on the clinoform rollover (Hodgson et al., 2018). This somewhat disagrees with conventional models, which are based on the argument that river-dominated systems have the ability to rapidly prograde across the shelf and form large fluvial networks that incise the clinoform rollover and transfer significant volumes of coarse-grained sediment into bottomset deposits (e.g., Vail et al., 1977; Van Wagoner et al., 1988; Posamentier et al., 1992; Johannessen and Steel, 2005; Carvajal and Steel, 2006; Catuneanu et al., 2009; Sanchez et al., 2012). In this instance, the lack of any observable large incisional features on the clinoform

rollover (Fig. 2.2) instead suggests the presence of a network of smaller sediment distributary channels (Hodgson et al., 2018).

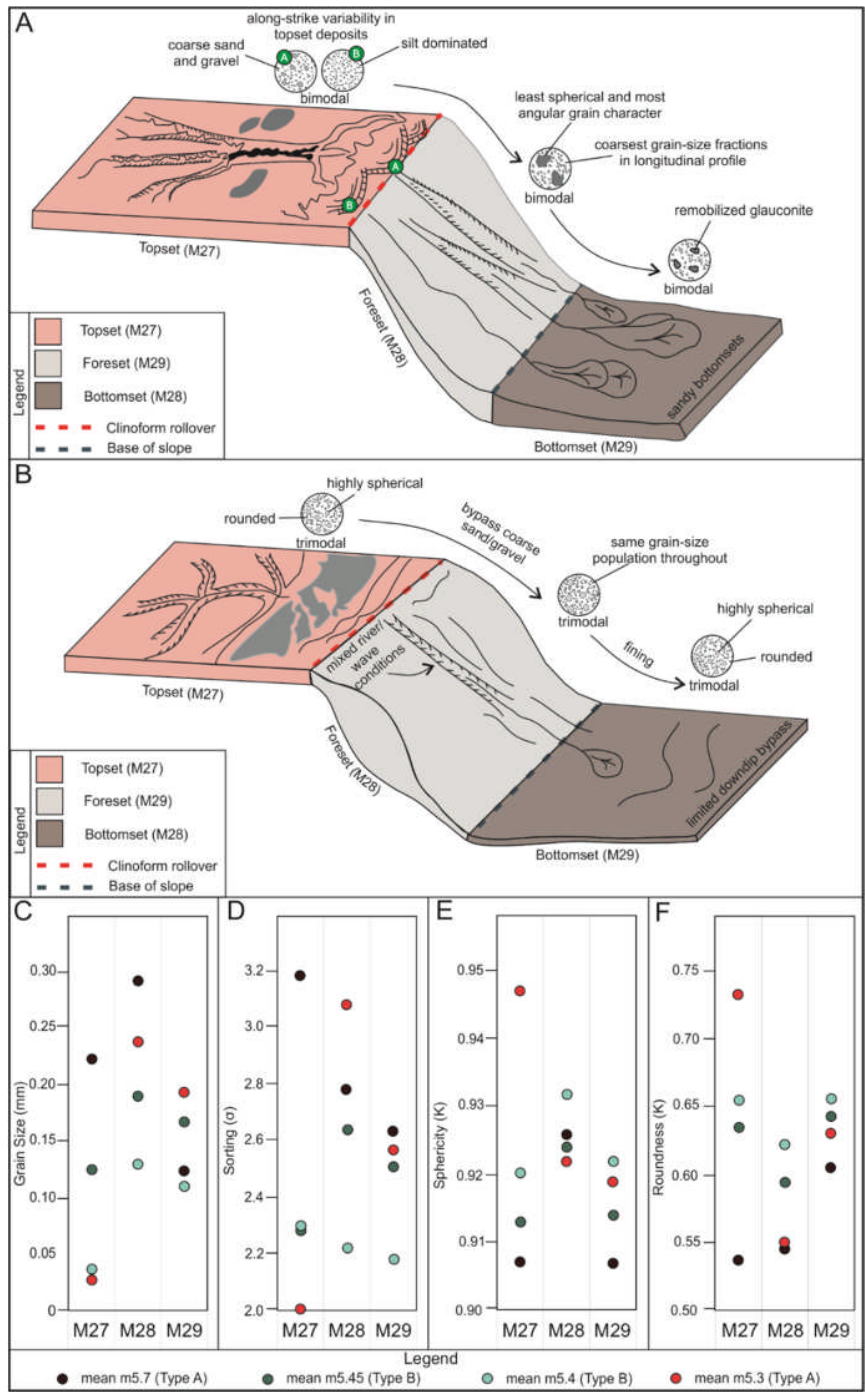


Figure 3.14: Idealised Type A and B clinothem sequences and associated downdip grain character changes. Part 3.14a shows an idealised Type A, river-dominated clinothem sequence. The topset illustrates a delta front containing glauconite-rich perched sands, which feed sandy foreset and bottomset deposits. The topset also illustrates the along-strike variability in the depositional environments of river-dominated clinothems. Part 3.14b shows an idealised Type B, wave-dominated clinothem sequence. The topset illustrates a characteristic wave-dominated shoreface. The delta front is dominated by longshore sediment drift, which prevents significant transport of sediment into bottomset deposits. The feeder channel illustrates episodic returns to river-dominated conditions, as observed in Sequence m5.45. c) Mean grain size, shown in millimetres, for Types A and B clinothems in Cores M27 – M29. d) Mean sorting, shown according to geometric Folk and Ward (1957) graphical measures, for Types A and B clinothem sequences in Cores M27 – M29. e) Mean sphericity, shown according to the Krumbein Scale (1941), for Types A and B clinothems in Cores M27 – M29. f) Mean roundness, shown according to the Krumbein Scale (1941), for Types A and B clinothems in Cores M27 – M29.

The fluvial distributary-channel network, supplying sediment to bottomset deposits, was likely to be active during periods of high sediment discharge (*sensu* Carvajal and Steel, 2006), and might have been associated with river flooding, storms, or combined events. However, the lack of evidence of subaerial exposure of the clinoform rollover (Mountain et al., 2010), suggests that river systems may not have transferred sediment directly into foreset and bottomset deposits. Instead river flooding, storm, or combined events may have triggered clinoform-rollover sediment failure, remobilizing glauconite- and quartz-rich sediment temporarily stored in topset deposits (*sensu* Chen et al., 2018). This mixed supply system may account for the consistent bimodal nature of Type A foreset and bottomset deposits (Fig. 3.13b, c), insofar as the very coarse-grained silt and very fine-grained sand component may reflect direct suspended riverine sediment discharge and the medium- and coarse-grained sand may reflect transient deposition of clinoform-rollover sands.

The bimodality of grain size in Type A clinothems highlights a paucity of grain size fractions spanning very fine to fine sand (0.088 – 0.18 mm) (Fig. 3.13b, c). This may reflect a scarcity of these grain size classes in the hinterland source area, i.e., these grain size classes are not delivered to the continental shelf. Alternatively, the absence of these grain sizes may reflect selective sediment bypass, such that these grain size fractions were preferentially bypassed into deeper-water than that sampled by Core M29 (*sensu* Stevenson et al., 2015).

This study indicates that, although the delivery of coarse-grained sediment can take place in river-dominated conditions under both rising and falling trajectories, fluvial entrenchment of the clinoform rollover is not required (e.g., Ryan et al., 2009; Dixon et al., 2012a). However, the lack of clinoform rollover incision may affect sediment distribution in the system. This is expressed in the longitudinal grain character profile, insofar as smaller distributary networks do not have the necessary energy to transport the coarsest-sediment fractions into bottomset deposits. This results in the largest, most angular grains being deposited within foresets (Fig. 3.14c, f).

3.6.3.2 Type B Clinothem Sequences

Type B clinothems (Sequences m5.45 and m5.4) consistently have rising clinof orm rollover trajectories (Fig. 3.2) and are characterised by wave-dominated process-regimes (Mountain et al., 2010; Fig. 3.14b). We observe relatively thin (< 20 m in thickness) bottomset deposits (Fig. 3.2), which contain no gravel and < 0.5 % coarse sand by percentage volume. This is interpreted to indicate limited bypass of coarse-grained sediments into bottomset deposits (Figs. 3.8, 3.10). The absence of coarse-grained sediment in bottomset deposits also reflects the lack of coarse-grained sediment fractions throughout the Type B depositional profile as whole (Figs. 3.8, 3.10). This suggests that, under wave-dominated conditions, the coarser sediment fractions are redistributed by shore-parallel processes, spreading coarse-grained sand over the nearshore margin. Thus, open-sea conditions under wave-dominated processes inhibit the transport of coarse-grained sediment to the clinof orm rollover, reducing the potential for downdip sediment transport. These observations conform to conventional sequence stratigraphic and rollover-trajectory models that predict limited bypass of coarse-grained sediment downdip under these circumstances, with preferential retention of sediment within shelf environments (Steel and Olsen, 2002; Deibert et al., 2003; Johannessen and Steel, 2005; Carvajal and Steel, 2009), and the development of shore-parallel sand bodies (e.g., Davis and Hayes, 1984; Bhattacharya and Giosan, 2003). Consequently such regimes have little potential to generate incisional features on the clinof orm rollover, limiting downdip transfer of coarse-grained sediment (Sydow and Roberts, 1994; Johannessen and Steel, 2005; Peng et al., 2017), provided that no canyon intersects the longshore-drift zone (Covault et al., 2007; Boyd et al., 2008; Dixon et al., 2012b).

The depositional profiles of Type B clinothems are dominated by very fine- and fine-grained sands, which are highly spherical and rounded relative to Type A river-dominated clinothems (Fig. 3.14e, f). This likely reflects wave-reworking and longshore-drift processes in the topsets of wave-dominated clinothems, which produce relatively clean shoreface sands (e.g., Roy et al., 1994; Bowman and Johnson, 2014). Grain rounding by additional wave resuspension processes produces a more uniform sediment grain size distribution in Type B clinothems (Fig. 3.14c), which lack the fine and coarse grain size outliers observed in Type A river-dominated clinothems (Fig. 3.13).

Type B clinothems exhibit intragroup variability, such that the foreset and bottomset deposits of Sequence m5.45 and m5.4 differ subtly (Figs. 3.8, 3.10). Sequence m5.45 has foreset and bottomset deposits that contain thin packages of coarse-grained sediments (e.g., Core M28, 523 – 528 mcd), associated with reworked glauconite (Fig. 3.8). These coarse-grained packages are absent in Sequence m5.4 (Fig. 3.10). The glauconitic, coarser packages account

for higher mean grain size observed in the foreset and bottomset deposits of Sequence m5.45 relative to Sequence m5.4 (Fig. 3.14c). In addition, the foreset deposits of Sequence m5.45 are more poorly sorted (Fig. 3.14d), and have less spherical (Fig. 3.14e) and more angular (Fig. 3.14f) grains relative to Sequence m5.4. The glauconite-rich, coarse-grained packages are associated mainly with turbiditic sedimentary features, including normally graded and cross-laminated glauconite sands (Hodgson et al. 2018). However, the topsets of both sequences are similar, displaying comparable up-core grain size patterns, grain size distributions, and sorting (Figs. 3.8, 3.10, 3.13-D). The divergence in grain character between Sequence m5.45 and m5.4 becomes greater downdip (Figs. 3.14d, e, f). This implies topset bypass of the glauconite-rich, coarse-grained sediment and/or its erosion and reworking beyond the clinoform rollover, but perhaps with larger sediment supply and coarse-grained sediment availability in Sequence m5.45. Under either of these circumstances (i.e., topset bypass and/or erosion beyond the clinoform rollover), a highly erosional turbidity current would be required to i) transport coarse-grained sediment across the topset, ii) bypass the high-energy coastal fence of longshore drift, and/or iii) erode and remobilize coarse-grained sediments from underlying foreset deposits. This implies one or multiple episodic returns to river-dominated process-regime conditions, suggesting that Sequence m5.45 is an example of mixed wave- and river-dominated clinoform rollover conditions (e.g., Gomis-Cartesio et al., 2017) (Fig. 3.14b).

3.7 Conclusions

High-resolution grain character analysis, integrated with core sedimentology and clinoform rollover-trajectory analysis of Miocene intrashelf clinothems, located offshore New Jersey, has allowed identification and detailed characterization of archetypal river- and wave-dominated longitudinal sedimentary profiles of clinothems for the first time (Fig. 3.14). River-dominated (Type A) clinothems, which display falling, flat, and rising clinoform rollover trajectories, are associated with considerable transport of coarse-grained sediment downdip. These conditions are associated with the following: i) inconsistent topset deposits, reflecting erosive conditions landward of the clinoform rollover; ii) delivery of coarse-grained sediment into foreset and bottomset deposits, via both turbiditic and debritic flow regimes, potentially triggered by river flooding remobilization or storm remobilization of glauconite-rich sands at the clinoform rollover; and iii) deposition of the coarsest, least spherical and most angular grains in foreset deposits, resulting from the rapid dissipation of energy, associated with multiple feeder channels and no major incision of the clinoform rollover. The largest volumes of coarse-grained sediment are delivered into downdip settings from river-dominated topsets.

Wave-dominated (Type B) clinothem sequences generally conform to traditional models, such that Sequences m5.45 and m5.4 have rising trajectories, relatively thin bottomset deposits, and minimal coarse-grained sediment throughout their depositional profiles. Wave-dominated conditions are associated with the following: i) longitudinal sediment profiles dominated by rounded, highly spherical very fine- and fine-grained sands, associated with wave reworking landward of the clinofom rollover; ii) minimal occurrence of coarse-grained sediment throughout the depositional profile, possibly associated with shore-parallel redistribution of coarse-grained sediment; and iii) a grain size distribution with limited downdip variation, associated with wave-resuspension grain size sorting. Sequence m5.45 also shows non-end-member characteristics, including glauconite-rich, turbiditic sands, and represents a locally mixed wave-dominated and river-influenced process-regime. Through analysis of multiple clinothems the integrated dataset reveals a breakdown in the predicted relationship between clinofom trajectory and the delivery of coarse-grained sediment into deep-water settings. Process-regime in the topset or shelf setting is a key factor controlling basinward transfer of coarse-grained sediment, which can be bypassed into bottomset deposits in river-dominated clinothems under both rising and falling clinofom rollover trajectories. As such, clinofom trajectory alone is not a reliable predictor of the presence of coarse-grained sediment in the absence of a good facies and grain size distribution control. Identification of the dominant process-regime alongside clinofom trajectory analysis is a more effective approach in determining the presence or absence of coarse-grained sediment deposits. The integrated analysis of high-resolution grain character and clinofom trajectory presented in this paper highlights the need for ongoing critical evaluation of conventional sequence stratigraphic and clinofom-trajectory paradigms. This study clearly demonstrates that the physical processes in action on the shelf, i.e., the interaction between fluvial and wave processes, exert a fundamental control on grain character distributions, and therefore reservoir quality. Furthermore, not only do fluvial and wave processes impact the grain size, grain shape, and sorting of shelf deposits, they change the reservoir characteristics across the complete depositional profile from topset (shelf) to foreset (slope) to bottomset (basin floor). This new quantitative dataset will have widespread use and value for improving numerical models, which seek to accurately replicate the sediment-export properties of depositional systems under specific shelf process-regime conditions.

Chapter 4 Manuscript Two

High-resolution correlations of strata within a sand-rich sequence clinotherm using grain fabric data, offshore New Jersey, USA.

4.1 Abstract

Trajectories of successive clinoform rollovers are widely applied to predict patterns of spatio-temporal sand distribution. However, the detailed internal architecture of individual clinothems is rarely documented. Understanding the textural complexities of complete topset-foreset-bottomset clinothem sequences is a key factor in understanding how and when sediment is transferred basinward. This study used high-resolution, core-based analyses of 267 samples from three research boreholes from quasi-coeval topset, foreset, and bottomset deposits of a single Miocene intrashelf clinothem recovered during Integrated Ocean Drilling Program (IODP) Expedition 313, offshore New Jersey, USA. Topset deposits were subdivided into three sedimentary packages based on grain character and facies analysis, consisting of upper and lower river-dominated topset process-regime packages separated by a middle wave- and storm- dominated process-regime package. Temporal variability in topset process-regime exerts a quantifiable effect on grain character across the complete depositional profile, which was used here to correlate topset deposits with time-equivalent sedimentary packages in foreset and bottomset positions. River-dominated sedimentary packages have higher sand-to-mud ratios; however, the grain character of river-dominated sedimentary packages is texturally less mature than that of wave- and storm-dominated deposits. Differences in grain character between packages dominated by different process-regimes increase basinward. The novel use of quantitative grain-character data allows intraclinothem time lines to be established at a higher resolution than is possible using chronostratigraphic techniques. Additionally, stratigraphic changes in grain character were used to refine the placement of the basal sequence boundary. These results challenge the idea that clinoform trajectories and stacking patterns are sufficient to describe spatio-temporal sand-body evolution across successive clinothems.

4.2 Introduction

Clinothems form the principal architectural building blocks of many shelf-to-basin successions (e.g., Gilbert, 1885; Rich, 1951; Bates, 1953; Asquith, 1970; Mitchum et al., 1977; Pirmez et al., 1998; Adams and Schlager, 2000; Bhattacharya, 2006; Patruno et al., 2015), and they are routinely subdivided geometrically into topset, foreset, and bottomset deposits. Clinothems form valuable archives of basin-margin evolution; the trajectories and geometries of consecutive clinoform rollovers and their resultant stacking patterns are widely applied to predict spatio-temporal sand distribution, in both the subsurface and in outcrop (e.g., Steel and Olsen, 2002; Johannessen and Steel, 2005; Helland-Hansen and Hampson, 2009; Jones et al., 2015; Koo et al., 2016; Chen et al., 2017; Pellegrini et al., 2017). Clinoform trajectory

models have been developed to account for observed form in terms of the balance between the rates of sediment supply and the generation of accommodation space (e.g., Burgess and Hovius, 1998; Mellere et al., 2002; Steel and Olsen, 2002; Bullimore et al., 2005; Carvajal and Steel, 2006; Uroza and Steel, 2008; Helland-Hansen and Hampson, 2009; Ryan et al., 2009). The role of topset and shelf process-regime in determining clinof orm architecture and timing of sediment transfer has recently been emphasized as an important parameter to consider (e.g., Dixon et al., 2012a; Jones et al., 2015; Hodgson et al., 2018; Cosgrove et al., 2018).

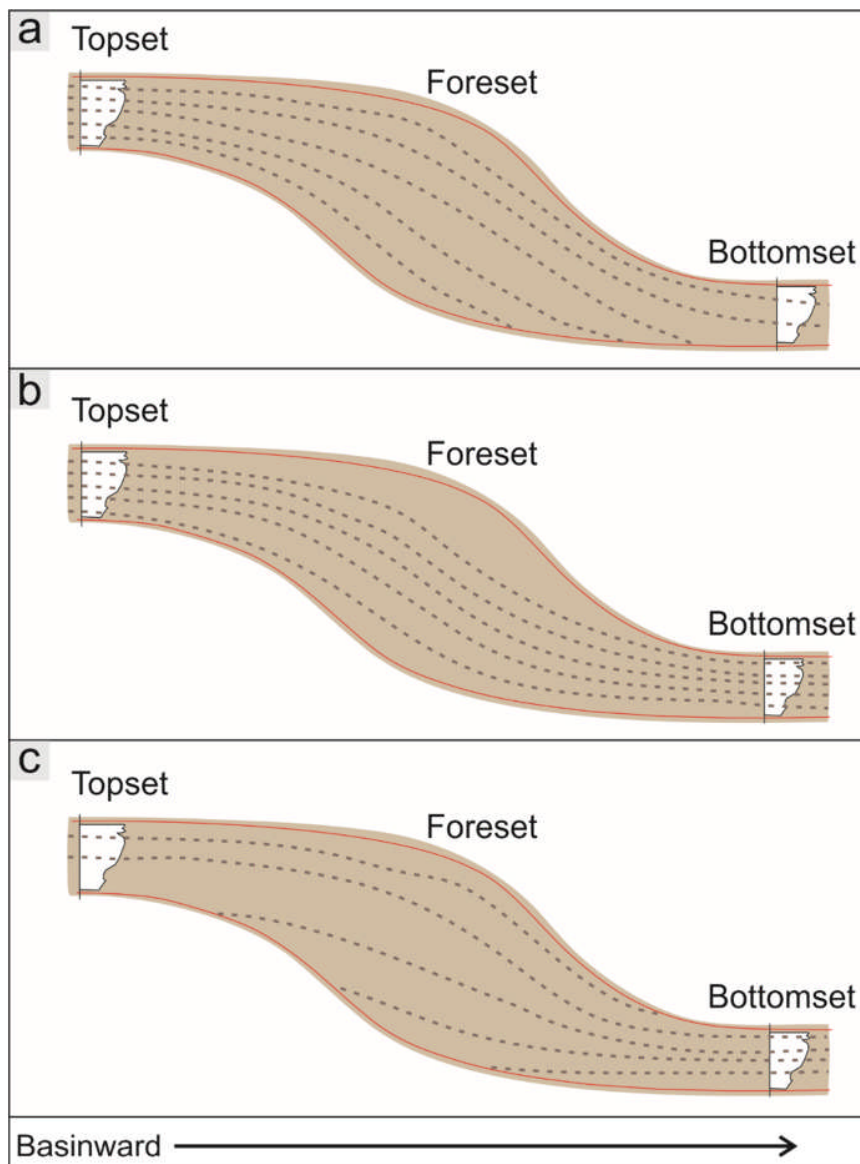


Figure 4.1: Schematic diagram of a clinof orm sequence, with different internal correlations. Sequence boundaries are shown in red. The dashed brown lines represent chronostratigraphic timelines from shallow- to deep-marine positions, illustrating permutations in intra-sequence architecture; a) strongly progradational clinof orm in which topset deposits are largely older than bottomset deposits; b) aggradational clinof orm in which topset deposits are the same relative age as bottomset deposits; c) clinof orm with strong early bypass, resulting in topset deposits that are largely younger than bottomset deposits.

Previous investigations of clinothem sequences have focused on understanding basin-scale relationships using multiple successive clinothems (e.g., Steel and Olsen, 2002; Johannessen and Steel, 2005; Helland-Hansen and Hampson, 2009; Dixon et al., 2012b; Koo et al., 2016; Chen et al., 2017; Pellegrini et al., 2017; Cosgrove et al., 2018). Understanding the internal architectural complexity of complete topset-foreset-bottomset clinothem sequences (including grain-size, grain shape and sand and mud content) is a key factor in understanding how and when sediment is transferred basinward, and in providing better constraint on the spatio-temporal sedimentary correlations of stratal units and their bounding surfaces. However, developing high-resolution intrasequence chronostratigraphic correlations is problematic, particularly in sand-rich successions. Stratigraphic changes in sedimentary facies can provide a means by which to correlate strata between wells, but this is fraught with uncertainty because of the transitional nature of facies change and the possibility for sediment bypass and nondeposition in one part of a clinothem that is time equivalent to deposits in other parts (Fig. 4.1). Biostratigraphic or chronostratigraphic constraints typically lack the necessary resolution to permit correlations of intrasequence surfaces. The limited understanding of intrasequence architecture is exacerbated by a paucity of sedimentological and stratigraphic documentation of individual clinothems with preserved coeval topset, foreset, and bottomset deposits (e.g., Carvajal and Steel, 2009; Carvajal et al., 2009; Wild et al., 2009; Grundvåg et al., 2014; Prélat et al., 2015; Koo et al., 2016).

To understand intraclinothem architecture at high resolution, both stratigraphically (up core) and longitudinally (dip parallel), and to determine linkages to topset process-regime, this study utilized samples from three research boreholes recovered during Integrated Ocean Drilling Program (IODP) Expedition 313, offshore New Jersey, USA (Fig. 4.2). The cored intervals targeted topset, foreset, and bottomset deposits of a single Miocene clinothem sequence (m5.4; Fig. 4.3) using integrated analysis of grain character (size and shape; cf. Fildani et al., 2018) and core-based interpretation of sedimentary textures and structures. The aim of this study was to highlight how quantitative grain-character data can be used to better understand the cause(s) of intrasequence textural complexities. Specific research objectives were as follows: (1) to understand how topset process-regime signals (including depositional architecture and grain character) are propagated downdip into foreset and bottomset deposits; (2) to illustrate how topset process-regime variability impacts sediment texture down the complete two-dimensional (2-D), dip-parallel depositional profile; (3) to demonstrate the use of grain character to correlate intraclinothem, time-equivalent surfaces;

and (4) to discuss how high-resolution grain-character data can be used as an additional tool to refine the placement of sequence boundaries.

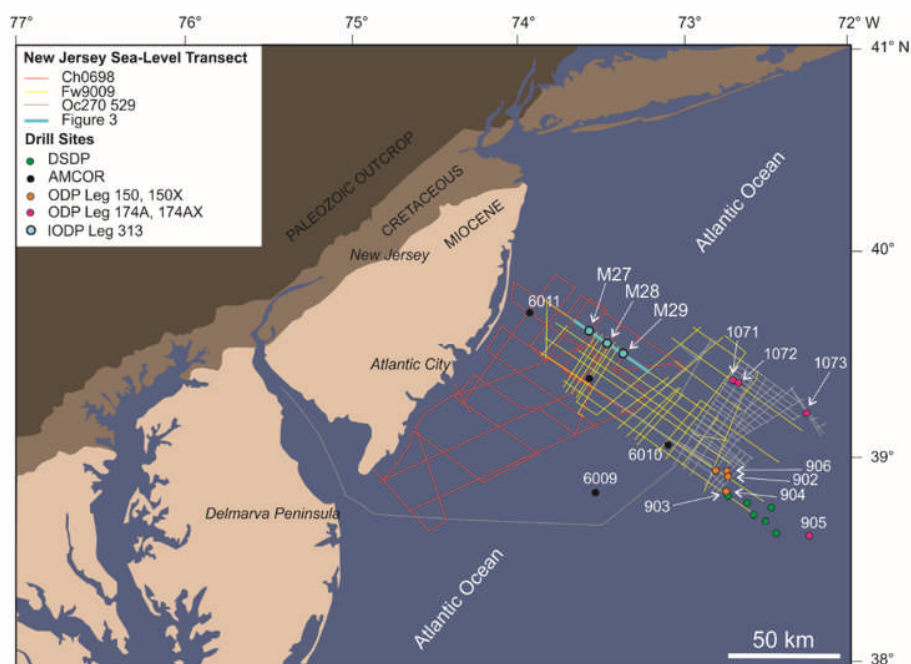


Figure 4.2: Location map of New Jersey sea level transect, modified from Expedition 313 Scientists (2010). Study sites used in this paper (Integrated Ocean Drilling Program [IODP] Expedition 313 Sites M27, M28 and M29) are presented as blue circles. The seismic profiles indicated represent data acquisition from three different cruises as part of the New Jersey sea-level transect (R/V Ewing cruise EW9009, R/V Oceanus cruise Oc270 and R/V Cape Hatteras cruise CH0698; Monteverde et al., 2008; Mountain et al., 2010; Miller et al., 2013a). The seismic line transecting the core sites M27-M29 (Oc270 529) is indicated in blue. This seismic transect is shown in Figure 4.3a.

4.3 Geological Setting

The Miocene United States (U.S.) middle Atlantic margin, spanning the shelf region offshore New Jersey, Delaware, and Maryland, is a siliciclastic-dominated prograding passive margin. This region has been tectonically quiescent since the opening of the Atlantic Ocean in the mid-Jurassic (Watts and Steckler, 1979). Therefore, the Mid-Atlantic margin offers a valuable natural laboratory in which to study mixed-energy coastal system successions in a tectonically stable setting (Katz et al., 2013). Furthermore, the succession preserves detailed microfossil and strontium isotope records, which provide good chronostratigraphic age control (Browning et al., 2013). Rifting commenced during the Late Triassic (ca. 230 Ma; Sheridan and Grow, 1988; Withjack et al., 1998), with seafloor spreading active from the Middle Jurassic (ca. 165 Ma). The Jurassic section, in the region of the Baltimore Canyon Trough (Fig. 4.2), is mainly composed of limestones of shallow-water origin (8–12 km thick). The margin was fringed by a barrier reef complex until the mid-Cretaceous (Poag, 1985). During the Cenozoic, the tectonic history was dominated by simple thermal subsidence, sediment loading, and crustal flexure (Watts and Steckler, 1979; Reynolds et al., 1991).

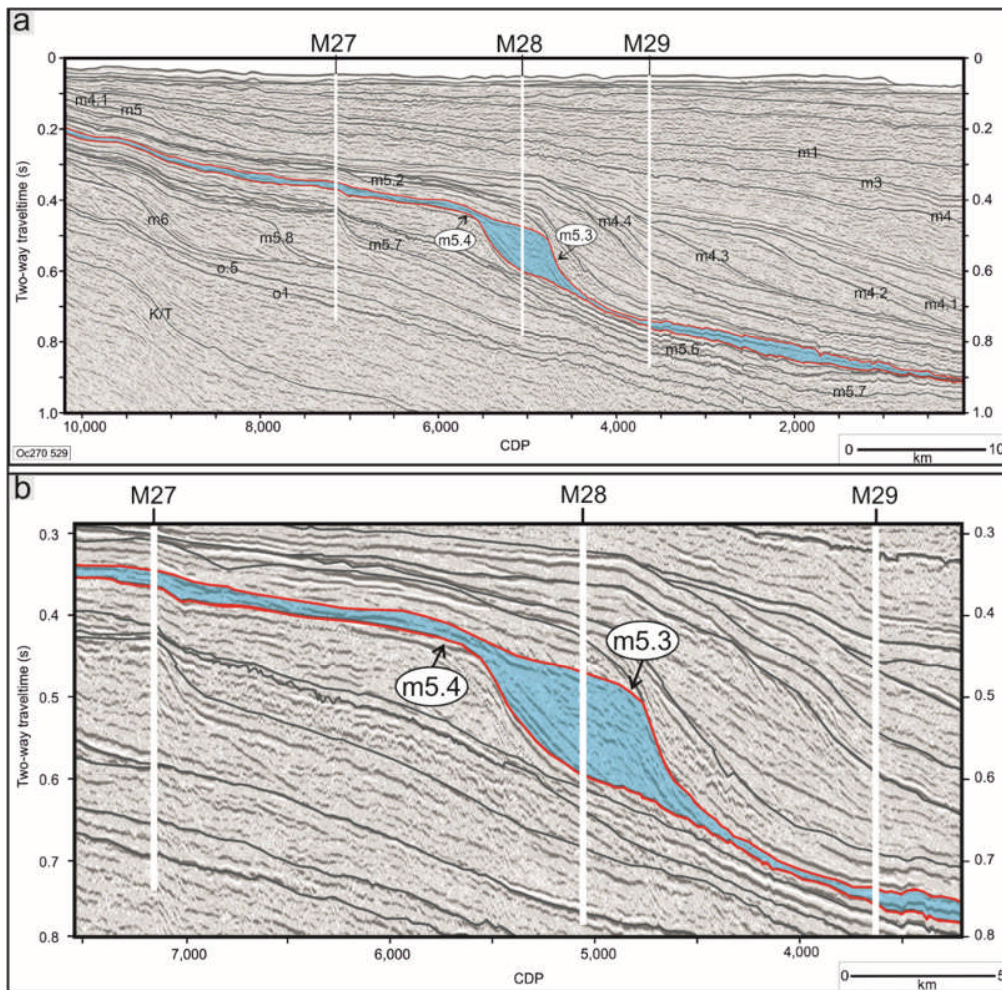


Figure 4.3: Location map of New Jersey sea level transect, modified from Expedition 313 Scientists (2010). Study sites used in this paper (Integrated Ocean Drilling Program [IODP] Expedition 313 Sites M27, M28 and M29) are presented as blue circles. The seismic profiles indicated represent data acquisition from three different cruises as part of the New Jersey sea-level transect (R/V Erwing cruise EW9009, R/V Oceanus cruise Oc270 and R/V Cape Hatteras cruise CH0698; Monteverde et al., 2008; Mountain et al., 2010; Miller et al., 2013a). The seismic line transecting the core sites M27-M29 (Oc270 529) is indicated in blue. This seismic transect is shown in Figure 3a.

The Late Cretaceous to Paleogene interval was marked by generally low rates ($\sim 5000 \text{ km}^3 \text{ m.y.}^{-1}$; shelf width $> 150 \text{ km}$) of siliciclastic and carbonate accumulation (Poag, 1985). Global and regional cooling resulted in a significant switch from carbonate ramp deposition to starved siliciclastic deposition during the late middle Eocene in onshore regions to earliest Oligocene further offshore on the slope (Miller and Snyder, 1997). The late Oligocene to Miocene interval was characterized by a dramatic increase in sedimentation rates (Poag, 1985; Miller and Snyder, 1997), the causes of which are poorly constrained, although some authors have suggested it was the result of tectonic activity in the hinterland (Poag and Sevón, 1989; Sugarman et al., 1993). The late Oligocene to Miocene increase in sedimentation rates resulted in the growth of a siliciclastic sedimentary prism, consisting of multiple clinothem sequences, which prograded over the low-gradient shelf. The clinothems accumulated in an

intrashelf setting, forming a seaward-thickening shelf prism (Hodgson et al., 2018). Intrashelf clinothems are situated seaward of the shoreline break and landward of the continental break and typically have reliefs of tens of meters (Helland-Hansen and Hampson, 2009; Henriksen et al., 2009; Helland-Hansen and Gjelberg, 2012; Patruno et al., 2015; Hodgson et al., 2018). IODP Expedition 313 drilled three research boreholes (Sites M27, M28, and M29), positioned to target the topset, foreset, and bottomset deposits of the Miocene intrashelf clinothems. The clinothems are well imaged on a grid of seismic profiles (Monteverde et al., 2008), which display the distinct sigmoidal geometries of the clinothem sequences (Fig. 4.3). Core sites M27, M28, and M29 were drilled in a transect along the trace of seismic line Oc270 529 (Fig. 4.2). Expedition 313 mapped 25 regional seismic surfaces of Oligocene to Miocene age, which correspond with changes in sedimentary facies in the associated core holes (Mountain et al., 2010). Integrated Sr-isotope stratigraphy and biostratigraphy (see Browning et al., 2013) was used to date sequences with a resolution of ± 0.25 – 0.6 m.y. This study focused on sequence m5.4, which is of Miocene age (Mountain et al., 2010; Browning et al., 2013), and it is discussed in detail below.

4.4 Sequence m5.4

Sequence m5.4 was deposited over ~ 1.1 m.y. (17.7–16.6 Ma), with brief depositional hiatuses at its base and top (Browning et al., 2013). Integrated seismic data and stratigraphy suggest m5.4 is a composite sequence, composed of three higher-order depositional sequences (m5.4–1, m5.34, and m5.33; Miller et al., 2013a) of ~ 100 k.y. duration; the higher-order sequences have been dated by regression of Sr-isotope data. Interpretations from previous studies of the stratigraphic depths of the composite sequence boundaries (m5.4 and m5.3) are illustrated in Figure 4.4, alongside interpretations of the higher-order sequence boundaries. For the purposes of this investigation, the placement of the m5.4 and m5.3 sequence boundaries will follow those presented in Miller et al. (2013a), who recognized sequence boundaries based on integrated core, seismic, and log data. The alternative published placements are described below.

4.4.1 Site M27

At site M27, the basal sequence boundary of m5.4 is placed at 295.01 meters composite depth (mcd) at an erosional surface (Miller et al., 2013a), which has been tied to synthetic seismogram data (Miller et al., 2013b). Originally, the m5.4 sequence boundary was placed at 271.23 mcd by Mountain et al. (2010). This surface was subsequently suggested by Miller et al. (2013a) to define the base of a higher-order sequence (m5.33). Sequence m5.4–1 is interpreted to have been cut out at Site M27 (Miller et al., 2013a); as such, m5.4 at Site M27 is

a composite sequence consisting of the m5.34 (23.88 m thick; 295.01 – 271.13 mcd) and m5.33 (15.04 m thick; 271.23 – 256.19 mcd) sequences. Sr-isotope age estimates are 17.0 – 16.9 Ma and 16.6–16.5 Ma for sequences m5.34 and m5.33, respectively (Browning et al., 2013). The placement of the overlying m5.3 sequence boundary is equivocal and has been placed at 236.15 mcd (Mountain et al., 2010), 249.76 mcd (Miller et al., 2013b), and 256.19 mcd (Miller et al., 2013a). The 256.19 mcd sequence boundary placement was favoured by Miller et al. (2013a) due to core expression, where a strongly bioturbated contact separates silt from an overlying coarse glauconite sand; this placement was also followed by Hodgson et al. (2018) and Proust et al. (2018).

4.4.2 Site M28

At Site M28, sequence m5.4 (151.30 m thick; 512.30 – 361.00 mcd) is bounded by two high-amplitude reflectors (m5.4 and m5.3) and has been recognized in previous studies (Monteverde et al., 2008; Monteverde, 2008; Mountain et al., 2010; Miller et al., 2013a, 2013b) based on termination styles of seismic reflectors at its base and top. Two alternative bases of sequence m5.4 were proposed by Mountain et al. (2010) at 495.20 mcd, where a thin sand bed overlies a clayey silt, and by Hodgson et al. (2018) at 519.70 mcd, where a sharp-based sand forms a fining-upward package of stratified sands with a deeply burrowed basal contact. M5.4-1 is differentiated from the m5.4 sequence boundary but shares the same basal reflector. Sequence m5.4-1 (512.30 – 479.00 mcd) is ca. 17.7 – 17.6 Ma in age (Browning et al., 2013). M5.34 (479.00 – 405.00 mcd; 17.6 – 17.4 Ma; Browning et al., 2013) is interpreted to be a sequence boundary, as determined from seismic reflector termination patterns, including onlap, downlap, and the erosional truncation of the m5.4 sequence boundary (Miller et al., 2013b; Miller et al., 2018). M5.33 (405.00 – 361.00 mcd) is 16.7–16.6 Ma in age and is associated with a basal unconformity representing a ~ 0.7 m.y. hiatus (Browning et al., 2013). Terminations onto adjacent seismic profiles (onlap and erosional truncation) are associated with the M5.33 sequence boundary, as illustrated by a strike line taken at Site M28 (Miller et al., 2018).

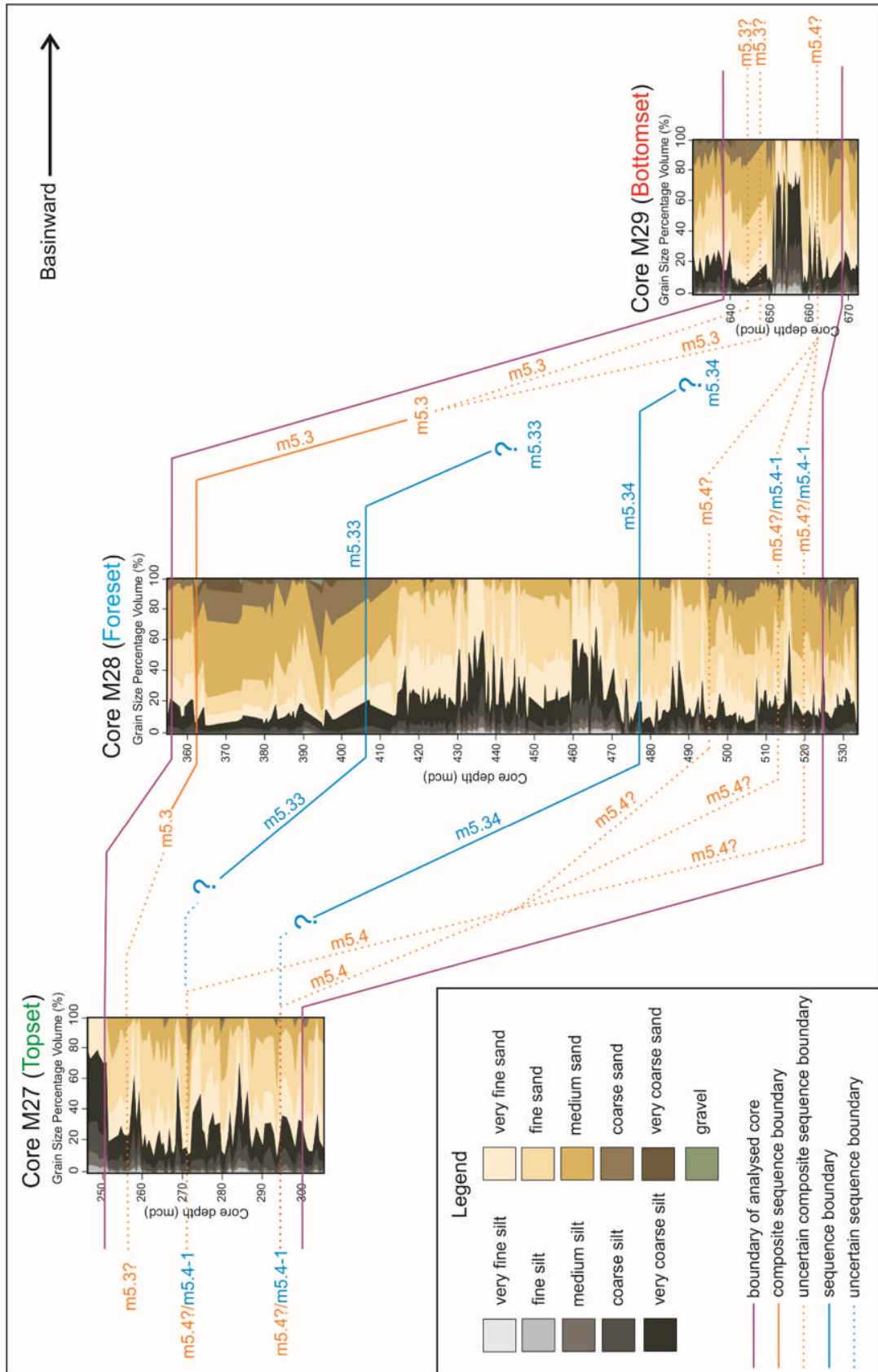


Figure 4.4: Correlation panel displaying various authors' composite sequence boundary (m5.3 and m5.4) and sequence boundary (m5.4-1, m5.34 and m5.33) interpretations (Mountain et al., 2010; Miller et al., 2013a, 2013b; Hodgson et al., 2018; Miller et al., 2018). The interpretations are overlain on new cumulative grain-size data plots from this study. The orange lines indicate composite sequence boundaries. The blue lines indicate intracolumn sequence boundaries. Dashed lines are used to illustrate uncertainty, where the same (composite) sequence boundary has been interpreted at multiple core depths. The additional core described below and above the m5.4 and m5.3 sequence boundaries respectively are illustrated by the purple lines.

4.4.3 Site M29

At Site M29 (19.18 m thick; 662.37 – 643.19 mcd; Miller et al., 2013b), Sr-isotope dating suggests sequence m5.4 has an age of 17.7 – 17.6 Ma; this age range corresponds to composite sequence m5.4-1 at Site M28, although this is poorly constrained (Browning et al., 2013). The basal m5.4 sequence boundary is placed at 662.37 mcd (Miller et al., 2013a), where a silty glauconite sand is overlain by a silt; the 662.37 mcd basal boundary is also supported by synthetic seismogram data (Miller et al., 2013b). Sequence m5.4 was originally interpreted by Miller et al. (2013a) to pinch out after Site M28 and reappear at Site M29, as per the preceding description. However, an alternative interpretation was provided by Hodgson et al. (2018), in which sequence m5.4 is not present at Site M29; that interval in the core (spanning at least 662.37 – 649.16 mcd, with a coring gap from 649.16 to 644.28 mcd) is interpreted to represent the upper part of underlying sequence m5.45. At Site M29, the upper sequence boundary (m5.3) is placed at 643.19 mcd, where a sharp-based glauconite sand is deeply burrowed into an underlying silt; this sequence boundary is also associated with a large impedance contrast (Miller et al., 2013b). However, synthetic seismograms place the m5.3 seismic sequence boundary in a coring gap at 648.00 mcd (Miller et al., 2013b).

4.5 Methods

This investigation employed two principal methodological approaches: (1) quantitative grain-character analysis and (2) palaeoenvironmental interpretations of lithofacies, based on the visual core descriptions by the Expedition 313 sedimentologists and original core observations of lithology and sedimentary structures. According to the Miller et al. (2013a) scheme, the seismic sequence targeted in this investigation, sequence m5.4, spans the depths 295.00 – 256.19 mcd (38.81 m thick), 512.33–363 mcd (149.33 m thick), and 662.37 – 643.19 mcd (19.18 m thick) in cores M27, M28, and M29, respectively. An additional ~ 5 m of stratigraphy was also described from below the basal m5.4 sequence boundary (300.00 – 295.00 mcd and 667.00 – 662.37 mcd in core M27 and core M29, respectively). In core M28, an additional ~ 12 m of stratigraphy has been described (525.00 – 512.33 mcd), in order to include the alternative m5.4 sequence boundary proposed by Hodgson et al. (2018) at 519.70 mcd. Similarly, above the overlying sequence boundary for m5.3, an additional ~ 5 m of stratigraphy is also described (256.19 – 251.00 mcd, 361.00 – 356.00 mcd, and 643.19 – 638.00 mcd in cores M27, M28, and M29, respectively).

4.5.1 Facies Associations and Depositional Environments

Here, we present interpretations of lithofacies and depositional environments based on assemblages of sedimentary structures, sedimentary texture and composition, fossil content, and ichnofabric. These lithofacies show variability up core within sequence m5.4.

Palaeoenvironmental interpretations were based on the following: (1) a classic wave-dominated shoreline model (e.g., Reineck and Singh, 1972; McCubbin, 1982; Browning et al., 2006), which recognises upper shoreface (0 – 5 m palaeo-water depth), lower shoreface (5 – 10 m palaeo-water depth), offshore transition (10 – 30 m palaeo-water depth), and offshore environments (> 30 m palaeo-water depth); and (2) mixed river/wave delta facies models (e.g., Galloway, 1975; Bhattacharya and Walker, 1992). These have been summarized in Mountain et al. (2010) and Proust et al. (2018).

4.5.2 Grain-Character Analysis

The semilithified samples were subjected to a mechanical and chemical disaggregation process to remove organic matter and prepare them for grain-character analysis (see Cosgrove et al., 2018). Grain-character analysis was undertaken using a CamsizerXT (Retsch Technology), which is an optically based dynamic image analysis instrument capable of measuring grain sizes from 0.001 to 8 mm with an accuracy of $\pm 1\%$ (Moore et al., 2011). The grain-character analysis of the CamsizerXT yielded: (1) a grain-size distribution for each individual sample, with 105 logarithmically divided grain size classes spanning 0.001–8 mm, and (2) a fully quantified grain-shape value (sphericity and roundness) for each grain-size class within that grain-size distribution. The raw output data of the CamsizerXT were subsequently analysed using GRADISTAT computer software (Blott and Pye, 2001). GRADISTAT allows rapid analysis of grain-size statistics from multiple sediment samples and provides values of the mean, mode, and sorting of the grain population, in addition to a grain-size cumulative frequency distribution for each sample. Grain-shape values were analysed with Microsoft Excel software.

Within sequence m5.4, 63, 219, and 49 sediment samples were recovered from cores M27, M28, and M29, respectively. Due to the downdip change in clinotherm thickness, the number of recovered samples varied between cores M27 and M29. Each core was subdivided into three sedimentary packages; this subdivision was based on the average grain-size distribution and corresponds to changes in sedimentary facies. The number of samples from each sedimentary package is displayed on the accompanying figures.

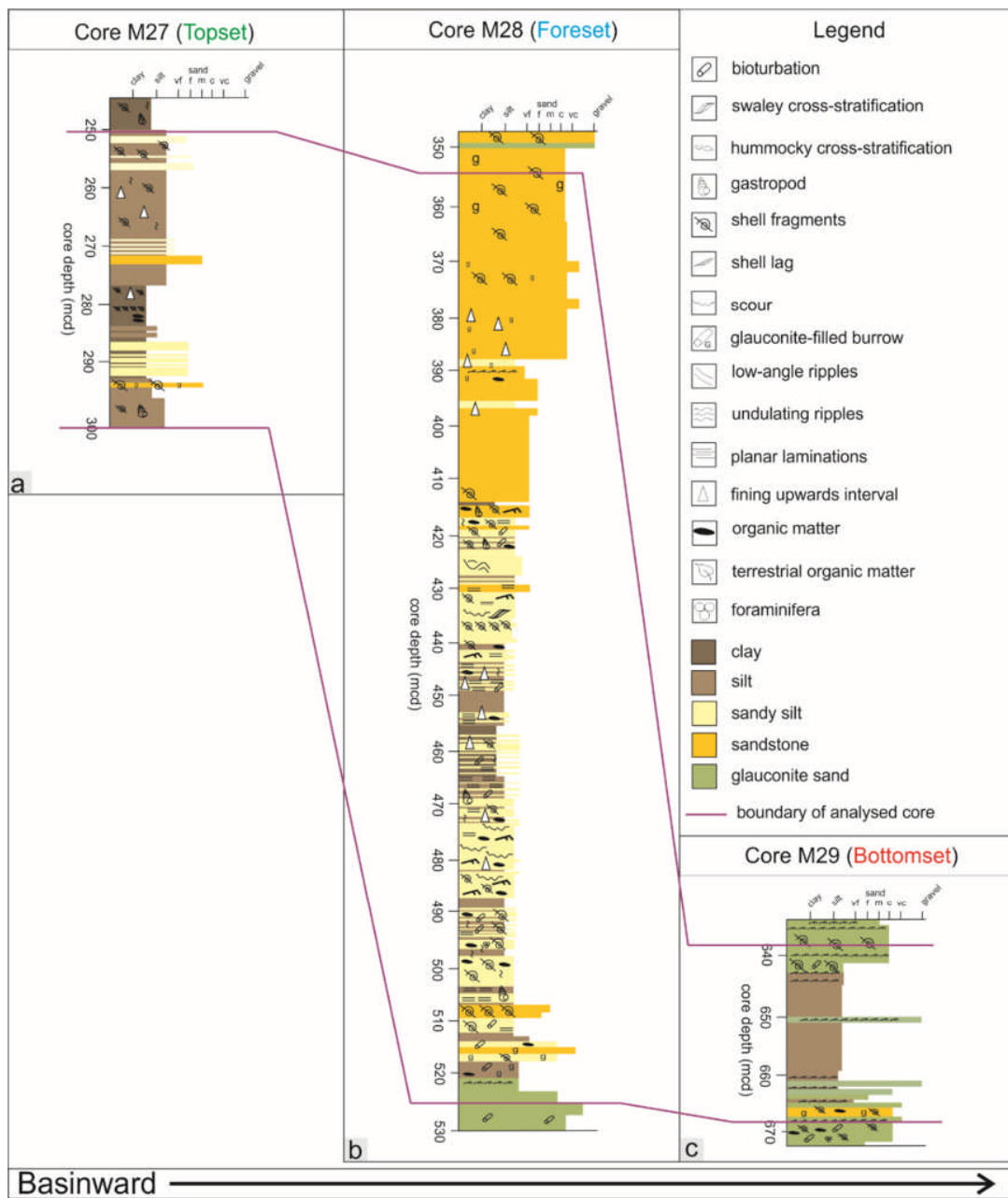


Figure 4.5: Simplified lithologic columns of Sites M27 (a), M28 (b) and M29 (c). The purple lines illustrate the boundaries of the core described in Tables 4.1 – 4.3.

4.6 Results

Core facies observations and descriptions are presented for sequence m5.4 at Sites M27, M28, and M29 in Tables 4.1 – 4.3, respectively. The tabulated lithofacies descriptions were supplemented by the sedimentary logs, which are presented in Figures 4.5a, 4.5b, and 4.5c for Sites M27, M28, and M29, respectively, and representative core photos (Fig. 4.6).

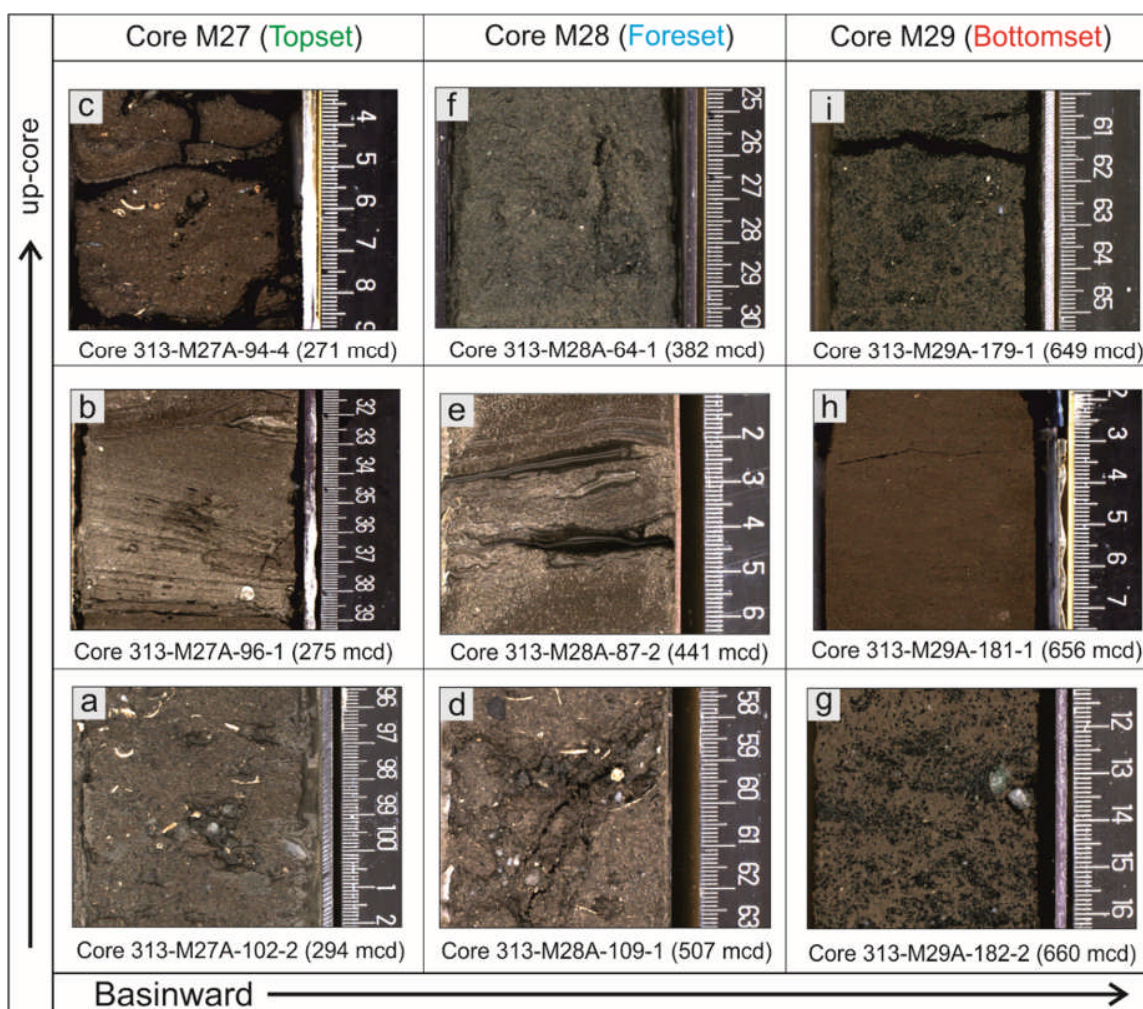


Figure 4.6: Representative core photographs: a) coarse-sand containing detrital quartz and glauconite grains and shell-fragments; b) hummocky cross stratification; c) fine sand containing detrital quartz and glauconite grains; d) coarse sand containing detrital quartz and glauconite grains; e) swaley cross stratification; f) structureless coarse glauconite sand; g) silty-sand containing quartz and glauconite; h) structureless silt; i) structureless coarse sand. The numerical code associated with each core photo refers to the expedition number (e.g. 313), the core location (e.g. M29), and the core number (e.g. 181-1). The core depth is also shown.

4.6.1 Topset Deposits (Core M27): Description

The core observations and descriptions are presented in Table 4.1.

4.6.2 Topset Deposits (Core M27): Interpretation

The topset deposits of sequence m5.4 form two broad facies associations: a coarser-grained facies (295.00 – ~ 294 mcd and 273.00 – 256.19 mcd; Figs. 4.6a and 4.6c) and an intervening finer-grained facies (~ 294 – 273.01 mcd; Fig. 4.6b). Within the coarse facies, the cross-lamination separated by undulating surfaces is interpreted as asymmetrical ripples formed by a unidirectional flow of fluvial origin. A fluvial source for the coarse facies is also supported by the presence of significant quantities of terrestrial material, including wood chunks and plant debris, concentrated within these stratigraphic intervals (e.g., Plink-Björklund and Steel,

2004; Rossi and Steel, 2016). The sand-rich nature of the coarse facies and the presence of gravel-sized detrital mineral grains (quartz and glauconite; Figs. 4.6a and 4.6c) suggest periods when river-flood events dominated, during which coarse sediment was rapidly deposited in a shoreface setting (e.g., Cosgrove et al., 2018). Within the fine facies (Fig. 4.6b), the sand and silt interbeds are interpreted to be storm beds in a lower shoreface setting; convex-up laminations are interpreted to be hummocky cross-stratification. The presence of storm-beds, hummocky cross-stratification, and frequent shell-debris supports a wave- and storm-dominated process-regime (e.g., Dott and Bourgeois, 1982; Harms et al., 1982).

4.6.3 Foreset Deposits (Core M28): Description

The core observations and descriptions are presented in Table 4.2.

4.6.4 Foreset Deposits (Core M28): Interpretation

The deposits of core M28 present either a coarse- or a fine-grained facies association with transitional changes observed between the facies. The foreset deposits of core M28 display a coarse-grained, glauconite-bearing facies (512.33 – ~ 495 mcd and ~ 420.80 – 361.00; Figs. 4.6d and 4.6f) and an intervening fine-grained facies (~ 495 – ~ 420.8 mcd; Fig. 4.6e). The coarse-grained facies is predominantly expressed as medium-grained muddy sand that contains gravel-sized quartz and glauconite grains (Fig. 4.6d), and it represents deposition by mixed sediment gravity flows. The poorly sorted and unstratified nature of the coarse-grained facies suggests deposition by debris flows (Mulder and Alexander, 2001; Fig. 4.6f).

Additionally, the presence of mud-chips and large volumes of detrital mineral grains (quartz and glauconite) suggests updip erosion and entrainment (Hodgson et al., 2018). Rare coarse-grained beds that display normal grading, and cross- and parallel-laminations, are interpreted to be the result of high-concentration turbidity currents (Mulder and Alexander, 2001). The abundant terrestrial debris and amount of mica suggest that fluvial processes at the shelf edge were responsible for the deposition of the coarse-grained facies. The dominant fluvial processes responsible for the deposition of the coarse-grained facies are suggested to be river-flood events that induced remobilization of shelf-edge deposits (cf. Normark and Piper, 1991; Zavala et al., 2006).

Depth (mcd)	Thickness (m)	Lithology			Sedimentary Structures	Glauconite/quartz	Terrestrial organic matter	Bioturbation index	Notes	Facies	Facies Transition
		Grain size	Sorting	Grading							
300*	~5	Clayey-silt	average	Normal		Not present	Abundant and finely disseminated lignite	3/5	Clayey-silt containing abundant terrestrial organic matter. The upper bounding surface at 295.01 is an erosional surface demarcating m5.4 sequence boundary (Miller et al., 2013b).	N/A	Abrupt
295.01*	~0.75	Coarse sand, fines upwards to sandy-mud	Poor	Normal	Generally massive	Abundant angular glauconite and quartz grains (1–3 mm in diameter)	Abundant macroscopic plant fragments and lignite dispersed throughout	4	Poorly sorted coarse-grained glauconite sand. The stratigraphic interval fines-upwards to sandy-mud and contains abundant shell fragments and terrestrial organic matter.	Coarse grained	Transitional
294.24	~272.99	Coarse silt	Average	Normal	Low angle laminations; convex-up laminations; planar laminations	Very rare gravel-sized glauconite found within convex-up laminations	Rare	2/3	Coarse-grained silt. The lower part of this stratigraphic interval is dominated by interbedded coarse-grained silts and sharp based sands, associated with shell debris. The upper part of this unit is dominated by planar laminated silt with rare fine-grained sand beds.	Fine grained	Abrupt
273.00	256.19 [‡]	Medium to coarse sand	Poor	Normal	Asymmetrical ripples; undulating laminations	Rare rounded quartzite pebbles and sub-rounded glauconite granules (1–8 mm in diameter)	Macroscopic plant fragments throughout and a large wood-chunk (~3 cm)	1	Poorly sorted coarse-grained glauconite sand. Coarsening upwards sand package with dispersed glauconite and quartz coarse-grained sand-sized grains. The upper bounding surface of this unit is the m5.3 sequence boundary; the m5.3 sequence boundary is placed where an underlying silt is separated from a coarse-grained glauconite-sand by a bioturbated contact (Miller et al., 2013a).	Coarse grained	Abrupt
256.19	251*	Silty sand	Good	Normal	Subhorizontal laminations	Localised medium-grained sand-sized glauconite grains	Finely disseminated organic matter	3	Laminated silty-sand with concentrated shell debris.	N/A	Abrupt

Table 4.1: Summary of the observed lithology and sedimentary texture of the Core M27 (topset) deposits. Note mcd - metres composite depth; *arbitrary point 5 m below m5.4 sequence boundary; †m5.4 sequence boundary; Miller et al., 2013b; ‡m5.3 sequence boundary Miller et al., 2013a; #arbitrary point 5 m above m5.3 sequence boundary. The yellow colour represents the coarse-grained, river-dominated facies; the blue colour represents the finer-grained, wave-dominated facies; no colour indicates the arbitrary core descriptions above and below a sequence boundary.

Depth (mcd)	Thickness (m)	Lithology		Sedimentary Structures	Glauconite/quartz	Terrestrial organic matter	Bioturbation index	Notes	Facies	Facies Transition
		Grain size	Sorting							
525*	5.3	Silty-clay	Poor	Generally massive	Medium-grained sand to gravel-sized (0.25 – 4 mm) quartz and glauconite grains. Glauconite forms between 1 and 25 % of the total sediment volume.	Not present.	4/5	Poorly sorted silty-clay containing abundant glauconite and quartz grains. The stratigraphic fines upwards and terminates at a bioturbated contact at 519.7 mcd (alternative m5.4 sequence boundary, Hodgson <i>et al.</i> , 2018).	N/A	Transitional
519.7*	2.7	Coarse-grained sand	Poor	Generally massive	Abundant medium-grained sand to gravel-sized glauconite (0.25 – 4 mm). Glauconite forms between 7 – 40 % of the total sediment volume.	Not present.	2/5 (highly variable)	Poorly sorted glauconite sand.	N/A	Abrupt
~517	~ 4.67	Sandy-silt	Average	Parallel laminations	Not present.	Finely disseminated organic matter is concentrated into ~ 2 mm thick laminae.	4/5	Sandy-silt. The stratigraphic interval fines upwards and terminates at a bioturbated contact at 512.33 mcd (m5.4 sequence boundary, Miller <i>et al.</i> , 2013a).	N/A	Abrupt
512.33	~ 17.3	Fine- to coarse-grained sand	Poor	Parallel laminations; rip-up clasts (mud chips)	Local gravel and pebble sized (3 – 8 mm), sub-rounded to sub-angular quartz and glauconite grains.	Common throughout; found both dispersed and concentrated into ~ 2 mm thick laminae. Rare larger wood chunks are found in association with glauconite and quartz grains.	4	Poorly sorted micaceous sand, containing localised glauconite- and quartz-rich sands.	Coarse grained	Transitional
~ 495	~ 74.2	Coarse-grained silt	Average	Parallel laminations; low-angle cross-laminations; convex-up laminations; scours	Not present.	Very finely disseminated organic matter is present.	2	Coarse-grained silt. The base of this stratigraphic interval is dominated by a fine-grained sand that fines upwards to a coarse-grained silt. The sandy base of this stratigraphic interval is associated with the preceding coarse-grained stratigraphic interval. Within the coarse-grained silt there are commonly occurring interbeds of coarse-grained silt and normally-graded fine-grained sand (1–3 mm in thickness).	Fine grained	Transitional
420.8	57.8	Medium- to coarse-grained sand	Poor	Rare parallel laminations at base	Local gravel- and pebble-sized (3 – 8 mm), sub-rounded quartz and glauconite grains.	Organic matter increases upwards associated with coarsening. The coarse sand is associated with larger wood chunks	1	Poorly sorted medium- to coarse-grained glauconite sand. The unit coarsens upwards from coarse-grained silt at the base to a coarse-grained sand. The silty base of this stratigraphic interval is associated with a transitional facies change with the preceding fine-grained stratigraphic interval.	Coarse grained	Transitional

361.00 ++	356 [†]	5	Medium- to coarse-grained sand	poor	Normal	Generally massive	Local medium-grained sand-sized (0.25 – 0.5 mm) glauconite grains. Glauconite forms between 1 – 3% of the total sediment volume.	Rare finely disseminated organic matter.	3/4	The expression of the m5.3 sequence boundary (361.00 mcd; Miller et al., 2013a; Miller et al., 2018) is subtle in core, but is associated with major gamma-log changes (Miller et al., 2013a).	N/A	Transitional
-----------	------------------	---	--------------------------------	------	--------	-------------------	--	--	-----	--	-----	--------------

Table 4.2 Summary of the observed lithology and sedimentary texture of the Core M28 (foreset) deposits Note mcd- metres composite depth; * arbitrary point 12 m below the m5.4 sequence boundary as presented in Miller et al., 2013a and 5 m below the alternative m5.4 sequence boundary as presented in Hodgson et al., 2018; # alternative m5.4 sequence boundary; Hodgson et al., 2018; **m5.4 sequence boundary, Hodgson et al., 2018; *#m5.4 sequence boundary; Miller et al., 2013a; ##m5.3 sequence boundary; Miller et al., 2013a; Miller et al., 2018; ** m5.3 sequence boundary; Miller et al., 2013a; #m5.3 sequence boundary. The yellow colour represents the coarse-grained, river-dominated facies; the blue colour represents the finer-grained, wave-dominated facies; no colour indicates the arbitrary core descriptions above and below a sequence boundary.

Depth (mcd)	Thickness (m)	Lithology			Sedimentary Structures	Glauconite/quartz	Terrestrial organic matter	Bioturbation index	Notes	Facies	Facies Transition
		Grain size	Sorting	Grading							
667*	4.63	Coarse-grained sand.	Moderate	Normal	Generally massive	Abundant coarse-grained sand-sized (0.5 – 1 mm) quartz and glauconite grains. Quartz and glauconite forms between 20 – 70 % of the total sediment volume	Not present	1	Coarse-grained glauconite sand. This stratigraphic interval terminates at the m5.4 sequence boundary (662.37 mcd; Miller et al., 2013a), where glauconite sand is overlain by a silty-clay.	N/A	Abrupt
662.37 [§]	10.87	Coarse-grained sand.	Poor	Normal	Generally massive; rare parallel laminae	Abundant coarse-grained sand to gravel sized (0.5 – 4 mm) quartz and glauconite grains. Locally the glauconite content can reach up to ~70 % of the total sediment volume, where glauconite is concentrated into ~2-cm-thick parallel laminae. Glauconite is also found concentrated in burrows.	Terrestrial organic matter is concentrated locally in laminae	5	Coarse-grained glauconite and quartz sand.	Coarse grained	Transitional
658.01	6.41	Coarse-grained silt.	Moderate	Normal	Structureless	Not present.	Not present	3	Structureless coarse-grained silt. The base of the stratigraphic interval is a fine-grained sand, which fines-upwards to a coarse-grained silt. The sandy base of this interval is associated with a transitional facies change to the preceding coarse-grained stratigraphic interval.	Fine grained	Transitional
651.6	8.41	Medium-grained sand.	Poor	Normal	Generally massive	Abundant fine- to coarse-grained sand-sized (0.125 – 1 mm) glauconite and quartz are present within a sandy matrix. Locally, the glauconite can form up to ~80 % of the total sediment volume.	Finely disseminated organic matter is found concentrated locally	0/4 (variable)	Structureless glauconite and quartz sand. The base of this stratigraphic interval has a silty matrix, which contains glauconite and quartz grains of medium-grained sand size (0.25 – 0.5 mm). The matrix coarsens upwards throughout the stratigraphic interval. The relatively siltier base of this stratigraphic interval is associated with a transitional facies change between this stratigraphic interval and the preceding finer-grained stratigraphic interval. The bioturbation index varies according to glauconite content; where glauconite > 40 % of the total sediment volume, the bioturbation index is 1-0. Where glauconite < 40 % of the total sediment volume, the bioturbation index is 4. The stratigraphic interval terminates at the m5.3 sequence boundary (643.19 mcd; Miller et al., 2013a), where an overlying glauconite sand is deeply burrowed into an underlying silt.	Coarse grained	Transitional
643.19**	5.19	Silty-sand.	Poor	Normal	Generally massive	Medium- and coarse-grained sand-sized (0.25 – 1 mm) glauconite grains are found within a sandy-silt matrix. Glauconite can form up to ~80 % of the total sediment volume.	Not present	1/5 (variable)	Silty glauconite sand.	N/A	Abrupt

Table 4.3: Summary of the observed lithology and sedimentary texture of the Core M29 (bottomset) deposits Note mcd- metres composite depth *arbitrary point 5 m below m5.4 sequence boundary; Miller et al., 2013a; †m5.4 sequence boundary; Miller et al., 2013a; ‡m5.4 sequence boundary; Miller et al., 2013a; §m5.3 sequence boundary; Miller et al., 2013a; ¶m5.3 sequence boundary; Miller et al., 2013a; **m5.3 sequence boundary; Miller et al., 2013a; ††m5.3 sequence boundary; Miller et al., 2013a; †††m5.3 sequence boundary; Miller et al., 2013a; ††††m5.3 sequence boundary; Miller et al., 2013a. The yellow colour represents the coarse-grained, river-dominated facies; the blue colour represents the finer-grained, wave-dominated facies; no colour indicates the arbitrary core descriptions above and below a sequence boundary.

Within the finer-grained facies (Fig. 4.6e), the presence of both low-angle cross-laminations and convex-up laminations (hummocky cross-stratification) indicates wave and storm reworking (e.g., Dott and Bourgeois, 1982; Harms et al., 1982). Additionally, the discrete sharp-based, normally graded sand beds interbedded with coarse-grained silt indicate episodic sediment flux associated with storm events (Reineck and Singh, 1972). The finer-grained facies are interpreted to represent deposition on a wave- and storm-dominated shelf. This sedimentary package can be tentatively associated with the finer-grained package found in the topset deposits of core M27.

4.6.5 Bottomset Deposits (Core M29): Description

The core observations and descriptions are presented in Table 4.3.

4.6.6 Bottomset Deposits (Core M29): Interpretation

The deposits of core M29 present either coarse- or fine-grained facies associations; however, interpretations of the exact stratigraphic segregation of these facies are somewhat subjective because no abrupt facies changes are present. The bottomset deposits of core M29 display a coarse-grained, glauconite-bearing facies (662.37 – ~ 658.50 mcd and ~ 651.60 – 643.19 mcd; Figs. 4.6g and 4.6i) and an intervening fine-grained facies (~ 658.5 – ~ 651.6 mcd; Fig. 4.6h). The coarse-grained facies is typified by structureless glauconite-bearing sand interbedded with planar-laminated glauconite sand. The coarse-grained intervals are interpreted to represent rapid deposition of glauconitic sands from high-density turbidity currents and debris flows (Hodgson et al., 2018). The fine-grained facies is dominated by a structureless silt, predominantly representing deposition from suspension fallout, either from surface plumes or low-density turbidity currents.

4.6.7 Process Summary

Across the depositional profile, the fine-grained facies show a predominant wave and storm influence, recognized by: (1) abundant hummocky cross-stratification in the deposits of cores M27 and M28; (2) sandy-silt interbeds, representing episodic sediment flux associated with storm events; and (3) silt-dominated foreset and bottomset deposits, indicating an absence of direct fluvial sediment delivery. In contrast, the coarse-grained facies shows a predominant river influence, recognized by: (1) the strong terrestrial influence displayed by this facies (abundant plant and wood debris); (2) the grain-size variation (granule- and pebble-sized quartz and glauconite grains); (3) unidirectional current indicators (asymmetrical ripples); and (4) debritic and turbiditic deposits in foreset and bottomset deposits, interpreted to result from river-flooding events and hyperpycnal flows, respectively.

Core M27 (topset)		Sedimentary package M27a		Sedimentary package M27b		Sedimentary package M27c	
Number of samples	2	Number of samples	31	Number of samples	28	Number of samples	28
Mean grain size (mm)	0.103	Mean grain size (mm)	0.106	Mean grain size (mm)	0.123	Mean grain size (mm)	0.123
Median grain size (n_{50}) (mm)	0.103	Median grain size (n_{50}) (mm)	0.099	Median grain size (n_{50}) (mm)	0.119	Median grain size (n_{50}) (mm)	0.119
Maximum grain size (mm)	0.118	Maximum grain size (mm)	0.198	Maximum grain size (mm)	0.271	Maximum grain size (mm)	0.271
Minimum grain size (mm)	0.087	Minimum grain size (mm)	0.044	Minimum grain size (mm)	0.042	Minimum grain size (mm)	0.042
Standard deviation (σ)	0.223	Standard deviation (σ)	0.040	Standard deviation (σ)	0.049	Standard deviation (σ)	0.049
Mean sorting (σ)	2.345	Mean sorting (σ)	2.283	Mean sorting (σ)	2.204	Mean sorting (σ)	2.204
Median sorting (n_{50}) (σ)	2.345	Median sorting (n_{50}) (σ)	2.326	Median sorting (n_{50}) (σ)	2.158	Median sorting (n_{50}) (σ)	2.158
Maximum sorting (σ)	2.455	Maximum sorting (σ)	2.739	Maximum sorting (σ)	2.747	Maximum sorting (σ)	2.747
Minimum sorting (σ)	2.235	Minimum sorting (σ)	1.699	Minimum sorting (σ)	1.830	Minimum sorting (σ)	1.830
Standard deviation (σ)	0.156	Standard deviation (σ)	0.245	Standard deviation (σ)	0.196	Standard deviation (σ)	0.196
Mean sphericity (K)	0.919	Mean sphericity (K)	0.922	Mean sphericity (K)	0.912	Mean sphericity (K)	0.912
Median sphericity (n_{50}) (K)	0.919	Median sphericity (n_{50}) (K)	0.927	Median sphericity (n_{50}) (K)	0.916	Median sphericity (n_{50}) (K)	0.916
Maximum sphericity (K)	0.921	Maximum sphericity (K)	0.943	Maximum sphericity (K)	0.949	Maximum sphericity (K)	0.949
Minimum sphericity (K)	0.917	Minimum sphericity (K)	0.888	Minimum sphericity (K)	0.867	Minimum sphericity (K)	0.867
Standard deviation (σ)	0.002	Standard deviation (σ)	0.016	Standard deviation (σ)	0.019	Standard deviation (σ)	0.019
Mean roundness (K)	0.631	Mean roundness (K)	0.660	Mean roundness (K)	0.683	Mean roundness (K)	0.683
Median roundness (n_{50}) (K)	0.631	Median roundness (n_{50}) (K)	0.671	Median roundness (n_{50}) (K)	0.697	Median roundness (n_{50}) (K)	0.697
Maximum roundness (K)	0.654	Maximum roundness (K)	0.779	Maximum roundness (K)	0.776	Maximum roundness (K)	0.776
Minimum roundness (K)	0.607	Minimum roundness (K)	0.519	Minimum roundness (K)	0.532	Minimum roundness (K)	0.532
Standard deviation (σ)	0.033	Standard deviation (σ)	0.078	Standard deviation (σ)	0.059	Standard deviation (σ)	0.059

Table 4.4: Summary of grain character for topset deposits (sedimentary package M27a-c)

Core M28 (foreset)		Sedimentary package M28a		Sedimentary package M28b		Sedimentary package M28c	
Number of samples		32		Number of samples	146	Number of samples	41
Mean grain size (mm)		0.174		Mean grain size (mm)	0.112	Mean grain size (mm)	0.238
Median grain size (n_{50}) (mm)		0.181		Median grain size (n_{50}) (mm)	0.111	Median grain size (n_{50}) (mm)	0.210
Maximum grain size (mm)		0.214		Maximum grain size (mm)	0.235	Maximum grain size (mm)	0.429
Minimum grain size (mm)		0.092		Minimum grain size (mm)	0.039	Minimum grain size (mm)	0.124
Standard deviation (σ)		0.040		Standard deviation (σ)	0.042	Standard deviation (σ)	0.068
Mean sorting (σ)		2.475		Mean sorting (σ)	2.148	Mean sorting (σ)	2.411
Median sorting (n_{50}) (σ)		2.445		Median sorting (n_{50}) (σ)	2.074	Median sorting (n_{50}) (σ)	2.436
Maximum sorting (σ)		3.837		Maximum sorting (σ)	3.667	Maximum sorting (σ)	2.807
Minimum sorting (σ)		2.132		Minimum sorting (σ)	1.633	Minimum sorting (σ)	1.953
Standard deviation (σ)		0.294		Standard deviation (σ)	0.258	Standard deviation (σ)	0.229
Mean sphericity (K)		0.887		Mean sphericity (K)	0.922	Mean sphericity (K)	0.915
Median sphericity (n_{50}) (K)		0.888		Median sphericity (n_{50}) (K)	0.924	Median sphericity (n_{50}) (K)	0.914
Maximum sphericity (K)		0.910		Maximum sphericity (K)	0.962	Maximum sphericity (K)	0.941
Minimum sphericity (K)		0.780		Minimum sphericity (K)	0.847	Minimum sphericity (K)	0.898
Standard deviation (σ)		0.023		Standard deviation (σ)	0.019	Standard deviation (σ)	0.008
Mean roundness (K)		0.522		Mean roundness (K)	0.651	Mean roundness (K)	0.581
Median roundness (n_{50}) (K)		0.532		Median roundness (n_{50}) (K)	0.645	Median roundness (n_{50}) (K)	0.568
Maximum roundness (K)		0.591		Maximum roundness (K)	0.800	Maximum roundness (K)	0.735
Minimum roundness (K)		0.326		Minimum roundness (K)	0.293	Minimum roundness (K)	0.491
Standard deviation (σ)		0.057		Standard deviation (σ)	0.070	Standard deviation (σ)	0.053

Table 4.5: Summary of grain character for foreset deposits (sedimentary package M28a-c)

Core M29 (bottomset)		Sedimentary package M29a		Sedimentary package M29b		Sedimentary package M29c	
Number of samples	10	Number of samples	28	Number of samples	11	Number of samples	11
Mean grain size (mm)	0.156	Mean grain size (mm)	0.056	Mean grain size (mm)	0.212	Mean grain size (mm)	0.212
Median grain size (n50) (mm)	0.177	Median grain size (n50) (mm)	0.037	Median grain size (n50) (mm)	0.239	Median grain size (n50) (mm)	0.239
Maximum grain size (mm)	0.243	Maximum grain size (mm)	0.259	Maximum grain size (mm)	0.267	Maximum grain size (mm)	0.267
Minimum grain size (mm)	0.054	Minimum grain size (mm)	0.033	Minimum grain size (mm)	0.035	Minimum grain size (mm)	0.035
Standard deviation (σ)	0.073	Standard deviation (σ)	0.055	Standard deviation (σ)	0.068	Standard deviation (σ)	0.068
Mean sorting (σ)	2.066	Mean sorting (σ)	2.158	Mean sorting (σ)	2.308	Mean sorting (σ)	2.308
Median sorting (n50) (σ)	2.040	Median sorting (n50) (σ)	2.173	Median sorting (n50) (σ)	2.347	Median sorting (n50) (σ)	2.347
Maximum sorting (σ)	2.341	Maximum sorting (σ)	2.388	Maximum sorting (σ)	2.533	Maximum sorting (σ)	2.533
Minimum sorting (σ)	1.834	Minimum sorting (σ)	1.687	Minimum sorting (σ)	2.130	Minimum sorting (σ)	2.130
Standard deviation (σ)	0.214	Standard deviation (σ)	0.151	Standard deviation (σ)	0.118	Standard deviation (σ)	0.118
Mean sphericity (K)	0.907	Mean sphericity (K)	0.940	Mean sphericity (K)	0.890	Mean sphericity (K)	0.890
Median sphericity (n50) (K)	0.903	Median sphericity (n50) (K)	0.947	Median sphericity (n50) (K)	0.885	Median sphericity (n50) (K)	0.885
Maximum sphericity (K)	0.936	Maximum sphericity (K)	0.959	Maximum sphericity (K)	0.940	Maximum sphericity (K)	0.940
Minimum sphericity (K)	0.869	Minimum sphericity (K)	0.879	Minimum sphericity (K)	0.873	Minimum sphericity (K)	0.873
Standard deviation (σ)	0.024	Standard deviation (σ)	0.019	Standard deviation (σ)	0.018	Standard deviation (σ)	0.018
Mean roundness (K)	0.644	Mean roundness (K)	0.713	Mean roundness (K)	0.540	Mean roundness (K)	0.540
Median roundness (n50) (K)	0.637	Median roundness (n50) (K)	0.732	Median roundness (n50) (K)	0.519	Median roundness (n50) (K)	0.519
Maximum roundness (K)	0.751	Maximum roundness (K)	0.782	Maximum roundness (K)	0.722	Maximum roundness (K)	0.722
Minimum roundness (K)	0.549	Minimum roundness (K)	0.508	Minimum roundness (K)	0.475	Minimum roundness (K)	0.475
Standard deviation (σ)	0.084	Standard deviation (σ)	0.058	Standard deviation (σ)	0.075	Standard deviation (σ)	0.075

Table 4.6: Summary of grain character for bottomset deposits (sedimentary package M29a-c)

4.6.8 Grain Character

Grain-character data are presented for the topset, foreset, and bottomset deposits of sequence m5.4. The observed facies changes correspond with changes in grain-size distribution. The changes in grain-size distribution noted below were used to subdivide sequence m5.4 deposits into three subunits (a, b, and c) at each site.

4.6.8.1 Topset Deposits (M27)

The grain-size distribution of samples from 295.00–294.26 mcd displays two principal peaks at 0.057 mm (very coarse-grained silt) and 0.35 mm (medium-grained sand; Fig. 4.7a). In contrast, from 294.25 to 273.00 mcd, the grain-size distribution displays one broad peak spanning 0.098–0.21 mm (very fine- to medium-grained sand; Fig. 4.7b). From 272.99 to 256.19 mcd, the grain-size distribution displays two principal peaks at 0.063 mm (very fine-grained sand) and 0.27 mm (medium grained-sand; Fig. 4.7c). These changes in grain-size distribution define three sedimentary packages in the topset deposits (core M27) of sequence m5.4, informally referred to as M27a (295.00–294.26 mcd), M27b (294.25–273.00 mcd), and M27c (272.99.00–256.19 mcd; Fig. 4.8). Additional differences in grain character in sedimentary package M27b relative to sedimentary packages M27a and M27c include a finer mean grain size (Fig. 4.9a), a lower sand-to-mud ratio (M27b = 70:30 [Fig. 4.10b], M27a = 71:29 [Fig. 4.10a], M27c = 74:26 [Fig. 4.10c]), and a higher mean sphericity (Fig. 4.9a; Table 4.4).

4.6.8.2 Foreset Deposits (M28)

The grain-size distribution of samples from 512.33 – 495.00 mcd displays two principal peaks at 0.0625 mm (very fine sand) and 0.25 mm (medium sand; Fig. 4.7d). In contrast, from 494.99 to 415.00 mcd, the grain-size distribution of the samples displays one broad peak spanning 0.0682–0.193 mm (very fine- to fine-grained sand; Fig. 4.7e). From 414.99 to 63.00 mcd, the grain-size distribution comprises two principal peaks at 0.0625 mm (very fine-grained sand) and 0.297 mm (medium-grained sand; Fig. 4.7f). These changes in grain-size distribution were used to define three sedimentary packages within the foreset deposits (core M28) of sequence m5.4, informally referred to as M28a (512.33 – 495.00 mcd), M28b (494.99–415.00 mcd), and M28c (414.99–363.00 mcd; Fig. 4.8). Additional differences in grain character of M28b compared to M28a and M28c include a finer mean grain size (Fig. 4.11a), a lower sand-to-mud ratio (M28b = 73:27 [Fig. 4.10e], M28a = 88:12 [Fig. 4.10d], M28c = 84:16 [Fig. 4.10f]), better sorting (Fig. 4.11b), and more spherical (Fig. 4.11c) and well-rounded (Fig. 4.11c) grains (Table 4.5)

4.6.8.3 Bottomset Deposits (M29)

The grain-size distribution of samples from 662.37 – 658.50 mcd displays two principal peaks at 0.0625 mm (very fine sand) and 0.273 mm (medium sand; Fig. 4.7g). In contrast, from 658.49 to 651.64 mcd, the grain-size distribution displays one sharp, asymmetric peak at 0.0682 mm (very fine sand; Fig. 4.7h). A bimodal distribution returns from 651.63 to 643.19 mcd, where the grain-size distribution displays two principal peaks at 0.0682 mm (very fine sand) and 0.297 mm (medium grained-sand; Fig. 4.7i). The changes in grain-size distributions were used to define three sedimentary packages in the bottomset deposits of core M29, informally referred to as M29a (662.37 – 658.50 mcd), M29b (658.49 – 651.64 mcd), and M29c (651.63 – 643.19 mcd; Fig. 4.8). Additional differences in grain character of sedimentary package M29b, relative to sedimentary packages M29a and M29c, include a finer mean grain size (Fig. 4.12a), a lower sand-to-mud ratio (M29b = 37:63 [Fig. 4.10h], M29a = 84:16 [Fig. 4.10g], M29c = 81:19 [Fig. 4.10i]) and more spherical and rounded grains (Figs. 4.12c and 4.12d; Table 4.6).

4.6.9 Correlations Across Topset-Foreset-Bottomset Profiles

In lieu of higher-resolution biostratigraphic and chronostratigraphic age control, quantitative grain-character data were used here as a lithostratigraphic tool to objectively subdivide the stratigraphy, and to correlate genetically related sedimentary packages, from topset through foreset to bottomset deposits of seismic sequence m5.4 (Fig. 4.8). The sedimentary packages are separated by two intraclinothem surfaces, based on abrupt changes in grain-size distribution, informally referred to in this study as surfaces 2 and 3; an additional surface (surface 1) corresponds to the basal m5.4 composite sequence boundary. Surface 2 separates sedimentary packages M27 – M29a and M27 – M29b and occurs at 294.26, 495.00, and 658.50 mcd in cores M27, M28, and M29, respectively. Surface 3 separates sedimentary packages M27 – M29b and M27 – M29c and occurs at 272.99, 415.00, and 651.64 mcd in cores M27, M28, and 389 M29, respectively (Fig. 4.8). The correlated sedimentary packages between the surfaces are M27 – M29a and M27 – M29c, which correspond to the coarse-grained facies and topset deposits that have bimodal grain-size distributions, and which are coincident with river-dominated facies, and sedimentary package M27 – M29b, which has a unimodal grain-size distribution and corresponds to the fine-grained package in the topset deposits that are wave-dominated.



Figure 4.7: Average grain-size distribution profiles, which are used to subdivide m5.4 stratigraphy. Y and X axes are percentage volume (%) and grain size (mm), respectively. Alongside the numerical grain-size classes are the descriptive grain-size classes modified from Udden (1914) and Wentworth (1922). a) Sedimentary package M27a; b) sedimentary package M27b; c) sedimentary package M27c; d) sedimentary package M28a; e) sedimentary package M28b; f) sedimentary package M28c; g) sedimentary package M29a; h) sedimentary package M29b; i) sedimentary package M29c; j) average grain size distribution profiles of Core M27 (topset), Core M28 (foreset) and Core M29 (bottomset) deposits of sedimentary package M27-M29a overlain; k) average grain size distribution profiles of Core M27 (topset), Core M28 (foreset) and Core M29 (bottomset) deposits of sedimentary package M27-M29b overlain; l) average grain size distribution profiles of Core M27 (topset), Core M28 (foreset) and Core M29 (bottomset) deposits of sedimentary package M27-M29c overlain. The number of samples used to produce each grain-size distribution profile is shown by N = X.

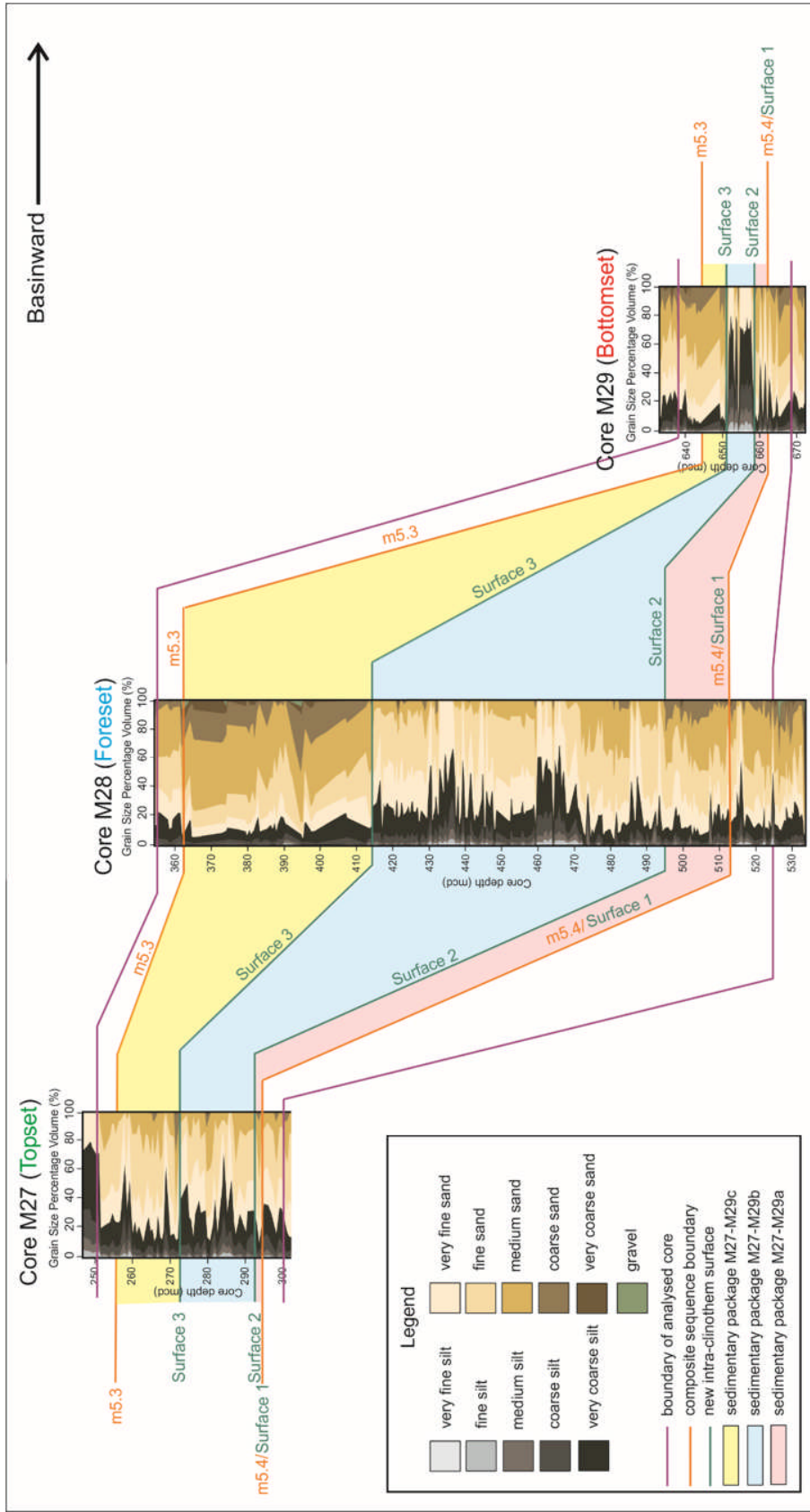


Figure 4.8: Correlation panel. The composite sequence boundaries (m5.4 and m5.3), as presented in Miller et al. (2013a), are shown in orange. Sedimentary package M27-M29a is highlighted in pink. Sedimentary package M27-M29b is highlighted in blue. Sedimentary package M27-M29c is highlighted in yellow. New interpreted intraclinothem surfaces (Surface 1, Surface 2, and Surface 3) are shown in green. The interpreted surfaces are overlain onto new cumulative grain-size data presented in this investigation. The boundaries of the additional core described below and above the m5.4 and m5.3 sequence boundaries respectively are shown in purple.

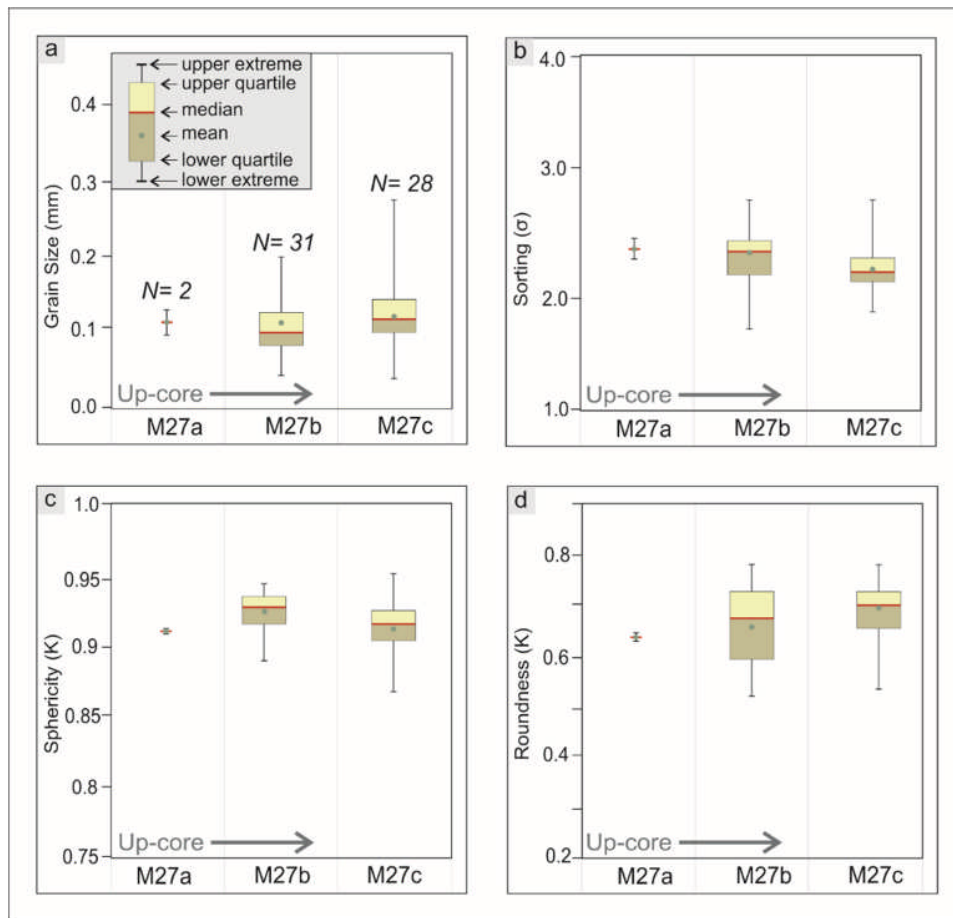


Figure 4.9: Box and whisker plot for sedimentary packages M27a, M27b and M27c (topset deposits); a) grain size; b) sorting; c) sphericity; d) roundness. The legend is shown in Part a. The number of samples used to produce each box and whisker plot is shown in Part a by $N = X$. Due to the low sample number for M27a, only the mean, median and standard deviation are shown.

4.6.9.1 Sedimentary package M27-M29a (coarse-grained facies)

A downdip transect through sedimentary package M27–M29a, which is bounded by surface 1 (m5.4 sequence boundary of Miller et al., 2013a) and surface 2 (Fig. 4.8), reveals the following: (1) an increase in mean grain size from topset (0.14 mm) to foreset (0.16 mm) to bottomset (0.16 mm) deposits (Figs. 4.13a); (2) an increase in sorting from foreset (2.4 s) to bottomset (2.0 s) deposits (Fig. 4.13b); (3) the lowest sphericity and most angular grains retained in foreset deposits (Figs. 4.13c and 4.13d); (4) consistently bimodal grain-size distribution throughout the depositional profile that varies minimally downdip (Fig. 4.7j); and (5) an increasing sand-to-mud ratio from topset (71:29; Fig. 4.10a) through to foreset (88:12; Fig. 4.10d) and bottomset (84:16; Fig. 4.10g) deposits.

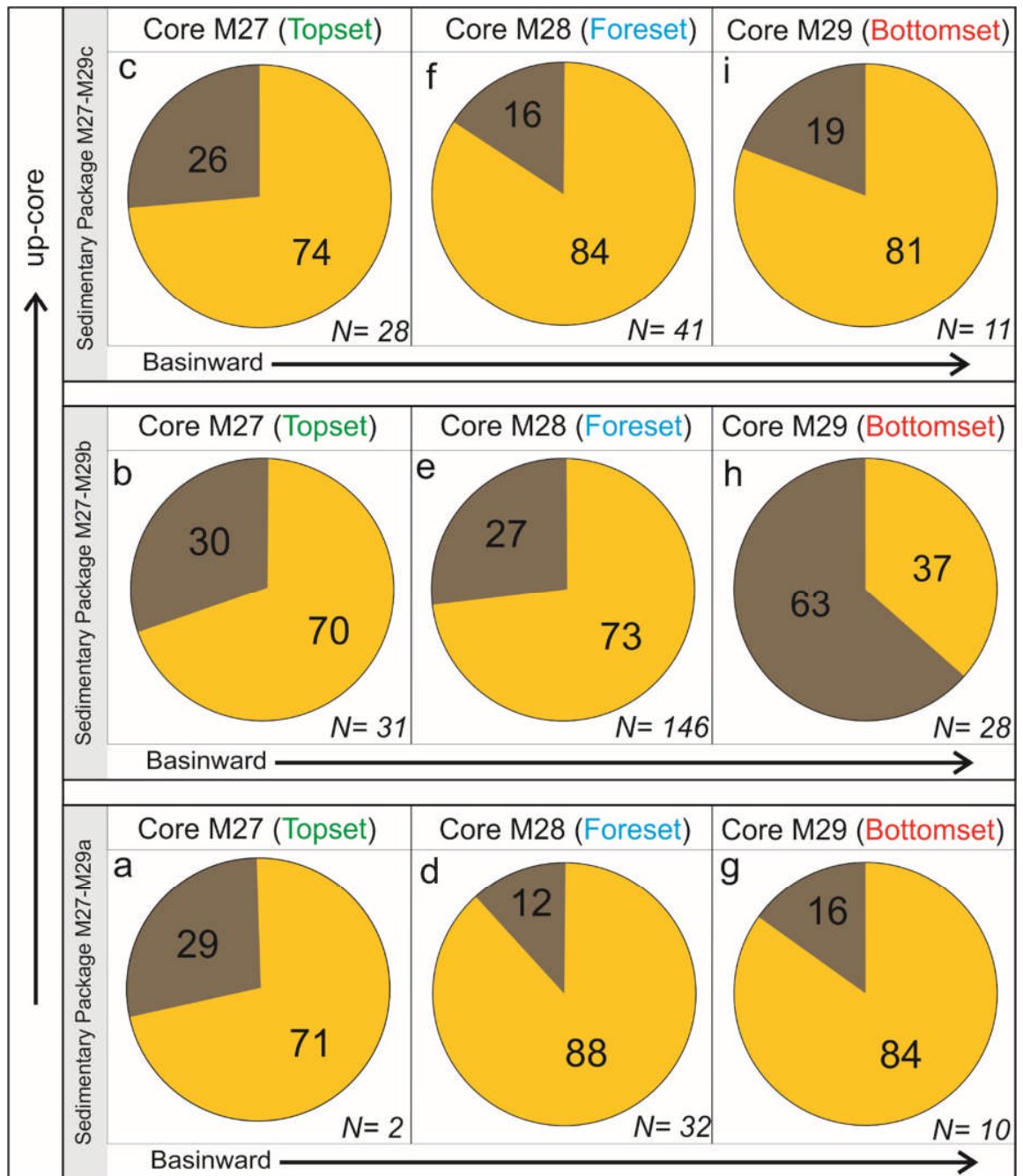


Figure 4.10: Pie charts showing average sand-to-mud composition by percentage volume. a) Sedimentary package M27a (topset); b) sedimentary package M27b (topset); c) sedimentary package M27c (topset); d) sedimentary package M28a (foreset); e) sedimentary package M28b (foreset); f) sedimentary package M28c (foreset); g) sedimentary package M29a (bottomset); h) sedimentary package M29b (bottomset); i) sedimentary package M29c (bottomset). The number of samples used to produce each pie-chart is shown by N= X.

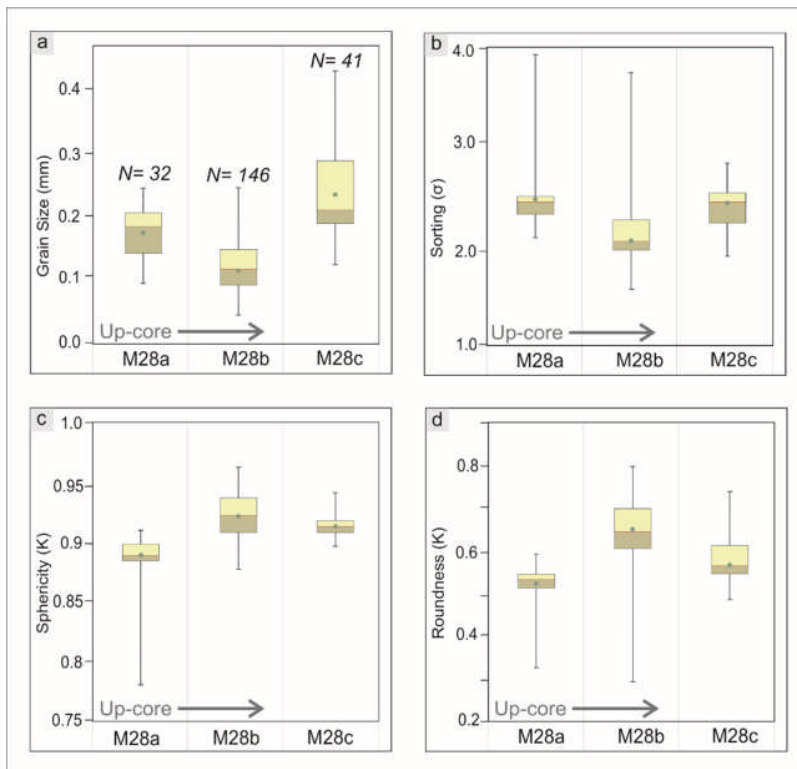


Figure 4.11: Box and whisker plot for sedimentary packages M28a, M28b and M28c (foreset deposits); a) grain size; b) sorting; c) sphericity; d) roundness. The legend is shown in Figure 4.9a. The number of samples used to produce each box and whisker plot is shown in Part a by $N = X$.

4.6.9.2 Sedimentary package M27-M29b (fine-grained facies)

The downdip profile of sedimentary package M27–M29b, which is bounded by surfaces 2 and 3 (Fig. 4.8), reveals the following: (1) a decrease in mean grain size from topset (0.11 mm) and foreset (0.11 mm) to bottomset deposits (0.061 mm; Fig. 4.14a); (2) an increase in sorting from topset to foreset and bottomset deposits (Fig. 4.14b); (3) an increase in sphericity and roundness downdip (Figs. 4.14c and 4.14d); (4) a grain-size distribution that is consistently unimodal and narrows and fines downdip (Fig. 4.7k); and (5) a variable sand-to-mud ratio from topset (30:70; Fig. 4.10b) through foreset (27:73; Fig. 4.10e) to bottomset deposits (37:63; Fig. 4.10h).

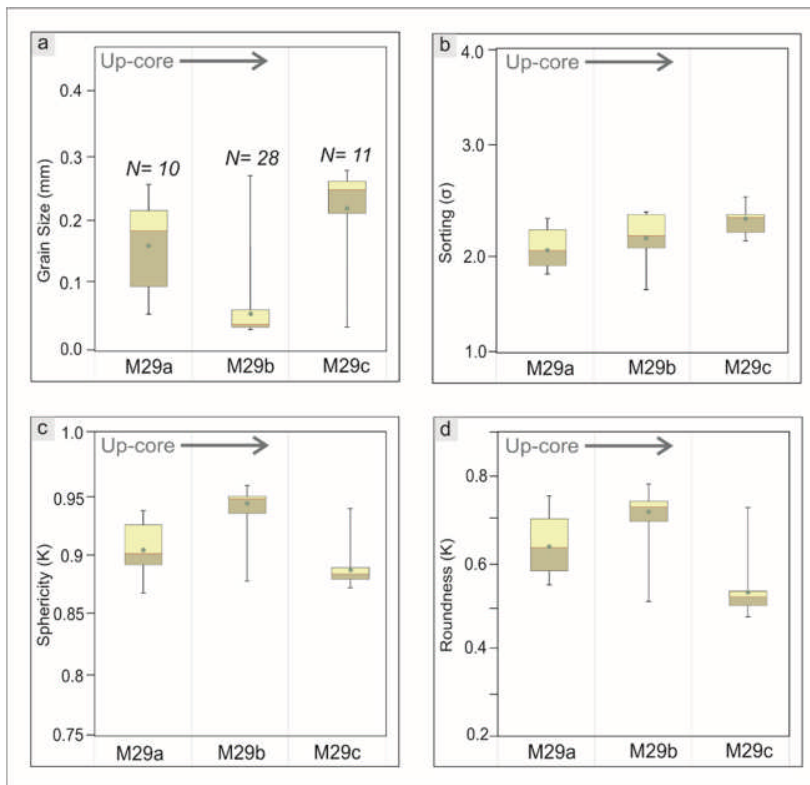


Figure 4.12: Box and whisker plot for sedimentary packages M29a, M29b and M29c (bottomset deposits); a) grain size; b) sorting; c) sphericity; d) roundness. The legend is shown in Figure 4.9a. The number of samples used to produce each box and whisker plot is shown in Part a by N= X.

4.6.9.3 Sedimentary package M27-M29c (coarse-grained facies)

The downdip profile of sedimentary package M27 – M29c, which is bounded by surface 3 and the overlying m5.3 sequence boundary (Miller et al., 2013a; see also Fig. 4.8 herein), reveals the following: (1) The coarsest grain sizes (0.24 mm) are found within foreset deposits relative to topset (0.13 mm) and bottomset (0.21 mm) deposits (Fig. 4.15a); (2) the most poorly sorted deposits are retained in the foreset deposits (Fig. 4.15b); (3) the least spherical and most angular grains are found within bottomset deposits (Fig. 4.15c and 4.15d); (4) the average grain-size distribution is consistently bimodal and varies minimally downdip (Fig. 4.71); and (5) the sand-to-mud ratio is lowest in topset deposits (26:74; Fig. 4.10c) and varies by < 5 % between foreset (84:16; Fig. 4.10f) and bottomset (81:19; Fig. 4.10i) deposits.

In summary, sedimentary package M27 – M29b displays: (1) a finer mean grain size; (2) better sorting; and (3) higher mean values of sphericity and roundness, and it consistently displays a unimodal average grain-size distribution (Figs. 4.7 and 4.8) relative to sedimentary packages M27 – M29a and M27 – M29c. The foreset and bottomset deposits of sedimentary package M27 – M29b are significantly more mud-prone relative to sedimentary packages M27 – M29a and M27 – M29c, which contain > 80 % sand (Fig. 4.10).

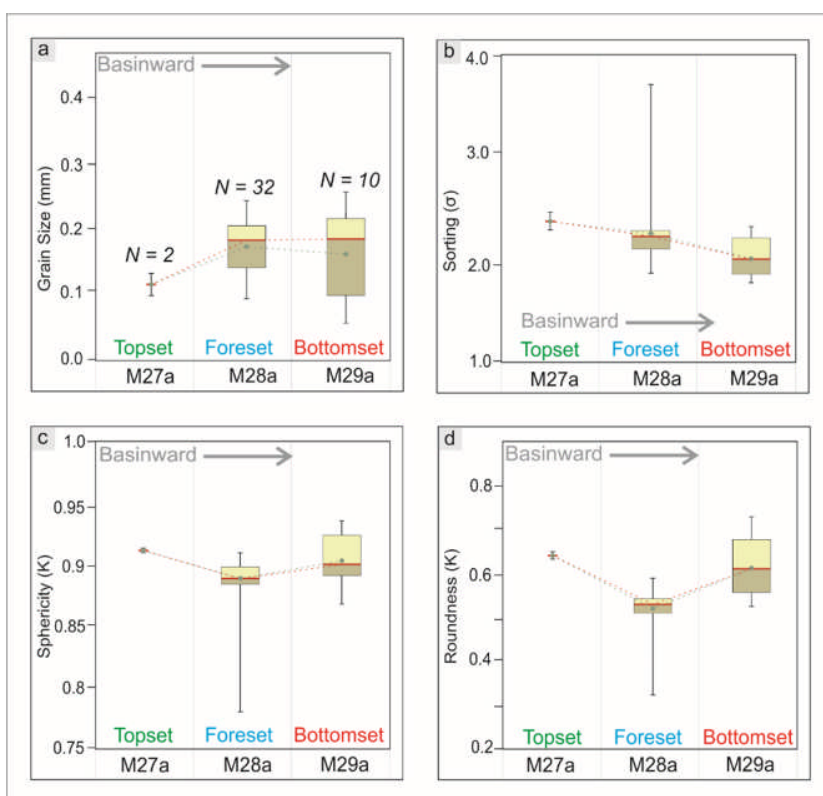


Figure 4.13: Box and whisker plot for sedimentary packages M27-M29a (topset-bottomset profile); a) grain size; b) sorting; c) sphericity; d) roundness. The legend is shown in Figure 4.9a. The number of samples used to produce each box and whisker plot is shown in Part a by $N = X$. Due to the low sample number for M27a, only the mean, median and standard deviation are shown.

4.6.10 Up-Core Grain-Size Patterns

The new high-resolution, quantitative grain-size data presented in this investigation are shown in Figure 4.8.

4.6.10.1 Site M27

From 300.00 mcd to 295.00 mcd, the dominant grain size is fine-grained sand, which typically makes up $\sim 60\%$ of the total grain-size composition. At 298.19 mcd, the grain size coarsens abruptly, associated with an increase in the medium sand content from $\sim 10\%$ to $\sim 30\%$, and the introduction of coarse sand, which forms $\sim 7\%$ of the overall grain-size composition. At 295 mcd, there is the surface 1 to m5.4 sequence boundary (Miller et al., 2013a), which is overlain by a sand-rich package, and an abrupt increase in the medium sand content (Fig. 4.8).

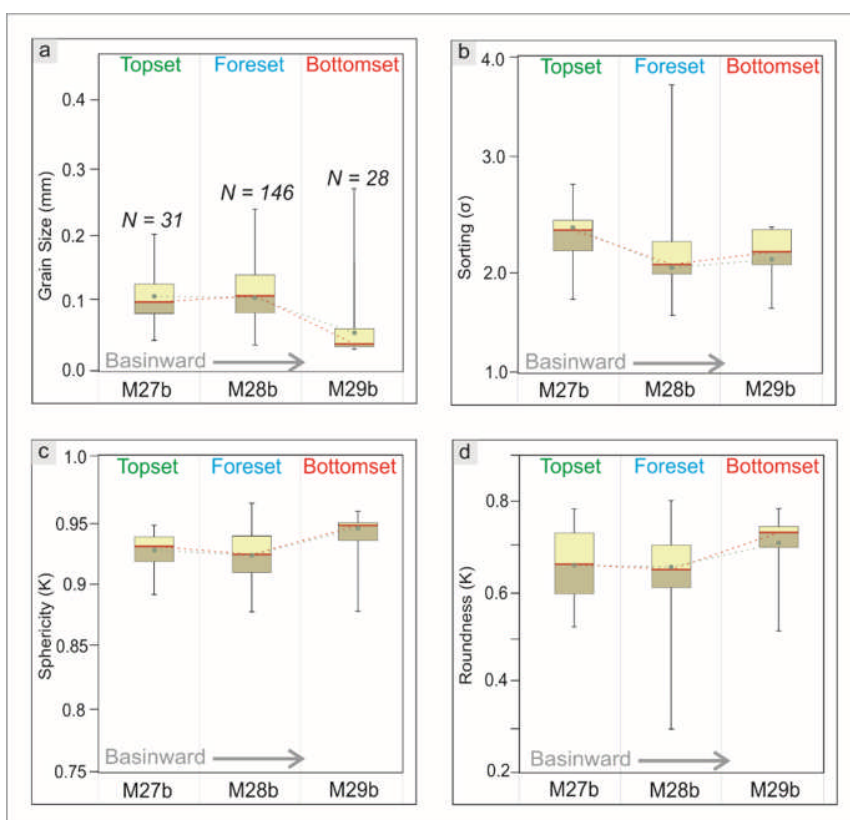


Figure 4.14: Box and whisker plot for sedimentary packages M27-M29b (topset-bottomset profile); a) grain size; b) sorting; c) sphericity; d) roundness. The legend is shown in Figure 4.9a. The number of samples used to produce each box and whisker plot is shown in Part a by $N = X$.

The coarse-grained sandy package (composed of $\sim 45\%$ and $\sim 10\%$ medium- and coarse-grained sand, respectively) terminates at 294.26 mcd (surface 2). Immediately overlying surface 2, there is an increase in the overall silt content (from $\sim 15\%$ to $\sim 30\%$) and a decrease in the medium sand content (from $\sim 45\%$ to $\sim 10\%$) within a fining-upward trend (294.26–285.06 mcd); this is overlain by a coarsening-upward package (285.05–279.78 mcd). A final fining-upward package (279.78–272.99 mcd) terminates at surface 3 (272.99 mcd; this study). Surface 3 is marked by a decrease in silt content ($\sim 55\%$ to $\sim 18\%$) and increase in coarse and very coarse sand, which form $\sim 30\%$ of the total sediment composition. Grain-size trends overlying surface 3 show a general fining-upward motif (272.98–256.19 mcd), which terminates at the overlying sequence boundary m5.3 (256.19 mcd). Overlying the Miller et al. (2013b) m5.3 sequence boundary, there is general coarsening-upward trend to 251 mcd, and there is an increase in the medium sand content from $\sim 5\%$ below the m5.3 sequence boundary to a maximum of $\sim 25\%$ at 251.52 mcd (Fig. 4.8).

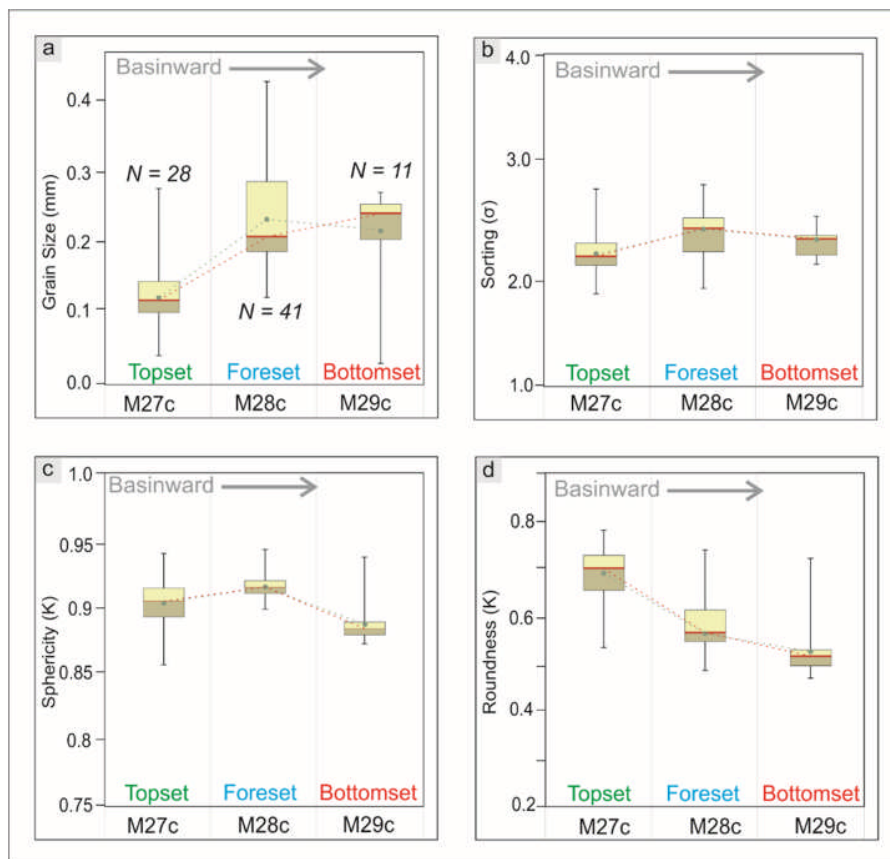


Figure 4.15: Box and whisker plot for sedimentary packages M27-M29c (topset-bottomset profile); a) grain size; b) sorting; c) sphericity; d) roundness. The legend is shown in Figure 4.9a. The number of samples used to produce each box and whisker plot is shown in Part a by $N = X$.

4.6.10.2 Site M28

From 525 to 519.7 mcd, there is a fining-upward sandy package, which typically consists of ~ 35 % medium sand. At 519.7 mcd (alternative m5.4 sequence boundary as proposed by Hodgson et al., 2018), there is a marked increase in medium sand content (~ 55 %). From 519.7 to 515.89 mcd, there is a fining-upward trend that results in an increase in the overall silt content from ~ 12 % at 516.8 mcd to ~ 52 % at 514.74 mcd (Fig. 4.8). From 514.71 to 512.33, there is a general coarsening-upward trend. The 512.33 mcd sequence boundary (Miller et al., 2013a) is shared by surface 1 (this study) and immediately overlies a very coarse sand at 512.97 mcd. Grain-size trends overlying surface 1 show a general coarsening-upward trend to 495.00 mcd (surface M28b; this study). Surface 2 is associated with an overlying fining in mean grain size and the disappearance of the coarse sand fractions. Surface 1 corresponds with the placement of the original m5.4 surface identified in Mountain et al. (2010) at 495.2 mcd, where a thin sand bed overlies a clayey silt. Grain-size trends overlying surface 2 show two fining-upward packages (495.00 – 459.95 and 459.94 – 432 mcd), which are overlain by a package of fine sand (432.00 – 415.00 mcd) that terminates at surface 3

(415.00 mcd; this study). Surface 3 is associated with a marked increase in medium sand content from ~ 7 % to ~ 45 % of the total sediment composition. Overlying surface 3, there are two coarsening-upward packages (415.00 – 392.00 and 392.00 – 363.00 mcd), which terminate at sequence boundary m5.3 (363.00 mcd; Miller et al., 2013a). Directly overlying the m5.3 sequence boundary, the gravel and very coarse sand are no longer present. From 363.00 to 358.00 mcd, the grain-size composition is dominated by fine and medium sand (Fig. 4.8).

4.6.10.3 Site M29

From 667.00 to 662.37 mcd, there is a general fining-upward trend; at this stratigraphic interval, the grain-size composition is dominated by fine and medium sand. At 662.37 mcd, there is the m5.4 sequence boundary (Miller et al., 2013a), shared by surface 1 (this study). Directly overlying surface 1, there is a decrease in silt content from ~ 50 % to ~ 12 % and an increase in the medium sand content from ~ 10 % to ~ 60 %. From 662.37 to 658.50 mcd, there is a sedimentary package dominated by medium sand, which forms ~ 50 % of the total sediment composition (Fig. 4.8). The sand-rich package terminates at surface 2 (658.50 mcd; this study). Directly overlying surface 2, there is a marked increase in the silt content (from ~ 5 % to ~ 75 %). Overlying surface 2, the grain size is dominated by silts (658.50 – 651.64 mcd), which form ~ 60 % to ~ 80 % of the total sediment composition; the silts are occasionally punctuated by thin lenses of medium and coarse sand (Fig. 4.8). The silt-rich package terminates at surface 3 (651.64 mcd). Directly overlying surface 3, the silt content drops from ~ 75 % to ~ 5 %, and coarse sand is present, forming ~ 25 % of the total sediment composition. Overlying surface 3, there is a fining-upward trend (651.64–649.51 mcd), followed by a coarsening-upward package (649.50–643.19), which terminates at the overlying sequence boundary m5.3 (643.19 mcd). From 643.19 to 638 mcd, there is an overall fining-upward trend (Fig. 4.8).

4.7 Discussion

4.7.1 How Does Intraclinothem Topset Process-Regime Influence Downdip Grain Character?

4.7.1.1 Vertical Process Variability and Grain Character

The core expression of sequence m5.4 topset deposits indicates that either fluvial-dominated (M27a and M27c) or wave- and storm-dominated (M27b) processes were active within the same seismic sequence. The presence of both fluvial and wave-and-storm process-regimes within one seismic sequence indicates that sequence m5.4 is an example of a mixed-energy system (e.g., Ainsworth et al., 2008, 2011; Olariu, 2014; Gomis-Cartesio et al., 2017), rather

than a clinothem described by a single process-regime (see examples cited in Dixon et al., 2012a). Concomitant changes in quantitative grain character occur in association with changes in the dominant process-regime.

4.7.1.2 River-dominated sedimentary packages

The sand-to-mud ratios show river-dominated sedimentary packages are dominated by bypass of sand-grade sediment across topsets and preferential deposition within foreset and bottomset deposits (Fig. 4.10). The shapes of the grain-size distribution profiles vary minimally between foreset and bottomset deposits (Figs. 4.7j and 4.7l); this suggests the bulk transfer of sand fractions across topsets. However, the foreset deposits are relatively coarser, indicating preferential deposition of the coarser grain-size fractions (0.25 – 0.75 mm; medium- and coarse-grained sand) in the slope setting. This may reflect the rapid dissipation of gravity-flow energy, resulting in slope deposition of the coarsest grain-size classes.

The high sand-to-mud ratios are associated with debritic and turbiditic foreset and bottomset deposits, which are typically glauconite-bearing sands. The association between reworked glauconite and river-dominated topsets was documented by Mountain et al. (2010), who interpreted clinoform sequences that had poorly sorted glauconitic sand in the clinoform rollover position as river-dominated features. The presence of recycled glauconite within foreset and bottomset deposits supports topset glauconitic sands as a sediment source for downdip deposits (Hodgson et al., 2018; Proust et al., 2018). Although the sand content is relatively high within the river-dominated sedimentary packages, river-dominated deposits are less well sorted, and grain shapes tend to be less spherical and more angular than that of the wave- and storm-dominated sedimentary package (Figs. 4.13, 4.14, and 4.15). The lower textural maturity of the river-dominated deposits reflects a shorter transport time from hinterland erosion to deposition within foreset and bottomset deposits (Hodgson et al., 2018). The river-dominated deposits exhibit a consistent bimodality in average grain-size distribution (Figs. 4.7j and 4.7l), which suggests a dual sediment source. This is interpreted to reflect a fine sand component associated with hinterland erosion and a coarser glauconite sand component associated with reworking from topset and clinoform rollover deposits. The bimodality in average grain-size distribution is present throughout the topset to bottomset profile in both river-dominated packages (Figs. 4.7j and 4.7l). In both cases, there is a slight coarsening from topset to foreset deposits, and then the average grain-size distribution remains constant between foreset and bottomset deposits (Figs. 4.7j and 4.7l). The coarsest grains are not sequestered in topset deposits, suggesting bypass of the coarsest-grained sediment fractions, possibly through channels. The average grain-size distribution profile of

the river-dominated deposits reflects sourcing of the coarsest grain-size fractions (typically reworked glauconite and quartz) from the clinoform rollover seaward of the core M27 intersection. Additionally, the average grain-size distribution profiles also indicate relatively efficient sediment transport beyond the shelf break, associated with sediment bypass (cf. Stevenson et al., 2015).

4.7.1.3 Wave-and-storm-dominated sedimentary packages

The sand-to-mud ratios of the wave- and storm-dominated sedimentary package (M27–M29b) are consistently lower than those of the river-dominated packages; the difference in sand content becomes greater downdip, where the bottomsets of the river-dominated packages contain up to 47 % more sand than the wave- and storm-dominated sedimentary package (Fig. 4.10). The sand-to-mud ratios of the wave- and storm-dominated sedimentary package show the retention of sand-grade sediment within topset and foreset deposits, with limited basinward sand bypass (Fig. 4.10). The bottomset deposits are associated with mud-grade sediment, attributed to deposition from suspension fallout. Compared to the river-dominated deposits, the foreset and bottomset deposits of the wave- and storm-dominated sedimentary package are less sand-rich (foreset and bottomset deposits contain an average of 13 % and 45.5 % less sand, respectively; Fig. 4.10), but the textural maturity is higher (Figs. 4.13, 4.14, and 4.15). The relatively higher textural maturity displayed by the wave- and storm-dominated deposits reflects reworking processes landward of the shelf edge, associated with the redistribution of sediment and a longer residence time within the sediment transport system (Bhattacharya and Walker, 1992; Deibert et al., 2003; Li et al., 2015).

The downdip average grain-size distribution profiles of wave and storm deposits display prominent fining from topset to bottomset (Fig. 4.7k). This reflects the inefficiency of wave- and storm-dominated systems at transferring sand beyond the shelf edge, and the dominance of shore-parallel sediment redistribution (Coleman and Wright, 1975; Bhattacharya and Giosan, 2003), resulting in relatively thick, sand-prone topset deposits. The documentation of significant variability in sediment composition and texture within the bottomset deposits of a single clinotherm sequence suggests that nuanced changes in topset process regime may represent a hitherto overlooked contributing factor in the depositional evolution of clinotherm sequences.

4.7.1.4 Lateral variability in process-regime

The core data set presented here is from a single 2-D dip-parallel transect and captures only one portion of the along-strike variability; however, a network of 2-D seismic reflection lines permits the three-dimensional (3-D) architecture of sequence m5.4 to be constrained (Monteverde et al., 2008). Recent studies have highlighted that shallow-marine systems, both modern and ancient, can display prominent lateral variability associated with changes in the interactions among fluvial, wave, and tidal processes (Ta et al., 2002; Ainsworth et al., 2008, 2011; Olariu, 2014; Jones et al., 2015). The propensity for systems to exhibit lateral variability, associated with changes in the dominant process-regime, has the potential to increase grain-character heterogeneity both along strike and downdip. In the context of improved prediction of downdip facies from updip sedimentary facies, the interactions of temporal and lateral process-regime change could introduce significant variability not only in sand content, but also in grain character. For example, the influence of shore-parallel variability may be expressed as a lateral transition from a river-dominated topset system to a wave-dominated system further along strike; however, downdip of the wave-dominated system, a fan fed by the river-dominated system could be intersected.

Despite this, sequence m5.4 is a rare example of a chronostratigraphically constrained clinotherm, in which the sedimentological and stratigraphic characteristics of coeval topset, foreset, and bottomset deposits have been documented. Future studies of the relationship between along-strike variability in process-regime and grain-character variability will require exceptional outcrop control, or integrated 3-D seismic reflection data sets and core-hole data with strike and dip control.

4.7.1.5 Classification of mixed process-regime clinotherms

Cosgrove et al. (2018) determined that sequence m5.4 formed a rising clinof orm trajectory and was a wave-dominated feature. Across seismic sequence m5.4, the majority of the cored topset, foreset, and bottomset deposits preserve indicators consistent with wave-dominated topset deposits, including minimal transport of coarse-grained sediment into deep-water settings (e.g., Helland-Hansen and Hampson, 2009). However, designating the entire sequence as belonging to this end-member category fails to accurately describe the stratigraphic or geographic variability. The stratigraphic intervals in sequence m5.4 that have a river-dominated topset process-regime (sedimentary correlations M27 – M29a and M27 – M29c) are associated with the effective transport of coarse sand into the deep-water setting. Therefore, characterizing a clinotherm by a single process or a clinof orm trajectory fails to account for the inherent stratigraphic and lateral variability in mixed process-regime systems.

4.7.1.6 Autogenic and Allogenic Topset Process-Regime Change

The cause of changes in topset process-regime may be controlled by allogenic or autogenic forcing mechanisms. Allogenic controls, i.e., those which are external to the sedimentary unit, primarily document the effects of eustatic variability and changes in hinterland climatic and tectonic regime, which modulate the production and discharge of sediment from source regions (e.g., Castelltort and Van Den Driessche, 2003; Armitage et al., 2011). The effects of allogenic forcing mechanisms could feasibly result in changes in the topset process-regime and consequently account for the stratigraphic expression of the surfaces and sedimentary packages displayed in sequence m5.4. The scenario in which allogenic processes result in the observed intraclinothem surfaces, in addition to their regional basinward extent, would support their interpretation as sequence boundaries within a m5.4 composite sequence (Miller et al., 2013a, 2013b; Miller et al., 2018).

The intraclinothem surfaces could also be the result of autogenic controls, such as river avulsion and/or switching of wave-dominated delta lobes (e.g., Olariu, 2014; Hampson, 2016); this would mean that the intraclinothem surfaces are not sequence boundaries. Autogenic mechanisms have been shown to generate surfaces and stratigraphic architectures that are challenging to distinguish from those generated through allogenic processes (e.g., Muto and Steel, 2002). The identification of autogenic and/or allogenic generation of the intraclinothem surfaces, in this instance, remains tentative given the lack of strike control to test the regional extent of the surfaces and resolution of the chronostratigraphic data.

4.7.2 How Can High-Resolution Grain Character Data Be Used As An Additional Correlation Tool?

Miller et al. (2013a) determined sequence m5.4 to be a composite sequence, composed of three higher-order sequences (m5.4-1, m5.34, m5.33) of ~ 100 k.y. duration. However, the placement of the intraclinothem stratigraphic surfaces was associated with varying degrees of uncertainty (Fig. 4.4). The placement of the intraclinothem sequence boundaries at Site M27 is primarily based on stacking pattern analysis. However, trends above the m5.33 sequence boundary are acknowledged to be unclear (Miller et al., 2013b). Furthermore, the Sr-isotope error margins and the single sample used to date sequence m5.33 (Browning et al., 2013) render the chronostratigraphic data weak.

At Site M28, sequence boundary m5.4-1 (17.7 – 17.6 Ma; Browning et al., 2013) is suggested to share its basal reflector with sequence boundary m5.4 (Miller et al., 2013a). Sequence boundary m5.34 (479 mcd; Miller et al., 2013a) is interpreted from seismic reflector terminations; however, only a minor impedance contrast, a weak core expression (Miller et

al., 2013b), and no significant chronostratigraphic hiatus (Browning et al., 2013) are present. The placement of the m5.33 sequence boundary is based on the criteria of onlap and downlap (Miller et al., 2013a), which coincides with a coring gap (~ 405 mcd; Miller et al., 2013a). In light of the coring gap and the error associated with Sr-isotope data ($\pm 0.61 - 0.4$ m.y.; see Browning et al., 2013), the placement is ambiguous.

At Site M29, the correlation of sequence boundaries m5.4-1, m5.34, and m5.33 is more tentative. Sr-isotope data permit correlation with both the m5.4-1 and m5.34 sequence boundaries (17.7 – 17.6 Ma; Browning et al., 2013; Miller et al., 2013a). Additionally, there are weak/no core sequence boundaries proposed for m5.34 and m5.33, respectively, which, combined with chronostratigraphic data, provides unconvincing evidence for a composite sequence at M29.

Grain-character data provide an alternative approach to the subdivision of clinothems (Fig. 4.10). The alternative intraclinotem surfaces presented here were correlated across the complete depositional profile and correspond to changes in facies, grain size (Figs. 4.13 – 4.15), grain shape (Figs. 4.13 – 4.15), grain-size distribution (Fig. 4.7), sand-to-mud ratios (Fig. 4.10), and stratigraphic stacking pattern (Fig. 4.8). The placement of the intraclinotem surfaces in this investigation differs from those proposed previously (m5.4-1, m5.34, and m5.33; Miller et al., 2013a). The differences in the stratigraphic placement of the intraclinotem surfaces between previous investigations and this study are attributed to (1) the different methodologies used to identify the intraclinotem surfaces and (2) the stratigraphic resolution available to each investigation. The intraclinotem surfaces that separate the sedimentary packages presented in this investigation are attributed to changes in the dominant topset process-regime. The results presented here highlight the potential application of quantitative grain-character data sets as supplementary correlation tools. Abrupt changes in grain size (often qualitatively observed) are widely used as a means of subdividing the stratigraphic record; however, additional grain-character attributes (including sorting, sphericity, and roundness) are overlooked. The lack of data sets that utilize sorting, sphericity, and roundness as additional correlation tools reflects the general lack of quantitative data sets in the wider literature.

4.7.3 How Can High-Resolution Grain Character Data Be Used As An Additional Tool To Refine Sequence Boundaries?

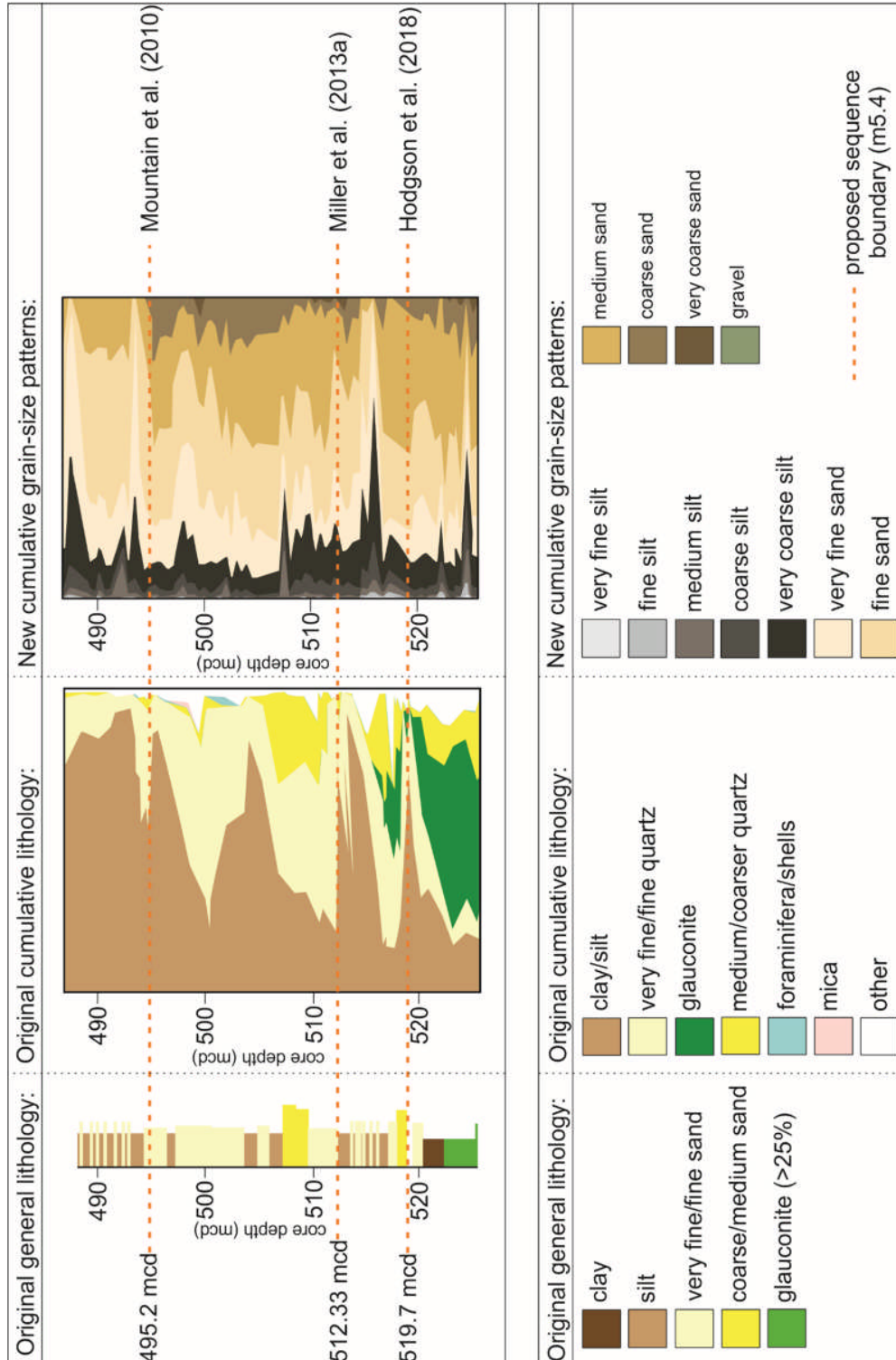


Figure 4.16: Comparison of the 'original general lithology' (Mountain et al., 2010), 'original cumulative lithology' (Miller et al., 2013b) and 'new cumulative grain-size patterns' (this study). The candidate m5.4 sequence boundaries (from Mountain et al., 2010; Miller et al., 2013a and Hodgson et al., 2018) are overlain in dashed orange lines.

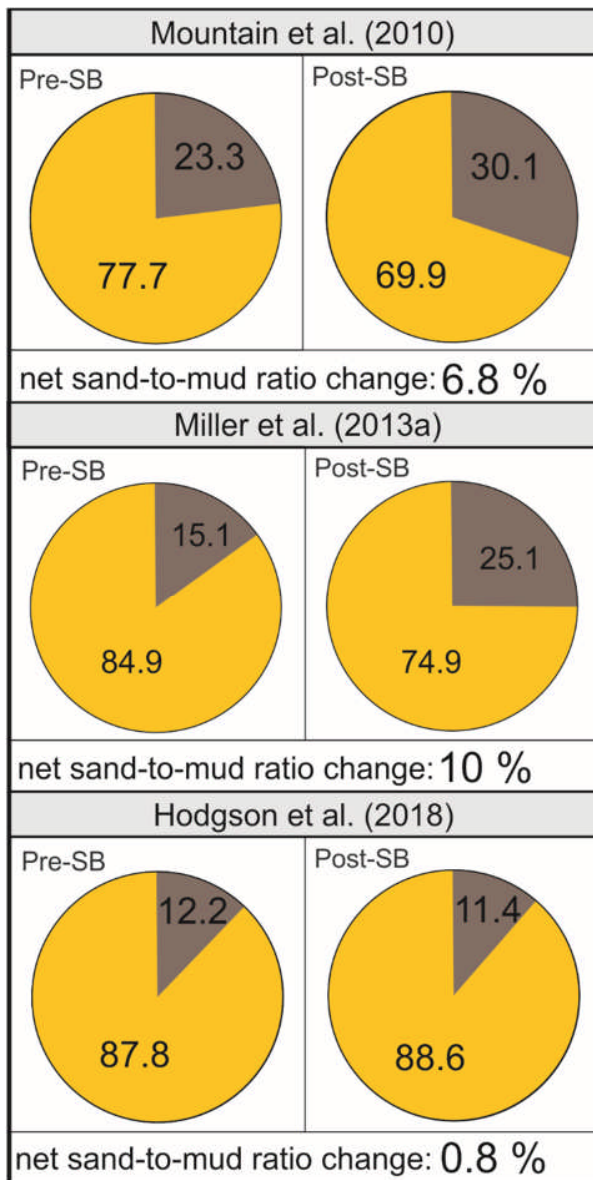


Figure 4.17: Pie-charts showing average sand-to-mud composition by percentage volume across the candidate sequence boundaries. The percentage difference in the sand: mud ratio has been calculated using the values of the samples closest to the proposed sequence boundary (i.e. the closest sample below and above the candidate sequence boundary). For the Mountain et al. (2010) candidate sequence boundary the samples are from 495.3 (below) and 494.8 (above) mcd. For the Miller et al. (2013a) candidate sequence boundary the samples are from 512.97 (below) and 512.23 (above) mcd. For the Hodgson et al. (2018) candidate sequence boundary the samples are from 519.8 (below) and 519.3 (above) mcd.

Different approaches exist for the placement of sequence boundaries across depositional profiles (e.g., Catuneanu et al., 2009; Hodgson et al., 2016; Barrett et al., 2018). However, in this instance, previous authors have followed a similar approach (Monteverde et al., 2008; Monteverde, 2008; Mountain et al., 2010; Miller et al., 2013a, 2013b; Hodgson et al., 2018; Miller et al., 2018) to place sequence boundaries within the Expedition 313 data set. Despite the integrated data set, which has identified sequence boundaries in multichannel seismic profiles and in core and sedimentary logs, uncertainty remains regarding the placement of the

m5.4 sequence boundary (Fig. 4.4). At Site M28, sequence boundary m5.4 has been placed at 495.2 mcd by Mountain et al. (2010), at 512.33 mcd by Miller et al. (2013a), and an alternative at 519.7 mcd by Hodgson et al. (2018). The ambiguity surrounding the exact placement of the sequence boundary m5.4 is exacerbated by the absence of strong supporting seismic impedance contrast and chronostratigraphic data, and the non-uniqueness of core-based approaches to identify sequence boundaries (e.g., Browning et al., 2006). The surface of Mountain et al. (2010) corresponds to a thin sand bed overlying a clayey silt. The surface of Miller et al. (2013a) corresponds to a contact of fine sand overlying clayey silt; this is associated with a minor impedance contrast and a minimal chronostratigraphic time gap (ca. 17.9 Ma below and 17.7 Ma above). The alternative surface of Hodgson et al. (2018) corresponds to a bioturbated contact, where an upward-fining, sharp-based sand is overlain by silt.

4.7.3.1 Grain-Size Trends

Mountain et al. (2010), Miller et al. (2013a), and Hodgson et al. (2018) used abrupt changes in stacking patterns and grain size to aid placement of the m5.4 sequence boundary. The higher-resolution, fully quantitative grain-size data presented in this investigation reveal more detailed up-core grain-size trends and stacking patterns (Fig. 4.16). In the original semi-quantitative cumulative lithology, the Hodgson et al. (2018) alternative sequence boundary (519.7 mcd) appears to immediately overlie a clay- and silt-rich horizon, which forms part of a fining-upward package. However, the candidate sequence boundary does not directly correspond with a prominent change in stacking pattern when the detailed cumulative grain-size data presented in this investigation are considered (Fig. 4.16). The new cumulative grain-size data do not indicate the presence of a large clay/silt peak directly underlying the proposed sequence boundary (Fig. 4.16). Instead, the total silt content remains relatively low (12 %), and a more subtle increase in the very fine and fine sand content is observed. This subtle but significant difference in grain size is likely a product of the different (quantitative and semi-quantitative) methodologies used in this investigation versus those presented in Miller et al. (2013b). The candidate sequence boundary proposed by Hodgson et al. (2018) does correspond with an increase in the medium sand content (30 % and 47 % directly below and above the proposed surface, respectively; Fig. 4.16). However, this does not correspond with an overall change in stacking pattern, as is suggested by the original semi-quantitative cumulative lithology. The new data presented here place the candidate sequence boundary proposed by Hodgson et al. (2018) within a fining-upward package, which peaks at 515.89 mcd and corresponds with a large peak in the silt content. The ~ 1.5 m sampling interval used

to produce the original semi-quantitative cumulative lithology was not of sufficient resolution to capture this.

The candidate sequence boundary proposed by Mountain et al. (2010; 495.00 mcd) was placed using general lithology alone, and it was placed within a very fine to fine sand package. The new cumulative grain-size data presented here indicate that the candidate sequence boundary of Mountain et al. (2010) corresponds to a broad change in stacking pattern and falls where a coarsening-upward package (containing coarse and very coarse sand) abruptly transitions into a relatively finer-grained package (Fig. 4.16). The abrupt change in grain size at 495.00 mcd is interpreted to represent intraclinothem surface 2, associated with a change in the topset process-regime and the depositional style associated with this change.

In the original semi-quantitative cumulative lithology, the candidate sequence boundary proposed by Miller et al. (2013a; 512.33 mcd) appears to overlie a coarsening-upward package and was placed at the junction between a clay/silt peak and very fine/fine sand package (Fig. 4.16). The new cumulative grain-size data presented here show the same overall stacking pattern: a coarsening-upward package that terminates at the 512.33 mcd and is overlain by a blocky, sand-rich package. There is also a peak in the fine sand content (40 % of the total sediment composition) directly overlying the candidate sequence boundary of Miller et al. (2013a). The clay/silt content presented in the original semi-quantitative cumulative lithology is significantly higher than that of the new high-resolution grain-size data; this is attributed to differences in technique used for data acquisition. The candidate sequence boundary at 512.33 mcd broadly corresponds with a change in stacking pattern across the original qualitative general lithology, the original semi-quantitative cumulative lithology, and the new high-resolution grain-size data presented here, which supports this position as the m5.4 sequence boundary.

From the lower-resolution, semi-quantitative cumulative lithology, it is clear that previous authors have identified potential sequence boundaries based upon perceived abrupt changes in grain size and lithology, alongside core-based criteria (Fig. 4.16). The higher-resolution quantitative data set presented here displays the same broad-scale (approximately tens of metres) trends in stacking as those presented by Mountain et al. (2010) and Miller et al. (2013b), but it refines and improves: (1) the accuracy of the grain-size composition and (2) the stratigraphic locations of changes in stacking pattern.

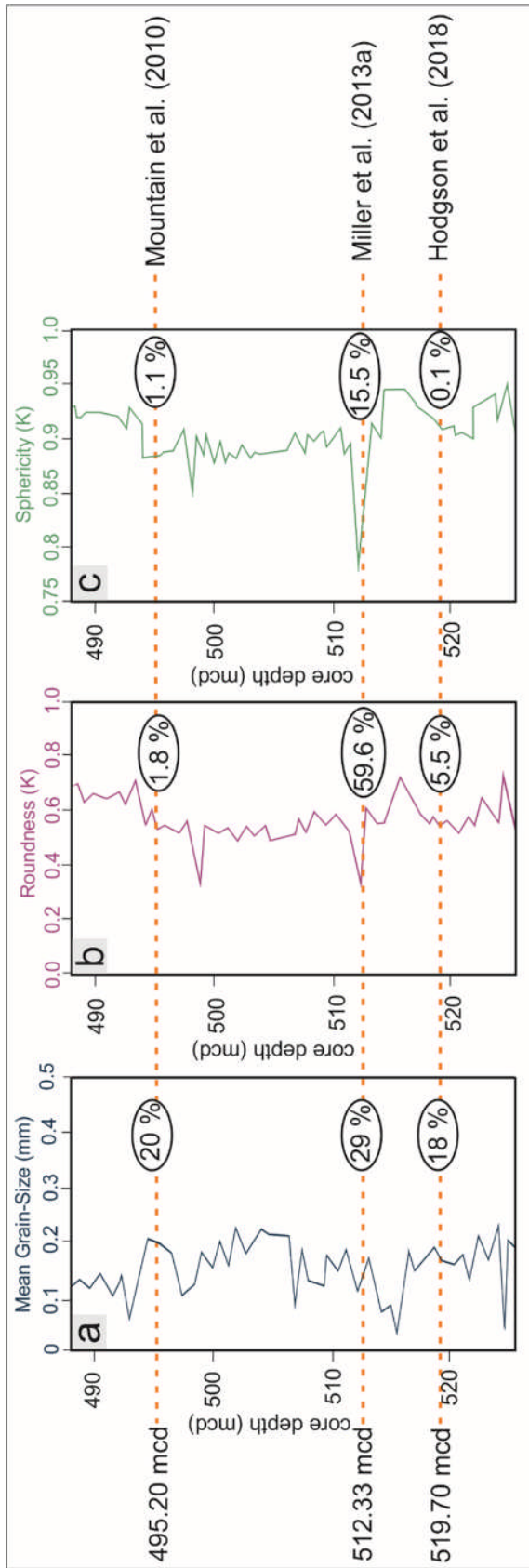


Figure 4.18: Percentage difference in grain character across candidate sequence boundaries. The percentage differences have been calculated using the values of the samples closest to the proposed sequence boundary (i.e. the closest sample below and above the candidate sequence boundary). See Figure 4.17 caption for sample positions; a) mean grain size; b) mean grain roundness; c) mean grain sphericity

4.7.3.2 Grain-Character

The fully quantitative nature of this data set enables changes grain size (including sand-to-mud content and mean grain size) to be calculated across the three candidate sequence boundaries. Of the three proposed sequence boundaries, the greatest change in sand-to-mud content occurs at the Miller et al. (2013a) boundary at 512.33 mcd, where a net change of 10 % in sand-to-mud content is recorded, compared to 6.8 % and 0.8 % change at the Mountain et al. (2010) and Hodgson et al. (2018) boundaries, respectively (Fig. 4.17). In addition to the changes in sand-to-mud ratios, changes in mean grain size across the proposed sequence boundaries have been calculated (Fig. 4.18). The largest change in mean grain size across the three candidate sequence boundaries again occurs across the 512.33 mcd sequence boundary (Miller et al., 2013a), where a 29 % change in mean grain size is observed, compared to a 20 % and 18 % change at the 495.2 mcd (Mountain et al., 2010) and 519.7 mcd (Hodgson et al., 2018) boundaries, respectively (Fig. 4.18a). One of the fundamental tenets for determining sequence boundaries is based upon the identification of abrupt stratigraphic changes in grain size; hitherto, a quantitative assessment of these parameters has been unavailable due to the relatively low sampling densities and qualitative/semiquantitative methodologies employed by previous authors. Quantitative analysis of sand-to-mud ratios and mean grain-size changes across the three proposed sequence boundaries supports a preferred sequence boundary at 512.33 mcd (Miller et al., 2013b), which displays the greatest overall change in grain size (Figs. 4.17 and 4.18a).

Up-core grain-shape characteristics (sphericity and roundness; Figs. 4.18b and 4.18c) are also shown alongside the potential sequence boundaries proposed by Mountain et al. (2010), Miller et al. (2013a), and Hodgson et al. (2018). Similarly, the grain-shape data support placement of the Miller et al. (2013a) sequence boundary at 512.33 mcd. The grain shapes become increasingly angular and less spherical up core to the 512.33 mcd sequence boundary; at the 512.33 mcd sequence boundary, there is a significant drop in both grain sphericity (from 0.91 to 0.78; 15.5 %) and grain roundness (from 0.61 to 0.33; 59.6 %) to their lowest levels within the stratigraphic section (Fig. 4.18). The dramatic difference in grain shape across this stratigraphic horizon supports a fundamental change in sediment source and/or transport regime, consistent with a depositional hiatus and sequence boundary; this is supported by the core expression of the 512.33 mcd sequence boundary (see Miller et al., 2013a). The other candidate sequence boundaries exhibit significantly less change in grain shape across the proposed sequence boundaries: 1.8 % and 5.5 % change in roundness and

1.1 % and 0.1 % change in sphericity for the Mountain et al. (2010) and Hodgson et al. (2018) candidate sequence boundaries, respectively (Fig. 4.18).

The high-resolution grain-character data presented here may provide an additional, complementary approach, to be used in conjunction with core criteria, to refine the placement of sequence boundaries, and/or to determine the most statistically likely sequence boundary from a number of candidate sequence boundaries. Additionally, the higher-resolution up-core grain-size data presented here highlight the fact that lower-resolution, semi-quantitative lithological data may dramatically oversimplify grain-size trends and promote the somewhat arbitrary placement of sequence boundaries in core sections.

4.8 Conclusions

Integrated grain-character data and core facies have been used to describe a mixed process-regime Miocene clinothem sequence offshore New Jersey, USA. The quantitative, high-resolution grain-character data have enabled the topset, foreset, and bottomset deposits to be subdivided into three sedimentological packages, based on shared grain-character attributes. The topset core expression indicates that sedimentary packages M27–M29a and M27–M29c were deposited under a river-dominated process-regime, as indicated by (1) widespread topset asymmetric ripple lamination; (2) terrestrial, woody organic matter; and (3) abundance of detrital quartz and glauconite sand grains. The topset core expression indicates that sedimentary package M27–M29b was deposited under a wave- and storm-dominated process-regime, as indicated by (1) widespread hummocky cross-stratification; (2) rhythmically laminated topset deposits; and (3) symmetrical ripple lamination.

The correlations of sedimentary packages across the topset-foreset-bottomset profile using high-resolution grain-character data provides a unique perspective into intraclinotem architecture and basin fill within a single seismic-scale clinotem. The dominant topset process-regime exerts a fundamental control on the distribution of grain character. In this system, the sedimentary packages associated with river-dominated topset conditions have higher sand-to-mud ratios across the downdip profile; however, the grain character is texturally less-mature relative to the wave- and storm-dominated sedimentary package. The differences in grain character between the river-dominated and wave- and storm-dominated sedimentary packages are exaggerated downdip.

The sedimentary packages are separated by intraclinotem surfaces, which were determined objectively using changes in the average grain-size distribution, and which are concomitant with stratigraphic changes in the facies, grain-size composition, and grain shape and sorting parameters. The identification of coeval sedimentary packages at subseismic resolution from grain character alone is a novel methodology for subdividing the stratigraphic record and

provides a high-resolution correlation of strata within a sand-rich sequence. However, the dataset does not resolve whether the intraclinothem surfaces are formed through autogenic or allogenic controls.

The high-resolution, quantitative grain-character data are also shown here to be an additional tool to help refine the placement of sequence boundaries. In this instance, the grain-character data were used to support the preferred placement of a sequence boundary position from three previously postulated candidate sequence boundaries. This was achieved by quantitatively assessing grain-size and grain shape change across the proposed sequence boundaries. Additionally, the new data presented here helped to refine and improve interpretations of stacking patterns and grain-size trends.

Chapter 5 Manuscript Three

Grain Character and Process-Regime Change Recorded down Clinotherm Slope Profiles

5.1 Abstract

Shelf-margin clinothem successions can archive process interactions at the shelf-to-slope transition, and their architecture provide constraints on the interplay of factors that control basin-margin evolution. However, detailed textural analysis and facies distributions from shelf-to-slope transitions remain poorly documented. This study uses quantitative grain-size and sorting data from coeval shelf and slope deposits of a single clinothem that crops out along a 5 km-long, dip-parallel transect of the Eocene Sobrarbe Deltaic Complex (Ainsa Basin, south-central Pyrenees, Spain). Systematic sampling of sandstone beds tied to measured sections have captured vertical and basinward changes in sedimentary texture and facies distributions at an intra-clinothem scale. Two types of hyperpycnal flow, related slope deposits, both rich in mica and terrestrial organic matter, are differentiated according to grain size, sorting and bed geometry: 1) sustained hyperpycnal flow deposits, which are physically linked to coarse channelised sediments in the shelf setting and which deposit sand down the complete slope profile; 2) episodic hyperpycnal flow deposits, which are disconnected from, and incise into, shelf sands and which are associated with sediment bypass of the proximal slope and coarse-grained sand deposition on the medial and distal slope. Both types of hyperpycnites are interbedded with relatively homogenous, organic- and mica-free, well-sorted, very fine-grained sandstones, which are interpreted to be remobilised from wave-dominated shelf environments; these wave-dominated deposits are found only on the proximal and medial slope. Coarse-grained sediment bypass into the deeper-water slope settings is therefore dominated by episodic hyperpycnal flows, whilst sustained hyperpycnal flows and turbidity currents remobilizing wave-dominated shelf deposits are responsible for the full range of grain-sizes in the proximal and medial slope, thus facilitating clinoform progradation. This novel dataset highlights previously undocumented intra-clinothem variability related to updip changes in the shelf process-regime, which is therefore a key factor controlling downdip architecture and resulting sedimentary texture.

5.2 Introduction

Clinothems typically form progradational basin margin successions (e.g., Gilbert, 1885; Rich, 1951; Asquith, 1970; Mitchum et al., 1977; Pirmez et al., 1998; Adams and Schlager, 2000; Bhattacharya, 2006; Patruno et al., 2015). Seismic reflection and well-log data have been used extensively to study subsurface clinothem successions (e.g., Ross et al., 1995; Pinous et al., 2001; Donovan, 2003; Jennette et al., 2003; Hadler-Jacobsen et al., 2005). However, outcrop

examples of clinothems offer a higher-resolution record of stratigraphic and downslope clinothem evolution (e.g., Helland-Hansen, 1992; Dreyer et al., 1999; Pyles and Slatt, 2007; Pontén and Plink-Björklund, 2009; Hubbard et al., 2010; Dixon et al., 2012a; Jones et al., 2013; Poyatos-Moré et al., 2019). Exhumed clinothem successions provide the opportunity to document patterns of facies distribution and sedimentary texture. This information can be used to help constrain the interplay of controls on clinothem evolution (e.g., Mellere et al., 2002; Plink-Björklund and Steel, 2003; Carvajal and Steel, 2006; Pyles and Slatt, 2007; Jones et al., 2015; Laugier and Plink-Björklund, 2016). However, predicting facies distributions and sedimentary textures within individual clinothems, both vertically and along depositional dip, remains challenging (Cosgrove et al., 2018). In part, this is due to the lack of detailed, quantitative grain size and sorting datasets recovered from clinothem sequences, which has left down-clinothem changes in grain size and sorting as poorly constrained and largely unquantified parameters (Catuneanu et al., 2009).

Prediction of sedimentary texture along a continuous clinothem depositional profile is further complicated by changes in the dominant shelf process-regime (cf. Dixon et al., 2012b; Laugier and Plink-Björklund, 2016; Cosgrove et al., 2018). Process-regime affects how and when sediment of different calibre and maturity is transferred downdip (Dixon et al., 2012b; Cosgrove et al., 2018). Sudden changes in shelf process-regime can occur over intra-clinothem timescales (Ta et al., 2002; Ainsworth et al., 2008; Plink-Björklund, 2008; Carvajal and Steel, 2009; Vakarelov and Ainsworth, 2013; Jones et al., 2015). Despite this, mixed-energy clinothems systems are under-represented in the literature (see Ainsworth et al., 2011; Olariu, 2014; Rossi and Steel, 2016) and clinothems are therefore commonly designated as being end-member types (i.e. river-, wave-, or tide-dominated, systems) (e.g., Dreyer et al., 1999; Plink-Björklund et al., 2001; Plink-Björklund and Steel, 2002; Deibert et al., 2003; Crabaugh and Steel, 2004; Plink-Björklund and Steel, 2004; Johannessen and Steel, 2005; Petter and Steel, 2006; Sylvester et al., 2012). As such, the impact of mixed process-regime conditions on downslope sedimentary texture remains relatively understudied (e.g., Cosgrove et al., in press).

To improve understanding of process and textural variability within individual clinothem sequences, we focus on the Sobrarbe Deltaic Complex, an outcrop example of well-constrained clinothems, located in the Eocene Ainsa Basin, south-central Pyrenees, Spain (Fig. 5.1). This system is ideal for studying quantitative changes in grain size and sorting at high spatial resolution, due to the presence of a series of well-exposed and accessible clinothem sequences, which can be directly correlated from coeval fluvio-deltaic shelf to distal slope deposits (Dreyer et al., 1999). This investigation uses detailed facies analyses and quantitative

changes in grain size and sorting to address three overarching questions: i) How do changes in the dominant shelf process regime affect facies distribution within an individual clinothem sequence? ii) How do changes in sedimentary texture (including grain size and sorting) vary up-stratigraphy and along depositional dip? iii) Can quantitative grain-size data be used to identify sediment bypass at the cliniform rollover? This outcrop-based study provides new insights into the evolution of individual clinothems and may be used as a predictive reference for subsurface exploration and basin evolution models.

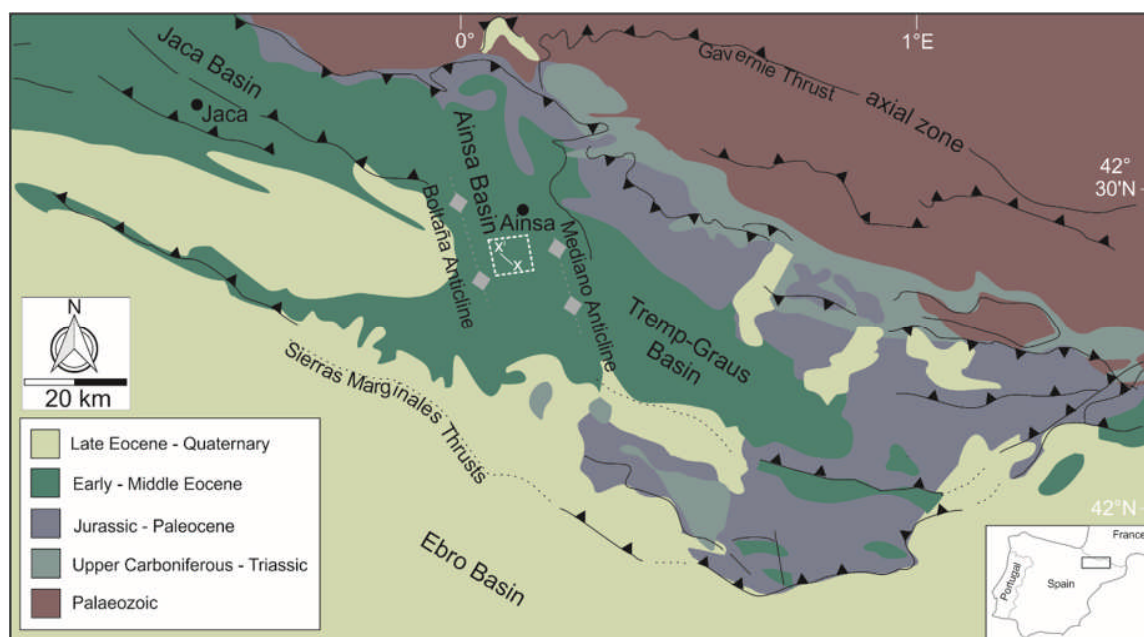


Figure 5.1: Map showing the location of the Ainsa Basin and the key neighbouring structural features, within the geological setting of the northern-Spanish South Pyrenean Foreland Basin. The dashed box shown in white, located in the Ainsa Basin, illustrates the area of study within the Sobrarbe Deltaic Complex. Line X-X' indicates the location of the approximately dip-parallel outcrop transect sampled in this investigation. Adapted from Dreyer et al. (1999).

5.2.1 Nomenclature

The term cliniform is used to describe sinusoidal basinward-dipping chronostratigraphic stratal surfaces, whereas the term clinothem is used to describe the sedimentary packages that occur between these surfaces (e.g. Gilbert, 1885; Rich, 1951; Mitchum et al., 1977; Pirmez et al., 1998; Patruno et al., 2015). Clinothems are typically composed of three constituent parts: a geometric shelf (topset deposits; updip, gently basinward dipping), a geometric slope (foreset deposits; central component, seaward-dipping typically at $\sim 1-3^\circ$) and a geometric basin-floor (bottomset deposits; downdip, gently dipping) (Gilbert, 1885; Steel and Olsen, 2002). The zone of the cliniform rollover denotes an area of gradient increase and is the site of the uppermost break-in-slope between the shelf and slope segments (Van Wagoner et al., 1990; Pirmez et al., 1998; Plink-Björklund et al., 2001; Glørstad-Clark et al., 2010; Glørstad-Clark et al., 2011; Anell and Midtkandal, 2015; Jones et al., 2015). Clinothems develop at scales

ranging from subaerial delta clinothem (∼ 10s of m in height), to basin-margin clinothem (ranging from ∼ 100s of m to > 1 km in height) (e.g., Pirmez et al., 1998; Steel and Olsen, 2002; Helland-Hansen and Hampson 2009; Henriksen et al., 2009; Anell and Midtkandal, 2015; Patruno et al., 2015; Patruno and Helland Hansen, 2018).

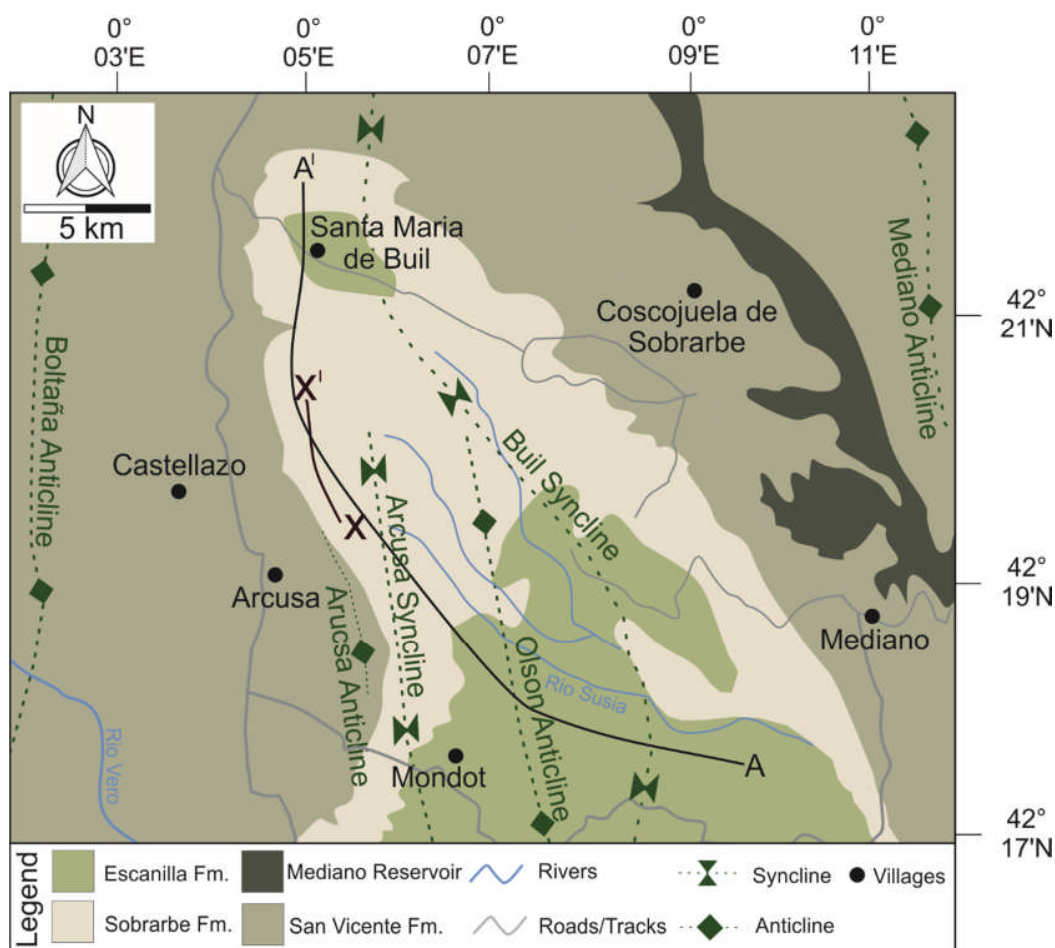


Figure 5.2: Simplified Geological map of the study area. Line X-X' shows the location of Las Gorgas Cycle 1 (Cycle LG-1), which is the dip-parallel outcrop transect sampled in this investigation. Line A-A' shows a regional dip-parallel cross-section as shown in Figure 5.3.

5.3 Geological Setting

The Sobrarbe Deltaic Complex crops out in the western part of the Eocene Ainsa Basin, north-eastern Spain (Fig. 5.1). The Ainsa Basin in the Upper Eocene is a piggyback basin, located in and on top of the easternmost portion of the Gavarnie thrust-sheet-complex, and forms the central sector of the South Pyrenean foreland basin (Vergés and Muñoz, 1990; Muñoz, 1992; Fernández et al., 2004). The Ainsa Basin is bordered to the west by the Jaca-Pamplona Basin and to the east by the Tremp-Graus Basin (Puigdefàbregas, 1975; Brunet, 1986). The western part of the basin is characterised by several fold structures that were active during

deposition: the Añiselo anticline to the north; the Peña Montañesa thrust to the northeast; the Mediano anticline to the east; the Boltaña anticline to the west (Fig. 5.2; Poblet et al., 1998; Dreyer et al., 1999; Fernández et al., 2004; 2012).

The fill of the western Ainsa Basin is dominated by a ~ 5 km-thick succession of Upper Eocene sediments. As part of these, the Sobrarbe Deltaic Complex (typically ~ 800 m-thick) comprises the uppermost part of the San Vicente Formation (marley slope deposits and turbiditic sandstones), the Sobrarbe Formation (shallow-marine deposits), and up to the middle part of Mondot Member of the Escanilla Formation (alluvial red-bed succession) (Van Lunsen, 1970; DeFrederico, 1981; Dreyer et al., 1993; Wadsworth, 1994). These deltaic successions accumulated over a period of ~ 3 million years during the middle Lutetian to lower Bartonian, reaching a maximum thickness of ~ 1 km (Muñoz et al., 1998).

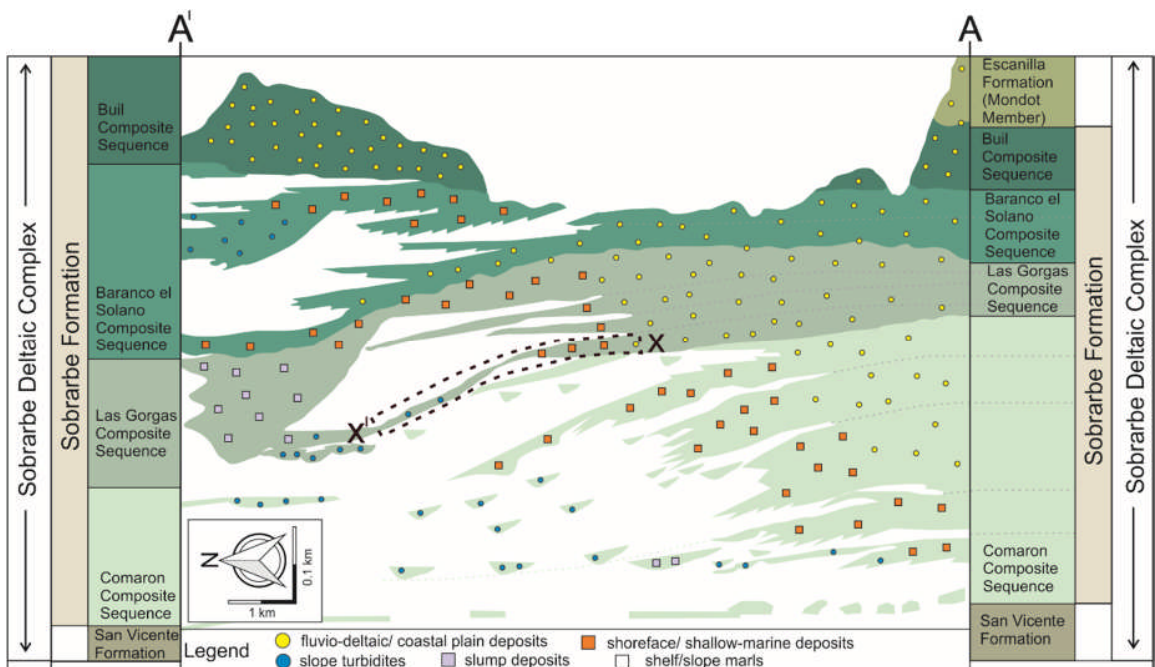


Figure 5.3: Regional cross-section showing the Sobrarbe Deltaic Complex stratigraphy (Line A-A'; Figure 5.2). The Sobrarbe Deltaic Complex is comprised of the uppermost part of the San Vicente Formation, the Sobrarbe Formation and up to the middle part of Mondot Member of the Escanilla Formation. The Sobrarbe Formation comprises several composite sequences: Comaron, Las Gorgas, Baranco el Solano and Buil. Highlighted in the burgundy box is line X-X' (see Figure 5.4), which is the study site of this investigation (Cycle LG-1). A simplified facies distribution is overlain. Adapted from Dreyer et al. (1999).

The Sobrarbe Deltaic Complex comprises a series of well-exposed, ~ 100 m-thick clinothems, which crop-out in a > 5 km-long transect, in an approximately dip-parallel orientation. These clinothems show the transition from fluvio-deltaic deposits (Escanilla Formation) in the south to progressively deeper shelf- and slope-deposits (Sobrarbe and San Vicente formations) in the north (Dreyer et al., 1999). Dreyer et al. (1999) subdivided the Sobrarbe Deltaic Complex into five composite sequences: the Comaron, the Las Gorgas, the Barranco el Solano, the Buil, and the Mondot Member of the Escanilla Formation (Fig. 5.3). These composite sequences are

separated by major unconformities, which represent fluctuations in relative sea-level (Dreyer et al., 1999).

The composite sequences are in turn subdivided into 'minor sequences' (Dreyer et al., 1999), which comprise sandstones units interbedded with mudstones and marls. The minor sequences are described as genetic sequences, bounded by transgressive surfaces (*sensu* Galloway, 1989). The first minor sequence of the Las Gorgas composite sequence is the specific focus of this study (Fig. 5.3).

5.4 Methods

The rock samples used in this investigation were acquired from the oldest clinothem of the Las Gorgas composite sequence (Figs. 5.2, 5.3), hereafter referred to as Cycle LG-1 (Fig. 5.4), which is continuously exposed in depositional dip for ~ 5 km and which reveals a shelf-to-slope transect. In Cycle LG-1, 7 sample locations were chosen along the continuous depositional profile to provide even down-dip coverage of the shelf-to-slope transition (Fig. 5.4).

At each sampling site, detailed sedimentary logs were collected, and between 4 and 7 rock samples were recovered. In total, 36 samples were recovered from Cycle LG-1. The locations of the rock samples were recorded using a handheld GPS and photographed; georeferenced sample locations are included in the Supplementary Material. To ensure consistency and repeatability, and to avoid impact of mudstone clasts, rock samples were recovered from ~ 0.1 m above the base of each sandstone-package.

Small blocks (~ 25 mm x 25 mm X 10 mm) were cut from each rock sample; samples were then polished and impregnated with epoxy resin, carbon-coated and placed on a scanning electron microscope (SEM) mount using conductive copper tape. Photomicrographs of samples were taken using a Tescan SEM at the University of Leeds Electron Microscopy and Spectroscopy Centre. All SEM photomicrographs were taken in backscatter mode at a similar contrast to ensure comparability. The photomicrographs were imported into the image processing and analysis program ImageJ, which was used to identify grain boundaries and to calculate grain diameters (e.g., Sumner et al., 2012). Measured grain-diameters ascertained from thin section, or photomicrographs, are smaller than the true maximum grain diameter (e.g., Chayes, 1950, Greenman, 1951; Kellerhals et al., 1975). However, due to the fully-lithified nature of the recovered rock-samples, photomicrograph analysis was deemed to be the most effective grain-sizing methodology. The statistical analysis of all ImageJ results was completed using GRADISTAT computer software (Blott and Pye 2001), which enables the

rapid analysis of grain-size and sorting statistics (e.g., St-Onge et al., 2004; Gammon et al., 2017).

Extensive unmanned aerial vehicle (UAV) photography was collected. Using georeferenced photographs, acquired using a DJI Phantom 3, a photorealistic three-dimensional outcrop model was constructed using the photogrammetric software Agisoft PhotoScan. The resulting model was analysed using the LIME visualisation software (www.virtualoutcrop.com). UVA-footage has enabled the construction of a high-resolution outcrop model, in which Cycle LG-1 can be traced laterally and the sampling locations can be illustrated (Fig. 5.4).

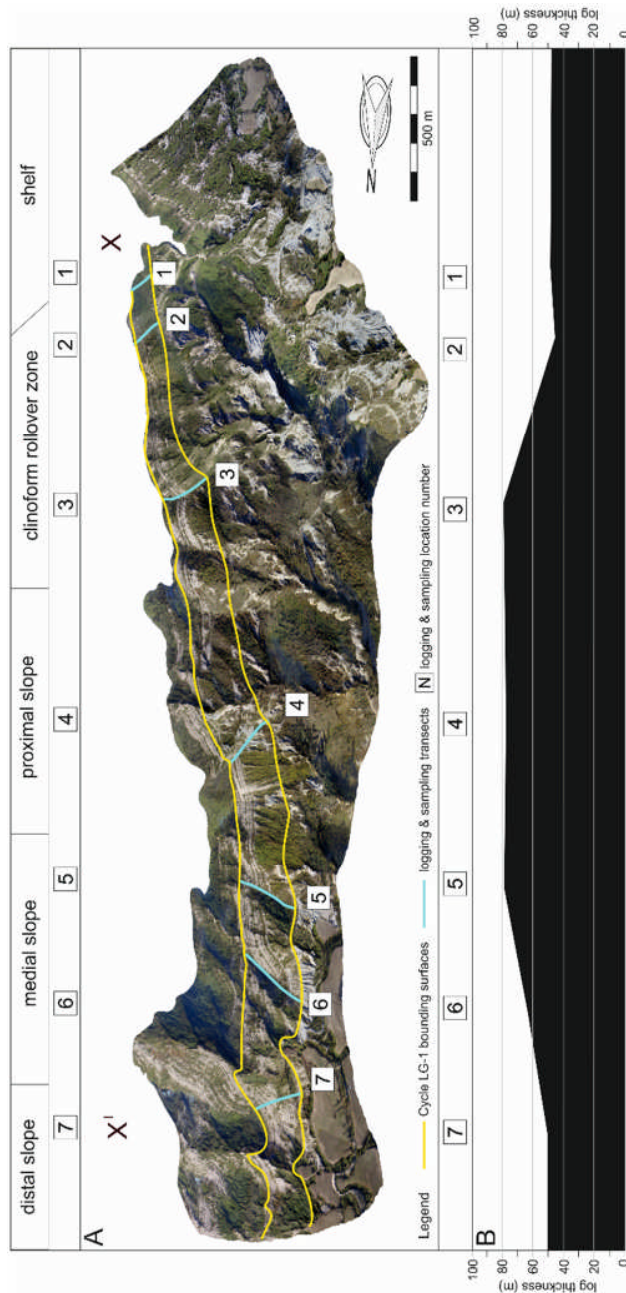


Figure 5.4: A) Outcrop model constructed from UAV photographs showing the study site (line X-X' in Figure 3); the upper and lower bounding surfaces of Cycle LG-1 are highlighted in yellow. The sedimentary log locations and sampling transects are highlighted in blue and are numbered. B) Total log thickness at each logging and sampling location.

5.5 Clinothem Geometry

The large-scale and well-exposed nature of the Sobrarbe Deltaic Complex allows the palaeobathymetric position of the shelf, clinofrom rollover and slope to be constrained (Fig. 5.4). Clinothem gradients, as outlined below, are averaged from UAV digital outcrop models (Fig. 5.4), which represent compacted stratigraphy.

5.5.1 Description

From Location 1 to 2, Cycle LG-1 has sub-horizontal geometry. From Location 2 to 3, there is an increase in average clinofrom gradient, from sub-horizontal to $\sim 4^\circ$, associated with an increase in clinothem thickness (Fig. 5.4). From Location 3 to 4 there is an increase in average clinofrom gradient to $\sim 8^\circ$. From Location 4 to 6 there is a decrease in average clinofrom gradient to $\sim 5^\circ$. From Location 6 to 7, average clinofrom gradient decreases to $\sim 2^\circ$ (Fig. 5.4).

5.5.2 Interpretation

The relatively flat clinothem geometry observed from Location 1 to 2 suggests a shelf (topset) environment (e.g., Steel and Olsen, 2002; Patruno et al., 2015; Laugier and Plink-Björklund, 2016). The prominent increase in gradient from Location 2 to 3 is interpreted to define the zone of clinofrom rollover (e.g., Pirmez et al., 1998; Glørstad-Clark et al., 2010; Anell and Midtkandal, 2015); this is further supported by the prominent stratigraphic thickening (Fig 4b; cf. Dixon et al., 2012b). Thus, locations 4 to 7, associated with a basinwards-dipping profile, represent slope deposits (e.g., Van Wagoner et al., 1990; Pirmez et al., 1998; Plink-Björklund et al., 2001; Glørstad-Clark et al., 2010). The slope is further sub-divided into proximal, medial and distal locations, based on proximity to the clinofrom rollover and slope gradient. The most steeply-dipping portion of the clinothem (represented by Location 4), is therefore interpreted as the proximal slope; the medial slope is represented by Locations 5 and 6, and is associated with a minor gradient-decrease; the distal slope (represented by Location 7) is associated with a further gradient decrease (e.g., Steel and Olsen, 2002; Glørstad-Clark et al., 2010; Anell and Midtkandal, 2015). This clinofrom geometry interpretation is supported by the distribution of facies, as outlined below.

5.6 Facies Associations and Descriptions

Five facies associations have been determined within Cycle LG-1, which are distinguishable by differences in sedimentary structure, bed-scale architecture, bed geometry and quantitative differences in grain size and sorting.

Facies Association (FA)	Total Thickness (m)	Bed Thickness (m)	Lithology		Grading	Sedimentary Structures	Fossil Content	Terrestrial Organic Matter	Bioturbation Index [*]	Description	Geometry	Interpretation
			Mean Grain size (mm)	Mean Sorting (σ)								
A	0.25 - 18	0.2 - 0.6	0.34 (medium-grained sand)	1.50 (moderately well sorted)	Normal	Planar bedding; tough cross bedding; rare asymmetric current ripple bedding.	Rare disarticulated bivalves.	Common as finely comminuted detritus; rarely as identifiable plant remains	0/1	Erosionally based, fining-upwards, medium-grained sandstone units, with basal granules and pebbles and rip-up clasts.	Crops out in Locations 1 (shelf rollover) and 2 (clinoform rollover). Lenticular appearance with highly variable stratigraphic thickness.	Fluvial channel-fill.
B	1 - 2	0.05 - 0.1	0.10 (very fine-grained sand)	1.73 (moderately sorted)	Ungraded	Parallel laminations; ripple-topped beds.	-	Finely comminuted detritus	0/1	Sharp, to erosionally based, very fine-grained sandstone, with parallel laminations and rippled bed-tops.	Crops out in Location 1 (shelf). Beds are tabular and sheet-like.	Crevasse splay deposits.
C	0.5-10	0.05 - 0.4	0.12 (very fine-grained sand)	1.51 (moderately well sorted)	Ungraded and normal	Parallel and current-ripple lamination.	Foraminifera, Gastropods, bivalves	-	1	Sharp based, very fine-grained sandstone with 'clean' appearance (composed predominantly of quartz and contains no organic matter or mica).	Crops out in Locations 2 (clinoform rollover zone) to 6 (medial slope). Beds are tabular. Overall stratigraphic thinning downdip.	Turbidity current deposits, associated with remobilised sediment from a wave-dominated shelf edge.
D	1.75 - 10	0.4 - 2.5	0.12 (very fine-grained sand)	1.50 (moderately well sorted)	Normal, inverse and normal	Structureless, parallel and current-ripple lamination.	-	Finely comminuted detritus	1/2	Erosionally based, very fine-grained sandstone with 'dirty' appearance (contains abundant organic matter and mica).	Crops out in Locations 2 (clinoform rollover zone) to 7 (distal slope). Overall stratigraphic thinning downdip.	Sustained hyperpycnal flow associated with a river-dominated shelf-edge.
E	0.5 - 10	0.5 - 6	0.39 (medium-grained sand)	1.43 (moderately well sorted)	Normal, inverse and ungraded	-	-	Finely comminuted detritus	1-3	Erosionally, or sharp based, deformed, medium-grained sandstone with 'dirty' appearance (contains abundant organic matter and mica).	Crops out in Locations 2 (clinoform rollover zone) to 7 (distal slope). Beds can remain at the same thickness or thin downdip.	Hyperpycnal flow associated with a river-dominated shelf-edge.
F	0.5 - 14	-	Very fine-grained silt	-	-	Structureless, faint parallel lamination.	-	-	0-4	Structureless to faintly laminated siltstone.	Crops out predominantly in Locations 5-7 (medial to distal slope).	Dilute turbidity currents.

* See Bioturbation Index of Taylor and Goldring (1993)

Table 5.1: Descriptions and interpretations of shelf and slope facies associations (FA A – FA F).

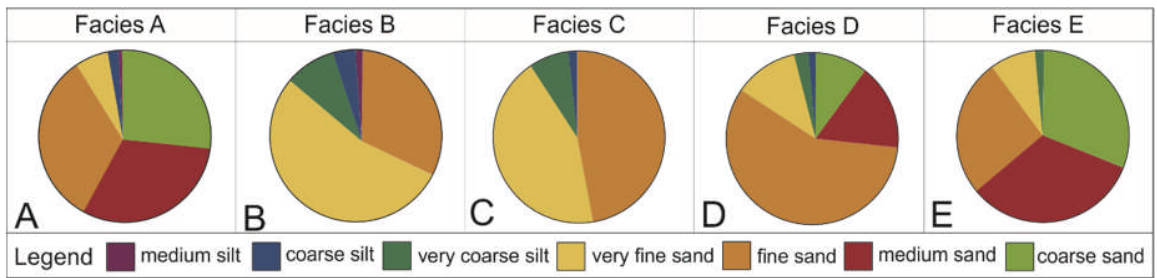


Figure 5.5: Pie charts illustrating differences in grain-size composition between Facies A-E. Sample numbers for each facies are shown in Figure 6A. Facies A = fluvial channel-fill deposits; Facies B = crevasse splay deposits; Facies C = very fine-grained clean turbidites; Facies D = fine-grained micaceous turbidites; Facies E = medium-grained, deformed turbidites.

5.6.1 Shelf Deposits

5.6.1.1 Facies Association A: fluvial channel fill deposits

5.6.1.1.1 Description (see Table 5.1)

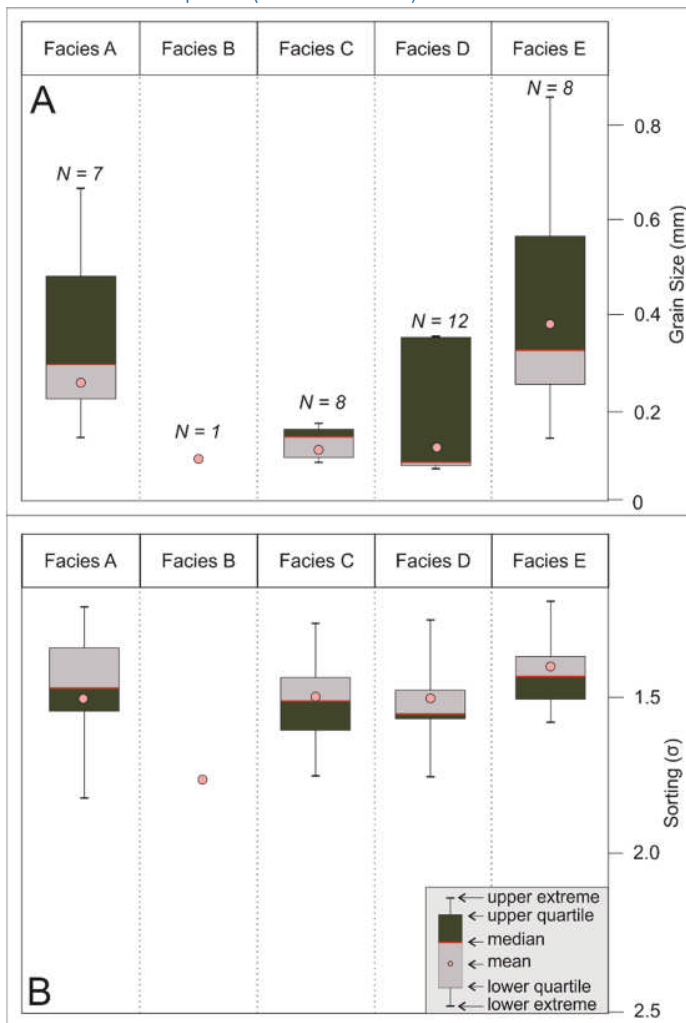


Figure 5.6: Grain size and sorting for Facies A-E. A) Box and whisker plot illustrating differences in grain size between Facies A-E. B) Box and whisker plot illustrating differences in sorting between Facies A-E. Sample numbers for each facies are shown in Part A. Facies A = fluvial channel-fill deposits; Facies B = crevasse splay deposits; Facies C =

very fine-grained clean turbidites; Facies D = fine-grained micaceous turbidites; Facies E = medium-grained, deformed turbidites.

Facies Association A (FA A) is predominantly composed of fine- and medium-grained sandstone (34 % and 31 % respectively, Fig. 5.5a) with a mean grain size of 0.34 mm (medium-grained sand; Fig. 5.6a). FA has a large intra-facies grain-size variability, and can be locally very coarse-grained, although it is generally moderately well-sorted (1.50σ mean sorting; Fig. 5.6b). Typically, grains are subangular to rounded. FA A varies from 0.25 – 18 m in thickness (Fig. 5.7), and has a highly discontinuous, lenticular geometry (Fig. 5.8a). The base of FA A is erosional, cutting up to 0.5 m deep into underlying siltstones (Fig. 5.8b). The base of FA A is often associated with mudstone rip-up clasts. FA A typically shows a fining-upwards trend and is bounded by flat to concave-up surfaces. Sedimentary structures include planar and trough cross-stratification; rare asymmetric current ripple cross-lamination is observed. Typically, cross-strata sets are 0.5 – 1.0 m thick, and dip uniformly; sets are bounded by flat surfaces, which dip in the same direction as the cross beds (Fig. 5.8c). Sandstones can contain sub-rounded granules and pebbles (20 – 50 mm in size) of extraformational origin concentrated at the base of FA A, or parallel to stratification, which are dominantly quartz, with subordinate feldspar and lithic clasts (Fig. 5.8d). Locally, plant matter is present as detritus, or rarely as identifiable plant remains; disarticulated bivalve shells are also common. FA A crops out in Locations 1 and 2, stratigraphically thickening at Location 2 (Figs. 5.4 and 5.7).

5.6.1.1.2 Interpretation

The presence of lenticular sand bodies, bounded by basal erosion surfaces and containing decimetre-scale cross-bedding with dominant unidirectional palaeocurrents indicates a channel-fill environment for FA A (Farrell, 1987; Collinson et al., 2006); the fluvial nature of the infill is further supported by the presence of terrestrial plant fragments and detritus. The planar and trough cross-stratified sedimentary structures record the migration of dune-scale bedforms, and the occurrence of basal granules and pebbles indicates relative high-energy conditions. The fining-upwards trends suggest progressive flow velocity decrease during the channel infill (e.g., Williams and Rust, 1969; Bridge et al., 1986).

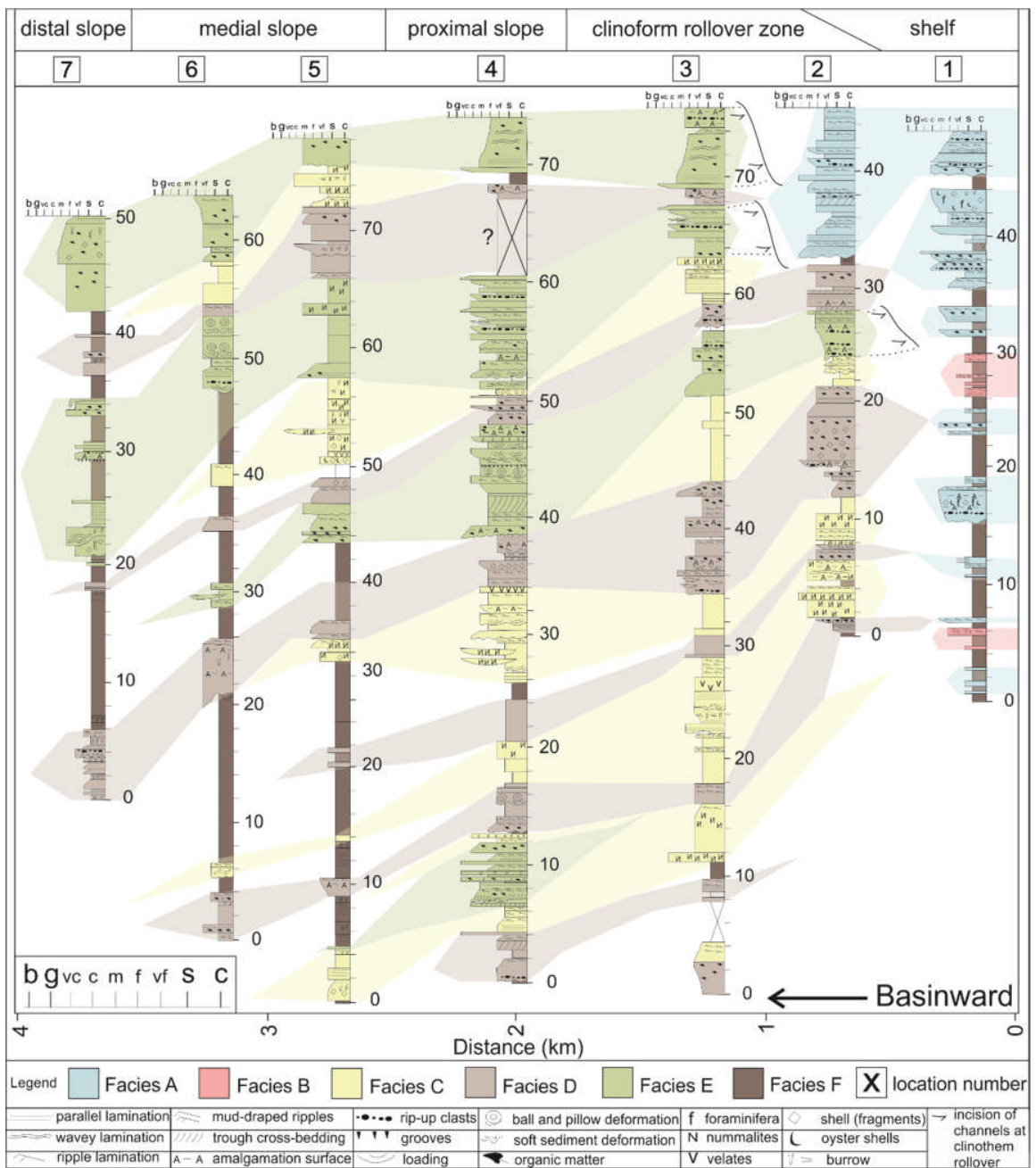


Figure 5.7: Sedimentary logs showing stratigraphic and dip-parallel facies distributions in Cycle LG-1. The inset shows an enlarged grain size scale: c = clay; s = silt; vf = very fine-grained sand; f = fine-grained sand; m = medium-grained sand; c = coarse-grained sand; vc = very coarse-grained sand; g = gravel; b = boulders.

5.6.1.2 Facies Association B: crevasse splay deposits

5.6.1.2.1 Description (see Table 5.1)

Facies Association B (FA B) is predominantly composed of very fine and fine-grained sandstone (54 % and 32 % respectively, Fig. 5.5b), and has a mean grain size of 0.10 mm (very fine-grained sand; Fig. 5.6a). FA B is moderately sorted (1.73 σ mean sorting; Fig. 5.6b), with subrounded grains. Bedsets are 1 – 2 m thick, and composed of 0.05 – 0.1 m-thick and

relatively tabular sandstone beds, interbedded with thin (0.05 – 0.2 m thickness) structureless siltstones (Fig. 5.8e). Tabular sandstone beds have sharp bases and are parallel-laminated (Fig. 5.8e), passing upward into very fine-grained ripple-bedded tops. FA B contains finely comminuted plant detritus. FA B crops out only in Location 1 and thins towards Location 2 (Figs. 5.4 and 5.7).

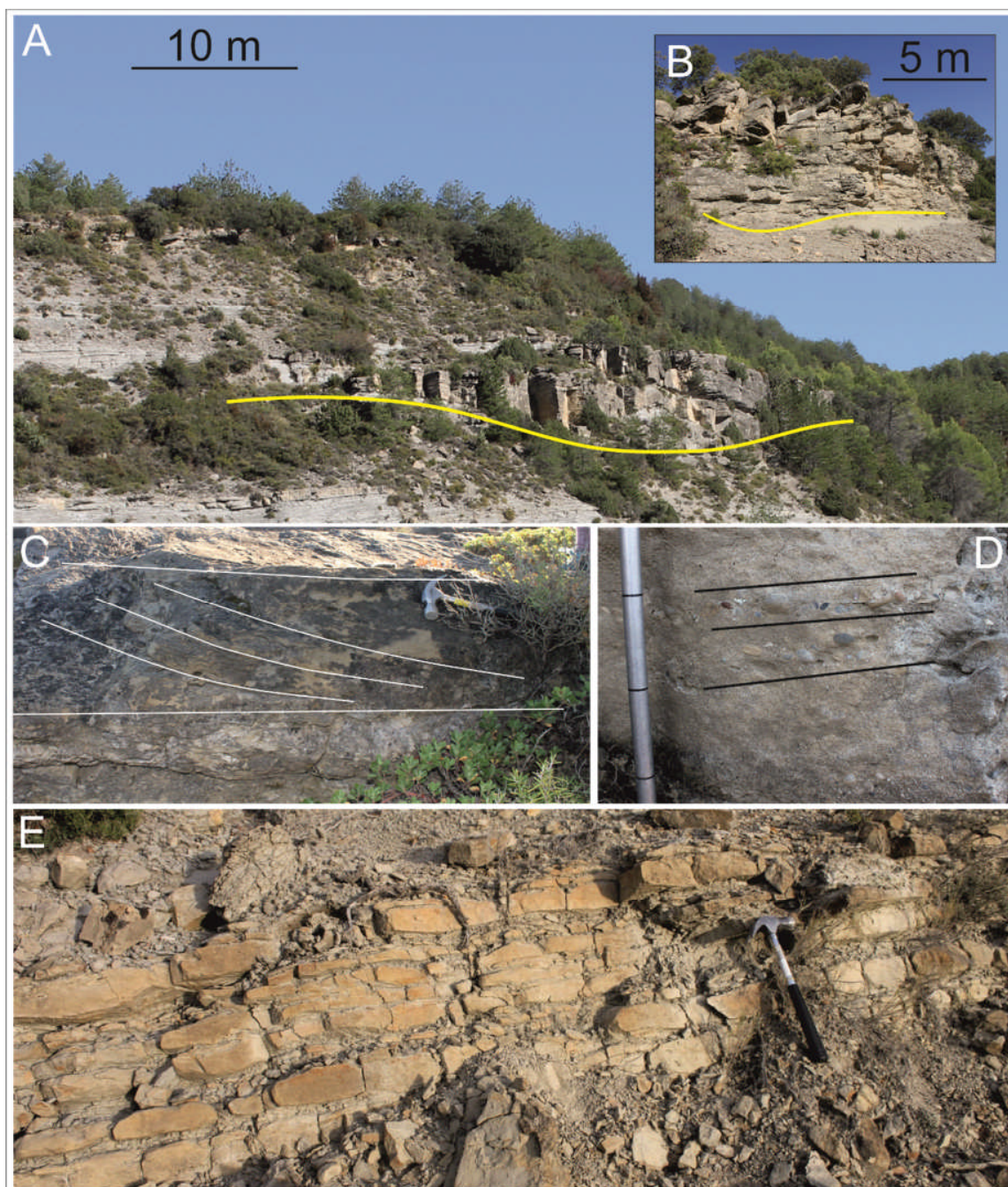


Figure 5.8: Representative facies photographs. A) Lenticular sand-body geometry (FA A). B) Close-up of channel-fill within lenticular sand-body (FA A). C) Trough cross-bedding with uniformly dipping foresets (FA A); hammer for scale. D) Sub-rounded granules and pebbles of extraformational origin aligned parallel to stratification (FA A); marks on Jacob's Staff denote 10 cm intervals. E) Tabular sandstone beds, interbedded with structureless silt (FA B).

5.6.1.2.2 Interpretation

FA B was deposited by low velocity, unidirectional currents. The planar and current ripple lamination and siltstone interbeds indicate changes in velocity and sediment load. The fine-grained nature of FA B and the sharp bases of the sandstone elements support interpretation as crevasse splay deposits (Ethridge et al., 1981; Gersib and McCabe, 1981; Bridge, 1984). This interpretation is strengthened by the proximity and close association of FA B to FA A, suggesting deposition in a lower delta plain environment.

5.6.2 Slope Deposits

5.6.2.1 Facies Association C: very fine-grained clean turbidites

5.6.2.1.1 Description (see Table 5.1)

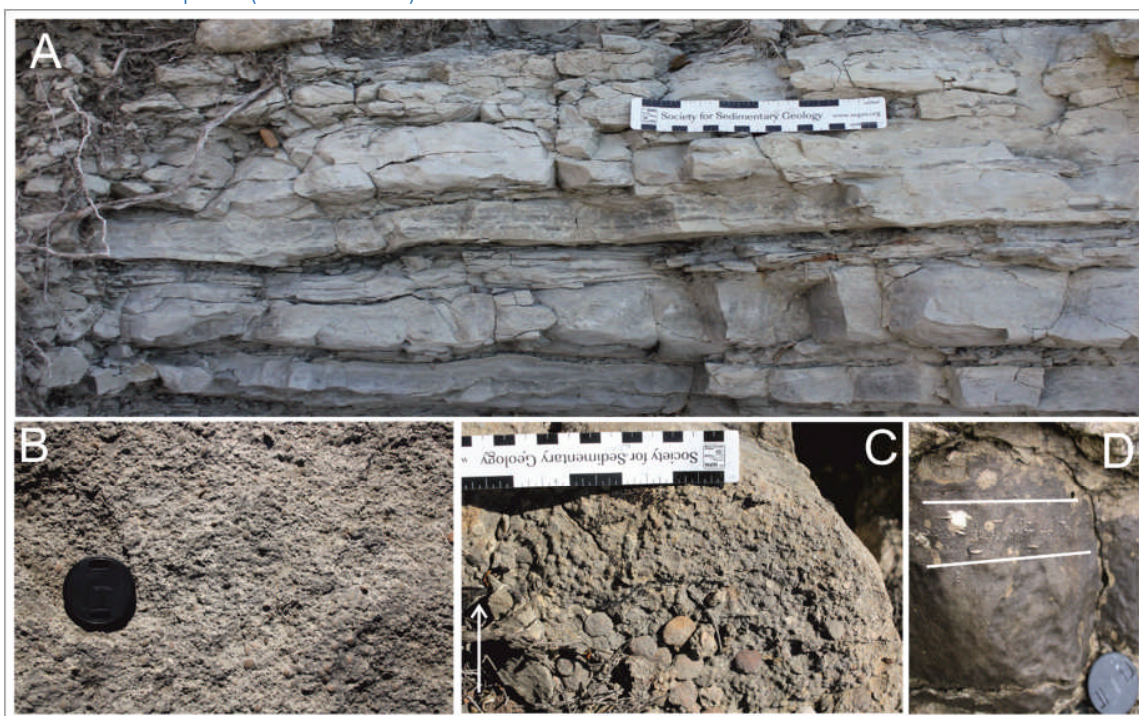


Figure 5.9: Representative facies photographs (FA C). A) Tabular beds of plane-parallel laminated, very fine-grained, quartz-rich, clean sandstone. B) Structureless Foraminifera-dominated bioclastic sandstone (found in Location 2; see Figs. 5.4 and 5.7); lens cap for scale. C) Normally graded Foraminifera-dominated bioclastic sandstone (found in Locations 3-6; see Figs. 5.4 and 5.7); arrow indicates fining direction. D) Foraminifera aligned parallel to laminations (found in Locations 3-6; see Figs. 5.4 and 5.7); lens cap (50 mm diameter) for scale.

Facies Association C (FA C) is predominantly composed of very fine- and fine-grained sandstone (44 % and 47 % respectively, Fig. 5.7c) and has a mean grain size of 0.12 mm (very fine-grained sand; Fig. 5.6a). FA C is moderately well sorted (1.51 σ mean sorting; Fig. 5.6b). Grains are rounded to well-rounded and predominantly quartz. FA C varies in thickness from 0.5 – 10 m, and individual beds are 0.05 – 0.4 m thick with a tabular appearance (Fig. 5.9a). Typically, bed bases are flat (Fig. 5.9a), although some are erosional, cutting up to 0.2 m-deep

into underlying siltstones. Typically, beds are ungraded, with local weak normal grading. The dominant sedimentary structures are current-ripple and plane-parallel lamination. FA C has a 'clean' appearance, lacks observable plant detritus or organic matter, and is mica-poor (Fig. 5.9a). The very fine-grained sandstone beds are interbedded with bioclastic sandstone beds (0.5 – 2 m thick) dominated by Nummulites (Figs. 5.9b-d) (see Mateu-Vicens et al., 2012). In Location 2 (Figs. 5.4 and 5.7), bioclastic sandstones are dominantly structureless (Fig. 5.9b), but in Locations 3-6 (Figs 5.4 and 5. 7) they are normally graded (Fig. 5.9c); foraminifera are also found aligned parallel to internal laminations (Fig. 5.9d). Basinwards, the mean grain-size of FA C varies slightly from 0.084 mm (very fine-grained sand) in Location 2, to 0.10 (very fine-grained sand) in Location 6 (Fig. 5.10a). Sorting shows an overall basinward decrease from 1.26 σ (very well sorted) in Location 2, to 1.59 σ (moderately well sorted) and 1.52 σ (moderately well sorted) in Locations 5 and 6, respectively (Fig. 5.10b). FA C crops out from Location 2 to Location 6 (Fig. 5.7), showing an overall basinward-thinning. FA C pinches out and terminates at Location 6. FA C shows no obvious vertical stratigraphic thickening or thinning trend.

5.6.2.1.2 Interpretation

The presence of both flat and erosive bed bases and abundant traction structures (including plane-parallel and current-ripple lamination) is consistent with deposition by turbidity currents (Hiscott et al., 1997). The significant basinward thinning of FA C suggest deposition by gradual aggradation from decelerating turbidity currents (Kneller, 1995). The normal grading observed in FA C is also characteristic of waning turbidity currents (Bouma 1962, Walker 1967, Lowe 1982, Middleton 1993, Kneller 1995), which are deposited from transient, surge-type turbidity currents that progressively lose sediment carrying-capacity downslope (Lowe 1982, Hiscott 1994, Kneller and Branney 1995). These turbidites would be expected to show a basinward-fining trend (Kneller, 1995). However, the grain size of FA C shows minimal basinwards change (< 0.016 mm) from the zone of the clinoform rollover (Location 2) to the medial slope (Location 6) (Fig. 10a); this almost constant grain-size profile may reflect the original narrow grain-size range available for remobilisation and basinward transport. The 'clean' appearance of FA C (i.e. its negligible mica and terrestrial organic matter content), in combination with its high textural maturity (i.e. FA C is very fine-grained, well sorted, well rounded and quartz-rich) suggests sediment remobilisation from a wave-dominated shallow marine shelf deposit (e.g., Cosgrove et al., 2018). This is supported by the direct correlation of outer shelf to shelf-edge (Location 2) structureless foraminifera-bearing bioclastic sandstones with normally-graded bioclastic sandstones in the proximal and medial

slope (Locations 3 – 6) (Figs. 5.4 and 5.7). The structureless bioclastic sandstones represent in-situ wave-dominated shallow-marine shelf deposits (Mateu-Vicens et al., 2012) and their basinward-equivalent, normally-graded bioclastic sandstones suggest the reworking and basinwards transport of foraminifera-rich sands from the contemporaneous shelf.

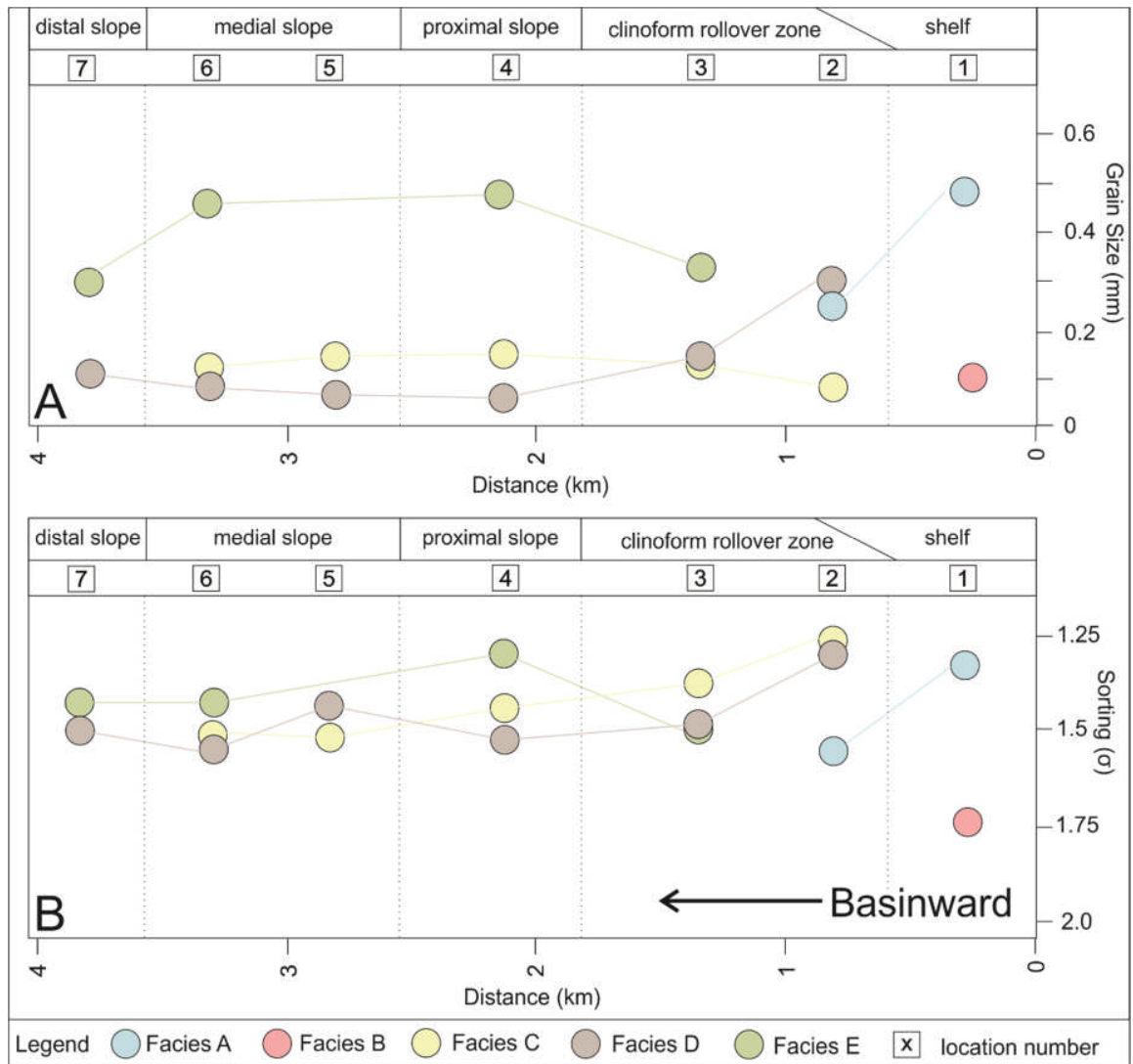


Figure 5.10: Basinward trends in grain size and sorting for Facies A-E of Cycle LG-1. Sampling locations are illustrated in the numbered boxes. Sample numbers for each facies are shown in Figure 5.6a.

5.6.2.2 Facies Association D: fine-grained micaceous turbidites

5.6.2.2.1 Description (see Table 5.1)

Facies Association D (FA D) is predominantly composed of very fine- and fine-grained sandstone (45 % and 43 % respectively, Fig. 5d) with a mean grain size of 0.12 mm (very fine-grained sand; Fig. 5.6a). FA D is moderately well sorted (1.50 σ mean sorting; Fig. 5.6b). FA D varies in thickness from 1.75 – 10 m (Fig. 5.7); individual beds are typically 0.4 – 2.5 m thick

(Fig. 5.11a) and interbedded with 0.25 m-thick siltstone beds (Fig. 5.11b). Typically, the base of FA D is erosional and contains abundant rip-up clasts (Fig. 5.11c). FA D deposits typically thin and fine upwards. Beds show normal, inverse, and inverse-to-normal grading, and can be structureless, but most commonly display traction structures, including plane-parallel and current-ripple lamination (Fig. 5.11d). FA D has a ‘dirty’ appearance, i.e. it has a high observable mica-content and contains finely comminuted plant detritus. Basinwards, grain size shows a prominent fining trend, with mean grain diameter decreasing from 0.34 mm (medium-grained sand; Location 2) to 0.10 mm (very fine-grained sand; Location 7) (Fig. 5.10a). Sorting shows an overall downdip decrease from 1.35 σ (well sorted; Location 2) to 1.5 σ (moderately well sorted; Location 7) (Fig. 5.10b). FA D crops out from Location 2 to Location 7 (Figs. 5.4 and 5.7). At Location 2, FA D can be correlated laterally to the fluvial channel-fill associated with FA A. FA D shows a marked basinward thinning trend (Fig. 5.7) and is commonly interbedded with FA C throughout the study area. Stratigraphically, FA D tends to thicken up-section.

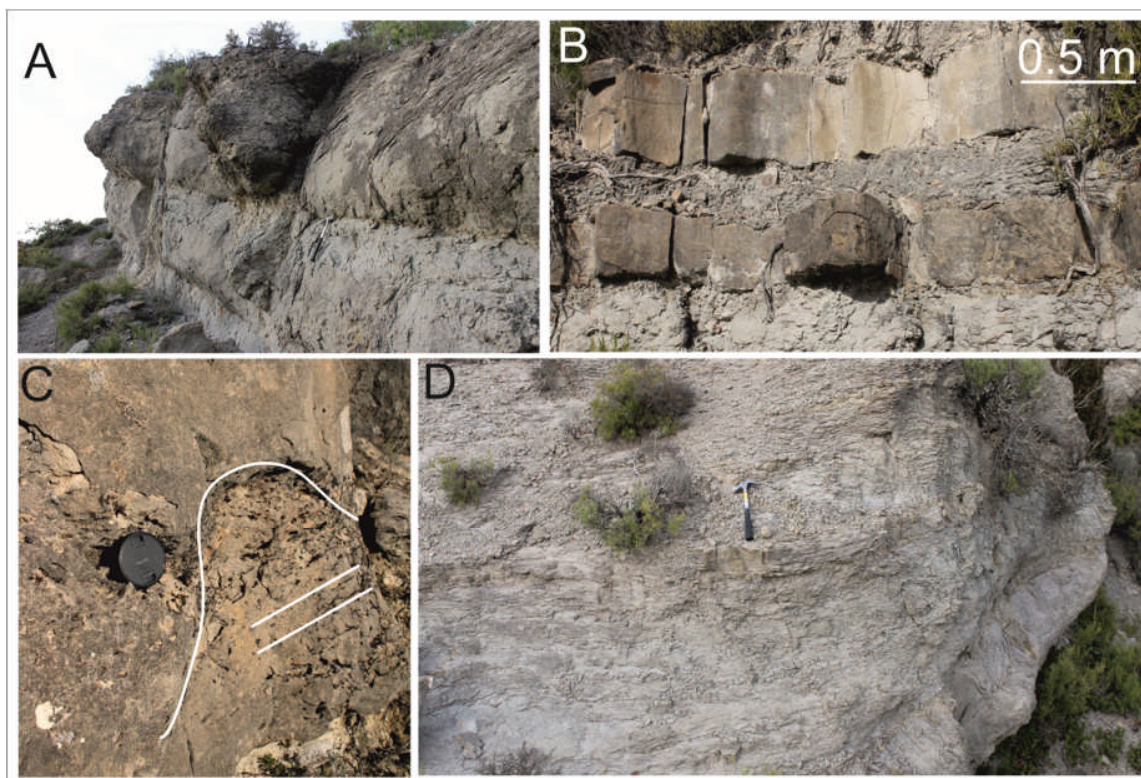


Figure 5.11: Representative facies photographs (FA D). A) 0.75 to 1.5 m-thick fine-grained sandstone beds, note the micaceous appearance; hammer for scale. B) 0.5 m-thick beds of FA E, interbedded with 0.25 m-thick siltstone beds. C) Concave upwards bed-base with aligned mudstone rip-up clasts; lens cap for scale. D) Plane-parallel laminated sandstone.

5.6.2.2.2 Interpretation

The erosive bases of FA D, with aligned mudstone clasts and abundance of traction structures (including plane-parallel and current-ripple laminations) support an interpretation of deposition by turbidity currents (Hiscott et al., 1997). The thick beds (up to 2.5 m) with traction structures are indicative of deposition from sustained turbidity currents, through gradual aggradation (Kneller, 1995). The significant thickness of individual turbidites may be indicative of deposition via hyperpycnal flows (e.g., Piper and Savoye, 1993; Mulder et al., 1998; Kneller and Buckee; 2000, Mulder and Alexander; 2001; Plink-Björklund and Steel; 2004), as river discharge can be sustained at a quasi-constant rate for hours, days or weeks (e.g., Wright et al., 1986; Hay, 1987; Prior et al., 1987; Wright et al., 1988; Nemec, 1990; Wright et al., 1990; Chikita, 1990; Zeng et al., 1991; Mulder et al., 1998; Piper et al., 1999). However, bed thickness cannot be used as a diagnostic criterion alone, as sustained flows can be triggered by various other mechanisms than river discharge (including volcanic eruptions, seismic activity and storm surges).

The physical connection from fluvial channel-fill (FA A) into slope deposits (FA D) suggests that the fluvial feeder system was directly depositing sediment onto the slope (e.g., Steel et al., 2000; Plink-Björklund et al., 2001; Plink-Björklund and Steel, 2002; Mellere et al., 2002; Plink-Björklund and Steel, 2004); this supports an interpretation of river-discharge-generated hyperpycnal flows that deposited their sediment load across the proximal to distal slope. The presence of high amounts of plant debris and mica within FA D also supports a direct linkage between the fluvial and marine depositional environment (e.g., Mulder et al., 2003; Plink-Björklund and Steel, 2004; Lamb et al., 2008; Zavala and Arcuri, 2016). Terrestrial organic matter and high concentrations of mica are widely used as indicators of hyperpycnal flows (e.g., Normark and Piper, 1991; Mulder and Syvitski, 1995; Mulder et al., 2003; Plink-Björklund and Steel, 2004; Zavala et al., 2011, 2012; Hodgson et al., 2018), associated with sustained river-derived flows during periods of high river discharge.

The basinward thinning and fining of FA D also supports deposition via hyperpycnal flows. As discussed in Plink-Björklund and Steel (2004), following flood termination coarser grain-size fractions are progressively deposited in a landward direction, and finer grain-size fractions are progressively deposited in a basinward direction, as flow velocity and sediment concentration decrease.

Repeated transitions between inverse and normal grading at intra-bed - scale, suggests the presence of accelerating (waxing) and decelerating (waning) flow regimes (cf. Kneller, 1995). As hyperpycnal flow beds are suggested to record variations in the flood hydrograph (e.g.,

Mulder and Alexander, 2001), the waxing episode of river-mouth discharge deposits an inversely graded division and a waning episode deposits a normally graded division, although these trends will not be present across an entire deposit (Mulder et al., 2001). However, inverse and normal grading at bed-scale may also reflect autogenic process, such as fluctuations in plunge-point position, which shred river discharge signals (Lamb et al., 2008, 2010).

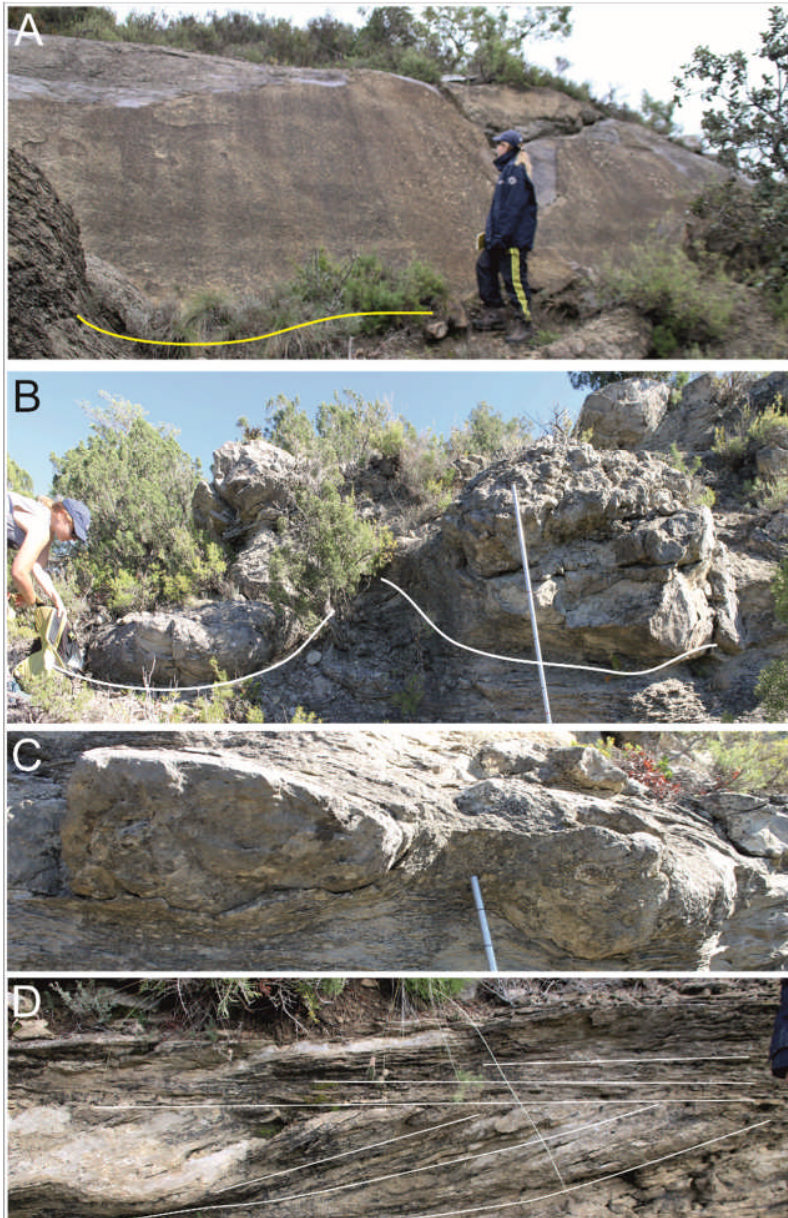


Figure 5.12: Representative facies photographs (FA E). A) 4 m-thick medium-grained sandstone bed, with erosive base cutting into underlying deposits; human for scale. B) Contorted units; 1.5 m Jacob's Staff for scale. C) Ball and pillow deformation structures; marks on Jacob's Staff denote 10 cm intervals. D) Trough cross-stratification; 20 cm notebook for scale.

5.6.2.3 Facies Association E: medium-grained, deformed turbidites

5.6.2.3.1 Description (see Table 5.1)

Facies Association E (FA E) is predominantly composed of medium- and coarse-grained sandstone (33 % and 31 % respectively, Fig. 5.5e) and has a mean grain size of 0.39 mm (medium-grained sand; Fig. 5.6a). FA E is moderately well sorted (1.43σ mean sorting; Fig. 5.6b). FA E varies in thickness from 0.5 – 10 m; individual beds are 0.5 – 6 m thick (Fig. 5.12a). Bed-bases are commonly sharp and flat. However, erosional bed-bases are observed, cutting up to 0.3 m deep into underlying siltstone deposits; these surfaces are overlain directly by beds containing mudstone rip-up clasts. Beds show normal and inverse grading or may be ungraded. FA E also shows extensive folding and ball-and-pillow structures (Fig. 5.12b, c). Where deformation is less intense primary sedimentary structures are preserved including trough cross-stratification (Fig. 5.12d), parallel and ripple lamination and abundant internal amalgamation surfaces. FA A has a 'dirty' appearance, and contains abundant finely comminuted plant detritus and is highly micaceous. FA E exhibits a basinward coarsening trend from Locations 3 to 6 (Fig. 5.10a), where grain size increases from 0.33 mm (medium-grained sand) to 0.45 mm (medium grained sand); at Location 7, grain-size decreases to 0.31 (medium-grained sand). The basinward sorting trend of FA E across the sampled profile shows an initial increase from 1.5σ (moderately well sorted) to 1.3σ (well sorted) at Locations 3 and 4, respectively, and then decreases to 1.44σ (moderately well sorted) in Locations 6 and 7 (Fig. 5.10b). FA E crops out from Locations 2 to 7 (Figs. 5.4 and 5.7) and can either thin in a basinward direction or remain at approximately the same thickness (Fig. 5.7). At Location 2, FA E cuts into and truncates FA A. FA E is interbedded with FA C and FA D throughout the study area; FA E becomes thicker and more common up-section.

5.6.2.3.2 Interpretation

Erosional bases with aligned mudstone clasts, and the abundance of traction structures (including plane-parallel and ripple lamination) suggest deposition via turbidity currents (Hiscott et al., 1997). The unidirectional cross stratification suggests that current velocities were relatively high (Plink-Björklund et al., 2001). Trough cross-stratification is associated with migration of 3-D dunes (Plink-Björklund et al., 2001; Stevenson et al., 2015; Hodgson et al., 2018). Similar to FA D, the significant thickness of individual turbidites (up to 6 m thick) may be indicative of deposition via hyperpycnal flows (e.g., Piper and Savoye, 1993; Mulder et al., 1998; Kneller and Buckee, 2000; Mulder and Alexander, 2001; Plink-Björklund and Steel, 2004). The presence of abundant terrestrial organic matter and high concentrations of mica might also support the interpretation of these deposits as hyperpycnites (e.g., Normark and Piper, 1991; Mulder and Syvitski, 1995; Mulder et al., 2003; Plink-Björklund and Steel, 2004;

Zavala et al., 2011, 2012). FA E shows repeated transitions between inverse and normal grading at bed-scale (similarly to FA D, see above), suggesting the presence of accelerating (waxing) and decelerating (waning) flow regimes (cf. Kneller, 1995).

The folds and extensive contorted units indicate slope-induced deformation or slumping. The rapid deposition of sediment associated with hyperpycnal flows can lead to liquefaction processes, resulting in soft sediment deformation (e.g., Pontén and Plink-Björklund 2009; Plink-Björklund and Steel, 2004).

Unlike FA D, FA E deposits cannot be directly correlated updip to coeval fluvial channel-fill deposits (FA A), as FA E deposits start in the clinoform rollover zone (Location 2) and erodes into underlying fluvial channelized facies (FA A) (Fig. 5.7). This suggests strong bypass of the contemporaneous shelf and the active erosion and entrainment of underlying deposits, which may correspond with individual surges in river discharge (e.g., Talling, 2014). Additionally, the overall basinward-coarsening trend and general lack of obvious thinning suggests significant proximal bypass, flow acceleration (cf. Kneller et al., 1995), and preferential sediment deposition in the medial and distal slope setting. The erosive nature of FA E and significant shelf-edge bypass suggests that flow velocity of FA E may have been higher, relative to FA D and supports a more catastrophic input of sediment associated with major river flooding events, rather than the sustained hyperpycnal flows associated with FA D.

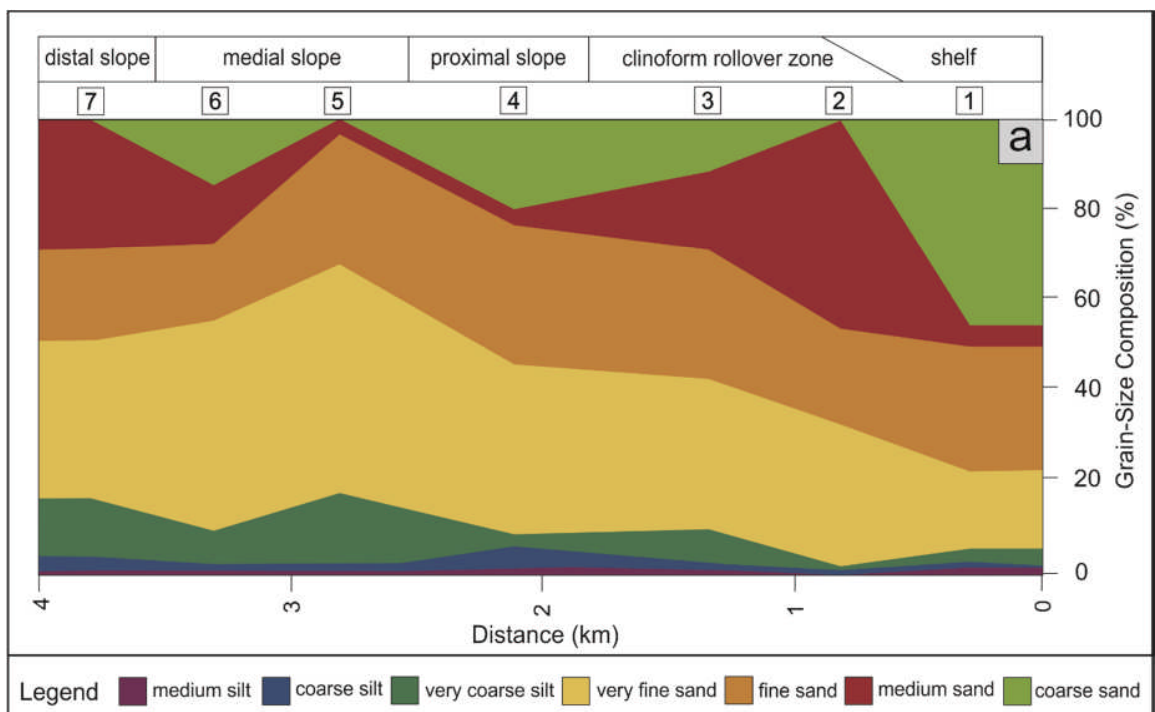


Figure 5.13: Grain-size cumulative frequency plot showing basinward changes in grain size at each sampling location.

5.7 Process-Regime Variability

The distribution of slope facies within Cycle LG-1 shows the stratigraphic alternation between FA C, D and E. The sedimentary texture and structure of FA D and FA E suggest deposition under river-dominated shelf conditions. This is consistent with the interpretation of Dreyer et al. (1999) who interpreted the Sobrarbe Deltaic Complex overall to record a river-dominated system. However, the 'clean' and texturally mature nature of FA C is suggestive of a wave-dominated shelf process-regime. As such, this new dataset documents intra-clinothem process-regime variability, in which river-dominated conditions are episodically punctuated by wave-dominated conditions.

5.8 Basinward Change

Grain size and sorting have been averaged for each sampling location to illustrate basin-scale changes in grain character (Figs. 5.13, 5.14).

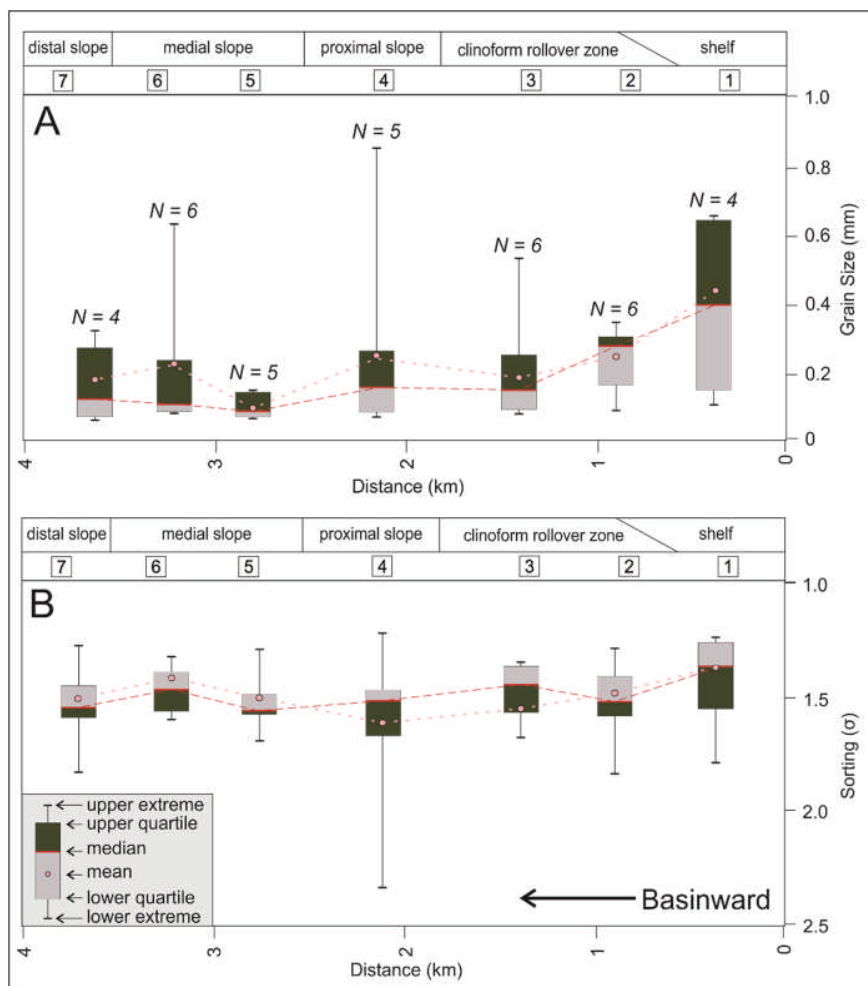


Figure 5.14: Basinward trends in grain-size and sorting data. A) Box and whisker plots showing basinward changes in grain size at each sampling location. B) Box and whisker plots showing basinward changes in sorting at each sampling location.

5.8.1 Grain Size

The grain-size variability in Cycle LG-1 is shown in Figures 5.13 and 5.14a. From Locations 1 to 3, there is a decrease in mean grain size from 0.46 mm (medium-grained sand; Location 1) to 0.21 mm (fine-grained sand; Location 3; Fig 5.14a). Location 1 has the highest inter-quartile grain-size variability (Fig. 5.14a). From Locations 4 to 7, mean grain size varies between sampling locations; mean grain-size is 0.25 mm (medium-grained sand), 0.10 mm (very fine-grained sand), 0.21 mm (fine-grained sand) and 0.18 mm (fine-grained sand) in Locations 4, 5, 6 and 7, respectively (Fig. 5.14a).

5.8.2 Sorting

The variation in sorting is illustrated by the box and whisker plots in Figure 5.14b; it has a limited range from 1.4 (well sorted, Location 1) to 1.58 (moderately well sorted, Location 4), with a weak overall basinward decrease in sorting (Fig. 5.14b).

5.9 Discussion

5.9.1 Mixed-Process Clinothem Evolution

All clinothems within the Sobrarbe Deltaic Complex, including Cycle LG-1, have been previously interpreted to be 'river-dominated' (see Dreyer et al., 1999). However, detailed analysis of facies reveals a more complicated stratigraphic evolution of process-regime at an intra-clinotherm scale. Changes in shelf process-regime result in prominent internal variability in sedimentary texture and structure across the complete depositional profile.

The documented process-regime change between river- and wave-dominated affects the downdip geometric distribution of sedimentary bodies; in this case, sedimentary packages associated with a river-dominated process-regime (FA D and FA E), are distributed across the complete sampled profile, from the shelf (topset) to the distal slope (foreset). In contrast, sand-dominated sedimentary packages associated with a wave-dominated process-regime (FA C), are deposited only in the proximal and medial slope environments. As such, distal slope deposits show prominent stratigraphic variability in grain-size; sand-rich packages are interbedded with >10 m silt-rich deposits. The termination, and downlap, of the wave-dominated, sand-facies on the medial slope results in the coeval deposition of silt in the lower slope setting. As such, only silt-grade sediment fractions are transported into the distal slope setting under a wave-dominated process-regime; intra-clinotherm variability in shelf process-regime thus directly influences the architecture and sand-content of downdip deposits. The maximum basinward extent of FA C on the medial slope may reflect the maximum down-slope distance at which turbidity currents associated with coeval wave-dominated process regimes

can transport their sand-fraction and illustrates their attenuated coarse-grained sediment transport capacity relative to turbidity currents associated with a river-dominated shelf. Many clinothem systems are designated as being river-, wave-, or tide-dominated (e.g., Dreyer et al., 1999; Pink-Björklund et al., 2001; Plink-Björklund and Steel, 2002; Deibert et al., 2003; Crabaugh and Steel, 2004; Plink-Björklund and Steel, 2004; Johannessen and Steel, 2005; Petter and Steel, 2006; Sylvester et al., 2012; Ryan et al., 2015). The use of end-member descriptors (i.e. river-, wave-, or tide-dominated) has led to the under-recognition of mixed-energy clinothem systems in the ancient record (see Ainsworth et al., 2011; Olariu, 2014; Rossi and Steel, 2016). As such, relatively few ancient clinothems have been interpreted to document spatial and temporal variability in shelf (topset) process-regime (e.g., Ta et al., 2002; Ainsworth et al., 2008; Plink-Björklund, 2008; Carvajal and Steel, 2009; Vakarelov and Ainsworth, 2013; Jones et al., 2015; Gomis-Cartesio et al., 2017). Assigning a clinothem with a dominant shelf (topset) process-regime is also associated with discrete sedimentary processes and facies associations, which are used to inform archetypal river-, wave- or tide-dominated clinothem models (e.g., Elliott, 1986; Bhattacharya and Walker, 1992; Dalrymple, 1992; Walker and Plint, 1992). A traditional model of a prograding river-dominated clinothem is associated with a broadly coarsening-upwards grain-size trends in shelf, slope and basin-floor deposits (Bhattacharya and Walker, 1992; Steel et al., 2008; Carvajal and Steel, 2009; Dixon et al., 2012b). However, as it is clearly documented in this case, applying an end-member shelf process-regime classification system to clinothem classification systems fails to adequately account for internal vertical and downdip variability in sedimentary texture associated with variability in topset process-regime conditions. This study highlights the internal textural variability of an individual clinothem, using detailed grain characterisation, with potential implications for future studies of basin-margin successions. An additional factor to consider is lateral variability in shelf process regime, which will influence the along-strike distribution of facies and their associated grain character and stratigraphic thicknesses on the clinothem slope.

5.9.2 Sediment Bypass at the Cliniform Rollover

In Cycle LG-1, the clinothem rollover (Locations 2 and 3) marks a prominent zone of grain-size fining (Figs. 5.13, 5.14a). Beyond the cliniform rollover zone, there is a basinward coarsening trend (Location 4), suggesting the presence of strongly bypassing flows across the shelf-edge. However, the bypass of coarse-grained sediment varies prominently between facies, according to i) the dominant process-regime in operation at the coeval shelf, and ii) the hyperpycnal flow-style.

Turbidite beds of FA C (associated with wave-dominated shelf process-regime conditions), do not bypass coarse-grained sand downdip (Fig. 5.10a); in FA C grain size does not vary significantly at the clinoform rollover or along the depositional profile. The uniformity in grain size observed in FA C across the depositional profile reflects the well-sorted sediment source, possibly associated with previous reworking and winnowing processes at the shelf-edge under wave-dominated conditions (e.g., Roy et al., 1994; Bowman and Johnson, 2014; Cosgrove et al., 2018).

Although FA D and FA E are both associated with river-dominated shelf process-regimes, sediment bypass styles beyond the clinoform rollover vary between the two facies. This is attributed to their variable flow-styles. FA D (interpreted to represent sustained hyperpycnal flows) shows a general fining trend beyond the clinoform rollover and does not bypass large volumes of coarse-grained sand into the distal slope setting. The calibre of sand available at the river-mouth is likely to be a dominant factor controlling grain-size uniformity in FA D. Additionally, the lack of shelf incision associated with FA D indicates a low erosion and entrainment capacity, which attenuates the ability of sustained hyperpycnal flow deposits to incorporate coarser-grained sand-fractions from underlying deposits. In contrast, FA E (interpreted to represent episodic hyperpycnal flows associated with major flooding events) bypasses the shelf setting and deposits coarse-grained sand in the medial and distal slope setting. The high-energy nature of the episodic hyperpycnal flows of FA E promotes bypass of the shelf and clinoform rollover (e.g. Petter and Steel, 2006), associated with erosion and entrainment of coarser-grained sand from underlying shelf deposits; this is evidenced by the incision of FA E into the underlying shelf deposits of FA A. In FA E, deposition of the coarsest sediment fractions occurs on the proximal and medial slope; at the distal slope there is a decrease in mean grain size, associated with slope-gradient decrease and consequent flow deceleration (Figs. 5.8 and 5.15).

In addition to influencing grain size across the depositional profile, the hyperpycnal flow type also influences the stratigraphic thicknesses of the resulting deposits. Episodic hyperpycnal flow deposits (FA E) are generally thicker, relative to their sustained hyperpycnal flow counterparts (FA D); this potentially implies that episodic hyperpycnal flows, associated with major flooding events, are able to transport and deposit higher sediment volumes relative to sustained hyperpycnal flows. However, this might seem counter-intuitive, as sustained hyperpycnal flows are likely to last longer and should thus result in greater stratigraphic bed-thicknesses compared to episodic hyperpycnal flows (e.g., Piper and Savoye; 1993; Mulder et al., 1998; Kneller and Buckee, 2000; Mulder and Alexander, 2001; Plink-Björklund and Steel,

2004). However, the relative thickness of FA E (episodic) relative to FA D (sustained) may be localised and represent an artefact of sampling along a 2-D depositional profile. Additionally, this may imply that some of the sediment volume associated with FA D is bypassed further downslope into the basin-floor environment, which doesn't crop-out in this locality (Fig. 5.15).

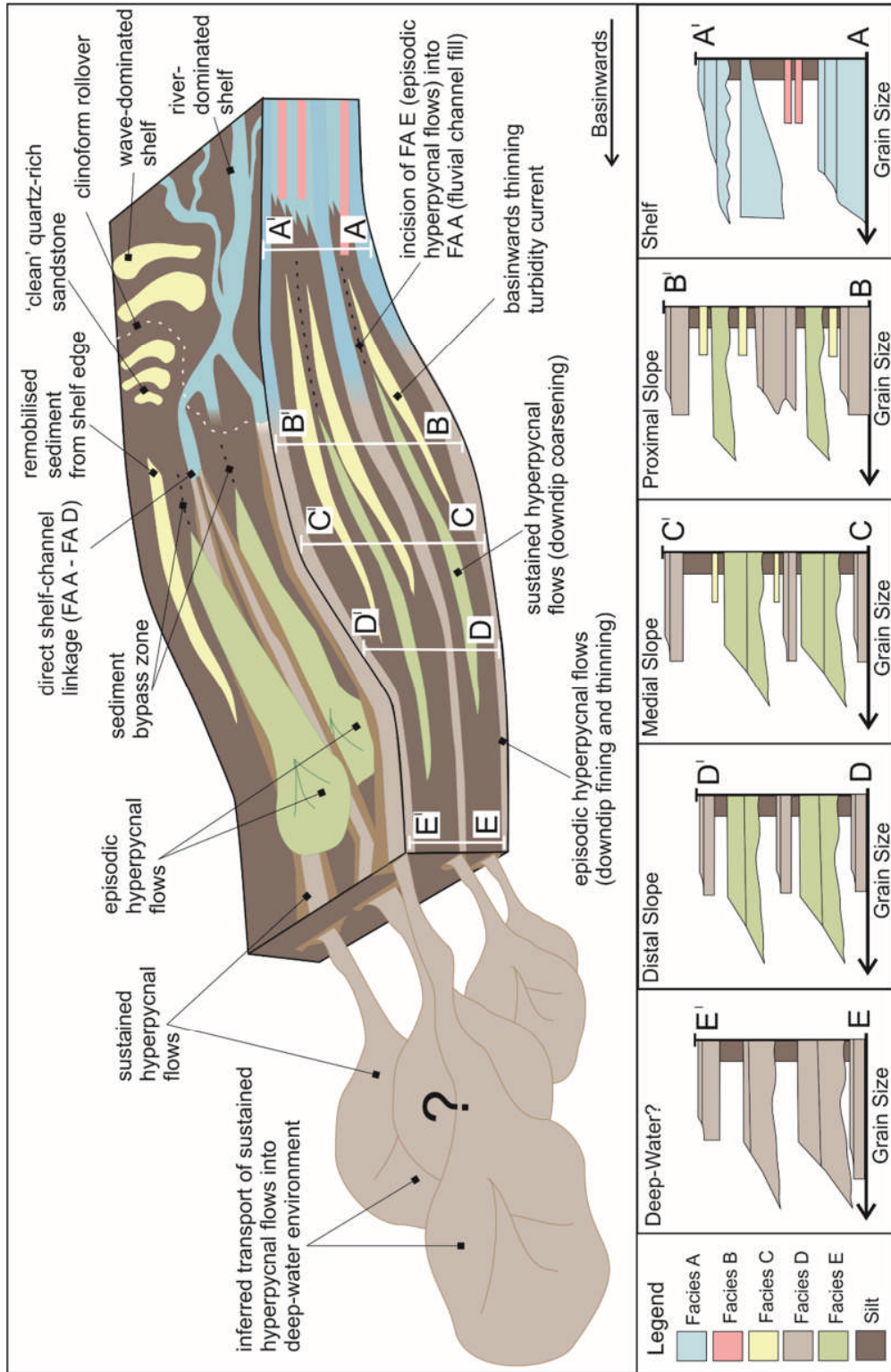


Figure 5.15: Clinoform model based on Cycle LG-1, including schematic grain-size logs; both grain size and the distribution of sand and mud vary downdip and through the stratigraphy at an intra-clinoform scale. Variability occurs according to processes operating in the shelf, including the dominant process-regime in operation at the shelf-edge (interpreted to relate to autogenic river avulsion), and the flow style (i.e. sustained versus episodic hyperpycnal flows). Inferred bypass of the sustained hyperpycnal flows (FA D) further downslope into the deep-water (basin-floor) environment is also illustrated.

5.9.3 Allogenic and Autogenic Process Regime Variability

Intra-clinothem process-regime variability may be driven by allogenic or autogenic forcings (e.g., Muto and Steel, 1997; Muto and Steel, 2014; Olariu, 2014). The duration of each cycle within the Sobrarbe Deltaic Complex is on the order of hundreds of thousands of years (Dreyer et al., 1999); as such within Cycle LG-1, intra-clinothem process regime variability occurred over timescales of tens of thousands of years. Allogenic variability, associated with small-scale relative sea-level variations, may account for the observed process-regime change in Cycle LG-1; this possibility is supported by the interpretations of Dreyer et al. (1999), who attribute intra-clinothem unconformities in the underlying Comaron composite sequences to high-frequency episodes of forced regression, associated with repeated small-scale tectonic tilting of the basin-floor. Variations in sediment supply rate provide an alternative allogenic cause of intra-clinothem process regime change. The river-dominated facies (FA D and E) may potentially be the result of climatically-activated river floods; as such, periods of heightened precipitation would have resulted in enhanced physical and chemical weathering, associated with increased terrestrial run-off (Schmitz, 1987; Peterson, et al., 2000). In contrast, wave-dominated facies (FA C) would be associated with periods of reduced sediment influx, associated with relatively drier climatic conditions. Variations in Eocene orbital cyclicity, related to the precessional (c. 25 ky period cycles) influence on precipitation patterns (e.g., Berger, 1978; Kutzbach and Otto-Bliesner, 1982), provide another potential allogenic mechanism of regulating sediment transport over the timescales observed in Cycle LG-1 (cf. Middle Eocene, Ainsa Basin; Cantalejo and Pickering, 2014).

Alternatively, autogenic processes such as river-channel avulsion, can result in a transient along-strike shut-down of the direct connectivity between the river-dominated shelf and deep-water system. Immediately downdip of the delta lobe switching and abandonment, a temporary shift to wave-dominated conditions at the shelf-edge may occur. The case for an autogenic cause of process regime variability is strengthened by the apparent rapidity (10 – 20 thousand years) at which alternating river- and wave-dominated conditions are recorded in the stratigraphic record (e.g., Amorosi and Milli, 2001; Amorosi et al., 2003; 2005; Correggiari et al., 2005; Olariu, 2014).

Both allogenic and autogenic drivers of process regime change are plausible for Cycle LG-1 and are difficult to distinguish in the absence of additional strike-parallel exposure. However, based on the abrupt intra-clinothem facies changes, and the localised preservation of wave-dominated facies (i.e. wave-dominated conditions are not documented at intra-clinothem scales in other minor sequences; Dreyer et al., 1999), autogenic river-avulsion is the favoured mechanism of intra-clinothem process regime variability in this case.

5.10 Conclusions

This study integrates quantitative analysis of grain size and sorting with a traditional outcrop-based study of a single topset-to-bottomset clinothem within the Las Gorgas composite sequence of the Eocene Sobrarbe Deltaic Complex. In Cycle LG-1, five sandstone-dominated facies have been identified, based on sedimentary texture and structure, and bed geometry. The sandstone-dominated facies associations show quantitative differences in grain size and sorting. Slope deposits are dominated by organic-rich and micaceous hyperpycnal flow deposits (FA D and E); these are associated with coeval river-dominated topset deposits (FA A and B). Two depositional styles are observed in FA D and E, related to the nature of the hyperpycnal flooding events: sustained (FA D), versus episodic (FA E). Sustained hyperpycnal flow deposits show direct river connectivity between the outer-shelf and proximal slope and result in the deposition of fine-grained sand across the complete depositional profile. Episodic hyperpycnal flows mostly bypass the clinoform rollover and incise underlying shelf deposits; deposition of medium- and coarse-grained sand occurs mostly on the proximal to distal slope. Episodic flows are interpreted to have higher flux rates, and ultimately may transport more sediment into distal slope settings than lower flux rate sustained flows of longer duration. Hyperpycnal-flow deposits are interbedded with much cleaner (terrestrial organic matter- and mica-poor), finer-grained turbidites (FA C), which do not show characteristics consistent with their hyperpycnal counterparts. The clean and relatively fine-grained nature of FA C suggests strong reworking or deposition under a wave-dominated process regime, under which clean shelf-edge sands are remobilised as turbidity currents. The wave-dominated regime deposits are entirely absent from the distal slope. The facies distributions documented in Cycle LG-1 are therefore the result of rapid temporal changes in the dominant process regime, occurring over timescales of tens of thousands of years; these transitions are interpreted to be the result of autogenic variability at an intra-clinothem scale, and mostly associated with river-avulsion processes.

Quantitatively-documented basinward changes in grain size, alongside facies distributions, indicate that coarse-grained sediment bypass at the clinoform rollover varies according to both the dominant process-regime in operation at the shelf-edge (i.e. wave- versus river-dominated) and the flow-style of river-dominated deposits (i.e. sustained versus episodic hyperpycnal flows). In Cycle LG-1, bypass into the deeper-water setting is driven by episodic hyperpycnal flows; sustained hyperpycnal flows and turbidity currents associated with a wave-dominated shelf do not bypass coarse-grained sediment downdip. Instead, all grain sizes are deposited across the slope setting, facilitating clinoform progradation. As such,

heterogeneity in grain size is documented not only at a process-regime scale, but variability in coarse-grained sand bypass can be introduced based on the dominant flow-style.

This study applies integrated quantitative grain size and sorting data and sedimentology in order to understand the evolution of an individual clinothem sequence. This novel dataset highlights hitherto undocumented intra-clinotem variability, which is directly related to changes in the shelf process-regime. Updip shelf process-regime is a fundamental factor controlling downdip architecture and sedimentary texture. The outcrop example from Cycle LG-1, also highlights the complexity and heterogeneity of different flow-types, such that flows associated with sustained and episodic hyperpycnal flows also modulate the distribution, calibre and maturity of sediment transported downdip. This novel outcrop-based study of grain character may be used as a predictive reference for subsurface exploration and provides new insights into the evolution of individual clinotem sequences.

5.11 Supplementary Information

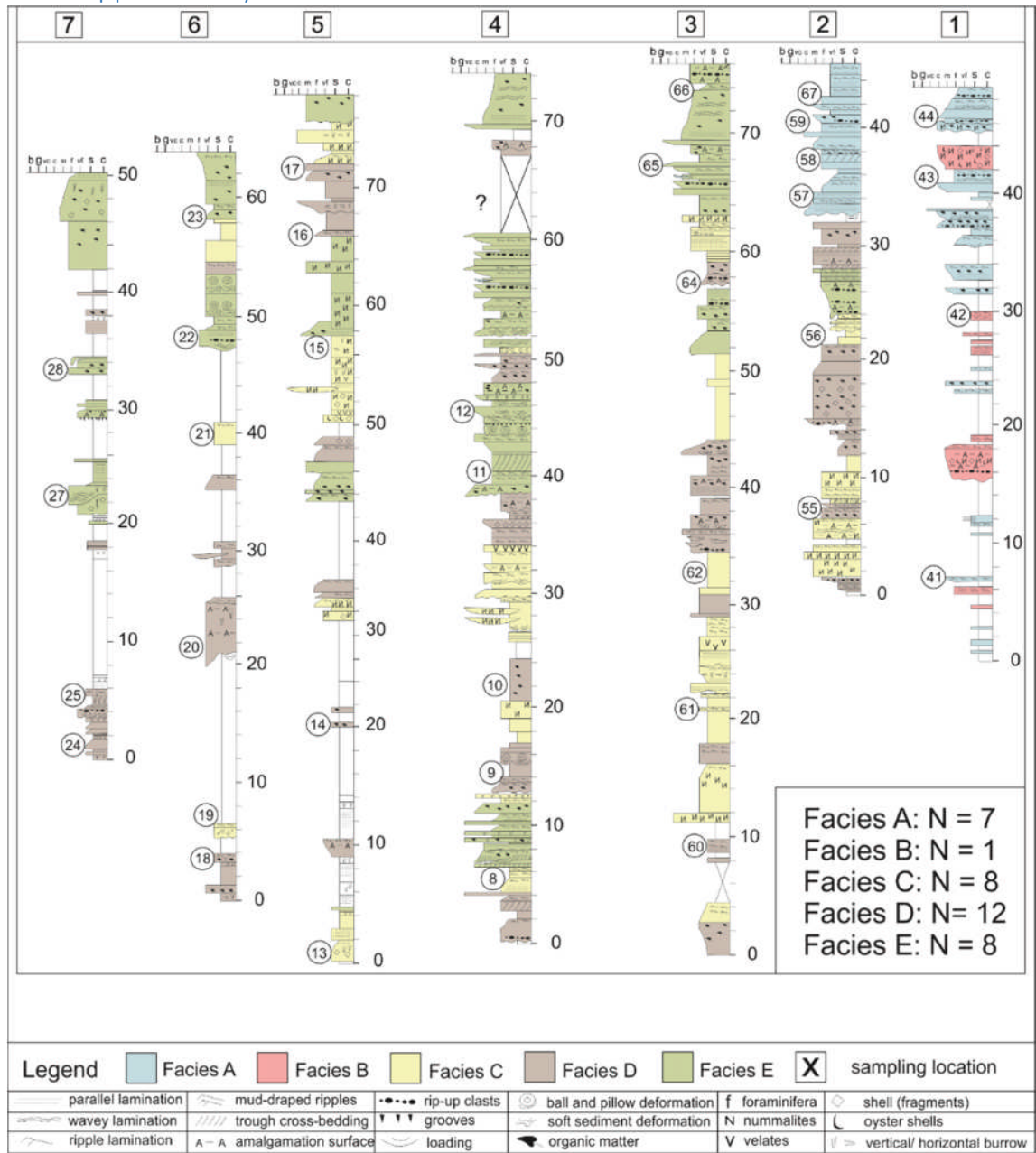


Figure 5.16: Supplementary information illustrating sample numbers and sample locations within sedimentary logs.

Sampling Location	Sample Number	Lat/Long Coordinates
1	41	42°19'44.73"N 0°05'22.56"E
1	42	42°19'45.56"N 0°05'22.90"E
1	43	42°19'46.27"N 0°05'22.92"E
1	44	42°19'46.65"N 0°05'23.44"E
2	67	42°19'59.37"N 0°05'10.63"E
2	59	42°19'58.36"N 0°05'10.47"E

2	58	42°19'57.87"N 0°05'10.14"E
2	57	42°19'56.93"N 0°05'09.73"E
2	56	42°19'54.67"N 0°05'09.16"E
2	55	42°19'51.91"N 0°05'08.65"E
3	66	42°20'16.04"N 0°05'00.08"E
3	65	42°20'16.01"N 0°05'00.43"E
3	64	42°20'15.96"N 0°05'00.05"E
3	62	42°20'15.66"N 0°04'58.97"E
3	61	42°20'15.25"N 0°04'57.60"E
3	60	42°20'14.96"N 0°04'56.43"E
4	12	42°20'43.73"N 0°04'44.98"E
4	11	42°20'43.23"N 0°04'44.93"E
4	10	42°20'42.74"N 0°04'45.00"E
4	9	42°20'41.96"N 0°04'45.72"E
4	8	42°20'40.68"N 0°04'43.29"E
5	17	42°20'59.19"N 0°04'35.75"E
5	16	42°20'58.86"N 0°04'34.33"E
5	15	42°20'58.93"N 0°04'34.18"E
5	14	42°20'59.02"N 0°04'33.90"E
5	13	42°20'59.41"N 0°04'31.31"E
6	23	42°21'07.59"N 0°04'34.67"E
6	22	42°21'08.28"N 0°04'34.15"E
6	21	42°21'09.05"N 0°04'33.89"E
6	20	42°21'09.04"N 0°04'32.66"E
6	19	42°21'10.92"N 0°04'32.08"E
6	18	42°21'10.88"N 0°04'32.01"E
7	28	42°21'17.57"N 0°04'32.59"E
7	27	42°21'16.79"N 0°04'32.98"E
7	25	42°21'17.28"N 0°04'30.66"E
7	24	42°21'17.27"N 0°04'30.42"E

Table 5.2: Supplementary information showing the georeferenced sample locations. The sampling locations and sampling numbers are shown in Figure 5.18.

Chapter 6 Discussion, Conclusions and Future Work

This chapter combines the findings of the previous chapters in order to address the four research questions outlined in Chapter One. A succinct conclusion is also provided, to summarise the overall findings of the project. Finally, recommendations are made for potential future research endeavours, which would build upon the findings presented and discussed in this thesis.

6.1 Discussion

6.1.1 Research Question One

What are intermediate-scale clinothems?

6.1.1.1 The Nomenclatural Class of the New Jersey Clinothems

The scale and architecture of the Miocene New Jersey clinothems, and their location on the continental shelf, relative to the palaeoshoreline and structural shelf-edge, means that they do not fit simply into current clinothem classification schemes. They exhibit a variety of features that cross-over a number of clinothem categories (Table 6.1, Fig. 6.1). This is reflected in the variety of nomenclatural terms used by various authors, including ‘subaqueous delta clinothems’ (Cosgrove et al., 2018; Hodgson et al., 2018), ‘midshelf clinothems’ (Proust et al., 2018), ‘shelf-prism clinothems’ (Patruno et al., 2015a) and ‘shelf-edge clinothems’ (Patruno and Helland-Hansen 2018). These issues are discussed below.

6.1.1.1.1 Subaqueous Delta Clinothems?

In a recent publication, Hodgson et al. (2018) described the New Jersey clinothems as being features developed at a scale similar to subaqueous delta clinothems. However, the New Jersey clinothems only share one clear commonality with subaqueous clinothems, their relative locations landward of the structural shelf-edge break and seaward of a clastic shoreline (Patruno et al., 2015a; Hodgson et al., 2018; Helland-Hansen and Patruno, 2018). Subaqueous delta clinothems are recognised on modern shelves (e.g., offshore southern Iberia, south-eastern Australia, and Monterey Bay, California; Mitchell et al., 2012) and are associated with highstands or stillstands of sea level (see Patruno et al., 2015a and references therein), however, ancient subaqueous delta clinothems are recognised rarely in the stratigraphic record (e.g., Jackson, 1964; Hampson, 2010; Hampson et al., 2015; Patruno et al., 2015b).

Considering a number of key characteristics, the New Jersey clinothems do not equate closely with either ancient or modern subaqueous delta clinothems. Most significantly, the New Jersey clinothems are of a larger scale than both modern and ancient examples of subaqueous delta clinothems (Table 6.1). The foreset heights of the New Jersey clinothems vary between ~60 – 200 m (Mountain et al., 2010). Modern subaqueous delta clinoforms are typically only a few 10s of m in height; maximum foreset heights of 46 m and 43 m have been recorded in modern muddy and sandy subaqueous delta clinothems, respectively (Patruno et al., 2015a; Patruno and Helland-Hansen; Table 6.1). Ancient outcrop examples of subaqueous clinothems have maximum foreset heights < 70 m, but are typically only a few tens of metres in height (e.g., Jackson, 1964; Hampson, 2010; Hampson et al., 2015; Patruno et al., 2015b). The New

Jersey clinothems and the other ancient examples of subaqueous clinothems have not been corrected for the effects of sediment compaction, and so foreset heights are likely to be attenuated.

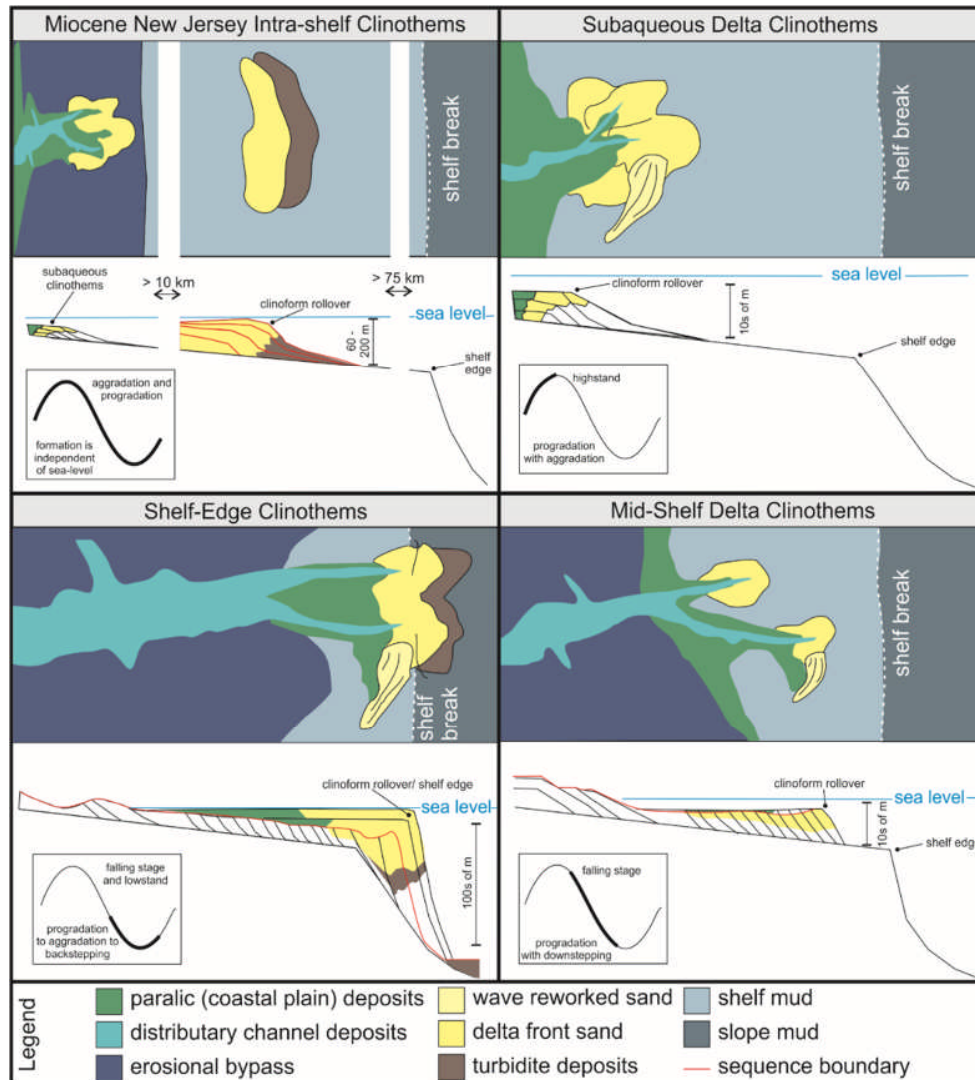


Figure 6.1: Comparison of the scale, architecture and relative position on the shelf, of the New Jersey clinothems with subaqueous, shelf-edge and mid-shelf clinothems. Adapted from Porębski and Steel, (2003)

Additionally, lithofacies and benthic foraminifer assemblages suggest the topset deposits of the Miocene intrashelf clinothems were deposited in maximum water depths of ~ 60 m (Mountain et al., 2010; Katz et al., 2013). In ancient examples, rollover depths of subaqueous clinofoms, derived from lithofacies and benthic foraminifer assemblages, are typically < 20 m (Patruno et al., 2015b), placing the rollover of the New Jersey clinothems well outside of this bracket. The rollover depths of modern subaqueous delta clinothems range from 6-59 m and 27-57 m for muddy and sandy subaqueous delta clinothems, respectively (Patruno et al., 2015a). These observations also similarly place the rollover depths of the New Jersey clinothems (just) outside of this bracket; modern subaqueous clinothems are, however,

highstand features and thus may not be suitable for direct comparison with the New Jersey clinothems.

Finally, Field and Roy (1984) suggest that both a steep shoreface profile and an extended period of stable sea level are required to develop subaqueous delta clinothems; neither of these prerequisites can be applied to the New Jersey clinothems. The New Jersey clinothems were deposited on a wide, gently sloping shelf (Steckler et al., 1999) and were deposited during repeated cycles of sea-level rise and fall (Mountain et al. 2010; Browning et al., 2013; Miller et al., 2013a).

Table 6.1	New Jersey	Muddy subaqueous clinoform	Sandy subaqueous clinoform (>20 kyr)	Mid-shelf delta clinoform	Shelf-edge delta clinoform
Rollover water depth (m)	~ 60	< 60	< 60	< 60	~ 60 – 420
Foreset height (m)	60 – 200	< 50	< 50	< 50 (as high as mid-shelf water-depth)	~ 300
Foreset gradient (°)	1 – 4	< 1	< 1 – 27.0	< 0.5 – 8	0.6 – 4.8
Basinward length (km)	5 – 15	1 – 12	0.05 – 2		2 – 17
Time scale (kyr)	10 ¹	10 ⁻¹ – 10 ¹	10 ¹ – 10 ²	10 ¹ – 10 ²	10 ² – 10 ⁴
Progradation rate	10 ¹	10 ² – 10 ⁴	10 ¹ – 10 ²	10 ¹ – 10 ²	10 ⁻¹ – 10 ¹
Clinoform trajectory	- 0.7 – + 22*	0 – + 0.5	- 0.5 – + 2.0	Sub-horizontal	- 0.4 – + 2.4

Table 6.1: Comparison of various clinothem parameters between clinothem classes. Adapted from Steckler et al., 1999; Porębski and Steel, 2003; Porębski and Steel, 2006; Mountain et al., 2010; Patruno et al., 2015; Kominz et al., 2016; Patruno and Helland-Hansen, 2018.

6.1.1.1.2 Mid-Shelf Clinothems?

In efforts to produce a depositional model describing the formation of the Miocene New Jersey clinothems, Proust et al. (2018) state that the New Jersey clinothems conform ‘to the main basic characteristics of mid-shelf deltas’ (Proust et al., 2018, p. 1582), sensu Porębski and

Steel (2006). Proust et al. (2018) make this assertion based on the following claims: i) the New Jersey clinoforms follow a progradational horizontal trajectory; ii) there are no paralic or coastal plain deposits; iii) the New Jersey clinoforms have turbiditic deposits in foresets and bottomsets. However, a series of significant observations preclude the New Jersey clinoforms as being mid-shelf delta clinoforms (sensu Porębski and Steel, 2006), these are outlined below.

1) The New Jersey clinoforms are of a larger size than mid-shelf delta clinoforms (Table 6.1); the clinoform height of the Miocene New Jersey deposits is ~ 60 – 200 m (Mountain et al., 2010). However, mid-shelf deltas are only a few tens of metres in scale (Porębski and Steel, 2003; Table 6.1). 2) The New Jersey clinoforms were deposited during repeated cycles of sea-level rise and fall (Mountain et al. 2010; Browning et al., 2013; Miller et al., 2013a). However, mid-shelf delta clinoforms prograde to a mid-shelf setting under conditions of falling relative sea-level and represent falling stage systems tracts (Porębski and Steel, 2003, 2006; Fig. 6.1). 3) The rollover trajectory of the New Jersey clinoforms varies from slightly negative (falling) to strongly positive (rising) (Cosgrove et al., 2018). However, mid-shelf clinoforms have sub-horizontal clinoform rollover trajectories (Porębski and Steel, 2003, 2006). The New Jersey clinoforms have not been systematically decompacted, therefore the trend and angle of rollover trajectory should not be used as a pivotal argument (see Klausen and Helland-Hansen, 2018). 4) The New Jersey clinoforms are well developed, with distinct sigmoidal clinoform morphologies; mid-shelf clinoforms are typically thin and patchily developed (Suter and Beryhill, 1985). 5) The New Jersey clinoforms show no evidence of any major incisional features of the clinoform rollover (Mountain et al., 2010; Cosgrove et al., 2018; Hodgson et al., 2018); mid-shelf deltas typically have an erosional ravinement surface (Porębski and Steel, 2003, 2006). 6) The New Jersey clinoforms do not record open-shelf mud-blanketing; even in interpreted transgressive deposits, the sand content typically remains > 45 % (Cosgrove et al., 2018). However, sand-rich deposits associated with mid-shelf clinoforms are typically blanketed by open-shelf transgressive muds (Suter and Beryhill, 1985; Porębski and Steel, 2003, 2006).

6.1.1.1.3 Shelf-Edge Clinoforms?

The Miocene New Jersey clinoforms have been described by Patruno and Helland-Hansen (2018) as shelf-edge clinoforms based only on the scale of the New Jersey clinoforms, which corresponds with their shelf-edge clinoform category (Fig. 6.1). The heights of shelf-edge clinoforms are typically ~ 100 – 300 m (Table 6.1), which corresponds to the scale of the New Jersey clinoforms, which are ~ 60 – 200 m in height (Mountain et al., 2010). However, to

Age	Miocene	Eocene	Eocene	Jurassic	Cretaceous	Miocene	Permian
Maximum Rollover water depth (m)	< 60	< 50 m	< 50 m	~ 20	~ 40	-	-
Foreset height (m)	~ 150	~ 100	~ 200	< 70	~ 400	< 400	< 140
Foreset gradient (°)	1 - 4	2 - 12	~ 3 - 6	~ 1 - 16	1 - 25	2 - 3	< 1
Basinward extent (km)	5 - 15	< 10	< 10	0.2 - 3	30 - 40	< 10	> 35 km
Time scale (kyr)	10 ¹	10 ¹	10 ¹	10 ¹	10 ¹		
Climofor m trajectory	Variable: slightly descending to strongly rising (-0.7 - +22)	Moderately rising	Variable	Variable: slightly descending to strongly rising (+0.2 - +0.5 (Series 2 and 3); +90 (Series 3 and 4); -0.01	Variable, overall moderately rising	Sub-horizontal	Moderately to strongly rising

				(Series 4 and 5))			
Shelf Width (km)/ Basin Size	> 100	Deposition in a tectonically constrained basin	1 -10	< 60	Deposition restricted to a ~ 8000 km ² circular depression	Deep lacustrine foreland basin	> 20
Classification	Subaqueous/mid-shelf/intra shelf/shelf-edge	Shelf-edge	Shelf-edge	Subaqueous	Shelf-edge	Lacustrine shelf-edge	Shelf-edge
Subaerial Exposure of the clinoform rollover?	No	Yes	Yes	No	Yes	Yes	No
Dominant Process-Regime	Wave- and river-dominated	River-dominated. Minor wave-influence	River-dominated. Minor wave-influence	Wave- and tide-dominated	River-dominated	River-dominated	Wave- and river-dominated
classification	Ramp	Slope	Ramp	Ramp	Ramp	Ramp	Slope

Table 6.2: Comparison of various clinothem parameters between a series of intermediate-scale clinothems. Adapted from: Dreyer et al., 1999; Steel et al., 2000; Mellere et al., 2003; Dreyer et al., 2005; Pyles and Slatt, 2007; Mountain

et al., 2010; Pyles et al., 2010; Patruno et al., 2015b; Kominz et al., 2016; Patruno and Helland-Hansen, 2018; Cosgrove et al., 2018.

With the exception of the Sognefjord Formation (the Sognefjord Formation is classified as series of subaqueous clinoforms), the intermediate-scale clinothems chosen for comparison here, have all been classified as shelf-edge clinothems (*sensu* Dixon et al., 2012b). However, some uncertainty exists surrounding this shelf-edge classification, due to the difficulty in discerning the location of the contemporaneous structural shelf-edge break in ancient outcrop examples. In the chosen examples, there is no evidence of draping a true structural shelf-edge (Dreyer et al., 1999; Petter and Steel, 2006; Pyles and Slatt, 2007; Pyles et al., 2010).

Additionally, these intermediate-scale clinothems are not associated with extensive growth faulting at the rollover, which is typically considered to be a diagnostic criteria of true shelf-edge clinothems (Dixon et al. 2012b; Patruno and Helland-Hansen, 2018). The lack of definitive proof of clinothem deposition at the true shelf-edge, leaves open the possibility that these intermediate-scale clinothems may have also been deposited in an intrashelf setting, in a manner similar to the New Jersey clinothems. If these intermediate-scale clinothems are not true shelf-edge clinothems (*sensu* Dixon et al., 2012b), then how and why are clinothems of this scale are able to develop landwards of the true shelf-edge?

6.1.1.2.1 Eocene Sobrarbe Deltaic Complex (Spain)

The syn-tectonic Sobrarbe Deltaic Complex crops out in the western part of the Eocene Ainsa Basin, north-eastern Spain. The Ainsa Basin is a piggyback basin, located in and on top of the easternmost portion of the Gavarnie thrust-sheet-complex, and forms the central sector of the South Pyrenean foreland basin (Vergés and Muñoz, 1990; Muñoz, 1992; Fernández et al., 2004). The Sobrarbe Deltaic Complex overlies channelised delta-plain and proximal and marginal marine sandstones (Dreyer et al., 1999). The Sobrarbe Deltaic Complex shows cyclic variations between muddy delta slope deposits and sandy delta front deposits (Dreyer et al., 1999). The average foreset height of the Sobrarbe Deltaic Complex clinothems is ~ 100 m; see Table 6.2.

6.1.1.2.2 Eocene Tertiary Basin (Spitsbergen, Norway)

The Eocene Central Basin of Spitsbergen comprised a small foreland basin, which developed in front of the contemporaneous West Spitsbergen fold and thrust belt (e.g., Kellog, 1975; Steel et al., 1985). The Eocene clinothems of Spitsbergen are interpreted to represent regressive and transgressive cycles across relatively narrow (1 – 10 km) and shallow (< 50 m) shelves. The Eocene clinothems are classified as shelf-edge deltas (e.g., Steel et al., 1985; Helland-Hansen, 1990; Mellere et al., 2002; Plink-Björklund and Steel, 2003), with sand-prone, actively accreting shelf-edge delta clinothems interbedded with mudstone-dominated

clinothems (Helland-Hansen, 1992; Steel et al., 2003; Uroza and Steel, 2006; Grundvåg et al., 2014). The average foreset heights of Eocene Spitsbergen clinothems are ~ 200 m; see Table 6.2.

6.1.1.2.3 Jurassic Sognefjord Formation (Norwegian shelf)

The upper Jurassic Sognefjord Formation comprises delta-scale, regressive-transgressive clinothems that were deposited on the eastern flank of the Northern North Sea rift system (Dreyer et al., 2005). The Sognefjord Formation is located on the < 60 km wide Horda Platform, which is bounded by a series of normal faults, associated with the North Sea rift system (Patruno et al., 2015b). The Sognefjord Formation internal stratigraphic architecture is dominated by aggradational and progradational stacking of sand-dominated clinothems, which are bounded by regional flooding-surfaces (Patruno et al., 2015b). The Sognefjord Formation clinothems have foreset heights of < 70 m. During the initial phase of progradation, the Sognefjord Formation prograded across the eastern part of the Troll Field; during a later phase of progradation, the Sognefjord Formation continued prograding west, onto a sloping sea-floor (Patruno et al., 2015b); see Table 6.2.

Although the amplitudes of the Sognefjord Formation clinothems are relatively small compared with other examples, they fall within the range of foreset heights exhibited by the New Jersey clinothems, and are located in an intrashelf setting; as such, the Sognefjord Formation clinothems are considered for comparison in this study. The Sognefjord Formation clinothems are deeply buried (Patruno et al., 2015b), and preserved foreset heights may be less than original heights due to the effects of sediment compaction (see Klausen and Helland-Hansen, 2018); see Table 6.2.

6.1.1.2.4 Cretaceous Lewis Shale (Wyoming, USA)

The Lewis Shale Formation is composed of relatively large-scale (~ 400 m height) progradational clinothems, interpreted to be deposited at the shelf-edge. The clinothems were deposited in a restricted basin, associated with regional subsidence, following the denudation of the Lost Soldier and Granite Mountain areas (Pyles and Slatt, 2007). The clinothems of the Lewis Shale rapidly prograded; accumulation rates exceeded basin subsidence approximately twofold (Pyles and Slatt, 2007). The Lewis Shale clinothems were deposited along the floor of the interior Cretaceous seaway of North America (Carvajal and Steel, 2006; Pyles and Slatt, 2007); see Table 6.2.

6.1.1.2.5 Permian Waterford Formation (Western Cape, South Africa)

The lower Waterford Formation comprises eight regionally correlated stratigraphic units (named Waterford clinothems 1-8; Jones et al., 2013; 2015). The Waterford Formation

clinothems vary laterally in foreset thickness (20 -140 m) and have low gradient foresets (< 0.7 °). The Waterford Formation clinothems shown a strong stratigraphic variability in dominant process-regime from river- to wave-dominated (Poyatos-More et al., 2016; Gomis-Cartesio et al., 2017). The Waterford Formation clinothems overlie a channelised slope succession (the Fort Brown Formation); see Table 6.2.

6.1.1.2.6 Miocene Para-Tethyan deep lake basin (Dacian Basin, Romania)

The Dacian Basin (Late Miocene – present) is situated in the foreland basin of the South Carpathian Mountains. Initially (Stage 1; Fongngern et al., 2016), the deltaic system prograded into a deep depocentre, generating high-gradient clinoforms, with closely spaced, < 2 km wide v-shaped canyons on clinoform foresets (Fongngern et al., 2016). During the second phase (Stage 2; Fongngern et al., 2016) of basin infill, clinoform foresets show < 4 km wide canyons and erosion of the lacustrine shelf-edge. During the final phase (Stage 3; Fongngern et al., 2016) of basin-fill, smaller clinoforms are present, with smoother foresets and less erosion of the lacustrine shelf-edge. The clinothems prograde into a flat-bottomed foreland basin. These lacustrine clinoforms reach heights of up to 400 m and show broadly horizontal growth trajectories (Fongngern et al., 2016); see Table 6.2.

6.1.1.2.7 Seismic Datasets

A number of intrashelf seismic datasets exist. However, these datasets lack depositional facies and lithological data. 1) Carbonate shelf, Australia (Upper Miocene; Adams and Schlager, 2000). 2) Florida Hatteras Slope (Post-Top Tithonian; Schlee et al., 1979). 3) Southeast South Island, New Zealand (Cenozoic; Adams and Schlager, 2000). 4) Shelf off Guadiana River (Pleistocene; Hernández-Molina et al., 2000). The foreset heights of the seismically imaged intermediate-scale clinothems vary between ~ 200 – 400 m; characteristics of these seismically imaged clinothems are summarised in Table 6.3.

Table 6.3	Carbonate shelf, Australia	Florida Hatteras Slope	Southeast South Island, New Zealand	Shelf off Guadiana River
Age	Upper Miocene	Post-Top Tithonian	Cenozoic	Pleistocene
Foreset height (m)	< 400	< 400	< 400	~ 200
Basinward extent (km)	< 20	~ 50	< 20	-

Clinoform trajectory	+0.8° to +2.5°	+1.3°	+1.5	Regressive descending
Tectonic Setting	Passive Margin	Passive Margin	Active Margin	Active Margin
Classification	Ramp	Ramp	Slope	Slope

Table 6.3: Comparison of various clinothem parameters between a series of seismically imaged intermediate-scale clinothems. Table Adapted from: Schlee et al., 1979; Adams and Schlager, 2000; Hernández-Molina et al., 2000. Clinoform trajectories taken from Patruno et al., 2015a. Foreset heights and basinward extents measured from published seismic sections in Schlee et al., 1979; Adams and Schlager, 2000; Hernández-Molina et al., 2000.

6.1.1.3 Sub-dividing Intermediate-scale Clinothems

The aforementioned intermediate-scale clinothems can be subdivided into end-members, here termed ‘ramp’ and ‘slope’ (Tables 6.2 and 6.3). The end-members are differentiated according to the water-depth of the basin into which they are prograding, and the inherited bathymetry and architecture of the underlying shelf over which they prograde. The morphological shelf in this context is defined as an aerially extensive, (sub-) horizontal to low-gradient, sub-aqueous surface that borders a deeper basin (*sensu* Porębski and Steel, 2003).

6.1.1.3.1 Ramp-type Intermediate-scale Clinothems

Ramp-type intermediate-scale clinothems describe the progradation of clinothems across a low-gradient shelf; progradation is typically directed towards a structural shelf-edge break, associated with a significant increase in water-depth (Fig. 6.2). This depositional environment can be described by foreland basin settings (e.g., Steel et al., 1985; Helland-Hansen, 1990; Mellere et al., 2002; Plink-Björklund and Steel, 2003; Carvajal and Steel, 2006; Pyles and Slatt, 2007; Patruno et al., 2015b; Fongngern et al., 2016) and passive margin settings (without deep-seated faulting, rotation, or other significant tectonic disturbances). This style of intermediate-scale clinothem deposition is typified by the Miocene New Jersey clinothems (e.g., Steckler et al., 1999; Mountain et al., 2010); the Eocene Tertiary Basin clinothems (e.g., Steel et al., 1985; Helland-Hansen, 1990; Mellere et al., 2002; Plink-Björklund and Steel, 2003); the Sognefjord Formation (Patruno et al., 2015b); the Lewis Shale Formation (Carvajal and Steel, 2006; Pyles and Slatt, 2007); the Dacian Basin (Fongngern et al., 2016); the

Carbonate shelf, Australia (Adams and Schlager, 2000) and the Florida Hatteras Slope (Schlee et al., 1979).

In ramp-type intermediate-scale clinothems, progradational wedges stack successively in a basinwards direction, over a gently sloping ramp ($< 1^\circ$). Ramp clinothems show relatively thin topset deposits, with thick, often aggradational foreset wedges (Fig. 6.2). The thin topset deposits presented by ramp clinothems suggest efficient topset-bypass, this is evidenced by the common occurrence of foreset and bottomset deposits associated with bypassing turbidity currents (e.g., New Jersey, Hodgson et al., 2018) and hyperpycnal flow deposits (e.g., Dacian Basin, Fongngern et al., 2016; Eocene Tertiary Basin, Mellere et al., 2002; Plink-Björklund and Steel, 2003). The relatively flat relief of the inherited topography and strong topset-bypass results in minimal stratigraphic climb (*sensu* Helland-Hansen et al., 2012), within ramp intermediate-scale clinothems.

6.1.1.3.2 Slope-type Intermediate-Scale Clinothems

Slope-type intermediate-scale clinothems describe the progradation of clinothems into gradually deeper water, across a basinward-directed channelised slope succession; this style of intermediate-scale clinothem deposition is typified by the Waterford Formation (Jones et al., 2013; 2015; Fig. 6.4); the Sobrarbe Deltaic Complex (Dreyer et al., 1999; Pyles et al., 2010; Fig. 6.4); the shelf off Guadiana River (Hernández-Molina et al., 2000); and Southeast South Island, New Zealand (Adams and Schlager, 2000). In 'slope' intermediate-scale clinothems, progradational wedges stack successively in the basinwards direction, over a channelised slope, and show no stratigraphic climb (*sensu* Helland-Hansen et al., 2012). The slope intermediate scale clinothems are associated with relatively small foreset heights (< 150 m). The smaller foreset heights may reflect the depositional environments of the slope intermediate-scale clinothems, which are often associated with deposition in a restricted basin; as such, available accommodation space may be a factor determining foreset height. Additionally, the channelised nature of the underlying deposits may provide a less stable platform for clinothem outbuilding and consequently attenuate foreset height.

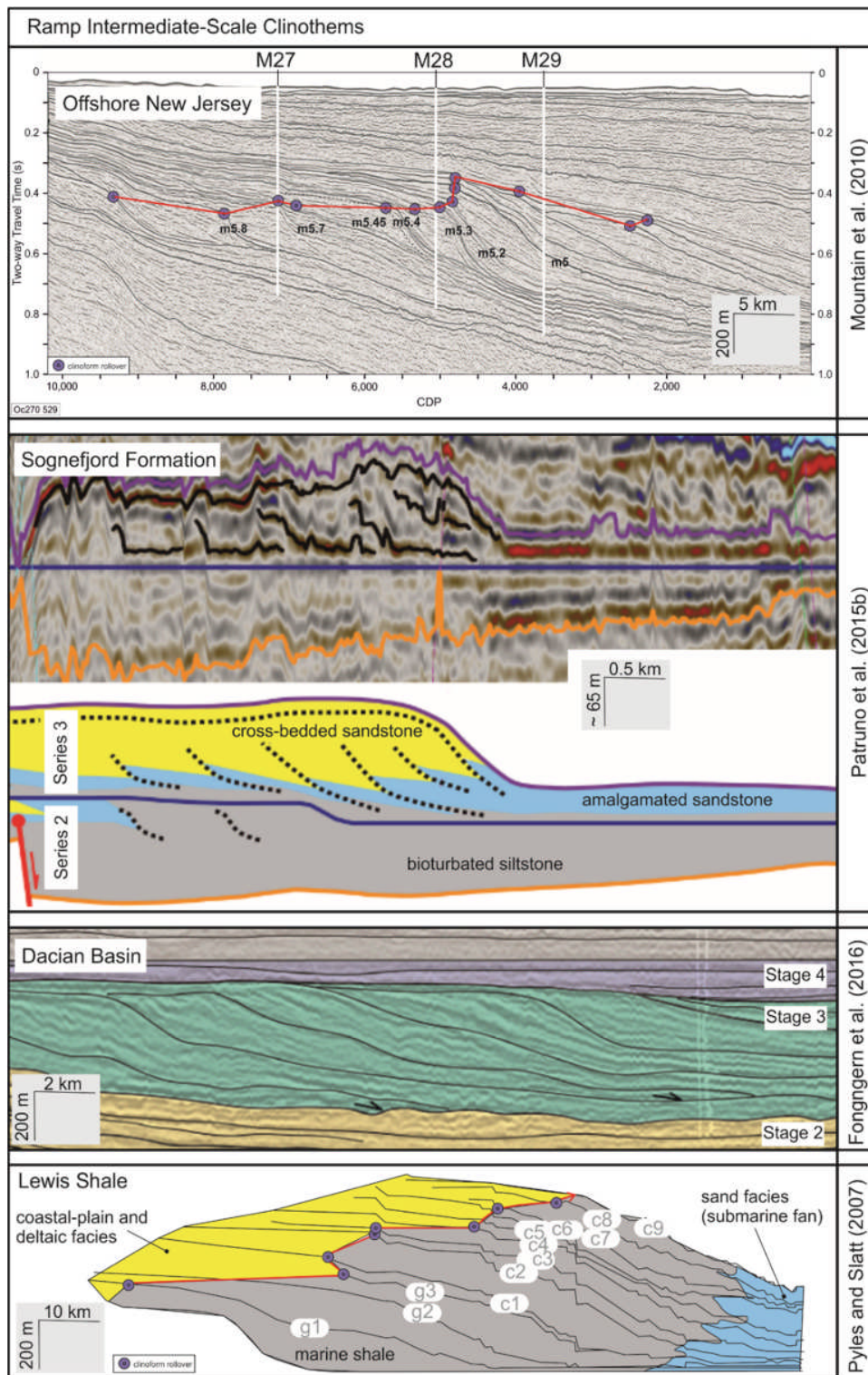


Figure 6.2: Examples of ramp style intermediate-scale clinothems. Adapted from Pyles and Slatt, (2007); Mountain et al. (2010); Patrino et al. (2015b) and Fongngern et al. (2016).

Slope-type intermediate-scale clinothems are associated with slumping at the clinoform rollover (e.g., Bullimore et al., 2005). The presence of widespread slumping at the clinoform rollover is largely absent from ramp-type intermediate-scale clinothems. This suggests that

the slumping observed in slope clinothems is an artefact of the inherited topography onto which these clinothems prograde, such that the entrenched slope valleys and channelised deposits underlying slope clinothems may promote instability at the clinoform rollover.

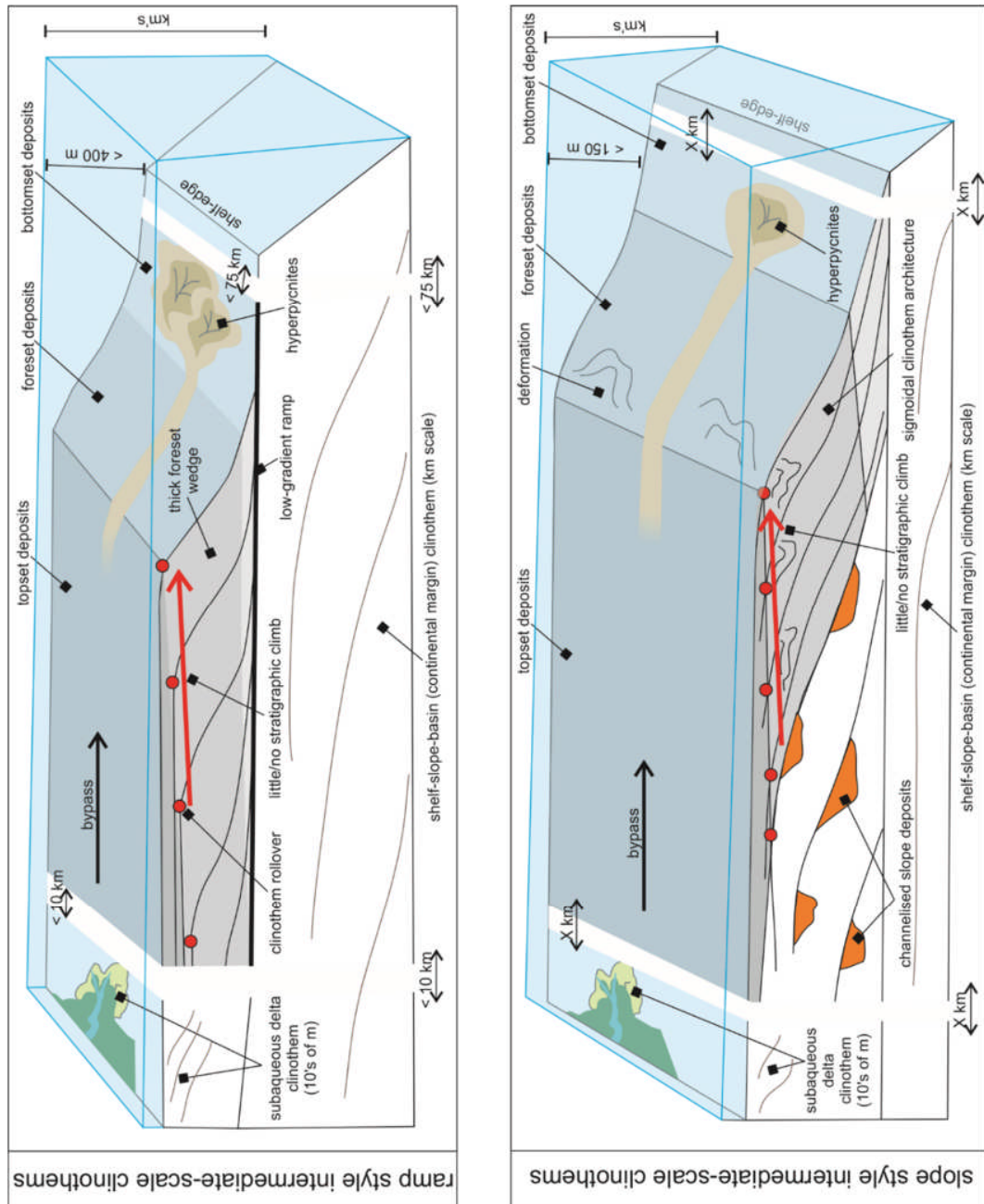


Figure 6.3: Idealised ramp and slope style clinothems.

Intermediate-scale slope clinothems exhibit more classical sigmoidal architectures, and lack the relatively thick and aggradational foreset wedges observed in ramp clinothems (Fig. 6.4); as such, slope clinothems display more even sediment-distribution across the complete depositional profile. The lack of a thick foreset wedge in slope clinothems suggests efficient foreset sediment bypass (e.g., Hadler-Jacobsen et al., 2005), reflecting a strong basinward-directed fluvial-drive, associated with proximity to a major river-system. In the Sobrarbe Deltaic Complex, the exposure of terrestrial fluvial deposits directly updip of shallow marine facies (Dreyer et al., 1999) supports this.

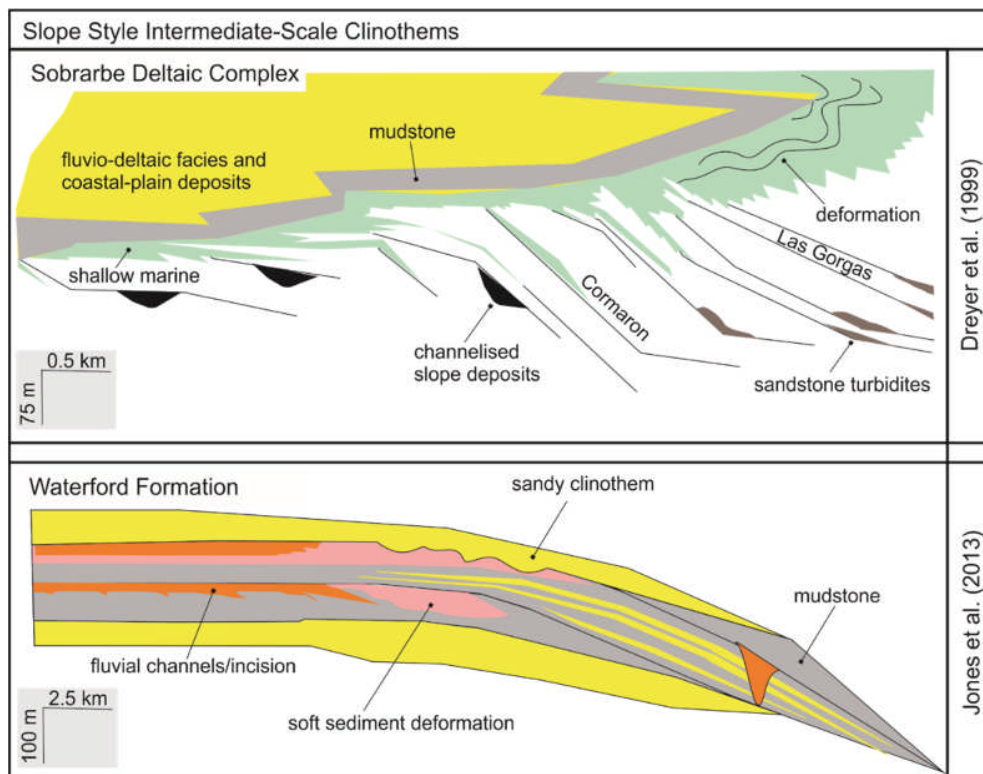


Figure 6.4: Examples of slope intermediate-scale clinothems. Adapted from Dreyer et al. (1999) and Jones et al. (2013).

6.1.1.4 Common characteristics of Intermediate-scale Clinothems

Despite the sub-division of intermediate-scale clinothems into ‘ramp’ and ‘slope’ types, intermediate-scale clinothems share a number of pervasive commonalities (see Table 6.2). 1) Comparable foreset heights, of ~ 100 – 400 m. 2) The maximum water-depth of the clinoform rollover is < 60 m. 3) Sandy foreset and bottomset deposits are often hyperpycnal in origin and associated with a river-dominated shelf process-regime. 4) Clinothem deposition occurs on scales of ~100,000 kyr. 5) Successive clinoforms show little to no stratigraphic climb (sensu Helland-Hansen et al., 2012); clinothem outbuilding is dominated by strong basinward progradation. These parameters are outlined in Table 6.2.

6.1.1.5 *Formation of Intermediate-scale Clinothems*

The formation of intermediate-scale clinothems is currently attributed to the interactions between shoreline (subaerial) clinothems and subaqueous clinothems, which are suggested to superimpose and interact to aggrade shelf strata (e.g., Hernandez-Molina et al., 2000; Oliveira et al., 2011; Proust et al., 2018). Delta-scale shoreline clinofolds are relatively small in scale (10s m in height) and occur where a river system feeds into a standing body of water (including the open sea, lakes, lagoons and bays), where the rate of sediment deposition exceeds the rate of sediment erosion (e.g., due to wave-action); the rollover of a subaerial delta corresponds with the junction between terrestrial and aqueous environments (Coleman and Wright, 1975; Galloway, 1975; Bhattacharya and Giosan, 2003). In this scenario, the cyclic regression and transgression of shoreline and subaqueous clinofolds is suggested to result in continental shelf outbuilding and lead to the formation of larger scale clinothems. This depositional scenario is here challenged to account for the observed common characteristics of intermediate-scale clinothems.

Accurately constraining clinofold rollover depths in ancient successions can be challenging; rollover depths vary through the lifecycle of a clinofold, and across successive clinofolds, with accommodation and sediment supply. Of the intermediate-scale clinofolds analysed in this study, maximum clinofold rollover water-depths, typically determined by faunal assemblages, vary between 20 and 60 m (Table 6.2). Excluding the New Jersey and Sognefjord clinofolds, minimum clinofold rollover depths of 0 m are recorded in all examples, as evidenced by the subaerial exposure of the clinofold rollover (Dreyer et al., 1999; Steel et al., 2000; Mellere et al., 2003; Dreyer et al., 2005; Pyles and Slatt, 2007). The lack of evidence for subaerial exposure in the New Jersey and Sognefjord Formation clinofold rollovers may, however, be an artefact of the datasets; in both cases limited core data sampling topset deposits is available (Dreyer et al., 2005; Mountain et al., 2010; Patruno et al., 2015b). During periods of relative sea-level highstand, where maximum rollover depths of ~ 20 - 60 m are recorded, sediment deposition would typically occur below the average fair-weather wave-base (e.g., Reineck and Singh, 1972; McCubbin, 1982; Browning et al., 2006), allowing the active accretion of sandy deposits and inhibiting the lateral dispersal of sediment through wave-reworking (e.g., Plink-Björklund and Steel, 2004; Petter and Steel, 2006; Dixon et al., 2012a). During periods of relative sea-level fall, with potential exposure of the clinofold rollover, hyperpycnal flows, associated with a river-dominated shelf, facilitate the bypass of sand-grade sediment across the shelf (e.g., Mulder and Syvitski, 1995; Nemec, 1995; Mulder and Alexander, 2001; Carvajal and Steel, 2006; Helland-Hansen and Hampson, 2009) and into the intrashelf setting; hyperpycnal flows would also erode and entrain underlying shoreface

sand, deposited under relative highstand conditions (e.g., Cosgrove et al., 2018; Hodgson et al., 2018). The inherited relief of underlying subaqueous delta clinothems provides basinwards accommodation space within the intrashelf-setting, within which the accretion of hyperpycnites can nucleate. With each phase of hyperpycnite deposition, the foreset gradient increases, allowing the formation of increasingly sigmoidal clinothems. During relative sea-level rise, the hyperpycnites become blanketed in hemipelagic muds. For example, in the Eocene Spitsbergen succession (e.g., Helland-Hansen, 1992; Steel and Olsen, 2002; Uroza and Steel, 2008), the Lewis Shale (Pyles and Slatt, 2007) and the Sobrarbe Formation (e.g., Dreyer et al., 1999; Pyles et al., 2010), underlying sand-rich clinothems are draped in mudstones; these deposits are interpreted to represent transgressive and regressive depositional phases, respectively.

On modern continental margins, active sediment accretion is concentrated at, or near, the shoreline; sediment delivery beyond the clinoform rollover is restricted (Swift and Thorne, 1991), excepting examples with a narrow shelf physiography (e.g., Walsh and Nittrouer, 2003; Boyd et al., 2008; Romans et al., 2009). Modern patterns of sediment delivery do not correspond with the strongly progradational intermediate-scale clinothems outlined in this study, which would require significant sediment delivery into the slope setting, in order to facilitate clinothem outbuilding. This suggests that the presence of a strong fluvial drive, associated with hyperpycnal flows may be a key factor determining the formation of intermediate-scale clinothems.

Although river-dominated conditions can occur at any relative sea-level stand, they are most likely to occur during periods of relative sea-level fall. The subaerial exposure of clinoform rollovers of the majority of the intermediate-scale clinothems (Dreyer et al., 1999; Petter and Steel, 2006; Pyles and Slatt, 2007) suggests that episodes of significant relative sea-level fall may be a driving factor determining the formation of intermediate-scale clinothems. Changes in relative sea-level would be amplified in the Sobrarbe Formation, the Eocene Tertiary Basin and Lewis Formation, which were all deposited in narrow shelf settings or restricted basins. The deposition of intermediate-scale clinothems on roughly 100,000-year cycles may also support a eustatic component contributing to the formation of intermediate-scale clinothems, although this would vary according to time of clinothem deposition (icehouse vs greenhouse) and tectonic setting.

The Miocene New Jersey clinothems exhibit a number of key differences from other intermediate-scale clinothems (see Table 6.1). 1). Intermediate-scale clinothems are typically associated exclusively with a river-dominated shelf process-regime (e.g., Sobrarbe Formation, Lewis shale, Spitsbergen); the New Jersey clinothems have clinothems that are both river- and

wave-dominated. 2) Intermediate-scale clinothems are associated with subaerial exposure of the clinoform rollover, associated with relative sea-level fall; the New Jersey clinothems show no evidence of subaerial exposure and are associated with deposition under variable sea-levels. 3) Intermediate-scale clinothems are deposited on narrow shelves, or within restricted basins; the New Jersey clinothems are deposited on a wide (> 100 km) ocean-facing passive margin. The formation of intermediate scale, intrashelf clinothems are also documented in passive margin settings by Adams and Schlager (2000, their Figure 8b) on a carbonate shelf in Australia, and the Florida Hatteras Slope (Schlee et al., 2000, their Figure 13). However, these subsurface datasets lack the necessary depositional facies and lithological data to inform depositional models.

6.1.1.6 The Formation of the New Jersey Clinothems

The apparent differences (process regime, subaerial exposure and depositional setting) between the New Jersey clinothems and many of the other examples of intermediate scale, intrashelf clinothems necessitates a slightly modified depositional scenario to describe the formation of the New Jersey clinothems. Below, a depositional scenario describing the formation of New Jersey clinothems, as presented in Proust et al. (2018), is outlined and critiqued, and an original depositional scenario is suggested.

6.1.1.6.1 Depositional Scenario of Proust et al. (2018)

One suggested scenario for the formation of the New Jersey clinothems presented in Proust et al. (2018) is that subaerial and subaqueous deltas are intercalated with what they term as shelf-edge deltas. Note that the term shelf-edge delta is erroneously used by Proust et al. (2018) to refer to a delta built on the edge of a morphological slope; this differs from the definition used in this paper, where a shelf-edge delta refers to one built at the continental shelf-break (*sensu* Dixon et al., 2012b).

The model presented by Proust et al. (2018) invokes changes in relative sea-level as the primary mechanism of intrashelf clinothem formation. The model presented by Proust et al. (2018) is summarised by the following steps. 1) Normal regression during a sea level highstand results in the low-angle progradation of a subaerial delta and its associated muddy subaqueous delta. 2) The subaerial delta gradually oversteps the muddy subaqueous delta during a period of relative sea-level fall. 3) During the forced regression, wave and storm currents transport sand to the clinoform rollover, building shelf-edge deltas at the subaqueous delta rollover. 4) During relative sea-level rise, clean sands accumulate in wave-dominated shoreface deposits, as the shelf-edge rollover progrades and then backsteps. 5) The subaqueous deltas are truncated by wave ravinement surfaces and draped by mud.

6.1.1.6.2 Points of Contention Regarding the Depositional Scenario of Proust et al. (2018)

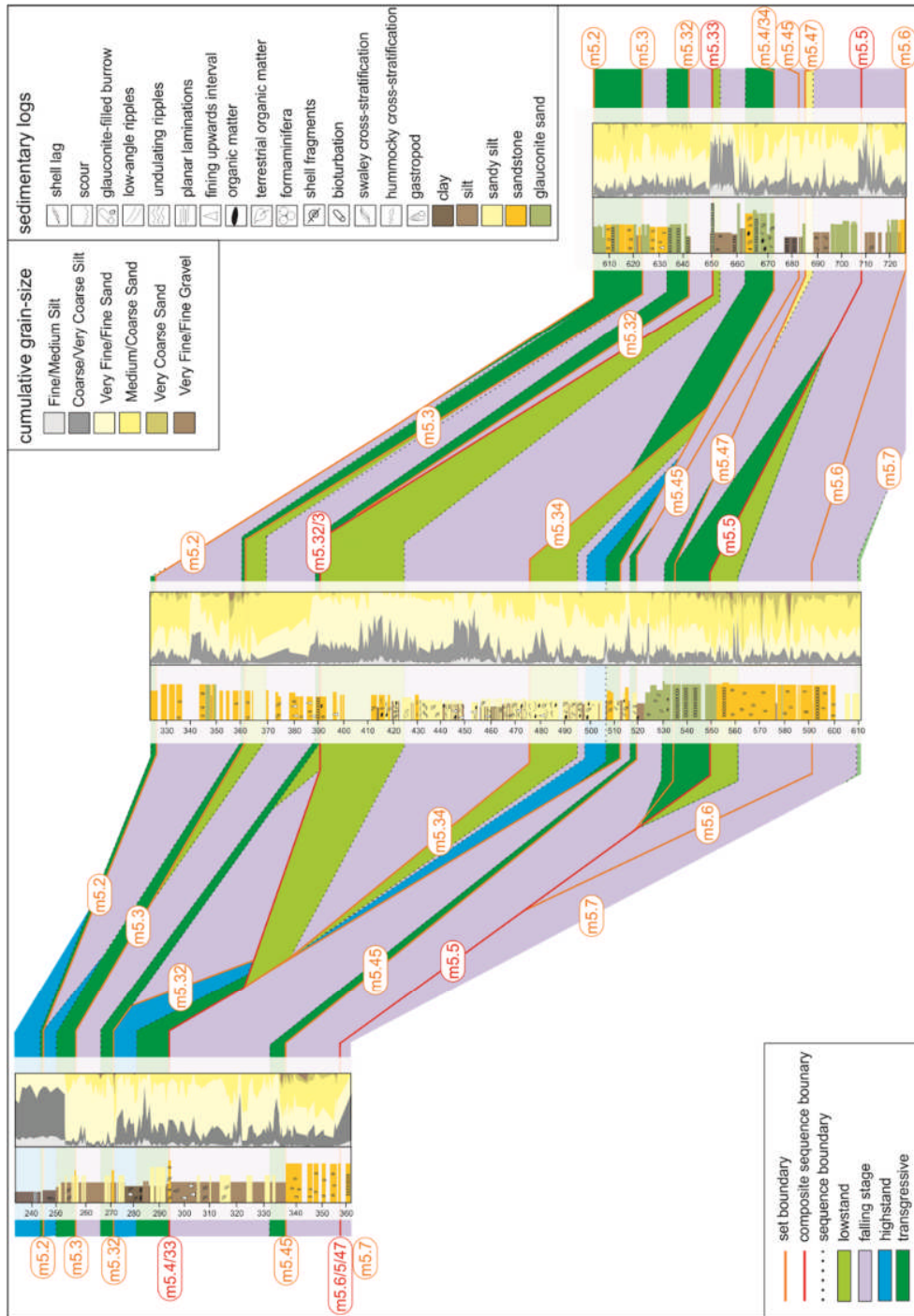


Figure 6.5: Interpreted systems tracts (as per Proust et al. 2018), overlain onto sedimentary log (Mountain et al., 2010) and quantitative cumulative grain size data (this thesis).

The model presented by Proust et al. (2018) to explain the formation of the New Jersey intrashelf clinothems is problematic. Outlined below are series of points, which contest the depositional scenario as presented in Proust et al. (2018). Firstly, the depositional model of Proust et al. (2018) requires the formation of a shelf-edge delta at the rollover of a muddy

subaqueous delta. However, databases from modern, muddy, subaqueous delta clinoforms indicate that those situated on wide (23-376 km) and gently sloping ($0.01 - 0.38^\circ$) shelves- as in the case of the Miocene New Jersey clinoforms- have gently dipping foreset slopes ($0.03 - 0.76^\circ$; Patruno et al. 2015a). The model of Proust et al. (2018) would require significantly steeper foreset slopes, and greater foreset relief, to invoke the formation of 'shelf-edge' deltas. The muddy subaqueous clinoforms would provide no significant break in slope for rollover outbuilding to take place. The Miocene intrashelf clinoforms have a foreset dip of $1-4^\circ$ (Mountain et al., 2010), which is a much steeper angle than the subaqueous delta clinoforms. Furthermore, the vertical relief of the Miocene intrashelf clinoforms (60 – 200 m) are significantly larger than muddy subaqueous delta clinoforms (< 50 m); as such, the scale of subaqueous delta clinoforms would not provide sufficient bathymetric relief to host the outbuilding of 'shelf-edge deltas' of the scale observed in the New Jersey clinoforms (Table 6.1).

Secondly, in order to support their depositional model, Proust et al. (2018) suggest that the New Jersey clinoforms are composed of ~ 70 % clay and silt fractions (i.e. all grain-sizes < 62 μm), and that these sediment fractions are concentrated at the clinoform rollover and toe of slope (Fig. 6.5). However, the quantitative grain-size analysis presented in this study (Chapters Three and Four) shows that in clinoforms m5.2 – m5.7 this is not the case. The clinoforms analysed in this study contain significantly less silt than that suggested by Proust et al. (2018; Fig. 6.5). The suggested abundance of mud is significant in the Proust et al. (2018) model, as they use this to evidence a 'detached subaqueous delta clinoform' (see Walsh and Nittrouer, 2009; Amazon River) or a shelf mud wedge (see Walsh and Nittrouer, 2009; Eel River), which is integral to their model.

Proust et al. (2018) suggest that the New Jersey clinoforms follow a broadly horizontal clinoform trajectory. However, analysis of clinoform trajectory shows deposition under both strongly rising clinoform trajectories (Sequence m5.3), slightly rising (Sequences m5.45 and m5.4) and flat to falling clinoform trajectories (Sequence m5.7) (Fig. 6.2; Chapter Three, Cosgrove et al., 2018). This is significant as Proust et al. (2018) use this horizontal trajectory to defend a comparison with mid-shelf delta clinoforms (sensu Porębski and Steel, 2006), which typically have a sub-horizontal clinoform trajectory (Table 6.1).

6.1.1.6.3 An Alternative Model of Formation of the New Jersey Clinothems

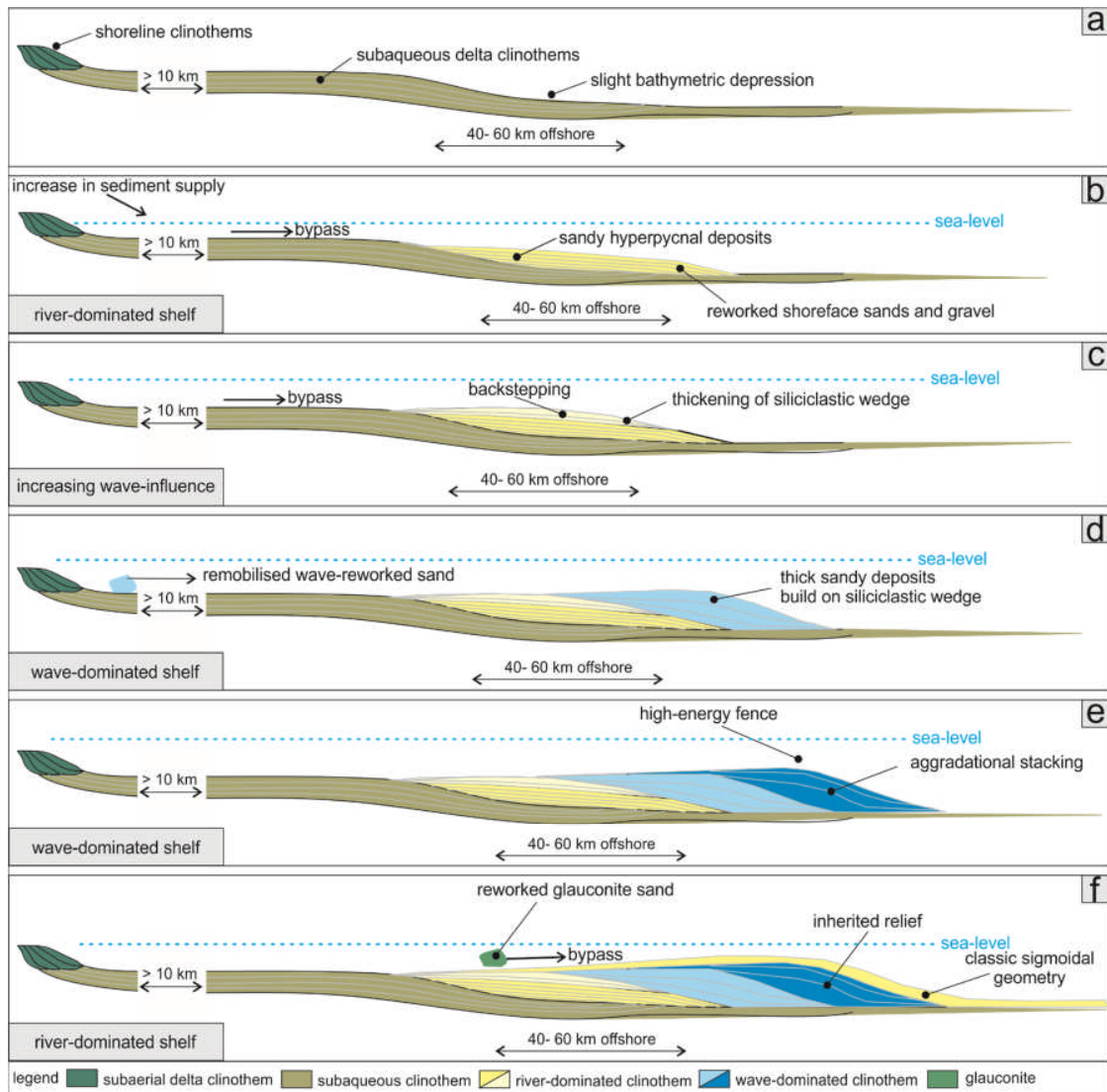


Figure 6.6: Alternative scenario of New Jersey clinothem formation.

The New Jersey clinothems formed above a shallowly dipping ($< 1^\circ$), carbonate ramp of Eocene age, which had no significant siliciclastic input until the late Oligocene (Steckler et al., 1999) and was controlled by differential subsidence. The attenuated sediment supply preceding the late Oligocene created a wide, dipping shelf, with a deep shelf-edge (Fig. 6.6a). During the late Oligocene to early Miocene, cooling of the global climate, and the associated increase in sediment supply, resulted in delta progradation. The deposition of the mid-Miocene clinothems analysed in this study correspond with a dramatic (20-fold) increase in sediment supply, suggested by Poag and Sevon (1989) to correspond with the rapid tectonic uplift, weathering and erosion of the Central Appalachian Highlands, which supply terrigenous sediment to the New Jersey shelf via the ancient Hudson and Delaware Rivers. The formation of the New Jersey clinothem is suggested to be linked to the occurrence of an

initial phase of sediment starvation during thermal subsidence (Steckler et al., 1999), proceeded by a second phase of rapid sediment influx (Poag and Sevon, 1989). The first phase generates the necessary accommodation in a wide shelf-setting, upon which the outbuilding of intrashelf clinothems can occur; the second high-supply phase provides the necessary sediment flux to facilitate clinothem construction. In sequence m5.7, during relative sea-level fall, the strong fluvial input (associated with the increase in mid-Miocene sediment supply; Poag and Sevon, 1989) generates sandy hyperpycnal flows (e.g., Mulder and Syvitski, 1995; Nemeč, 1995; Mulder and Alexander, 2001; Plink-Björklund et al., 2001; Mellere et al., 2002; Plink-Björklund and Steel, 2004). Hyperpycnal flows bypass the innermost shallow shelf, which is subaqueous delta clinothem-dominated (Fig. 6.6a, b); muddy subaqueous delta clinoforms are often sites of sediment bypass due to high near-bed shear stress (Helland-Hansen and Hampson, 2009). Deposition along subaqueous clinoform topsets is often inhibited in shallow-marine environments marked by high-energy waves, tides and currents; this results in sediment bypass through the processes of lateral advection and resuspension of sediment (Pirmez et al., 1998, Driscoll and Karner, 1999, Swenson et al., 2005, Cattaneo et al., 2007).

The hyperpycnal turbidites are deposited ~ 40 – 60 km from the shoreline (Katz et al., 2013) in the gentle slope of the underlying muddy subaqueous delta clinoforms, which generate basinward accommodation space (see Patruno et al., 2015a; Fig. 6.6b). During forced regression, hyperpycnal flows erode and rework shoreface glauconite sands and gravels (Cosgrove et al., 2018; Hodgson et al., 2018), which are deposited within this basinward accommodation space. During relative sea-level rise, the frequency and intensity of bypassing turbidity currents decrease, due the increasing dominance of wave currents on the inner shelf (Dixon et al., 2012). The attenuated flow-regime of the turbidity currents results in backstepping, which thickens the upper portion of the siliciclastic wedge and increases the angle of the slope (Fig. 6.6c).

In Sequence m5.45 and the overlying Sequence m5.4, there is a change in the dominant process-regime on the shelf, from river- (m5.7) to wave- (m5.45 and m5.4) dominated (Mountain et al., 2010; Cosgrove et al., 2018). During relative sea-level fall in the wave-dominated sequences, the heightened intensity of wave currents and storm action remobilises significant quantities of relatively well-sorted sand from the inner shelf to the middle shelf (Dixon et al., 2012a). Thick sandy topset and foreset deposits build on top of, and on the slope of, the siliciclastic wedge respectively (Figs. 6.6d, e). During relative sea-level rise, the mean-storm wave base creates a high-energy fence (Katz et al., 2013), which promotes along-strike sediment transport (Davis and Hayes, 1984; Bhattacharya and Giosan, 2003; Deibert et al.,

2003; Johannessen and Steel, 2005; Carvajal and Steel, 2009). This inhibits the bypass of the significant volumes of sand down the slope of the siliciclastic wedge of underlying Sequence m5.7 and sandy deposits are aggradationally stacked at the rollover and on the upper slope. The deposition of large volumes of sand on the upper slope creates a thick foreset prism and increases the relief of the slope (Fig. 6.6e)

In Sequence m5.3, the dominant process-regime changes from wave- (m5.45 – m5.4) to river- (m5.3) dominated. During relative sea-level fall and regression, erosive conditions are dominant landward of the clinoform rollover (Cosgrove et al., 2018; Hodgson et al., 2018), this is evidenced by the presence of significant quantities of reworked glauconite in the foreset and bottomset deposits of Sequence m5.3, likely reworked from transgressive shoreface sands in topset deposits (Fig. 6.6f). The inherited relief of the underlying wave-dominated deposits permit Sequence m5.3 to develop a classic, sigmoidal clinothem geometry (Fig. 6.6f).

6.1.1.7 A new class of clinothem?

Previous classification schemes have failed to adequately account for intermediate-scale clinothems. As such, many examples of intermediate-scale clinothems have been systematically ‘force-fitted’ into a variety of inappropriate nomenclatural classes (e.g., Patruno and Helland-Hansen, 2018). This study proposes a new nomenclatural class to encompass intermediate-scale clinothems. This proposed class of clinothem are termed ‘intrashelf’ clinothems (Table 6.4). The diagnostic criteria of intrashelf clinothems are as follows. 1) A geographic location on a morphological shelf, landwards of a morphological shelf-edge break, and basinwards of the (palaeo-)shoreline (and associated subaerial and subaqueous delta clinothems). 2) An intermediate scale, where foreset heights typically vary between ~ 100 – 400 m. 3) A strong fluvial drive, associated with the deposition of sand prone turbidity currents in foreset and bottomset deposits.

Despite the commonly shared characteristics, this proposed class of clinothem exhibits variability between clinothem systems (Table 6.4). This includes depositional setting (which vary from passive margins, to active margins, to foreland basins, to restricted basins, to lacustrine basins; Table 6.2), foreset gradients (which vary from $< 1 - 25^\circ$; Table 6.2), and basinward extent (which vary from $< 1 - >35$ km; Table 6.2). The variability exhibited by intrashelf clinothems is, perhaps, one of the reasons why this complex class of clinothem has been overlooked, or misidentified, in previous literature. The variability exhibited by intrashelf clinothems may also highlight that this proposed scheme may require further refinement in the future. However, it represents a first step towards understanding this complex scale of clinothem.

Increasing wider awareness that intermediate-scale clinothems can, and do, form in an intrashelf setting may have important implications for interpreting ancient outcrop datasets. As outlined in the preceding discussion, many ancient clinothem successions of an intermediate scale, have been classified as shelf-edge clinothems (e.g., Steel et al., 1985; Helland-Hansen, 1990; Mellere et al., 2002; Plink-Björklund and Steel, 2003; Dreyer et al., 1999; Petter and Steel, 2006; Carvajal and Steel, 2006; Pyles and Slatt, 2007; Pyles et al., 2010; Jones et al., 2013, 2015). However, identifying the true shelf-edge rollover in outcrop is notoriously difficult without the vertical exaggeration seen in seismic datasets; the commonly limited aerial extent of outcrop successions is also a limiting factor when attempting to identify the true structural shelf-break. These factors may have led to the under-recognition of intrashelf clinothems in the ancient record, where authors have favoured the interpretation of deposition at the shelf edge.

Intrashelf and shelf-edge clinothems share common characteristics, including their similar scales; as such, discerning between true intrashelf and true shelf-edge (sensu Dixon et al., 2012b) clinothems from ancient outcrop successions may be challenging. Therefore, misidentification of intrashelf clinothems as shelf-edge clinothems could be commonplace. As clinothems, at various scales, form the principal architectural elements of many deltaic-to-continental slope successions (e.g., Gilbert, 1885; Rich, 1951; Bates, 1953, Asquith, 1970; Mitchum et al., 1977; Pirmez et al., 1998; Adams and Schlager; Bhattacharya, 2006; Patruno et al., 2015b), correctly identifying and understanding the formation of clinothems of all scales, has important implications for understanding wider basin-margin evolution.

Table 6.4	Intrashelf clinothems	Muddy subaqueous delta clinoform	Sandy subaqueous delta clinoform (>20 kyr)	Mid-shelf delta clinoform	Shelf-edge delta clinoform
Rollover water depth (m)	< 60	< 60	< 60	< 60	~ 60 – 420
Foreset height (m)	~ 100 – 400	< 50	< 50	< 50 (as high as mid- shelf water- depth)	~ 300

Foreset gradient (°)	< 1.0 – 25.0	< 1.0	< 1.0 – 27.0	< 0.5 – 8.0	0.6 – 4.8
Basinward length (km)	~ 5- 40	1 – 12	0.05 – 2		2 – 17
Time scale (kyr)	10 ¹	10 ⁻¹ – 10 ¹	10 ¹ – 10 ²	10 ¹ – 10 ²	10 ² – 10 ⁴
Progradation rate	10 ¹	10 ² – 10 ⁴	10 ¹ – 10 ²	10 ¹ – 10 ²	10 ⁻¹ – 10 ¹
Clinoform trajectory	0 - +22	0 – + 0.5	- 0.5 – + 2.0	Sub- horizontal	- 0.4 – + 2.4

Table 6.4: Comparison of various clinothem parameters between clinothem classes; modified from Table 6.1, with the intrashelf clinothem class included. Adapted from Steckler et al., 1999; Porębski and Steel, 2003; Porębski and Steel, 2006; Mountain et al., 2010; Patruno et al., 2015; Kominz et al., 2016; Patruno and Helland-Hansen, 2018.

6.1.2 Research Question Two

What role does process-regime play in regulating the timing and grain character of sand transfer to slope and basin-floor settings?

6.1.2.1 Introduction

The data and associated interpretations presented in this thesis have advanced understanding of the pivotal role played by shelf process-regime in three fundamental ways, by presenting; i) interactions between process-regime, clinoform rollover trajectory and the downdip distribution of sand and mud (mud comprises all grain sizes of 62 µm or less; see Chapter Three and Cosgrove et al., 2018); ii) the first ever fully quantitative grain character database comparing wave- and river-dominated clinothem sequences (see Chapter Three and Cosgrove et al., 2018); and iii) prototype models comparing the architectural, sedimentological, facies and grain character attributes of river- and wave-dominated conditions across the depositional profile (see Chapter Three, Chapter Five, Cosgrove et al., 2018 and Cosgrove et al., in review). These novel quantitative datasets should find widespread use, including calibration of numerical models designed to predict the sediment-export properties of depositional systems under specific shelf process-regime conditions.

6.1.2.2 Basin-Scale Clinoform Trajectory

Clinoform rollover trajectories have been interpreted across seismic line Oc270 529 (Fig. 6.7a). The expected distribution of sand- and mud-dominated bottomset deposits, according to the traditional clinoform trajectory paradigm (see Burgess and Hovius, 1998; Mellere et al., 2002; Steel and Olsen, 2002; Bullimore et al., 2005; Carvajal and Steel, 2006; Uroza and Steel, 2008; Helland-Hansen and Hampson, 2009; Ryan et al., 2009), is shown on Figure 6.7b.

However, the actual distribution of sand- and mud-dominated within bottomset deposits significantly differs from what would be expected by the established clinoform trajectory model (Fig. 6.7c). The New Jersey clinothems show examples where sand-dominated bottomsets can be associated with rising clinoform rollover trajectories, and examples where mud-dominated bottomsets can be associated with flat-to-falling clinoform rollover trajectories; as such, the actual distribution of sand within bottomset deposits does not always agree with the simple clinoform trajectory model (Fig. 6.7).

The New Jersey clinothems show a direct correlation between the distribution of sand- and mud-dominated bottomsets and the dominant process-regime in operation at the shelf-edge (Chapter 3; Cosgrove et al., 2018a). Across seismic line Oc270 529, river-dominated clinothems are associated with sand-dominated bottomsets and wave-dominated clinothems are associated with mud-dominated bottomsets. The interpretations of the dominant process-regime and the distribution of sand and mud are from Mountain et al. (2010). Furthermore, the new grain character dataset presented and discussed in this thesis, which pertains only to clinothems m5.7 – m5.3, allows the relationship between process-regime and sediment distribution to be considered at finer scale and quantitatively; this is discussed in the section 6.1.2.5 (entitled Grain Character and Process Regime).

Trajectory analysis of wave-dominated clinothems (Sequences m5.45 and m5.4) have clinoform rollover trajectories that are rising. Trajectory analysis of river-dominated clinothems (Sequences m5.7 and m5.3) have flat-to-falling and rising clinoform rollover trajectories, respectively. Despite this variability in clinoform rollover trajectory, both sequences have foreset and bottomset deposits that are dominated by debrites and hyperpycnites, and contain substantial quantities of coarse-grained sediment. As such, in the river-dominated clinothems, the downdip transport of coarse-grained sediment occurs regardless of the clinoform rollover trajectory. The grain-size data show a greater overall proportion of coarse-grained sediment in Sequence m5.3 (rising trajectory) relative to Sequence m5.7 (falling trajectory). This is discussed in detail in Cosgrove et al. (2018) (see Chapter Three).

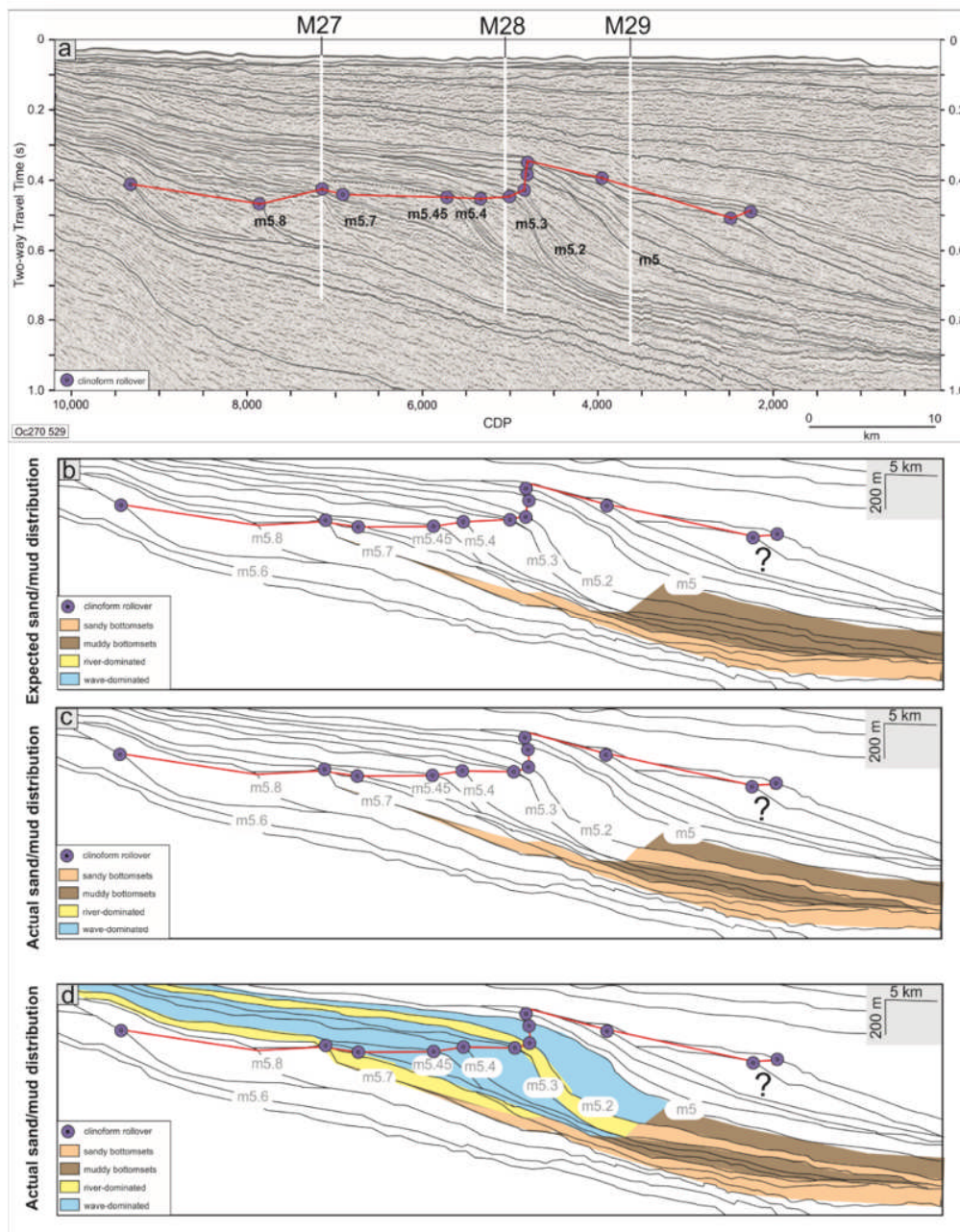


Figure 6.7: Relationship between clinoform rollover trajectory, process-regime and sand- and mud distribution. a) Seismic line Oc270 597; the clinoform rollover trajectory is illustrated. b) Expected distribution of sand and mud according to the established clinoform trajectory model. c) Actual distribution of sand and mud across successive clinothem sequences. d) Actual distribution of sand and mud across successive clinothem sequences and the associated topset (shelf) process-regime. Sequences m5.7 – m5.3 are highlighted, where a sequence is named according to its underlying reflector.

6.1.2.3 Clinoform Trajectory and Intraclinothem Variability

The dominant process-regime has been shown in the preceding discussion to be an important factor governing the distribution of sand and mud across multiple successive clinothem. The importance of the dominant process-regime in determining the distribution of sand and mud within an individual clinothem sequence is also apparent when Sequence m5.4 is considered

(see Chapter Four and Cosgrove et al., 2019). This clinotherm sequence has a rising clinof orm rollover trajectory (Fig. 6.7a) and was originally determined to have a wave-dominated shelf process-regime (Mountain et al., 2010; Cosgrove et al., 2018). However, new detailed sedimentological and grain character analysis suggests that the process-regime varies stratigraphically; Sequence m5.4 is shown to have a secondary river-influence (Cosgrove et al., 2019).

The stratigraphic process-regime variability in Sequence m5.4 results in the wave- and river-dominated portions of the clinotherm having different transport capacities; as such, the sand- and mud-distribution within bottomset deposits vary according to the updip shelf process-regime (Fig. 6.8). The wave-dominated sedimentary package within Sequence m5.4 contains > 45 % less sand in the bottomset deposits, relative to the river-dominated sedimentary packages; the average sand-to-mud ratios for the river- and wave-dominated packages within Sequence m5.4 are 82:18 and 37:63, respectively (Fig. 6.8, Chapter Four, Cosgrove et al., 2019). Thus, the sand-content varies stratigraphically within the bottomset deposits of Sequence m5.4 according to the updip shelf process-regime. As such, attempting to determine the coarse-grained sand content within an individual clinotherm sequence using clinof orm trajectory alone fails to account for the inherent stratigraphic variability associated with process-regime change.

6.1.2.4 Summary

The clinof orm trajectory paradigm, which remains widely used to predict the presence or absence of sand in the deep-water setting (e.g., Steel and Olsen, 2002; Johannessen and Steel, 2005; Helland-Hansen and Hampson, 2009), is challenged by the new dataset presented here (see Chapter Three and Cosgrove et al., 2018a). The occurrence of coarse-grained sediment in foreset and bottomset deposits, under both rising and falling clinof orm rollover trajectories, implies that a river-dominated process regime at the clinof orm rollover may be a more important factor in determining the delivery of coarse-grained sediment than clinof orm trajectory alone (e.g., Dixon et al., 2012a; Cosgrove et al., 2018a).

6.1.2.5 Grain Character and Process-Regime

Sedimentological analysis indicates that the New Jersey clinotherms have two clinotherms, m5.7 and m5.3, which are river-dominated. Clinotherms m5.45 and m5.4, in the New Jersey dataset are wave-dominated, with a secondary river-influence. Cycle LG-1 of the Sobrarbe Deltaic Complex, is river-dominated, with a secondary wave-influence. It is important to acknowledge, and this is discussed in detail in Section 6.1.3 (entitled Research Question Three), that designating a clinotherm sequence as river- or wave-dominated may overlook internal process-regime change within an individual clinotherm. However, the end-member

classification scheme is useful to understand the evolution and grain characteristics of clinothem sequences at basin-scale. The determination of the dominant process-regime, through detailed sedimentological analysis, for each of the analysed clinothem sequences allows comparisons of clinothem architecture and grain character attributes, under end-member process-regime conditions.

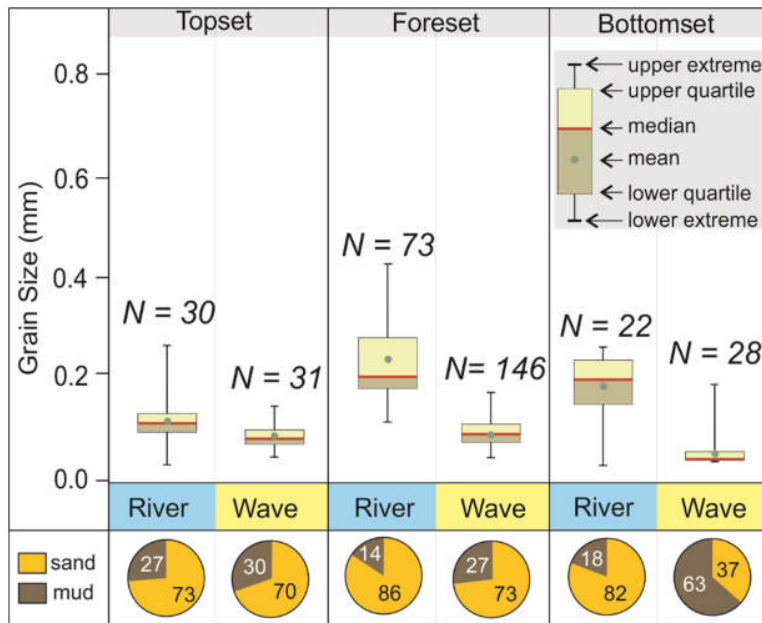


Figure 6.8: Box and whisker plots illustrating the difference in grain-size across topset (M27), foreset (M28) and bottomset (M29) deposits between the river- and wave-dominated portions of an individual clinothem sequence (Sequence m5.4). The sand-to-mud ratios across topset, foreset and bottomset deposits between the river- and wave-dominated portions of Sequence m5.4 are also illustrated.

The grain character attributes of clinothems deposited under river- and wave- dominated conditions vary. In general, deposits associated with a river-dominated shelf process-regime, relative to their wave-dominated counterparts, tend to be: i) coarser in mean grain-size across the complete depositional profile (Fig. 6.9); ii) more poorly sorted (Fig. 6.10); and ii) less rounded and spherical (Figs. 6.11, 6.12). The variable grain character attributes are reflective of the depositional environments of river- and wave-dominated clinothems, respectively (see Chapter Three, Chapter Five, Cosgrove et al. 2018 and Cosgrove et al., in review).

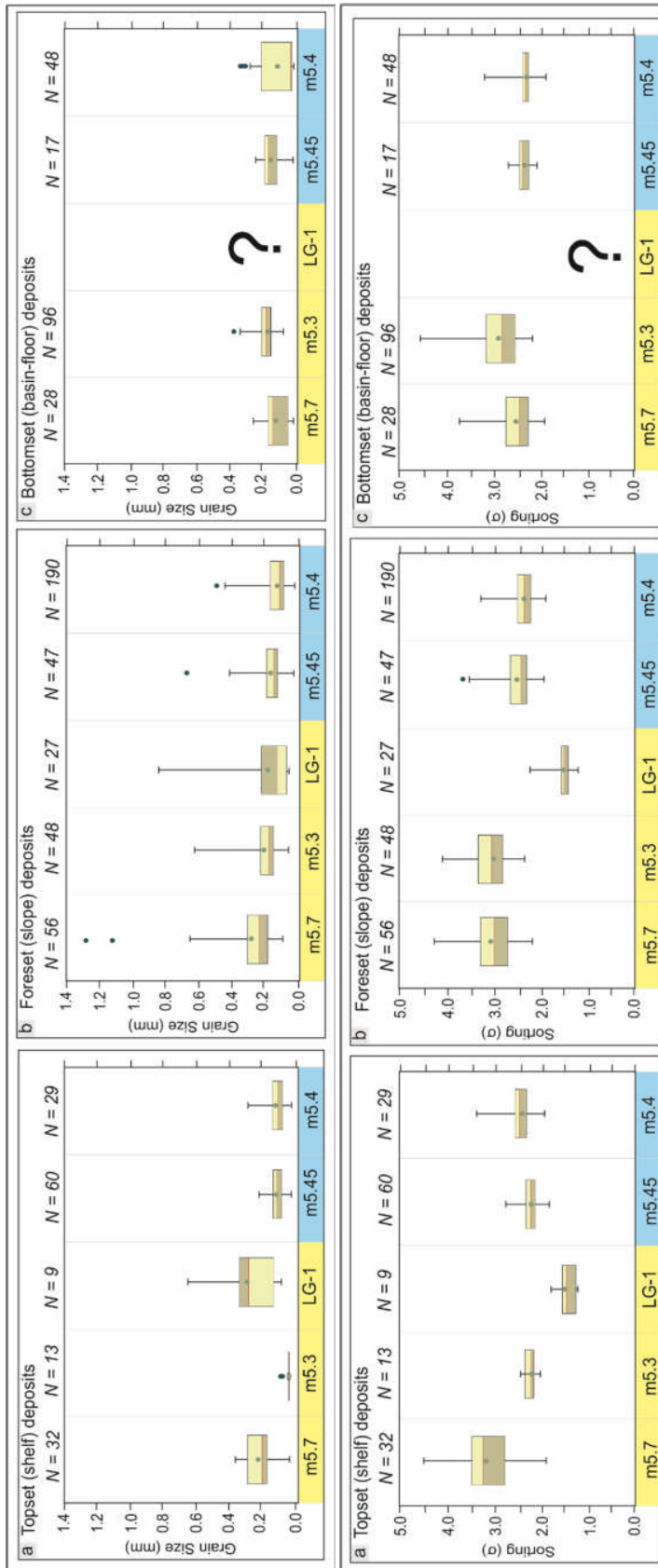


Figure 6.9: Box and whisker plots illustrating the grain size and sorting of topset (shelf), foreset (slope) and bottomset (basin-floor) deposits in river-dominated and wave-dominated clinothems. Sequences m5.7 and m5.3 and Cycle LG-1 are river-dominated and illustrated in yellow. Sequences m5.45 and m5.4 are wave-dominated and illustrated in blue. The number of samples used to construct the box and whisker plots is illustrated by $N = X$ and is shown in Part a. The legend describing the box and whisker plots is shown in Figure 6.8.

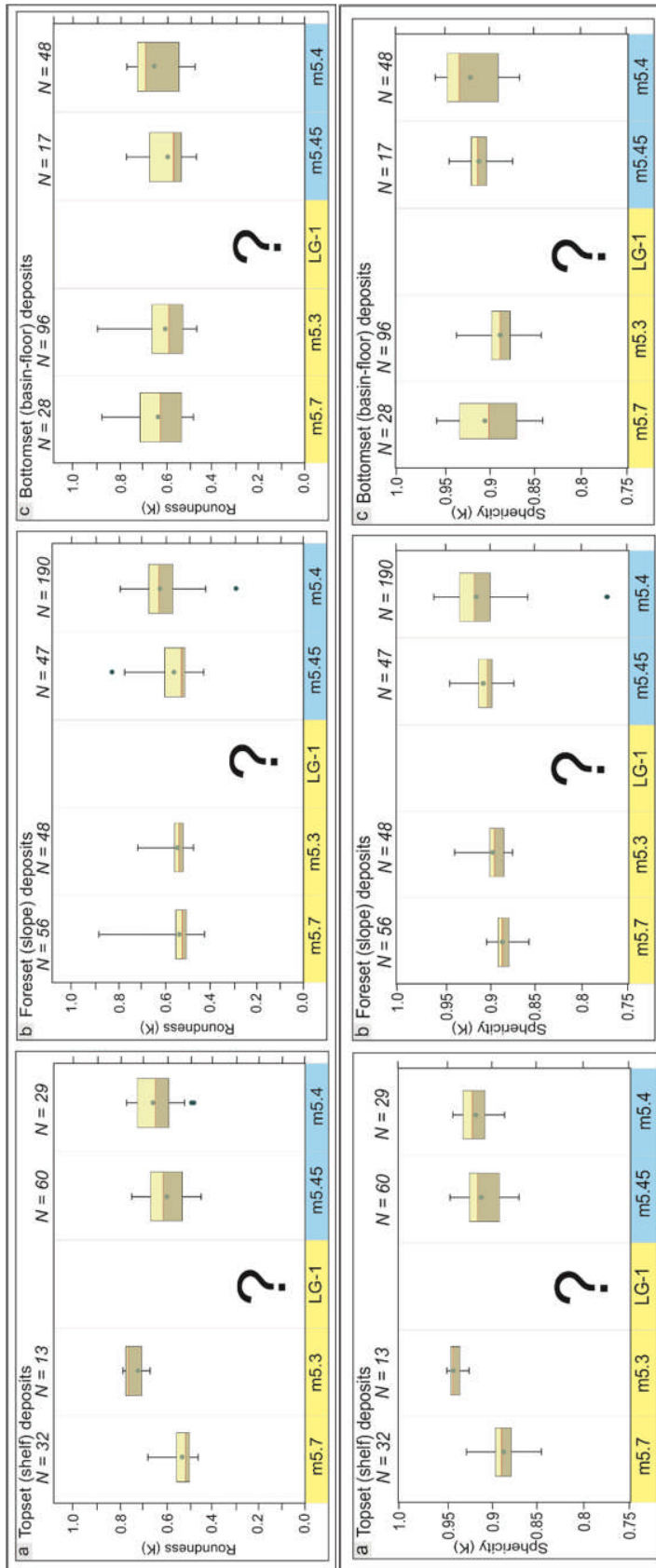


Figure 6.9: Box and whisker plots illustrating the grain sphericity and roundness of topset (shelf), foreset (slope) and bottomset (basin-floor) deposits in river-dominated and wave-dominated clinothems. Sequences m5.7 and m5.3 are river-dominated and illustrated in yellow. Sequences m5.45 and m5.4 are wave-dominated and illustrated in blue. The number of samples used to construct the box and whisker plots is illustrated by N = X and is shown in Part a. The legend describing the box and whisker plots is shown in Figure 6.8.

Wave-dominated clinothems are dominated by very fine- and fine-grained sands (Fig. 6.9), which are more rounded (Fig. 6.11) and spherical (Fig. 6.12) relative to river-dominated clinothems. This likely reflects wave-reworking and longshore-drift processes in the topsets of wave-dominated clinothems, which produce relatively clean shoreface sands (e.g., Roy et al., 1994; Bowman and Johnson, 2014). Grain rounding by additional wave resuspension processes produces a better-sorted deposit (Fig. 6.10). Despite the relative differences in the grain character attributes of the river- and wave-dominated deposits, the absolute differences in grain character are relatively small (Figs. 6.9 – 6.12). This is likely due to the strong secondary river-influence in the wave-dominated clinothems, and as such, Sequences m5.45 and m5.4 do not represent true end-member wave-dominated clinothem sequences. This is discussed in detail in Section 6.1.3 (entitled Research Question Three).

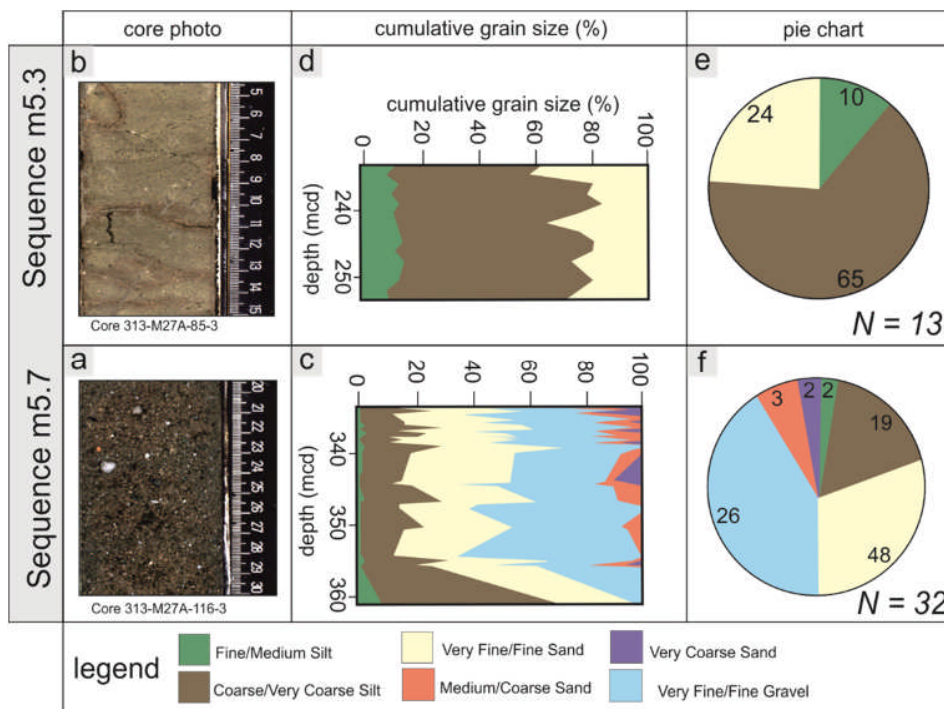


Figure 6.10: Heterogeneity within river-dominated topset deposits (Core M27) in Sequences m5.7 and m5.3. a) Gravelly glauconite- and quartz-rich sand. b) Organic-rich silt deposit. c) Sequence m5.7 up-core grain size composition. d) Sequence m5.3 up-core grain size composition. e) Pie-chart showing average grain size composition in Sequence m5.7. f) Pie-chart showing average grain size composition in Sequence m5.3.

In general, river-dominated deposits tend to show greater interquartile ranges across all grain character attributes, reflecting greater heterogeneity within river-dominated deposits (Figs. 6.9 – 6.12). This is highlighted by a comparison of the outcrop and core river-dominated clinothem sequences. Cycle LG-1 of the Sobrarbe Deltaic Complex is significantly coarser and better sorted, relative to Sequences m5.7 and m5.3 of the New Jersey clinothems (Figs. 6.9, 6.10). The large difference in grain size and sorting between Cycle LG-1 and Sequences m5.7

and m5.3 reflects a variety of parameters; these include: i) sediment provenance; ii) transport regime (e.g., hyperpycnal flows versus mass-transport of remobilised sediment at the clinoform rollover; ii) relative position within the source-to-sink system. Sequences m5.7 and m5.3 are fully subaqueous and are deposited in an intra-shelf setting; the Sobrarbe Deltaic Complex shows evidence of subaerial exposure, including paleosols in underlying clinothems, suggesting a more proximal location, relative to the New Jersey deposits.

The heterogeneity within river-dominated deposits is clearly reflected by the topset deposits (Core M27) of Sequence m5.7 and m5.3 (Fig. 6.13, 6.14). Sequence m5.7 has a silt-rich base (355 – 361 mcd), which progressively coarsens upwards, to contain ~20% very coarse sand and gravel by percentage volume (336 – 355 mcd; Fig. 6.13). By contrast, the topset deposits of Sequence m5.3 are dominated by silt-prone sediments and lack the coarse-grained sediment components observed in Sequence m5.7 (Fig. 6.13).

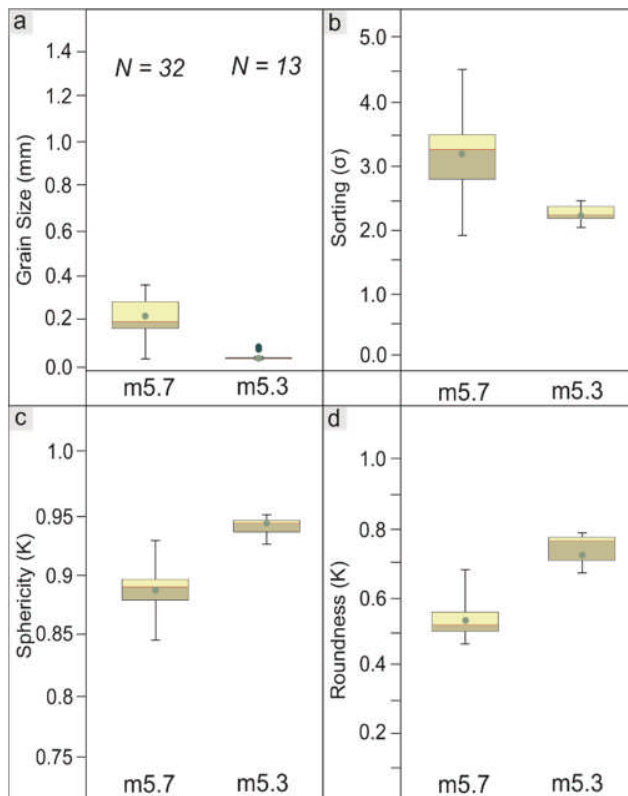


Figure 6.11: Box and whisker plots illustrating the difference in grain character attributes between the topset (Core M27) deposits of river-dominated Sequences m5.7 and m5.3. a) Grain size. b) Grain sorting. c) Grain sphericity. d) Grain roundness. The number of samples used to construct the box and whisker plots is illustrated by $N = X$ and is shown in Part a. The legend describing the box and whisker plots is shown in Figure 6.8.

The variable nature of the topset deposits of river-dominated clinothem sequences may reflect along-strike variability in depositional environments of river-dominated process regimes; examples of such lateral variability in shelf systems is documented in both modern and ancient delta systems (e.g., Ta et al., 2002; Gani and Bhattacharya, 2007; Carvajal and

Steel 2009; Olariu, 2014; Li et al., 2015). Alternatively, or in addition to this, the inter-sequence topset grain size variability (Fig. 6.14) may reflect erosive conditions landward of the clinoform rollover, such that the upper topset deposits of Sequence m5.3 may have been eroded during regression or transgression, removing the coarser sediment fractions and the erosion-generated accommodation infilled with finer-grained sediment.

6.1.2.6 Summary

The data presented here represents the beginning of grain character database (Figs. 6.9 – 6.12), which can help predict grain character attributes (including grain size, sorting and grain shape) under wave- and river-dominated conditions. However, the database presented here needs to be augmented by grain character data from variety of river- and wave-dominated clinothem.

6.1.2.7 Downdip Grain Character Variability

The quantification of grain character at different points along the depositional profile has been hitherto poorly constrained and largely unquantified in the context of a specific shelf process regime. This is, in part, due the paucity of datasets that sample genetically linked topset (shelf), foreset (slope) and bottomset (basin-floor) deposits. The offshore New Jersey and Sobrarbe Deltaic Complex study sites provide rare core and outcrop examples, respectively, in which components of downdip grain character variability can be captured (Chapters Three and Five, Cosgrove et al., 2018, Cosgrove et al., in review). The New Jersey core-dataset samples the topset, foreset and bottomset deposits of four successive clinothem sequences (Sequences m5.7, m5.45, m5.4 and m5.3), thus sampling the complete depositional profile at three discrete points. The Sobrarbe Deltaic Complex (Cycle LG-1) outcrop-dataset samples the topset (shelf) to foreset (slope) transect at ~ 1 km intervals along the depositional profile of a single clinothem sequence providing a valuable archive of grain character change across the shelf to slope transition; the genetically linked bottomset deposits are not exposed at this location.

River-dominated conditions in Sequences m5.7 and m5.3 are associated with the following attributes: 1) development of heterogeneous topset deposits (variable grain-size distributions, sorting values and grain shapes), reflecting erosive conditions landward of the clinoform rollover; 2) delivery of coarse-grained sediment into foreset and bottomset deposits, via both turbidity currents and debris flows, potentially triggered by river flooding remobilization or storm remobilization of glauconite-rich sands at the clinoform rollover; 3) deposition of the coarsest, least spherical and most angular grains in foreset deposits, resulting from the rapid dissipation of energy, associated with multiple feeder channels and

no major incision of the clinoform rollover (Fig. 6.15). Coarse-grained sediment is delivered in the largest volumes into downdip settings via river-dominated topset deposits. River-dominated conditions in Cycle LG-1 are associated with the following attribute: 1) basinward coarsening beyond the clinoform rollover; 2) transport of coarse-grained sediment into the lower slope setting, under hyperpycnal flow regimes triggered by river flooding events; 3) development of slightly poorer sorting basinward (Fig. 6.16).

Wave-dominated conditions in Sequences m5.45 and m5.4 are associated with the following attributes: 1) development of longitudinal sediment profiles which marked by the predominance of rounded, highly spherical very fine- and fine-grained sands, associated with wave reworking landward of the clinoform rollover; 2) a minimal occurrence of coarse-grained sediment throughout the depositional profile, possibly associated with shore-parallel redistribution of coarse-grained sediment; 3) limited downdip variation in grain-size distribution, associated with wave-resuspension - controlled grain-size sorting (Fig. 6.17).

The New Jersey river- and wave-dominated clinothem sequences can also be differentiated based on their average grain-size distributions, which are dominantly bimodal and trimodal in river- vs. wave-dominated clinothems, respectively (Figs. 6.15, 6.17).

6.1.2.8 Summary

The high-resolution grain character analysis, integrated with sedimentological analysis, has allowed the identification and detailed characterisation of river- and wave-dominated longitudinal sedimentary profiles of clinothems for the first time. The results presented and discussed in this thesis demonstrate that the physical processes in action on the shelf, i.e., the interaction between fluvial and wave processes, exert a fundamental control on grain character (including grain size, grain shape, and sorting) across the complete depositional profile from topset (shelf) to foreset (slope) to bottomset (basin floor).

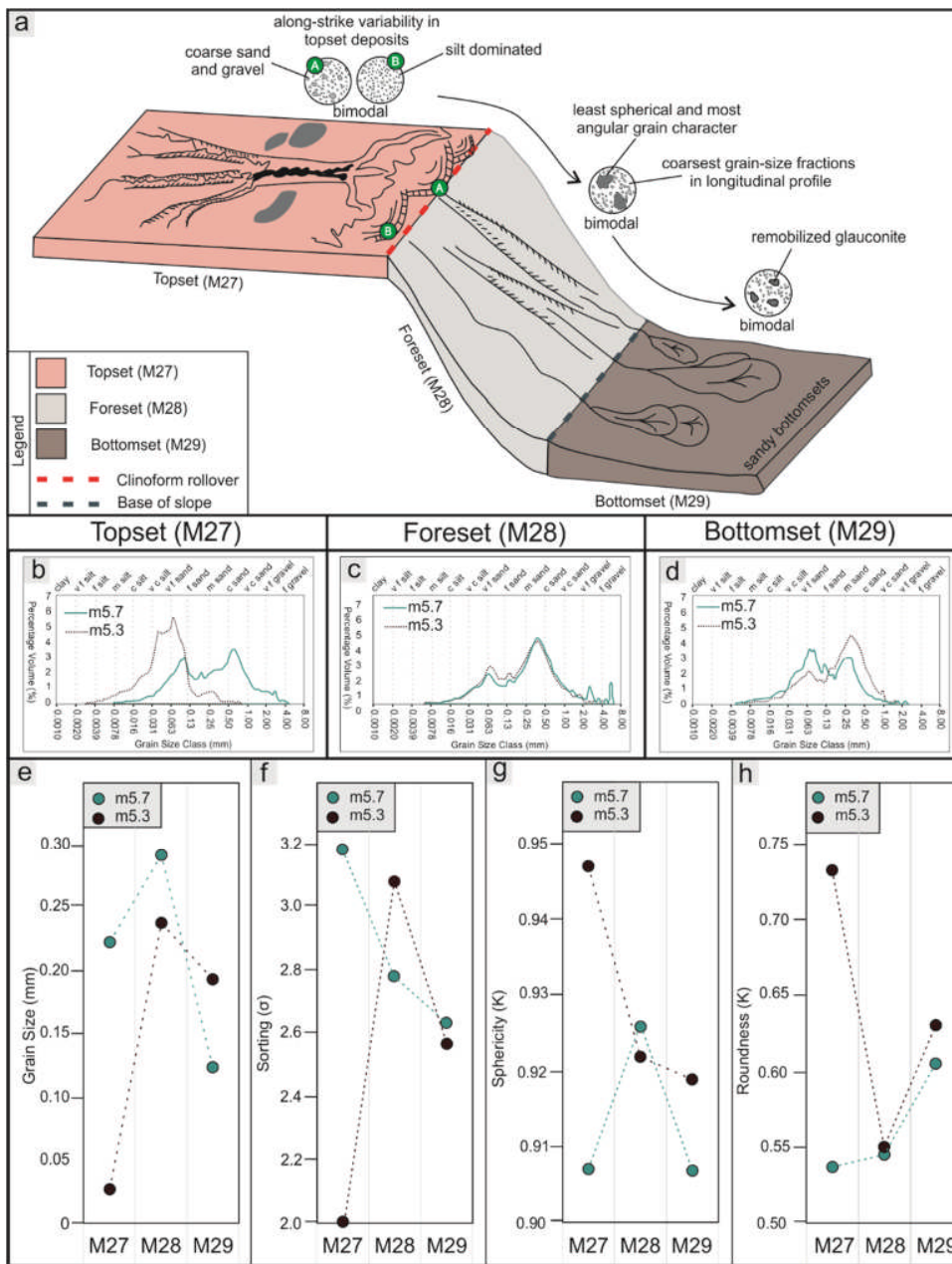


Figure 6.12: a) Summary diagram illustrating the sedimentological, architectural and grain character attributes of river-dominated Sequences m5.7 and m5.3. b) Average grain-size distribution of topset deposits of Sequences m5.7 and m5.3. c) Average grain-size distribution of foreset deposits of Sequences m5.7 and m5.3. Average grain-size distribution of bottomset deposits of Sequences m5.7 and m5.3. e) Mean grain size of Sequences m5.7 and m5.3. f) Mean sorting of Sequences m5.7 and m5.3. g) Mean sphericity of Sequences m5.7 and m5.3. h) Mean roundness of Sequences m5.7 and m5.3.

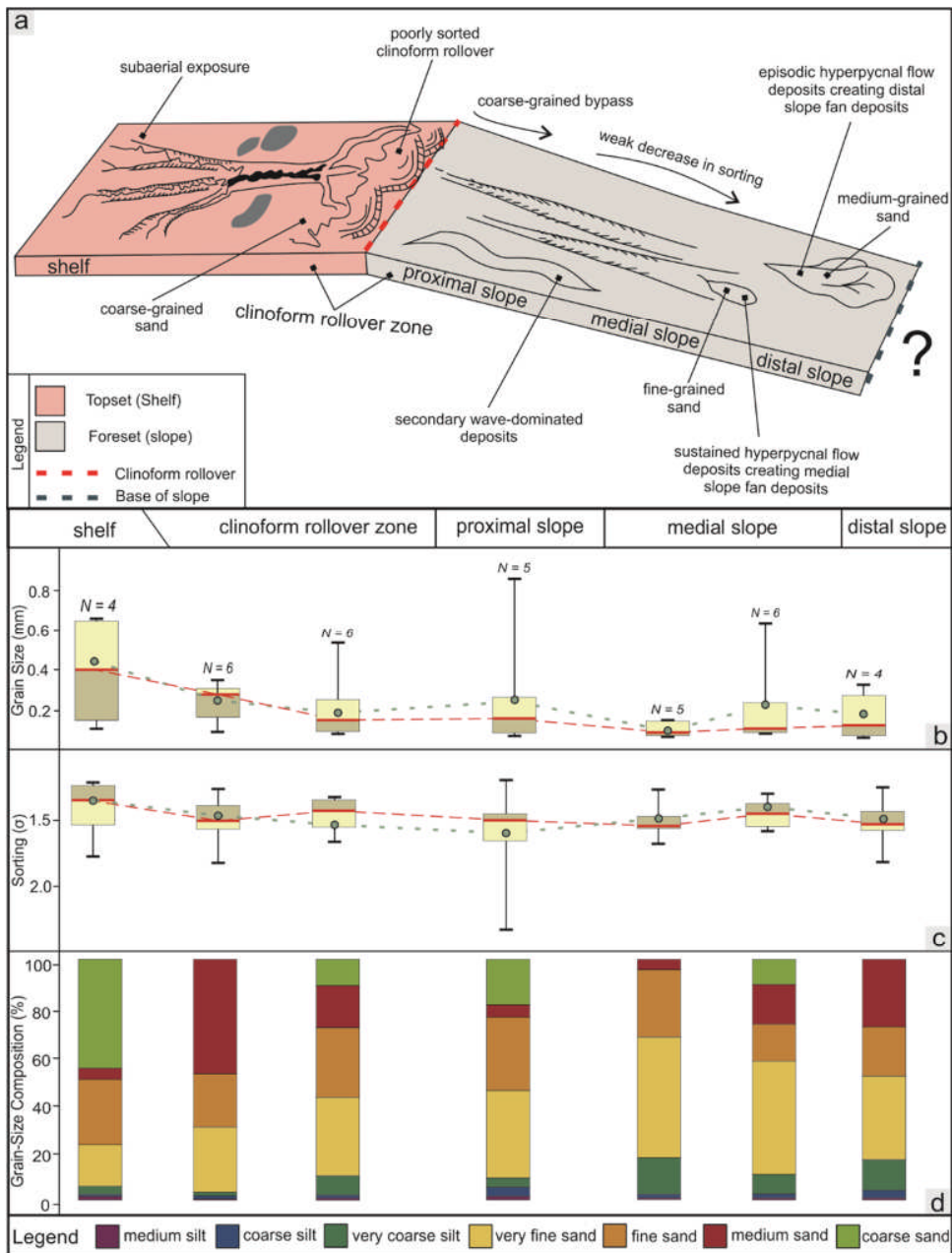


Figure 6.13: a) Summary diagram illustrating the sedimentological, architectural and grain character attributes of river-dominated Cycle LG-1. b) Box and whisker plots illustrating grain size composition across shelf and slope deposits. c) Box and whisker plots illustrating sorting across shelf and slope deposits. The number of samples used to construct the box and whisker plots is illustrated by $N = X$ and is shown in Part b. The legend describing the box and whisker plots is shown in Figure 6.8. d) Cumulative grain size composition across shelf and slope deposits.

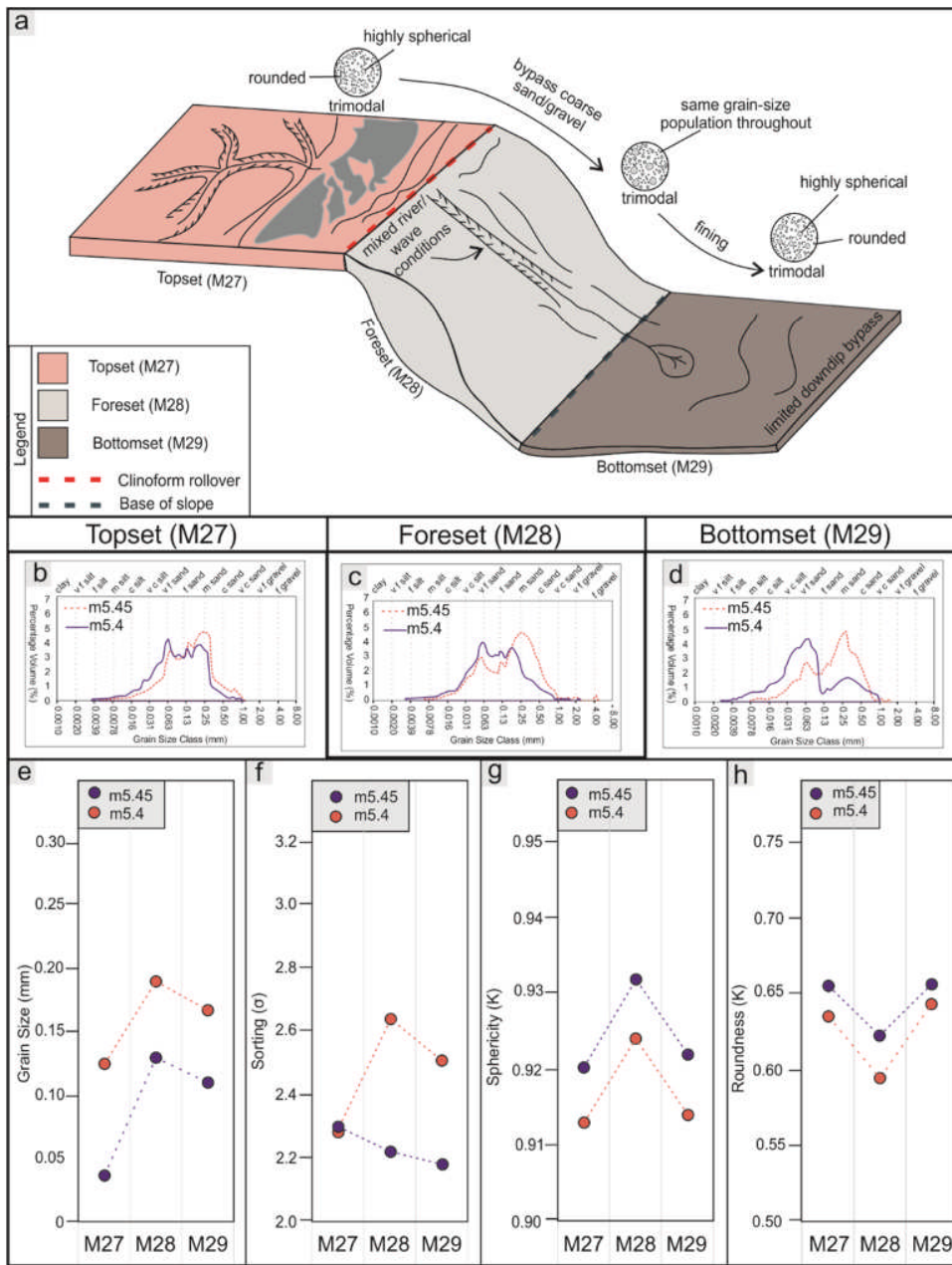


Figure 6.14: a) Summary diagram illustrating the sedimentological, architectural and grain character attributes of wave-dominated Sequences m5.45 and m5.4. b) Average grain-size distribution of topset deposits of Sequences m5.45 and m5.4. c) Average grain-size distribution of foreset deposits of Sequences m5.45 and m5.4. Average grain-size distribution of bottomset deposits of Sequences m5.45 and m5.4. e) Mean grain size of Sequences m5.45 and m5.4. f) Mean sorting of Sequences m5.45 and m5.4. g) Mean sphericity of Sequences m5.45 and m5.4. h) Mean roundness of Sequences m5.45 and m5.4.

6.1.3 Research Question Three

How can grain-character be used to improve understanding of clinothem evolution?

6.1.3.1 Introduction

The data and interpretations presented in this thesis have been used to: i) re-categorise Sequence m5.4 (offshore New Jersey, Chapter Four, Cosgrove et al., 2019) and Cycle LG-1

(Sobrarbe Deltaic Complex, Chapter Five, Cosgrove et al., in review) as mixed-energy clinothems; ii) document changes in intraclinotem grain character, and tie them to changes in the dominant topset (shelf) process-regime and flow style; and iii) correlate intraclinotem sedimentary packages across the complete depositional profile using grain character. The results have helped advance our understanding of the evolution of individual clinotem sequences at a resolution greater than that which is achieved through typical seismic- or outcrop-based investigations.

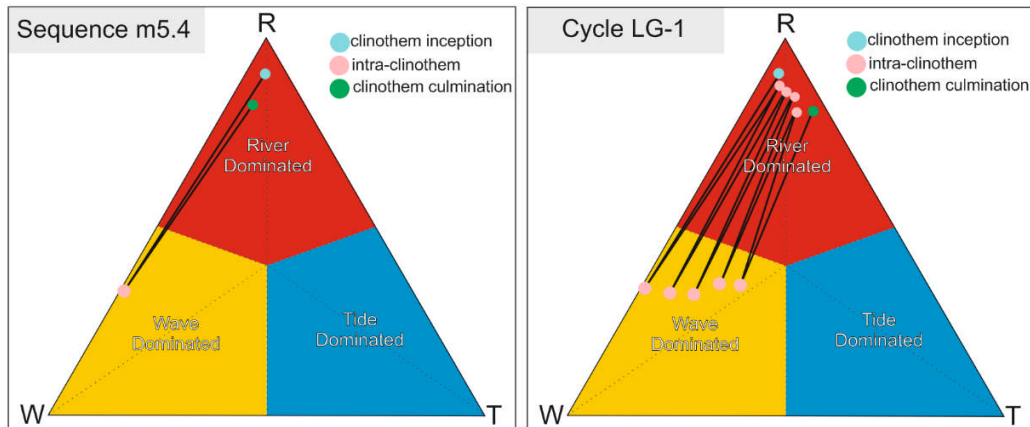


Figure 6.15: Tripartite classification scheme of Galloway (1975). The black lines illustrate the stratigraphic evolution of the dominant process-regime within Sequence m5.4 and Cycle LG-1.

6.1.3.2 Mixed Process-Regime Conditions

Mixed-energy systems, in which more than one process-regime is dominant in a single clinotem sequence, are being increasingly recognised in both the modern and ancient record (e.g., Ainsworth et al., 2008; 2011; Olariu, 2014; Gomis-Cartesio et al., 2017). Modern and ancient shallow-marine systems can exhibit high levels of process-regime variability, both laterally and stratigraphically, related to the relative importance of fluvial, wave, and tidal processes (Ta et al., 2002; Bhattacharya and Giosan, 2003; Ainsworth et al., 2008; 2011; Vakarelov and Ainsworth, 2013; Olariu, 2014; Jones et al. 2015).

Sequence m5.4 (offshore New Jersey) and Cycle LG-1 (Sobrarbe Deltaic Complex) have previously been classified according to the scheme of Galloway (1975), and determined to be wave- (Mountain et al., 2010; Cosgrove et al., 2018) and river-dominated (Dreyer et al., 1999) respectively. However, the detailed stratigraphic sedimentological characterisation of topset (shelf) deposits from both of these clinotem sequences provides strong evidence of stratigraphic and, by inference, temporal variability in the dominant process-regime. In both clinotem systems, abrupt stratigraphic transitions from river- to wave-dominated facies (and vice versa) are observed (Fig. 6.18).

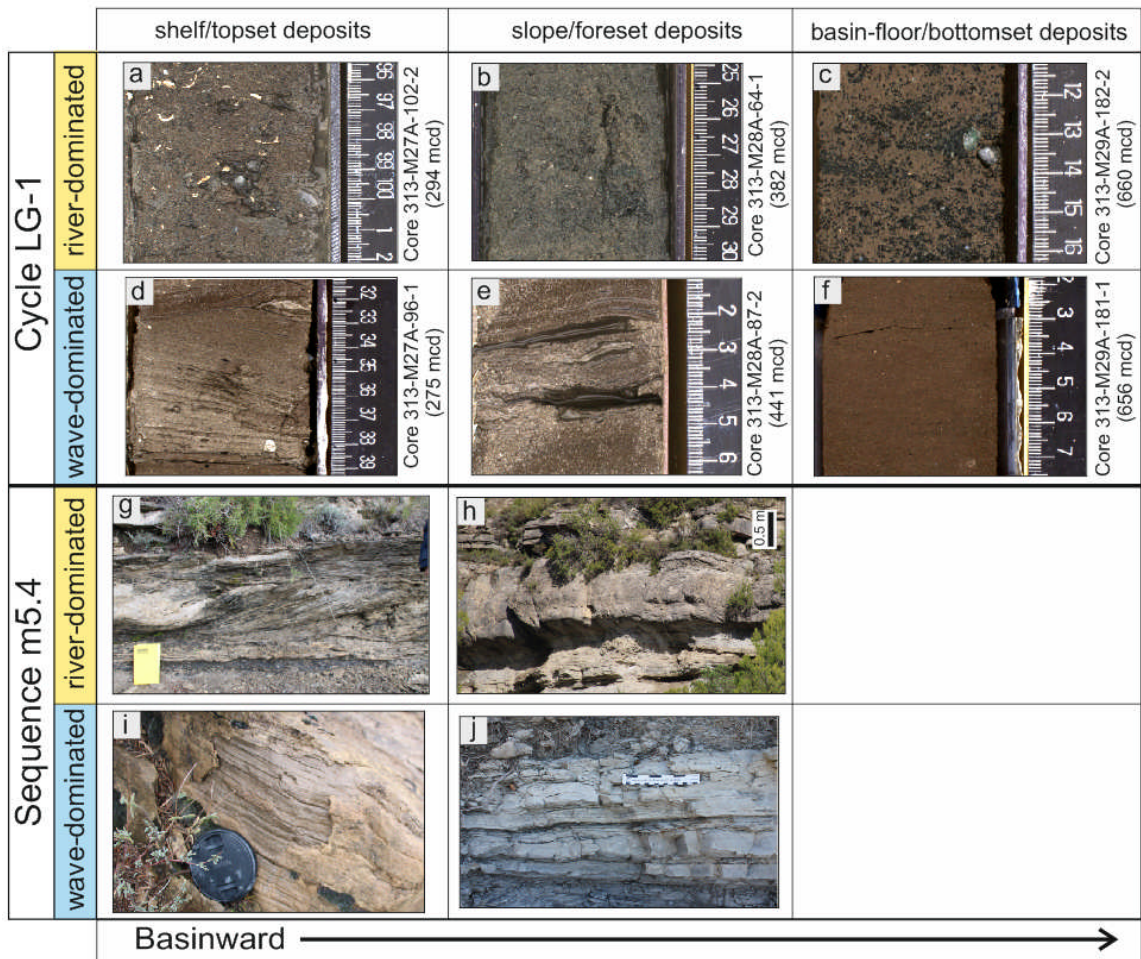


Figure 6.16: Core (a-f) and outcrop (g-j) facies photos, showing river- and wave-dominated facies within Sequence m5.4 and Cycle LG-1. a) glauconite sand containing shell debris; b) structureless glauconite sand; c) very fine-grained sand containing ~ 4 mm glauconite and quartz grains; d) hummocky cross-stratification; e) swaley cross-stratification; f) structureless fine-grained silt; g) trough cross-strata and asymmetric ripple lamination; h) fine-grained coarsening-upwards sandstone beds bodies (~0.3 – 0.75 m thickness); i) parallel laminated very-fine sandstone ; j) tabular beds of very fine-grained 'clean' sandstone beds (~ 0.5 – 1.5 m thickness).

The observations of abrupt stratigraphic facies change (based on analysis of sedimentary texture and structure), and associated changes in the dominant shelf process-regime, had been hitherto undocumented in both examples. In both clinothems, fluvial- and wave-processes may dominate the shelf (topset) environment, at a given location in time and space; as the process-dominance varies during clinothem evolution (Fig. 6.18), the end-member delta classification scheme of Galloway (1975) does not adequately describe either Sequence m5.4 or Cycle LG-1. It follows that the use of the tripartite classification scheme cannot enable prediction of the architectural complexities observed at an intraclinothem scale within Sequence m5.4 or Cycle LG-1. Outcrop and core photos demonstrating river- and wave-dominated facies within individual clinothem sequences are shown in Figure 6.19.

6.1.3.3 *Process-Regime and Grain Character*

In Sequence m5.4 and Cycle LG-1, process-regime change in the topset environment fundamentally impacts the grain character of the resulting deposits. This tangible effect on grain character is observed not only in the topset deposits, but can be traced across the depositional profile. The effect of the dominant process-regime in the shelf setting is thus one of the fundamental controlling factors determining the downdip distribution of sediment of different calibre and maturity within individual clinothem sequences.

Differences in grain size and sorting, for the river- and wave-dominated portions of Sequence m5.4 and Cycle LG-1, respectively are shown in Figure 6.20. From the box and whisker plots, it is clear that the grain-size and sorting can be statistically differentiated for the river- and wave-dominated portions of either Sequence m5.4 or Cycle LG-1. In general, across the depositional profile the river-dominated portions of clinothems Sequence m5.4 and Cycle LG-1 have coarser mean grain sizes and are more poorly sorted relative to the wave-dominated portions of the clinothem (Fig. 6.20; Chapters Four, Five). Additionally, the river-dominated portions tend to display a greater spread of grain-size and sorting values, indicating higher levels of heterogeneity relative to wave-dominated deposits (Fig. 6.20).

As demonstrated by box and whisker plots, shown in Figure 6.20 (Chapters Four, Five, Cosgrove et al., 2019, Cosgrove et al., in review), the topset process-regime can introduce significant stratigraphic and downdip heterogeneity in grain character at an intraclinothem scale. As different process-regimes can be in operation at the shelf-edge under any clinof orm trajectory (i.e. rising, falling, standstill), the results of these two studies highlights the need for caution when attempting to predict the distribution of coarse-grained sand deposits in the deep-water setting using conventional sequence stratigraphic or clinof orm trajectory models alone; a prerequisite for effective prediction of grain character across the depositional profile is an understanding of the shelf process-regime, and its evolution through stratigraphy.

6.1.3.4 *Sequence m5.4*

In Sequence m5.4, process-regime change in the topset (shelf) environment is associated with a coeval change in grain-size distribution (Fig. 6.21). In Sequence m5.4, topsets deposited under river-dominated conditions are dominantly bimodal; topsets deposited under wave-dominated conditions are dominantly unimodal (Fig. 6.21). The average grain-size distribution can be used to define sedimentary packages, alongside changes in facies. In addition to impacting the grain-size distribution, changes in the topset process-regime affect grain shape (sphericity (Fig. 6.22) and roundness (Fig. 6.23)) and sand-to-mud ratios (Chapter Four, Cosgrove et al., 2019). River-dominated sedimentary packages have higher

sand-to-mud ratios and coarser mean grain-sizes; however, the grain character of river-dominated sedimentary packages is texturally less-mature than that of wave-dominated deposits (Figs. 6.21-6.23). Differences in grain character between packages dominated by different process-regimes become greater in a basinwards direction. In the context of reservoir heterogeneities, this is most prominently expressed by the sand-to-mud ratios; river-dominated packages are > 45 % richer in sand, relative to the wave-dominated package.

6.1.3.5 Geometric Distribution of Facies in Cycle LG-1

In Cycle LG-1, process-regime change affects the downdip geometric distribution of sedimentary packages; in this case, sedimentary packages associated with a river-dominated process-regime, show distribution across the complete sampled profile, from the shelf (topset) to the distal slope (foreset) (Fig. 6.24; Chapter Five, Cosgrove et al., in review). In contrast, sand-dominated sedimentary packages associated with a wave-dominated process-regime, are deposited only in the proximal and medial slope environments. The termination, and downlap, of the wave-dominated sand-dominated facies on the medial slope results in suspension fallout of silt in the lower slope setting; such that only silt-grade sediment fractions are transported into the distal slope setting under a wave-dominated process-regime. As such, distal slope deposits vary stratigraphically; sand-rich packages (associated with a river-dominated shelf) are interbedded with > 10 m silt-rich deposits (associated with a wave-dominated shelf process-regime) (Fig. 6.24; Chapter Five, Cosgrove et al., in review). Shelf process-regime thus directly influences the architecture and coarse-grained sand-content of downdip deposits.

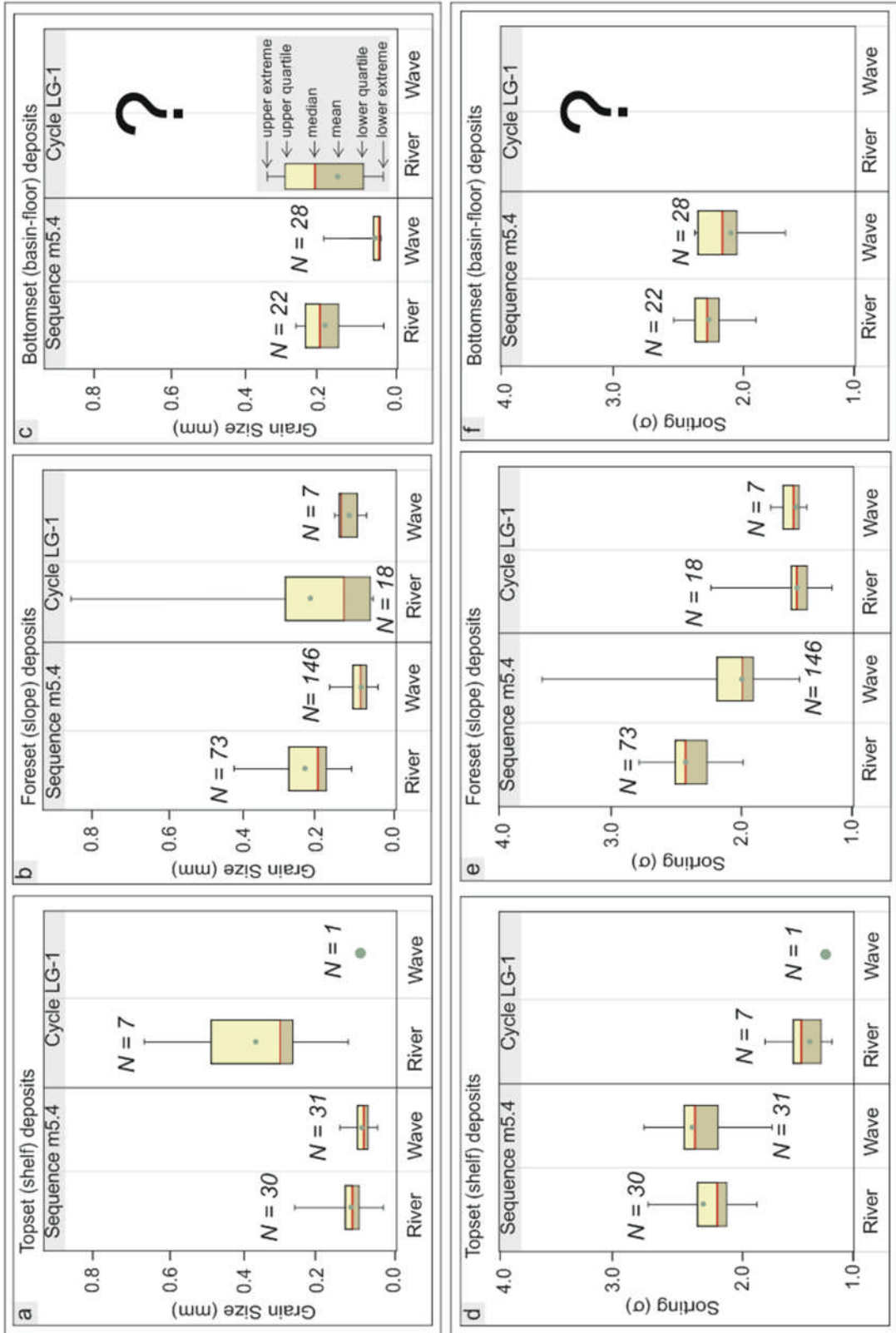


Figure 6.17: box and whisker plots illustrating grain size (a-c) and sorting (d-f) in the topset (shelf), foreset (slope) and bottomset (basin-floor) deposits of Sequence m5.4 and Cycle LG-1, comparing the river- and wave-dominated portions of each clinothem, respectively. The legend for the box and whisker plots is illustrated in part c. The sample numbers for the box and whisker plots are illustrated by N = X.

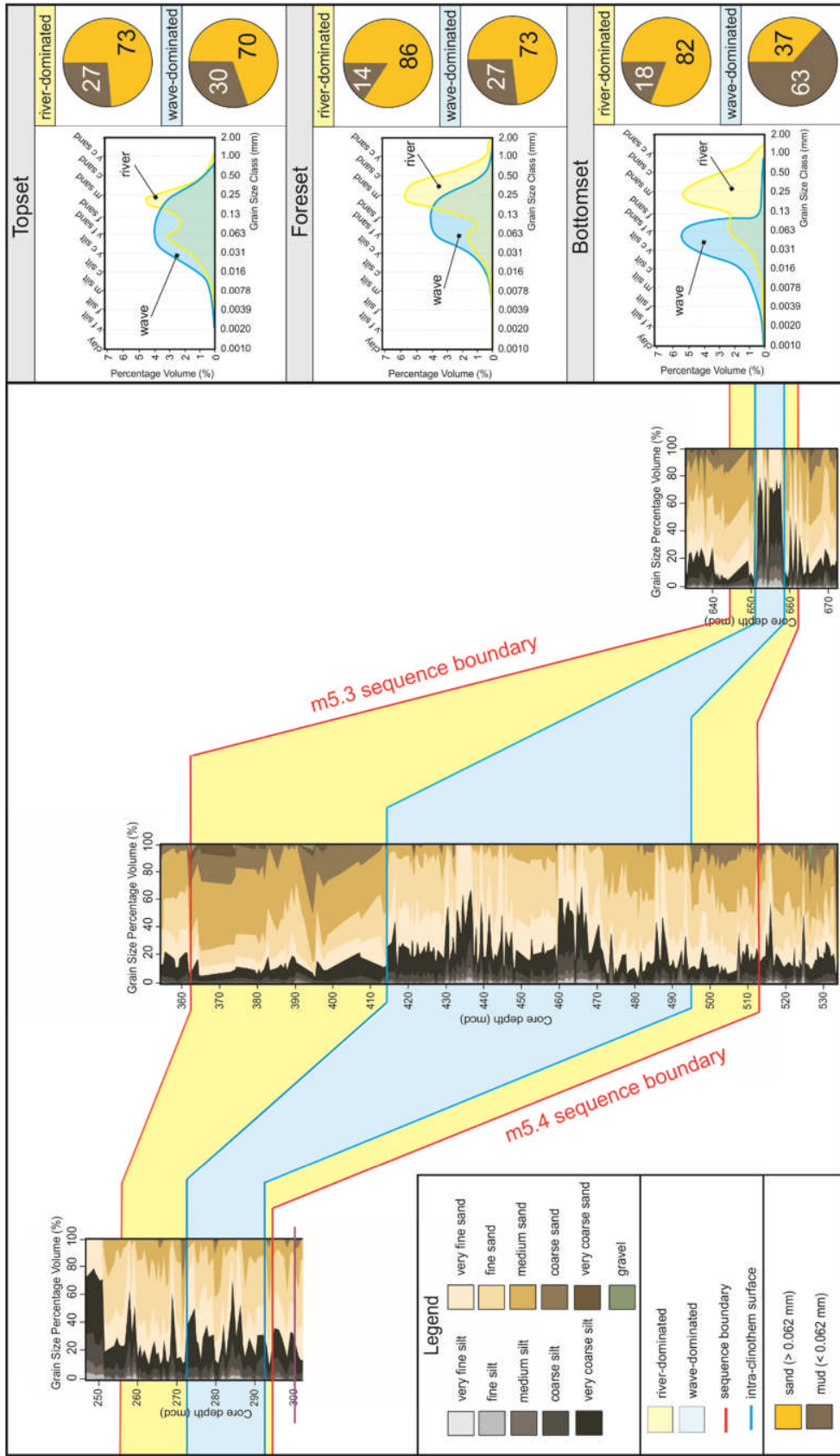


Figure 6.18: Summary diagram illustrating the differences in grain-size composition between river- and wave-dominated deposits within a single clinothem (Sequence m5.4). Grain-size distributions and sand-to-mud ratios are also shown for the river- and wave-dominated packages, with topset, fore- and bottomset locations. Note the bimodal (river-dominated) and unimodal (wave-dominated) grain-size distributions and relatively mud-rich fore- and bottomset deposits of the wave-dominated package, relative to the river-dominated packages.

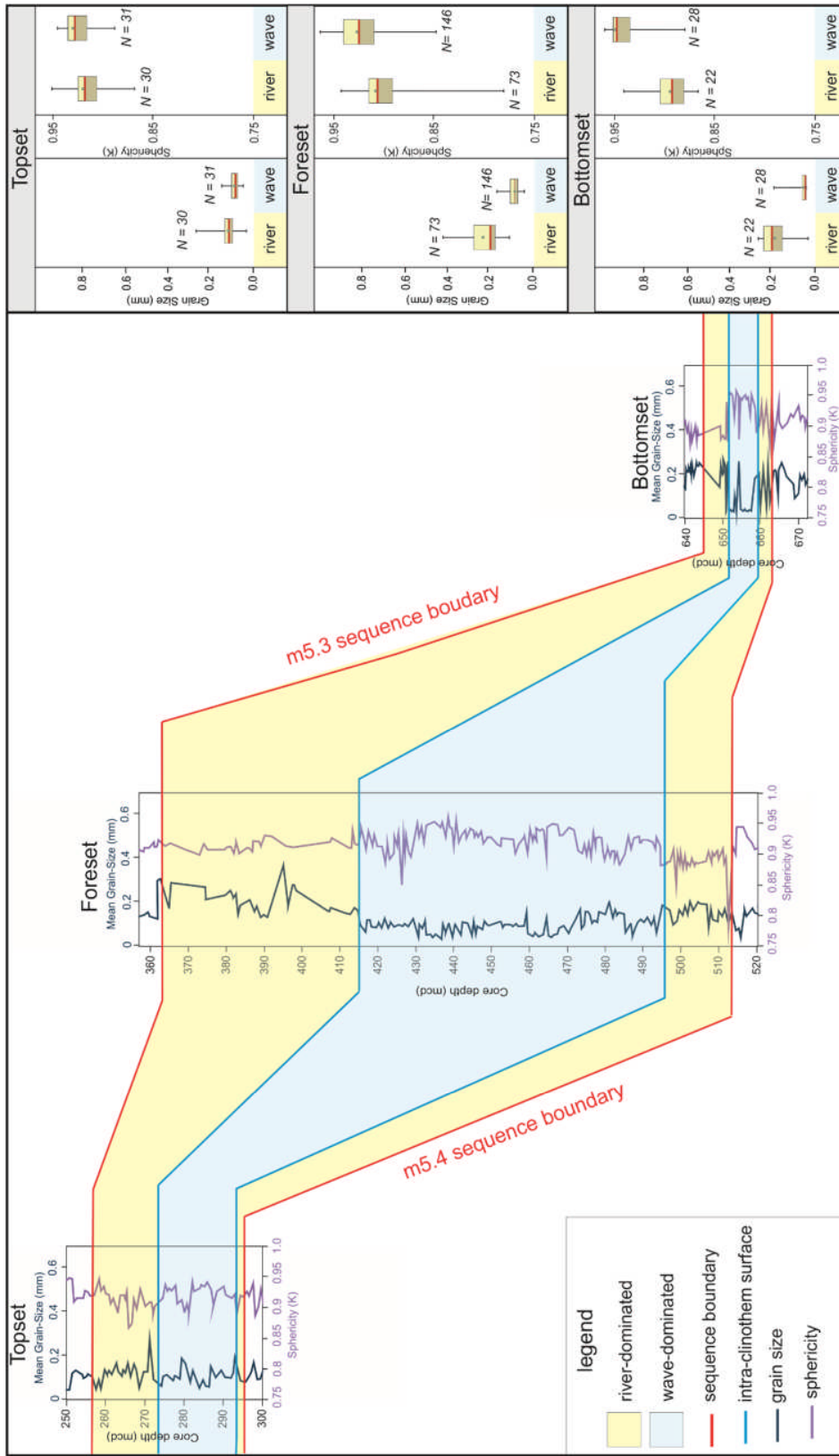


Figure 6.19: Summary diagram illustrating the differences in mean grain-size and sphericity between river- and wave-dominated deposits, within a single clinothem (Sequence m5.4). Box and whisker plots are also shown for the river- and wave-dominated packages, with topset, foreset and bottomset locations. Note the lower grain size and higher sphericity of the wave-dominated package, relative to the river-dominated packages. The legend for the box and whisker plots is illustrated in Figure 6.8. The sample numbers for the box and whisker plots are illustrated by N = X.

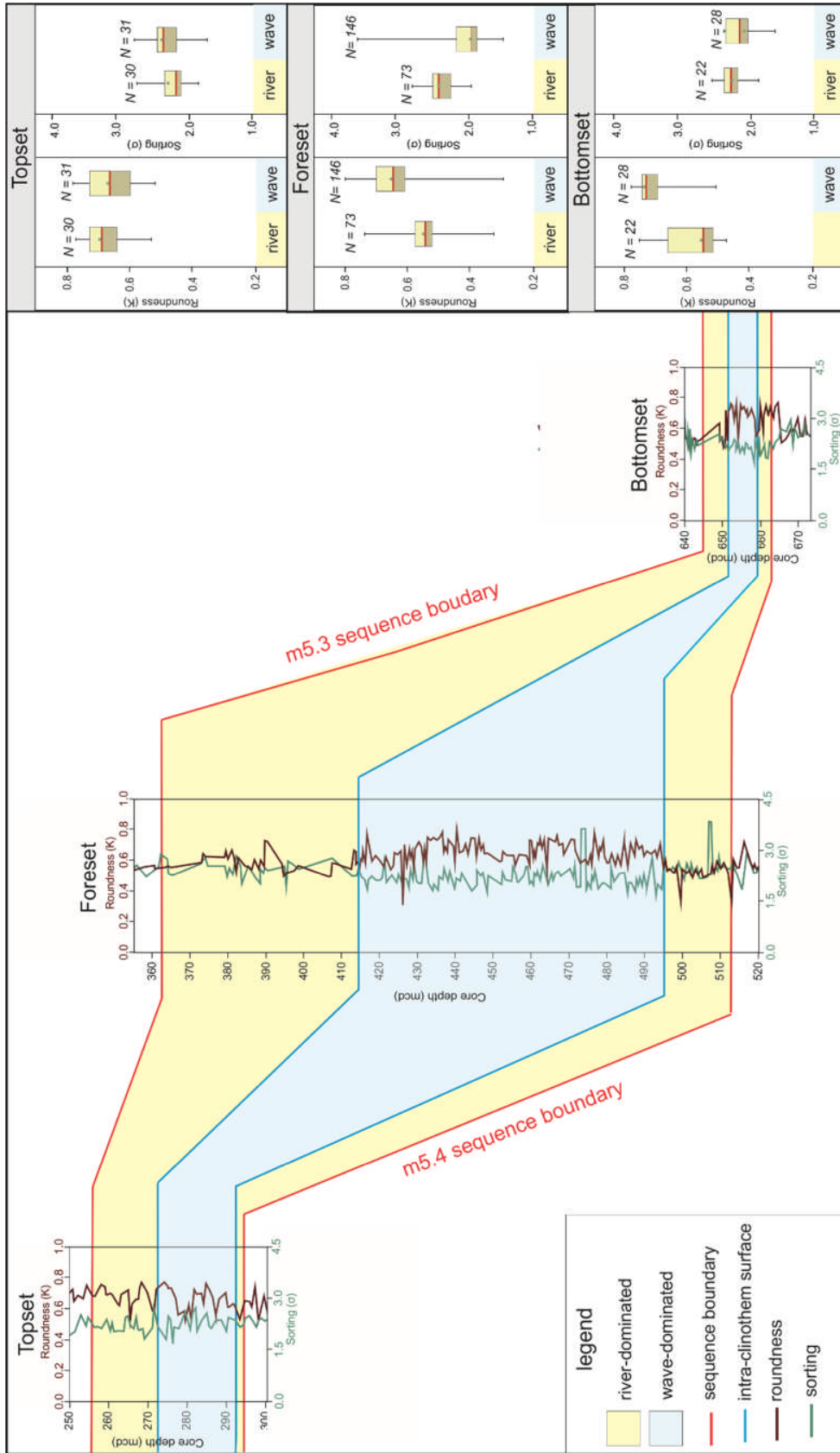


Figure 6.20: Summary diagram illustrating the differences in mean roundness and sorting between river- and wave-dominated deposits, within a single clinothem (Sequence m5.4). Box and whisker plots are also shown for the river- and wave-dominated packages, with topset, foreset and bottomset locations. Note the higher roundness and better sorting of the wave-dominated package, relative to the river-dominated packages. The legend for the box and whisker plots is illustrated in Figure 6.8. The sample numbers for the box and whisker plots are illustrated by N = X.

6.1.3.6 Bypass and Flow Regime in Cycle LG-1

The river-dominated clinothems from both offshore New Jersey (Sequences m5.7 and m5.3) and the Sobrarbe Deltaic Complex (Cycle LG-1), show evidence of sediment transport via hyperpycnal flows (Chapter Five, Cosgrove et al., in review). The presence of hyperpycnal flows is evidenced in both datasets by: i) repeated transitions between inverse and normal grading at bed-scale, suggesting accelerating (waxing) and decelerating (waning) flow regimes (cf. Kneller, 1995) and ii) high concentrations of plant debris and mica, suggesting a relatively direct linkage between the fluvial and marine depositional environment (e.g., Normark and Piper, 1991; Mulder and Syvitski, 1995; Mulder et al., 2003; Plink-Björklund and Steel, 2004; Lamb et al., 2008; Zavala and Arcuri, 2016).

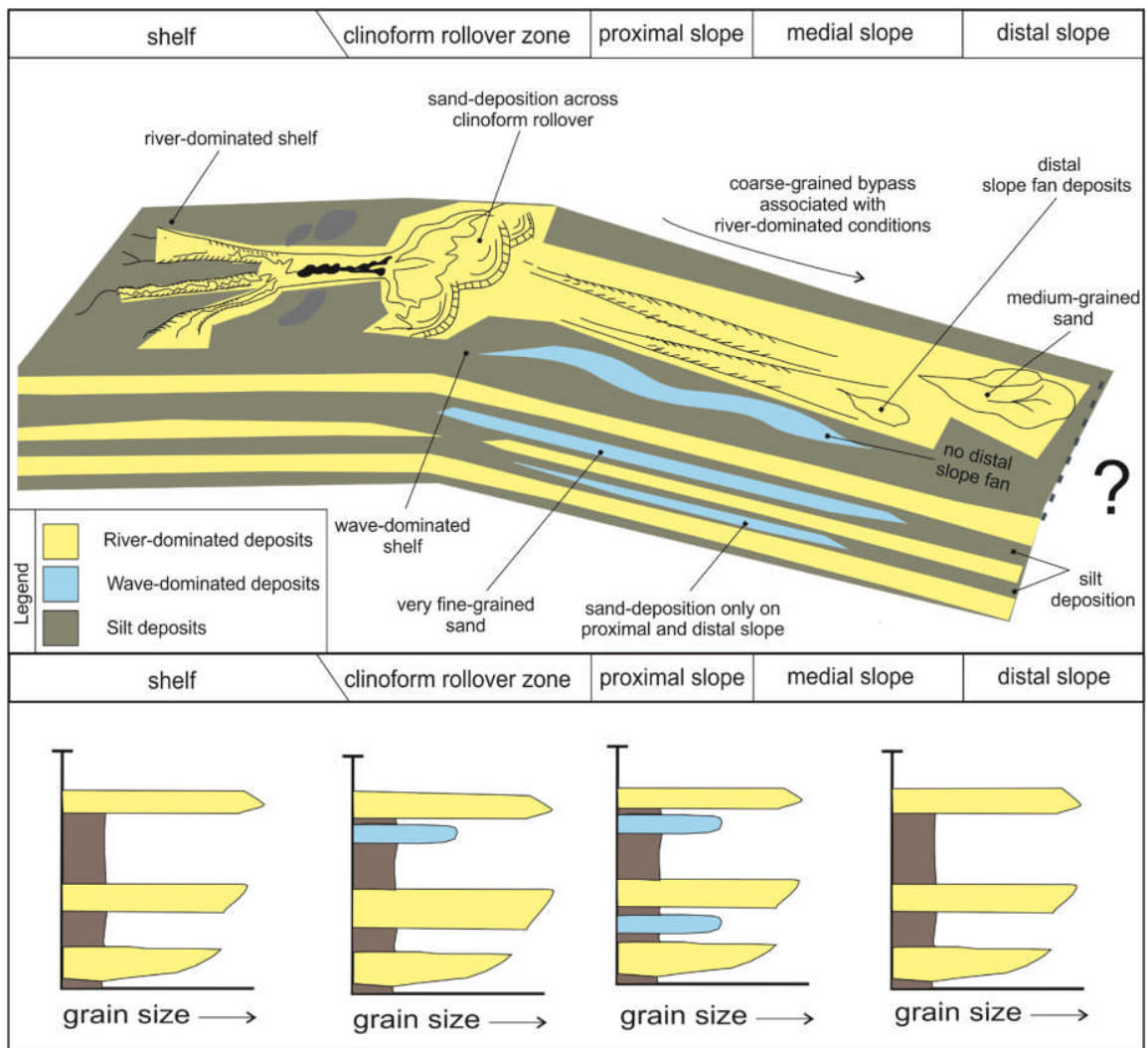


Figure 6.21: Summary diagram showing the geometric, downdip and stratigraphic distribution of river- and wave-dominated facies with Cycle LG-1. River-dominated facies distribute medium- and coarse-grained sand from the shelf to the distal slope environment. Wave-dominated facies distribute very fine-grained sand only on the proximal and medial slope, and are associated with silt deposition in the distal slope environment. Schematic logs are also shown, illustrating the stratigraphic distribution of facies, and corresponding grain-sizes, at different positions along the depositional profile.

In both the core and outcrop examples, hyperpycnites are associated with the transport of the coarsest grain-size fractions into the deeper-water setting; in both cases hyperpycnal deposits are associated with a river-dominated topset (shelf) process-regime (Chapters Three, Five, Cosgrove et al., 2018, Cosgrove et al., in review). In the case of the New Jersey clinothems, the direct bed-scale correlation of updip hyperpycnal flow deposits with genetically linked deposits downdip is not possible with any degree of certainty, as packages of beds cannot be directly traced across the depositional profile. However, the continuous downdip exposure of Cycle LG-1 within the Sobrarbe Deltaic Complex, permits hyperpycnal flow deposits to be directly correlated from topset (shelf) deposits to the foreset (lower slope) deposits (Chapter Five, Cosgrove et al., in review).

In Cycle LG-1, hyperpycnal flow deposits are subdivided into two families, based on geometric facies distribution, and organic matter- and mica-content. Type A hyperpycnal flows show deposition across the complete shelf-to-slope transect and have relatively lower mica- and organic matter-contents. Type B hyperpycnal flows deposit sand only on the cliniform rollover and slope settings and have relatively higher mica- and organic matter-content. As is shown in Figure 6.25, the bypass of coarse-grained sediment varies according to the hyperpycnal flow-style (Chapter Five).

Type A hyperpycnal deposits show a general fining trend beyond the cliniform rollover and do not bypass large volumes of coarse-grained sand into the distal slope setting (Fig. 6.25). In contrast, Type B hyperpycnal flows bypass the shelf setting and deposit coarse-grained sand in the medial and distal slope setting (Fig. 6.25). The relatively coarser grain size of the Type B hyperpycnal flows, in combination with the relatively higher organic matter content, and shelf-bypass suggest an episodic nature of deposition associated with large river-flooding events. The relatively finer-grained Type A hyperpycnal flows may be associated with more sustained river flooding events.

Coarse-grained sand-bypass varies according to: i) the dominant process-regime, which directly impacts the distribution of facies within Cycle LG-1 and their resulting grain sizes, and ii) the flow-style of river-dominated deposits (i.e. sustained versus episodic hyperpycnal flows). As such, heterogeneity in grain size is documented not only at a process-regime scale, but additionally, under the umbrella of 'river-dominated deposits', significant variability in

coarse-grained sand bypass can be introduced, based on the dominant flow-style (Fig. 6.25; Chapter Five, Cosgrove et al., in review).

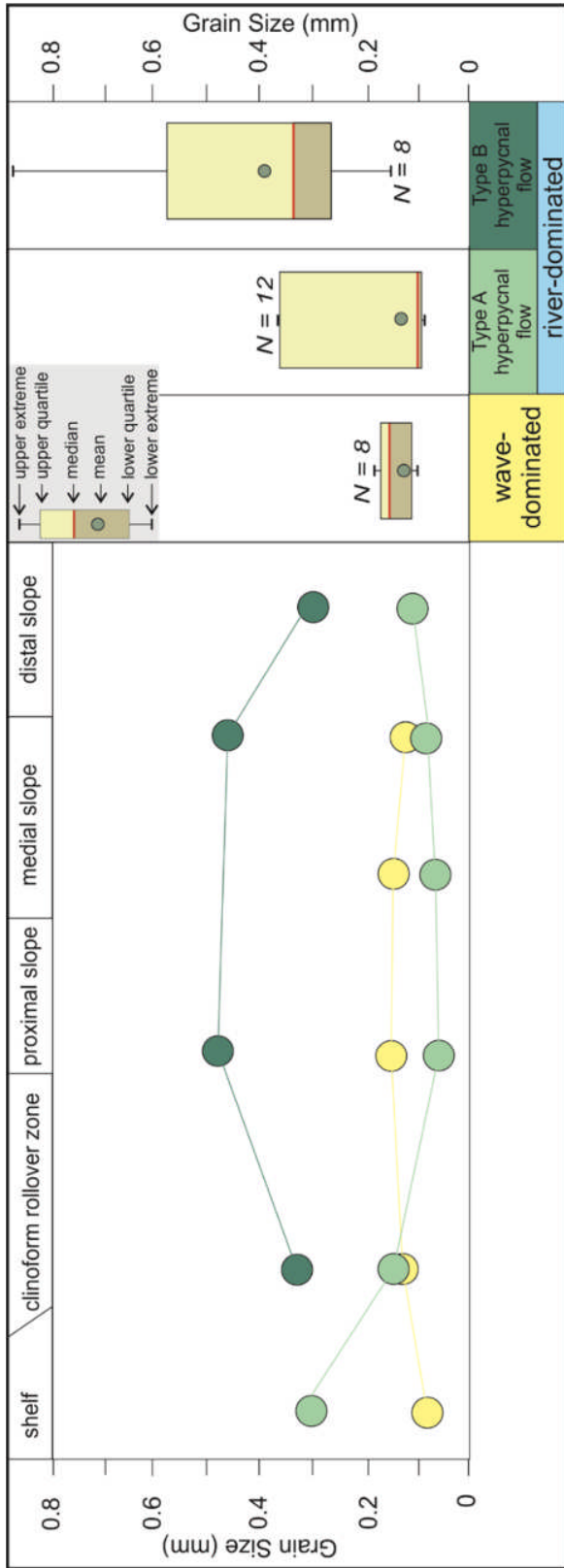


Figure 6.22: Difference in grain size for wave-dominated and river-dominated sedimentary packages. The river-dominated sedimentary packages are subdivided into sustained and episodic hyperpycnal flows. Changes in grain size are shown across the depositional profile. Box and whisker plots illustrated the bulk differences in grain size for the wave-dominated deposits versus hyperpycnal flow (sustained and episodic) deposits. The legend for the box and whisker plots is illustrated. The sample numbers for the box and whisker plots are illustrated by N = X.

6.1.3.7 *Summary*

Both datasets use a novel methodology and application of integrated quantitative grain character data and sedimentology, in order understand the evolution of individual clinothem sequences (Chapters Four, Five). The novel datasets highlight hitherto undocumented intraclinothem variability, which are directly related to changes in the topset (shelf) process-regime. In both cases, it is apparent that updip shelf process-regime is a significant factor controlling downdip architecture and grain character. The outcrop example from Cycle LG-1, also highlights the complexity and heterogeneity that fall under the wide umbrella of 'river-dominated deposits', such that flows associated with sustained and episodic hyperpycnal flows also modulate the distribution, and calibre and maturity, of sediment transported downdip.

6.1.3.8 *Allogenic and Autogenic Variability*

In Cycle LG-1, stratigraphic process-regime change occurs within a single transgressive-regressive cycle, on timescales of ~10s of thousands of years (Chapter Five, Cosgrove et al., in review). In Sequence m5.4, stratigraphic process-regime change occurs within a clinothem originally interpreted to be a composite sequence (Chapter Four, Cosgrove et al., 2019), composed of three higher order sequences (Miller et al., 2013), each deposited over a ~100,000 year timescale (Browning et al., 2013). In both sequences, the changes in shelf process-regime may be accounted for by either allogenic or autogenic variability.

Allogenic controls, i.e. those external to the sedimentary unit, primarily document the effects of eustatic variability and changes in hinterland climatic- and tectonic-regime, which modulate the production and discharge of sediment from source regions (e.g., Castelltort and Van Den Driessche, 2003; Armitage et al., 2011). Typically, process-regime change is considered to be driven by unsteady external forcing conditions. Allogenic forcings, in both cases, cannot be discounted as the mechanism for driving shelf (topset) process-regime change at the observed intraclinothem scale.

In Sequence m5.4, allogenic-driven process-regime change on 100,000 year timescales is feasible; this would support the interpretations of Miller et al. (2013) and Miller et al. (2018) who determined the intraclinothem surfaces to be sequence boundaries. In Cycle LG-1, process-regime change through either sea-level change or sediment supply are both considered. The active tectonic setting of the Sobrarbe Deltaic Complex could provide a mechanism for driving high-frequency, small-scale eustatic sea-level variations (see Dreyer et al., 1999). Variations in Eocene orbital cyclicity, relating to the precessional influence on patterns of precipitation (e.g., Berger, 1978; Kutzbach and Otto-Bliesner, 1982), also provides

a potential allogenic mechanism of regulating sediment supply over the timescales observed in Cycle LG-1 (cf. Middle Eocene, Ainsa Basin; Cantalejo and Pickering, 2014).

Autogenic controls, i.e. changes in stratigraphy or morphology that occur against a backdrop of steady external forcing conditions (see Muto et al., 2007), may account for the intraclinothem process-regime change within Sequence m5.4 and Cycle LG-1. Autogenic variability, such as river avulsion and/or switching of wave-dominated delta lobes (e.g., Olariu, 2014; Hampson, 2016) would provide plausible mechanisms for driving intraclinothem variability.

The rapidity of process-regime change in Cycle LG-1 (~ 10s of thousands of years) supports an autogenic interpretation (e.g., Amorosi and Milli, 2001; Amorosi et al., 2003; Amorosi et al., 2005; Correggiari et al., 2005; Olariu, 2014). Modern deltas (including the Mississippi, Mekong, Danube and Mahakam) exhibit significant autogenic process-regime change over short temporal scales (100s – 1,000s of years) during Holocene progradation (see Olariu, 2014), despite steady external forcings. These modern examples may be analogous with Cycle LG-1.

Distinguishing between allogenic and autogenic process-regimes in the stratigraphic record is problematic; autogenic forcings have been shown to generate surfaces and stratigraphic architectures that are challenging to distinguish from those generated through allogenic processes (e.g. Muto and Steel 2002). In the two examples presented here, Sequence m5.4 is most likely to be the result of allogenic variability, due to the timescale and basinward extent of the intraclinothem surfaces generated by the process-regime variability (Chapter Four, Cosgrove et al., 2018). In contrast, the rapid timescale of process-regime change in Cycle LG-1, is more likely to be the result of autogenic forcing mechanisms (Chapter Five, Cosgrove et al., in review). Although we suggest an allogenic and autogenic mechanism for Sequence m5.4 and Cycle LG-1 respectively, this remains tentative given the lack of strike control to test the regional extent of the key surfaces. This is discussed in detail below.

6.1.3.9 Lateral Variability

Many modern and ancient systems exhibit significant lateral variability in depositional facies, and dominant process-regime, related to the relative importance of fluvial, wave, and tidal processes (Ta et al., 2002; Bhattacharya and Giosan, 2003; Ainsworth et al., 2008; 2011; Vakarelov and Ainsworth, 2013; Olariu, 2014; Jones et al., 2015). The core (New Jersey) and outcrop (Sobrarbe Deltaic Complex) datasets presented and discussed, however, both lack

strike-parallel data; in both datasets, the dip-parallel orientation of wells/exposure precludes observation of along-strike variability.

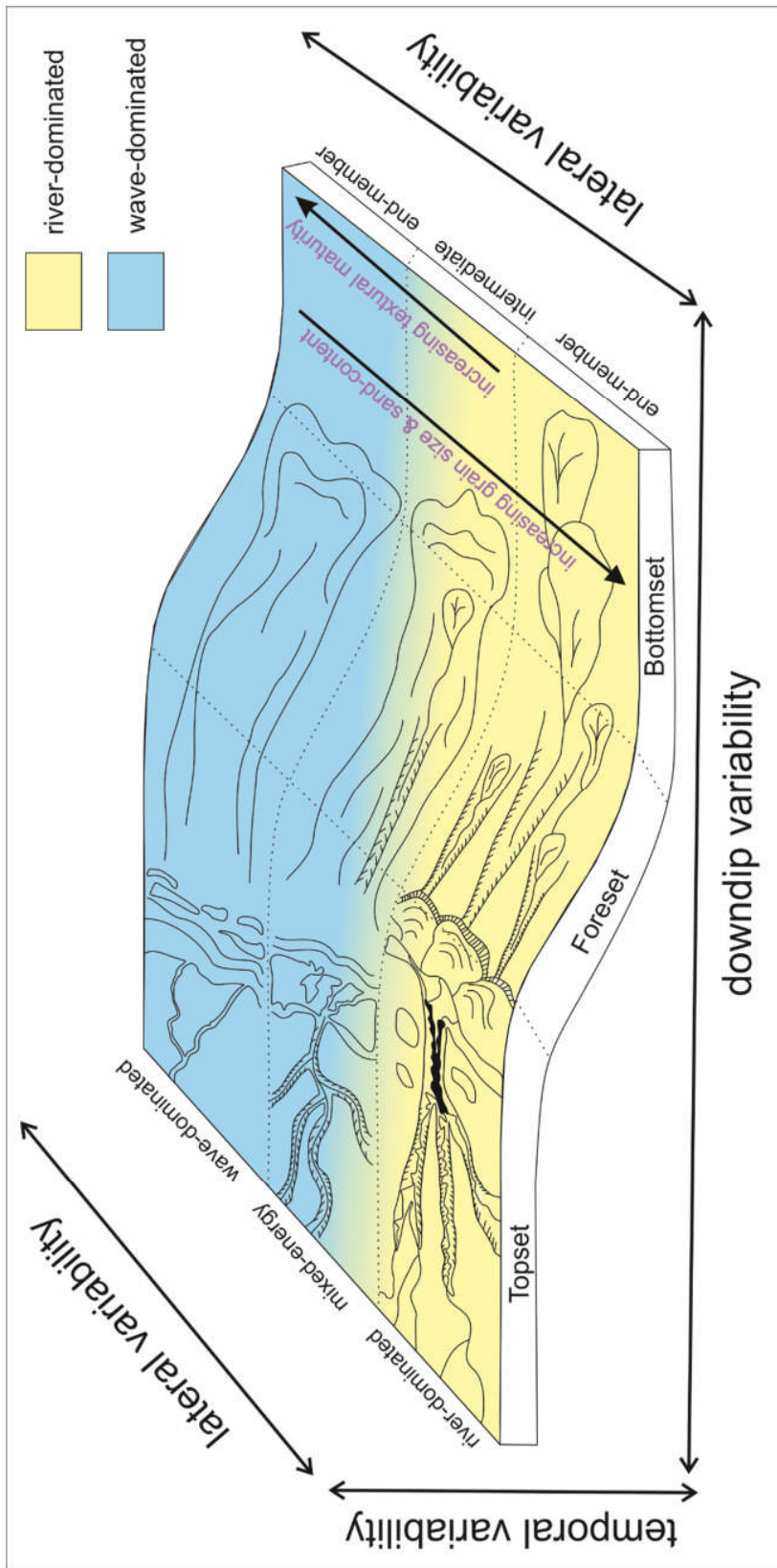


Figure 6.23: Summary diagram showing lateral (along strike), temporal (stratigraphic) and down-dip variability associated with river-dominated, mixed-energy and wave-dominated clinothem sequences. Variations in the topset process-regime, at a variety of scales, introduces significant heterogeneity in grain character within an individual clinothem sequence, and across multiple successive clinothems. River-dominated conditions are associated with coarse-grained bypass, and sediments of lower textural maturity. Wave-dominated conditions are associated with the deposition of silt in the deep-water environment but have high textural maturities.

The propensity for systems to exhibit lateral process-regime variability along the same shoreline, would likely impact the grain character of associated deposits (Fig. 6.26). This 3-D, strike-parallel variability has the potential to introduce additional sedimentological heterogeneities down-dip, directly impacting grain character. For example, the influence of shore-parallel variability may be expressed as a lateral transition from a wave-dominated topset system to a river-dominated system further along-strike. However, down-dip of the river-dominated system, sedimentary deposits fed by the wave-dominated system could be intersected. As such, lateral changes in the process-regime could impact the timing of sand delivery into the deeper basin (Madof et al., 2016), the location of coarse-grained deposits (Carvajal and Steel 2009; Koo et al., 2016), and the spatial distribution of grain character within foreset and bottomset deposits.

The prominent stratigraphic variability in process-regime, and associated grain character variability in both systems, may be indicative of associated lateral variability (Fig. 6.26). However, this supposition cannot be addressed using these datasets alone. Future investigations into the interplay of lateral variability in process-regime and grain character heterogeneity will require exceptional exhumed systems with 3-D control, or integrated subsurface datasets of 3-D reflection seismic data and additional research core holes.

6.1.3.10 Summary

The new datasets presented and discussed in this thesis highlight the importance of constraining, and understanding the causes of architectural variability within individual clinothems. In both the core (New Jersey) and outcrop (Sobrarbe) examples, process-regime plays a crucial role in determining the internal sedimentological and grain character variations observed within individual clinothem sequences.

6.1.4 Research Question Four

What value do high-resolution quantitative grain character datasets offer to sedimentology and stratigraphy?

6.1.4.1 Introduction

The preceding discussion has outlined the wide and varied use of quantitative datasets to better understand the evolution of successive clinothem sequences and individual clinothem sequences. In addition to what has already been previously outlined, two further novel applications of quantitative databases can be identified that have application to the broader field of sedimentology. Firstly, quantitative grain-size data can be compared with qualitative grain-size data to determine the differences in the outputs of these methodologies. Secondly,

the quantitative database can be used as an additional tool to aid the placement of sequence boundaries.

6.1.4.2 Comparison to Traditional Methods

Quantitative grain-size datasets can be used as a means to test the accuracy and consistency of traditional qualitative and semi-quantitative sedimentary log data and cumulative lithology summaries. The New Jersey dataset is ideal for this, as both qualitative sedimentary logs (Mountain et al., 2010) and semi-quantitative cumulative lithologies have been produced from the same core deposits (Fig. 6.27). For example, quantitative grain-size data from a section of the foreset deposits (Core M28) of Sequence m5.4, are shown alongside the semi-quantitative cumulative lithology presented in Browning et al. (2013). The semi-quantitative dataset presented in Browning et al. (2013) used samples recovered at ~ 1.5 – 3 m intervals. Samples were semi-quantitatively analysed, using both traditional sieving techniques and visual estimations of grain-size.

When the two cumulative lithologies are compared at a broad-scale (i.e. over ~ 10s of m in scale), the same overall trends in stacking pattern are apparent. In this example, an overall coarsening upwards trend can be observed in both sequences (Fig. 6.27). However, when the two cumulative lithologies are viewed in high-resolution, clear differences are apparent. Firstly, the methodology used by Browning et al. (2013) cannot differentiate coarser silt-fractions from very fine-grained silt fractions; this leads Browning et al. (2013) to significantly over-state the silt content, and under-state the sand content, throughout the complete section, by as much as ~ 60 % (see core depth ~ 497 mcd; Fig. 6.27). Additionally, the sampling resolution has a clear impact upon the recognition of up-core grain-size patterns; the resolution of Browning et al. (2013) is between three and six times lower than that achieved in this thesis. Higher resolution stratigraphic sampling reveals hitherto undocumented bed-scale changes in grain-size composition. An example of this can be observed comparing the interval observed between core-depths ~ 508 and ~ 501 mcd; Browning et al. (2013) represent this interval as a blocky silt-dominated mass, whereas in this study higher resolution sampling reveals a number of silt-rich event beds that produce a fining-upwards trend (Fig. 6.27).

The comparison of the quantitative data with the lower-resolution qualitative data highlights significant differences in the apparent and actual grain-size composition. Because qualitative sedimentary logs and qualitative/ semi-quantitative cumulative lithologies compilations are fundamental tools, the potential errors associated with their use may affect interpretations. It follows that caution must be used when attempting to interpret patterns of sediment

dispersal, sediment bypass, stacking patterns and sequence boundaries from qualitative and semi-quantitative data alone.

6.1.4.3 Extracting Data from Sedimentary Logs

The use of sedimentary logs, based on visual estimations of grain-size, amongst other sedimentological and textural attributes, is a staple of many outcrop and core-based studies. Thus the analysis of grain-size trends as determined from sedimentary logs is central to clastic sedimentology, and the interpretations arising are used to determine the depositional histories of sedimentary successions.

Reynolds (2018) suggests that conventional sedimentary logs could be digitised and analysed to generate quantitative data. However, the analysis above shows that using a qualitative source (i.e. sedimentary logs) to produce nominally quantitative data is highly likely to produce unreliable metadata. This is because the quality of the derived data depends on the accuracy of visual estimations of grain size grain-size recorded within each sedimentary log. The difference between visual, and even semi-quantitative, estimations of grain-size versus truly quantitative data has been clearly demonstrated in the previous discussion of Sequence m5.4; data derived from visual estimation commonly differ from genuinely quantitative data, and likely vary from vary from person-to-person, such that there is significant potential for the introduction of human error in any grain size estimation. The methodology suggested by Reynolds (2018), highlights that the drive for quantitative datasets, and the use of machine learning approaches, in sedimentology risks precision and accuracy if the approaches adopted are not quantitative throughout.

6.1.4.4 Applications of High Resolution Datasets

The practical applications of the accurate determination of grain-size composition at high-resolution is demonstrated when the basal composite sequence boundary of Sequence m5.4 (Core M28) is considered. Three potential sequence boundary placements have been attempted: sequence boundary m5.4 has been placed at 495.2 mcd by Mountain et al., 2010; at 512.33 mcd by Miller et al. (2013); and an alternative at 519.7 mcd by Hodgson et al. (2018). Using lower-resolution, qualitative lithology data and semi-quantitative cumulative lithology data, previous authors identified potential sequence boundaries based upon abrupt perceived changes in grain-size, lithology and stacking patterns, alongside core based criteria. However, the new data presented here suggests that such abrupt, apparent changes in stacking-pattern and grain-size may be an artefact of the low-sampling density and of the semi-quantitative methodology used to produce cumulative lithology data.

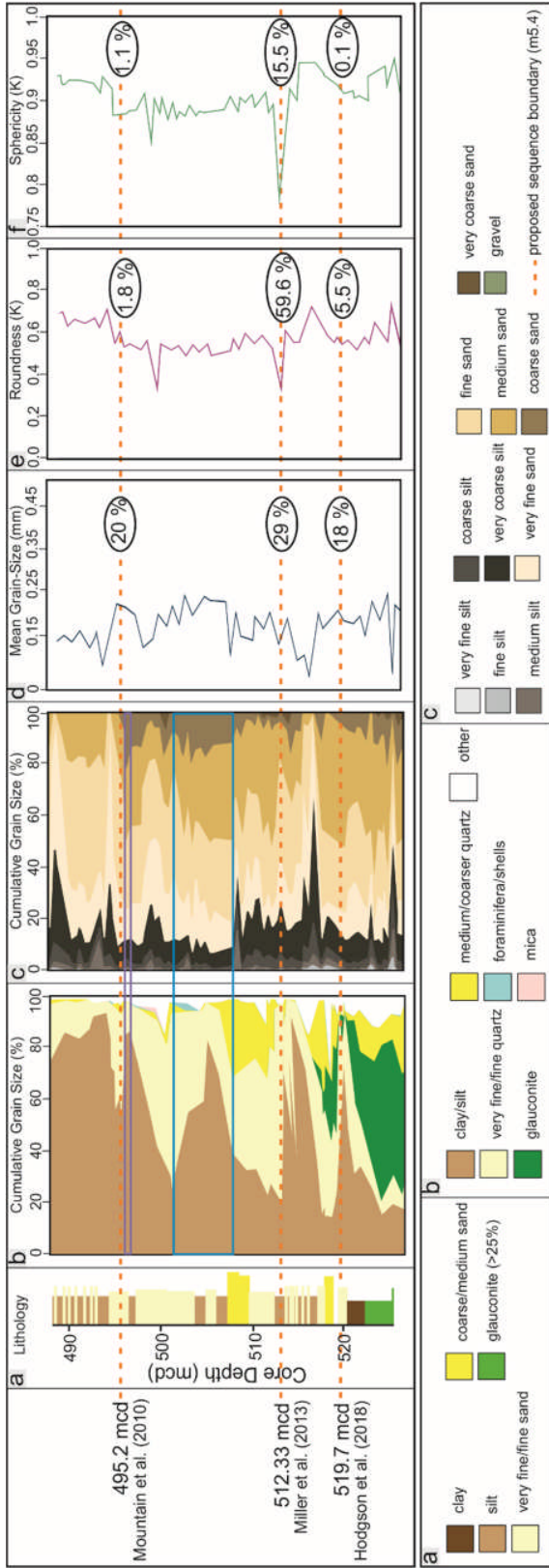


Figure 6.24: Summary diagram showing the differences in grain-size composition between a) sedimentary logs (qualitative; Mountain et al., 2010), b) cumulative lithologies (qualitative/ semi quantitative; Browning et al., 2013) and c) the new quantitative dataset presented in this thesis. The purple box (~497 mcd) highlights differences in the apparent (Part b; Browning et al., 2013) and actual (Part c; this thesis) silt-content; which varies by > 60%. The blue box (~508 - 501 mcd) highlights the difference in sampling resolution between traditional sedimentary logging (Part a) and the original cumulative lithology (Part a) and the high-resolution methodology presented in this thesis (Part c); note the event-bed scale changes in grain-size composition in Part c. Parts, d, e and f show changes in mean grain size (d), roundness (e) and sphericity (f) across three proposed sequence boundaries.

In order to identify the most likely position of the candidate sequence boundaries, the fully quantitative dataset can be used to calculate changes in sand-to-mud ratio and mean grain size, roundness and sphericity across the candidate sequence boundaries. In this case, the sequence boundary location proposed by Miller et al. (2013) at 512.33 mcd corresponds to the depth where the greatest change in grain size and shape are seen. Because the associated changes in sediment source and/or transport regime are most consistent with the depositional hiatus represented by a sequence boundary, the Miller et al. (2013) boundary is preferred. The grain-size data presented here therefore highlight that lower resolution, semi-quantitative lithological data may dramatically oversimplify grain-size trends and promote the somewhat arbitrary placement of sequence boundaries in core, whereas high-resolution grain-character datasets can be used in conjunction with core criteria to refine the placement of sequence boundaries and to determine the statistically most likely placement where a number of candidates exist.

6.1.4.5 Summary

The field of sedimentology moves away from models based on observation alone (e.g., Vail et al., 1977; Van Wagoner et al., 1988; Posamentier et al., 1992; Johannessen and Steel, 2005; Catuneanu et al., 2009), to those more founded on quantitative approaches and datasets (e.g., Burgess and Hovius, 1998; Harris et al., 2016; Fildani et al., 2018). Quantitative measurement of grain character will play an integral role in this transition. The use of quantitative datasets, such as those presented in this thesis, currently remain relatively limited in modern sedimentology. This may be due to the labour-intensive methodologies required in their generation in terms of sample collection, preparation and analysis, and the relatively high cost of laboratory analyses. However, the advantages, and numerous potential applications of such datasets, justifies the financial cost and time required.

6.2 Conclusions

This thesis presents high-resolution grain character data, integrated with sedimentological analyses, from core-based (offshore New Jersey) and outcrop (Sobrarbe Deltaic Complex) examples. The novel datasets presented here represent the first archives of grain character, which capture: i) genetically linked topset (shelf), foreset (slope) and bottomset (basin-floor) deposits across multiple successive clinothems, and ii) the topset-to-foreset transition within a single clinothem sequence. The unique datasets presented and discussed in this thesis have been used for a variety of applications, which span many broad fields of modern sedimentology, including clinof orm trajectory analysis, sequence stratigraphy, shelf (topset) process-regime and clinothem evolution. The overarching aim of the project has been to

better understand the role played by the continental shelf as a conveyor or filter of sediment of different calibre and maturity into the deep-water setting; this has been facilitated by addressing four key research questions. Concluding remarks, answering these four key research questions, are outlined below.

6.2.1 What are intermediate-scale clinothems?

This study defines a new class of intermediate-scale clinothem: intrashelf clinothems. The intrashelf clinothem class is defined by an intermediate-scale (~ 100 – 400) and a location landwards of a morphological shelf-break. Intrashelf clinothems can be deposited in a variety of depositional settings and show variable foreset gradients and basinwards extents.

Intrashelf clinothems exhibit two dominant depositional styles, here termed 'ramp' and 'slope.' In ramp intermediate-scale clinothems, progradational wedges stack successively in a basinwards direction, over gently sloping ($< 1^\circ$) topographies, as observed in passive margin or foreland basin settings. 'Ramp' clinothems show little stratigraphic climb; the relatively flat relief of the inherited topography, and strong topset bypass, results in clinothem deposits with relatively thin topset deposits and relatively thick, aggradational foreset-wedges. Slope intermediate-scale clinothems describe the progradation of clinothems into gradually deeper water, across a basinward-directed channelised slope succession. Intermediate-scale slope clinothems exhibit more sigmoidal architectures, and lack relatively thick foreset wedges observed in ramp clinothems, suggesting a stronger foreset bypass component in ramp clinothems, associated with proximity to a major river-system.

The Miocene offshore New Jersey clinothems provide an example of intrashelf clinothems, associated with a characteristic intermediate-scale and a location demonstrably on the shelf, landwards of the shelf-break. The formation of the New Jersey intrashelf clinothems is suggested to be a function of an initial phase of sediment starvation, during Oligocene thermal subsidence of the Atlantic passive margin. A second phase of rapid sediment influx proceeded this. The first phase generates the necessary accommodation within which the outbuilding of intrashelf clinothems can take place; the second high-supply phase provides the necessary sediment flux to facilitate clinothem construction. Intrashelf clinothem construction is facilitated by sandy hyperpycnal flows, associated with a river-dominated shelf process-regime, which bypass the innermost shallow shelf.

The definition of an intrashelf class of clinothem will remove the nomenclatural confusion surrounding intermediate-scale clinothems, which have hitherto been variably termed subaqueous, mid-shelf, shelf-prism and shelf-edge clinothems. The definition of an intrashelf class of clinothem may be significant for the interpretation of ancient intermediate-scale

clinothems, which are overwhelmingly classified as shelf-edge clinothems; this shelf-edge classification is typically determined in the absence of strong evidence of a position at the true structural shelf-edge. Clinothems represent the fundamental building blocks of many deltaic-to-continental slope successions, correctly identifying and understanding the formation of intermediate-scale clinothems, has important implications for understanding basin-margin evolution.

6.2.2 What role does process-regime play in regulating the timing of sand transfer, and in controlling the character of grains delivered, to the slope and basin-floor settings?

The New Jersey and Sobrarbe datasets provide excellent core and outcrop based case-studies, in which the effect of the shelf process-regime on the downdip distribution, and grain character, of sediment can be assessed. The datasets presented and discussed in this thesis, suggest that the clinoform trajectory paradigm, widely used to predict the presence or absence of sand in the deep-water setting, is not sufficient to predict the distribution of coarse-grained sand, either across successive clinothems or within individual clinothem sequences. River-dominated conditions in the topset or shelf setting are a key factor determining the basinward transfer of coarse-grained sediment; river-dominated clinothems under both rising and falling clinoform rollover trajectories are associated with the basinward transfer of coarse-grained sediment; as such, river-dominated conditions are effective sediment conveyors. Wave-dominated conditions are associated with attenuated delivery of coarse-grained sediment into the deep-water setting; as such, wave-dominated process-regimes are effective sediment filters.

Additionally, high-resolution grain character analysis, integrated with sedimentological analysis, has allowed the production of novel, archetypal grain character profiles for end-member, wave- and river-dominated conditions. The detailed characterisation of river- and wave-dominated longitudinal sedimentary profiles demonstrate that the physical processes in action on the shelf exert a fundamental control on grain character (including grain size, grain shape, and sorting) across the complete depositional profile from topset (shelf) to foreset (slope) to bottomset (basin floor).

6.2.3 How can grain-character be used to improve understanding of clinothem evolution?

The detailed sedimentological analyses undertaken on individual clinothem sequences has allowed the reclassification of Sequence m5.4 (offshore New Jersey) and Cycle LG-1 (Sobrarbe Deltaic Complex) as mixed-energy systems; both clinothems show a complex history of stratigraphic process-regime change. The stratigraphic variability in shelf process-regime, at

an intraclinothem scale, directly impacts every aspect of grain character, including grain size, grain shape, sorting and sand-to-mud ratios.

Grain character variations, associated with changes in the dominant topset or shelf process-regime, can be traced across the complete sampled depositional profile, using facies associations and grain-size distributions. Within an individual clinothem, the sedimentary packages corresponding with a wave-dominated topset or shelf process-regime have: i) finer mean grain-sizes; ii) better sorted sediment compositions; iii) more rounded and spherical grains; and iv) lower sand-to-mud ratios, relative to their river-dominated counterparts. Additionally, the topset process-regime influences the geometric distribution of facies. In Cycle LG-1 (Sobrarbe Deltaic Complex), river-dominated facies are deposited over the complete depositional profile, from the shelf to the distal slope setting; wave-dominated facies are deposited only on the proximal and medial slope. The relative influence of fluvial- and wave-processes thus controls the distribution of facies, and grain character, within a single clinothem.

The new datasets presented and discussed in this thesis, highlight the importance of constraining, and understanding the causes of architectural variability within individual clinothems. In both the core and outcrop examples, process-regime plays a crucial role in determining the internal architectural evolution, and the sedimentological and grain character attributes of individual clinothem sequences. Critically, these new datasets highlight the heterogeneous nature of grain character within individual clinothems. Basin-scale approaches, for example those which utilise clinoform trajectory to infer the presence or absence of sand in deep-water settings, cannot account for the observed stratigraphic and downdip variability in grain character observed in these examples, and therefore their use in isolation results in predictive uncertainty.

6.2.4 What value do high-resolution quantitative grain-character datasets offer to sedimentology and stratigraphy?

As the field of sedimentology moves away from models based on observation, to those more firmly based on numerical datasets, quantitative grain character datasets will play an integral role in this transition. The methodology of high-resolution sampling and quantitative grain character data collection presented in this thesis provides a unique database of grain size, grain shape, and sorting statistics, which may be used to test and refine numerical forward models that seek to improve prediction of reservoir characteristics in both mature and frontier hydrocarbon basins. The datasets presented and discussed in the three manuscripts accompanying this thesis, have been used in a variety of novel ways to understand the role

played by the continental shelf in determining the timing of sediment delivery to the deep-water setting; these are outlined below.

1) Archetypal depositional models for river- and wave-dominated clinothem systems are presented; downdip changes in sediment texture and grain character are shown to relate to updip changes in process-regime. 2) Process-regime is determined to be a more significant control on delivery of coarse-grained sediment to deeper-water settings and its timing, than is clinoform trajectory, both across successive clinothem sequences and within individual clinothem sequences. 3) We discuss the major controls determining clinothem architecture in order to produce an improved model of clinothem evolution, which does not rely on the simple tripartite shelf-slope-basin (topset-foreset-bottomset) subdivision. 4) The causes of variable sediment bypass at the clinoform rollover, such as the dominant shelf process-regime, and flow type are identified. 5) Intraclinothem, time-equivalent surfaces are proposed. 6) Grain-character data are used to help refine the placement of sequence boundaries.

6.2.5 Final Remarks

This study uses a novel quantitative approach to determine the impact of process-regime change on grain character both across multiple successive clinothems, and within individual clinothem sequences, which has been used to develop models describing clinothem evolution. The datasets presented and discussed in the three manuscripts accompanying this thesis, and in the four research questions outlined in the discussion, have been used in a variety of novel ways to understand the critical role played by the continental shelf as a conveyor or filter of sediment to deep-water. Throughout this thesis, the dominant shelf process-regime has been shown to be a key parameter, influencing the distribution of sedimentary facies and the grain character of deposits, across the complete depositional profile. The results of this study challenge conventional sequence stratigraphic and clinoform trajectory paradigms, which cannot adequately account for the observed stratigraphic and downdip variability in grain character observed in these examples.

6.3 Future Work

6.3.1 Lateral Variability

One of the key, but unavoidable, limitations of the core and outcrop datasets presented in this thesis is the lack of strike-parallel data. The offshore New Jersey dataset comprises a 2-D dip-parallel transect of seismic reflection data and three cores, intersecting the topset, foreset, and bottomset deposits of prograding Miocene clinothems. The Sobrarbe Deltaic Complex dataset comprises samples recovered from a sandy Eocene clinothem, which crops out effectively

only in a 2-D, dip-parallel transect. In fact many outcrop studies of dip-parallel variability are limited by their lack of strike-parallel control (e.g., the Lewis Shale, Wyoming (Pyles and Slatt, 2007), the Magallanes Basin, Chile (Covault et al., 2009) and the Battfjellet Formation, Spitsbergen (Helland-Hansen, 2010)). The studies presented in this thesis therefore stand in the tradition of using 2-D profiles, usually oriented in the direction of sediment transport, which is widespread in the literature (see also Dreyer et al., 1999; Pyles and Slatt, 2007; Covault et al., 2009; Helland-Hansen, 2010; Mountain and Proust, 2010, Browning et al., 2013; Miller et al., 2013).

Although 2D studies provide valuable archives of basin-margin evolution, a number of publications have highlighted their limitations and have used 3-D seismic datasets to refine understanding of spatio-temporal variability in basin-margin architecture and sedimentary processes, in both a dip- and strike-orientation (e.g., Suter and Berryhill, 1985; Matteucci and Hine, 1987; Poag et al., 1990; Tesson et al., 1990; Allen and Posamentier, 1994; Sydow and Roberts, 1994; Martinsen and Helland-Hansen, 1995; Morton and Suter, 1996; Driscoll and Karner, 1999; Kolla et al., 2000; Hiscott, 2001; Pinous et al., 2001; Krassay and Totterdell, 2003; Johannessen and Steel, 2005; Houseknecht et al., 2009; Ryan et al., 2009; Moscardelli et al., 2012). However, outcrop examples that offer both lateral (> 10 km) and dip-parallel variability are relatively rare (e.g., Wild et al., 2009; Charvin et al., 2010; Jones et al., 2015). In order to investigate both dip- and strike-parallel variability, an alternative outcrop analogue would have to be found. One potential location, in which genetically linked shelf and slope deposits can be sampled, is the lower Waterford Formation (Karoo Basin, South Africa; Fig. 6.28). Eight successive clinothems crop out, capturing both along-strike variability and the shelf-to-slope transition. The lower Waterford Formation is discussed in Jones et al. (2015), in which three dip-parallel transects were produced, approximately 6 km apart along strike (Fig. 6.28). Despite similar clinof orm rollover trajectories significant along-strike variability was documented, and interpreted to influence patterns of sediment distribution beyond the clinof orm rollover. Jones et al. (2015) produced their findings based on traditional sedimentary logging along. This leaves open the possibility to produce a fully quantitative grain character dataset, within the context of the wealth of previously published material regarding the sedimentology of the lower Waterford Formation (e.g., Rubidge et al., 2012; Jones et al., 2013; Jones et al., 2015).

Sampling of the lower Waterford Formation would provide the opportunity to expand the grain character dataset presented in this thesis and to assess how grain character can vary both along depositional dip and in a strike-parallel direction. Additionally, sampling the lower Waterford Formation would represent a first step towards producing a comprehensive database of grain character statistics. In the future, the findings would need to be compared to additional core and outcrop examples, from a variety of clinothem systems, which vary by setting (e.g., intrashelf versus basin-margin) and location (e.g., latitude, climatic conditions). This database would find application in numerical models (e.g., DionisosFlow, Delft2D) which seek to improve prediction of reservoir characteristics in both mature and frontier hydrocarbon basins.

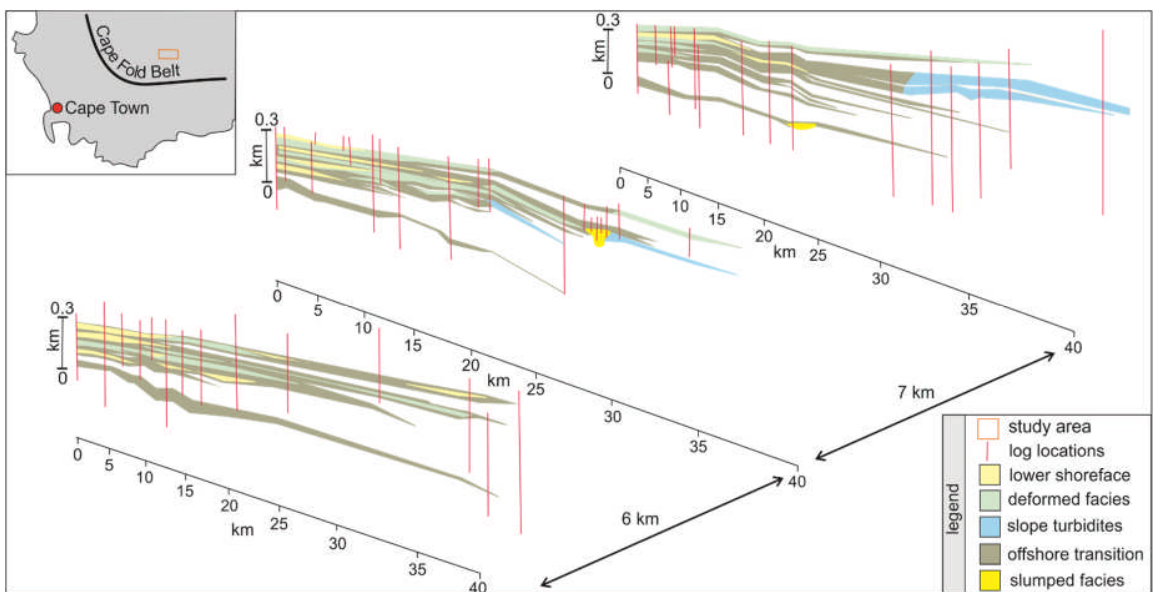


Figure 6.25: Three dip-parallel cross-sections of the lower Waterford Formation, capturing along-strike variation in sedimentary facies. Inset shows the location of the lower Waterford Formation. Adapted from Jones et al. (2015).

6.3.2 Expanding the New Jersey Dataset

The offshore New Jersey grain character dataset may have the potential to be placed within a high-resolution 3-D context. In 2014, it was announced that US National Science Foundation funding would enable Rutgers University and the University of Texas to undertake a 3-D seismic survey, which encompasses the Expedition 313 core sites (M27, M28 and M29; Fig. 6.29). When this dataset is made available to the public, the acquired strike parallel acoustic images could be tied to the core-based grain character dataset and high-resolution dip-parallel seismic dataset, to produce a truly unique integrated 3-D seismic and grain character dataset.

Strike parallel (3-D) acoustic images would enable the extraction of true dip-parallel sections, from which any lateral variability in clinoform trajectory could be assessed. As clinoform trajectory can vary along strike (e.g., Henriksen et al., 2009; Jones et al., 2015), this would enable the results of integrated rollover trajectory and grain character presented in Cosgrove et al. (2018) (Chapter Three) to be tested. Additionally, the 3-D dataset would enable different lateral scales of variability in topset, foreset and bottomset deposits to be constrained. The 3-D seismic dataset will be able to help address some of the fundamental questions regarding lateral variability raised in Chapters Three and Four; particularly the causes of process-regime change (i.e. allogenic versus autogenic forcing mechanisms) within the successive Miocene intrashelf clinothems could be illuminated should this 3-D dataset become available.

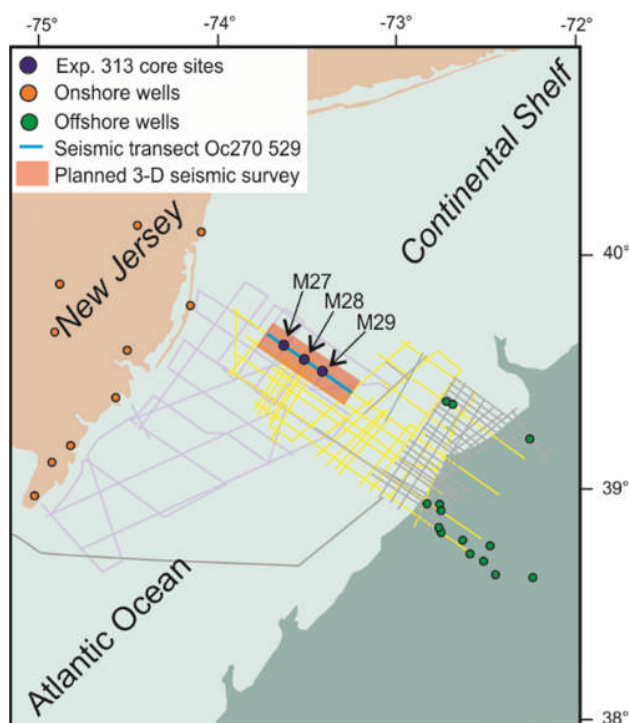


Figure 6.26: Location map illustrating location of planned 3-D seismic survey, which encompasses the IODP Expedition 313 drill sites. The Expedition 313 drill sites exist within grids of 2-D seismic profiles (violet, yellow and grey lines).

6.3.3 Expanding the Sobrarbe Deltaic Complex Dataset

Despite the lack of strike-parallel outcrop within the Sobrarbe Deltaic Complex, it is still an extremely valuable outcrop example, capturing the transition from fluvio-deltaics to lower slope settings. This outcrop could be sampled more extensively to further enhance the quantitative grain character dataset already presented in this thesis. Only one clinothem was originally sampled, leaving open the option to sample consecutive clinothems, in order to constrain grain character variability across successive clinothems, within a basin-scale context. Also, the original sampling strategy only targeted sandy packages within Cycle LG-1;

it would be possible to sample systematically, taking samples at a pre-designated vertical interval (as per the New Jersey dataset); in the case of the Sobrarbe dataset sampling could be undertaken, for example at 0.5 – 1 m intervals. This approach would capture grain character variability at a far greater stratigraphic resolution and would provide insight into the grain character of siltstone deposits, as well as adjacent sandstones. Finally, the grain character dataset presented in this thesis could be expanded through decreasing the sampling intervals across depositional dip; this would provide a greater constraint on spatial grain character variability between shelf and slope deposits.

6.3.4 Geochemical Datasets

Another potential avenue of possible future research involves the integration of the grain character datasets with geochemical data, in order to provide additional insight into the depositional histories of the New Jersey and Sobrarbe case-studies. Original core and rock samples have been retained and carefully stored for both the New Jersey and Sobrarbe case-studies respectively, should such geochemical work be possible in the future.

6.3.4.1 *Glauconite (offshore New Jersey)*

Throughout the sampled stratigraphic sections of the New Jersey clinothem, autochthonous (in-situ) and allochthonous (detrital) glauconite is present in variable concentrations (Mountain et al., 2010). Autochthonous glauconite formation (glauconitisation) occurs when potassium-rich crystal aggregates are precipitated onto, or within, a host-grain; the host-grain is typically a phyllosilicate mineral grain, a foraminiferal test or a faecal pellet (Huggett and Gale, 1997). Autochthonous glauconite has long been established as an important tool for the identification and interpretation of condensed sections (and maximum flooding surfaces) within sequence stratigraphy (Table 6.5). In particular, sedimentary units enriched in glauconite are strong indicators of low sedimentation rates or sediment starvation within the marine realm (e.g., McCracken et al., 1996; Huggett and Gale, 1997; Amorosi, 1997; Hesselbo and Huggett, 2001). In a general sense, analysis of both the quantity and maturity of autochthonous glauconite through the New Jersey core would provide a supplementary tool to support the placement of major sequence stratigraphic surfaces. With specific reference to this thesis, data derived from the glauconite grains could be integrated with the grain character dataset presented, to ascertain if stratigraphic sections containing highly-evolved glauconite correspond with major changes in grain size, grain shape and sand-to-mud ratios. With specific reference to Chapter 4, this would provide valuable additional data to support the placement of the m5.4 sequence boundary.

Depositional setting	Sequence-stratigraphic framework setting	Maturity of Glauconite
Lowstand fan complex	Lowstand Systems Tract	Varying
Proximal lowstand wedge	Lowstand Systems Tract	Varying
Shelf margin wedge	Lowstand Systems Tract	Nascent - slightly evolved
Lower part of parasequence	Transgressive Systems Tract	Nascent - evolved
Upper part of parasequence	Transgressive Systems Tract	Nascent - evolved
Incised valley fill	Transgressive Systems Tract	Nascent - evolved
Ravinement surface	Transgressive Systems Tract	Varying
Uppermost Transgressive Systems Tract to lowermost Highstand System Tract; surface of maximum sediment starvation	Condensed Section	Evolved- highly evolved
Maximum flooding surface	Condensed Section	Evolved- highly evolved
Lower part of parasequence	Highstand System Tract	Nascent- slightly evolved
Upper part of parasequence	Highstand System Tract	Nascent-highly evolved

Table 6.5: Glauconite maturity in relation to depositional setting and the sequence stratigraphic framework. Adapted from Amorosi (1995).

The process of glauconitisation is divided into four stages, reflecting: i) the crystalline structure of the glauconite grain; ii) grain morphology and iii) the potassium content (Odin and Fullagar, 1988). The four stages of glauconite evolution are: nascent, slightly evolved, evolved and highly evolved (Fig. 6.30). The stage of glauconite evolution reflects the amount of time the glauconite grain has remained at the sediment-water interface (McCracken et al., 1996). As glauconitisation advances, the potassium-content within a glauconite grain increases; this process results in significant variability in the chemical composition of glauconite grains at different stages of evolution, which can be identified using XRD (X-ray diffraction)-analysis (Amorosi, 1997; Fig. 6.30). The formation of highly evolved glauconite can be achieved in $\sim 10^5$ years, provided that the grain remains near to the sediment-water

interface; glauconite evolution ceases after grain-burial to more than ~10-20 cm depth within the sedimentary column.

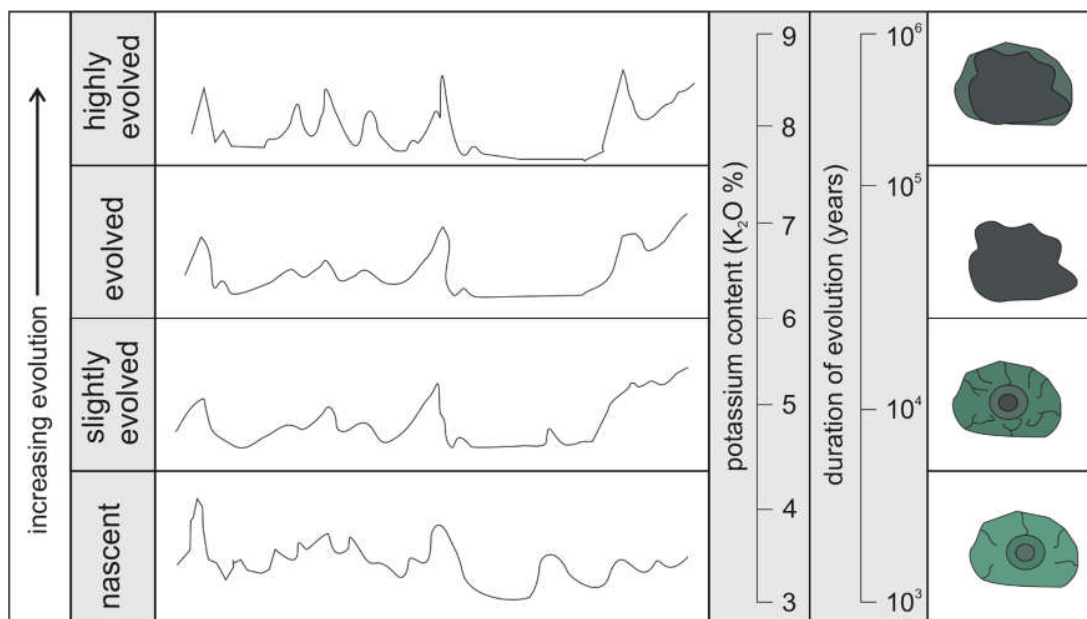


Figure 6.27: Progressive stages of glauconitisation, showing the four stages of glauconite evolution. X-ray diffractogram for glauconite evolution are shown, as are cartoons of glauconite grains at various stages of evolution. Adapted from Odin and Matter (1981) and McCracken et al. (1996)

Once autochthonous-glauconite bearing horizons have been identified, representative glauconite grains would be chosen for XRD-analysis. The relative maturity of the representative glauconite grains could then be inferred from the resulting X-ray diffractogram peaks, which vary according to the potassium-content (Odin and Matter, 1981; Fig. 6.30).

6.3.4.2 Carbon and Nitrogen Ratios (Sobrarbe Deltaic Complex)

Cycle LG-1 of the Sobrarbe Deltaic Complex is interpreted to show cyclical variations between river- and wave-dominated shelf process-regime conditions. Additionally, two families of hyperpycnal flow deposit are proposed ('sustained' and 'episodic'; see Chapter Five, Manuscript Three). One method of testing interpretations of process-regime variability, and of differentiating hyperpycnal flows deposits, would be through the analysis of carbon to nitrogen ratios (C/N ratios) of organic matter (OM) found within sediment samples. Ratios of carbon to nitrogen can be used to constrain original sources of OM within a sediment sample (Bertrand et al., 2009). Fragments of OM are derived from two end-member sources: aquatic or terrestrial OM, which are characterised by low (varying from 4 – 12) and high C/N ratios (typically > 20), respectively (Meyers, 1994; Meyers and Lallier-Verges, 1998; Sterner and Elser, 2002; Bertrand et al., 2009). The relative contributions of OM from terrestrial and marine end-members to sediment samples recovered from the Sobrarbe Deltaic Complex

could be used as a proxy for the dominant process-regime in operation at the clinoform rollover. The depositional facies associated with a river-dominated shelf process-regime would be expected to have relatively high C/N ratios. In this circumstance, OM would be derived primarily from terrestrial plant debris transported into the shelf- and slope-setting via hyperpycnal flows. In contrast, the depositional facies associated with a wave-dominated shelf process-regime would be expected to have relatively low C/N ratios, as OM would be derived primarily from marine phytoplankton. As such, the C/N ratios would provide an independent methodology of testing the interpretations of process-regime variability in the shelf-setting. Particularly, the C/N ratios would be useful in determining to what extent sediment delivery from the terrestrial environment is curtailed during the process of autogenic switching from river- to wave-dominated shelf process-regimes.

Additionally, C/N ratios and the total organic carbon content (TOC) could be used as a means of testing the interpreted differentiation of two families of hyperpycnal flow deposits within the Sobrarbe Deltaic Complex. These geochemical indices could be used as proxies for precipitation and terrestrial run-off (see Meyers, 1994; Meyers and Lallier-Verges, 1998; Sterner and Elser, 2002; Bertrand et al., 2009); heightened precipitation would be associated with relatively higher TOC content and higher C/N ratios. As such, hyperpycnal flow deposits interpreted to be 'sustained' or 'episodic' (see Chapter Five, Manuscript Three) would be expected to have relatively lower and relatively higher C/N ratios, respectively. These palaeoclimatic proxies could then be used to infer variations in Eocene orbital cyclicity, relating to the precessional influence on patterns of precipitation (e.g., Berger, 1978; Kutzbach and Otto-Bliesner, 1982), which would provide a potential mechanism of regulating sediment transport (cf. Middle Eocene, Ainsa Basin; Cantalejo and Pickering, 2014).

6.3.5 Conclusions

In summary, the grain character datasets presented in this thesis provide valuable archives of sedimentary fabric, tied to clinothem architecture, at both interclinothem and intraclinothem scales. At present these datasets provide the only examples of quantitative, high-resolution grain character sampling within genetically linked clinothem sequences. However, these datasets have the potential to be advanced through the incorporation of samples recovered from dip- and strike-parallel outcrop and core examples. Additionally, geochemical datasets could be integrated with grain character datasets to test or strengthen interpretations. However, in the broadest sense, the major research endeavour would be to extend these grain character datasets and to develop new datasets from other clinothems. This would involve data-collection from additional core and outcrop examples, from a variety of clinothem

systems, which vary by setting (e.g., intrashelf versus basin-margin) and location (e.g., latitude, climatic conditions) to produce a database of grain character statistics. This database would find application in the numerical modelling of sedimentary systems to predict the distribution of reservoir quality of mature and frontier hydrocarbon systems, and would provide insights into the natural variability of these systems and the controls upon their development.

Chapter 7 References

Adams, E.W., and Schlager, W., 2000, Basic types of submarine slope curvature: *Journal of Sedimentary Research*, v. 70, p. 814-828.

Ainsworth, R. B., Flint, S.S., and Howell, J.A., 2008, Predicting coastal depositional style: Influence of basin morphology and accommodation to sediment supply ratio within a sequence-stratigraphic framework, in Hampson, G.J., Steel, R.J., Burgess, P.M., and Dalrymple, R.W., eds., *Recent Advances in Models of Shallow-Marine Stratigraphy: SEPM Special Publication 90*, p. 237-263.

Ainsworth, R.B., Vakarelov, B.K., and Nanson, R.A., 2011, Dynamic spatial and temporal prediction of changes in depositional processes on clastic shorelines: toward improved subsurface uncertainty reduction and management: *American Association of Petroleum Geologists, Bulletin*, v. 95, p. 267-297.

Allen, P.A., 1997, *Earth Surface Processes*, Blackwell, London.

Allen, P.A., 2005, Striking a chord: *Nature*, v. 434, p. 961.

Allen, P.A., 2008, From landscapes into geological history: *Nature*, v. 451, p. 274-276.

Allen, G. P., and Posamentier, H. W., 1994, Transgressive facies and sequence architecture in mixed tide and wave-dominated incised valleys: example from the Gironde estuary, France, in Dalrymple, R.W., Boyd, R.J., and Zaitlin, B.A., eds., *Incised valley systems: Origin and sedimentary Sequences. Society of Sedimentary Geology Special Publication*, v. 51, p. 226-240.

Amorosi, A., 1997, Detecting compositional, spatial, and temporal attributes of glaucony: a tool for provenance research: *Sedimentary Geology*, v. 109, p. 135-153.

Amorosi, A., Centineo, M. C., Colalongo, M. L., and Fiorini, F., 2005, Millennial-scale depositional cycles from the Holocene of the Po Plain, Italy: *Marine Geology*, v. 222, p. 7-18.

Amorosi, A., Centineo, M. C., Colalongo, M. L., Pasini, G., Sarti, G., and Vaiani, S. C., 2003, Facies architecture and latest Pleistocene–Holocene depositional history of the Po Delta (Comacchio area), Italy: *The Journal of Geology*, v. 111, p. 39-56.

- Amorosi, A., and Milli, S., 2001, Late Quaternary depositional architecture of Po and Tevere river deltas (Italy) and worldwide comparison with coeval deltaic successions: *Sedimentary Geology*, v. 144), p. 357-375.
- Ando, H., Oyama, M., and Nanayama, F., 2014, Data report: grain-size distribution of Miocene successions IODP Expedition 313 Sites M0027, M0028 and M0029, New Jersey shallow shelf, in Mountain, G., Proust, J.-N., McInroy, D., Cotterill, C., and the Expedition 313 Scientists: *Proceedings of the Integrated Ocean Drilling Program*, vol. 313.
- Anell, I., and Midtkandal, I., 2015, The quantifiable clinothem- types, shapes and geometric relationships in the Plio-Pleistocene Giant Foresets Formation, Taranaki Basin, New Zealand: *Basin Research*, v. 29, p. 277-297.
- Anell, I., and Midtkandal, I., 2017, The quantifiable clinothem – types, shapes and geometric relationships in the Plio-Pleistocene Giant Foresets Formation, Taranaki Basin, New Zealand: *Basin Research*, v. 29, p. 277-297.
- Armitage, J.J., Duller, R.A., Whittaker, A.C. and Allen, P.A., 2011, Transformation of tectonic and climatic signals from source to sedimentary archive: *Nature Geoscience*, v. 4, p. 231–235.
- Asquith, D.O., 1970, Depositional topography and major marine environments, Late Cretaceous, Wyoming: *American Association of Petroleum Geologists Bulletin*, v. 54, p. 1184–1224.
- Austin, J.A., and 27 others, 1998, Initial reports of the Ocean Drilling Program, Leg 174A: College Station, Texas, Ocean Drilling Program, p. 324.
- Barrett, B.J., Hodgson, D.M., Collier, R.E.L., and Dorrel, R.M., 2018, Novel 3D sequence stratigraphic numerical model for syn-rift basins: Analysing architectural responses to eustasy, sedimentation and tectonics: *Marine and Petroleum Geology*, v. 92, p. 270-284.
- Bates, C.C., 1953, Rational theory of delta formation, *American Association of Petroleum Geologists Bulletin*, v. 37, p. 2119–2162.

Battarbee, R.W., 1986, Diatom analysis, in Berglund, B. E., ed., *Handbook of Holocene Palaeoecology and Palaeohydrology*: Toronto, John Wiley and Sons, p. 527-570.

Battarbee, R.W., Jones, V.J., Flower, R.J., Cameron, N.G., and Bennion, H., 2001, Diatoms, in Smol, J.P., Birks, H.J.B. and Last, W.M., eds., *Tracking Environmental Change Using Lake Sediments, Volume 3: Terrestrial, Algal and Siliceous Indicators*: Dordrecht, Kluwer Academic Publishers, v. 3, p. 155-202.

Beelen, D., Jackson, C.A.L., Patruno, S., Hodgson, D.M., and Trabuco Alexandre, J.P., 2018, Rising not falling? Differential compaction of shelf-edge trajectories and clinothem geometries, in press, DOI: [10.31223/osf.io/8a93m](https://doi.org/10.31223/osf.io/8a93m).

Berger, A., 1978, Long-term variations of caloric insolation resulting from the Earth's orbital parameters: *Quaternary Research*, v. 9, p. 139-167.

Bertrand, S., Sterken, M., Vargas-Ramirez, L., De Batist, M., Vyverman, W., Lepoint, G., and Fagel, N., 2009, Bulk organic geochemistry of sediments from Puyehue Lake and its watershed (Chile, 40°S): Implications for paleoenvironmental reconstructions: *Journal of Palaeolimnology*, v. 294, p. 56-71.

Bhattacharya, J.P., 2006, Deltas, in Walker, R.G., and Posamentier, H., eds., *Facies Models Revisited*: Society for Sedimentary Geology (SEPM) Special Publication, v. 84, p. 237-292.

Bhattacharya, J.P., and Giosan, L., 2003, Wave-influenced deltas: geomorphological implications for facies reconstruction: *Sedimentology*, v. 50, p. 187-210.

Bhattacharya, J.P., and Walker, R.G., 1992, Deltas, in Walker, R.G., and James, N.P., eds., *Facies Models: Response to Sea Level Change*: St. John's, Newfoundland, Geological Association of Canada, p. 157-177.

Blott, S.J., and Pye, K., 2001, GRADISTAT: a grain-size distribution and statistics package for the analysis of unconsolidated sediments: *Earth Surface Processes and Landforms*, v. 26, p. 1237-1248.

Bouma, A.H., 1962, *Sedimentology of Some Flysch Deposits: A Graphic Approach to Facies Interpretation*. Elsevier, Amsterdam. 168.

Bowman, A.P., and Johnson, H.D., 2014, Storm-dominated shelf-edge delta successions in a high accommodation setting: The palaeo-Orinoco Delta (Mayaro Formation), Columbus Basin, South-East Trinidad: *Sedimentology*, v. 61, p. 792-835.

Boyd, R., Dalrymple, R. W., and Zaitlin, B. A., 1992, Classification of clastic coastal depositional environments: *Sedimentary Geology*, v. 80, p. 139-150.

Boyd, R., Dalrymple, R. W., and Zaitlin, B. A., 2006, Estuarine and incised valley facies models, in Posamentier, H.W., and Walker, R.G., eds., *Facies models revisited: Society for Sedimentary Geology Special Publication 84*, p. 171-235.

Boyd, R., Ruming, K., Goodwin, I., Sandstrom, M., and Schröder-Adams, C., 2008, Highstand transport of coastal sand to the deep ocean: a case study from Fraser Island: *Southeast Australia Geology*, v. 36, p. 15-18.

Brenchley, P.J., and Newall, G., 1977, The significance of contorted bedding in the Upper Ordovician sediments of the Oslo region, Norway: *The Journal of Sedimentary Petrology*, v. 47, p. 819-833.

Bridge, J.S., 1984, Large-scale facies sequences in alluvial overbank environments: *Journal of Sedimentary Research*, v. 54, p. 85-170.

Bridge, J. S., Smith, N.D., Trent, F., Gabel, S. L. and Bernstein, P. (1986) Sedimentology and morphology of a low-sinuosity river: Calamus River, Nebraska Sand Hills. *Sedimentology*, **33**, 851-870.

Brooks, H.L., Hodgson, D.M., Brunt, R.L., Peakall, J., Hofstra, M., and Flint, S.S., 2018, Deep-water channel-lobe transition zone dynamics: Processes and depositional architecture, an example from the Karoo Basin, South Africa: *Geological Society of America Bulletin*, v. 130, p. 1723-1746.

Browning, J.V., Miller, K.G., McLaughlin, P.P., Kominz, M.A., Sugarman, P.J., Monteverde, D., Feigenson, M.D., and Hernández, J.C., 2006, Quantification of the effects of eustasy, subsidence, and sediment supply on Miocene sequences, mid-Atlantic margin of the United States: Geological Society of America, Bulletin, v. 118, p. 567-588.

Browning, J.V., Miller, K.G., Sugarman, P.J., Barron, J., McCarthy, F.M.G., Kulhanek, D.K., Katz, M.E. and Feigenson, M.D., 2013, Chronology of Eocene-Miocene sequences on the New Jersey shallow shelf: Implications for regional, interregional, and global correlations: Geosphere, v. 9, p. 1434-1456.

Brunet, M.F., 1986, The influence of the Pyrenees on the development of the adjacent basins: Tectonophysics, v. 129, p. 343-354.

Bullimore, S., Henriksen, S., Liestøl, F.M., and Helland-Hansen, W., 2005, Clinoforms stacking patterns, shelf-edge trajectories and facies associations in tertiary coastal deltas, offshore Norway: implications for the prediction of lithology in prograding systems: Norwegian Journal of Geology, v. 85, p. 167-187.

Burgess, P.M., and Hovius, N., 1998, Rates of delta progradation during highstands: consequences for timing of deposition in deep-marine systems: Geological Society of London, Journal, v. 155, p. 217-222.

Burgess, P.M., and Steel, R., 2008, Stratigraphic forward modelling of basin-margin clinoform systems: implications for controls on topset and shelf width and timing of formation of shelf-edge deltas, in Hampson, G.J., Steel, R.J., Burgess, P.M., Dalrymple, R.W., eds., Recent Advances in Models of Siliciclastic Shallow-Marine Stratigraphy, Society for Sedimentary Geology Special Publication 90, p. 35-45.

Burns, C.E., Mountney, N.P., Hodgson, D.M., and Colombera, L., 2017, Anatomy and dimensions of fluvial crevasse-splay deposits: Examples from the Cretaceous Castlegate Sandstone and Neslen Formation, Utah, U.S.A.: Sedimentary Geology, v. 351, p. 21-35.

Cantalejo, B., and Pickering, K.P., 2014, Climate forcing of fine-grained deep-marine systems in an active tectonic setting: Middle Eocene, Ainsa Basin, Spanish Pyrenees: Palaeogeography, Palaeoclimatology, Palaeoecology, v. 410, p. 351-371.

Carvajal, C., and Steel, R., 2006, Thick turbidite successions from supply-dominated shelves during sea-level highstand: *Geology*, v. 34, p. 665-668.

Carvajal, C., and Steel, R., 2009, Shelf-edge architecture and bypass of sand to deep water: influence of shelf-edge processes, sea level and sediment supply: *Journal of Sedimentary Research*, v. 79, p. 652-672.

Carvajal, C., Steel, R., and Petter, A., 2009, Sediment supply: The main driver of shelf-margin growth: *Earth-Science Reviews*, v. 96, p. 221-248.

Castelltort, S., and Van Den Driessche, G., 2003, How plausible are high-frequency sediment supply-driven cycles in the stratigraphic record?: *Sedimentary Geology*, v. 157, p. 3-13.

Cattaneo, A., Trincardi, F., Asioli, A., and Correggiari, A., 2007, The western Adriatic shelf clinoform: energy-limited bottomset: *Continental Shelf Research*, v. 27, p. 506-525.

Catuneanu, O., Abreu, V., Bhattacharya, J.P., Blum, M.D., Dalrymple, R.W., Eriksson, P.G., Fielding, C.R., Fisher, W.L., Galloway, W.E., Gibling, M.R., Giles, K.A., Holbrook, K.A., Jordon, J.M., Kendall, R., Macurda, C.G. St., Macurda, C.B., Martinsen, O.J., Miall, A.D., Neal, J.E., Nummedal, D., Pomar, L., Posamentier, H.W., Pratt, B.R., Sarg, J.F., Shanley, K.W., Steel, R.J., Strasser, A., and Tucker, M.E.C., 2009, Towards the standardization of sequence stratigraphy: *Earth- Science Reviews*, v. 92, p. 1-33.

Charvin, K., Hampson, G.J., Gallagher, K.L., and Labourdette, R., 2010, Intra-parasequence architecture of an interpreted asymmetrical wave-dominated delta: *Sedimentology*, v. 57, p. 760-785.

Chayes, F., 1950, On the bias of grain-size measurements made in thin-section: *The Journal of Geology*, v. 58, p. 156-160.

Chikita, K., 1990, Sedimentation by river-induced turbidity currents: field measurements and interpretation: *Sedimentology*, v. 37, p. 891-905.

Chen, S., Steel, R., Olariu, C., Li, S., 2018, Growth of the paleo-Orinoco shelf margin prism: Process-regimes, delta evolution, and sediment budget beyond the shelf edge: *Geological Society of America, Bulletin*, v. 130, p. 35-63.

Coe, A. L., Bosence, D.W.J., Church, K.D., Flint, S.S., Howell, J.A., Wilson, R.C.L., 2003, *The Sedimentary Record of Sea Level Change*: Cambridge, UK, Cambridge University Press and the Open University, p. 288-340.

Coleman, J.M., Prior, D.B., and Lindsay, J.F., 1983, Deltaic influences on shelf edge instabilities processes, in Stanley, D.J., and Moore, G.T., eds., *The Shelf break, Critical Interface on Continental Margins: Society of Economic Palaeontologists and Mineralogists, Special Publication*, 33, p. 121-137

Coleman, J. M., and L. D. Wright, 1975, Modern river deltas: Variability of processes and sand bodies, in Broussard, M.L., ed., *Deltas: Models for exploration: Houston, Texas*, Houston Geological Society, p. 99–149.

Coleman, J.M., 1988, Dynamic changes and processes in the Mississippi River delta: *Geological Society of America Bulletin*, v. 100, p. 999-1015.

Collinson, J.D., Mountney, N. P. and Thompson, D. B., 2006, *Sedimentary Structures*. 3rd edition, Terra Publishing, Harpenden, 292 pp.

Correggiari, A., Cattaneo, A., and Trincardi, F., 2005, The modern Po Delta system: lobe switching and asymmetric prodelta growth: *Marine Geology*, v. 222, p. 49-74.

Cosgrove, G.I.E., Hodgson, D.M., Poyatos-Moré, M., Mountney, N.P., McCaffrey, W.M.D., 2018, Filter or conveyor? Establishing relationships between clinoform rollover trajectory, sedimentary process-regime, and grain character within intrashelf clinotherms, offshore New Jersey, U.S.A.: *Journal of Sedimentary Research*, v. 88, p. 917-941.

Cosgrove, G.I.E., Hodgson, D.M., M., Mountney, N.P., McCaffrey, W.M.D., 2019, High-resolution correlations of strata within a sand-rich sequence clinothem using grain fabric data, offshore New Jersey, USA.: accepted *Geosphere*

Cosgrove, G.I.E., Poyatos-Moré, M., Lee, D., Hodgson, D.M., McCaffrey, W.M.D., Mountney, N.P., Grain Character and Process-Regime Change Recorded down Clinothem Slope Profiles: in review *Sedimentology*

Covault, J.A., and Fildani, A., 2014, Continental shelves as sediment capacitors or conveyors: source-to-sink insights from the tectonically active Oceanside shelf, southern California, USA, in Chiocci, F.L., and Chivas, A.R., eds., *Continental Shelves of the World: Geological Society of London, Memoirs* 41, p. 315-326.

Covault, J.A., Normark, W.R., Romans, B.W., and Graham, S.A., 2007, Highstand fans in the California borderland: the overlooked deepwater depositional systems: *Geology*, v. 35, p. 783-786.

Covault, J.A., and Graham, S.A., 2010, Submarine fans at all sea-level stands: tectono-morphologic and climatic controls on terrigenous sediment delivery to the deep sea: *Geology*, v. 38, p. 939-942.

Crabaugh, J.P. and Steel, R.J., 2004, Basin-floor fans of the Central Tertiary Basin, Spitsbergen: relationship of basin-floor sand-bodies to prograding clinoforms in a structurally active basin: *Geological Society of London Special Publication*, v. 222, p. 187-208.

Cummings, D.I., Arnott, R.C.W., and Hart, B.S., 2006, Tidal signatures in a shelf margin delta: *Geology*, v. 34, p. 249-252.

Dalrymple, R.W., 1992, Tidal depositional systems, in Walker, R.G., and James, N.P., Eds., *Facies Models: Response to Sea-Level Change: Geological Association of Canada*, p. 195-218.

Davis, R.A., and Hayes, M.O., 1984, What is a wave-dominated coast?: *Marine Geology*, v. 60, p. 313-329.

DeFederico, A., 1981, La sedimentacion de talud en el sector occidental de la cuenca Paleogena de Ainsa, Autonoma de Barcelona: *Publicaciones de Geolocalionia*, v. 12, p. 270.

Deibert, J.E., Benda, T., Løseth, T., Schellpeper, M., and Steel, R.J., 2003, Eocene clinoform growth in front of a storm-wave-dominated shelf, Central Basin, Spitsbergen: No significant sand delivery to deepwater area: *Journal of Sedimentary Research*, v. 23, p. 546-558.

Densmore, A.L., Allen, P.A., and Simpson, G., 2007, Development and response of a coupled catchment fan system under changing tectonic and climatic forcing: *Journal of Geophysical Research- Earth Surfaces*, v. 112, v. 16.

- Dixon, J.F., Steel, R.J., and Olariu, C., 2012a, Shelf-edge delta regime as a predictor of the deep-water deposition: *Journal of Sedimentary Research*, v. 82, p. 681-687.
- Dixon, J.F., Steel, R.J., and Olariu, C., 2012b, River-dominated shelf-edge deltas: delivery of sand across the shelf break in the absence of slope incision: *Sedimentology*, v. 59, p. 1133-1157.
- Donovan, A., 2003, Depositional topography and sequence development, in: Roberts, H.H., Rosen, N.C., Fillon, R.H., and Anderson, J.B., eds., *Shelf margin deltas and linked down slope petroleum systems: Global significance and future exploration potential: Society for Sedimentary Geology Gulf Coast Section Special Publication*, p. 493-522.
- Dott, R.J., and Bourgeois, J., 1982, Hummocky stratification: Significance of its variable bedding sequences: *Geological Society of America Bulletin*, v. 93, p. 663-680.
- Dreyer, T., Fält, L.M., Høy, T., Knarud, R., Steel, R.J., and Cuevas, J.L., 1993, Sedimentary architecture of field analogue for reservoir information (SAFARI): a case study of the fluvial Escanilla Formation, Spanish Pyrenees, in: Flint, S., Bryant, I.D., eds., *The Geological Modelling of Hydrocarbon Reservoirs and Outcrop Analogue: International Association of Sedimentology, Special Publication 15*, p. 57-80.
- Dreyer, T., Corregidor, J., Arbues, P., and Puigdefabregas, C., 1999, Architecture of the tectonically influenced Sobrarbe deltaic complex in the Ainsa Basin, northern Spain: *Sedimentary Geology*, v. 127, p. 127-169.
- Dreyer, T., Whitaker, M., Dexter, J., Flesche, H., and Larsen, E., 2005, From spit system to tide dominated delta: integrated reservoir model of the upper Jurassic Sognefjord Formation on the Troll West Field, in Doré, A.G., and Vining, G., *Petroleum Geology of North-West Europe and Global Perspectives: Proceedings of the 6th Petroleum Geology Conference*, Geological Society of London, London, p. 1-26.
- Driscoll, N. W., and Karner, G. D., 1999, Three-dimensional quantitative modeling of clinoform development: *Marine Geology*, v. 154, p. 383-398.
- Droz, L., Marsset, T., Ondréas, H., Lopez, M., Savoye, B., and Spy-Anderson, F. L., 2003, Architecture of an active mud-rich turbidite system: The Zaire Fan (Congo-Angola margin

southeast Atlantic): Results from ZaiAngo 1 and 2 cruises: American Association of Petroleum Geologists Bulletin, v. 87, p. 1145-1168.

Edwards, M.B., 1981, Upper Wilcox Rosita delta system of South Texas: growth-faulted shelf-edge deltas: American Association of Petroleum Geologists Bulletin, v. 65, p. 54-73.

Einsele, G., 1996, Event deposits: the role of sediment supply and relative sea level changes—overview: Sedimentary Geology, v. 104, p. 11–37.

Elliott, T., 1986, Deltas, in Reading, H.G., ed., Sedimentary Environments and Facies, Oxford, U.K., Blackwell Scientific Publications, p. 113–154.

Embry, A.F., 2002, Transgressive-Regressive (T-R) Sequence Stratigraphy, in Armentrout, J., and Rosen, N., eds., Sequence Stratigraphic Models for Exploration And Production: Evolving Methodology, Emerging Models and Application Histories, 22nd Annual Gulf Coast Society for Sedimentary Geology Special Publication, 151-172.

Embry, A. and Johannessen, E.P., 1992, T-R sequence stratigraphy, facies analysis and reservoir distribution in the uppermost Triassic-lower Jurassic succession, western Sverdrup Basin, Arctic Canada, in Vorren, T.O., Bergsager, E., Dahl-Stamnes, Ø.A., Holter, E., Johansen, B., Lie, E., and Lund, T.B., eds., Arctic Geology and Petroleum Potential: Norwegian Petroleum Society Special Publication 2, p. 121-146.

Ethridge, F.G., Jackson, T.J. and Youngberg, A.D., 1981, Floodbasin sequence of a fine-grained meander belt subsystem: the coal-bearing Lower Wasatch and Upper Fort Union Formations, Southern Powder River Basin, Wyoming, in Ethridge, F.G., ed., Recent and Ancient Nonmarine Depositional Environments: Society of Economic and Palaeontologists and Mineralogists Special Publication 31, p. 191-209.

Expedition 313 Scientists, 2010, Site M0028, in Mountain, G.S., Proust, J-N., McInroy, D., Cotteril, C., and the Expedition 313 Scientists, 2010, Proceedings of the Integrated Ocean Drilling Program, Expedition 313: Tokyo, Integrated Ocean Drilling Program Management, Inc.

Fairbanks, R.G., 1989, A 17,000-year glacio-eustatic sea-level record: influence of glacial melting rates on the Younger Dryas event and deep-ocean circulation: *Nature*, v. 342, p. 637-641.

Farrell, K.M., 1987, Sedimentology and facies architecture of overbank deposits of the Mississippi River, False River region, Louisiana. In Ethridge, F.G., and Flores, R.M., *Recent Developments in Fluvial Sedimentology: Society of Economic and Palaeontologists and Mineralogists Special Publication 39*, p. 111-120.

Fernández, O., Muñoz, J.A., Arbues, P., and Marzo, M., 2004, Three dimensional reconstruction of Geological surfaces: An example of growth strata and turbidite systems from the Ainsa Basin (Pyrenees, Spain): *American Association of Petroleum Geologists Bulletin*, v. 88, p. 1049-1068.

Fildani, A., Clark, J., Covault, J.A., Power, B., Romans, B.W., and Aiello, I.W., 2018, Muddy sand and sandy mud on the distal Mississippi fan: Implications for lobe depositional processes: *Geosphere*, v. 14, p. 1051-1066.

Field, M.E., and Roy, P.S., 1984, Offshore transport and sand-body formation: evidence from a steep, high-energy shoreface, southeastern Australia: *Journal of Sedimentary Petrology*, v. 54, p. 1292-1302.

Fleming, R.H., and Revelle, R., 1939, Physical Processes in the Ocean, in Trask, P.D., ed., *Recent Marine Sediments: Tulsa, Oklahoma, American Association of Petroleum Geologists*, p. 48-141.

Folk, R.L., and Ward, W.C., 1957, Brazos River bar: a study in the significance of grain-size parameters: *Journal of Sedimentary Petrology*, v. 27, p. 3-26.

Fongngern, R., Olariu, C., Steel, R.J., and Krézsek, C., 2016, Clinoform growth in a Miocene, Para-tethyan deep lake basin: thin topsets, irregular foresets and thick bottomsets: *Basin Research*, v. 28, p. 770-795.

Frey, M.H., and Payne, D.A., 1996, Grain-Size effect on Structure and Phase Transformations for Barium Titanate: *Physical Review*, v. 54, p. 3158-3168.

Friedrichs, C.T., and Wright, L.D., 2004, Gravity-driven sediment transport on the continental shelf: implications for equilibrium profiles near river mouths: *Coastal Engineering Journal*, v. 51, p. 795–811.

Galloway, W.E., 1975, Process framework for describing the morphologic and stratigraphic evolution of deltaic depositional systems, in Broussard, M.L., ed., *Deltas: Models for Exploration*: Houston Geological Society, p. 87-98.

Galloway, W.E., 1989, Genetic stratigraphic sequences in basin analysis 1: architecture and genesis of flooding-surface bounded depositional units: *American Association of Petroleum Geologists Bulletin*, v. 73, p. 125-142.

Galloway, W.E., 1998, Genetic stratigraphic sequences in basin-analysis I: Architecture and genesis of flooding bounded depositional units: *American Association of Petroleum Geologists Bulletin*, v. 73, p. 125-142.

Galloway, W.E., 1998, Siliciclastic slope and base-of-slope depositional systems: component facies, stratigraphic architecture, and classification: *American Association of Petroleum Geologists Bulletin*, v. 82, p. 569–595.

Gamero, H., Perdomo, J.L., Laporte, L., Rodriguez, F., Rahn, T.C. and Isakson, C., 2006, Three-dimensional reservoir and simulation modelling workflow of hyperpycnal systems: a case study of LAG-3047, Block X, Misoa Formation, Maracaibo Basin, Venezuela: *Integrating Technology and Business Practices*, 26th Annual Gulf Coast Society for Sedimentary Geology Special Publication, p. 223–270.

Gammon, P.R., Neville, L.A., Patterson, R.T., Savard, M.M., and Swindles, G.T., 2017, A log-normal spectral analysis of inorganic grain-size distributions from a Canadian boreal lake core: Towards refining depositional process proxy data from high latitude lakes: *Sedimentology*, v. 64, p. 609-630.

Gani, M.R., and Bhattacharya, J.P., 2007, Basic building blocks and process variability of a Cretaceous delta: internal facies architecture reveals a more dynamic interaction of river, wave, and tidal processes than is indicated by external shape: *Journal of Sedimentary Research*, v. 77, p. 284-302.

Gersib, G.A., and McCabe, P.J., 1981, Continental coal-bearing sediments of the Port Hood Formation (Carboniferous), Cape Linzee, Nova Scotia, Canada: *Society of Economic Palaeontologists and Mineralogists* 31, p. 95-108.

Gilbert, G.K., 1885, The topographic feature of lake shores: U.S. Geological Survey, Annual Report, v. 5, p. 104-108.

Glørstad-Clark, E., Faleide, J.I., Lundschie, B.A., Nystuen, J.P., 2010, Triassic seismic sequence stratigraphy and paleogeography of the Western Barents Sea area: *Marine and Petroleum Geology*, v. 27, p. 1448-1475.

Glørstad-Clark, E., Birkeland, E.P., Nystuen, J.P., Faleide, J.I., Midtkandal, I., 2011, Triassic platform-margin deltas in the Western Barents Sea: *Marine and Petroleum Geology*, v. 28, p. 1294- 1314.

Goldstein, G.I., Newbury, D.E., Echlin, P., Joy, D.C., Fiori, C., and Lifshin, E., 1981, Scanning electron microscopy and x-ray microanalysis: New York, Plenum Press, ISBN: 0-306-40768-X.

Gomis-Cartesio, L.E., Poyatos-Moré, M., Flint, S.S., Hodgson, D.M., Brunt, R.L., and Wickens, H.D.V., 2017, Anatomy of a mixed-influence shelf edge delta, Karoo Basin, South Africa, in Hampson, G.J., Reynolds, A.D., Kostic, B., and Wells, M.R., eds., *Sedimentology of Paralic Reservoirs: Recent Advances: Geological Society of London Special Publications* 444, p. 393-418.

Gong, C., Steel, R.J., Wang, Y., Lin, C., and Olariu, C., 2016, Grain-size and transport regime at shelf edge as fundamental controls on delivery of shelf-edge sands to deepwater: *Earth-Science Reviews*, v. 157, p. 32-60.

Goodbred, S., and Saito, Y., 2011, Tide-dominated deltas, in Davis, R.A., Dalrymple, R.W., *Principles of Tidal Sedimentology*, 2012th Edition, Springer, New York

Gray, J., 1965, Extraction Techniques, in Kummel, B., and Raup, D., eds., *Handbook of Paleontological Techniques*, San Francisco: W. H. Freeman and Co, p.852.

Gray, A.B., Pasternack, G.B., and Watson, E.B., 2009, Hydrogen peroxide treatment effects on the particle size distribution of alluvial and marsh sediments: *The Holocene*, v. 20, 293-301.

Green, O.R., 2001, Disaggregation and Dispersal of Partially Consolidated and Unconsolidated Sediments, in: *A Manual of Practical Laboratory and Field Techniques in Palaeobiology*, Springer, Dordrecht, p. 127-137.

Greenman, N.N., 1951, On the bias of grain-size measurements made in thin-section: a discussion: *The Journal of Geology*, v. 59, p. 268-274.

Grundvåg, S.A., Johannessen, E.P., Helland-Hansen, W., and Plink-Björklund, P., 2014, Depositional architecture and evolution of progradationally stacked lobe complexes in the Eocene Central Basin of Spitsbergen: *Sedimentology*, v. 61, p. 535–569.

Hadler-Jacobsen, F., Johannessen, E.P., Ashton, N., Henriksen, S., Johnson, S.D., and Kristensen, J.B., 2005, Submarine fan morphology and lithology distribution: a predictable function of sediment delivery, gross shelf-to-basin relief, slope gradient and basin topography, in Dore, A.G., Vinin, B.A., Eds., *Petroleum Geology: North-west Europe and Global Perspectives: Proceedings of the 6th Petroleum Geology Conference*, Geological Society, London, p. 1121-1145.

Hall, M.T., 1997, *Sequence stratigraphy and early diagenesis: Unpublished PhD Thesis*, University of Manchester.

Hay, A.E., 1987, Turbidity currents and submarine channel formation in Rupert Inlet, British Columbia: The roles of continuous and surge-type flow: *Journal of Geophysical Research*, v. 92 p. 2883-2900.

Hampson, G.J., 2010, Sediment dispersal and quantitative stratigraphic architecture across an ancient shelf: *Sedimentology*, v. 57, p. 96–141.

Hampson, G.J., 2016, Towards a sequence stratigraphic solution set for autogenic processes and allogenic controls: Upper Cretaceous strata, Book Cliffs, Utah, USA: *Journal of the Geological Society*, v. 173, p. 817-836.

Hampson, G.J., Morris, J.E., and Johnson, H.D., 2015, Synthesis of time-stratigraphic relationships and their impact on hydrocarbon reservoir distribution and performance,

Bridport Sand Formation, Wessex Basin, UK, in Smith, D. G., Bailey, R. J., Burgess, P. M., and Fraser, A. J, eds., *Strata and Time: Probing the Gaps in Our Understanding*. Geological Society, London, Special Publications, 404, p. 199–222.

Hansen, L.J.J., Daoussi, R., Vervaet, C., Remon, J.-P., and De Beer, T.R.M., 2015, *Freeze-Drying of Live Virus Vaccines: A Review: Vaccine*, v. 33, p. 5505-55019.

Harms, J.C., Southard, J.B., and Walker, R.G., 1982, *Structures and sequences in clastic rocks: Society for Sedimentary Geology (SEPM) Short Course 9*, p. 249.

Harris, A.G., and Sweet, W.C., 1989, Mechanical and chemical techniques for separating microfossils from rock, sediment and residue matrix, in Feldman, R.M., Chapman, R.E., and Hannibal, J.T., eds., *Paleotechniques: The Paleontological Society Special Publication 4*, p. 70-86.

Harris, P.T., Hughes, M.G., Baker, E.K., Dalrymple, R.W., and Keene, J.B., 2004, Sediment transport in distributary channels and its export to the pro-deltaic environment in a tidally dominated delta: Fly River, Papua New Guinea: *Continental Shelf Research*, v. 24, p. 2431–2454.

Harris, A.D., Covault, J.A., Madof, A.S., Sun, T., Sylvester, Z., Granjeon, D., 2016, Three-dimensional numerical modeling of eustatic control on continental-margin sand distribution: *Journal of Sedimentary Research*, v. 86, p. 1434-1443.

Helland-Hansen, W., 1990, Sedimentation in Paleogene foreland basin, Spitsbergen, *American Association of Petroleum Geologists Bulletin.*, v. 74, p. 260–272.

Helland-Hansen, W., 1992, Geometry and facies of Tertiary clinothems, Spitsbergen: *Sedimentology*, v. 39, p. 1013-1029.

Helland-Hansen, W., 2010, Facies and stacking patterns of shelf-deltas within the Palaeogene Battfjellet Formation, Nordenskiöld Land, Svalbard: implications for subsurface reservoir prediction: *Sedimentology*, v. 57, p. 190-208.

Helland-Hansen, W., and Gjelberg, J.G., 1994, Conceptual basis and variability in sequence stratigraphy; a different perspective: *Sedimentary Geology*, v. 92, p. 31-52.

Helland-Hansen, W., and Gjelberg, H., 2012, Towards a hierarchical classification of clinofolds: American Association of Petroleum Geologists Annual Convention and Exhibition, April 22-25, 2012, Long Beach, California, U.S., Search and Discovery Article #90142.

Helland-Hansen, W., and Hampson, G.J., 2009, Trajectory analysis: concepts and applications: *Basin Research*, v. 21, p. 454-483.

Helland-Hansen, W., and Martinsen, O.J., 1996, Shoreline trajectories and sequences: description of variable depositional-dip scenarios: *Journal of Sedimentary Research*, v. 66, p. 670-688.

Helland-Hansen, W., and Steel, R.J., 2012, Trajectory analysis: concepts and analysis: *Basin Research*, v. 21, p. 454-483.

Helland-Hansen, W., Steel, R.J., and Sømme, T.O., 2012, Shelf genesis revisited: *Journal of Sedimentary Research*, v. 82, p.133-148.

Henriksen, S., Hampson, G.J., Helland-Hansen, W., Johannessen, E.P., Steel, R.J., 2009, Shelf edge and shoreline trajectories, a dynamic approach to stratigraphic analysis: *Basin Research*, v. 21, p. 445-453.

Hernández-Molina, F.J., Somoza, L., and Lobo, F., 2000, Seismic stratigraphy of the Gulf of Cadiz continental shelf: a model for Late Quaternary very high-resolution sequence stratigraphy and response to sea-level fall, in Hunt, D., and Gawthorpe, R.L., eds., *Sedimentary Responses to Forced Regressions: Geological Society Special Publications*, 172, p. 329-362

Hesselbo, S.P., and Huggett, J.M., 2001, Glauconite in ocean-margin sequence stratigraphy (Oligocene-Pliocene, Offshore New Jersey, U.S.A.; ODP LEG 174A): *Journal of Sedimentary Research*, v. 71, p. 599-607.

Hiscott, R.N., 1994, Loss of capacity, not competence, as the fundamental process governing deposition from turbidity currents: *Journal of Sedimentary Research*, v. 64, p. 209-214.

Hiscott, R. N., 2001, Depositional sequences controlled by high rates of sediment supply, sea-level variations, and growth faulting: the Quaternary Baram Delta of northwestern Borneo: *Marine Geology*, v. 175, p. 67-102.

Hiscott, R.N., Pickering, K.T., Bouma, A.H., Hand, B.M., Kneller, B.C., Postma, G. and Soh, W., 1997, Basin-floor fans in the North Sea: sequence stratigraphic models vs. sedimentary Facies: discussion: *American Association of Petroleum Geologists*, v. 81, p. 662-665.

Hodgson, D.M., Browning, J.V., Miller, K.G., Hesselbo, S., Poyatos-Moré, Mountain, G.S., and Proust, J.-N., 2018, Sedimentology, stratigraphic context, and implications of Miocene bottomset deposits, offshore New Jersey, 2017: *Geosphere*, v. 14, p. 95-114.

Hodgson, D.M., Kane I.A., Flint, S.S., Brunt R.L., and Ortiz-Karpf, A., 2016, Time-transgressive confinement on the slope and the progradation of basin-floor fans: Implications for the sequence stratigraphy of deep-water deposits: *Journal of Sedimentary Research*, v. 86, p.73-86.

Houseknecht, D. W., Bird, K. J., and Schenk, C. J., 2009, Seismic analysis of clinoform depositional sequences and shelf-margin trajectories in Lower Cretaceous (Albian) strata, Alaska North Slope: *Basin Research*, v. 21, p. 644-654.

Hubbard, S.M., Fildani, A., Romans, B.W., Covault, J.A. and McHargue, T.R., 2010, High-relief slope clinoform development: insights from outcrop, Magallanes Basin, Chile: *Journal of Sedimentary Research*, v. 80, p. 357-375.

Huggett, J.M., and Gale, A.S., 1997, Petrology and paleoenvironmental significance of glaucony in the Eocene succession at Whitecliffe Bay, Hampshire Basin, UK: *Journal of the Geological Society*, v. 154, p. 897-912.

Hunt, D., and Tucker, M.E., 1992, Stranded parasequences and the forced regressive wedge systems tract: deposition during base-level fall: *Sedimentary Geology*, v. 81, p. 1-9.

ImageJ, v. 142, 2009, Research Services Branch, National Institute of Mental Health Bethesda, MD, USA

Ito, M., and Masuda, F., 1988, Late Cenozoic deep-sea to fan-delta sedimentation in an arc–arc collision zone, central Honshu, Japan: sedimentary response to varying plate tectonic regime, in Nemec, W., Steel, R.J., eds., *Fan Deltas: Sedimentology and Tectonic Settings*, Blackie and Son, Glasgow, UK, p. 400–418.

Jackson, W.E., 1964, Depositional topography and cyclic deposition in west-central Texas: *American Association of Petroleum Geologists*, v. 48, p. 317–328.

Jennette, D.C., Wawrzyniec, T., Fouad, D., Dunlap, D., Munoz, R., Barrera, D., Williams-Rojas, C., and Escamilla-Herra, A., 2003, Traps and turbidite reservoir characteristics from a complex and evolving tectonic setting, Veracruz Basin, southeastern Mexico: *American Association of Petroleum Geologists Bulletin*, v. 87, p. 1599-1622.

Jervey, M. T., 1988, Quantitative geological modelling of siliciclastic rock sequences and their seismic expressions, in Wilgus, C.K., Hastings, B.S., Ross, C.A., Posamentier, H.W., Van Wagoner, J.C. and Kendall, C.G.St.C., eds., *Sea-level changes: An integrated approach: Society of Economic Palaeontologists and Mineralogists Special Publication*, v. 42, p. 47-69.

Jiang, Z., and Liu, L., 2011, A pre-treatment method for grain-size analysis of red mudstones: *Sedimentary Geology*, v. 241, p. 13-21.

Johannessen, E.P., and Steel, R.J., 2005, Shelf-margin clinoforms and prediction of deepwater sands: *Basin Research*, v. 17, p. 521-550.

Johnson, S.D., Flint, S., Hinds, D., and Wickens, H.D.V, 2001, Anatomy, geometry and sequence stratigraphy of basin floor to slope turbidite systems, Tanqua Karoo, South Africa: *Sedimentology*, v. 48, no. 5, p. 987-1023.

Jones, G.E.D., Hodgson, D.M., and Flint, S.S., 2013, Contrast in the process response of stacked clinothems to the shelf-slope rollover: *Geosphere*, v. 9, p. 299-316.

Jones, G.E.D., Hodgson, D.M., and Flint, S.S., 2015, Lateral variability in clinoform trajectory, process-regime, and sediment dispersal patterns beyond the shelf-edge rollover in exhumed basin margin-scale clinothems: *Basin Research*, v. 27, p. 657-680.

Katz, M.E., Browning, J.V., Miller, K.G., Monteverde, D.H., Mountain, G.S., and Williams, R.H., 2013, Paleobathymetry and sequence stratigraphic interpretations from benthic foraminifera: Insights on New Jersey shelf architecture, IODP Expedition 313: *Geosphere*, v. 9, p. 1488-1513.

Kellerhals, R., Shaw, J., and Arora, V.K., 1975, On grain size from thin sections: *The Journal of Geology*, v. 83, p. 79-86.

Kellog, H.E., 1975, Tertiary stratigraphy and tectonism in Svalbard and continental drift: *American Association of Petroleum Geologists Bulletin*, v. 59, p. 465-485.

Kim, Y., Kim, W., Cheong, D., Muto, T., Pyles, D.R., 2013, Piping coarse-grained sediment to a deep water fan through a shelf-edge delta bypass channel: tank experiments: *Journal of Geophysical Research*, v. 118, p. 2279-2291.

Klausen, T.G. and Helland-Hansen, W., 2018, Methods for restoring and describing ancient clinoform surfaces: *Journal of Sedimentary Research*, v. 88, p. 241-259.

Kneller, B., 1995, Beyond the turbidite paradigm: physical models for deposition of turbidites and their implications for reservoir prediction, in: Hartley, A.J., and Prosser, D.J., eds., *Characterization of Deep Marine Clastic Systems: Geological Society Special Publication 94*, p. 31-49.

Kneller, B.C., and Branney, M.J., 1995, Sustained high-density turbidity currents and the deposition of thick ungraded sands: *Sedimentology*, v. 42, p. 607-616.

Kneller, B. and Buckee, C., 2000, The structure and fluid mechanics of turbidity currents: a review of some recent studies and their geological implications: *Sedimentology*, v. 47, p. 62-94.

Kolla, V., 1993, Lowstand deep-water siliclastic depositional systems: Characteristics and terminologies in sequence stratigraphy and sedimentology: *Bulletin des Centres de Recherche Exploration Production*, v. 17, p. 67-78.

Kolla, V., Biondi, P., Long, B., and Fillon, R., 2000, Sequence stratigraphy and architecture of the Late Pleistocene Lagniappe delta complex, northeast Gulf of Mexico: *Geological Society, London, Special Publications*, v. 172, p. 291-327.

Kolla, V., and Macurda, D.B. Jr., 1988, Sea-level changes and timing of turbidity-current events in deep-sea fan systems, in Wilgus, C.K., Hastings, B.S., Kendall, C.G.St.C., Posamentier, H.W., Ross, C.A., and Van Wagoner, J.C., eds., *Sea-Level Changes: An Integrated Approach*, Society for Sedimentary Geology Special Publication 42, p. 71-108.

Kolla, V., and Perlmutter, M. A., 1993, Timing of turbidite sedimentation of the Mississippi Fan: *American Association of Petroleum Geologists Bulletin*, v. 77, p. 1129-1141.

Kominz, M.A., Miller, K.G., Browning, J.V., Katz, M.E., and Mountain, G.S., 2016, Miocene relative sea level on the New Jersey shallow continental shelf and coastal plain derived from one-dimensional backstripping: A case for both eustasy and epeirogeny: *Geosphere*, v. 12, p. 1437-1456.

Koo, W.M., Olariu, C., Steel, R.J., Olariu, M.I., Carvajal, C.R., and Kim, W., 2016, Coupling between shelf-edge architecture and submarine fan growth style in a supply-dominated margin: *Journal of Sedimentary Research*, v. 88, p. 613-628.

Krassay, A. A., and Totterdell, J. M., 2003, Seismic stratigraphy of a large, Cretaceous shelf margin delta complex, offshore southern Australia: *American Association of Petroleum Geologists Bulletin*, v. 87, p. 935-963.

Krumbein, W.C., 1933, The dispersion of fine-grained sediments for mechanical analysis: *Journal of Sedimentary Petrology*, v. 3, p. 121-135.

Krumbein, W. C., 1940, Flood gravels of San Gabriel Canyon, California: *Geological Society of America Bulletin*, v. 51, p. 639-676.

Krumbein, W.C., 1941, Measurement and geological significance of shape and roundness of sedimentary particles: *Journal of Sedimentary Petrology*, v. 11, p. 64-72.

Krumbein, W.C., and Pettijohn, F.J., 1938, *Manual of Sedimentary Petrography*: *Geologiska Föreningen i Stockholm Förhandlingar*, v. 61, p. 197 - 225.

Krumbein, W.C., and Sloss, L.L., 1951, *Stratigraphy and Sedimentation*, San Fransisco: Freeman, p. 297-500.

Kuehl, S.A., Nittrouer, C.A., and DeMaster, D.J., 1986, Nature of sediment accumulation on the Amazon continental shelf: *Continental Shelf Research*, v. 6, p. 209–225.

Kutzbach, J.E., and Otto-Bliesner, B.L., 1982, The sensitivity of the African-Asian monsoonal climate to orbital parameter changes for 9000 years BP in a low-resolution general circulation model: *Journal of Atmospheric Science*, v. 39, p. 1177-1188.

Lamb, M.P., Myrow, P.M., Lukens, C., Houck, K., and Strauss, J., 2008, Deposits from wave-influenced turbidity currents: Pennsylvanian Minturn Formation, Colorado, USA: *Journal of Sedimentary Research*, v. 78, p. 480-498.

Lamb, M.P., McElroy, B., Kopriva, B., Shaw, J. and Mohrig, D., 2010, Linking river-flood dynamics to hyperpycnal-plume deposits: Experiments, theory, and geological implications: *Geological Society of America Bulletin*, v. 1222, p. 1389-1400.

Laugier, F.J., and Plink-Björklund, P., 2016, Defining the shelf edge and the three-dimensional shelf-edge to slope facies variability in shelf-edge deltas: *Sedimentology*, v. 63, p. 1280-1320.

Lebauer, L.R., 1964, Petrology of the Middle Cambrian Wolsey Shale of southwestern Montana: *Journal of Sedimentary Petrology*, v. 34, p. 503-511.

Li, Z., Bhattacharya, J., and Schieber, J., 2015, Evaluating along-strike variation using thin-bedded facies analysis, Upper Cretaceous Ferron Notom Delta, Utah: *Sedimentology*, v. 62, p. 2060-2089.

Li, W., Bhattacharya, J.P., and Wang, Y., 2011, Delta asymmetry: concepts, characteristics, and depositional models: *Petroleum Geoscience*, v. 8, p. 278–289.

Lowe, D.R., 1982, Sediment gravity flows: II. Depositional models with special reference to the deposits of high-density turbidity currents: *Journal of Sedimentary Petrology*, v. 52, p. 279-297.

Maceachern, J.A., Bann, K.L., Bhattacharya, J.P., and Howell, C.D., 2005, Ichnology of deltas: organism responses to the dynamic interplay of rivers, waves, storms, and tides, in Giosan, L., and Bhattacharya, J.P., eds., *River Deltas: Concepts, Models, and Examples*: Society for Sedimentary Geology Special Publication 83, p. 49-85.

Madof, A.S., Harris, A.D., and Connell, S.D., 2016, Nearshore along-strike variability: Is the concept of the systems tract unhinged?: *Geology*, v. 44, p. 315-318.

Martinsen, O. J., and Helland-Hansen, W., 1995, Strike variability of clastic depositional systems: Does it matter for sequence-stratigraphic analysis?: *Geology*, v. 23, p. 439-442.

Mateu-Vicens, G., Pomar, L. and Ferràndez-Cañadell, C. , 2011, Nummulitic banks in the upper Lutetian 'Buil level', Ainsa Basin, South Central Pyrenean Zone: the impact of internal waves: *Sedimentology*, v. 59, p. 527-552.

Matteucci, T. D., and Hine, A. C., 1987, Evolution of the Cape Fear Terrace: A complex interaction between the Gulf Stream and a paleo-shelf edge delta: *Marine Geology*, v. 77, p. 185-205.

Martinsen, O.J., Sømme, T.O., Thurmond, J.B., Helland-Hansen, W., and Lunt, I., 2011, Source-to-sink systems on passive margins: theory and practice with an example from the Norwegian continental margin: *Petroleum Geology: From Mature Basins to New Frontiers—Proceedings of the 7th Petroleum Geology Conference*, v. 7, p. 912-920.

Marzo, M., and Steel, R. J., 2000, Unusual features of sediment supply-dominated, transgressive-regressive sequences: Paleogene clastic wedges, SE Pyrenean foreland basin, Spain: *Sedimentary Geology*, v. 138, p. 3–15.

Mayall, M.J., Yeilding, C.A., Oldroyd, J.D., Pulham, A.J., and Sakurai, S., 1992, Facies in a shelf-edge delta an example from the subsurface of the Gulf of Mexico, Middle Pliocene, Mississippi Canyon, Block 109: *American Association of Petroleum Geologists Bulletin*, v. 76, p. 435–448.

McCracken, S.R., Compton, J., and Hicks, K., 1996, Sequence stratigraphic significance of glauconite-rich lithofacies at site 903, in Mountain, G.S., Miller, K.G., Blum, P., Poag, C.W., Twichell, D.C., eds., *Proceedings of the Ocean Drilling Program, Scientific Results*, v. 15, p. 171-187.

McCubbin, D.G., 1982, Barrier-island and strand-plain facies, in Scholle, P.A., and Spearing, D., eds., *Sandstone Depositional Environments: American Association of Petroleum Geologists, Memoir 31*, p. 247-279

Meade R. H., 1972, Sources and sinks of suspended matter on continental shelves, in Swift D. J. P., Duane D. B., and Pilkey O. H., eds., Shelf Sediment Transport, Dowden, Hutchinson and Ross, Stroudsburg, p. 249–262.

Meade R. H., 1982, Sources, sinks, and storage of river sediment in the Atlantic drainage of the United States: *Journal of Geology*, v.90, p.235–252.

Mellere, D., Plink-Björklund, P., Steel, R., 2002, Anatomy of shelf deltas at the edge of a prograding Eocene shelf margin, Spitsbergen: *Sedimentology*, v. 49, p. 1181-1206.

Mellere, D., Breda, A., Steel, R.J., 2003, Fluvially-incised shelf-edge deltas and linkage to upper-slope channels (Central Tertiary Basin, Spitsbergen), in Roberts, H.H., Rosen, N.C., Fillon, R.H., and Anderson, J.B., eds., Shelf-Margin Deltas and Linked Downslope Petroleum Systems; Global Significance and Future Exploration Potential: 23rd Annual Gulf Coast Society for Sedimentary Geology Special Publication, Houston, Texas, p. 231–266

Meyers, P. A., 1994, Preservation of elemental and isotopic source identification of sedimentary organic-matter: *Chemical Geology*, v. 114, p. 289-302.

Meyers, P.A., and Lallier-Verges, E., 1998, Lacustrine sedimentary organic matter records of Late Quaternary paleoclimates: *Journal of Paleoclimatology*, v. 21, p. 345-372.

Middleton, G.V., 1993, Sediment deposition from turbidity currents: *Annual Review of Earth and Planetary Science*, v. 21, p. 89-114.

Miller, K.G., and Mountain, G.S., 1994, Global sea-level change and the New Jersey margin, in Mountain, G.S., et al., eds., *Proceedings of the Ocean Drilling Program, Initial Reports, Volume 150*: College Station, Texas, Ocean Drilling Program, p. 11-20.

Miller, K.G., and Snyder, S.W., Eds, 1997, *Proceedings ODP Scientific Results, 150X*, College Station, TX (Ocean Drilling Program), 374 p.

Miller, K.G., Browning, J.V., Mountain, G.S., Bassetti, M.A., Monteverde, D., Katz, M.E., Inwood, J., Lofi, J. and Proust, J.-N., 2013a, Sequence boundaries are impedance contrasts: core–seismic–log integration of Oligocene–Miocene sequences, New Jersey shallow shelf: *Geosphere*, v. 9, p. 1257–1285.

Miller, K.G., Mountain, G.S., Browning, J.V., Katz, M.E., Monteverde, D., Sugarman, P.J., Ando, H., Bassetti, M.A., Bjerrum, C.J., Hodgson, D.M., Hesselbo, S., Karakaya, S., Proust, J-N., and Rabineau, M., 2013b, Testing sequence stratigraphic models by drilling Miocene foresets on the New Jersey Shallow Shelf: *Geosphere*, v. 9, p. 1236-1256.

Miller, K.G., Lombardi, C.J., Browning, J.V., Schmelz, W.J., Gallegos, G., Mountain, G.S., Baldwin, K.E., 2018, Back to basics of sequence stratigraphy, Early Miocene and Mid-Cretaceous examples from the New Jersey palaeoshelf: *Journal of Sedimentary Research*, v. 88, p. 148-176.

Milliman, J.D., and Syvitski, J.P.M., 1992, Geomorphic/tectonic control of sediment discharge to the ocean: the importance of small mountainous rivers: *Journal of Geology*, v. 100, p. 525-544.
Mitchell, N.C., Masselink, G., Huthnance, J.M., Fernández-Salas, L.M., and Lobo, F.J., 2012, Depths of modern coastal sand clinoforms: *Journal of Sedimentary Research*, v. 82, p. 469-481.

Mitchum, R.M. Jr., and Vail, P.R., 1977, Seismic stratigraphy and global changes in sea level, part 7: stratigraphic interpretation of seismic reflection patterns in depositional sequences: *Memoir of the American Association of Petroleum Geologists*, v. 39, no. Seismic Stratigraphy - Applications to Hydrocarbon Exploration, p. 116-139.

Mitchum, R.M. Jr., Vail, P.R., and Thompson, S., 1977, Seismic stratigraphy and global changes in sea level, part 2: the depositional sequence as the basic unit for stratigraphic analysis, in Payton, C.E., ed., *Seismic Stratigraphy: Applications to Hydrocarbon Exploration: American Association of Petroleum Geologists Memoir 26*, p. 53-62.

Mitchum, R., M., Jr., and Van Wagoner, J.C., 1990, High-frequency sequences and eustatic cycles in the Gulf of Mexico basin: *Proceedings, 11th Annual Gulf Coast Society for Sedimentary Geology Special Publication*, p. 257-267.

Monteverde, D.H., Mountain, G.S., and Miller, K.G., 2008, Early Miocene sequence development across the New Jersey margin: *Basin Research*, v. 20, p. 249-267.

Moore, G.T., 1969, Interaction of rivers and oceans; Pleistocene petroleum potential: *American Association of Petroleum Geologists Bulletin*, v. 53, p. 2421-2430.

Moore, A., Goff, J., McAdoo, B.G., Fritz, H.M., Gusman, A., Kalligeris, N., Kalsum, K., Susanto, A., Suteja, D., and Synolakis, C.E., 2011, Sedimentary Deposits from the 17 July 2006 Western Java Tsunami, Indonesia: Use of Grain-size Analyses to Assess Tsunami Flow Depth, Speed, and Traction Carpet Characteristics: *Pure and Applied Geophysics*, v. 168, p. 1951-1961

Morton, R. A., and Suter, J. R., 1996, Sequence Stratigraphy and Composition of Late Quaternary Shelf-Margin Deltas, Northern Gulf of Mexico: *American Association of Petroleum Geologists Bulletin*, v. 80, p. 505-530.

Moscardelli, L., Wood, L. J., and Dunlap, D. B., 2012, Shelf-edge deltas along structurally complex margins: A case study from eastern offshore Trinidad: *American Association of Petroleum Geologists Bulletin*, v. 96, p. 1483-1522.

Moss-Russell, A.C., 2009, The stratigraphic architecture of a prograding shelf-margin delta in outcrop, the Sobrarbe Formation, Ainsa Basin, Spain: Unpublished Master of Science Thesis, Colorado School of Mines.

Moston, R.P., Johnson, A.I., 1964, Ultrasonic Dispersion of Samples of Sedimentary Deposits, in: Nolan, T.B., *Geological Survey Research, Part 3*, p. 159-160.

Mountain, G., and Proust, J. N., 2010, The New Jersey margin scientific drilling project (IODP Expedition 313): Untangling the record of global and local sea-level changes: *Scientific Drilling*, no. 10, p. 26-34.

Mountain, G.S., Proust, J.-N., McInroy, D., Cotterill, C. and the Expedition 313 Scientists, 2010, Initial Report: Proceedings of the International Ocean Drilling Program, Expedition 313, College Station, Texas, 885 p.

Mulder, T., and Alexander, J., 2001, The physical character of subaqueous sedimentary density flows and their deposits: *Sedimentology*, v. 48, p. 269-299.

Mulder, T., and Chapron, E., 2011, Flood deposits in continental and marine environments: character and significance, in Slatt, R.M., and Zavala, C., eds., *Sediment transfer from shelf to deep water- Revisiting the delivery system: American Association of Petroleum Geologists, Studies in Geology*, p.1-30.

Mulder, T., Migeon, S., Savoye, B., and Faugères, J.-C., 2001, Inversely graded turbidite sequences in the deep Mediterranean. A record of deposits from flood-generated turbidity currents?: *Geo-Marine Letters*, v. 21, p. 86–93.

Mulder, T., and Syvitski, J.P.M., 1995, Turbidity currents generated at river mouth during exceptional discharges to the world's oceans: *Journal of Geology*, v. 103, p. 285–299.

Mulder, T., Syvitski, J.P.M., Migeon, S., Faugeres, J.C. and Savoye, B., 2003, Marine hyperpycnal flows: initiation, behavior and related deposits: a review: *Marine and Petroleum Geology*, v. 20, p. 861-882.

Mulder, T., Syvitski, J.P.M. and Skene, K.I., 1998, Modeling erosion and deposition by turbidity currents generated at river mouths: *Journal of Sedimentary Research*, v. 68, p. 124-137.

Muñoz, J.A., 1992, Evolution of a continental collision belt: ECORS-Pyrenees crustal balanced cross section, in McClay, K.R., ed., *Thrust Tectonics*, Chapman and Hall, London, p. 235-246.

Muñoz, J.A., Arbues, P., and Serra-Kiel, J., 1998, The Ainsa Basin and the Sobrarbe oblique thrust system: sedimentological and tectonic processes controlling slope and platform sequences deposited synchronously with a submarine emergent thrust system, in Hevia, A.M., Soria, A.R., eds., *Field Trip Guidebook of the 15th International Sedimentological Congress*, Alicante, p. 213–223.

Muto, T., and Steel, R.J., 1997, Principles of regression and transgression: the nature of the interplay between accommodation and sediment supply: *Journal of Sedimentary Research*, v. 67, p. 994–1000.

Muto, T., and Steel, R.J., 2002, In defence of shelf-edge delta development during falling stage and lowstand: *Journal of Geology*, v. 110, p. 421 – 436.

Muto, T., and Steel, R.J., 2014, The autostratigraphic view of responses of river deltas to external forcing: Development of the concept: *International Association of Sedimentologists Special Publication 47*, p. 139-148.

Mutti, E., Tinterri, R., Benevelli, G., DeBiase, D. and Cavanna, G., 2003, Deltaic, mixed and turbidite sedimentation of ancient foreland basins: *Marine and Petroleum Geology*, v. 20, p. 733–756.

Nakajima, T., 2006, Hyperpycnites deposited 700 km away from river mouths in the Central Japan Sea: *Journal of Sedimentary Research*, v. 76, p. 59–72.

Nelson, T.A., 1983, Time and Method Dependent Size distributions of Fine-Grained Sediment: *Sedimentology*, v. 30, p. 249-259.

Nemec, W., 1990, Aspects of sediment movement on steep delta slopes, in Colella, A., and Prior, D.B., *Coarse-Grained Deltas: International Association of Sedimentologists Special Publication 10*, p.29–73.

Nemec, W., Steel, R.J., Gjelberg, J., Collinson, J.D., Prestholm, E., and Oxnevad, I.E., 1988, Anatomy of collapsed and re-established delta front in Lower Cretaceous of eastern Spitsbergen: gravitational sliding and sedimentation processes: *American Association of Petroleum Geologists Bulletin*, v. 72, p. 454-476.

Normark, W.R., and Piper, D.J.W., 1991, Initiation processes and flow evolution of turbidity currents: implications for the depositional record, in Osborne, R.H., ed., *From Shoreline to Abyss: Contributions in Marine Geology in Honour of Francis Parker Shepard: Society for Sedimentary Geology Special Publication*, v. 46, p. 207–230.

Normark, W.R., Piper, D.J.W., Romans, B.W., Covault, J.A., Dartnell, P., and Sliter, R.W., 2009, Submarine canyon and fan systems of the California Continental Borderland, in Lee, H.J., and

Normark, W.R., eds, *Earth Science in the Urban Ocean: The Southern California Continental Borderland*, Geological Society of America Special Paper 454, p. 141-168.

Odin, G.S., and Matter, A., 1981, De glauconiarum origine: *Sedimentology*, v. 28, p. 611-641.

Odin, G.S., and Fullagar, P.D., 1988, Geological Significance of the Glauconite Facies, in Odin, G.S., ed., *Green Marine Clay*, Elsevier, Amsterdam, p. 295–332.

Olariu, C., 2014, Autogenic process change in modern deltas: lessons from the ancient, in Martinius, A.W., Ravnås, R., Howell, J.A., Steel, R.J., and Wonham, J.P., eds., *From Depositional*

Systems to Sedimentary Successions on the Norwegian Continental Margin: International Association of Sedimentologists, Special Publication 46, p. 149-166.

Olariu, C., and Bhattacharya, J.P., 2006, Terminal distributary channels and delta front architecture of river-dominated delta systems: *Journal of Sedimentary Research*, v. 76, 212–233.

Olariu, C., and Steel, R.J., 2009, Influence of point-source sediment-supply on modern shelf – slope morphology: implications for interpretation of ancient shelf margins: *Basin Research*, v. 21, p. 484- 501.

Olariu, C., Steel, R.J. and Petter, A.L., 2010, Delta-front hyperpycnal bed geometry and implications for reservoir modeling: Cretaceous Panther Tongue delta, Book Cliffs, Utah: *American Association of Petroleum Geologists Bulletin*, v. 94, p. 819–845.

Olariu, M.I., Carvajal, C., Olariu, C., and Steel, 2012, Deltaic process and architectural evolution during cross-shelf transits- Fox Hills Deltas, Washakie Basin, Wyoming: *American Association of Petroleum Geologists Bulletin*, v. 96, p. 1931-1956.

Oliveira, C.M.M., 2008, Soft-sediment deformation processes and products in shelf to base slope settings: Unpublished Ph.D. thesis, University of Liverpool, p. 327.

Oliveira, C.M.M., Hodgson, D.M., and Flint, S.S., 2011, Distribution of soft-sediment deformation structures in clinoform successions of the Permian Ecca Group, Karoo Basin, South Africa: *Sedimentary Geology*, v. 235, p. 314-330.

Patruno, S., Hampson, G.J., and Jackson C, A-L., 2015a, Quantitative characterisation of deltaic and subaqueous clinoforms: *Earth-Science Reviews*, v. 142, p. 79-119.

Patruno, S., Hampson, G.J., and Jackson C, A-L., Whipp, P.S., 2015b, Quantitative progradation dynamics and stratigraphic architecture of ancient shallow-marine clinoform sets: a new method and its application to the Upper Jurassic Sognefjord Formation, Troll Field, offshore Norway: *Basin Research*, v. 27, p. 412-452.

Patruno, S., and Helland-Hansen, W., 2018, Clinoform systems: Review and dynamic classification scheme for shorelines, subaqueous deltas, shelf edges and continental margins: *Earth Science Reviews*, v. 185, p. 202-233.

Payton, C.E., 1977, Seismic stratigraphy - application to hydrocarbon exploration: *American Association of Petroleum Geologists Memoir*, v. 26, p. 516.

Pellegrini, C., Maselli, V., Gamberi, F., Asioli, A., Bohacs, K.M., Drexler, T.M., and Trincardi, F., 2017, How to make a 350-m-thick lowstand systems tract in 17,000 years: The late

Pleistocene Po River (Italy) lowstand wedge: *Geological Society of America, Bulletin*, v. 45, p. 327-330.

Peng, Y., Steel, R.J., and Olariu, C., 2017, Transition from storm wave-dominated outer shelf to gullied upper slope: The mid-Pliocene Orinoco shelf margin, South Trinidad: *Sedimentology*, v. 64, p. 1511-1539.

Peterson, L.C., Haug, G.H., Hughen, K.A., and Rohl, U., 2000, Rapid changes in the hydrologic cycle of the Tropical Atlantic during the last glacial: *Science*, v. 290, p. 1947-1951.

Petter, A.L., and Steel, R.J., 2006, Hyperpycnal flow variability and slope organization on an Eocene shelf margin, central basin, Spitsbergen: *American Association of Petroleum Geologists, Bulletin*, v. 90, p. 1451-1472.

Pinous, O.V., Levchuck, M.A., and Sahagian, D.L., 2001, Regional synthesis of the productive Neocomian complex of West Siberia: sequence stratigraphic framework: *AAPG Bulletin*, v. 85, p. 1713-1730.

Piper, D.J.W., and Savoye, B., 1993, Processes of late Quaternary turbidity current flow and deposition on the Var fan, north-west Mediterranean Sea: *Sedimentology*, v. 40, p. 557-582.

Piper, D.J.W., Hiscott, R.N., and Normark, W.R., 1999, Outcrop-scale acoustic facies analysis and latest Quaternary development of Hueneme and Dume submarine fans, offshore California: *Sedimentology*, v. 46, p. 47-78.

Pirmez, C., Pratson, L.F., and Steckler, M.S., 1998, Cliniform development by advection-diffusion of suspended sediment: modelling and comparison to natural systems: *Journal of Geophysical Research*, v. 103, p. 141-157.

Plink-Björklund, P., 2008, Wave-to-tide facies change in a Campanian shoreline complex, Chimney Rock Tongue, Wyoming-Utah, USA, in Hampson, G.J., Steel, R.J., Burgess, P.M., Dalrymple, R.W., eds., *Recent Advances in Models of Siliciclastic Shallow Marine Stratigraphy: Society for Sedimentary Geology Special Publication 90*, p. 265-291.

Plink-Björklund, P., Mellere, D., and Steel, R.J., 2001, Turbidite variability and architecture of sand-prone, deep-water slopes: Eocene cliniforms in the central basin, Spitsbergen: *Journal of Sedimentary Research*, v. 71, p. 895-912.

Plink-Björklund, P., and Steel, R.J., 2002, Perched-delta architecture and the detection of sea level fall and rise in a slope-turbidite accumulation, Eocene Spitsbergen: *Geology*, v. 30, p. 115-118.

Plink-Björklund, P., and Steel, R.J., 2004, Initiation of turbidity currents: outcrop evidence for Eocene hyperpycnal flow turbidites: *Sedimentary Geology*, v. 165, p. 29-52.

Plink-Björklund, P., Steel, R., and Mellere, D., 2001, Turbidite variability and architecture of sand-prone, deep-water slopes: Eocene cliniforms in the Central Basin, Spitsbergen: *Journal of Sedimentary Research*, v. 71, p. 895-912.

Plint, A.G., and Nummedal, D., 2000, The falling stage systems tract: recognition and importance in sequence stratigraphic analysis; in *Sedimentary Responses to forced regressions*, in Hunt, D., and Gawthorpe, R., eds., Geological Society of London, Special Publications, 172, p. 1-17.

Poag, C.W., 1985, Depositional history and stratigraphic reference section for central Baltimore Canyon trough, in Poag, C.W., ed, *Geologic Evolution of the United States Atlantic Margin: New York (Van Nostrand Reinhold)*, p. 217-264.

Poag, C.W., Sevon, W.D., 1989, A record of Appalachian denudation in postrift Mesozoic and Cenozoic sedimentary deposits of the U.S. middle Atlantic continental margin: *Geomorphology*, v. 2, p. 119-157.

- Poag, C. W., Swift, B. A., Schlee, J. S., Ball, M. M., and Sheetz, L. L., 1990, Early Cretaceous shelf-edge deltas of the Baltimore Canyon Trough: Principal sources for sediment gravity deposits of the northern Hatteras Basin: *Geology*, v. 18, p. 149-152.
- Poblet, J., Muñoz, J.A., Yrave, A., and Serra-Kiel, 1998, Quantifying the kinematics of detachment folds using three-dimensional geometry: Application to the Mediano anticline (Pyrenees, Spain): *Geological Society of America Bulletin*, v. 110, p. 111-125.
- Pontén, A., and Plink-Bjorklund, P., 2009, Process regime changes across a regressive to transgressive turnaround in a shelf-slope basin, Eocene central basin of Spitsbergen: *Journal of Sedimentary Research*, v. 79, p. 2-23.
- Porębski, S.J., Pietsch, K., Hodiak, R and Steel, R.J., 2002, Origin and sequential development of Upper Badenian-Sarmatian clinofolds in the Carpathian Foredeep Basin, SE Poland: *Geologica Carpathica*, v. 54, p. 119-136.
- Porębski, S.J., and Steel, R.J., 2003, Shelf-margin deltas: their stratigraphic significance and relation to deepwater sands: *Earth-Science Reviews*, v. 62, p. 283–326.
- Porębski, S.J., and Steel, R.J., 2006, Deltas and sea-level change: *Journal of Sedimentary Research*, v. 76, p. 390-403.
- Posamentier, H.W., and Allen, G., 1999, Siliciclastic sequence stratigraphy – concepts and applications: *Society of Economic Paleontologists and Mineralogists Concepts in Sedimentology and Paleontology*, v. 7, p. 210.
- Posamentier, H.W., Allen, G.P., James, D.P., and Tesson, M., 1992, Forced regressions in a sequence stratigraphic framework: Concepts, examples, and exploration significance: *American Association of Petroleum Geologists, Bulletin*, v. 76, p. 1687-170.
- Posamentier, H.W., Jervey, M.T., and Vail, P.R., 1988, Eustatic controls on clastic deposition I— Conceptual framework, in Wilgus, C.K., Hastings, B.S., Posamentier, H., Van Wagoner, J., Ross, C.A., and Kendall, C.G.St.C., eds., *Sea-Level Changes: An Integrated Approach: Society of Economic Paleontologists and Mineralogists Special Publication 42*, p. 109–124.

Posamentier, H.W. and Kolla, V., 2003, Seismic geomorphology and stratigraphy of depositional elements in deep-water settings: *Journal of Sedimentary Research*, v. 73, p. 367-388.

Posamentier, H.W., and Vail, P., 1988, Eustatic controls on clastic deposition II- sequence and systems tract models, in Wilgus, C., Hastings, B.S., Kendall, C.G., Posamentier, H.W., Ross, C.A. and Van Wagoner, J.C., eds., *Sea level changes: an integrated approach*: Society of Economic Paleontologists and Mineralogists Special Publication 42, p. 125-154.

Postma, G., 1995, Sea-level-related architectural trends in coarse-grained delta complexes: *Sedimentary Geology*, v. 98, p. 3-12.

Poyatos-Moré, M., Jones, G.E.D., Brunt, R.L., Hodgson, D.H., Wild, R.J., Flint, S.S., 2016, Mud-dominated basin-margin progradation: process and implications: *Journal of Sedimentary Research*, v. 86, p. 863-878.

Poyatos-Moré, M., Jones, G.D., Brunt, R.L., Tek, D., Hodgson, D.M., and Flint, S.S., 2019, Clinoform architecture and facies distribution through an erosional to accretionary basin margin transition: *Basin Research*: In Press: <https://doi.org/10.1111/bre.12351>

Puigdefàbregas, C., 1975, La sedimentacion molasica en la Cuenca de Jaca: *Monografia del Instituto de Estudios Pirineos*, v. 104, p. 1-88.

Pratson, L.F., Nittrouer, C.A., Wiberg, P.L., Steckler, M.S., Swenson, J.B., Cacchione, D.A., Karson, J.A., Murray, A.B., Wolinsky, M.A., Gerber, T.P., Mullenbach, B.L., Spinelli, G.A., Fulthorpe, C.S., O'Grady, D.B., Parker, G., Driscoll, N.W., Burger, R.L., Paola, C., Orange, D.L., Field, M.E., Friedrichs, C.T. and Fedele, J.J., 2007, Seascape evolution on clastic continental shelves and slopes, in: Nittrouer, C.A., Austin, J.A., Field, M.E., Syvitski, J.M., Wiber, P.L., *Continental Margin Sedimentation: From Sediment Transport to Sequence Stratigraphy*: International Association of Sedimentologists Special Publication 37, 339-380.

Pratson, L.F., Ryan, W.B.F., Mountain, G.S., and Twichell, D.C., 1994, Submarine canyon initiation by downslope eroding sediment flows: evidence in Late Cenozoic strata on the New Jersey continental slope: *Geological Society of America Bulletin*, v. 106, p. 395-412.

Prélat, A., Pankhania, S.S., Jackson, C.A.-L., and Hodgson, D.M., 2015, Slope gradient and lithology as controls on the initiation of submarine slope gullies: Insights from the North Carnarvon Basin, Offshore NW Australia: *Sedimentary Geology*, v. 329, p. 12–17.

Prior, D.B., Bornhold, B.D, Wiseman Jr., W.J., and Lowe, D.R., 1987, Turbidity current activity in a British Columbia fjord: *Science*, v. 237, p. 581-584.

Proust, J.N., Pouderoux, H., Ando, H., Hesselbo, S.P., Hodgson, D.M., Lofi, J., Rabineau, M., and Sugarman, P.J., 2018, Facies architecture of Miocene subaqueous clinothems of the New Jersey passive margin: Results from IODP-ICDP Expedition 313: *Geosphere*, v. 14, p. 1564-1591.

Puigdefàbregas, C., 1975, La sedimentacion molasica en la Cuenca de Jaca: *Monografia del Instituto de Estudios Pirineos*, v. 104, p. 1-88.

Pyles, D.R., and Slatt, R.M., 2007, Stratigraphic evolution of the Upper Cretaceous Lewis Shale, Southern Wyoming: Applications to understanding shelf to base-of-slope changes in stratigraphic architecture of mud-dominated, progradational depositional systems, in: Nilsen, T.H., Shew, R.D., Steffebd, G.S., Studlick, J.R.J., eds., *Atlas of Deepwater Outcrops: American Association of Petroleum Geologists Studies in Geology*, v. 56, p. 19.

Pyles, D., Moss-Russell, A., Silalahi, H., Clark, J., Bracken, B., Bouroullec, R., Anderson, D., and Moody, J., 2010, Integrating outcrop data to define regional reservoir-scale patterns in prograding shelf-slope-basin systems, Sobrarbe Formation Spain: *American Association of Petroleum Geologists Annual Meeting Program with Abstracts*, v. 20.

Reineck, H.E., and Singh, I.B., 1972, Genesis of laminated sand and graded rhythmites in storm-sand layers of shelf mud: *Sedimentology*, v. 18, p. 123-128.

Reynaud, J.Y., and Dalrymple, R.W., 2011, Shallow-marine tidal deposits, in Davis, S., and Dalrymple, R.W., eds., *Principles of Tidal Sedimentation*: Springer, Berlin, p. 335–369.

Reynolds, T, 2018, The Analysis of Grain-Size in Siliciclastic Systems- a Step Forward? Applications to Paralic Systems: *British Sedimentological Research Group Annual Meeting*, Edinburgh, UK, Abstract.

Reynolds, D.J., Steckler, M.S., and Coakley, B.J., 1991, The role of the sediment load in sequence stratigraphy: the influence of flexural isostasy and compaction: *Journal of Geophysical Research (Solid Earth)*, v. 96, p. 6931–6949.

Rich, J.L., 1951, Three critical environments of deposition and criteria for recognition of rocks deposited in each of them: *Geological Society of America, Bulletin*, v. 62, p. 1-20.

Richards, M., Bowman, M., and Reading, H., 1998, Submarine-fan systems I: characterization and stratigraphic prediction: *Marine and Petroleum Geology*, v. 15, p. 689-717.

Roberts, H.H., 1997, Dynamic changes of the Holocene Mississippi River delta plain: the delta cycle: *Journal of Coastal Research*, v. 13, p. 605-637.

Roberts, H.H., 1998, Delta switching, early responses to the Atchafalaya River diversion: *Journal of Coastal Research*, v. 14, p. 882-899.

Romans, B.W., and Graham, S.A., 2013, A Deep-Time Perspective of Land-Ocean Linkages in the Sedimentary Record: *Annual Review of Marine Science*, v. 5, p. 69-94.

Romans, B.W., Hubbard, S.M., and Graham, S.A., 2009, Stratigraphic evolution of an outcropping continental slope system, Tres Pasos Formation at Cerro Divisadero, Chile: *Sedimentology*, v. 56, no. 3, p. 737-764.

Ross, W.C., Halliwell, B.A., May, J.A., Watts, D.E., and Syvitski J.P.M., 1994, Slope readjustment; a new model for the development of submarine fans and aprons: *Geology*, v. 22, p. 511–514.

Ross, W.C., Watts, D.E., and May, J.A., 1995, Insights from stratigraphic modelling: mud-limited versus sand-limited depositional systems: *American Association of Petroleum Geologists Bulletin*, v. 79, p. 231-258.

Rossi, V.M., Perillo, M.M., Steel, R.J., and Olairu, C., 2017, Quantifying mixed-process variability on shallow marine depositional systems: what are sediment structures really telling us?: *Journal of Sedimentary Research*, v. 87, p. 1060 – 1074.

Rossi, V.M., and Steel, R.J., 2016, The role of tidal, wave and river currents in the evolution of mixed-energy deltas: example from the Lajas Formation (Argentina): *Sedimentology*, v. 63, p. 824-864.

Roy, P.S., Cowell, P.J., Ferland, M.A., and Thom, B.G., 1994, Wave-dominated coasts, in Carter, R.W.G., and Woodroffe, C.D., eds., *Coastal Evolution: Late Quaternary Shoreline Morphodynamics*: Cambridge, UK, Cambridge University Press, p. 121.

Rubidge, B.S., Hancox, P.J., Mason, R., 2012, Waterford Formation in the south-eastern Karoo: Implications for basin development: *South African Journal of Science*, v. 108, p. 598-623.

Ryan, M., Helland-Hansen, W., Johannessen, E.P., and Steel, R.J., 2009, Erosional vs accretionary shelf margins: the influence of margin type on deepwater sedimentation- an example from the Porcupine Basin, offshore western Ireland, in Henriksen, S., Hampson, G.J., Helland-Hansen, W., Johannessen, E.P., and Steel, R.J., *Trajectory Analysis in Stratigraphy: Basin Research*, v. 21, p. 676-703.

Sahu, B.K., 1964, Depositional Mechanisms for the Size Analysis of Clastic Sediments: *Journal of Sedimentary Petrology*, v. 34, p. 73-83.

Sanchez, C.M., Fulthorpe, C.S., and Steel, R.J., 2012, Middle Miocene – Pliocene siliciclastic influx across a carbonate shelf and influence of deltaic sedimentation on shelf construction, northern Carnarvon Basin, Northwest Shelf of Australia: *Basin Research*, v. 24, p. 664-662.

Savage, E.L., 1969, Ultrasonic Disaggregation of Sandstones and Siltstones: *Journal of Sedimentary Research*, v. 39, p. 375-378.

Schellpeper, M., and R.J. Steel, 2001, A shelf edge delta-to-estuary couplet in the Eocene Battfjellet Formation, Central Basin, Spitsbergen: Abstract, American Association of Petroleum Geologists, Annual Meeting, Denver.

Schlager, W., 1993, Accommodation and supply: a dual control on stratigraphic sequences: *Sedimentary Geology*, v. 86, p. 111-136.

Schlee, J.S., Dillon, W.P., and Grow, J.A., 1979, Structure of the continental slope off the eastern United States, in Doyle, L.J., and Pilkey, O.H., eds., *Geology of Continental Slopes: Society of Economic Paleontologists and Mineralogists Special Publication*, 27, p. 95-117.

Schmitz, B., 1987, The TiO_2/Al_2O_3 ratio in the Cenozoic Bengal Abyssal Fan sediments and its use as a paleostream indicator: *Marine Geology*, v. 76, p. 195-206.

Schumacher, B. A., 2002, *Methods for the Determination of Total Organic Carbon (TOC) in Soils and Sediments*. Ecological Risk Assessment Support Centre, Office of Research and Development, US Environmental Protection Agency, Las Vegas.

Shanley, K.W., and McCabe, P.J., 1994, Perspectives on the Sequence Stratigraphy of Continental Strata: *American Association of Petroleum Geologists Bulletin*, v. 78, p. 544-568.

Shanmugam, G., Bloch, R.B., Mitchell, S.M., Damuth, J.E., Beamish, G.W.J., Hodgkinson, R.J., Straume, T., Syvertsen, S.E., and Shields, K.E., 1996, Slump and debris-flow dominated basin-floor fans in the North Sea: an evaluation of conceptual sequence-stratigraphical models based on conventional core data: *Geological Society of London Special Publication* 103, p. 145-176.

Sheridan, R.E., and Grow, J.A., 1988, U.S. Atlantic Continental Margin; A typical Atlantic-type or passive continental margin in Sheridan, R.E., and Grow, J.A., *The Atlantic Continental Margin: Geological Society of America, Geology of North America Series*, v. I-2, p. 1-7.

Shiers, M.N., Hodgson, D.M., Mountney, N.P., 2017, Response of a coal-bearing coastal-plain succession to marine transgression: Campanian Neslen formation, Utah, U.S.A.: *Journal of Sedimentary Research*, v. 87, p. 168-187.

Simon, A., Bennett, S.J., and Castro, J.M., 2013, *Stream Restoration in Dynamic Fluvial Systems: Scientific Approaches, Analyses and Tools: Geophysical Monograph Series*, v. 194, p. 1892-1902.

Slingerland, R., Selover, R. W., Ogston, A. S., Keen, T. R., Driscoll, N. W., and Milliman I. D., 2008, Building the Holocene clinothem in the Gulf of Papua: An ocean circulation study: *Journal of Geophysical Research*, v. 113, p. F01S14.

Sømme, T.O., Helland-Hansen, W., Martinsen, O.J., Thurmond, J.B., 2009, Relationships between morphological and sedimentological parameters in source- to-sink systems: a basis for predicting semi-quantitative characteristics in subsurface systems: *Basin Research*, v. 21, p. 361-387.

Southard, J.B., and Stanley, D.J., 1976, Shelf-break processes and sedimentation, in Stanley, D.J., and Swift, D.J.P., eds., *Marine Sediment Transport and Environmental Management*: New York, Wiley-Interscience, p. 351-377.

St-Onge, G., Mulder, T., Piper, D.J.W., Hillaire-Marcel, C., and Stoner, J.S., 2004, Earthquake and flood-induced turbidites in the Saguenay Fjord (Quebec): a Holocene paleoseismicity record: *Quaternary Science Reviews*, v. 23, p. 283-294.

Steckler, M.S., Mountain, G.S., Miller, K.G., and Christie-Blick, N. 1998, Reconstruction of Tertiary progradation and clinoform development on the New Jersey margin by 2-D backstripping: *Marine Geology*, v. 154, p. 399-420.

Steel, R.J., Carvajal, C., Petter, A.L., and Uroza, C., 2008, Shelf and shelf-margin growth in scenarios of rising and falling sea level, in Hampson, G.J., ed., *Recent Advances in Models of Siliciclastic Shallow-Marine Stratigraphy*, Society for Sedimentary Geology Special Publication 90, p. 47-71.

Steel R.J., Crabaugh, J., Schellpeper, M., Mellere, D., Plink-Bjorklund, P., Deibert, J., and T. Loeseth, 2000, Deltas versus rivers on the shelf edge: their relative contributions to the growth of shelf margins and basin-floor fans (Barremian and Eocene, Spitsbergen): 20th Annual Gulf Coast Society for Sedimentary Geology Special Publication, *Deepwater Reservoirs of the World*, Houston, Dec. 2000, pp. 981-100.

Steel, R.J., Gjelberg, J., Helland-Hansen, W., Kleinspehn, K.L., Nøttvedt, A. and Rye-Larsen, M., 1985, The Tertiary strike-slip basins and orogenic belt of Spitsbergen, in Biddle K.T., and Christie-Blick N., eds., *Strike-Slip Deformation, Basin Formation and Sedimentation*, Society of Economic Palaeontologists and Mineralogists, Special Publication, 37, p. 339-359.

Steel, R., Mellere, D., Plink-Björklund, P., Crabaugh, J., Deibert, J., Loeseth, T., and Shellpeper, M., 2000, Deltas v rivers on the shelf edge: their relative contributions to the growth of shelf-

margins and basin-floor fans (Barremian and Eocene, Spitsbergen): Gulf Coast Society for Sedimentary Geology Special Publication, 20th Annual Research Conference Special Publication, p. 981–1009.

Steel, R.J., and Milliken, K.L., 2013, Major advances in siliciclastic sedimentary geology, 1960–2012, in Bickford, M.E., ed., *The Web of Geological Sciences: Advances, Impacts, and Interactions*: Geological Society of America Special Paper 500, p. 121-167.

Steel, R.J., and Olsen, T., 2002, Clinoforms, clinoform trajectory and deepwater sands, in Armentrout, J.M., and Rosen, N.C., eds., *Sequence Stratigraphic Models for Exploration and Production: Evolving Methodology, Emerging Models and Application Histories: Proceeding of the 22nd Annual Bob F. Perkins Research Conference, Gulf Coast Section, (Dallas, TX), USA*: Society of Economic Paleontologists and Mineralogists (GCS-SEPM), p. 367-381.

Steel, R.J., Porębski, S.J., Plink-Björklund, P., Mellere, D., and Schellpeper, M., 2003, Shelf-Edge Delta Types and their Sequence-Stratigraphic Relationships, in Roberts, H.H., Rosen, N.C., Fillon, R.H., Anderson, J.B., eds., *Shelf Margin Deltas and Linked Down Slope Petroleum Systems*: Society for Economic Paleontologists and Mineralogists, v. 23, p. 205-230.

Sterner, R.W., and Elser, J.J., 2002, *Ecological Stoichiometry: the Biology of Elements from Molecules to the Biosphere*, Princeton University Press, Princeton: ISBN 9781400885695

Stevenson, C., Jackson C. A.-L., Hodgson, D.M., Hubbard, S.M., and Eggenhuisen, J.T., 2015, Deep-water sediment bypass: *Journal of Sedimentary Research*, v. 87, p. 1058-1081.

Stow, D., 1994, Deep sea processes of sediment transport and deposition, in: Pye, K., *Sediment Transport and Depositional Processes*, Blackwell Scientific Publications, Oxford, p. 257–291.

Sugarman, P.J., Miller, K.G., Owens, J.P., and Feigenson, M.D., 1993, Strontium-isotope and sequence stratigraphy of the Miocene Kirkwood Formation, southern New Jersey: *Geological Society of America Bulletin*, v. 105, p. 423-436.

Sumner, E.J., Talling, P.J., Amy, L.A., Wynn, R.B., Stevenson, C.J., and Frenz, M., 2012, Facies architecture of individual basin-plain turbidites: Comparison with existing models and implications for flow processes: *Sedimentology*, v. 59, p. 1850-1887.

Suter, J. R., and Berryhill, H. L., 1985, Late Quaternary shelf-margin deltas, Northwest Gulf of Mexico: *American Association of Petroleum Geologists Bulletin*, v. 69, p. 77-91.

Swenson, J.B., Paola, C., Pratson, L., Voller, V.R., and Murray, A.B., 2005, Fluvial and marine controls on combined subaerial and subaqueous delta progradation: morphodynamic modelling of compound-cliniform development: *Journal of Geophysical Research*, v. 110, p. 1-16.

Swift, D.J.P., and Thorne, J.A., 1991, Sedimentation on continental margins, I: a general model for shelf sedimentation, in Swift, D.J.P., Oertel, G.F., Tillman, R.W., and Thorne, J.A., eds., *Shelf Sand and Sandstone Bodies; Geometry, Facies and Sequence Stratigraphy*: Society for Economic Palaeontologists and Mineralogists, Special Publication 14, p. 3-31.

Sydow, J., Finneran, J., and Bowman, A.P., 2003, Stacked shelf-edge delta reservoirs of the Columbus Basin, Trinidad, West Indies, in Roberts, H., ed., *Shelf-Margin Deltas and Linked Downslope Petroleum Systems: Global Significance and Future Exploration Potential*, Gulf Coast Society for Sedimentary Geology Special Publication, p. 441-465.

Sydow, J., Roberts, H., 1994, Stratigraphic framework of a Late Pleistocene shelf-edge delta, northeast Gulf of Mexico: *American Association of Petroleum Geologists Bulletin*, v. 78, p. 1276-1312.

Sylvester, Z., Deptuck, M.E., Prather, B.E., Pirmez, C., and O'Byrne, C., 2012, Seismic stratigraphy of a shelf-edge delta and linked submarine channels in the northeastern Gulf of Mexico, in Prather, B.E., Deptuck, M.E., Mohrig, D., Van Hoorn, B., and Wynn, R.B., eds., *Application of the Principles of Seismic Geomorphology to Continental-Slope and Base-of-Slope Systems: Case Studies from Seafloor and Near-Seafloor Analogues*: Society for Sedimentary Geology Special Publication 99, p. 31-59.

Syvitski, J.P.M., 2003, Supply and flux of sediment along hydrological pathways: research for the 21st Century: *Global and Planetary Change*, v.39, p. 1-11.

Ta, T.K.O., Nguyen, V.L., Tateishi, M., Kobayashi, I., Saito, Y., Nakamura, T., 2002, Sediment facies and Late Holocene progradation of the Mekong River Delta in Bentre Province, southern Vietnam: an example of evolution from a tide-dominated to a tide- and wave-dominated delta: *Sedimentary Geology*, v. 152, p. 313-325.

Talling, P.J., 2014, On the triggers, resulting flow types and frequencies of subaqueous sediment density flows in different settings: *Marine Geology*, v. 352, p. 155-182.

Taylor, A.M., and Goldring, R., 1993, Description and analysis of bioturbation and ichnofabric: *Journal of the Geological Society*, v. 150, p. 141-148.

Tesson, M., Gensous, B., Allen, G. P., and Ravenne, C., 1990, Late Quaternary deltaic lowstand wedges on the Rhône continental shelf, France: *Marine Geology*, v. 91, p. 325-332.

Thorne, J., 1995, On the scale independent shape of prograding stratigraphic units, in Barton, C.B., La Point, P.R., eds., *Fractals in Petroleum Geology and Earth processes*, Plenum Press, New York, p. 97-112.

Udden, J.A., 1914, Mechanical composition of clastic sediments: *Geological Society of America Bulletin*, v. 25, p. 655-744.

Uroza, C.A., and Steel, R.J., 2008, A highstand shelf-margin delta system from the Eocene of West Spitsbergen, Norway: *Sedimentary Geology*, v. 203, p. 229-245.

Vaasma, T., 2008, Grain-size analysis of lacustrine sediments: a comparison of pre-treatment methods: *Estonian Journal of Ecology*, v. 57, 231-243.

Vail, P. R., Audemar, F., Bowman, S. A., Eisner, P. N., and Perez-Cruz, C., 1991, The stratigraphic signatures of tectonics, eustasy and sedimentology - and overview, in Einsele, G., Ricken, W., and Seilacher, A., eds., *Cycles and Events in Stratigraphy*, Springer-Verlag, Berlin Heidelberg, p. 617-659.

Vail, P.R., Mitchum, R.M., Jr., and Thompson, S., 1977, Seismic stratigraphy and global changes of sea level, part 4, global cycles of relative changes of sea level, in Payton, C.E., ed., *Seismic Stratigraphy, Application to Hydrocarbon Exploration: American Association of Petroleum Geologists, Memoir 26*, p. 83-97.

Vail, P.R., and Todd, R.G., 1981, Northern North Sea Jurassic unconformities, chronostratigraphy and sea-level changes from seismic stratigraphy, in Illing, L.V., and Hobson, G.D., eds., *Petroleum Geology of the Continental Shelf of Northwest Europe*, Proceedings of the Second Conference, Heyden, London, p. 216-235.

Vakarelov, B.K., and Ainsworth, R.B., 2013, A hierarchical approach to architectural classification in marginal-marine systems: bridging the gap between sedimentology and sequence stratigraphy: American Association of Petroleum Geologists, Bulletin 97, p. 1121-1161.

Van Lunsen, H., 1970, Geology of the Ara-Cinca region, Spanish Pyrenees, province of Huesca: *Geologica Utraiectana*, v. 16, p. 1-119.

Van Wagoner, J.C., 1985, Reservoir facies distribution as controlled by sea-level change: Abstract and Poster Session, Society of Economic Paleontologists and Mineralogists Midyear Meeting, Golden, Colorado, p. 91-92

Van Wagoner, J.C., Mitchum, R.M., Jr, Posamentier, H.W., and Vail, P.R., 1987, Seismic stratigraphy interpretation using sequence stratigraphy: Part 2. Key definitions of sequence stratigraphy, in Bally, A.W., ed., *Atlas of Seismic Stratigraphy: American Association of Petroleum Geologists, Studies in Geology 27*, p. 11–14.

Van Wagoner, J.C., Posamentier, H.W., Mitchum, R.M., Vail, P.R., Sarg, J.F., Loutit, T.S., and Hardenbol, J., 1988, An overview of the fundamentals of sequence stratigraphy and key definitions: *The Society of Economic Paleontologists and Mineralogists: Society for Sedimentary Geology*, v.42

Van Wagoner, J.C., Mitchum, R.M. Jr., Campion, K.M., and Rahmanian, V.D., 1990, Siliciclastic sequence stratigraphy in well logs, cores and outcrops: concepts for high-resolution correlation of time and facies: American Association of Petroleum Geologists, *Methods in Exploration Series*, v.7

Verges, J., and Muñoz, J.A., 1990, Thrust sequences in the southern Central Pyrenees: *Bulletin de la Societe Geologique de France*, v. 8, p. 265-271

Wadsworth, J.A., 1994, Sedimentology and Sequence Stratigraphy in an Oversteepened Ramp Setting: Sobrarbe Formation, Ainsa Basin, Spanish Pyrenees: Unpublished Ph.D. Thesis, University of Liverpool, p. 195

Walker, R.G., 1967, Turbidite sedimentary structures and their relationship to proximal and distal depositional environments: *Journal of Sedimentary Petrology*, v. 37, p. 25-43.

Walker, R.G. and Plint, A.G., 1992, Wave- and storm-dominated shallow marine systems, in

Walker, R.G., and James, N.P., *Facies Models: Response to Sea-level Change: Geological Association of Canada*, 219–238 pp.

Walling, D.E., and Horowitz, A.J., 2005, *Sediment Budgets: Technology and Engineering*, Vol. 1, p. 367- 382.

Walsh, J.P., and Nittrouer, C.A., 2003, Contrasting styles of off-shelf sediment accumulation in New Guinea: *Marine Geology*, v. 196, p. 105-125.

Walsh, J.P., and Nittrouer, C.A., 2009, Towards an understanding of fine-grained river-sediment dispersal on continental margins: *Marine Geology*, v. 263, p. 34-45.

Watson, E.B., Pasternack, G.B., Gray, A.B., Goñi, and Woolfolk, A.M., 2013, Particle size characterization of historic sediment deposition from a closed estuarine lagoon, Central California: *Estuarine, Coastal and Shelf Science*, v. 126, p. 23-33.

Watts, A.B., and Steckler, M.S., 1979. Subsidence and eustasy at the continental margin of eastern North America, in Talwani, M., Hay, W., and Ryan, W.B.F., eds, *Deep Drilling Results in the Atlantic Ocean: Continental Margins and Paleoenvironment*, Maurice Ewing Series, v. 3, p. 218–234.

Wear, C.M., Stanley, D.J., and Boula, J.E., 1974, Shelf break physiography between Wilmington and Norfolk canyons: *Journal of Marine Science and Technology*, v. 8, p. 37-48.

Weber, M.E., Wiedicke, M.H., Kudrass, H.R., Hübscher, C., and Erlenkeuser H., 1997, Active growth of the Bengal fan during sea-level rise and highstand: *Geology*, v. 25, p. 315-318.

Weimer, P., and Posamentier, H.W., 1994, *Siliciclastic Sequence Stratigraphy. Recent developments and Applications: American Association of Petroleum Geologists Memoir 58*, p. 492-523.

Wentworth, C.K., 1922, A scale of grade and class terms for clastic sediments: *Journal of Geology*, v. 30, p. 377-392.

Wermund, E.G., 1961, Glauconite in early Tertiary sediments of Gulf Coast Province, *American Association of Petroleum Geologists, Bulletin* 45, p. 1667-1696.

Westermann, J., 2013, Particle Characterisation with Dynamic Image Analysis, *Whitepaper European Pharmaceuticals Review*.

Wild, R., Flint, S.S., and Hodgson, D.M., 2009, Stratigraphic evolution of the upper slope and shelf edge in the Karoo Basin, South Africa: *Basin Research*, v. 21, p. 502-527.

Wilgus, C.K., Hastings, B.S., Posamentier, H., Van Wagoner, J., Ross, C.A., and Kendall, C.G.St.C., 1988, Sea Level Changes: An Integrated Approach: *Society for Sedimentary Geologists Special Publication* 42, p. 407-426.

Williams, P.F., and Rust, B.R., 1969, The sedimentology of a braided river: *Journal of Sedimentary Petrology*, v. 39, p. 649-679.

Willis, B., 2005, Deposits of tide-influenced river deltas, in Giosan, L., and Bhattacharya, J.P., eds., *River Deltas: Concepts, Models and Examples: Society for Sedimentary Geologists Special Publication* 83, p. 87-129.

Wilson, M.D., and Pittman, E.D., 1977, Authigenic Clays in Sandstones: Recognition and Influence on Reservoir Properties and Palaeoenvironmental Analysis: *Journal of Sedimentary Petrology*, v. 47, p. 3-31.

Winker, C. D., 1982, Cenozoic shelf margins, northwestern Gulf of Mexico basin: *Gulf Coast Association of Geological Societies*, v. 32, p. 427-448.

Withjack, M.O., Schlische, R.W., and Olsen, P.E., 1998, Diachronous rifting, drifting, and inversion on the passive margin of Eastern North America: an analogue for other passive margins: *American Association of Petroleum Geologists Bulletin*, v. 82, p. 817-835.

Wright, L.D., and Friedrichs, C.T., 2006, Gravity-driven sediment transport on continental shelves: a status report: *Continental Shelf Research*, v. 26, p. 2092–2107.

Wright, L.D., Yang, Z.-S., Bornhold, B.D., Keller, G.H., Prior, D.B., and Wiseman Jr., W.J., 1986, Hyperpycnal plumes and plume fronts over the Huanghe (Yellow River) delta front: *Geo-Marine Letters*, v. 6, p. 97-105.

Wright, L.D., Wiseman, W.J., Bornhold, B.D., Prior, D.B., Suhayda, J.N., Keller, G.H., Yang, L.S., and Fan, Y.B., 1988, Marine dispersal and deposition of Yellow River silts by gravity-driven underflows: *Nature*, v. 332, 629- 632.

Yang, Y., and Aplin, A.C., 1997, A method for the disaggregation of mudstones: *Sedimentology*, v. 44, pp. 559-562.

Zamagni, J., Mutti, M., and Košir, A., 2008, Evolution of shallow benthic communities during the Late Paleocene-earliest Eocene transition in the Northern Tethys (SW Slovenia): *Facies*, v. 54, p. 25-43.

Zavala, C. and Arcuri, M., 2016, Intrabasinal and extrabasinal turbidites: origin and distinctive characteristics: *Sedimentary Geology*, v. 337, p. 36–54.

Zavala, C., Arcuri, M., and Blanco Valiente, L., 2012, The importance of plant remains as diagnostic criteria for the recognition of ancient hyperpycnites: *Revue de Paléobiologie*, v. 11, p. 457-469.

Zavala, C., M. Arcuri, M. Di Meglio, H. Gamero Diaz, and C. Contreras, 2011, A genetic facies tract for the analysis of sustained hyperpycnal flow deposits, in: Slatt, R.M., and Zavala, C., eds., *Sediment transfer from shelf to deep water—Revisiting the delivery system: AAPG Studies in Geology* 61, p. 31–51.

Zavala, C., H. Gamero, and M. Arcuri, 2006, Lofting rhythmites: A diagnostic feature for the recognition of hyperpycnal deposits (abs): *Geological Society of America Abstracts with Programs*, v. 38, no. 7, p. 541.

Zavala, C. and Pan, S.X., 2018, Hyperpycnal flows and hyperpycnites: Origin and distinctive characteristics: *Lithologic Reservoirs*, v. 30, p. 1-27.

Zeng, J., Lowe, D.R., Prior, D.B., Wiseman Jr., W.J., and Bornhold, B.D., 1991, Flow properties of turbidity currents in Bute Inlet, British Columbia: *Sedimentology*, v. 38, p. 975-996.